PROCEEDINGS OF THE 9th INTERNATIONAL CLOUD PHYSICS CONFERENCE

VOLUME II

ТРУДЫ 9-Й МЕЖДУНАРОДНОЙ КОНФЕРЕНЦИИ ПО ФИЗИКЕ ОБЛАКОВ

ТОМ II

TALLINN, ESTONIAN SSR, USSR

21—28 August, 1984

PROCEEDINGS OF THE 9th INTERNATIONAL CLOUD PHYSICS CONFERENCE

ТРУДЫ 9-Н МЕ)КАУНАРОАНОJ1 КОН<I>ЕРЕНЦJ1J1 по ФНЗИКЕ 0БЛАК0В

INTERNATIONAL. COMMISSION ON CLOUD PHYSICS

INTERNATIONAL ASSOCIATION OF
METEOROLOGY AND ATMOSPHERIC PHYSICS

PROCEEDINGS OF THE 9th INTERNATIONAL CLOUD PHYSICS CONFERENCE

TALLINN,ESTONIAN SSR, USSR 21-28 AUGUST, 1984

VOLUME II

SPONSORS ACADEMY OF SCIENCES OF THE USSR,
SOVIET GEOPHYSICAL COMMIITEE
ACADEMY OF SCIENCES OF THE ESTONIAN SSR,
INSTITUTE OF ASTROPHYSICS AND ATMOSPHERIC PHYSICS
USSR STATJi' COMMIITEE FOR HYDROMETEOROLOGY AND
CONTROL OF NATURAL ENVIRONMENT,
CENTRAL AEROLOGICAL OBSERVATORY

TALLINN „VALGUS" 1984

53
P78

UDK 551.576

Chairman of the Conference
Yu.S. Seciunov

International Scientific
Programme Coramittee (ISPC)

I.P. Mazin - Chairman (USSR)
O.A. Avaste (USSR)
A.A. Chernikov (USSR)
G.B. Foote (USA)
W.F. Hitschfeld - President ICCP
P.V. Hobbs (USA)
P.R. Jonas (United Kingdom)
W. King (Australia)
H.R. Pruppacher (?RG)
R.R. Rogers. (Canada)
Yu. S. Sedunov (US.SR)
R.G. Soulage (France)

National Organizing Committee

I.P. Opik (Chairman)
O.A. Avaste (Vice-Chairman)
I. P. Mazin .Vice-Chairraan)
U.R. Mullamaa (Vice-Chairman)
N.O. Plaude (Sec etary)
I.I. Burtsev
A.A. Chernikov
A.G. Kallis
A.Kh. Khrgian
A.D. Povzner
V.A. Unt
Ch.J. Villmann
V.M. Voloschuk

Local Organizing Committee:

U.R. Mullamaa (Chairman)
Institute of Astrophysics and
Atmospheric Physics,
202444 Toravere, Tartu, Estonia, USSR

Cover by R. Hagar
Edited by V. Russak

P $\frac{1903040000 - 214}{М\ 902\ (1'6) - 84}$ Заказное

ВНП;,t:leHO ТПО 3аКа3у АКageМНН НауК
3СТОНСКОН ССР

Tipegce aTeJib KOH@epeH:O:HH
[J.C. CegyHOB

Me>K'AYHapogHH!'.1: Hay'!HHH
nporpaMMHHH KOMHTeT (MHIIK)

H.TI. Ha3HH - rrpegcegaTeJib (CCCP)
O.A. ABaCTe (CCCP)
TI.P. ,J:\)!:<CHac(BeJIHK06pHTaHH.f!)
B. KHHr (ABCTpaJIH.f!)
X.P. Ilpyrrrraxep (Pr)
P.P. Pog epc (KaHaga)
,0.C. CegyHOB (CCCP)
P.r. Cyna (<I>paH:O:HH)
r.E. <I>yT (C[;JA)
B- - XHT'I eJib'A - rrpe3HgeHT MK O
rr.B. Xo6c (C[;JA)
A.A. qepHHKOB (CCCP)

Национальный организационный
KOMHTeT

H.Il. 3rrHK (rrpegcegaTenb)
O.A. ABacTe (3aM. npegcegaTenH)
H. rr. 1-la3HH (3aM. rrpegcegaTeJIH)
IO.P. MynnaMaa (3aM rrpegcegaTenH)
H.O. Ilnayge (ceKpeTap)
H.H. Byp:o;eB
q.fi. BHJIJIMaHH
B. M. BOJIOf:r.\YK
A. r. KaJIJIHC
A.,!l;. TIOB3Hep
B.A. YHT
A.X. XprHaH
A.A. qepHHKOB

MeCTHHH oprKOMHTeT:

Iv.P. 1-1ynnaMaa (npegcega TeJib)
HHCTHTYT aCTpO H3HKH H H3HKH
aTMOC epH
202444 THpaBepe, TapTy, 3CCP

06JIO Ka P. MHrap
PegaKTOP B. PyccaK

© Academy of Sciences of the Eston.ian SSR,
1934

C O N T E N T S

SESSION III

MESO- AND MACROSTRUCTURE OF CLOUDS AND CLOUD SYSTEMS

Subsession III-I

Storms, sqall lines

STRUCT RE AND EVOLUTION OF A CONTINENTAL WEST-AFRICAN SQUALL LINE

J.P. CHALON, G. JAUBERT and D. ROSSTAUD

Etablissement d'Etudes et de Recherches Meteorologiques
Direction de la Meteorologie
CNRM/Toulouse - FRANCE

1. INTRODUCTION

A curate descriptions of tropical squall lines are difficult due to the scarcity of meteorological observations in the.Tropics. Experiments over the Caribbean sea in 1968 (Ref.1), GATE over the Tropical Atlantic in 1974 (Ref.2) and VIMHEX in Venezuela in 1972 (Ref.3) h;,ve allowed to obtain a better description and a better understanding of processes involved in the formation and evolution of maritime and South-American tropical squall lines. An experiment for the study of the African tropical convection (COPT 81) has been conducted in the North of Ivory Coast in May-June 1981 by French and Ivorian research Institutes. A radiosounding station, a dual Doppler radar system (Ro sard) and two mesoscale networks of automated meteorological stations (4M and Alice) were operated. Reports from the African meteorolqgical stations and pictures from the NOAA6 satellite were available. This experiment was described with details (Ref.4), it allowed the observation of several African Continental tropical squall lines. As maritime squall lines in the Tropics, continental ones have an important contribution to energy exchanges at the global circulation scale, moreover, in sub-Saharan Africa they also provide most of the rainfall.

A-squall line which crossed over the experiment field during the night of June 23 to 24 has been studied. We will essentially discuss here the characteristics of the environment, the structure and evolution of the squall line through satellite pictures and radar reflectivity data and its signature as recorded by the network of automated stations. Its dynamics obtained from the Ronsard system data will be presented during this conference by Roux (Ref.5). The evolution of the convective part of the system has been simulated and results will be presented by Lafore and Redelsperger (Ref.6).

2. LARGE SCALE CHARACTERISTICS

a) Synoptic scale observations

On June 22 and 2'3, the synoptic field was mainly characterized by low pressures centered over tte Algerian Sahara at low level and high pressures at 20"0 mb. The Intertropical Front ondulated between the 15 N and 20 N latitudes. The studied squall lin developped under such conditions on June 22 over Nigeria. Available data from the African meteorological.network and pictures from the NOAA6 sat.ellite allowed to analyse its large scale structure and trajectory from June 23 at 00:00 GMT to June 24 at 06:00 GMT (time used throughout this paper is GMT).

The cloud system associated with this line was aboul: 700 km long (North to South) and 250 to 500 km wide (East to West) (Figure 1). Its width increased with time. We can notice on Figure 1 that the clouds wer restricted to the rear of the squall in th early stage (06:00) and that a frontal anvil appeared later (18:00) in the evolution of. the system. Howeverl, a part of the clouds seen on the picture at 18:00 !were associated with diurnal corivection which devélopped West of the squall line.

,At larx e s c? l (Figure 22 , tl) prop'!filitj21, of. the

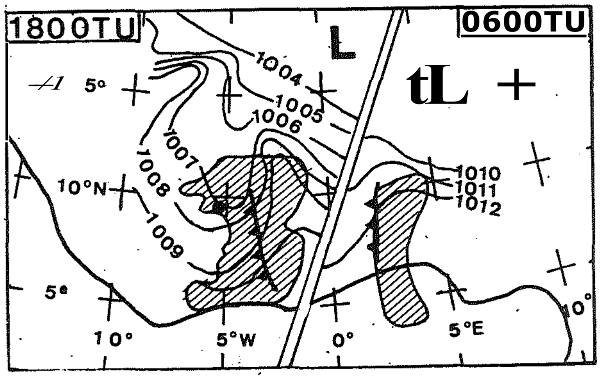

Fi gWte 1. ·rhe da.c,hed.Mecv., nepnv.,en,,t the doud coven a.c,1.,oucu:ed wdh :the .s:tuMed 1.iqu.a.il line 1iy1.item and ,ob1.ienved by :the NOAA6 1.icu:e.W,te on June 23 a: 08:0v and f9:00. ContoUM nepnv.,e.n,;,: :the 1.iUJt6ace ,tJ.iObMJ.i MJ.iOUCU:d wdh :the'env onment 06 :the 1.iqua.U 1iy1.i- :te and ob1.ienved by ,:the Wv.,:t-A6can me:teonolog,i_cal ne:twonk.. The 1.imaU black. unde ,i.nMccu:e :the po1.i,i-tion 06 :the Mud ex.pen,i.men:t.

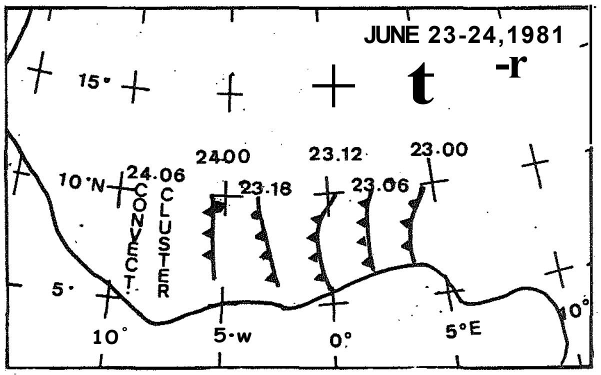

EigUJte 2. Succv.,1.i,i.ve po1.i,ttioYL1.i 06 :the leadfog edge. 06 :the 1.iqua.U deduced 6Mm J.iWtoace and 1.ia:telu:te obli enva;t,i.o Yi .

;squall was essentially towards West with a mean speed-lof 12 m.s-1.Thisisquite less th;m the average of 17 µi.s-1 usually recorded for squall- lines in this area. The line was over Niamey (Niger) at 5:00 on June 23, was over Korhogo at 23:40 and turned into a conve - tive cluster when it arrived over the Fouta-Djallon mountains. Ground observations are in agreement with position of the line. Cumulonimbus and thunderstorms were observed below the system. The surface signa-_ ture •of the squall (SSS) was a line slightly concqve, making an angle of +20 to -20 degrees with respect to the meridian lines and it was active enough to be Jbserved over a length of 400 to 500 km. Ondulations in the pressure field were present at all levels above the syste and travelled at the speed of the ·sss. At 06:00 and 18:00 on June 23, the axis of the thalweg and through associated with the squall were parallel 'to i:he.SSS and distant by 300 km. These ondulaticns were weak in the morning and well :marked at 18:00 lilt.b. a_re.Ja.ti.us....minimrn.c<anU!r-- f-.1006- mb—a•t·-t-he··NW

of the line. The wave amplitude was about 1000 km .

Pressure variations relative to the squall .Position were studied. In .order to reduce effects due to the geographical position of the stations and to these-mi-diurnal oscillations, we used the pressure variations recorded through 24 hours at the same location. Observed variations were negative (about -2.3 mb) in front of the line and positive at the rear (about +2.6 mb). So at lar5e scale the maximum pressure jump may have been of the order of 5 mb. However, these values may be skewed due to the occurence on June 22 of another squall line.

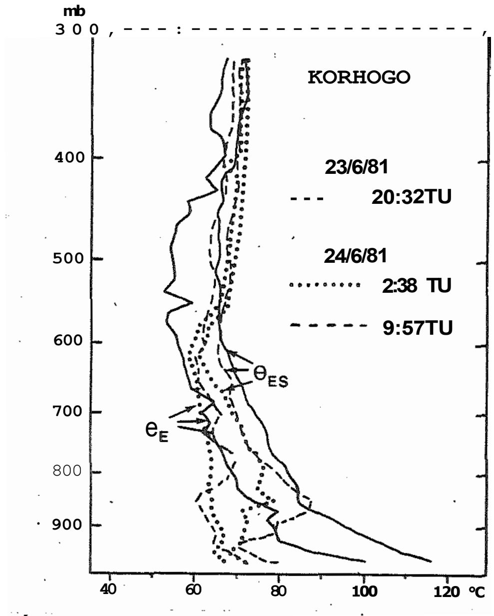

FiguJte 3. EqU,{.valen.:tpo;t:rn.;t,i,a,tt:empvi.a.:tWtet!E a.nd .t,a.;t:wc.a.:ti,eaqU-{.valen.:tpo;t:en.;t,i,a,l;t:empe/1.a.;t:Wtet!ES Ob.t.e11.ved 6nom Konhogo .t.ounding.t..

h) Time evolution of the vertical structure above Korhogo

Frequent soundings were performed at Korhogo over the whole experimental period. In the vertical the main features of the atmosphere during this period were associated with the frequent presence of a Monsoon flux (about 7 m.s-1) below 1000 m A.G.L. (heights used throughout this paper are Above Ground Level : AGL), the African Easterly Jet (about 10 m.s-1) centered at 4000 m and the Tropical Easterly Jet (about 30 m.s-1) centered between 12000 and 15000 m. An 'inte ediate jet (22 m.s-1) also occasionaly appeared around 8800 m. Soundings were launched before (20:32), at the front (23:33), during (02:38) and after (8:00 and 9:57) the passage of the system,

figure 3 displays equivalent potentiel temperature SE and saturation equivalent potentiel temperature SES recorded during the vertical soundings launched before (20:32), during (2:38) and after (09:57) the passage of the system. The first sounding shows a strong conditional vertical instability of the atmosphere. Static energy had been accumulated in the low levels and a dynamic effect was needed to trigger the instability. At 02:38 the atmosphere has been homogenized by convective transferts and was then stable. It had been cooled below the 700 mb level and warmed above. Air below 600 mb had an equivalent po,tentiel temperature nearly constant indicating a probable common origin, air of the same equivalent temperature was found at 23:33 at 600 mb which .also. corresponded .to the=melting level. ..This saunding does not display any layer of warm and dry air as found at low level behind the squall in other cases (Ref.1). At 09:57, the.soundin? had a diamont sh pe as refered by Zipser (Ref. 1). It was characterized by the presence of a strong subsidence in the 1'50-750 mb layer and moi t air close to the ground. Its maximum difference between .temperature and dew point temperature (12 °C) was reached near 850 mb. The squall iine strongly stabilized the atmosphere, carrying static energy from the low levels to the higher half of the troposphere through vertical air transports. The stabilization took place through the whole troposphere depth and at large scale. It was still effective far behind the system. In this area, this was not the case for the observed diurnal convectioE which effects were not obvious.

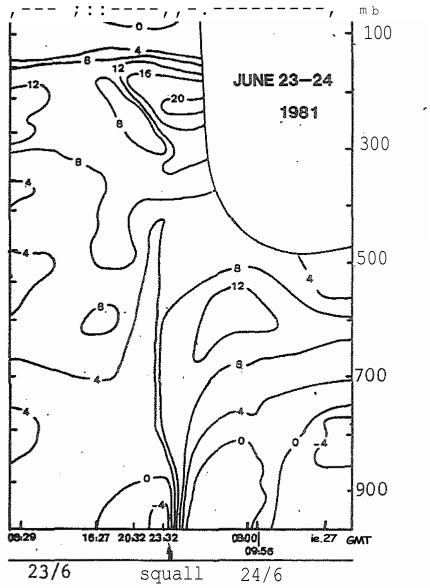

FigMe 4- Ven;t:,i,cal.t.une eno.t..t.-.6ee;t:iono0 wind component u·pcvr.a.lle..l;t:o;t:he .t.qua.U u n e pnopa.ga.uon veuon a.nd ob.t.e.nved onom .t.oundingl., a.t Konhogo. Po.t..-i..;uve valuu indicate wind componen;t:J.,;t:owMd/2 SW in ;t:he dinee;t:ion 06 ;t:he .t.qua.U u n e pnopa.ga.:tion·a.l.,i l Mo.6.5ed oven ;t:he e:x.pa.l.,(,men;t1.,ile.

Ihe wind components U parallel to the propagation vector of the line were drawn using the wind soundings available on June 23 and 24 (Figure 4). Values found at the ground stations were used to draw the perturbation associated with the line. The winds were directed from rear to front of the line (positive component) but at low lev ls. At 23:33, air Lelow 1100 m with a negative component (up to -7 m.s-1) and a high static energy corresponded to the monsoon flux which fed convection in the system. Winds relative to the line were directed from the front towards the rear of the system almost everywhere (winds of U component lower than 12 m.s-1) but in the high altitude jet present between 90G0 and 14000 m and behind the line around 4000 mat a level corresponding to the 0°C isotherm. The 23:33 sounding was launched near the. gust front and penetrated rapidly in the system. Air with a small positive component found at this time between 5G00 and 6000 m probably corresponds to low level air from the monsoon flux which has been transported upwards in a convective updraft. Inversely, ir with a strong positive speed and a low static energy which was found on the ground just behind the squall(after 23:40) may corresponds to air which was transported downwards from 4000 m (meltinR level) where the air had similar properties. Air of nearly constant U component was also found at

09:00 at the rear of the system between 850 and 750 mb where we already noticed the presence of a strong subsidence. Large positive speeds around 14000 m a t 23:33 and 20:32 allowed the rapid extension of the forward anvil. If we assume a nearly bi-dimensionnal flow t the scale of the system, differences between the speed values found before and behind the squall may indicate the levels of convergence and divergence. Computations at a scale of 500 km were possible only up to 5500 m. Three main regions appeared : a region of convergence (-2x1 o-Ss--1) below 700 m, a region of divergence (+2xlo-5s-1) from 700 m to 3000 m and a region of convergence (-3x10-ss-1) from 3000 to 5500m. Then it seems that the system was essentially fed from the front at low level (feeding of the convective part by the monsoon flux) and from both front and rear at an intermediate level (3000 to 5500m) corresponding to the African Easterly Jet level and including the melting level (feelfing of the downdrafts).

3. MESOSCALE CHARACTERISTICS

a) Surface mesa-network

Data from 7 Automated meteorological stations were used to analyse the surface small scale signature_ of the squall Jine. Data from station D, 4 are displayed on Figure 5. Six hours before the arrival of th line, at 18:UO, the temperature started to decrease due to the end of solar heating. At 21 :00, it reached a level of 25 to 26 °C. During the.same period relative humidity increased to 84% due to the temperature decrease. Temperature and humidity kept then nearly constant values for almost 3 hours (up to the arrival of the squall).

Pressure which was increasing slowly due to the semi diurnal cycle had a relative maximum at 23:10 then decreased slightly up to 23:47. At this time, the U component of the wind (parallel to the squall propagation vector) wh_ich was negative (towards the rear of the system) s_tarted to increase rapidly with pressure. These variations corre ponded to the beginning of a strong convergence zone whi-ch nay have develop convective updrafts.

S· to 8 minutes iater, the V component (perpendicular to the squall propagation vector) made a sudden change rapidly followed by a first temperature drop to 21 .5 °C. At this time, the air was a little dryer (down to 74% in relative humidity) in spite of the temperature drop. Pressure and U component reached a maximum value at 24:00 when the V component gradient was maximum. The pressure jump was about 0.8 mb. The U maximum value on the network was about 12m.s-1. This value is closed to the squall propagation speed at the same time _and suggests that the system was essentially drived by the convective downdrafts. The maximum variation of the U component was of the order of .14m.s-1. We can notice that the maximum variation of U was recorded before having any significant charr ge in the V coraponent. Variations up to 10m.s-1 within 5 mn were recorded at some of the stations in the absence of any signifi.cant changes in the V component. This corresppnds to a convergence of 2.8x10-3s-1. The pressure jump of 0.8 mb was certainly essentially dynamical ; a dynamic pressure of 0.8 mb corresponding through the Berriouilli equation to a wind variation of 11 m.s-1 which is of the order of the recorded one.

After 24:00, the pressure decreased until 00:06 when the V component reached its maximum negative value indicating the end of the convergence region. Both pressure, U and V components of the wind reached a new maximum under the convective shower which occured from 00:18 to 00:50. The beginning of the shower coincided to a new temperature drop. Temperature rapidly reached a minimum of 20.2 °C while relative humidity increased nearly to saturation. Then for 2 hours both parameters kept a nearly constant value and pressure stayed high. The convective shower lasted for about 30 mn and was followed by stratiform rains. The maximum precipitation intensity recorded on a 2 mn 30 integration time was 115 mm.h-1. Air found in the first 100 km behind the gust front had the same equivalent potential temperature (66 to 68 °C) as air found just below the melting level in the 800-620 mb layer from which it may originate. We may also notice that just behind the squall line, the wind had a prefered orientation directed towards WSW which also corresponds to the wind direction recorded at 23:33 between 1500 and 6000 m (850 to 500 mb).

About 100 km behind the squall front, temperature <1hich had been nearly constant for almost 2 hours showed a sudden jump (+0.5 °C). This was associated with a pressure decrease and an inversion in the U component which decreased and became negative corresponding then to a flow towards the rear of the system. The associated.divergence was of the order of 0.3x10-3s-1 on a scale of 30 km. Behind this region, the temperature fell to 19.5 °C.

All rain stopped at 05:10. Up to 47 mm were recorded at one of the stations. The mean value was 30 mm, &0% of it having occured in the convective shower.

Advection over the network of pressur , temperature, relative humidity and wind perturbations associated with the squall was quite regular and followed straigpt lines making a 127 degrees angle with North and propagating towards the 217 with a speed of 11 to '13.Sms-1. The time-lags between this different parameters were as described previously. On the contrary, the.advection of the precipitation and radar reflectivity zones were more erratic both in time and space.

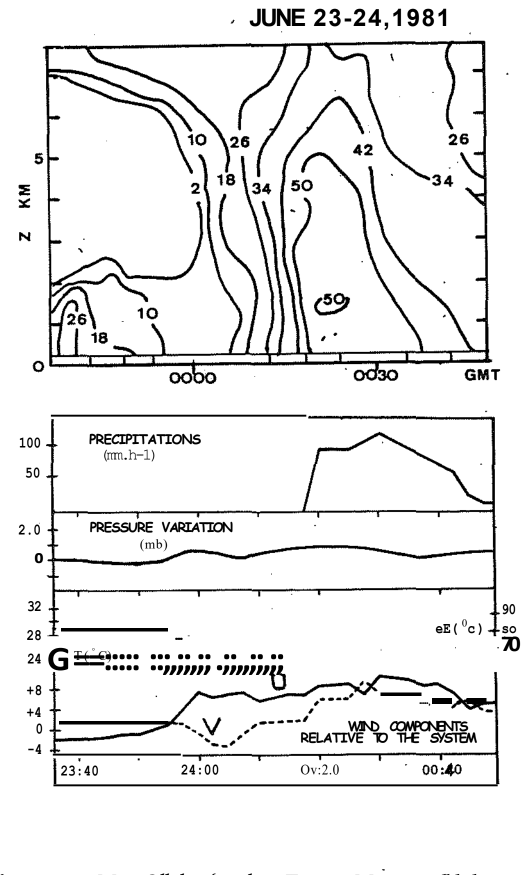

F{gU/Le 5. Me:teOllolog{.c.a,l paJLame:teM 11.ec.Ollded at .the A4 1.,ta;t-{.on .toge:the!L wdh .the· 11.eMeilivily data. ob1.,e11.ved above i11 loc. on

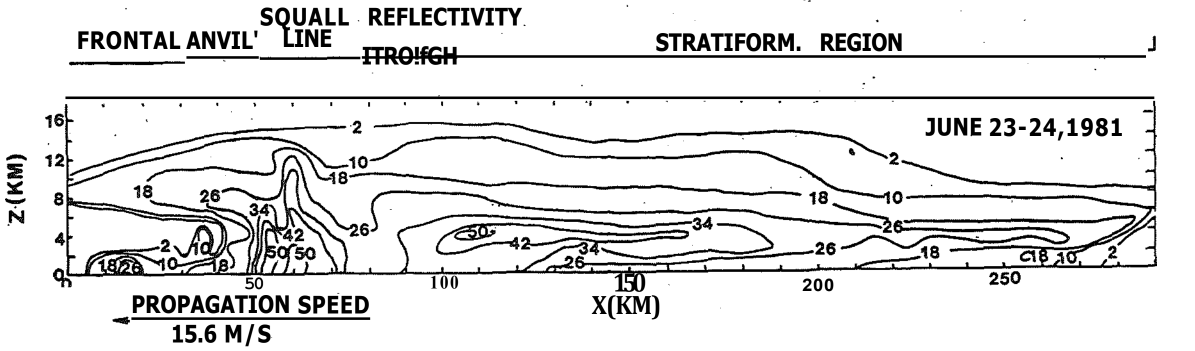

FigWLe 6. Vvr..t.i.c.a.£ c.ompo-0.Ue pic.:tWLe 06 :the M.daJt 1te6,temv.Uy ob:ta_i_ned w.Uh veJttic.a.£ c.JtoM--0 ec;t,<.onJ, pe1t601tmed while :the <1y<1tem .1uw cito0-0<ng oveJt :the expvumen:t -0.Ue

b) Raoar reflectivity analysis

Reflectivity data were recorded with the Ronsard system which was operated by the Centre de Recherches en Physique de l'Environnement terrestre et planetaire (CRPE).
Figure 5 and Figure 6 both display a composite picture obtained by integration of successive vertical cross-sections observed at different times while the system crossed over the experiment site. At this time, the squall line was composed of four distinct regions :

- a forward anvil preceding the squall front and detectable by the radar on more than 40 km between 6000 and 14000 m. At low levels, below this anvil, small cells of reflectivity lower than 30 dBZ were present. They were organized into lines parallel to the squali front and distant by 25 to 35. km. They be ame.more numerous and more intense as the squall was approaching.
- a convective region 10 to 30 km wide, 16 km thick, with reflectivity values greater than 35 dBZ and made up of individual cells (50 dBZ or more). These cells were highly convective and closely organized along a straight line.
- a low reflectivity region (25 to 35 dBZ), 10 to 30 km wide, 16 km thick and separating two regions of higher reflectivity : the convective and stratiform regions.
- a stratiform region spreading on about 200 km with a depth going from 16 km close to the low reflectivity region to 8 km at the rear of the system. It had a very low reflectivity gradient everywhere but near the 0°C level where a higher reflectivity zone (sometimes more than 50 dBZ) was associated to a bright band indicating the presence of melting in stratiform conditions.

The convective line was oriented NW-SE and propagated towac·ds SW with a speed fluctuating from 8 to 23 m.s-1.

The mean speed was 15.6 m.s-1 and its component along the large scale propagation axis (towards West) **was** of the order of the system speed observed at large scale (12 m.s-1 towards West). While it crossed over.the mesoscale network, the system slowed down to about 10 m.s-1 ; this speed is also in agreement with the one computed through the advection of the surface squall signature. The advection direction and speed has been also computed for cifferent indi vidual cells in front of the squall and in the convective region. In front of the squall, the cells were almost stationnary and when the squall met them, they rapidly intensified forming.a new cell which joined the convective region. In this later region, the cells propagation direction was towards 230° relative to the North and so.made a 5° angle with the line propagation vector. This implies a slight slipping of the cells with respect tci the system. Their speed slightly slower thari the squall speed implies that the cells developping in front of the squall were moving towards the rear of the convective region where they dissipated. At low level, the convective and stratiform regions wer always separated. by a low reflectivity region and seemed to be independent one from the other at the low levels.

Exchanges seem. to have taken place only well above the mixing layer.

4. SYNTHESIS OF OBSERVED CliARACTERISTICS

The obs·erved squall syst,em was composed of a forward anvil, a convective ·region, a reflectivity trough and a stratiform regi·on. Updrafts ,,ere fed by conditionaly instable air : the mon,soon flux. Downdrafts associated with the prec{pitations were essentially fed from both front and rear by air from a layer centered around 600 mb corresponding to the melting level and to the position of .the African Easterly Jet. The squall system was drive'q. by the convective downdrafts which formed a lar.ge sc le sqc:all front. Small cells were present at some distance in front of the squall where they moved slowly. They developped when they came close·to the gust front and then became active elements of the convective region.. Later they dissipa_ted at the rear of this region.

5. ACKNOWLEDGt;ENTS

Financial and logistical sl,pports of ·the COPT 81 (Convection Profonde Tropicale)- experiment have been provided by the Institut National d'Astronomie et de Geophysique (France), the Direction des Recherches, Etudes et Techniques (France) and the Ivorian Government. The Centre de Recherches en Physique de l'Environnement terrestre et planetaire provided the radar reflectivity d·ata. Mrs G.Froment typed the **manuscript.**

6. REFERENCES

1. Zipser E. I.• 1977 : Mesoscale and convective-scale downdrafts as distinct components of squall-line structure. Mon.Wea.Rev..!.Ql, 1568-1589.

2? Houze R.A., 1977 : Structure and dynamics of tropical squall-tine system. Mon.Wea.Rev. .!.Ql, 1540-1567

3. Betts A.K., R.W. Grover and M.W. Moncrieff, 1976: St.ructure and motion of tropical squall-lines over Venezuela. Quart. J. Roy; Meteor. Soc. , 395-404.

4. Roux F., 1984 : Three dimensional structure of a West African continental squall line observed during the experiment. COPT 81. Preprints volume. IX Int.ernational Conf. on Clouds Physics, Tallinn. URSS.

5. Lafore J.P. and J.L. Redelsperger, 1984 : Numerical simulation of a tropical squall line. Preprints volume. IX Int.ernational Conf. on Clouds Physj.cs, Tallinn. URSS.

VERTICAL STRUCTURE OF A NOTABLE CLOUD SYSTEM OVER THE SEA OF JAPAN UNDER WINTER MONSOON

Tatsuo Endoh, Kunihiko Hozumi
and, Choji Magano

Institute of Low Te perature Science, Hokkaido University,
Sapporo 060, Japan

1. INTRODUCTION

It may be considered that the activity of an individual cloud depends on the stage of the life cycle with many limited cond tions and it also depends on its position in the entire cloud system which. is caused by the atmospheric field in a synoptic scale.

To understand the pro.perties of clouds, predict their behaviors and estimate the amount of precipitation, it is necessary to investigate the relationship between the morphological distribution features of individual clouds and the motion structure of the entire cloud system.

Most of the severe heavy snowfalls occur in association with the pressure distriqution of monsoon type. When cold monsoon bursts spread aloft over the Sea of Japan, numerous cloud bands can be observed aligned in parallel from the continental coast to the Japanese Archipelago. Each of the .cloud bands is accompanied by a constant and locally concentrated snowfall on the west coast of the Islands where it arrives.

After a cyclone has passed over the Japanese Islands and departs toward the east, we have the pressure field of monsoon type and a cold air mass aloft over the Sea of Japan where the warm water of the Tsushima stream spreads over the surface of the sea. Therefore, an unstable condition of the atmosphere builds up and numerous cloud·bands can be.a served over the entire area.

Then a notable cloud system is observed to grow and align itself in an intermediate scale from the north east base of the Korean Peninsu+a to the west coast of the Japanese Islands as shown in Figs. 1 and 2. Such cloud systems and the area observed are called the convergence cloud system of the Sea of Japan and the convergence zone respectively.

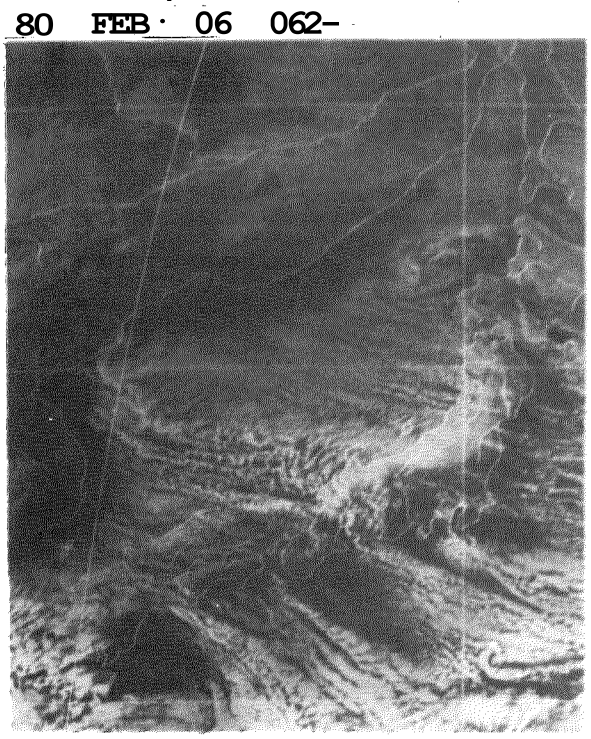

Figure_ 1. A typical picture of convergence cloud system observed by GMS-1 (06Z 6th Feb. 1980).

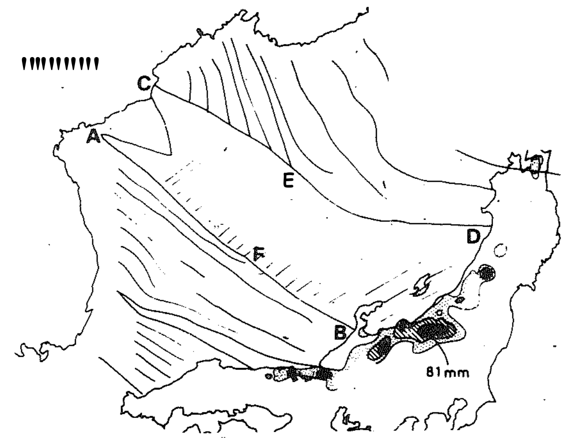

Figure 2. ·Relationship be-tween a convergence cl,oud system zone and corresponding areas in total snowfall amount.

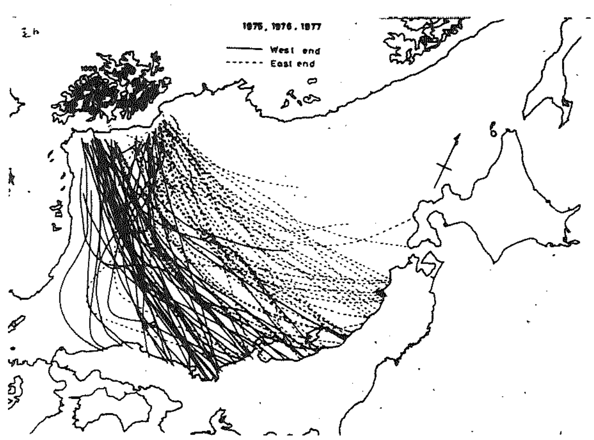

Figure 3. Southwest (solid line)·and northeast (broken line) peripheries of the convergence cloud system during three winter seasons.

2. METHOD

To investigate the generation mechanism and behavior of the convergence cloud system, some observations and analyses were carried out using aircrafts, balloons and cloud pictures by the satelite GMS. Fr m an aircraft on an air route, many air photographs of the cloud systems were taken at a constant time interval by a time lapse camera and analyzed stereoscopically (Ref. 1). They provided the dimensions of individual clouds. Another observation with free balloons provided wind profiles in the component of the vertical transverse section of the convergence cloud zone. Finally some series of successive pictures were taken at a short time interval by GMS and analyzed stereoscopically by means of Cameron's method (Ref. 2).

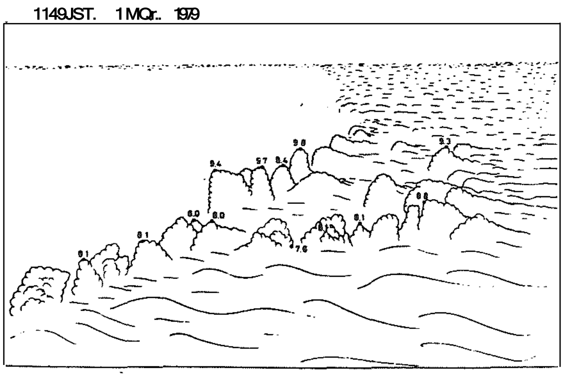

Figure 4. Aerial picture at the southwest periphery toward E from B in Fig. 2.

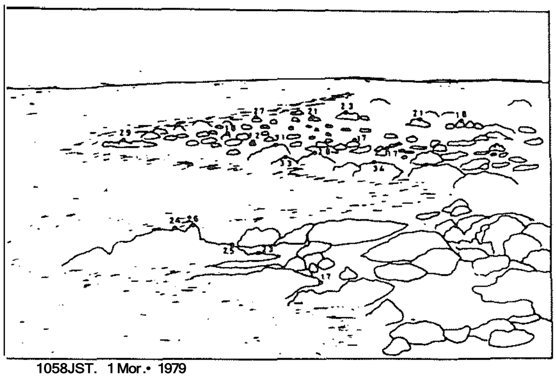

Figure 5. Same as Fig. 4 except at northeast periphery toward F from D.

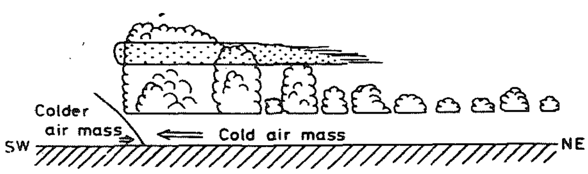

Figure 6. Schematic feature of vertical and transversal sec_tion of the convergence cloud system.

3. RESULTS

Figure 2 indicates that the clouds along the southwest edges of the .system (AB) bring the highest peak values of snowfalls on the coastal area of their arrival point. In Fig. 3 the southwest (as AB in Fig. 2) and northeas (as CD) edges are shown in solid and broken lines respectively, based on the summary of three winter statistics from 1975 to 1977. It is noted that southwest edge lines (solid line) start from a particular area around the southwest shoulder of the upstream mountain area.

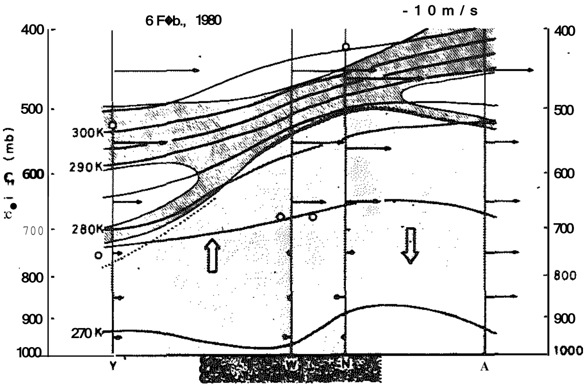

Figure 7. Profiles of wind aloft in the component of BD section in Fig. 2. The convergence cloud zone is thatched.

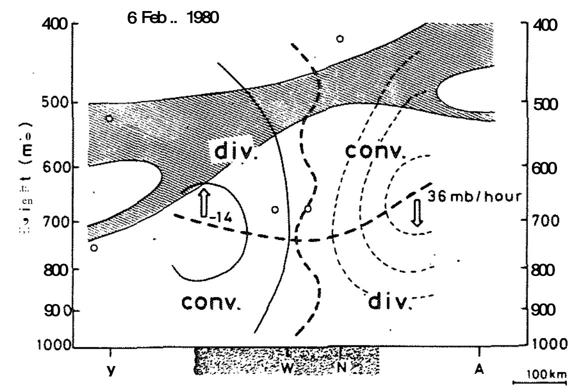

Figure 8. 2D-vergences and vertical motions deduced from Fig. 7.

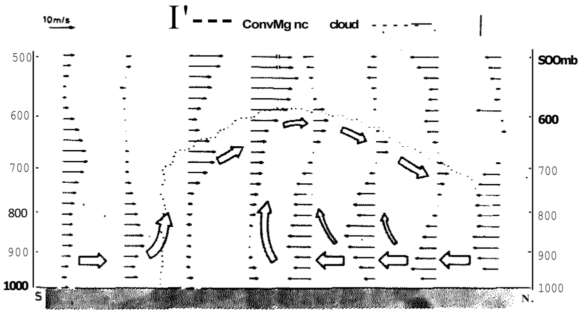

Figure 9. Circulations of air current in the section around the convergence cloud system.

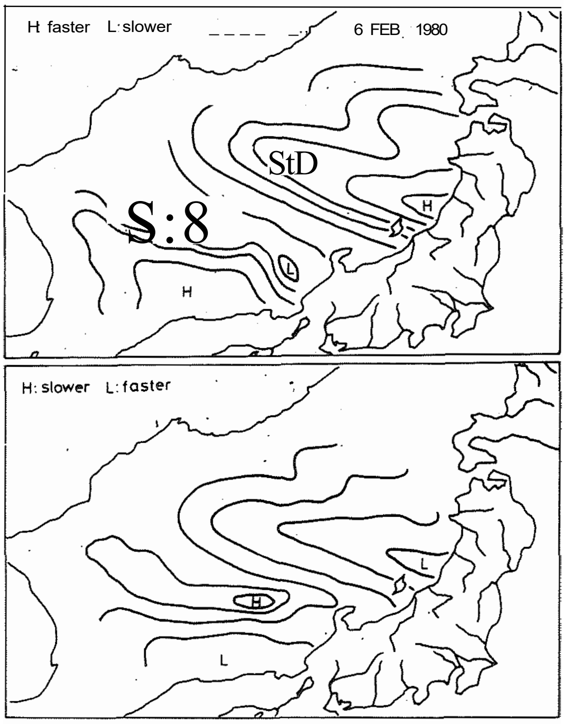

Figure 10. Qualltative isoplethes of relative velocity of the clouds in the component parallel to AB direction in Fig. 2.

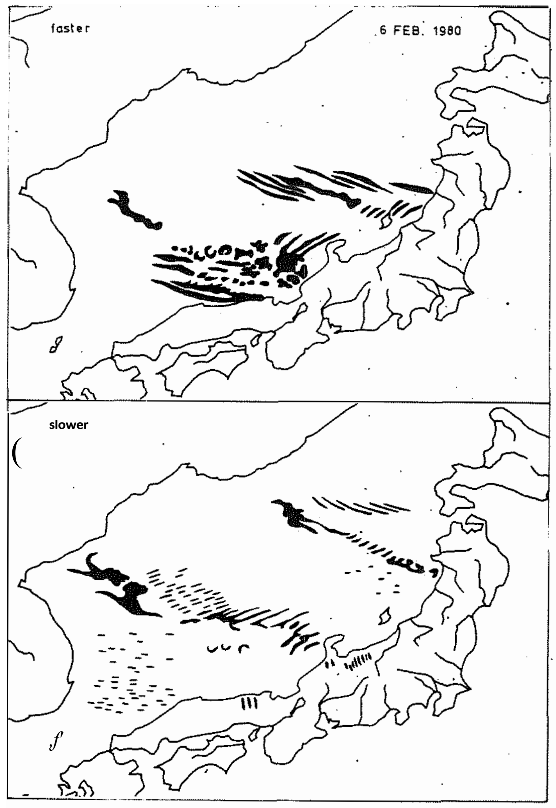

Figure 11. Typical cloud features corresponding to Fig. 10.

3.1. Air photographic observation

The stereoscopic analyses of overlapping parts between a pair of continuous pictures provided the heights of the cloud tops as shown in Figs. 4 and 5 taken at the southwest and northeast edges of the convergence cloud zone respectively. In Fig. 4, many turrets of cumuli (Cloud Top: 8000 9000 m) were observed to penetrate the widely spreading altostratus-(C.T. 5000 6000 m) along the southwest edge of the cloud zone.

In Fig. 5, the altostratus was observed to diffuse and many small cumuli with low level heights were found near sea surface under it. All pictures analyzed may be combined into a simple schematic feature of vertical transverse section of the convergence cloud system, which is shown in Fig. 6.

3.2. Free balloon observation

Another observation with released balloons was carried out using the .same kind of sondes and launched at the same time as routine work of the upper air station of Japan Meteorological Agency at another observation point.

This was done to achieve a more complete analysis of mesa-scale on the convergence cloud system. The results provided the wind profiles in the component of such vertical transverse sections of the convergence cloud zone which are shown in Fig. 7. Depending on the law of continuity of the atmosphere in the section,' an updraft and a downdraft are deduced from the results of- the two dimensional vergence analyses of the section which existed on the southwest edge and in the north-eastward area of the convergence zone respectively. The position of the convergence zone of that time is shown as hatched areas under the axis of the abscissa of Figs. 7 and 8.

Combining some resvlts at different relative positions to the convergence cloud system in soite of different time, a schematic circulation of air current in the section is illustrated over whole section around the cloud system in Fig. 9.

3.3. Analyses of successive satellite pictures

A series of successive pictures taken at intervals of seven minutes by GMS-1 were analyzed stereoscopically by means of Cameron's method (Ref. 2), which provides the qualitative difference in relative velocity of individual clouds. Qualitative isoplethes of the cloud velocity are shown in Fig, 1Q.

The upper and lower half of the figure are characterized with maximum and minimum values of velocity distribution respectively. Typical cloud features with such velocities are shown in Fig. 11 corresponding to the velocity distribution of Fig. 10.

It was possible to estimate the height of a cloud by comparison between the velocitie of the cloud obtained by the stereoscopic analyses and the velocity of wind obtained by the sounding data, since the velocity of wind aloft almost always increa?ed with the increase in height during the observations.

A schematic result analyzed is shown in Fig. 13. Within the confines of this convergence zone a large number of cloud rows were observed in a transverse mode, where the velocit.ies and the heights of clouds were seen lower than those of other areas. Numerous cloud bands were also observed to the northward area from the zone in a longitudinal mode, where the velocities and the heights of clouds were seen to be highest. To the southward area of the converg'fnce zone, a large number of open-cell clouds were observed to align themselves in.a .longitudinal mode in the upstream.part, which began meandering mosaically in the downstream part, wnere the velocities and the heights of clouds were moderately higher thifh. those in the convergence zone.

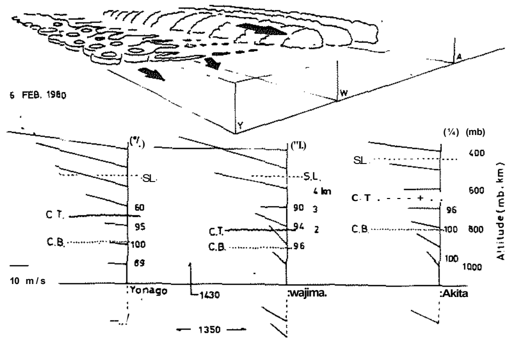

Figu:re 12. Features and thickness of three kinds of cloud zones around the system and corresponding sounding aloft profiles.

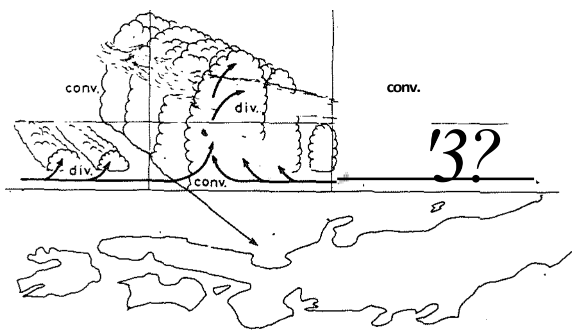

Figure 13. A schematic model and motional structure of the convergence cloud system in the vertical and ·transversal section.

4. DISCUSSION

As a whole, combining the results of Fig·s. 2, 6, 9 and 13, it may be coRsidered that the circulations of air current as shown with the arrows in Fig. 15, construct a simple model of the structure of the convergenc.e cloud system zone. On the southwest edge of the zone, it is considered that strong upward air motions make many tall convective clouds and a considerable amount of snow crystals and flakes are formed in the clouds which fall in concentrated fashion on the coastal area around the arrival point of the southwest edge line.

It is important to understand the behavior of the convergence cloud system for the prediction of snowfall.· One of the most important properties are described here.

rt may be considered that nowcast and forecast of a short time range can readily be performed regarding the snowfall area caused by the cloud systems under the monsoon type. It may be expected in the near future that useful information of snowfalls will be available for the inhabitants residing in the snowfall area regardles of time and place.

5. REFERENCES

1. Hozumi K et al., ·1982,. The size distribution of cumulus clouds as a function of cloud amount, J Meteor Soc Japan 60, 691-699.

2. Cameron H L 1'952, The measurements of water current velocities by parallax methods, Photogrammetric Engineering 18, 99.

HYDROMETEOR DISTRIBUTIONS IN CALIFORNIA RAINBANDS

Glenn L. Go.rdon, John D. Marwitz and Mark Bradford
university of Wyoming
Laramie, WY 82071

1. INTRODUCTION

Hydrometeor distributions were measured in a number of rainbands during the 1982 wintertime Sierra Cooperative Pi ot Project. The ground radar was used to vector the /yarning King Air (data system described by Cooper, 1978) to the top of the rainbands (-5 to 30°C) from whence an onboard computer afgorithm was initiated for making multiple penetrations of an ensembTe pf particles which are assumed to descend at 1 or 2 m/s while drifting downwind. The K'ing Air wa.s flown in an elongated figure-elght pattern. The rate Of descent was selected to approximate the fallspeed of ice crystals and yet have the aircraft descend below the 0°C level before the topography precluded such a descent .. The figure-eight was oriented normal to the orientation of the band and was about 20 km in length. This flight pattern was flown on 13 and 15 February and on 1 March 1982. A similar flight procedure and nalysis technique was first used by Lo and Passarelli (1982) in cyclonic storms except they did a spiral descent at a constant descent rate. Our data are averaged over each leg of the fiqure-eight pattern. The results of the 15 Februa y 1982 case study are presented.

2. DATA CO LECTION

Hydrometeor distributions were measured using 2D-C and 2D-P .PMs probes. The results shown here are from the 2D-P. Both probes, however, showed similar results with 2D-C concentrations being somewhat larger. Images from both probes were used for hydrometeor classification.

As mentioned above, the data were averaged over relatively long flight segments. To minimize statistical sampling errors we required that 10 particles be sampled in each bin for each leg in order for that bin size to be included in the data (Gordon and Marwitz, 1982).

3. RESULTS AND DISCUSSION

Figure 1 shows leg-averaged FSSP total concentration, FSSP concentration .for drops larger than 24 µm and FSSP liquid water content plotted as a function of temperature (and height). The numbers correspond to consecutive legs with 1 being at the top .of the ra inband. There appears to be very little liquid water above the -i0°C level. Small quantities of liquid water are present at warmer temperatures ,tith -values remaining less than .1 g/m^3 above the 0°C level. The concentration of droplets with diameters> 24 µm was 0.5 cm^{-3} ear the, 5°C level. Figure 1 has.been divided into 5. layers (a through e). The significance of these layers will be discussed below.

Figure 2 shows representative hydrometeor images from the 2D-C for each of the 5 layers indicated on Figure 1. In the first 4 legs where T < -22°C (Figure 2a) crystals are Small .. Small aggregates occasionally can be seen. Figure 2b shows representative images throughout layer b.in the temperature range from -11 to -22°C (legs 4 through 8). Dendrites and dendritic aggregates can be seen throughout layer b. Images from layer c where the temperature varies from -3 to -11°C (legs 8 through 14) are shown in Figure 2c. A large number of columnar type crystals are present along with some aggregates. The temperature range of layer d varied from 0 to -3°C (legs 14 through 17) (Figure 2d) and contained mostly forge aggregates with relatively few pristine crystals. Images from the final layer (e) sam.pled had a temperat.ure range from 0 to +3°C (leg 18) and showed mostly water drops with some aggregates still present (Figure 2e).

Figure 3 shows representative size spectra for levels a through e of the rainband. 1-nitia.1ly, the spectrum is very steep and narrow (T,;-25.5°c). The spectra evolve in a systematic manner as the temperature gets warmer. At T = -13.1°C the spectrum is a little bro.ader. By T = -5.6°C the spectrum seems fully developed with a broad range of sizes and an excess of particles w'ith sizes < 0. 1. cm. At T = -0.1°C large (> 0..2 cm) particles are sti 11 increasing in number while ttie smaller (< 0.1 cm) sizes are decreasing in number. There is a noticeable decrease in particle concentration by T = +1.2°C. Presumably this is the beginning of melting and collapse of ice p rticles.

Acy exponential distribution function of the form

$$N(D) = N_o \exp(-\lambda D)$$

was fitted.to the dat for each leg using a least squares technique. The values of the slope parameter (\) and the intercept parameter (N_o) are shown in Table 1 alona with the mean temperature and height for each leg. Slope and intercept values are determined only for that portion of the spectrum that behaved in an exponential manner (D > .05 cm). By requiring at least 10 particles in any given bin size legs with low concentrations of particles greater than 0;05 cm could not'have distribution parameters calculated for them.

The log of the slope is plotted against the. log of the intercept for each leg in Fig. 4. An increase in N_0 and a slrght increase in\ occurred between leqs 3 and 4 (layer a). According to Lo and Passare 11 .i (1982) deposit iona 1 growth wf 11 cause particles of all sizes to grow at the same rate (with respect to diameter) .which will cause\

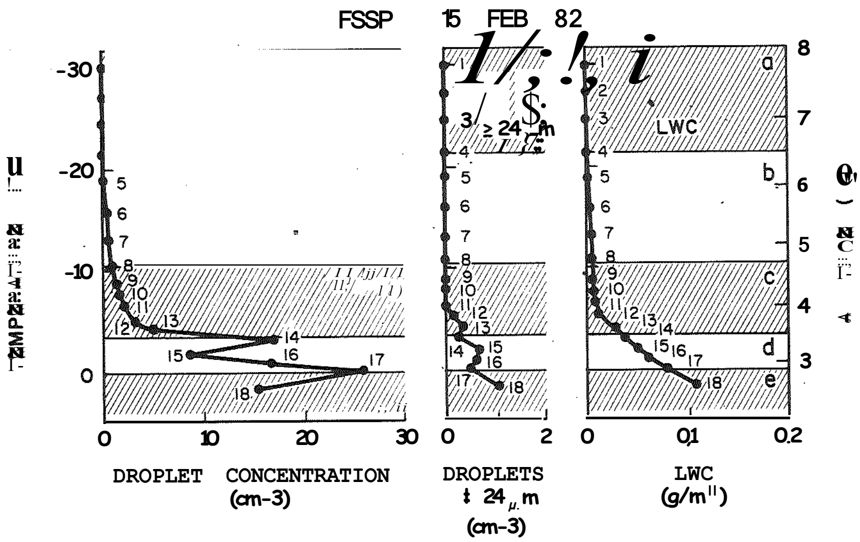

Fig. 1. FSSP droplet concentration, concentration of drops ≥ 24 μm and FSSP liquid water content plotted as a function of temperature and altitude. Numbered points represent flight leg averages. Lettered regions correspond to different hydrometeor growth regimes.

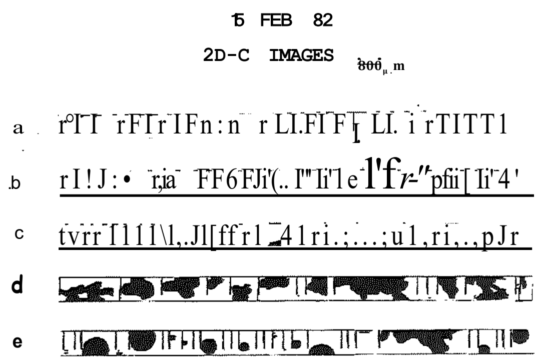

Fig. 2. 2D-C images collected at 5 regions of the rainband.

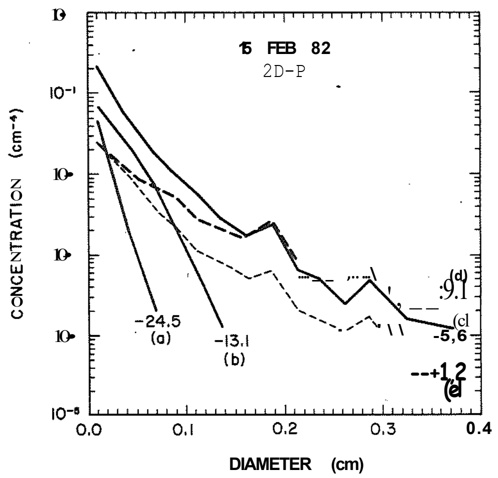

Fig. 3. 2D-P size distributions sampled at 5 regions of the rainband.

Table 1. Mean values of temperature (T), altitude (Z), and intercept, (N_0) values for each leg.

Leg #	T (°C)	Z (m)	λ (cm.-1)	N_0 (cm-4)
1	-30.5	7767	-----	-----
2	-27.4	7356	-----	-----
3	-24.5	6981	76.6	.043
4	-21.8	6563	107.9	-337
5	-18.9	6129	-----	-----
6	-16.0	5672	81.0	.308
7	-13.1	5167	47.2	.148
8	-10.7	4776	14.1	.010
9	-9.2	4529	18.7	.019
10	-8.1	4301	17.6	.022
11	-6.8	4089	18.1	.029
12	-5.6	3863	17.3	.043
13	-4.3	3636	17.0	.053
14	-3.3	3417	16.6	.059
15	-2.0	3197	13.5	.030
16	-1.1	3001	14.0	.032
17	-0.1	2756	11.2	.012
18	1.2	2546	15.6	.009

to remain constant and N_0 to increase due to more numerous smaller particles growing to larger particles. A slight increase in λ in addition to an increase in N_0 indicates that there was an input of small particles due to nucleation, secondary production, and/or small particles growing into detectable sizes. If the input of small particles was only due to growth to detectable sizes, than λ would remain constant. The fact that λ does increase slightly indicates that new particles were produced at a faster rate than depositional growth.

Further evidence of small particle input can be seen in Figure 5 which shows ice crystal concentration versus average temperature. Concentration shows a slight but steady increase from leg 1 to leg 4.

Figure 5 shows a drop in total concentration at leg 5. This is puzzling since, in addition, the 2D images were smaller and no aggregates were

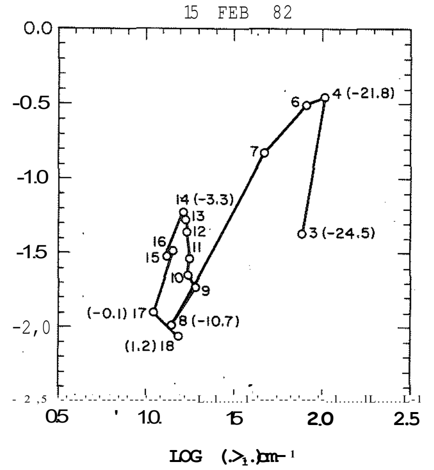

Fig. 4. 2D-P values of the logarithm of the intercept parameter N_0 plotted as a function of the logarithm of the slope parameter \ for the various flight legs.

apparent (they may have been too smal 1 to recognize;. One explanation for this might be that due to a slight horizontal variation in the flight track the aircraft may not have sampled the same ensemble of descending :ce crystals. The flight track with respect to the ground and with respect to the descending position reference suggested that the experiment was properly flown, however. Since the number of particles with D > .05 cm sampled was not greater tha 10 per bin;- no A or N_O was calculated for leg 5.

Both A and N_O show a decrease from leg 4 (-22°C) to leg 8 (-11°C) (layer b) (Figure 3). This represents a region of rapid aggregation. Small particles are increasing in number causing A to also decrease. There continued to be a slight increase in concentration (Figure 5) descending through laye, b (ignoring leg 5). The increase in concentration in layer b indicates an input of smaller particles possibly by the same process discussed above. 2D images show increased aggregates present wit sizes increasing through leg 8 (Fig. 2b).· The concentration of dendritic crystals increased from leg 4 (-22°C) to leg 7 (-13°C).

Leg 9 showed some peculiarities that again suggest that the aircraft may have been slightly out of position. 2D images showed no large aggregates and lots of smal 1 particles. At leg 10, however, the large aggregates were again evident. At this point there does not seem to be an expl nation for this observation.

Legs 8 (-11°C) through 14· (-3°c) (layer c) are character[zed by N_O increasing rapidly from leg 8 to 14 and A remaining relatively constant. This indicates aggregation is occurring with a major input of small particles. The presence of liquid water with some drops larger than 24 µm (Fig. 1) and the te perature of these legs would suggest a r me-splintering mechanism for secondary ice crystal production (Mossop, 1976). If aggregation was not occurring, then A would increase. This assumes depositional growth with respect to diameter is slow at large sizes. Figure 5 shows the total concentration increasing to a maximum at leg 12 (-6°C) and then decreasing through leg 14. 2D images .show many columnar type crystals throughout this region with the number and size of aggregates increasing· (Figure 2c).

Both N_O and A decrease from leg 14. (-3°C) through leg 17 (0°) (layer d) (Figure 4). This suggests more aggregational. growth with no inpwt of smaller particles. Total concentration is also decreasing from its maximum at leg i2 (-6°C) (Fig. 5). 2D images show fewer and fewer pristine·crystals with larger and more numerous aggregates (Figure 2d). Giant aggregates and a few water drops were observed in leg 17 (0°C).

By leg 18 (1°C) (layer e) the large aggregates are melting, collapsing and perhaps breaking up into smaller size categories. This causes A to increase and N_O to decrease due to the smaller crystals and aggregates melting and the resulting drops to be depelted by accretion and coalescence. Some drops may be small enough to not be detectable. 2D images show fewer aggregates and-more large water drops (Figure Se).

The log of A and the log of N are also plotted as a function of mean temperature ?or each leg in Figure 5. It can be seen that in general A increases with decreasing temperatu e. above the 0°C level. These results agree with those of Houze et al. (1979), Lo and Passarelli (1982) and Stewart et al. (1982). Houze et al. (1979) and Stewart et al. (1984) show that N_O also increased with. decreasing temperature above the 0°C level. As can be seen in Figure 5 such was not th case for these data. N_O increased at the co1der temperatures- as more smaller particles were being produced or detected. N_O then decrea?ed with increasing temperature through the aggregation region (legs 4 through 8). An increase in N_O is noted from legs 8 through 14. As mentioned above an increase in smaller particles was obser ed in this region due to secondary ice crystal production. N_O then shows· a decrease through the 0°C level as aggregation and melting become the dominate processes. These results are similar to those of Lo and Passarelli (1982).

4. CONCLUSIONS

The data presented on one rainband indicate that there were distinct regions in which different hydrometeor processes were domfnate. At temperatures colder than -22°C, ice crystal spectra were dominated by nucleation and deposition growth. From -11 to -22°C (the dendrttic temperature.regime) aggregational growth was dominate. From -4 to -10°C secondary ice crystal production and aggregational growth were the dominate processes and from -4 to 0°C only aggregation was apparent. The final stage (T > 0°C) was dominated by melting, accretion, coalescence a d perhaps breakup. Aggregation seems to be occurring throughout most of the rainband.

The •light procedure and analysis technique used here and that used by Lo and Passare1l i (1982) appears to be a very useful method for studying hydrometeor evolution.

5. ACKNOWLEDGEMENTS

This research was funded by the Division of Atmosoheric Hater Resources Management, Bureau of Reclamation, Department of Interior. Contract

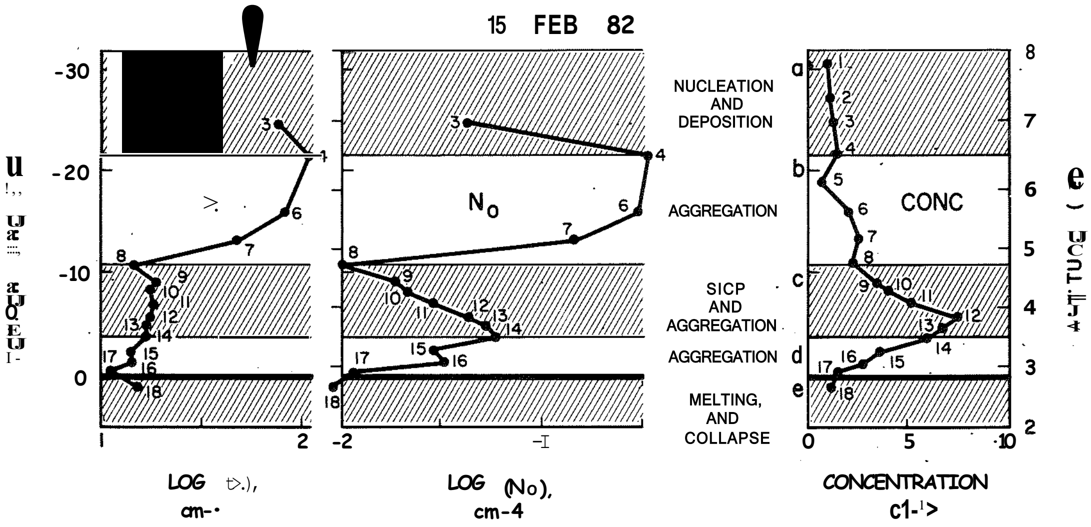

Fig, 5. 2D-P values of the Zoga:r>ithm of the slope parameter, A, loga:r>ithm of the interaept parameter, N_0 and aonaentration plotted as a funation of temperature and altitude. Lettered regions aorrespond to different hydrometeor growth regimes.

n-07-83-voool.

6. REFERENCES

Cooper,- W.A., 1978: Cloud physics investigations by the University of Wyoming, in HIPLEX 1977. Dept. of Atmos. Sci ., Laramie, \JY, 320 pp.

Gordon, G.L. and J.D. Marwitz, 1982: An airborne comparison of three PMS probes. Conference on Cloud Physics, Chicago, IL.

Houze, R.A., Jr., P.V. Hobbs, P.H. Herzegh and D.B. Parsons, 1979: Size distributions of precipitation particles in frontal clouds. J. Atmos. Sci., 36, 156-162.

Lo, K.K. and R.E. Passarelli, Jr., 1982: The growth of snow in winter storms: an airborne observational study. J. Atmos. Sci., 39, 697-706.

Stewart, R.E., et al, 1984: Characteristics through the melting layer of stratiform clouds. Submitted to J. Atmos. Sci.

OROGRAPHIC \/IMTER STORM STP.UCTURE IM CAL IFORM IA

John D. Marwitz
Department of Atmospheric Science
University of Wyoming, Laramie, 82071

1. INTRODUCTION

The Sierra Cooperative Pilot Project is a inter cloud seeding research program sponsored by the Bureau of Reclamation. The objectives of SCPP are to evelop a better understanding of the precipitation processes in the Sierra Nevada and to identify conditions that provide ·the best potential for enhancement of winter precipitation.

Over the American River Basin, where SCPP is centered, the barrier has a ne,rly constant slope of 3%. The barrier rises from 0.1 km to 3.0 km in 100 km. The Si,rra Nevada extends NNW/SSE for 400 km. The upwind barrier can be viewed as a two-dimensional inclined plane.

The University of Wyoming has operated the UH Kinq Air aircraft in this project for a number of years and ha developed a number of safe but effective flight routines for documenting the structure of the orographic storms. This paper will describe the observed hydrometeor characteristics of a typical stable oroqraphic storm. More detailed results are contained in Martner et al. (1983).

2. OBSERVED HYDROMETEOR CHARACTERISTICS

Fig. 1 contains the flight track of the King Air plotted in a vertical cross section oriented normal to the Sierra barrier (along the 070° azimuth). Fi 9. la contains the analyzed fields of Se (equivalent potential temperature) and U' ·(wind component normal · to the barrier·). Below 1 km the flow is blocked by the barrie·r. Above where the 0°C level impinges on the barrier the U' increases from 8 to 24 m/s. Se is a conservative parameter above the meltinq level (2 km) and can be assumed to be streamlines of the airflow. Multiplying the slope of the Se's above the melting layer by the U' indicates that W was 0.2 to 0.4 m/s.

The concentration of hydrometeors detected by the 2D-C probe and the temperature field are presented in Fig. lb. Below the melting layer the concentration was < 3/L. Numerous large aggreqates were resent immediately above the melting level. A ·peak concentration, > 100/L, originated near the -5°C level. Exa ination of the images revealed that many 9f these hydrometeors were needles. The.re were no graupel present, but many of the particles were moderately rimed with some heavily rimed particles present near the barrier. Since the peak concentration of ice particles was near the -S°C level and many of them were needles, this is sufficient evidence to onclude that a Hallett-Mossop type of secondary ice crystal production (SICP) process was active. We will see later that a few large·(> 24um) diameter cloud droplets were present bui there was no indication that small (< 13µm) ·diameter droplets were present. These observations reinforce the conclusion that a Hallett-Mossop type SICP process was active, but it certainly w9s not a classic H allett-Mossop SICP as speci·fied by Hallett and Mossop (1974) and Mossop (1976). The phrase "Hallett-Mossop tyoe SICP" is used because neither graupel nor smaTicloud droplets were observed. We suppose that ice crystals with fallspe ds of 1 to 2 m/s which rime·cloud ·droplets with diameters of 25um can oroduce a Hallett-Mossop type SICP as suggested by the lab results of Griggs and Choularton (1983).

The concentration of particles detected by h€ FSSP probe and the cloud water content over the barrier are presented in Fig. le.. The cloud water content was integrated from the FSSP cloud droplet spectra (3-45um). The FSSP will properly size cloud droplets but in the presence of ice particles the· laser light is scattered in an unpredictable manner such that an ice crystal is sized randomly. Two characteristics of the FSSP spectrum were therefore imposed to discriminate ice from water droplets. The spectrum from water droplets must exceed a concentration of $10/cm^3$ (10,000 ice crystals per liter is unrealistic) and the distribution must display a :Jistinct peak size concentration. The cloud water exceeded $0.1g/m^3$ above the melting level and close to the mountain barrier. A few values exceeding 0.2 gm^{-3} were encountered very close to the barrier at 3bout -2°C. There were a couple of regions away from the barrier where the concentrations exceeded $10/cm^3$ but the size distribution did not display a distinct peak in particle size. A significant numoer of those particles were probably ice. Close to the barrier and below the melting layer the r-ssp concentration exceeded $100/cm^3$ and decreased to $10/cm^3$ above the -4°C level.

The 6-s average FSSP spectral data are presented in Fig. 2. The spectra began qt 2000 GMT (-3°C) and continued during the descent into the wind at minimum obstruction clearance altitude until 2005 GMT (+2°C). From there we flew at a constant altitude unti 1 2008 GMT (+2°C). \le then began to climb and exited out of cloud droplets at 200930 (+0.5°C). The cloud droplet dist ibuiion during descent from 2000 GMT (-3°C) to 2003 GMT (0°C) is distinct and quite significant. The concentration was 10 to $20/cm^3$ and the mean droplet diameter was 25 to 30um with no droplets< 15µm. From 2003 GMT (0°C) to 2005 GMT (+2°C) the distribution abruptly changed. The ·concentration increased to - $100/cm^3$ and the mean droplet diameter decreased from 25 to Sum. During the climb which began at 2007 GMT (+2°C) the concentration decreased to< $5/cm^3$ and the mean droplet diameter increased to 13µm just prior to exiting the cloud droplets. This observed variation in cloud droplets along the barrier is not an atypical pattern. Several similar cases have been observed.

The vertical velocities near the barrier are similar above and below the 0°C layer. If anything, the vertical velocities above the 0°C layer are greater than below the 0°C layer. This is b(cause the slope of the barrier is. constant but recall the upslope component (U') increased rapidly above the· 0°C layer. The number of CCN activated during condensation is pro ortional to the vertical velocity. Since the observed cloud droplet concentration is inversely related to the derived vertical velocities, the differences must be due to the presence of two very different CCN populations. -Since the distinct change in cloud droplet distribution was observed near 0°C, possible explanatLons fo distinctly different CCN populations above and below 0°C 3re in order. Two explanations are proposed. A cloud of ice crystals is more effective at scavenqinq the sol id aerosols than a cloud of raindrops by virtue of the fact that the concentration of ice crystals exceeds the concentration of raindrops by 1 to 2 orders of magnitude and the scavenging rate is concentration dependent. The other explanation for different CCN populations is that the diabatic process of melting produces a stable layer above the melting layer which acts to stratify or decouple the primary source of aerosols (the ground) from the atmosphere above the melting layer during stratiform precipitation.

The fact that cloud droplets were observed up to the -3°C level along the barrier and only up to the +0.5°C level away from the barrier was probably due to weaker updrafts away from the barrier as compared to along- the barrier. Depletion of cloud droplets by accretional growth should not differ markedly as a function of distance from the barrier.

Since the collection efficiency by ice crystals of cloud droplets with diameters < 30um is exponentially dependent on cloud droplet size (Pruppacher and Klett, 1980, p. 498), the accretion of these large droplets above the melting level is a rapid and efficient proces .

References

Griggs, D. and T. Choularton, 1983: QJRMS, 109, 243-253.
Hallett, J. and S. Hossop, 1974: Nature, 249, 26-28.
Hossop, S., 1976: QJRMS, 102, 45-57.
Pruppacher, H. and J. Klett, 1980: Microphysics of Clouds and Precipitation, D. Reidel Publishing Co., Boston, p. 714.
Hartner, B. i l 21, 1983: Interim Progress Report t Bureau of Reclamation, Dept. of Interior, DS tt145, 94 pp.

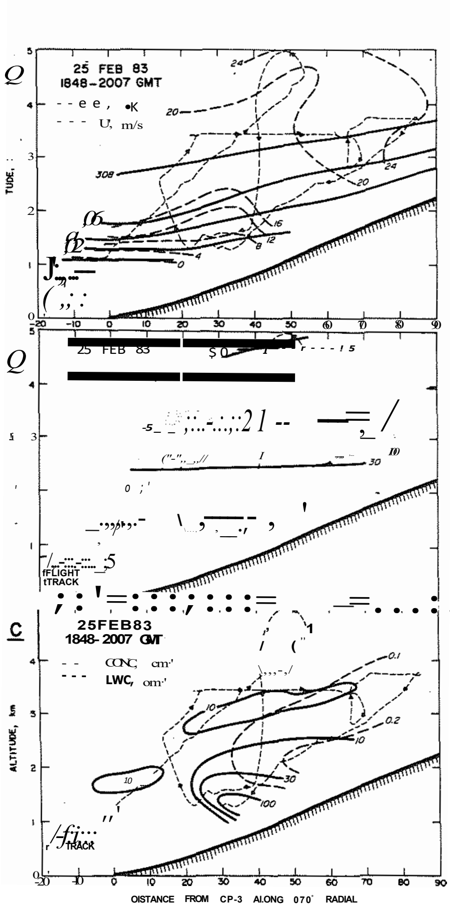

Fig. 1. Vertical cross-section of King Air data. The crest line is near 100 km.

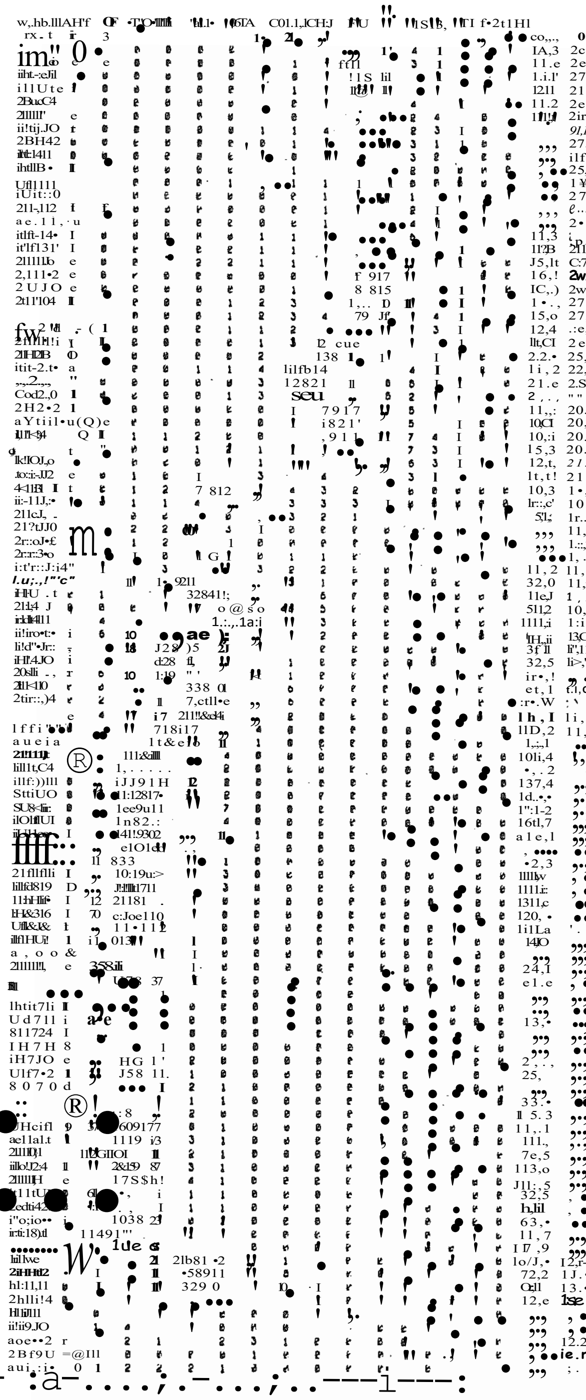

Fig. 2. FSSP 6s averaged spectra from 2000 to 2010 GMT. The columns of numbers from left to right are time in GMT R (_ignore), temperature in °C (lettered and circled), 3:6,9, --- 5 are range bins in um with total number of particles detected in 6s, total FSSP concentration (CONC) in cm-3 and mean droplet diameter (DBR). The DBR is plotted within the range bins as a dot.

G.Lu.DAL B'IELD uF CLCJUJ)I.NESS: .Pl:fYSICO-STATIS'.L'ICAL ANALYSIS, 3IMULAI'ION AND PAR,\.METRIZATION.

L.T.Matveev

Leningrad Hydrometeorological Institute. USSR

.OurinG tho p: st 1S-20 years the launching of satellites vlith phototelevision and infrared equipment on board. has provided c:mple opportunities .for investigating the ; lobal field of cloudiness. At present the 2.1;1ount of these satellite data on cloudiness (it is especially true for the data obtained over the oceans and scarcely populated land areas and also for the entire Southern Hemisphere) is already greater tha,,."lthe number of surface observations.

A report is S;iven of the o.nalysis of :catellite data on cloudiness during the peri od from 1960 to 19s·o. 'l.rhese data were first ta:cen from composite photographs and neph charts and then recorded on a magnetic tape. The amount of cloudiness (n) has been determined for spherical rectangles having the dimensions of 5° latitude and 10° longitude. Because of their higher quality and resolution observational data obtained over the USSR territory have been used for constructing the distribution functions of .

1 • THE ZONAL FIELD OF CLOUDINESS

According to both surface (Ref.1,2) and satellite (Ref.3,4-) data two cloud amount minimums (in high atitudes and subtropics) and two maximums (in temperate latitudes and within the tropical zone of convergence) are registered in both hemispheres when moving meridionally. This conclusion is true for all seasons, as well as for zonal rt on the oceans and the continents. Out of the great volume of cloud information (averaged for monthly, seasonal, one-year, five-year periods,seasons over the continents and the oceans) we shall briefly analyse variations of the position (latitude) of extreme values of n .during the year. The zones of these -n - values shift (though with a considerable lapse) in both hemispheres in the same direction as the sun noves away from the equator: towards the poles in spring an.a. surnner and towards the equator in autu= and winter. Thus the temperate latitude maximum of the Northern Hemisphere is situated near 4-5° (Lat.) in the latter part of 1,inter a d near 62,5° (Lat.) in late summer or in early autumn, the values of n_{max} being greater by 5-7% in summer than in winter. The variations of the :00-sition of subtropical depression (from 15°S.L. ln winter to 30° N.L. in summer in the Horthern :iemisphere and the intert1º0 ,iical convOrgence zone (from 30° S.L. in :J:<'ebru'lry to 10° N.L. in September) are nearly as· great as those ir. the temperate latitudes. L'l ti-ie 3outhern Hemisphere only tile annual change of ilosition of subtropical dcJression is pronounced (from 30° S.L, in December to 10° S.L in June), the position of nm , changing very.little in temperate latitudes. The zonal amount of clouds for the same latitude zone is greater over the oceans than the continents (as a rule by 10-15%) throughout the year. The annual changes of n are negligible over the ocean (their amplitude never exceeding 5%), and they are more noticeable over the continents, the values of n in summer are greater than tl1ose in winter by 8-10%. 'rhe annual values of n - averaged for oce-a;1s, lands and the Earth as a whole - are subject to considerable variations from year to year and even every five years. "l'hus, the mean monthly values of n resistered during the 1971-1976 period in the Southern Hemisphere are less than those recorded during the 1976-1980 period. For the Earth as a whole mean annual cloud amount constituted 55% during the first five-year period and 60% in the second ones. Du.ring a decade (1971-1980) mean annual cloud cover amounted to 50% over the Northern Hemisphere and 62% over the Southern Hemisphere.

2. ,.rHE DL3TRIBUTION FUNCTIONS.

-J:he distribution functions of n have a number of peculiarities. The basic difference in the shape of tne curves representing density distribution of n (V" -shaped for satellite dat;a) is, first of all, accounted for by the fact that the distribution of n depends greatly on the area subjected to averaging /5/. '.rable shows t.he empirical density of clo'.l.d amount distribution for the four seazons (expresGed as a percentage). To reduce the volume of the present paper this table : ives the ini'ormation on density distribution (P) of cloud amount obtained from catellites over USSR territory during the period of 1979-1981 only for 3 squares. Spherical sq uares (with a common cent.re) hc1ve been used, whose sides vary from 0,5° to 10° (in Lo. and Lat.). In case of determining n for small squares (0,5° x 0,5° ; 1°x1° ; 2°x2°) the distribution (of n) is of a V -. shaped character. '.rhe P,.,.,a, corresponds to small (0-10%) and large (80-100%) values of 1 • The P,,,..,;,.corresponds to n varing from 4-0% to 60%. ".rhe distribution of n for large square (8°x 3°;10°x 10°) is dome-shaped. In ·I-his case P has its maximum values for n varing from 30 to 70%, 1:iinimum values for n being equal to 0 m d '100%.

Table 1

The empirical density of cloud amount distrib tion for the four seasons(%).

n%	squares											
	0,5°x 0,5°				10:x:10				10°:x10°			
	W	Sp	S	A	W	Sp	S	A	W	Sp	S	A
0	17	34	50	35	11	26	39	26	1	5	2	2
10	6	7	12	7	7	10	18	10	2	5	16	4
20	5	7	10	7	5	8	9	7	3	7	19	8
30	2	2	2	2	5	5	6	5	9	14	23	16
40	3	3	1	2	4	5	2	4	10	14	12	15
50	2	2	0	1	2	2	1	2	8	9	8	10
60	4	2	1	3	4	3	2	4	12	14	6	12
70	4	3	2	3	6	5	2	4	19	14	6	15
80	4.	4	2	2	8	5	3	5	18	10	7	11
90	16	12	9	14	18	13	9	17	17	8	2	5
100	38	24	11	24	29	18	9	16	2	0	0	0

The list of abbreviations:

W - winter

Sp - spring

S - summer

A - autumn

In summer the frequency of a few cloud weather calculated for European territory pf the USSR is great. In the case of deter- Piing n. for the small squares tM main maximum of P corresponds to the clear sky and the secondary maximum to the continuous loudiness. These maximums decrease with increasing of the surveyd square. They gratlually shift in different directions. The main maximum moves to the great values of n. and the secondary to the less values (of n.). These mazj.mums become practically one if the dimensions of the square are greater or being equal to 6°x6° and the distribution of n. may be considered as dome-shaped.

In winter stratiform (frontal) cloudiness dominates in temperate latitudes. Therefore in the case of small squares (their dimensions never exeeding 1°x1°) the mai maximum of P corresponds to the continuous cloudiness and the secondary to the clear sky and the P,., corresponds to n, =50%. In the case of further increasing of dimensions of squares (2°x2° and greater) two additional deepening minimums of P are recorded. They correspond to n =0% and n., =100%. The curve of distribution becomes two-humped.

Several types of fllilctions for parametrization of empirical distribution functions have been tested (gamma-, Gramme-Charlier, exponential, power distribution and others) Parametrization using generalized log-normal distribution approximates empirical data best of all.

The analysis of spatial correlation functions leads us to a conclusion that the correlation of n, - values standardized according to IS.., is much closer along the parallels than along the meridians. Correlation coefficients calculated along parallels (x) are substantially greater than those calculated along meridians (y) at the same distance. Values of rc,(x,) and (y) decrease with distance in both hemispheres. However, (x) coefficients decrease more slowly and (y) coefficients decrease more quickly with growing and y in the Southern Hemisphere than in the Northern Hemisphere. This differenc can be accounted for by the following:

1) the predominance of claud fi lds;
2) a more pronounced zonality of these fields in Southern Hemisphere as compared with the Northern Hemisphere. The sp tial correlation scalep are as follows: x,... =. 3540 km and y,., 1430 km for the Northern Hemisphere and x.s= 4950 km and ys= 1094 km for the Southern Hemisphere. The longer the averaging period is the less distinct the anisotropy, of a cloud field becomes.

The results of modelling make it possible to draw a conclusion that vertical speed distribution plays an important part in the forma ion of cloud and temperature fields (particularfy in the growth of thermal instability of updrafts which is accompanied by the development of convective clouds and storms). Mention should also be made of cold advection which. is responsible for initiating cyclonic disturbances (tropical cyclones. being among them).

REFERENCES

1. Berljand T.G., Strokina .A., Greshnikova L.E., 1980, Zonal distribution of cloud amount over the Earth, Meteorology and eydrology, N° 3, p.15-23.
2. Kobysheva N.V., 1971, Indirect calculations of climatic cnaracteristics, L., Gicirometeoizdat, 19 pp.
3. Matveev L.T., 1981, Cloud dynamics, L., Gidromteoizdat, 311 pp.
4. Matveev J L., Statistical characteristics of global cloud field, 1981, Sem., "Atm.-ocean-space", Rep.N°15, AN USSR, m, 27pp.
5. Matveev J.L. Dependence of distribution functions of cloud amount on averaged and parametrization of cloudiness, 1982, Sb. Osnovnye voprosy met.obespechenija gr.av., L., OLAGA, p.122-128.

MESOSCALE ANALYSIS OF THUNDERSTORM SYSTEMS IN ALBERTA

Gerd Ragette

Zentralanstalt fur Meteorologie und Geodynamik,Hohe Warte 38,1190 Vienna,Austria

I.DATA AND DATA ANALYSIS

As part of the Alberta Hail Project serial radiosonde ascents were released during 1976 on certain summer days.Several fixed.sites and one mobile radiosonde station we e used (Ref.1).Soundings commenced early in the morning and were to be repeated throughout the day usually in intervals of 2 hours. They were all intended to reach the 150mb level.Computer programms convert the ordinate values according to baseline data into temperature and humidity;Temperatures are not corrected for radiation error. The observed humidities which are assumed to.refer to saturation with respect to water are modified by using a fictitious saturation vaJJor p·ressure es according to Eq. l,

$$es = eu + (ee - ew) F \qquad (1).$$

For temperatures above -15C only water saturation is allowed.Between -15C and -36C an· exponential variation of F from o to l is assumed. According to Ref. 2 an exponent of 0.576 is used.Below -36C only ice saturation is allowed to occur.For calculating the winds the curvature of the earth and the refraction are not taken into account.However,a fairly detailed error analysis - particularly for the wind components - has been incorporated into the analysis scheme.

Once all ascents of a given day have been analyzed they are combined by applying time-to-space conversion. All meteorological fields are assumed to move quasistationary with the same velocity which is independant of height but may vary with time.In case of convection the yelocity of the fields was identified with the motion of the storms.In the absence of radar echoes the motion of synpptic weather systems was used instead.For a given level the conversion of time series of observations taken at various locations yields a set of scattered data points.3-dimensional fields of temperature,humidity,wind and time are derived by objective interpolation on a regular grid. The.grid point data are used for further calculations.

The vertical velocity is computed from

$$\text{\II} = \cdot c./\backslash T.\backslash 1/T+AD.wD)/(AT+AD) \qquad m.$$

wT is the vertical velocity obtained from the temperature by using the first law of thermodynamics where the effects of evaporating precipitation and melting sn0\11 as well as the vertical eddy diffusion of sensible heat have been· neglected and wD the vertical ve-' locity obtatned from the divergence by integrating the continuity equation.The weights are essentially functions of the accuracy of the corresponding vertical velocity computed from the error estimates of the original observations.Upon ·averaging according to Eq.2 the resulting \IIis used as lower boundary vaiue of vertical velocity for the next integrational step in the calculation of·wo.

The rate of condensation (evaporation) is computed from :·

$$r = -\dot{q}s.\rho D.\delta \qquad (3).$$

qs, the derivative of the saturation mixing ratio, is obtained according to Ref. 3,D is the density of dry air·andJ a gradual onset function (Ref.4).A critical relative humidity of *95?(* and a power law with an exponent of 0.6 (Ref.5) are used.If the relative humidity exceeds this limit condensation or evaporation of clouds is allowed to take place.

Estimates of the rate of precipitation are calculated by vertically integrating the rate of condensation taking only positive contributions-into account,as Eq.3 is assumed to describe the evaporation of clouds only.The evaporation of precipitation is formulated according to Ref.6,which prohibits evapo ration in saturated air.This seems inadequate for saturated descending layers.In order to arrive at more realistic precipitation patternp radar data were incorporated for those storms which produced precipitation on the ground by setting the relative humidity equal to 100?, within the vertical extent of the echoes. For practical reasons it was not feasible to use at any grid point radar data of the appropriate i.J:iter-· polated time.Thus the times at which the radar echoes are drawn do not always correspond with those which apply to the soundings.

2.RESULTS

The case of August 12,1976 is presented as example. The horizontai dimensions of the· domain are 300x250km (Fig.1),with a corresponding average spacing of the observations of 40km.The internal grid length is 9.5km.

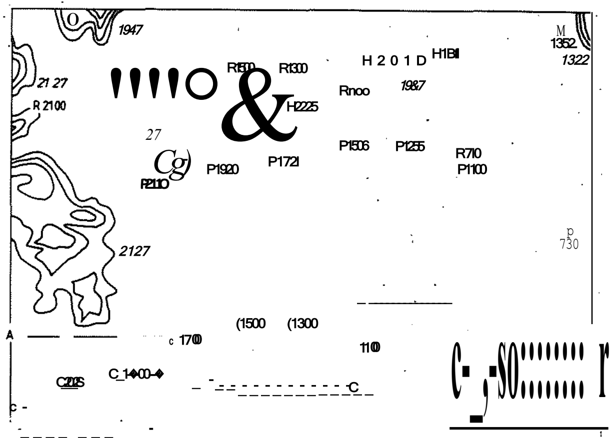

Figure I.Location of sites (letters) and release times.Echoes at indicated times (obl-ique) in steps of lOdBZ,outer contour at 20dBZ.

2.1.Mesoscale fields

The vertical section of6w (Fig.2) shows a 5km deep layer of low8w between 2 and 7 km which was humid except for the layers above 5km(Fig.3).Thus the storms of that day can be called air mass type storms, The low-level temperature distribution reflects the diurnal heating,the highest t.emperature occurring around 1700.At the 3km level,2km above ground,where tne diabatically induced temperature changes are less pronounced than near the surface,the temperature maxima are found ahead of the precipitation areas with temperatures about 2C higher than in the echo regions:A somewhat different picture emerges from the low-level distribution of 8w (Fig. 4) ,where areas of convective precipitation are warm regions. In the low levels all regions of high 8 w coinci ded with regions of high mixing ratio q (Fig.5) and in particular the echoes are seen to be closely related to the maxima of q.This ' seems to agree with Marwitz (Ref;7) llho states that updrafts of storms are typically co·ol·,moist and contain the highest El w. The pattern of calculated precipitation (Fig.6) may be compared with the radar data

(Fig.1).The storms of 1527 and 2127 come out reasonably well by the computations.Although the observed maximum rates which ranged between 12 and 50mm/h - corresponding to reflectivity maxima of 40 to 50dBZ - were one order of magnitude higher than the maximum computed rates of 1 to 4 mm/h, the agreement is encouraging.

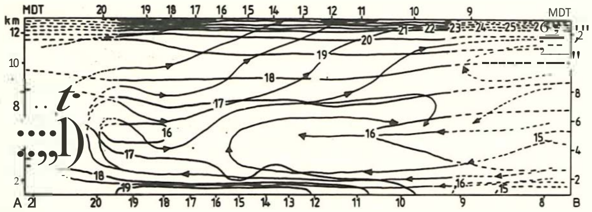

Figure 2.Time-height section of θ_w along AB with relative flow.

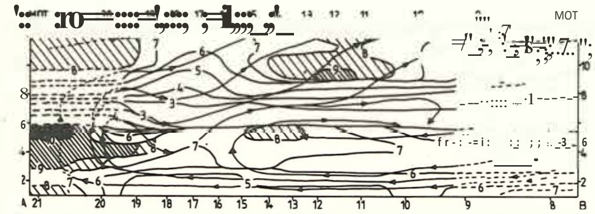

Figure 3. Time-height section of RH along AB in 10 %, with relative flow. RH ≥ 80%, hatched.

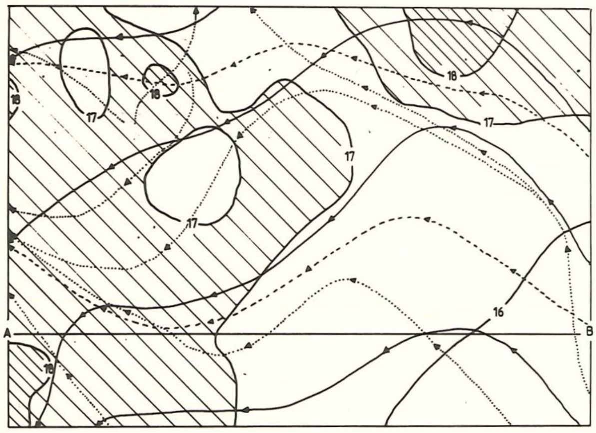

Figure 4.θ_w at 3kmMSL, θ_w ≥ 17C hatched.Streamlines at 1kmMSL ___ ,2kmMSL - - - ,3kmMSL:••••.

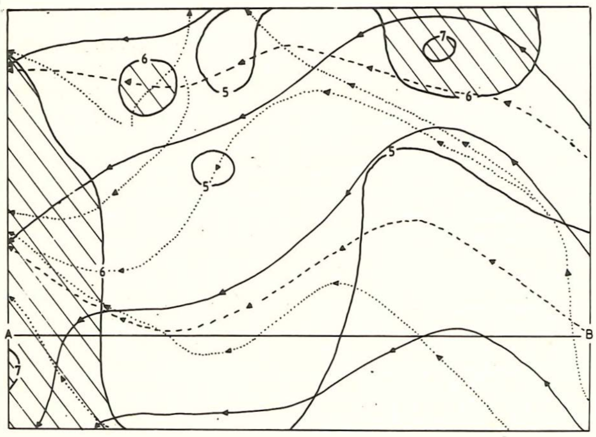

Figure 5.Mixing ratio q in 10^{-3} at 3kmMSL,q ≥ 0.006 hatched.Streamlines as in Figure 4.

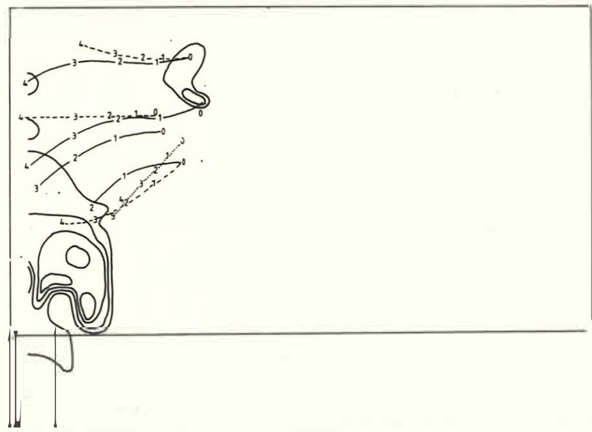

Figure 6.Calculated precipitation at ground in steps of 1mm/h.Horizontal trajectories at 1kmMSL —— ,2kmMSL - - - ,3kmMSL •..... with times in hours.

2.2.Storm of 2127

Although no soundings are available from the back of this storm and the echo drawn at 2127 is not representative for the times indicated in Figures 2 and 3, when it extended all the way to the edge of the domain,we shall discuss it in more detail.As the streamline analysis of Figure 2 suggests,low-level air originating later than 1600 from above the 2km level,not more than about 50km ahead of the subsequent precipitation,was eventually incorporated into the storm system. The increase of θ_w with time indicates that warm air from close to the ground was involved in the ascent towards the storm.Air parcels ascending prior to that time or further ahead of the still future storm, respectively,were not drawn towards it but were recirculated at mid-levels where Ac-clouds were reported in accordance with a humidity maximum(Fig.3).A horizontal θ_w-difference of more than 3C is apparent between low-θ_w air at mid-levels just ahead of the storm and the ascending warm air.The θ_w-minimum in 5km in front of the storm coincides with high θ_w at the surface pointing to considerable potential instability just ahead of the precipitation.The trajectories displayed in Figure 6 suggest possible interaction between the storm drawn at 1527 (Fig. 1) and the following system of 2127. Air originating from the precipitation area of the earlier storm at a time when it was at its most active stage (1400 to 1500) could have participated in the formation of the subsequent system from 1700 to about 1800.When the first storm had dissipated (no echo after 1645),air from the dying storm should have reached the cell on the left flank of the following system at a time when it was rising to more than 12km.

3. REFERENCES

1.Robitaille F E & Sackiw C 1977,storm environment, Current Research on Hailstorms and Their Modification,Atm. Sci. Rep. 77-3, Alberta Research Council,1-20.
2. Isaac G A & Douglas R H 1973, Ice Nucleus Concentrations at -20C During Convective Storms,J.Appl.Met. 12, 1183-1190.
3.Fulks J R 1935,Rate of Precipitation from Adiabatically Ascending Air,Mo. Weath. Rev. 63, 291-294.
4.Davies D & Olson M 1973,Precipitation forecasts at the Canadian Meteorological Centre, Tellus 25,43-57.
5.Twomey S & Wojciechowski TA 1969,Observations of the geographical variations of cloud nuclei,J.Atm. Sci. 26, 684-688.
6.Kessler E 1969,On the distribution and continuity of water substance in the atmospheric circulations, Met.Monogr.10(32),Am.Met.Soc.
7.Marwitz J D 1973,Trajectories Within the Weak Echo Regions of Hailstorms,J.Appl.Met.12, 1174-1182.

THREE-DIMENSIONAL STRUCTURE OF A WEST-AFRICAN SQUALL LINE OBSERVED DURING THE COPT 81 EXPERIMENT

Frank ROUX
CENTRE DE RECHERCHES EN PHYSIQUE DE L'ENVIRONNEMENT TERRESTRE ET'PLANETAIRE (CNET-CNRS)
38-40 rue du **General** Leclerc
92 ql ISSY-LES-MOULINEAUX
France

1. INTRODUCTION

It is widely recognized that cumulonimbus convection organized in mesoscale systems in the tropics (squall lines) plays an important role as contributor to tropical .rainfall budget and , through the vertical transport of momentum , heat and moisture , ,to the energetics of atmosphere on the scale of general circulation • However our lack of knowledge about their internal organization prevents satisfying parameterization in large scale prediction models .

Some field experiments (e.g. : VIHMEX 1972 , GATE 1974 ,WAMEX 1979 ••.) have been previously devoted to the observation of such events and have c_ontributed to clarify the concepts of squall line structure and to make them more ·quantitative . In the same goal the COPT81 (Convection Profonde Tropicale) experiment has been carried out in May and June 1981 at Korhogo (in the north of Ivory Coast) by french and ivorian research institutes (Ref.1) . Dual- Doppler radars , radiosounding and surface network stations were operated to provide detailed description of dync\lllics and thermodynamics of west-african squall lines .

The case study reported here refers to a squall line observed on 23-24 June 19_81 . This event was a very active one and rather different from the other observation previously reported (Ref.2) , concerning the 22 June 1981 squall line. Hereafter section 2 deals with the mesoscale structure deduced from satellite pictures , radiosounding and radar measurements . Detailed kinematic features are displayed in section 3 from dual-Doppler data obtained in the frontal region and compared with surface network observations •

2. MESOSCALE CHARACTERISTICS

2.1. Meteorological environment

NOAA6. satellite pictures taken on 23 June at 080017 and on 24 June at 073719 (all times are local times GMT) display very different features . On the first one , 15h before the arrival of the squall line at Korhogo , an ensemble of isolat·ed Cb clouds is observed 1000 to 1500 km eastward of the experimental site , but no structure could be identified as a squall line_. On the contrary the second picture , taken 7h30min after the arrival of the squall line , shows a cloud cover of 1000x1000 km^2 area over southwestern coast of West-Africa . Thus the observed squall line was probably a very young and active one which has developed during 23 June . This is corroborated by the observations of the Ivory Coast Meteorological Network which indicates increasing of the precipitations associated to this squall line during its displacement toward southwest .

θe and θes profiles (Fig.1) deduced from 6 radiosoundings launched on 23 and 24 June at Korhogo show a continuous increase of convective instability until the arrival of the squall line (gust front was observed at Korhogo at 2350) . one may note that influence of Cb clouds , observed between 1630 and 1800 near Korhogo ,was negligible while the squall line has completely changed the thermodynamic structure of atmo"sphere through high-levels wa,ming and low-levels cooling.

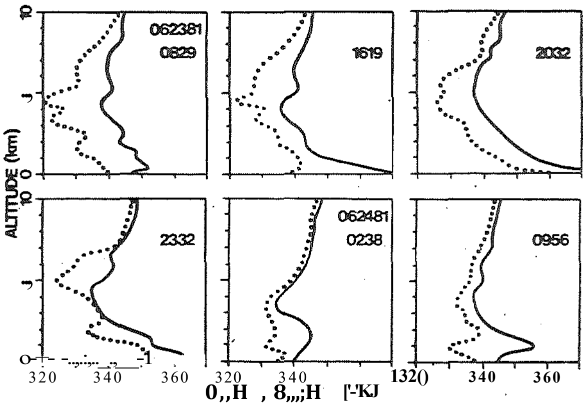

Figure 1 : Vertical profiles of equivalent θe (dotted lines) and saturated equivalent θes (solid lines) temperatures deduced from 6 radiosoundings on 23 and 24 June 1981 .

Detailed analysis of the 233250 sounding displays an unstable layer between ground and altitude 2500m (all altitudes are AGL) , t condensation level is at 1000m and the level of free co vection at 2000m, so an initial lifting is necessary for convection to develop • Once lifted, air parcel may reach altitude 15000m (equilibrium temperature level) with a maximum temperature excess of 5°C with respect to environment at 4500m . Wind profile deduced from the 233250 sounding indicates a weak (5 ms-')southwesterly flow between ground and 1000m (moonsoon flux) , above an easterly flow is observed with constant intensity (10 ms-1) between 1500 and 4500m and with a noticeable shear (3.5" 10-, s-•) between 5000 and 14000m.

2.2. Mesoscale radar observations

Reflectivity contours (Fig.2) deduced from a 100km range PPI scan display classical features· (Ref.3) : (i)The maximum- reflectivity values are found in the 40km wide convective region in front of the squall line . Peak values (>50dBZ) are not contiguous , but located within distinct cells . Minimum reflectivity values (20dBZ)follow immediately after ("reflectivity trough") (ii)an extensive precipitating stratiform region (250km wide) trails the squall line (only its forward part appears on Fig.2) where minima (30dBZ) and maxima (45dBZ) are wider than in the convect'ive region . The squall line front is oriented NW-SE and moves towards southwest at 16.5 ms-•. Although observations are limited to the radar range one may suppose the horizontal extent of this squall line is larger than the displayed 200km , so the present observations refer only to a limited **"slice" within the convective and stratiform** regions .

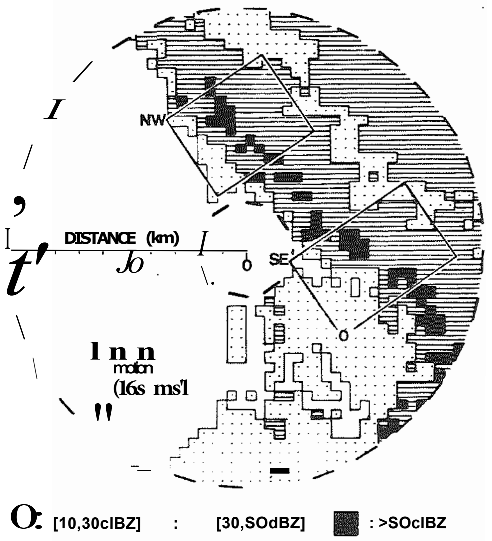

Figure 2 : Reflectivity contours deduced from a 100km range PPI scan at 1 elevation on 23 June 1981 at 2330 . Rectangles with m, and SE in the upper left indicate regions where 3D wind and reflectivi.ty fields are obtained from COPLAN data . North direction and squall line motion are ilulicated .

Combining the mean horizontal and vertical wind profiles deduced from COPLAN (in the convective region) and VAD (in the stratiform region) scans allows to reconstitute a vertical cross section , along the squall line displacement axis ,. of the mesoscale circulation (Fig.3) . The frontal region is characterized by an intense updraft (maximum mean upward velocity is 3.5 ms-1) which may be associated to the inflow of unstable air at low levels . Below 1000m a weak easterly flow forces the initial lifting or this entering air . Above 6000m air in front of the squall line flows forward due to the wind speed in the environment larger than the squall line motion ; this induces throwing of precipitations in a forward anvil between altitudes 6000 and 13000m . Within the " reflectivity trough " mean vertical motion is downward (-0 .4 ms-1) so that evaporation of precipitations condensed in the convective updraft should be important . In the stratiform region mesoscale updraft (0.5 ms^{-1}) and weak downdraft (-0.1 ms··) are observed on each side of the 0^{o}c isotherm (altitude 4000m) .

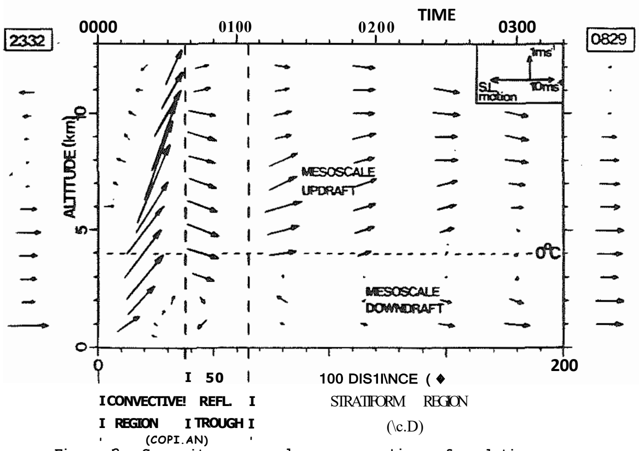

Figure 3 : Composite mesoscale cross-section of relative wind in the squall line deduced from COPLAN and VAD data . Wind profiles deduced from the 2332 (23 June) and 0829 (24 June) soundings a.re displayed on each side of the frame . Scale and squall line motion are indicated .

This mesoscale circulation is substantially different from that deduced for the 22 June 1981 squall line (Ref.2) since here the main vertical motions occur within .the convective region . The low-level easterly flow observed in the frontal region is weak and results probably from the " reflectivity trough " downdraft , although contribution from the stratiform region downdraft could be of lower influence . For the 22 June squall line a similar low-level easterly flow was more intense and deeper , and was analyzed as resulting merely from a -mesoscale downdraft . Moreover ,when compared to this previous observation , vertical motions are more intense in the convective region and " reflectivity trough " , and weaker in the stratiform region . These differences result probably from different maturity stages in squall l.ine evolution . The present event is a young and convectively active"one where upward motions result from convective instability of inflowing air ; the associated vertical fluxes contribute to stabilize the thermodynamic vertical structure of atmosphere in the inner regions of the squall line , then prevent development of intense vertical motions in the stratiform region . on the other hand the 22 June squall line was supposed to be in a decaying stage where upward motions in the frontal convective region were mainly forced by the propagation of a density current of cold air generated by a mesoscale downdraft in the stratiform region . As convective updafts were weaker in this previous case , air in the stratiform region was probably less stable and more intense mesoscale vertical motions (upward and downward) could develop .

3. DETAILED OBSERVATIONS OF THE FRONTAL REGION

Two sets of COPLAN scans , in the NW and SE of Korhogo (see Fig.1) , have been conducted in the frontal region of this squall line . For brevity we will only discuss here the results from the SW scans , including 4 sequences at respectively 2335 , 2341, 2347 and 2353 (the NW scans display very similar features) .

3.1. Cellular structure

As deduced from the location of ·the 10dBZ forward contour on successive- PPI scans , the squall line front diplaces toward southwest at 16.5 ms-1 . The convective region is composed of short-living high reflectivity cells which cannot be followed on the successive PPI scans . Intervals between successive COPLAN scans (6m-in) is short enough to permit tracking of these cells and their motion is found slower (J:1 ms-1) , though in the same direction , than the- squall line front propagation .Then , to minimize the effect of temporal evolution during data acquisition (Ref.4) , the moving frame to be considered in the data processing is that of the cells where dynamic processes really occur .

Evidence of cellular structure in the convective reg-ion clearly appears when superimposing (in the frame moving with the cells) vertical veiocity fields on reflectivity contours , e.g. at altitude. 5000m (Fig.4) . The fair correlation between high reflectivity cells (Z>40dBZ) and updrafts cores (w>+6ms-·) confirms reality of discrete convectively active elements . The cells are approximately aligned along a direction parallel to the squall line front ; the more intense reflectivity values (up to 60dBZ) and updrafts (up to +20 ms-1) are located in the frontal part while maxima in the rear part are less pronounced . As seen on the successive scans , the cells evolve rather rapidly through growing , decaying , splitting or merging ; but new cells preferentially form in front of the older decaying ones , with sometimes downdrafts (W<-3 ms-1) between them , associated to lower reflectivity values (Z<30dBZ) •.

In the rear part of the COPLAN scanning area (X>35 km) downward motions are associated to the region of minimum reflectivity values (Z<20dBZ) , representing the forward part of the "reflectivity trough" . Since these downdrafts are apparently distinct from 'the convective cells , their origin should be different from those observed between cells . Likewise weak downdrafts in front of the squall line (around X=lO km , at 2347 and 2353) seem disconnected from the region of main updrafts . Both points are detailed below.

.3.2. Dynamic features

The main dynamic phenomena in the convective region occur within small size (area less than 100 km) short-living cells . Fig.Sa displays , in the frame moving With the cells , vertical cross-sections along X axis for the 4 scans in the southernmost cell (at Y=9 km) , which is associated to the more intense reflectivity and vertical velocity values . Unfortunately its location near the edge of the scanning region prohibits complete views , especially for the 2335 and 2341 sequences .

Kinematic characteristics of the convective region diplayed on Fig.3 appear again : a low-level easterly flow up to altitude 2 km , an entering flow up to 5 km feeding the updraft and an easterly flow above 6 km·. The updraft is intense (up to +20 ms-' at altitude 7500m) and reaches altitude 13000m ; during the 4 scans its structure evolves .. At 2335 , although it is near he scanning limit , narrowness of the 40dBZ contour indicates that this updraft has probably just formed, but reflectivity values larger than 50dBZ already exist . The region of intense vertical motions broadens out at 2341 , reflectivity values larger than SOdBZ appear near altitude 5000m . At 2347 updraft and high reflectivity regions grow forward , vertical motions dimipishes in the high reflectivity region in altitude (Z>SOdBZ ; X=30 km) due probably to liquid water loading opposed to buoyancy , below this region weak downward motions appear . At 2353 a downdraft has formed (X=35 km) and is associated in the lower levels to low reflectivity values (Z< 20dBZ) ; this could imply that cooling due to evaporation of. precipitations acts together with liqui.d water loading to maintain downward motions . This downdraft feeds the low-level easterly flow so that the updraft base and ::onsequently the high r eflectivity region in altitude (Z>50dBZ ; X=25 km) are diplaced forwards . Through this mechanism new updraft regions may form in front of older ones . In the present case this forward displacement of the updraft base occurs continuously , but for other cells the easterly flow resulting from the convective downdraft may cross the updraft base instead of diplacing it . In such a situation the older updraft vanishes before a new one forms forwards .

Above altitude 6 km the forward part of the updraft (which has approximately the same inematic characteristics than the entering flow) is near an oppositely directed flow which entrains precipitations formed in the updraft to a forward anvil which extends some 30 km in front of the updraft base . Weak downward motions observed within this anvil (see also Fig.4) are probably due to cooling caused by evaporation of precipitations in this unsaturated easterly flow. The resulting downward humidity flux could then increase convective instability of the lower layers in front of the updraft base and facilitates creation of new updraft regions in front of the squall line .

Temporal measurements , conducted with a surface station located near these cross-sections , have been transformed in spatial measurements along the squall line displacement axis (Fig.Sb) . Owing to non-stationnarity of the convective region , the radar results from 2335 to 2353 may only be compared to surface measurements obtained simultaneously , i.e. from 2330 to 0000 or from X=O to X=25 km . Interface between inflowing air and easterly flow at ground is observed (through the change in wind direction , increase of the wind intensity and temperature drop) at X=lO km, about 8 km forward the beginning of intense upward motions . This shows that convective instability does not develop immediately , and the entering flow has to be lifted by the lowTlevel easterly flow, at least up to the condensation level (1000m) . Two steps appear in the temperature drop (2°C from X=lO to X=15 km; 2°C from X=20 to X=25 km) ; radar data are not available in the .first region, however this first drop should correspond to the temperature difference between inflowing air and low-level easterly flow ·, the 'second temperature drop results probably from the additional cooling caused by air coming from the convective downdraft . The maximum pressure pertubation occurs within this second drop and is characteristic of non-hydrostatic effect due to velocity gradients , however , as it is observed after 2353 , it is difficult to correlate with radar data. Intense precipitations (maximum : 112 mm.h-1) observed at ground are connected to the high reflectivity region (Z>40dBZ) diplayed on radar data .

Downward motions associated to low reflectivity values in,the rear part of the COPLAN scanning area (see Fig.4) are detailed on Fig.6 through vertical cross-sections along X axis (at Y=22, 19 and 18 km) for the 4 scans • These downdrafts differ noticably from those observed in the frontal part since they extend over the whole altitude range (0,15 km) . As they originate in the higher levels , they should result from negative buoyancy (inducing downward acceleration) of the high level easterly flow with respect to warmer air below, lifted up through the convective updrafts . Moreover the low reflectivity values (Z<20dBZ) could be a consequence of evaporation of precipitations in unsaturated air (as what o curs in the forward anvil , but on a larger scale here) . A.part of this downdraft feeds the low level easterly flow while the other one mixes with warmer air from the updraft , stabilizing the vertical thermodynamic structure of atmosphere in the inner regions of the squall line .

4. CONCLUSIONS

The squall line observed during COPT81 on 23-24 June 1981 is a large and convectively active one . Jue to instability of inflowing air , intense vertical motions develop and lead to important change in the vertical structure of· atmosphere . These upward motions occur in the frontal convective region within short-living cells aligned perpendicularly to the low-level inflow and the continuous generation of new cells in front of the older ones , through updraft-downdraft interaction , allows to maintain an intense convective activity . On the opposite, vertical motions in the extended stratiform region are weak .

Now comparisons between the 3D wind and reflectivity fields in the NW and SE scanning regions (see Fig.2) will permit to investigate horizontal homogeneity of the convective region . Results from 6 COPLAN scans conducted from 0010 till 0050 in the "reflectivity trough" will furnish detailed informations about this region , scarcely accessible from the present data . At least retrieval of pressure and temperature fields (Ref.5) should display dynamic and thermodynamic processes occuring in the frontal region of this squall line .

6. REFERENCES

1. COPT organizing committee (paper gathered by G. Sommeria and J.Testud), 1984 : "COPT.81" , a field experiment designed for the study of deep convection in continental tropical regions. , to appear in Bull. Amer. Meteor. Soc.

2. ROUX F. , J.Testud , B.Payrissaty and J-P.Chalon, 1982 : Dual-Doppler radar and surface network observations of a west-african squall line during the COPT81 experiment , conf. on Cloud Phys. , Amer. Meteor. Soc. , Chicago , Ill. , 547-550 .

3. Houze R.A. and A.K. Betts , 1981 : Convection in GATE , Rev. Geophys. Space Phy . , 19 , 541-576

4. Chong M. , J.Testud and F.Roux , 1983 : Three dimensional wind field analysis from dual-Doppler radar data . Part II .Minimizing the error due to temporal evolution , J. Clim. Appl. Meteor. , 22 , 1216-1226 .

5. Roux F. and J. Testud , 1982 : Pressure and temperature fields retrieved from dual-Doppler radar observation of a west-african squall line , 21st Conf. on Rad. Meteor. , Amer. Meteor. Soc. , Edmonton , Alta. , canada , 27-31 .

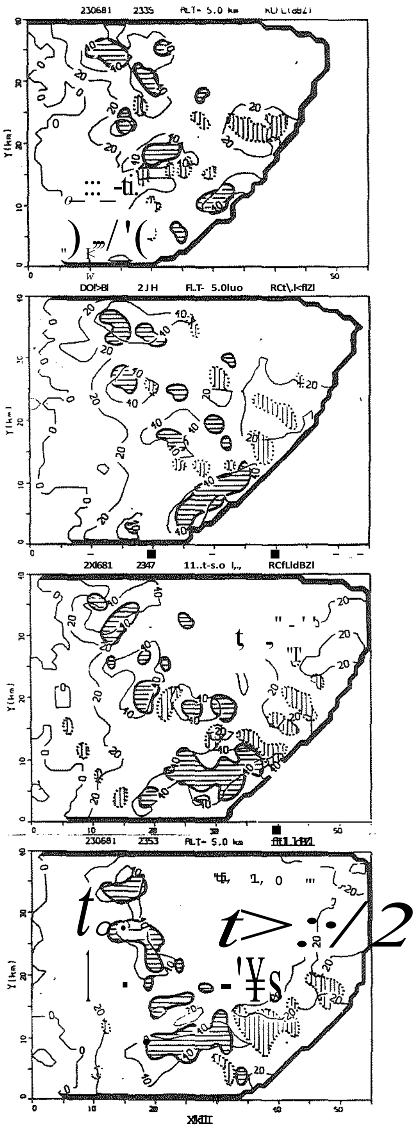

Figure 4 : Reflectivity (0,20,40dBZ) and vertical velocity (solid line contour and horizontal hatching : W>+6ms ; dotted line contour and vertical hatching : W<-3ms) contours for the 4 successive scans (2335,2341,2347,2353) at altitude 5 km in the frame moving with the cells . Thick solid line indicates scanning limit .

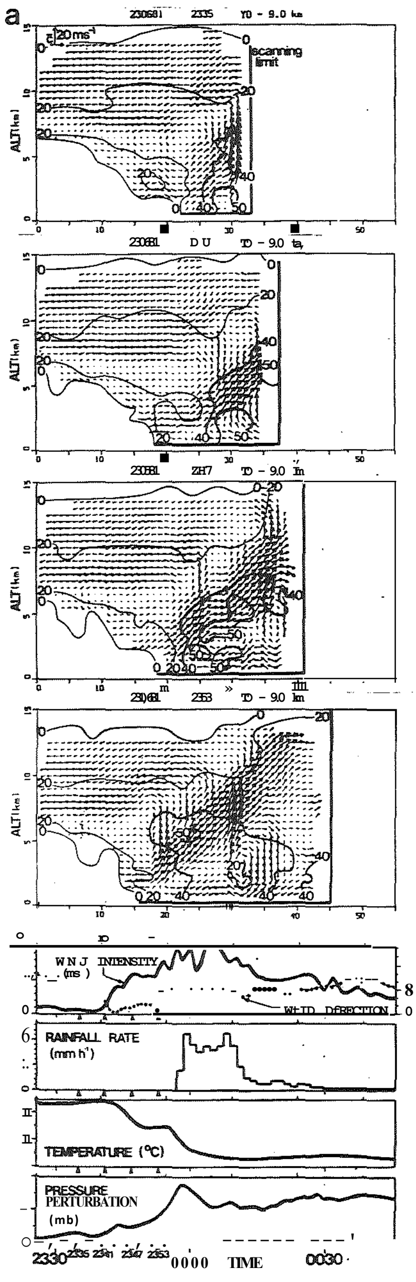

Figure 5a : Vertical cross section at Y=9km of wind and reflectivity in the frame moving with the cells for the 4 successive scans . Scale and cells motion are indicated in the upper left for 2335 . ----- 5b : Wind intensity and direction , rainfall rate , temperature and pressure perturbation profiles deduced from the ALICE 1B measurements .

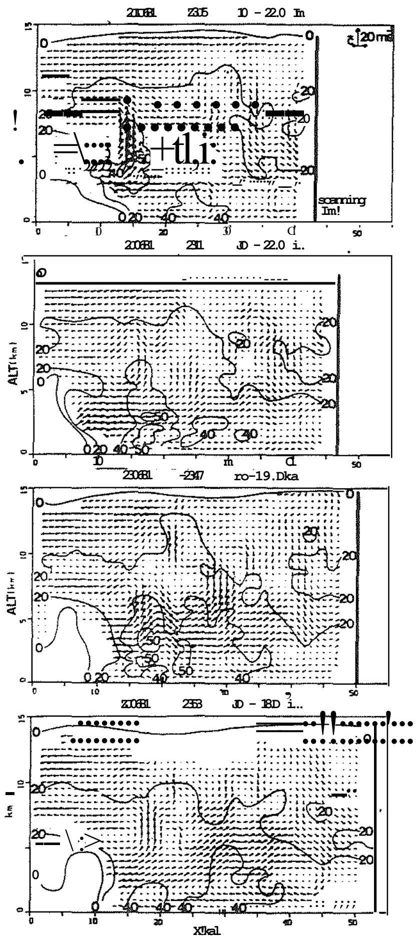

Figure 6 : Vertical cross section of wind and reflectivity in the "reflectivity trough" (Y=22, 19, 18km) in the frame moving with the cells for the 4 successive scans . Scale and cells motion are indicated in the upper right for 2335 .

A SQUALL-LINE OVER CENTRAL ARG NTINA

H.E. Saluzzi and E. Lichtenstein

National Commission on Space Research and National Weather Bureau
Buenos Aires, Argentina

1. INT:zODUCTION

In Argentina, north of 38° S and during the warmer half of the year - from October to Harch - the greater part of the precipitation occurs convectively.

With great frequency (Ref. 1), this convection is organized into a squall-line , usually close to a frontal system and to a disturbance in the synoptic scale. (Ref. 2). They increase in intensity in the presence of tropical air mass, warm, humid (0e = 350° Abs.) which penetrates beneath the superior mass of air (0e = 330⁹ Abs.), both separated by an inversion convectively unstable.

The orography besides plays an important role in the mechanism of formation.

The mesoscale studies carried out (Ref. 3 and 4) point out this circumstarce.

The squall-lines can produce torrential rains, strong gusts, destructive hail and even tornadoes. (Ref. 5).

In the present case, the storm formed in front of the squall-line over the Sierras of Cordoba and San Luis and created abundant hail of up to 4 cm in diameter, which was collected between 4:30 and 4:40 (local hour :·LH) in the city of Cordoba (31° 10'S, 64° 13'0).

The presente paper explains the mechanism of the formation of the storm and its intrinsec features.

2. 1"dE GENERAL CONFIGURATION

The days prior to November 17th, are characterized by a high index of circulation, with intense west winds up to the equatorial region in the superior troposphere.

On the day of the storm, two jets found inmersed in the current west, to 12 GUT.: one, at 150 km nol'.'th of the city of Cordoba, oriented WSW, with 60 m/s at 170 mb (probably the subtropical jet); the other, 1000 km.to the S of Cordoba, from the HNW with 48 m/s at 240 mb identifying the jet of the P£lar front. Both currents are diffluent over the central region of the country.

At that lati.tude, the west winds show markedly short waves, as long as 2700 km, so that a wedge (at 12 Gl'IT.) is found 200 km east of Cordoba while over the Pacific Ocean there is a trough which, in its migration towards the east, will increase its influenc on the region over which the storm ocurred.

3. THE SYNOPTIC SITUATION ON THE SURFACE

A mass of polar air had entered the Patagonia, quickly advancing towards to the north. Strong negative tendencies in the field of pressure in the north of Patagonia indicated the beginninf of frontal wave and, at OQ GMT. of November 17th, a frontal depression formed over the San 1'atias Gulf. To the northwest the quick advance of the cold front is detected, which at 12 GMT. on the 17th, has advanced noticeably, crossing from San Juan (31° 34'S, 68° 25'W) to Mar del Plata (37° 56'S, 57° 35'W), with typical orientation over the country's territory: N"w-SE. This front, considering the time of the year, is quite intense (at 850 mb, 19°C of difference between Mendoza (32° 50'S, 68° 47'W) and Puerto Lontt (41° 28'S, 72°56'W)).

The central region of the country -see Fig. 1- also is affected by the remainder of a previous cold front (associated with a depression in dissipation over the Bahia Santa Catalina) which adds some baroclinicity to the air masses present there which are the ones that interact for the formation of the storm.

A tongue of warm and very humid air penetrates from Brazil, through Paraguay, Formosa, Chaco, Santiago del Estero and Cordoba, in other words fron the north over the central zone without any jet in the lower layers.

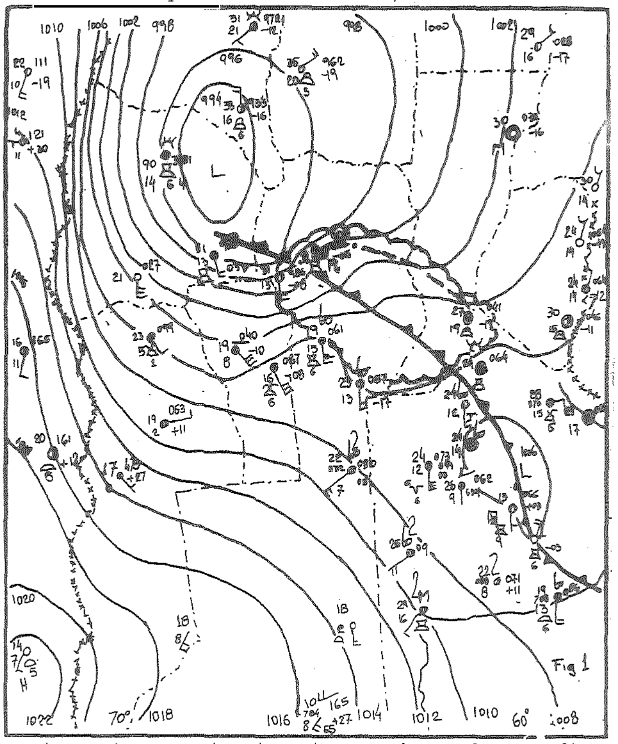

Figure 1. Synoptic situation on the surface at 21 GMT., 6 PM local hour.

4. CONVECTIVE ACTIVITY

Independently, storms break out in Mar del Plata (which are helped by the maritime breeze and later disappear) and in Santa Rosa (36° 44'S, 64° 16'W) at 21 GMT. This last storm expands affecting the north of La Pampa and the south of San Luis at 00 GET. but, in general, the activity continues dispe£sed at 12 Gl".T. on the 17th of November.

4.1. Development and intensification. Causes.

The reintensification of the convective activ_i ty is over the center of Argentina, where the penetration of mass of tropical air (characterized by θ_e 342° Abs. at 12 GMT.) existed. On Cordoba at 9 LH the Showalter index has a marked minimum of -7, the lowest of the country, and the K index is of 44. The increase produced by the entering trough causes the existence of humid air at 700 mb, (Td in Cordoba 7,5°C, in Mendoza 5°C and in Santa Rosa 2°C against the figures for Salta -3°C, Resistencia -11°C and Ezeiza -26°C) showing the way of penetration from the north of the 'tongue of very humid tr£. pical air. The Td of Cordoba, at 700 mb, is the highest of the country.

Also, as a kind of trigger for the vespertine convection, in the zone of Cordoba, the following factors interact:

a) The effect of the Sierras(2500 m a.s.l.) which extends from N to S, 80 km W of the city, whose peaks reflect the convective elements which are conducted towards the oriental plain by the aloft winds.
b) The advance of the cold, front, by then very close, from the south.

Both factors generate a field of convergence particularly intense which finally leads to the formation of a mesocyclone associated with the storm.- (See Fig. 2) •

The convection is helped by the vertical structure of the wind which was weak up to 500 mb but showed a strong shear between 500 and 200 mb.

At 12 QIT a stable layer is observed in the local radiosounding between 800 and 650 mb through which the ·equivalent potential temperature decreased from 342° Abs. to 328° Abs., revealing the mechanism mentioned in the introduction.

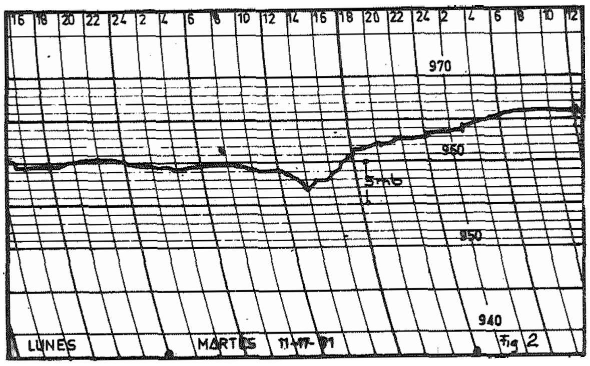

Figure 2. Barogram of the meteorological station of the city of Cordoba (11-17-81), showing the passage of the mesocyclone ..

5. THE CONVECTIVE CELL

Finally a large convective cloud develops, formed, as has already been mentioned, in front of the squall-line and is at its ext_reme left, according to the direction of the shifting. It IJ'at•iredover the .city of Cordoba, causing intense hail.

Its characteristics according to the graphic output of the modified Hirsh model (Ref. 6) is seen in Fig. 3, where it is observed that the updraft reache:,. maximum of 41 m/s, the top of the cloud is 12900 m a.s.l. and the maximum content of water is 5_.35 g/kg at 7300 ·with a temperature of -15. 7°C, in the cloud.

6. HAIL COLLECTED

The sall'ple of stones collected was very large (more than one hundred) and these were analyzed at the Laboratory of Cloud Physics at the Center of Atmospheric Physics of the National Weather Bureau

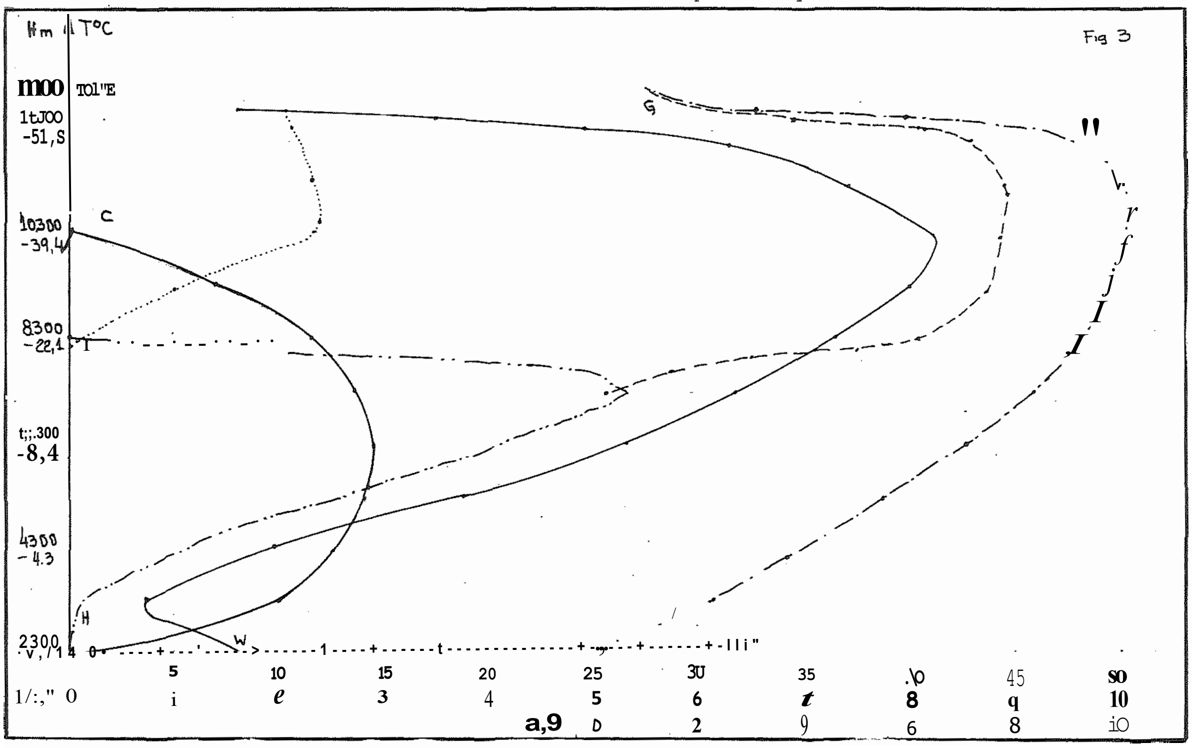

Figure 3. The profiles of the updraft and of the four categories of the water, according to the model of convective cloud used.
- W updraft (m/s) ;-··-H water of hydrometeors (g/kg); - C water of cloud (g/kg);
—··—I ice of cloud (g/kg); -·---9 total of water (g/kg); ----G water of graupel: hail. (g/kg).

Ref. 7.

Its characteristics were:

Shape : almost spherical
Radius : between 1 and 2 cm.
Embryos : 40% of visible frozen dro s
60% of conic polycristalline **structures.**

Very few embryos of frozen drops reach 7 mm. The smallest drops are surrounded by a layer of smaller opaque crystals.

Peripherical layers: reveal condition of humid growth and also generally present a zone of smaller surrounding crystals.

Table I shows the results of the structural analysis of some of the hailstones; it enables the observation, as was anticipated, that all the peripherical layers except one, fYOW in condition of humid growth, for temperature in the cloud between -10° to -24°C, the main requirements of water being 4.48 10-6 glcm³ and with a time of growth varying between 7 and 15 112 min. The maximum updraft calculated was 37 *mis.*

It thus seems possible to estimate, for this convective cloud, the following characteristics:

TABLE I

HAIL	PERIPHERICAL LAYERS	Ts (°C)	Ta (oc)	w(glcm³)	t (min.)	u *(mis)*
X37	Layer surrounding the center	0 (humid growth)	-13	2.93 10-6	10 112	
	Layer of small crystals	0 "	-22	3.53 "	2 113	
				Total	13 min.	
X32	Layer surrounding the center	0 "	-13	3.13 "	6	
	Layer of small crystals	0 "	-23	3.80 "	5	
				Total	**11** min.	
X56	B	0 "	-10	2.96 "	7 115	
	C	-6 (dry)	-20	2.26 "	3 112	
oB)C)D)	D	0 (humid)	-24	3.91 "	3 112	
				Total	14 115	
X39	B	0 "	-.17	4.48 "	3	19.3
	C	0 "	-10	2.05 "	7 114	33.3
oB)C)D)	D	0 "	-24	3.6 "	5 113	37.1
				Total	15 112	

Where X identifies the sample of stones and number
B, C, D. " the layers studied
Ts is the surface temperature calculated for the layer
Ta is the temperature of the cloud where the layer is growing
W is the liquid content in the cloud while the layer was growing
t is the time of growth for each layer and the total of all the layers
u is the velocity the updraft which keeps the stone in suspension

TABLE.I where the characteritics of the peripherical layers of the hailstones collected of the storm of November 17th, 1981 in Cordoba, are stated.

Top : 13000 m
Base : 2360 m
Temperature in the base: 14,2°C (warm base)
Maximum velocity of the updraft: 37 *mis,* as the majority of the hail analized required; 41 *mis* according to the model.
Maximum content of water: at the level of -17°C in the cloud, located at 7300 m according to the model and through the analyses of the stones: 4.48 10-6 glcm³, and according to the calculations of the model 5,4 glkg.

For the hailstorms collected in the north of the Province of Mendo.za, it was established that:

1. The zone of growth of the large hails.torms is situated between -15° and -25°C, between 400 to 350 mb.

2. Independently of embryos, which the majori½y are

conic, it is confinned that the hailstones grow su stantially during the stationary stage of involved cloud's life, and meanwhile relatively high tempera tures are maintained (Ta: -14° to -18°C). Besides-;- the possibility that there be growth in the lirr t of humid growth, that is, Ts = 0°C, is a decisive conditioning factor to achieve times of growth compati tible with the evolution shown by the clouds invol:-ved.

3. The time of growth of the stones in the cloud involved is variable and generally exceeds the 15 min. mark. It is usually between 20 and 25 min.

If these conclusions are compared with the results that are shown in Table I, it can be observed that the hail produced by the stonn being studied, located in another area of the country, shows similar characteristics with one exception: that some of the hail indicate that several of the peripheral layers grow at temperature slightly superior.

8. CONCLUSIONS

1) It has been possible to' study the genesis, dev lopment and culmination of the storm by considering it an ordinary case of the manifestation of the squall-lines over the center of the country.

2) The information obtained permits an understanding, upon a first approximation (with an estimated error of 10% in the figures) to the involved convective cell.

3) The data obtained from the study of the structure of the hail are comparable with the results obtained with the numerical model.

4) When comparing the results o(the studies of the structure of the storm's stones with the results obtained for the hail in Mendoza it is obser ved that, in spite of the large geographical dif-- ferences of both region, the characteristics of the products of .the large convection clouds, are similar.

5) In both regions, the great influence of the oro graphy on the genesis of the convective events can be observed, in spite of the great difference in magnitude between the Andes Cordillera and the Sierras of Cordoba.

Acknowledgements: 'The hail studied was analyzed by the professionals at the Laboratory of Cloud Physics at the Center of Atmospheric Physics of the National Weather Bureau; Technicians at the Climatological Center at the above-mentioned Bureau read the barographical and anemocinemographical registers of the meteorological stations in the region of Cordoba. The computation of the convective model and others were carried out at the San Higuel Space 'center (CNIE). The elaboration of the basic information which supports Ref. 8 was carried out by the professionals on the National Hail Suppression Program (CNIE). The authors thank all of them for their dedication.

9. REFERENCES

1. Lichtenstein, E.R., Schwarzkopf, M.L.A. 1974. Aspectos Estadisticos de la lineas de inestabilidad en la Argentina. Meteorologica. Vol. 1, N° 1. 3-13.

2. Lichtenstein, E.R. ,.Altinger, !LL. 1970. Condiciones meteorol6gicas asociadas a la ocurrencia de lineas de inestabilidad. Meteorol6gica. Vol. 1. N° 2. 79-89.

3. Schwarzkopf, M.L.A., Migliardo, R. 1973. El tornado de San Just , Provincia de Santa Fe, ocurrido el 10 de Enero de 1973. Meteorol6gica. Vol. IV. Nros. 1, 2, 3. 65-87.

4. Bullorini, S.B., Flores, I.V., 1979. Estudio del liesosistema del 13 de Abril de 1972. Meteorol6gica. Vol. X. N° 2. 43-53.

5. Benzaquen, R. 1974. Analisic de una lfnea de inestabilidad con la ayuda de imagenes proporcionada par satelites meteorol6gicos. Meteorol6gica. Vol. V. Nros. 1, 2 y 3. 5-31.

6. Ghidella, M.H., Saluzzi, M.E. 1979. 'Estudio de **un modelo numerico de nube convectiva. Geoacta.** Vol. 10. N° 1. 111-122.

7. Lubart, L., Saluzzi, M.E.; Nuii.ez, J.M. y Levi, L. 1979. Estudio comparado de la estructura de granizos. Geoacta. Vol. 10. N° 1. 41-50.

8. Saluzzi, M.E. 1983. Aspectos de la convecci6n severa en !1endoza. Departamento de 11eteorologfa. F.C.E.yµ. UBA. Tesis.

RESULTS OF HAILPAD MEASUREMENTS IN HUNGARY IURING 1978-83

Szekely cs. and Zoltan Cs.

Applied Cloud];'hysics Center, Meteorological Service of the Hmgarian People's Republic., 7601 P,ecs, Pf. 353, Hmgary

1. INTIDDUCTION

The hailpad is the rrost wide-spread instrurrent for neasurements of the hailfalls at the gromd surface. It is suitable to measure the number and sizes of hailstones falling onto its surface. Relatively large and dense networks can be produced using hailpads.

The present study aimed to outline the results of the hailpad measuranents in Hmgary and several prccedures of the hailpad data ")?reparations. The data of three different. networks /TABIF. l, Fig.l. / are presented and used for the analysis.

First we give the climatological description of m2asurements with networks 1. and 2. Naturally, the, data of netiwork 1. can not be o::insidered that or full value fran the point of view of-climatological description because of hail suppression. Afte it we deal with the problem of the deteDllin.ation of the true number of haildays and hailstreaks in cai;;e of ccmronlydense networks. A procedure is given to est.il!ate these true numbers. At the end two rreasurerrents of micronetwork 3. is shown. Studies of small scale variability of hailfalls are presented by the help of these rreasuranents.

Table 1

Characteristics of the hailpad networks in Hmgary

liailpad network	Area.size km2	Density pad/kIP.2	Period	Hail suppression	Size of a hailpad m^2
South-Baranya 1.	1780	0.16	1978-81	Yes	0.04
Bacs-Kiskm 2.	1260	0,11	1983	No	0.09
Hicmnetwork 3.	0,04	2025	1980	No	0.04

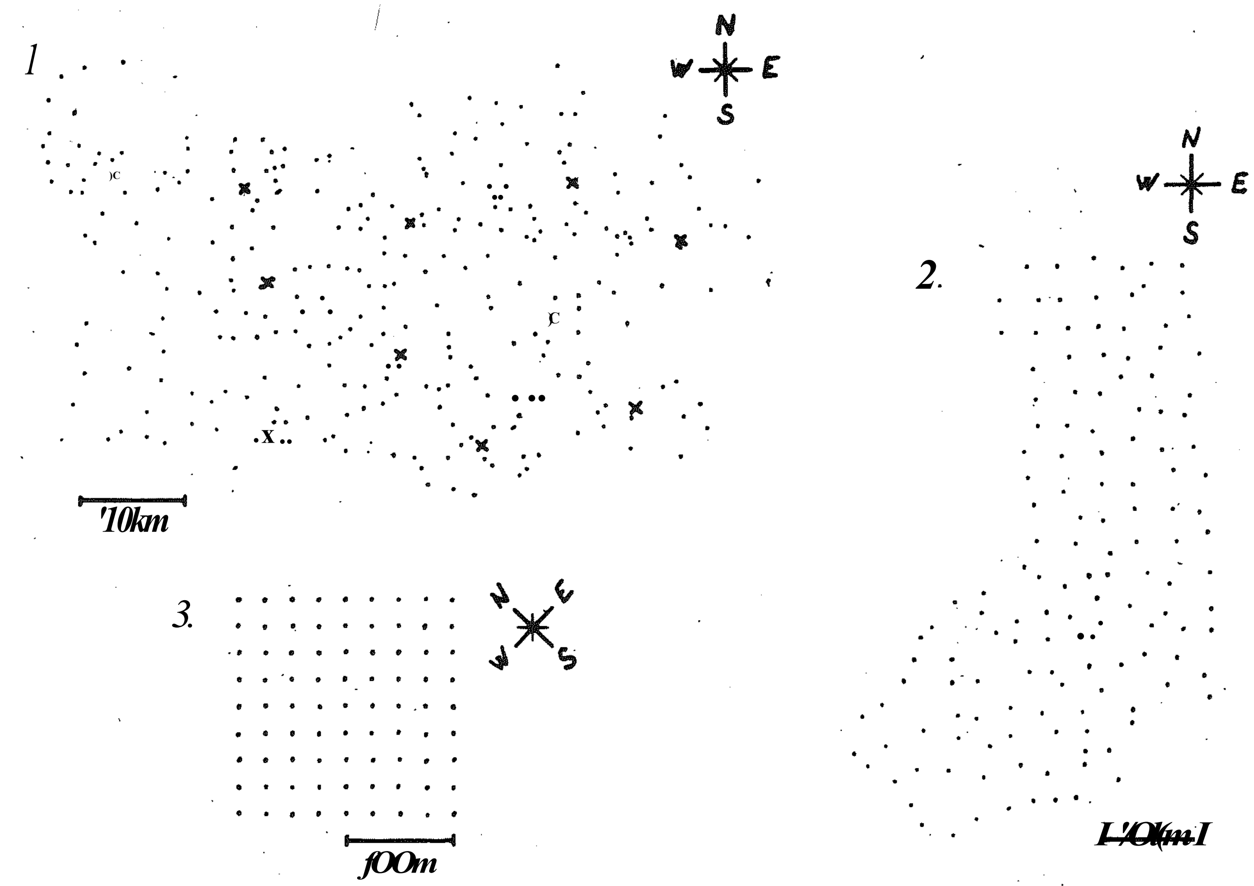

t'igure 1. Hailpad networks described in Table 1. Points mark hailpads and crosses mark lamching sites.

2 . CLIMATOLOGICAL DESCRIPI'ION

In period 1978-81 network 1. detected 63 hail-days. The rronthly distribution of these days can be seen in Fig. 2.1.

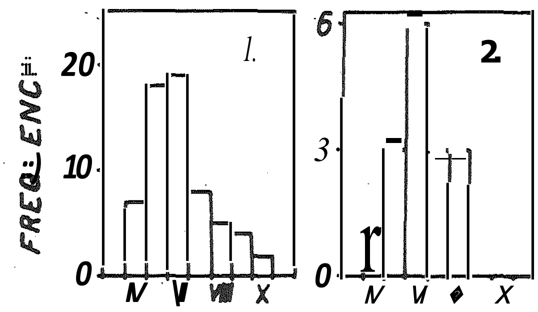

Figure 2. M::lnthly distribution of haildays detect-ed in peri-odS 1978 81'and 1983 on the te=itories of networks 1. and 2;, resl7ctively.

In case of finer division by ten days the peak of Hay-June na=ows to the end of Ilay and to the begin-ing of June. The hailfalls in lay and June are very varying. The detected rraximum hailstone diarreter fluctuates between 5 and.32,5rrm while in the early hailfalls /April/ it is between 5 and 15rrm and in hailfalls after June it is between 7,5 and 17,5rrm /Fig. 3/.

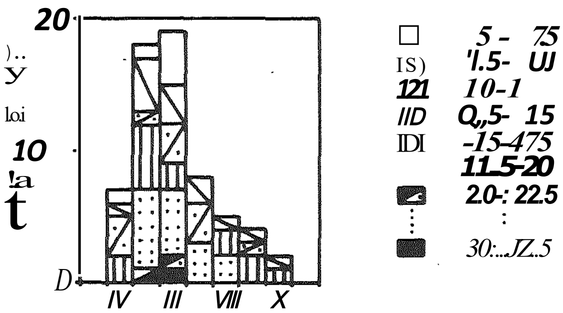

Figure 3. 1''.bnthly distribution of the maximum hailstone size freqUertcy on the territory of net-work 1. in period 1978-81.

Network 2. operated since April l to October 31 in 1983. In this period 15 haildays were detected. The m:mthly frequency of these haildays is shown in Fig-2. The maximum of June can be observed even in case of such little data set. The maximum hailstone dia-rreters can be found in Table 2.

The maximum hailfall frequency at the end of 1'lay and in J·une supposedly due to the following: this is the very tine interval when the wanning of the lower layers of the air does not effectively melt the hailstones and at this time the warming of the higher layers of the air is stil: late and the instaJ;>ility arising this way encourages the hail-stcrms in maturation.

The size distribution of hailstones detected by a hailpad presents capricious variability but the annual and rrulti - annual distributicns can be regarded exponential /Fef. 1, Fig. 4/.

The rrean annual point frequencies on te=ito-ries of network 1. and 2. were 0.35 and 0.85, re-spectively. The frequencies of point frequencies are presented in Fig. 5. The greater the point frequency the less its probability. This decrease is approximately exponential.

Table 2

The maximum hailstone size detected and the number of exposed hailpads di.rring a day on the bases of data of network 2. in 1983.

Date	No. <?f exp::,sed pacl	Max. diarreter mm
30 April	1	7.5-10.0
24 tlay	1	7.5-10.0
25 tlay	1	5.0- 7.5
26 !lay	11	7.5-10.0
6 June	3	10.0-12.5
13 June	2	7.5-10.0
14 June	3	5.0- 7.5
22 June	2	7.5-10.0
27 June	4	17.5-20.0
29 June	1	7.5-10.0
8 July	1	7.5-10.0
11 July	1	5.0- 7.5
24 July	80	75.0-80.0
3 August	2	7.5-10.0
19 August	8	12.5-15.0

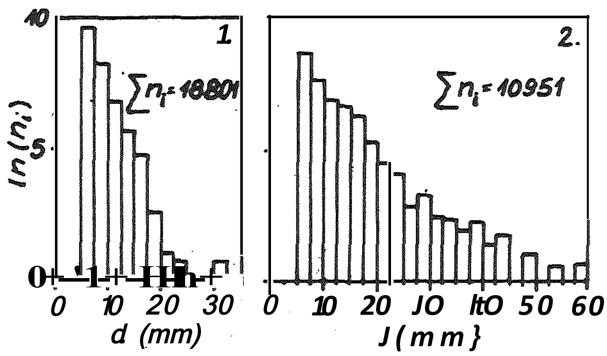

Figure 4. Multi-annual hailstone size distribution measured by network 1. in J:E!riod 1978-1981 and annu-al hailstcne size distributicn measured by network 2. in 1983.

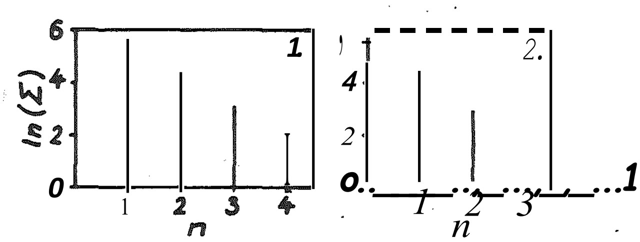

Figure 5. I.Ogarithrn of the number f hailpads Z: e;xposed n tirres in the whole rreasuring period.

3. A PROCEDURE TO ESTIMATE THE TRUE NUMBER OF HAILSTREAKS AND HAILDAYS

The density of hailpad networJc should be cho-sen unreasonably great if we wanted to detect each hailstreak on a large area /Fef. 2/. It is generally irrpossible mostly because of e=1ornical reascns. The true number of haildays and hailstreaks hi;i.sto be estimated because these values are very irrpor-tant climatological characteristics of a territcry and a period. L'l the following we give an estimaticn which can l::e applied in case of corrrronly dense hailpad networks. As a parergon we get also an estimation for the.expected area of hailstreaks.

Let N and F be measured number of haildays and hailstreaks, respectively, and let S denote the density of hailpad network. The empirical $N - S$ and $F - S$ relations can be determined by randanly reducing the number of hailpads. 1n the nature N(S)' an6 $F(S)$ are rronotonic increasing saturation functions an6 their upper limits are the true number of haildays and hailstreaks, respectively, if the mrnber of hailpads great enough and the network is uniformly dense. Also theoretical approximation can be 9iven for N(S) and F(S)/Fef. 3/.

Let us suppose that the probability of detecting a hailstreak having•an area A is

$$P = \begin{cases} 1 & \text{if } A \geq 1/S \\ AS & \text{if } A < 1/S \end{cases} \qquad /1/$$

If the distribution of .hailstreak area, the network density .S and the true number of hailstreaks F_0 were known, the' expected number of the detected hailstreaks(F) =u1d be estimated as follows

$$\langle F \rangle = F_0 \left(\int_0^{1/S} AS\, f(A)\, dA + \int_{1/S}^{\infty} f(A)\, dA \right) \qquad /2/$$

where .f(A) is -the density function of the above uistribution. After Ref. 1 f(A) can be taken as an exponential density function

$$f(A) = \frac{1}{\bar{A}} \exp\left(-\frac{A}{\bar{A}}\right) \qquad /3/$$

where A is. the cted area of the hailstreaks. Supposing that $\langle F \rangle = F(S)$ and substituting Eq. 3 into Eq. 2 F(S) becares:

$$F(S) = F_0 \bar{A} S \left(1 - \exp\left(-\frac{1}{\bar{A}S}\right)\right) \qquad /4/$$

The way to determine the function N(S) is the sarre

$$N(S) = N_0 \bar{B} S \left(1 - \exp\left(-\frac{1}{\bar{B}S}\right)\right) \qquad /5/$$

where N_0 is the true number of haildays and $\bar{B}$ denotes the expected area exposed by the hailfall during a day.

The empirical N-S and F-S functions were determined three times in each year for both hailpad networks. The different network densities were prodqced by randomly reducing the number of hailpads using a radom number generator providing uniformly distributed random numbers. The functions

Table 3

Summarised results of the estimation for the number of haildays and hailstreaks. N and F are the numbers of haildays and hailstreaks measured by network 1. or 2. N_0 and F_0 are the estimated true values. $\bar{A}$ and $\bar{B}$ denote the expected area of hailstreaks and the expected area exposed by hail on a day, respectively.

Network and year	N	N_0	$\bar{B}$	F	F_0	$\bar{A}$
1. 1978	20	23	27	52	72	9
1. 1979	11	15	8	19	29	6
1. 1980	19	20	48	88	110	11
1. 1981	13	17	10	34	48	7
2. 1983	15	21	13	24	35	10

N(S) and F(.S) were fitted to these points by the least-squares-method. An example is shown in Fig. 6. The results is summarised in Table 3. On the evidence of the data in Table 3 we conclude that the densities of our networks generally are not enough to measure the true number of haildays:

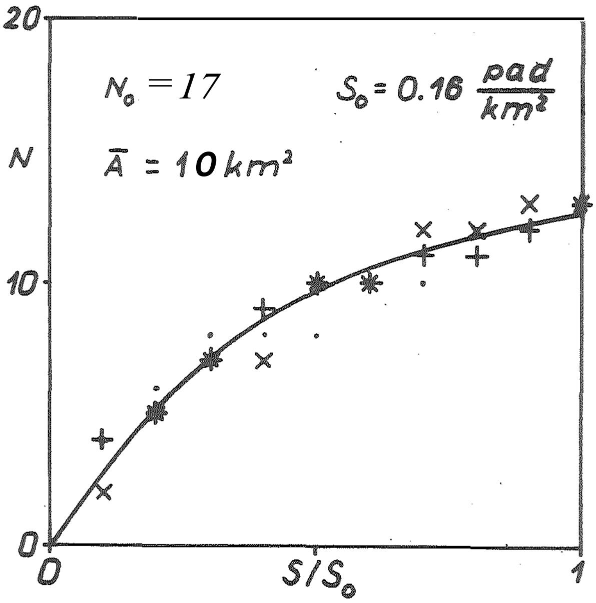

Figure 6. The number of haildays vs. the network density in 1979 on the bases of data network 1. Points, pluses and crosses mark the empirical N values using three different random number generator. The curve is the fitted theoretical function N(S).

4. SMALL SCALE VARIABILITY OF HAILFALLS

The micronetwork shown in the introduction operated in 1980. Two hailfalls were detected in this period /Fig. 7/. The possibility of the occurrence of small scale variability /Ref. 4, Ref. 5/ was studied in the mentioned two cases.

The next question was examined: does the expected number of hailstone concentration depend on place or not? In case of dependence, what is its magnitude?

Let $\lambda(x,y)$ be the hypothesis for the expected value of the hailstone concentration at point (x_i, y_i). If the distribution of the measured values is known at the measuring points, statistical test can be done to see whether $\lambda(x,y)$ contradicts the concrete measured values or not. It is well known from the literature that hailstone concentration follows Poisson distribution, provided that its expected value is great enough /Ref. 6/. Fortunately the only parameter of Poisson distribution is just the expected value.

This way we can perform the following test: let us divide the range of measurable values into three parts so that the measured values fall into intervals I_1, I_2, I_3 with probabilities P_1, P_2, P_3, $P_1+P_2+P_3=1$. The probability of falling N out of the N_0 measured values into the outer intervals I_1, I_3 is:

$$P_{N_0}(N) = \binom{N_0}{N} (P_1 + P_3)^N (1 - P_1 - P_3)^{N_0 - N} \qquad /6/$$

If N falls into $I_1 + I_3$ the probability of falling

21	19	14	15	9	8	4	3	6
6	5	9	6	12	9	7	8	11
3	9	16	7	7	9	7	9	18
8	7	12	16	12	12	9	13	13
7	5	7	9	11	3	5	15	9
7	7	9	8	14	18	14	11	17
7	8	6	9	10	12	3	11	6
10	8	7	16	12	4	8	13	0
17	10	2	6	11	11	16	13	14

a.

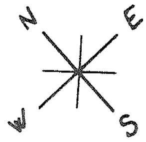

× 1

5	5	5	5	4	3	4	€	4
3	6	2	4	4	5		5	1
9	5	4	7	9	3	4	9	7
4	4	4	4	5	4	3	5	1
3	4	6	4	7	6	1	5	4
3	2	7	0	4	5	10	3	6
8	6	7	1	4	6	2	4	13
8	7	3	12	5	6	6	6	14
0	7	3	3	5	7	3	3	0

b.

li'igure 7. 'l.wo measurements made by raicronetwork 3. in 1980. 'l'he origin of the(.:(,) 12lane is in the tof'. left hand corner of the network. 'T'.henumbers are given in units of number of stones/12ad.

N' into I_1 is:

$$P_N(N') = \binom{N}{N'}\left(\frac{P_1}{P_1+P_3}\right)^{N'}\left(1-\frac{P_1}{P_1+P_3}\right)^{N-N'} \qquad /7/$$

Whereas the two events are independent, the probability of their simultaneous occurrence is:

$$P(N,N') = P_{N_0}(N)\,P_N(N') \qquad /8/$$

Knowing the values of N_0, P, , 7l, 1 one can c:cn-:st:ru.ct the confidence region of GI. percent from the 9reatest values of P(N,Pl)in (N,N')plane.

If the rreas point falls into this c:cnfiderice region the expression for iir::-.)is accepted to hold at a significance level of Q percent. If the poinj: falls out the confidence region we reject the hypothesis.

Haturally the test would be the same if the number. of measured values falling into the middle and to one of the side intervals were examined.

The test des=ibed was performed in case of JI„ =81, Q =90%, 1, =0.25, =0.5, 1s=0.25. The c:cnfrdence region can be seen in Fig. 8.

First we tried the place free case ii{l',ff}= C , using both measurerrents shown in Fig. 7. For the neasurerrent a. the interval 10.45 C 10.80 stone/pad was acceptable. For the rreasurerrent b. the interval S.15 S C 5.95 stone/pad was acceptable. In case of rreasurerrent a. we also examined which (1,8,() points could be acceptable, supposingh{X, J=AXt8 tC. ,.The variability can be des=ibed by the vector (A, B)! / ,;,....dii{(,f/))f. The length and the direction of the, accepted vector (A, BJ changes between 0.00 - 1.58 1/m^3 and 9o^0 - 233 , respectively.

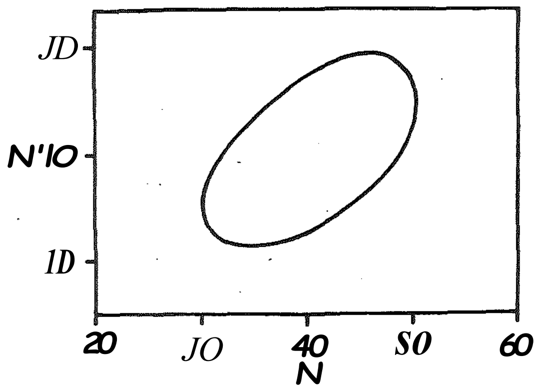

Figure 8. The 90% c:cnfidence range of c:cn-st:ru.cted fran the greatest values /see text fer details/.

5. REFERENCES

1. Federer B and v!aldvogel A 1975, Hail and Raindrop Size Distributions from a Swiss Multicell Storm, J Appl l'.leteor. 14,91-97.
2. Chagnon s A 1970, Hailstreaks, J Atm. Sci. 27,109-125.
3. Szekely Cs and Zoltan Cs 1984, A jegesoindikator es felhasznalasanak lehetosegei, Idojaras. 88, 32-45.
4. Gertzman H S and Atlas D 1977, Sampling errors in the rreasurernent of rain and hail parerneters, J Geophys Res. 82,4955-4966.
5. Joss J and Waldvogel A 1961, Raindrop size distribution and sampling size e=rs, J Atm Sci. 26, 566-569.
6. Szekely Cs and Zoltan Cs 1982, E=rs in hailpad measurerrents, Conference-vli:Jrkshop on hailstonns and hail prevention, Sofia.

RADAR ECHO AND AIRFLOW STRUCTURE OF THUNDERSTORi\\S IN XINJIANG

Ang Sheng Wang

Institute of Atmospheric Physics, Acadsmia Sinica
Beijing, The People's Republic of China

Wen Q,uan Shi   Jia Mo Fu

Meteorological Inrtitute of Xinjiang
Wulumuqui of Xinjiang, The People's Republic of China

ABSTRI\.CT

A new probing technique which can probe vertical two-dimensions radar profile and vertical airflow etc, data at same time by use of two radara was used in Xinjiang, and a great number of useful data was got, According to those data, the relations between updraft and overhang echo, airflow shear and gust front, and downdraft and divergence on the lower layer etc. had been studied in China. Some colour photographes of hailstone micro-structure were given in this paper, The form of hailstone was relative closely with the airflow of hailcloud.

[eywords: Thunderstorm, Hailcloud, Airflow, Radar echo-, Hailstone, Divergence.

1. INTRODUCTION

During recent 20 years, many scientists •studied thunderstorm and their structure, because of thunderstorms are an important damaging weather in the world. For example, K. A. Browing and F. H. Ludla.lll (1962, Ref, 1), G, K. Sula.kvelidz et. al (1965, Ref, 2), Ang Sheng Wang (1972, Ref J, D. Marwitz (1972, Ref, 4), J, Musil et. al (1973, Ref. 5), R.-H. Bushnell (1973, Re'f':"'67'and R. M. Lhermitte (1975, Ref. 7) et, al, already used diffe ent methods to probe storm and get a great number of useful results. Hovever, thunderstorms are a very complex phenomenon, many basic laws will be waited to discover,

A new probing technique which can measure vertical airflov, vertical two- dimensions radar profile etc, data had been used in Xinjiang of China (Ang Sheng **Wang**, 1982, Ref, 8; **Ang Sheng** Wang, Jia Mo Fu, Wen Qua. Shi e al, 1963, **Ref**, 9), Now, ve vill use those data to study the relations **batveen** updraft and overhang echo, airflov shear and gust front, and downdraft a.cd divergence,

2, THE UPDRAFT AND OVERHANG ECHO

Although the fact of thunderstorm. in which the updraft supports an overhang echo had been infered, then the datum which can proves above fact is a few, for example, D, J, Marwitz'e work (1972, Ref. 4). If we can get useful data a. d to prove **it**, we **think** that is very interesting, From 1976 to 1982, we used above method to got a lot of data, Sfd proved above phenomenon

One of above probing data has been given in Fig,1, This is a tY1Jie&l datum which has been got on August 6, 1977 in Xinjiang, According to horizontal airflow and vertical airflow (updraft, please see Fig, 2, left), we can find **that** th re is a updraft in Fig,1 right, **it** is stronger; the updraft comes in hailcloud from the,right side of the Fig, near the ground; and leaves out the hailcloud in higher altitude, From Fig, 1 and Fig, 2, it is very clear that the updraft supports the overhang radar echo, Due to the support of updraft, we can find that a stronger radar echo (**stronger** than 40dbz) are hanged in the median **height)**, we call the hanging stronger radar echo to **overhang** echo, Usually according to overhang echo, a stronger updr-dt will be decided,

It is well know, bigger raindrop or hailstone nas been supported in updraft of thunderstorm, and

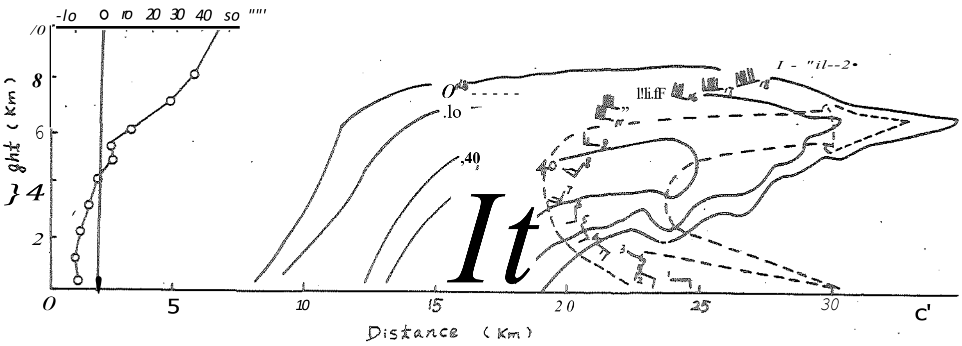

Fig, 1 Probing result of radar echo and airflow of hailcloud on August 6, 1977,
Left: The wind along moving direction of hailcloud.
Right: The airflow and echo on X--z plane•.

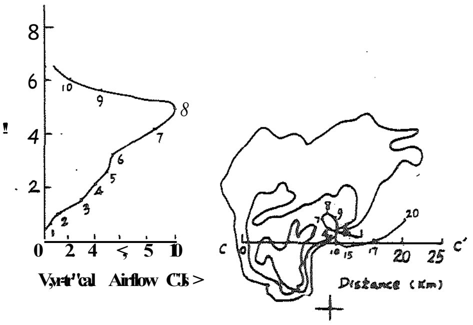

Fig. 2 The updraft profile (left), and ra.da.r echo (PPI, s0), and balloon trajectory (right) on August 6,. 1977 in Xinjiang.

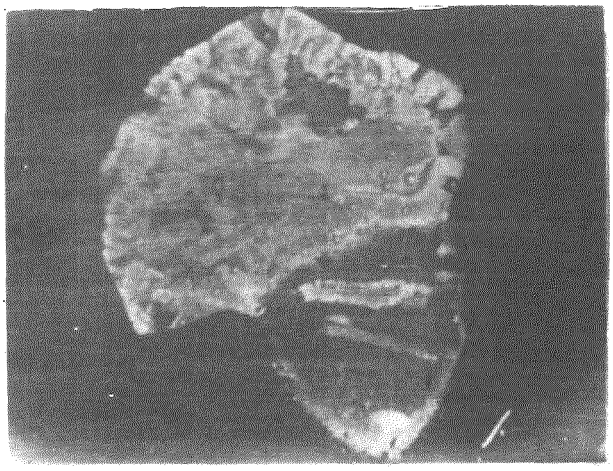

.Fig. 3. A photo of hailstone section qnder polarized light on July 16, 1982, in Xinjiang.

they grow rapidly in here, We already got a great number of hailstones in Xinjiang (Ang Sheng Wang and Wen Quan Shi, 1982, Ref, 10), In Fig, 3, we show a colour photograph of hailstone section under polarized light on July 16, 1982 in Xinjiang, The form of this hailstone is like mushroom or cone shape, Its length is about 8,1 mm, and its width is 7.2 mm. It is very clear tl:_Ja.t the top of hailstone is a freezing drop which consists of several bigger ices. According to Fig,3, we can believe that the embryo of this hailstone was a freezing drop; and when it fell in updraft, it grew and a cone hailstone formed in hailcloud,But, at same time, it had been influenced by side-blown updraft, so left side of hailstone grew faster than right side.

Now, we already got one thousand hailstones in Xinjiang, and cut them to get sections, shot their photographs under polarized and transmission light, From above data, we got some results, i.e. 51 % embryoes of hailstones belong to freezing drop; then the.positions of about 76 % freezing drops are in the top of cone. In Xinjiang, we fo︀UI?-d that th form of 59 % hailstones is the cone hail. So we think that the characteristic of hailstone growth is the growth along vertical direction. This phenomenon is relative closely with vertical airflow of hailcloud in Xinjiang•.

Two ra.da.r echo profiles and their enviromental horizontal winds along the profile has been shown in Fig. 4. They - r e got on July 28, 1980 (left) and August 23,1977 (right) in weste= Xinjiang. From Fig, 1 and Fig. 3, we can see three hailclouds have like-structure of radar echo and airflov, That means the updraft supports overhang echo.

3, THE GUST FRONT AND AIRFLOW SHEAR

In the lower altitude between updraft and downdraft, there is an important region in where strong wind usually happen near the ground and damage the buildings and crops. The research work of above region is very useful, In Xinjiang, we already got some data.

In Fig. 5, we got three cas,as about the gust front and airflow shear. Three cases of thunderstorm on August 28, 1980; July 15, 1980 and August 23, 19 77 has been shown in Fig. 5 left, medile and right respectively, They are very observable, w en balloon rises from the ground, the direction of wind changes rapidly between 1,4 - 3 km height, For example, in Fig, 5 left, when the thunderstorm moved into the observational station, the balloon left the ground, in that time, we measured west-north wind. Then, when the balloon rose to about 1,4 km height, the direction changed to east. In fact, we measured west-north wind in the iower layer which was outflow; and the east wind between 1,4 and 3 km height was inflow. There are a airflow shear in near 1 km height.

If we drew the horizontal projects of alti-wind in near the inflow region of thundercloud, we can find that the project of wind is rotation along the

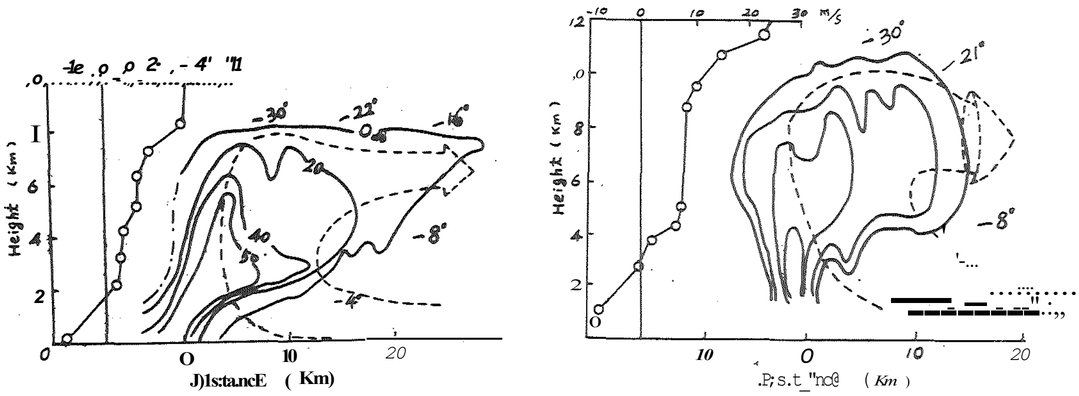

Fig. 4 The radar echo profiles and their enviromental horizontal winds along the profile.
Left: July 28, 1980. Right: August 23, 1977,

clock direction, as like as Fig. 6. In Fig. 6, we gave four cases, they are (1) at 18:40, on August 23, 1977; (2) at 17:00, on August 28, 1980; (3) at 18:43, on August 13, 1980; and (4) at 17:50, on July 15, 3980; in Xinjiang. In Fig. 6, the Arab number shows the time (minutes) of balloon leaving the ground. From Fig. 6, we can see clearly that when the balloon rises gradually from lower layer to high height in weak radar echo region, its movement is rotation along the clock direction.

According to above data, a model of gust front and airflow shear in thunderstorm has been given in Fig. 7. From this figure, we can see that if the balloon leaves the ground in second region (please see Fig. 7 near the ground) which is between updraft and downdraft, we will get the shear airflow as same as Fig. 5, and the movement of balloon will be rotation as same as Fig. 6.

4. THE W\o/NllRAFT AND DIVERGENCE

Although the measurement of downdraft in thunderstorm is a difficult thing, our system is a good method for measuring it, and got a lot of data (Ang Sheng Wang 1972, Ref. 3; 1982, Ref. 8; and Ang Sheng Wang, Jia Mo Fu and Wen Quan Shi et. al, 1983, Ref. 9). Now, we are interested for downdraft and divergence only.

In our system, we can use 3 cm and 5 cm radar to probe cloud hydrometeor field, and use radar wind system to measure airflow, and use a special anemometer to probe updraft (Ang Sheng Wang, Jia Mo Fu and Wen Quan Shi • 1983, Ref. 9) etc. data. As an example, a downdraft and its divergence near the ground has been shown in Fig. 8. That is severe th1,¥derstorm on August 23, 1977 in Xinjiang. The thunderstorm fell hailstones on the ground. In that day, we already measured downdraft, radar echo, divergence and enviromental conditions etc. So we can draw a synthetical structure of this thunderstorm as showing in Fig. 8. In Fig. 9, we give a data o'f downdraft on the day which had been got by use of relative vertical anemometex. From Fig. 9, we see that the balloon passed through downdraft below 1.5 km in thunderstorm. The ma.ti.mum velocity of downdraft was about 9 m/s at about 1 km height.

In Fig. 8, the structure of radar echo, downdraft and divergence etc. of thunderstorm on August 23, 1977 in Xinjiang tell us-that, the strong downdraft appears in the strongest radar echo region. Because of there are strong downdraft and heavy rain in lower height of stronger radar echo region, so strong divergence happen in na.er.the ground region according to continuity law, We can find thc.t the center of divergence is near the project point of the strongest downdraft as showing in Fig. 8. Of course, we have many cases which are like above case, they show the dynamic divergence of thundercloud is relation closely with heavy rain and strong downdraft, and it damdges crops and buildings at same time by the strongest wind near the gust front.

In a few word, we already used our new probing system to sound a lot of tlmnderstorms. In this pa.per, we introduce several phenomena. of severe storms, they are the relatiollS between updraft and-overhang echo, airflow shear and gust front, and downdraft and divergence etc. We think those data are useful for understanding the thunderstorm.

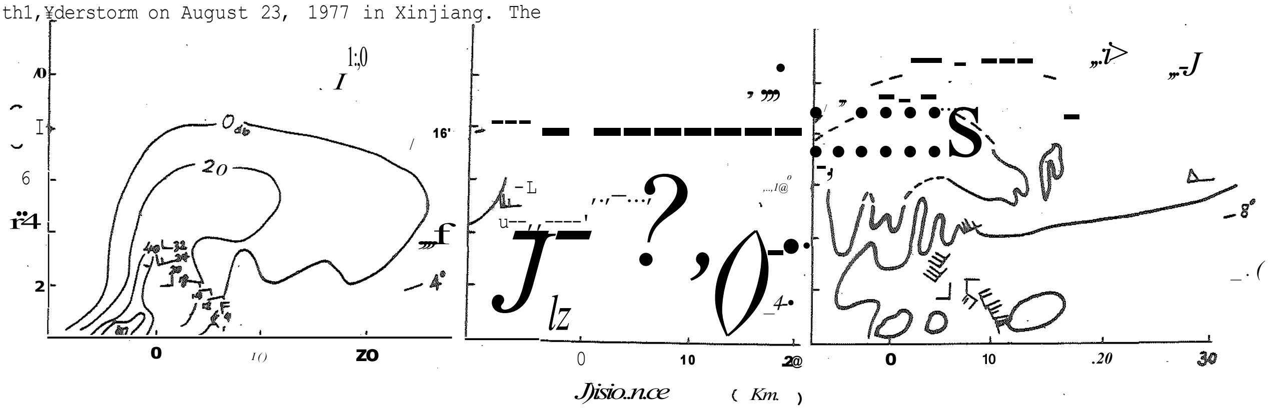

Fig. 5 The gust front and airflow shear in the thunderstorm.
Left: August 28, 1980; Medile: July 15, 1980; and Right: August 23, 1977 in Xinjiang.

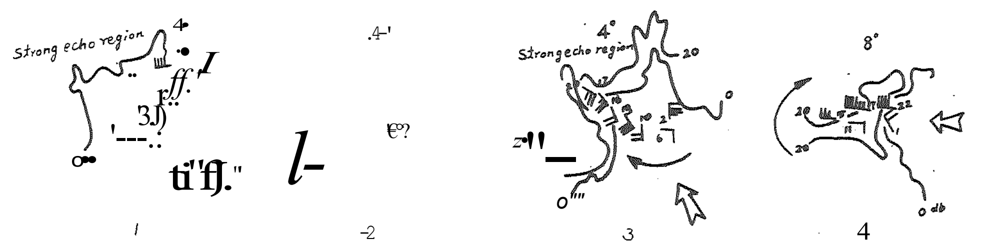

Fig. 6 The horizontal projects of alti - wind in near inflow region of thunderstorms:
1, at 18:40, on August 2}, 1977; 2. at 17:00, on August 28, 980;
3. at 18:43, on August 13, 1980; 4. at 17:50, on July 15, 1980,

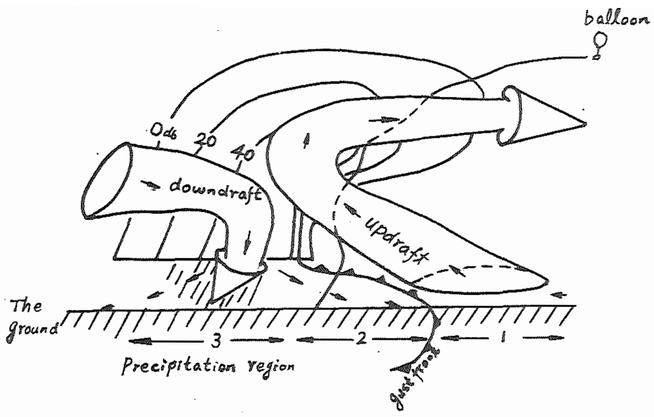

Fig. 7 ·The model of gust front and airfloi, shear.

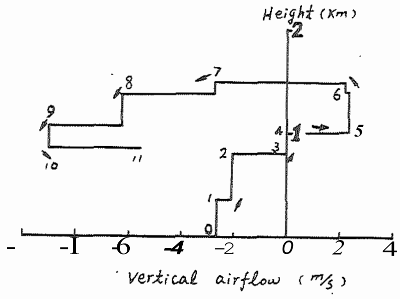

Fig. 9 The downdraft plotted as a function of the height.

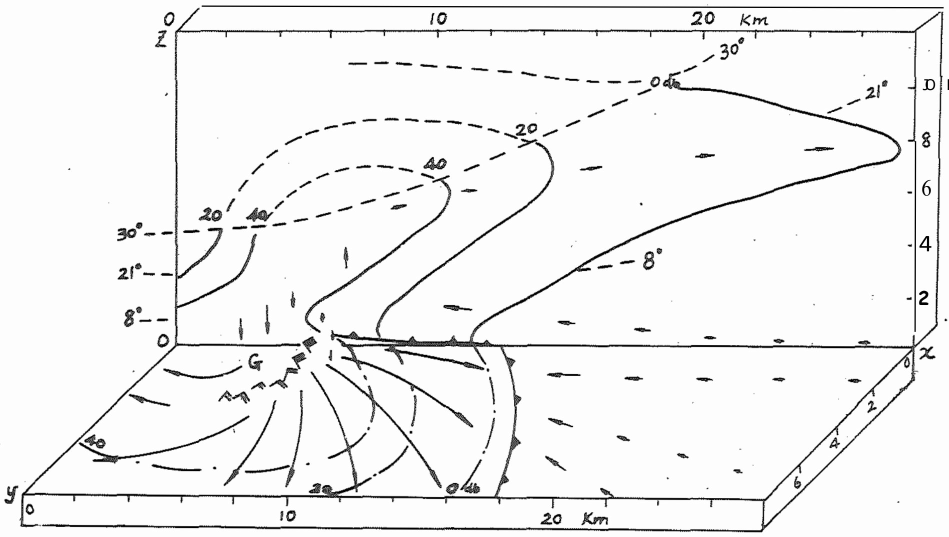

Fig. 8 The structure of radar echo, deldndraft .and divergence etc. data of thunderstonn on August 23, 1977 in Xinjia.ng.

5. REFERENCES

1. Browning, K. A. and F. H. Ludlam, 1962: Airflow in convective stonns. Quart. J. Rog. Meteor. Soc., . 117-'135.

2, Sula.kvelidz, G. K., X. S. Bibilashiveli and V. F. Lappjenva, 1965: The fomation of precipitation and modification of hail process. u.s.s.R. Hyd.rometeoroJ;ogical Press. Leninhrad. 262.

3. Wang Ang iheng, 1972: Probe of updraft in thunderstol.'111, Papers presented at the National Conf, on Hain Enhancement and Hail Suppression. No. 2, 169-179, Changsha of China.

4. rwitz, J, D., 1972: The structure and motion of severe hailstom. J, Appl. Met., 11, 166-201,

5. Musil, J., W.R. Sand and R, A. Schlcusener, 1973: Analysis of data from T-28 aircraft penetrations of a Colorado hailstom, J. Appl. Met,, 12, 1364-1370.

6. Bushnell, R. H., 1973: Vertical winds in thunderstoms measured by dropsondes. 8th Conf. on Severe Local Stems. AMS. 10-13,

7. Lhermitte, R. M., 1975: Real time velocity observations by multi-doppler radar. 16th Conf. on Radar Meteorology, AMS. 107-114,

8. Wang Ang Sheng, 1982: Vertical airflow sounding of severe convective cloud. Conf, on Cloud Physics. AMS. Nov. 15-18, 1982. Chicago, Ill. 543-546,

9. ______, Fu Jia Mo and Shi Wen Quan et, al, 1983: Cloud and vertical airflow sounding by use of two radars. 21st Conf. on Radar Meteorology, AMS. Sept. 19-23, 1983, Edmonton, Alta, canada.

10. and Shi Wen Quan, 1982: Analysis and re- of hailstone micro-structure, Conf,on Cloud Physics. AMS, Nov. 15-18, 1982. Chicago, Ill. 450-452,

SESSION III

MESO- AND MACROSTRUCTURE OF CLOUDS AND CLOUD SYSTEMS

Subsession 111-2

Other forms of clouds and cloud systems

MESOSCALE STRUCTURE OF ATMOSPHERIC FRONTS AND ASSOCIATED CLOUD AND PRECIPITATION SYSTEMS OVER THE EUROPEAN USSR

I.E. Belyakov, N.A. Bezrukova, S.N. Burkovskaya, A.A. Postnov, V. I. Silayeva , T. V. Trutko and V.M. Vostrenkov

Central Aerological Observatory, Moscow Region, USSR

1. INTRODUCTION

It is now generally accepted that frontal Ns-As cloud and precipitation systems are inhomogeneous on a wide range of scales (from several to hundreds of kilometers). In particular, bands of relatively heavy precipitation (so-called rainbands) have been observed both in warm and cold frontal regions (Refs. 1-3). Rainbands are approximately parallel to the frontal line and typically 50-100 km-wide, distance between their axes being 200-300 km. There is some evidence that formation of rainbands is caused by horizontal inhomogeneity of widespread uplifting, which, in its turn, has something to do with features in temperature field (Refs. 4-7).

The aim of this paper is to present some results of aircraft investigation of mesoscale structure of temperature and air motion (both horizontal and vertical) fields in warm frontal regions of the European USSR and their effect on cloud precipitation systems, A typical size of mesoscale structure elements is roughly equal to typical width of rainbands.

2. DESCRIPTION OF DATA AND METHODS OF ANALYSIS

The bulk of data came from the measurements of temperature, wind (both direction and vel'ocity), cloud water (both liquid and ice) content and radar reflectivity of clouds and precipitation, which were performed by the use of an instrumented IL-18D aircraft.

The measurements and observations were made as aircraft flew along horizontal runs. The runs were 300-700 km long, roughly normal to frontal line and lay one over another, 1-1*5 km apart. The number of runs, flown by the aircraft in each frontal region varied from 3 to 5 (Ref. 5).

Widespread vertical motion velocity was calculated by isentropic method based on the fact that if air motion field is stationary and processes are adiabatic, isotherms of pseudo-potentional temperature coincide with streamlines (Ref. 4) .

The aircraft data on 15 warm frontal regions were analysed. The fronts were observed mainly in autumn and spring in various parts of the European USSR and were linked to cyclones, which were at various stages of development. No deep convection was present in frontal regions.

Besides, mesoscale structure of 183 frontal' cloud systems in summer (19 of warm, 77 of cold fronts and 87 of occlusions) and 103 frontal cloud systems in winter (20 of warm, 33 of cold, 50 of occlusions) was studied by the use of satellite IR--pictures (Ref. 8) . Structure of precipitation field in 6 warm frontal regions. was also analysed using pluviographic network.

3. MESOSCALE THERMAL AND DYNAMICAL STRUCTURE OF WARM FRONTAL REGIONS

Temperature and air motion fields in warm air over the front were inhomogeneous. Horizontal changes of temperature were concentrated in narrow zones with relatively large baroclinicity, so called hyperbaroclinic zones (HBZ). On vertical cross-sections, HBZ looked like layers, tilted to Earth's surface, with relatively warm air above HBZ, and relatively cold beneath it (Fig. 1). Earlier the existence of HBZ had been noticed in occlusions (Ref. 7).

In a warm frontal region there were at least three HBZ, the horizontal distance between their axes was 200 km and vertical distance was 2 km.

At levels 1-2 km HBZ were almost parallel to the front, while at higher levels the angle of HBZ tilting was somewhat more than that of the front.

Average width of HBZ was 80 km, while relatively homogeneous portions of warm air mass between them were about 1.5 times wider. Horizontal gradient of temperature within HBZ did not differ much from that within the front. Average values of $\partial T/\partial x$ and their confidence intervals were $+(1.7 \pm 0.4) \cdot 10^{-5}$ °cm-1 in HBZ and (0.1 - 0.2) 10^{-5} °cm-1 between HBZ.

In HBZ wind component, normal to frontal line (U) is subjected to one-dimensional convergence ($\partial u/\partial x < 0$) while between HBZ little spatial changes of U occurred. As a result average values of $\partial u/\partial x$ and their confidence intervals were (-5 ± 1) 10^{-5}s-1 in HBZ and (1 ± 1) 10^{-5} s-1 between them.

Vertical motion field was also effected by HBZ. This is evident from configuration of streamlines (Fig. 1). Ai parcels are subjected to strong convergence while crossing HBZ and moved almost horizontally between HBZ.

Evaluation of vertical motion velocity, (W) by isentropic method gives W = 5-10 cms-1 in HBZ (precisely, at their upper boundaries) and W 1-2 cms-1 between HBZ.

So, upward widespread motion of warm air over the front is not uniform. Strong lifting is concentrated in relatively narrow zones, tilted to the Earth surface and separated by zones with very weak vertical motion. The tilting of the zones makes field of W inhomogeneous both in vertical and horizontal directions. Vertical distance between axes of the zones with strong lifting is about 2 km and horizontal distance is about 200 km.

Horizontal and vertical inhomogeneity of temperature and air motion fields forms the so-called "leaf" structure of warm frontal regions (Refs. 2, 7) .

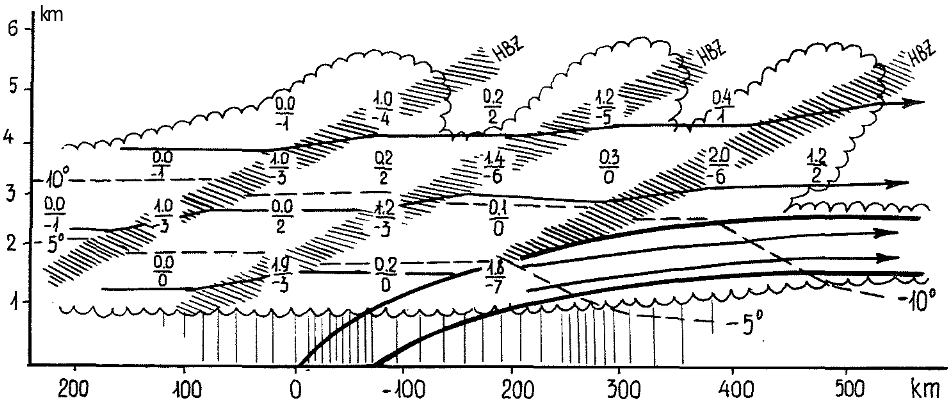

Fig. 1. Scheme of warm frontal region mesoscale structure. a Numerator and denominator are average values of , 10-5 °C m-1 and'ax, 10 s—1, respectively. Hyperbaroclinic zones are hatched. ":Lines with arrows are streamlines, festoons are cloud system boundaries. Hatching under lower cloud boundary represents precipitation, the density of hatching is proportional to precipitation intensity. Dashed lines are isotherms.

4. EFFECT OF HBZ ON THE STRUCTURE OF FRONTAL CLOUD AND PRECIPITATION SYSTEMS

Satellite IR-picture analysis has shown that banded structure of cloud systems was typical of all types of fronts (warm, cold and occlusions). Cloud upper boundary in cloud bands was higher than between the bands. The bands were almost parallel to frontal line; their width varied from 40 to 250 km (Fig. 2) and length varied from 200 to 600 km.

According to aircraft measurements, cloud water content (CWC) field in frontal Ns-As clouds contained zones with relatively large ewe, s.urrounded by volumes with relatively small ewe (Fig. 3). The zones with large ewe were tilted and parallel to the front.

Horizontal and vertical distances between their axes were about 200 km and 2 km, respectively (Fig. 3). This result verifies the earlier findings(Ref. 9).

According to pluviographic data, the field of warm frontal rain intensity had a banded structure. Rainbands were about 100 km wide and almost parallel to frontline (Fig. 4).

Rain in the rainbands was 2-4 times heavier than in the areas between them. One of the rainbands was located 200-300 km ahead of the warm frontal line while another almost coincided with the frontal line.

The facts, given above, testify that mesoscale structure of warm frontal cloud and precipitation systems in continental regions does not differ (at least qualitatively) from that on oceanic coasts (Refs. 1, 2). Hence, the structure is not a prJduct of any specific geographical conditions, but rather connected to mesoscale systems of vertical motion, inherent to frontal region itself.

An attempt was made to relate cloud and precipitation to "leaf" structure of thermodynamic fields. The existence of such a relation is suggested by layer-like con-

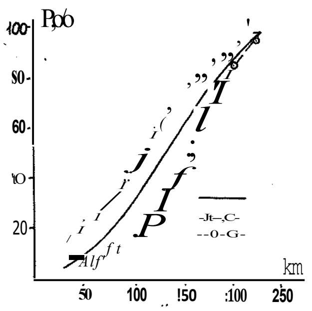

Fig. 2. Cumulative frequency of occurrence (P, %) of frontal cloud band width (derived from satellite IR-pictures). 1 - warm fronts, 2 - cold fronts, 3 - occlusioni.

figuration of zones with large ewe and also by the fact that distance between them coincides with the distance between HBZ.

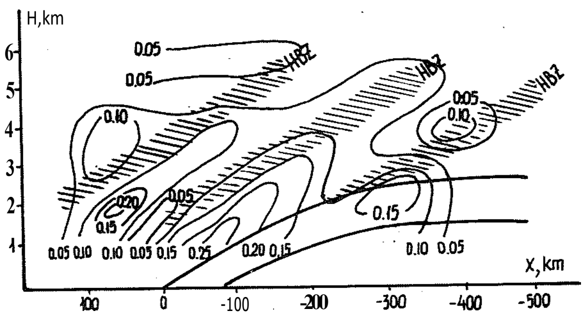

Fig. 3. Average cloud water content (g m-1) in warm frontal regions. Hyperbaroclinic zones are hatched.

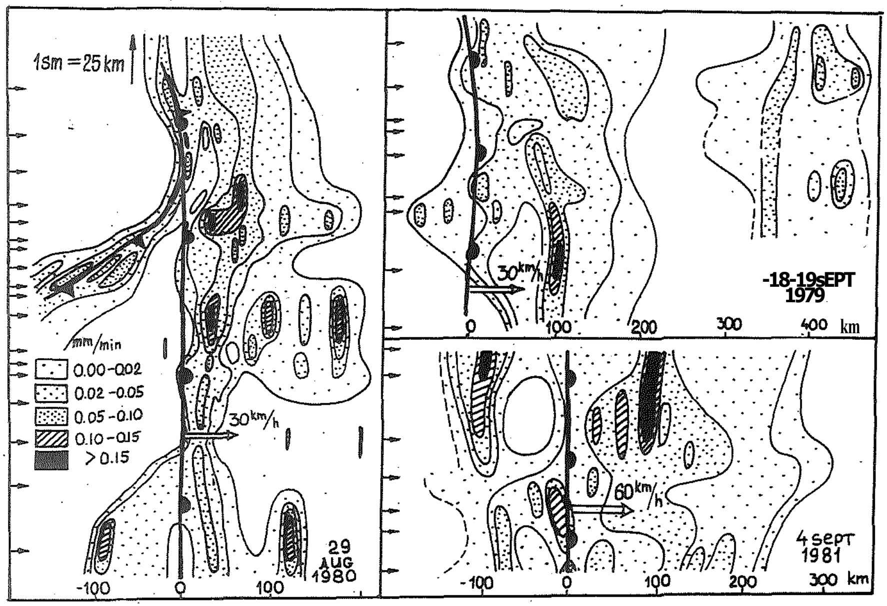

F.ig. 4 .. Precipitatio n intensity in warm frontal regions on 18 19 September; 1979, 20 August, 1980, 4 September, 1981

According to aircraft observations cloud layers in upper portions of Ns-As were tilted and coincided wi'th the upper boundary of HBZ, where widespread vertical lifting was the strongest, while cloudless zones were found between HB:3, where vertical motion was the weakest. This result casts some light upon the origin of cloudless zones in Ns-As, which are typical of Ns-As.

Cloud water content is poorly correlated with HBZ and vertical motion field (see Fig. 3). 'rt is no wonder, because ewe depends on the balance hetween water vapour condensation rate (which is proportional to vertical velocity) and precipitation particle production rate (which depends on microphysical processes).

According to Refs, 2,7, the formation of rainbands is caused by spatial inhomogene.ity of rEa alization of potential instability in "seeding" layer and, as a result, by formation of generating cells. To our mind, in formation of rainbands a large role is played by spatial inhomogeneity of widespread vertical motion in "feeding" layer, where temperature is -5° ..--15°. Vertical cross-sections of radar reflectivity (Fig. 5) showed that the zones with relatively large radar reflectivity (which means relatively high rain intensity) were obser'.red under the portions of HBZ and the front, where temperature was -5° -10°. It was likely to have been caused by 'the fact, that the Bergeron mechanism is the most effective at the mentioned temperatures: So the moisture, condensed by widespread vertical motion re-condensed on ice particals.

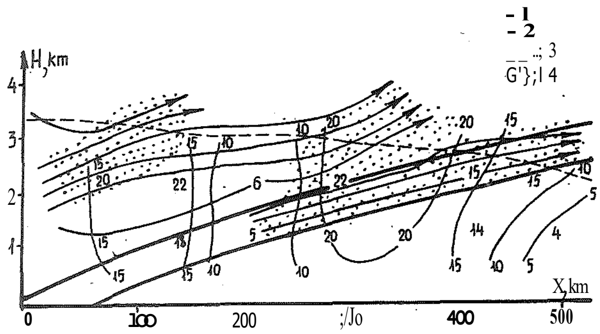

Fig. 5. Relation between zones with large radar reflectivity (with heavy precipitation) and air motion structure. Warm front on 2 June, 1981. 1-radar reflectivity, 2 - streamline, 3 - isotherm of -7°, - areas with w 5 cm s-1.

5. CONCLUSIONS

The results of investigation have led us to the following con lusions.

1. Temperature, wind and widespread vertical motion fields in warm airmass over the fronts are not homogeneous. There are zones (so called hyperbaroclinic zones - HBZ), in which major spatial changes of temperature occur. HBZ are tilted and almost parallel to the front; they are separated by relatively homogeneous portions of warm airmass. There are at least 3 HBZ in a warm frontal region.

2. In HBZ strong convergence of wind and widespread lifting are observed, while between HBZ there are divergence (or weak convergence) and almost no vertical motion. This forms "leaf" mesoscale structure of temperature, wind and widespread vertical motion in warm frontal regions.

3. Hesoscale structure of warm frontal cloud and precipitation systems in continental regions does not differ much from that on oceanic coasts. "Leaf" structure of vertical air motio makes it possirle to explain some features of frontal cloud system mesoscale structure, including inhomogeneity of cloud system upper boundary, layerlike structure-of ewe field, the existence of cloudless zones in Ns-As. andfo - mation of rainbands.

6. REFERENCES

1. Shakina, N.P., 1978. Onmesoscale structure of fronts and cyclones in middle latitudes. Meteorologya i hydrologya, No. 3.
2. Hobbs, P.V., 1981. Mesoscale structures in mid-latitude frontal systems. Proc. IAMAP Symposium, Hamburg.
3. Lyakhov, A.A., Shakina, N.P., 1981. Mesosccile structure of atmospheric fronts in European part of the USSR. Proc. IAJ'l!AR Symposium, Hamburg.
4. Matkovsky, B.fl., Shakina, N.P., 1982. Mesoscale structure of occlusion over the central European USSR according to special measurementS-.. Meteorologya i hydrologya, No. 1.
Sa Postnov, A.A., 1983. Mesoscale structure of wind field in warm frontal regions over the European USSR. Meteorologya i hydrologya, No. 2.
6. Bezrukova, N.A., 1982. "Conveyer belt" in cold frontal region over the European USSR. Trudy Tsentral. Aerolog. Obs., No. 148.
7. Kreitzberg, C.W., Brown, H.A., 1970. Mesoscale weather systems within an occlusion. Jour. Appl. Meteorol., v. 9. No. 3.
8. Trutko, T.V., 1982. Peculiarities of summer frontal cloudiness over Europe according to satellite observations. Trudy Tsentral. Aerolog. Obs., No. 148.
9. Burkovskaya, S.N., 1961. Spatial distribution of liquid water content in frontal ·clouds. Trudy Tsentral. Aerolog. Obs., No. 36.

A i\IDLTI-SCALE OBSERVATIONAL INVESTIGATION OF TIIE FOUATION lfflCB.ANISMS OF A lfflSOSCALE CONVECTIVE COlill'Ull

William R. Cotton, Ray L. McAnelly, Jerome M. Schmidt and Ming-Sen Lin
Dept. of Atmo•pheric Science
Colorado State University
Fort Collins, Colorado 80523
lJ.S .A.

1. INTRODUCTION

In recent year•, the Me,oscale Convective Complex (MCC) **ha** been identified•• a fundamentally **unique** atmo,pherio circulation system (Ref. 6) that **aignificantly** affects, if not domlnates, the **c'onTeotive** season'• precipitatio1> and severe veather climatololies over a **larle** portion of the central United States (Reh. 3, 10). Studies utilizing conventional surface and ravinsonde observations provide a basic picture of th@ MCC's meso-a-scale (200-2000 km) circulation, the envirol.lll!ento.l condit.ions. nece•sary for its formation, and its influence on the larger-seal@ envirolll!lent (Refs. ,7, 1·, 8, 12). However, the nechanisns .by **which** the nature ne•o a-scele system evolve• fron it• initial cumulonimbus building components are not vell understood. Quaiitativ@ radar studies of thi• up-scale transition stage (Refs. 2, 9) have noted that it typically involves the merger of (or interaction betveen) tvo or more meso- -•cale (20-200 km) lines or clusters of cumulonimbi. **Ref.** 5 provides a more detailed radar acc.oimt of a ll!CC'• formation, emphasizing its similarity to the precipitation structure that develops in tropical cloud clusters (Refs. 13, 4).

This paper examines **thi•** crucial but poorly understood formation staie of a MCC which developed out of eastern Montana on the evening of 2 Augu•t 1981. The tvo mmjor meso-!3-scah convective component• that evolved into the MCC passed directly **throulh** the 1981 **Cooperative** Convective Precipitation **Experillent (CCOPE)** ob,ervational netvod:, vhich **provided** extensive documentation on this up-scale **deTelop■ent.** Presented herein are the preliminary results of our continuing investigation.

2. LARGE-SCALE ENVIRONBIE?>UAL CONDITIONS

In Fil. la, the 500-mb **■ap** for 0000 GilT 3 A•lu•t (1700 looal 2 August), durinl th@ formative •tale of the JICC, •hovs the Montana region to be l':llder the influence of a moderate vest-southwesterly flow ahead of a itationary trough off **tke** west coast. A veak short-wave that had emanated from this trough is evident (from the temperature and height-change fields) in western Montana. This short-vave, **with** an attendant mesoscale band of cloudines,, **had** passed over the Continental Divide by this time, coupling vith and •upporting 1fternoon deep convection on the eo.stern slopes of the Montano. Rockies. The 700-mb map for the same time (Fig. lb) •.hows the short-wave in central Montana and a confluent geostrophic flow dovnstream over the MCC genesis region. Such 700-mb confluence has been seen in other MCC studies (Refs. 2, 9) and may be a mechanism helping to steer discrete me10- -scale convective components tovards a .meso-a-•cale organization.

An objective surface analysis of winds and **•q•ivalent** potential temperature **(8e)** at this time **(Fil.** 2) shows the lov-level **condition•** over the ll!illlhPlains that the eutwo.rd-propagating convection .generated on the .eastern slopes would be encoimtering. The dominant synoptic feature was a veak cold front that had moved slovly southvard across eastern Montana **and** North Dakota throuih the day, vith ;enerml orth@awtorlie• to th@ north a:ad. $OUtheasterli@$ to **tk• ao t•. A** eyelonie

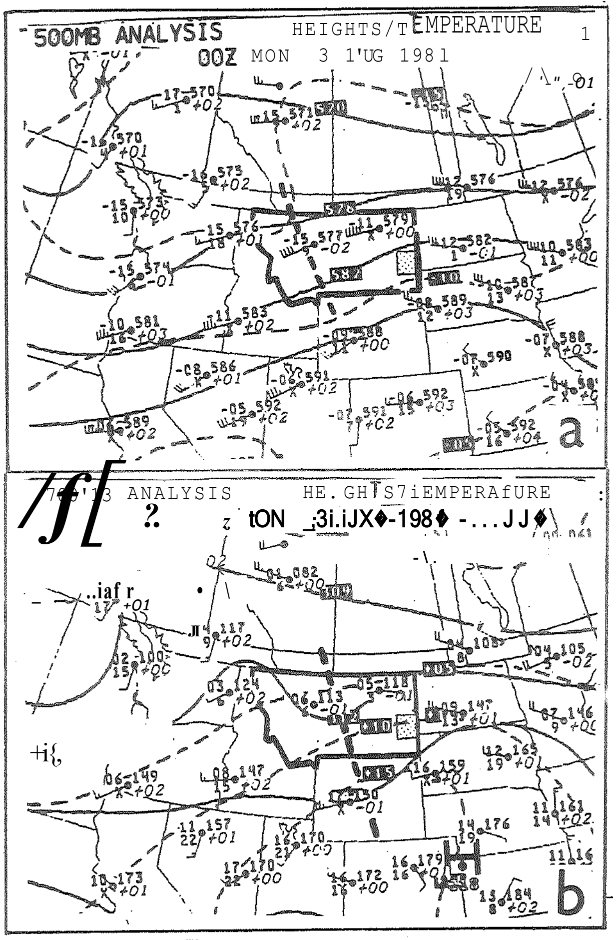

Fig. 1. Nationml Meteorological Center analyse• of height end temperature for (a) 500 ab and (b) 700 mb at 0000 GMT 3 August 1981. Short-wave axis is indicated. Montana and the CCOPE eree in •outheast Montana are outlined.

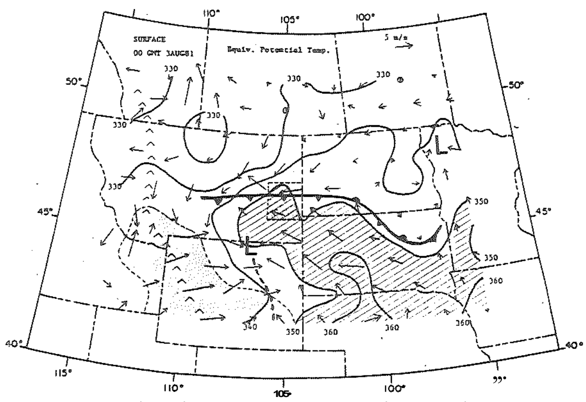

Fill. 2. Objective •urfeee analy•i• of vind• and equivalent potential temperature (Ge) for 0000 GIIT, 8_6 > 350 K is hatched. Shaded region in the southvest im terrain> 1600 m. Continent•l Divide is depicted.

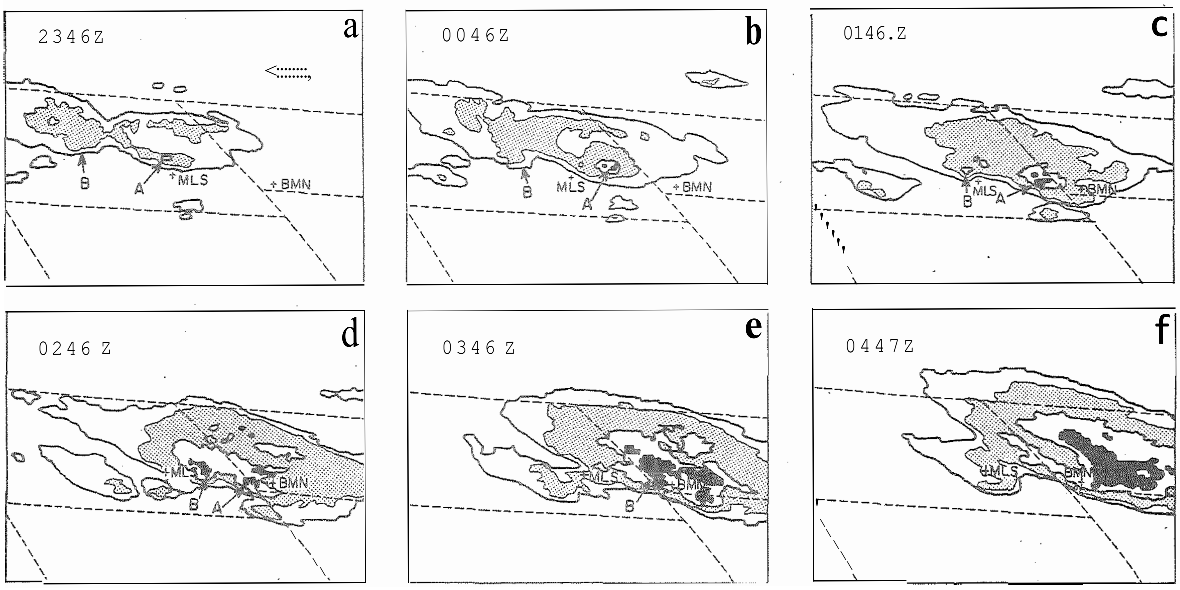

Fi&, 3. GOES-West **(IR) satellite sequence at hourly intervals boginnini ■t** 2346 GMT 2 **Aus •t.** IR **isotherm• enclosing** cloud-tops **colder than -40,** -50 (shaded), -55, -60 **(black), ■nd** -65° Care sho• . Miles City ()ILS), Montana, **at** the wost edge of the CCOPE area, and Bo,..an (Bil!N), North Dakota are sllown.

circulation around n low-pre1anre center in northorn **Yyo■ins** aided **a** rich flow of ki1h 0e-air into 1outhea1tern Montana towards a confluence with the northeasterly frontal flow. This boundary **was** very p:rom.1nii;:ed in visible aatollite iaagery as a thi• cloud line aud apparently acted **al** a trigger **■ecltanil■** for the twc major stor■ •y te■• of the **day,** ·which developed on the north ,ide cf the **bo-.Adary.**

In conjunction **with an** isentropic objectiv@ **an■ly•is/initialization p■ck•1• of o r** CSU m■somo■l■ n-■rio■l mod■l, wo are **investigating** th■te enviromnental **conditions** in **aoro detail.**

3, 1l!ESO-JHlCALE SATI!LLITE AND RADAR EVOLUTION

An hourly infrared (IR) **satellite** sequence **in** Fit, 3 provides an IR overview of the MCC's d@v@lopment **in** eastern **Kontana and** western North Dakota. The two **■ajor** storms, **labelled** A **and** B, formed to **th•** northw••t **of the** CCOPE area **on the torth** side of the cold front **and propagated** to **the** east-southe&st **on near-identical tracks.** Storm **A** was **nearins** tho CCOPE 7-radar Doppler array at 2346 ml:T (Fig. **3a; Kile$** City, J(LS, i$ **at** the **array's** southwe,t corned. For **the next two hours** it **1ras a •o•ero** storm with **tho** coldest IR **tops,** located **near** the southern **edge** of its **expanding anvil** cloud **(Fis.** 3b-c) .

Storm B **for■ed about** 2.5 **hand** 180 km **behind** the first storm. **Initially (Fig.** 3a), it **was at** t • southern edse of an anvil shield produced by a rather unorgani%ed group of cells. It beca■e more orsanized and intenle •• it approached the CCOPE **area** (Fi&, 3b-c), so that durin1 its period of exton1ive Doppler probin1 (02-03 GJIT) its inton•ity wa• co■parable to tho fir• systo■ (Fig. 3d).

The I aoquonce show, a con1olidation of tho two system'• anvil cloud shields, ,o that by 0246 GIl' (Fis, 3d) tho combined syste■ ■et tho MCC **,i%o** crl.toria (Rof. 6). The ■esoscalo core of the HCC continued o con1olidate •• the overall system **gre1r ia size through 0447 GMT (FiJ,** 3e-f). Beyond **thia** time, satellite **imagery** show• the mature MCC to track **ea1t 1outhoa1tward** thron1h the **Dakotas** (approximately **alons the 1urfaco front location** in Fi&, 2), **re.taiaing** its MCC **di■on1ions** until about 1200 GMT 3 **Ausust, when** it beian to decay as it entered Minnesota.

One factor possibly responsible for tho MCC's **deTelop..ent wa, tho faster** propagation speed of **Stor■** B **than A. This** is **eTidont** in th'e satellite **sequence as well as tho** composite radar sequence **saown** in **Fi&,** 4. Storm B moved **at** an average speed of 22 .,.:, **a$ it** track@d across southeiutern **Kontana, compared** to **an** avorale speed of 16 m/s for **Storm A.** The differential propagation speed was **■ost** pronounced after 0135 IDIT, so that during the **period** of most intense anvil cloud development (Fig, 3c-e), Storm B **was** rapidly approaching A (Fil. **4c-d).**

A third itorm, thou1h much weaker than A or B, may ■l•o h.ve **had a** •ignificant role in the MCC formation. **Thia** storm is evident in both Figs. 3 **and** 4 **... a** separate sy,tem (south of the .front) **which** developed over **the** Bighorn Mountain range of northcentral Wyoming. It tracked eastward and **1li1htly** northward through 0230 GMT (Fig. 4a-c), so that **a aorsing** tendency was displayea between the **three** storms. After this **ti■e,** new cell growth **occurred** .head of this **sy1to■** and to **tho** southeast **of** the weakening Storm A **(Fi&,** 4d). The final two **radar depictions** (Fig. 4e-f) show **tkc** new storm and Storm B to **be** the southemost cells of the MCC's **conTective** core (Fig. 3f), with **a** widespread weaker echo having developed into a meso-a-scale **precipitation** structure. This precipitation structure over **the** next several hours was characterized by a leading squall line with a large tr iling stratiform **area,** similar to tropical cloud clusters (Refs. 13, 4). Reflectivity data from the **variona** research radars are being analyzed in **1reater detail** to further investigate this **consolidation.**

4. STORM-SCALE RADAR AND SURFACE ANALYSIS

Storm A was an intense severe storm **haTin& 1upercoll** characteristics. Extensive multiple **Doppler and** multiple-aircraft data were collected on this **stor■, ■akins** it a top priority research **caae** from CCOPE. Other researchers **■re inv·ostigating this** storm **(e.g.,** Ref. 11), while our

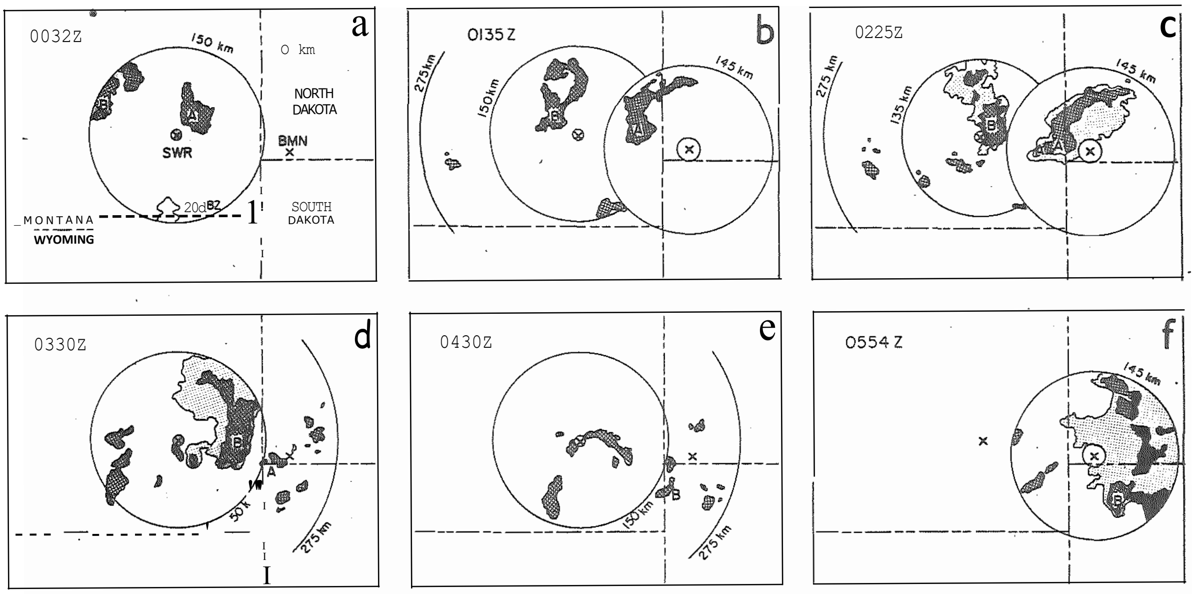

Fig. 4. Composite radar analyses a: apprc iiu,t.::: !1our}y inte::-va.ls. b.esinning at 0032 . 3 August Priit.ary rac...ars utiliz!cC arc: 5-cm r;;.aar 3t Eb;,..-mi.MD (BKN) and t:he -cm. Skywate:r radar (SlrR) about 10-:1:m west of Miles City MT. For SWR (a-e), dark shadea areas are vertically composited echoes) 30 dBZ inside the indicated nea:r-:renge mark and 10 PPI echoe• > 30 dBZ beyond. For BMN (b.c,f), da:rk shaded :regions are 4 :lmAGL echoes) 30 **dBZ.** **As** an indication of anvil precipitation, vertically composited echoes > 20 Z are indicated where available in (c,d,f).

storm-scale analysis is focusin1 on the second system, which was also well-documented by Doppler radar, but not by aircraft. We intend to collaborate with other :researchers in combining the various independent analyses into a more unified and comprehensive case study.

The second storm intensified and became more oraanized as a ·north-south convective line as it approached the CCOPE area (Fig. 4b-d). We have performed multiple-Doppler analyses for several tine periods on the most intense portion of this line, finding that the circulations within the stono are rather typical of a severe meso- -scale squall line.

The mid-level :reflectivity and horizontal relative flow at 0246 GMT is depicted in Fig. 5. Strong southeasterly inflow along the entire leading edge of the line (originating at levels just above the low-level outflow) is seen to extend up through this level (4.a km MSL, or 4.0 km AGL), feeding the strong updrafts which exist along a •ajor portion of the storm's eastern fled. r....ediately to the west of the main updraft region is a precipitation leden downdraft. A more widespread.and weaker downdraft in the western portion of the storm is associated with mid-level air feeding the storm from its :rae:r flank. The dow..draft origin and, perhaps, inflow are correlated with the melting level (~4.8 km), sqgesting that it :represents a me•oscale downdraft of tke type described in tropical squall lines (ltefs. 13, 4), with ,melting ac.tinl1 ,u " prime driving force.

In Fig. 6, two west-east cross-sections (along lines A-B, D-D in Fig. 5) provide more detail to this flow strncture. Across the southern portion of the squall lin.e (A-B), strong sontheute:rly inflow is entering the strongest npdrafts on the sontheaste:rn flank of the systere in a bou ded weak-echo region (reflectivity is not depicted) , with st:rong precipitation-laden do,rndr,fts just to the west in the reflectivity core. Lo -le7el m@rtheasterly outflow aRd upper-level 1outhealterl) ontflo dominate the :rear portion of th• stono.

Further north (C-D), the southeasterly iiaflOW on the storm's eastern flank feeds lo•s intense, through still highly organized, updrafts. Mid-level inflow is evident in the western portion, perhaps feeding the mesoscale downdrafts under the trailing anvil portion of the sto:rm'.

Fig. 7 is a schematic of the surface features and the :relationship between the two major storl11 systems at about 0230 GMT, as derived from the CCOPE mesonetwo:rk of surface stations (20-km •pacing). Storm A is the supercell-type syste,m with its attendant mesocyclone, tracking along t a pre-existing synoptic cold.front. This stono hal - direct access to the high ee air (l 350 K) of the storm's southeastern ambient environment. The storm produced low-level northeasterly outflow with 8_e of 330 to 340 K, not much different than the e_9 value, characteristic of the low-level northeasterly frontal flow ahead of the storm system. Thus, the surface air ahead of the see@ad system had reduced 8_e valueo, high 11.turation points (or lifting condensation levels), aRd very little conditional instability. We hypothesize that the air feeding the intense updrafts of the •quell line o:riginated in the 350 X 8• surface air ma••· Aircraft descent sou...tings between the twe storm• show an elevated layer of h gh 8_e-aii (- 341 K) several hundred meters above th@ • rfao• layer of outflow from Storm A. Thus, Storm B was effectively deconpled from the surface, not experiencing the surface friction, a u surface heat flnxes, and feeding off the high-0_0 air risint ver the first storm's outflow.

5. DISCUSSION

?.,,,l.nve provided a multi-scale overview of tit.• \.:.::"'cc c,i of and liiC in the :aortlt.cr• Hillt. Plai:,u. 'Cc:•.'tr::•n·c with th.ii formation, a:all pola ibly resp Jibl for it ••• tko clo5ing diztamo@s :;,ztween the two major storms (due to a faster ;:c:.opalation of the second storm) and with third, weaker storm to the ,outh. Factor$ po••ibly cau,inl this merging tendency between multiple

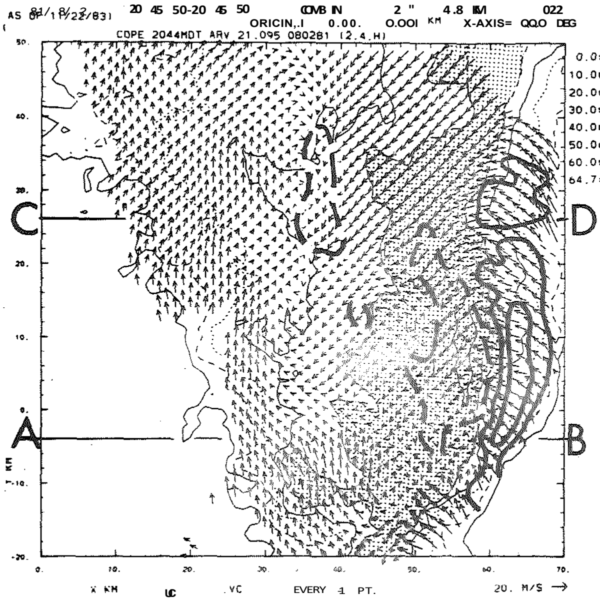

Fig. 5. Multiple Doppler radar analysis of reflectivity a u horizt:mtal relative flow (keys provided in picture) at 4.8 km MSL at 0246 Gi!T, on a 70 z 70-km grid. Region exceeding 40 dBZ is shaded. Updraft isotachs (heavy solid contours) of 5 and 15 m/s and downdraft isotach (heavy dashed contour) of j m/s are indicated. Lines A-B **and C-D** denote cross-sections in Fig. 6.

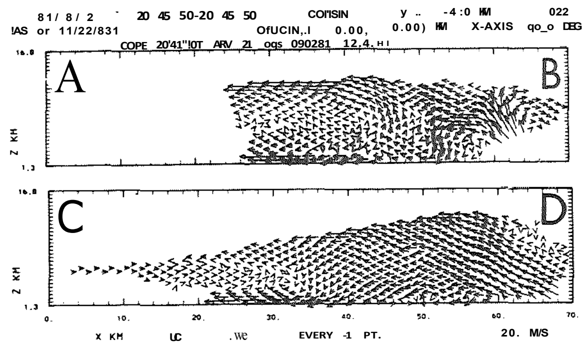

Fig. 6. Multiple Doppler radar analysis of relative flow in the vertical cross-section planes A-Band C-D of Fig. 5.

aeso-p-scale conyective features include: (1) weak confluence in the environaental steering-level flow; (2) the blocking of mid-level westerly flow by the second system, perhaps weakening the steering current for the first system; (3) the decoupling of the second system from the surface, with reduced surface fluxes and stresses favoring a faster propagation of the second system, and (4) the linkage of the second system to the upper-level short-wave, which could have had a faster wave propagation speed than the translation speed of the first system.

ACKNOWLEDGEMENTS

We thank Pat Laybe for his assistance in processing the satellite -\ata utilized in this study, and Judy Sorbie for her drafting. This research wa- sponsored by the National Science Foundation under Grants ATM-8312077 and ATM-8306521, by the National Oceanic and Atmos heric Ad.ministration Contract #NA82RAH00001. and by the Air • Force Office of Scientific Research under Grant AFOSR 82-0162. bdar and objective analysis computations were performed on the NCII Cray-1 coaputer. Neil is sponsored by the National Science Foundation.

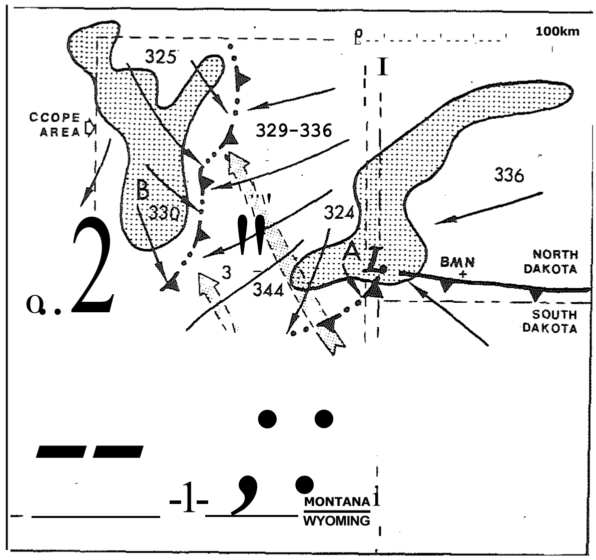

Fig. 7. Schematic surface features (fronts, outflow boundaries, streamlines and characteristic Θe values) over the CCOPE area at 0230 Gl<T, showing the relation between Storms A and B {low-level reflectivity> 30 dBZ is shaded). Broad arrows depict low-level flow decoupled from the surface.

!UIFE!IENCES

1. Boaart L.F. and Sanders F. 1981. The Johnstown Flood of J11.ly 1977: A long-lived convective system. J. Atmos. Sci. 38 (8). 1616-1642.
2. Cotton W.R. et m1 1983, A long-lived mesoscale convective complex.. Part I: The mountain-generated component, Mop. Wea. !!!!.. 111 (9), 1893-1918.
3. Fritsch J.M. et al 1981, The character of me oscale convective complex precipitation and its contribution to warm season rainfall in the U.S., Preprints. Fourth Conference on Hydrometeorolop;y. Reno, Nevada 7-9 October 1981, Amer. Meteor. Soc .• 94-99.
4. Leary C.A. and Houzc R.A, Jr. 1979, The structure and evolution. of convection in a tropical cloud cluster, J. Atmos. Sci- 36 (3). 437-457.
5. Leary C.A. and Rappaport E.N. 1983, Internal structure of a mesosc.ile convective complex, Preprints. 21st Cppf. on Radar Meteor., Edmonton, Alberta. Canada, 19-23 September 1983, Aaer. Meteor. Soc., 70-77.
6. Maddox R.A. 1980, Mesoscale convective complexes. Bull. Amer. ifpteor. Soc., 61 (11). 1374-1387.
7. Maddox R.A. 1983, Large-scale meteorological conditions associated with midlatitude mesoscale convective complexes, Mon. Ygp. m- 111 (7). 1475-1493.
8. Maddox R.A. and Doswell C.A., III 1982. An examination of jet stream configurations, 500 mb vorticity advection and low-level thermal advection patterns during extended periods of intense convection, Mon. Wea. Rev. 110 (3), 184-197.
9. McAnelly R.L. and Cotton W.R., 1981, The meso-B scale structure and precipitation characteristics of middle-latitude meso-a scale convective complexes. Preprints. Fourth Copf. on Hydrometeor., Reno, Nevada, 7-9 October 1981. Amer. Meteor. Soc., 81-87.
10. Rodgers 1 ıW. et al 1983, Mesoscale convective complexes over the United States during 1982, Mon. Wea. Rev., 111 (12), 2363-2369.
11. Wade C.G. 1982, A preliminary study of an intense thunderstorm. which moved across the CCOPE research network in southeastern Montana, Preprints. 9th Conf. on Wea. Forecasting and Analysis, Seattle, Washington, 28 June - 1 July 1982, 388-395.
12. Wetzel P.L ct al 1983, A long-lived mesoscale convective complei. Part II: Evolution and structure of the mature complex, Mon. Wea.·Rev. 111 (9), 1919-1937.
13. Zipscr E.J. 1977. Mesoacale and convective-scale down.drafts as distinct components of squall-line structure, Mon. Wea. R9v. 105 (12), 1568-1589.

MESO- AND MICROSCALE STRUCTURE OF WIND AND TEMPERATURE FIELDS IN JET STREAM CI CLOUDS

V.K. Dmitriev, T.P. Kapitanova, V.D. Litvinova, N.G. Pinus, G.A. Potertikova, G.N. Shur

Central Aerologica Observatory, Moscow, USSR

In recent years attention to Ci clouds has increased. This is due both to the role which these clouds play in atmospheric dynamics and to the necessity to meet tne requirements of aviation.

Cirrus-are mainly linked to atmospheric fronts ana jet streams. They cover the area up to hundreds of thousand km^2 , and their life period varies from several hours to 1-2 days.

There are very few and somewhat conflicting empirical data on microstructure of wind and temperature fields in cirrus clouds (Ref. 4).

Research flights were made in 1981-1982 to study turbulence within Ci clouds over the northern part of the USSR. The measurements were made at the altitude levels from 6 to 10 km. The CAO Il-18 aircraft was used, which was equipped with a variety of measuring, computing, and recording systems. Two groups of instruments were used to obtain data on temperature and wind field structure.

The first one consists of sensors of ground speed, static and dynamic pressure, total temperature, heading, roll, pitch angles and airborne computer; the second one, named "pulsation thermo-dynamic complex", made high accuracy measurements of wind components and temperature fluctuations (Ref. 5). Table 1 presents the characteristics of instruments on output parameters.

Nineteen flights were made in 1981-1982, in which 9400 km had been flown in Ci clouds and 43200 km in clear air.

Fig. 1 presents an example of vertical cross-sections of wind and temperature fields in Cs on anticyclone side of a jet stream (November 11, 1981). Dashing represents areas with dense Ci dlouds. Waved lines in the figure mark zones of turbulence. The zones were selected as the ones where standard deviations of vertical (w) and horizontal (v) velocity pulsation were equal to or exceeded 0.1 m s-1 (6w ≥ 0.1 m s-1). The vertical cross-s6 tion gives an impression of the structure of Cs, intermittency of turbulent zones with the undisturbed ones, inhomogeneity of wind and temperature fields. A cross-section of that kind was drawn for each of the research flights, utilizing the results of both measurements and observations. Averaged vertical p ofiles of turbulent characteristics (Gw, 6v, 6t) at various levels in Ci clouds and near their upper and lower boundaries are given in Fig. 2. The figure shows that as a rule profiles of all parameters are-

Table 1
Main characteristics of instruments on output parameters

Parameter	Range	Accuracy	Frequency range
Altitude bar.	-50÷12000 m	0.5 %÷30 m	0÷0.1 Hz
Ambient temperature	+40÷-70 °C	1 %÷0.5°	0÷0.1 Hz
Wind velocity	0÷100 ms-1	2 %÷3 ms-1	0÷0.1 Hz
Wind direction	0÷360°	±3°	0÷0.1 Hz
Air speed	150÷750 kmh-1	1 %÷5 kmh-1	0÷0.1 Hz
Vertical gust vel.	±10 ms^{-1}	5 %÷0.1 ms-1	0.01÷2 Hz

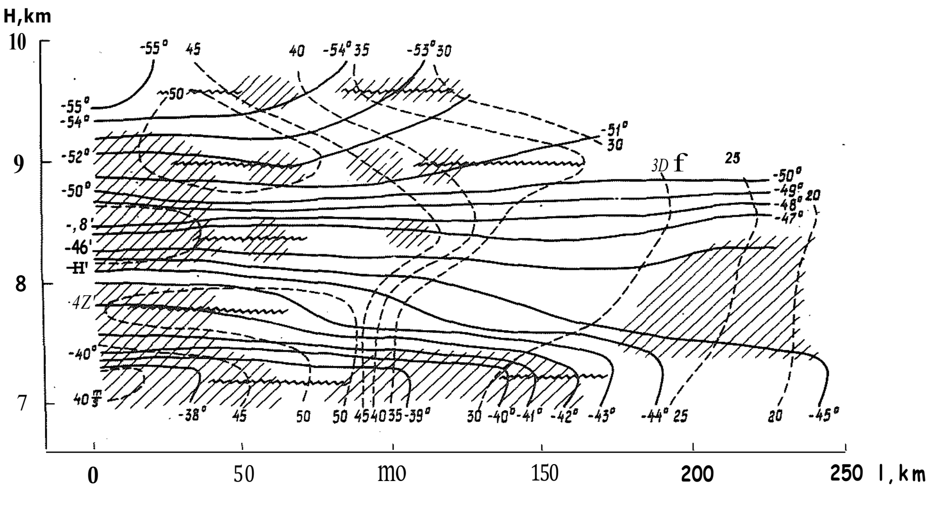

Fig. 1. vertical cross-section of wind and temperature fields on November 11, 1981

Table 1 (continued)

Para-meter	Range	Accuracy	Frequency range
Horizontal gust velocity	±10 ms^{-1}	5 %÷0.1 ms^{-1}	0.01÷2 Hz
Temperature fluctuations	±2 °c	3 %÷0.05°	0.0h-2 Hz

similar. The intensity of turbulence is the highest in the middle of Cs and lowest in their upper and lower portion. Mean turbulence intensity above Cs is a bit higher than on base level of clouds. Spectra of wind and temperature fluctuation were also computed. It is to mention that in general turbulence was weak.

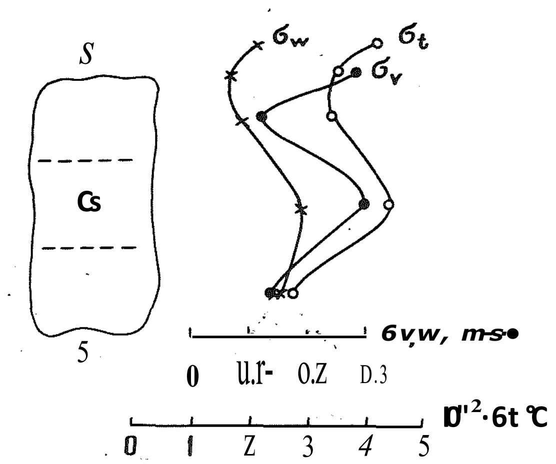

Fig. 2. Vertical profiles of σ_w, σ_v, σ_t in *Ci* clouds

The spectra of micro- and mesoscale pulsations at various levels averaged over the whole bulk of data, are given in Fig. 3. Hereafter, we shall refer to the scale of a kilometer to tens of kilometers as mesoscale and to the scale of hundreds of meters to kilometers as microscale.

Fig. 3 shows large variations of wind pulsation intensity on mesoscale. If intensity of wind mesopulsations is estimated by turbulent energy scale-to-scale transformation C , where k = $10^{-4}m^{-1}$, values of $e_{10^{-4}}$ ary from 5.0 to 5.10^{1} $cm^2 s^{-3}$.

Spectra of microscale pulsations in *Ci* clouds and in clear air are given separateiy. The spectra are fairly approximated by Kolmogorov-Obukhov's law Sv(k) = = $0.15E^{2/3}k^{-5/3}$. Turbulent energy dissipation rate can be evaluated by the use of the right wing of spectra, correspondin ly to k = $5.10^{-3}m^{-1}$. In Cs, *Ci* clouds E :::: 2 .2 $cm^2 s^{-3}$, whereas in clear air ϵ = =1 .4 $cm^2 s^{-3}$. This is more a tendency, than a regularity taking into account confidence-intervals, because of limited statistics.

The fact, that 6< $_{10^{-4}}$, perfectly corresponds to the idea of turbulent energy scale-to-scale transformation in stable thermal stratification conditions (Ref. 3). That is so because a portion of turbulent energy is spent on the work against buoyancy forces and does not reach viscous scale subrange where dissipations of turbulent kinetic energy ipto heat take place.

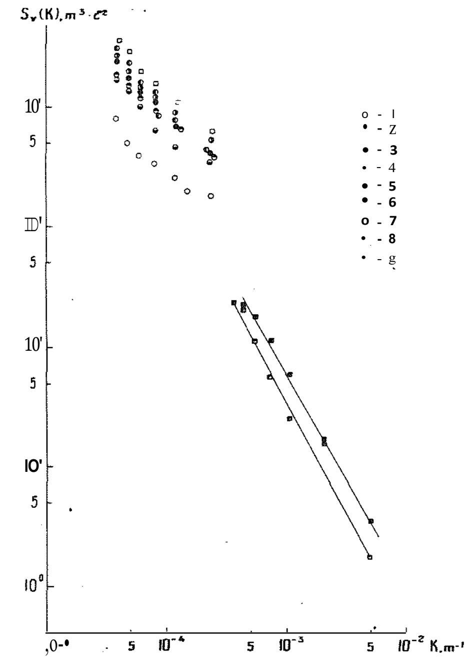

Fig. 3. Spectral density of wind fluctuations in meso- and microscales:
1 - 5.5 6.0 km; 2 - 6.5 7.0 km; 3 - 7. 7.5 km; 4 - 7.5 8.0 km; 5 - 8.0-8.5 km; 6 - 8.5 9.0 km; 7 - 9. 9. 5 km; 8 - CAT 9 - *Ci* clouds

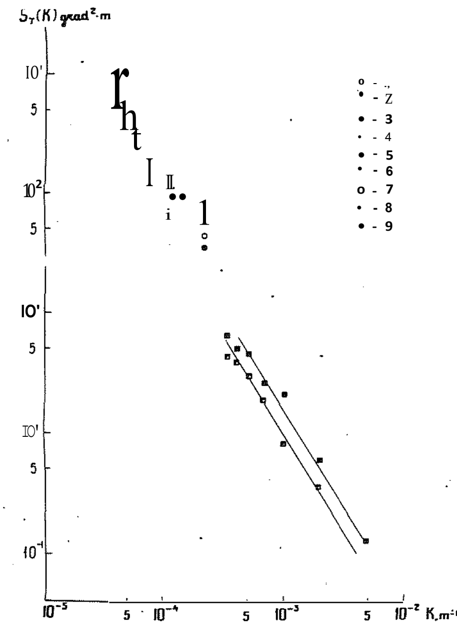

Fig. 4. Spectral density of temperature fluctuations (the same designations as in Fig. 3)

Table 2

Some characteristics of jet stream *Ci* clouds

Flight position in relation to jet -stream	Number of i:-uns	.S$_r$ (km)	Scl / S:i::: (%)	Sz: tb . (km)	Stb.r::l. (km)	stb.cl. / Scl. (km)	Lcl. (km)	LCAT (km)	ov ms^{-1}	6w in clouds- ms^{-1}	6 t grad;
Across jet stream on Zn side	31	14605	20	3507	2137	74	45	57	0.262	0.167	0.047
Across jet stream on AZ side	20	8056	11	2727	732	84	36	63	-	0.18_9	0.056
Along jet stream on Zn side	16	6079	15	1526	846	90	34	62	0.129	0.143	0.028
Along jet stream on Az side	10	4432	24	1336	966	93	37	62	-	0.180	0.036

Fig. 4 presents averaged data on temperature meso- and micropulsations. Mesoscale temperature pulsations can be describ_ed by expression ST (k) "'- k-n, where lnl ::: 2. Spectra in microscale range can be approximated by the same expression, but liil::: 5/3, and correspond to spectral Obukhov's law ST(k) = o.25C k-5/3. The data also allow to estimate values of structural charactBristics of temperature pulsations cl. The values of c in *Ci* clouds are a bit greater than in ciear air and on the average they are 1.4.10-6grad2cm-2;3 and 7.o-10-7grad2cm-2/3, correspondingly. Now we shall elaborate on turbulence in *Ci* clouds :i,njet stream zones. The data gathered in jet stream zones were devided into 4 groups. They included :!;lights along and across jet stream on its cyclonic and anticyclonic sides. Table 2 gives some characteristics of turbulence in Ci clouds of jet streams. The length of flights in clouds (S cloud) for each group was about 15-20 % of total fl ght length (SL).

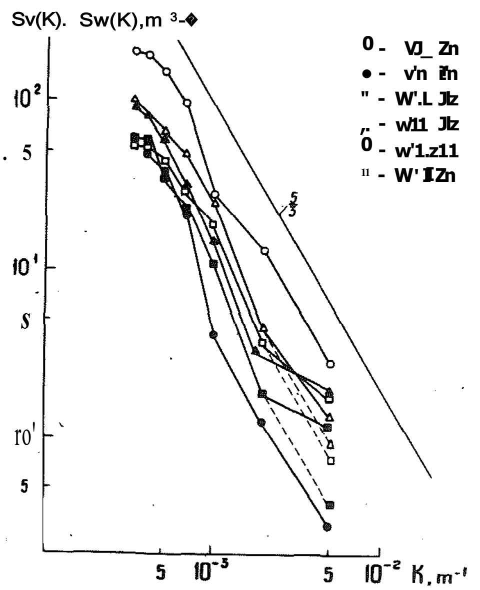

Fig. 5. Spectral densities of wind component pulsations in jet stream ci clouds

In all groups the occurrence of urbulence in clouds was 75-90 %, while in clear air it was only 10-20 %. Mean length of turbulent zones (Lcloudl in clouds for all groups is 40 km, while in clear air (LcAT) it is 60 km.

Meanwhile there is a difference in turbulent intensity encountered in flights across and along jet stream. The mean square values of wind component and-temperature pulsations are larger in cross-stream flights than in along-stream flights.

Fig. 5 gives averaged spectral densities of wind component pulsati•ons for different groups. The designations are as follows: V.1.zn - horizontal wind]1>ulsations in. flights across jet stream and its cyclonic side. Other designations are based on a similar principle.

The energy spectra of 2' and v', obtained in *Ci* clouds in the vicinity of jet streams, are of special interest. It is characteristic of spectra of W', that on cycloni,;: and anticyclonic sides of jet stream spectral density of pulsations (S_w) at "5/3" spectra subrange is higher in cross-stream flights than in along-stream flights. The same is also true for spectra of V', with SVL being an order of magnitude larger than Svl1 .

In Fig. 6 temperature pulsations spectra for all 4 groups are given. Similar peculiarities are observed in temperature spectra: both on cyclonic and anticyclonic sides of jet st.reams spectral density of temperature pulsations is a good bit larger in cross-stream flights than in along stream flights. It is no wonder, beca,:.se in stable stratification conditions, wrich are almost always present at those alt•.tudes, there should be a close correlat· on between W' and T' (Ref.2).

Table 3 presents turbulent energy dissipation rate f, and structural characteristics of temperature pulsation field C in jet-stream Ci clouds.

The fact, that intensity of turbulent pulsations of horizontal wind component is higher in cross-jet stream flights than in along-jet stream flights demonstrates the. spatial anisotropy of wind pulsation intensity.

Kao and Woods (Ref. 1), who studied clear air turbulence in "Jet stream" project, also showed that dispersion of wind pulsation is larger in flights across jet stream than in flights along the stream. Our data have demonstrated that in jet stream Ci clouds such a relationship is true not only for wind, but also for temperature fields. When analysing the experimental data, it should be taken into account that anisotropy like the one discussed above can be a result of the existence of not only turbulent, irregular in space and time motions in jet stream Ci clouds, but also of some. regular structures in cross-section of flying aircraft. So it is known that wind profile in jet stream is not smooth, but considerably jagged.

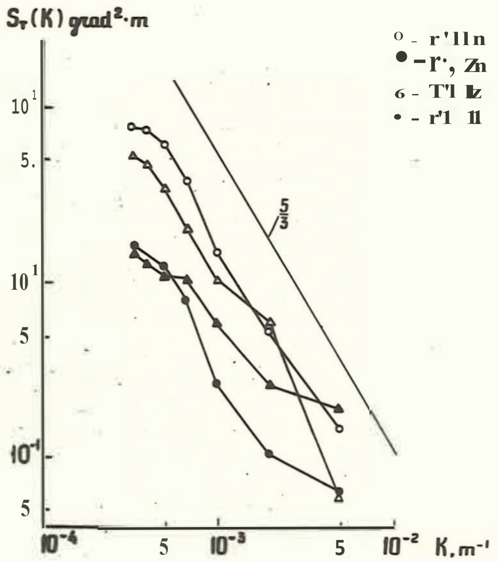

Fig. 6. Spectral densities of temperature pulsations in jet stream Ci clouds

Table 3

Averaged values of l and c_T^2 in Ci clouds

Wind velocity.fluctuations		e^2 cm^{2}s^{-3}	Temperature fluctuations		c^2 grad^2;m$^{-2/3}$
vl'	Zn	4.4	tl	Zn	1.4-10^{-6}
v,1	Zn	1.3-10^{-1}	tl1	Zn	2.7·10-7
'Wl	Zn	8.4•10-1	t'1	Az	9.0-10-7
Wl1	Zn	1.9·10^{-1}	td	Az	5.4·10-7
w'.t.	Az	1.3			
Wl1	Az	3.5•10-1			

REFERENCES

1. Kao, S.K., Woods; H.D. Energy spectra of mesoscale turbulence along and across the jet stream. Journ. Atm. Sci.; 1964, v. 21, 513-519.
2. Monin, A.S. Effect of thermal stratification of medivnt n turbulence, in: Internation l Colloquium on the Fine-Scale Structure of the Atmosphere and its Relation to Radio-Wave.Propagation. Nauka, Moscow, 1965, 113-127.
3. Shur, G.N. 'Energy transfer across turbulence spectrum in the free atmosphere, in: Turbulent Flows, Nauka, Moscow, 1970, 228-233.
4. Vasiliev, A.A., Kapitanova, T.P., Leshkevitch,. T.V., Pinus, N.S., Cherednichenko, V.S. Meteorological conditions of aircraft flights. 177 pp.
5. Vinnichenko; N.K., Pinus, N.z., Shmeter, S.M., and Shur, G.N; Turbulence in the Free Atmosphere. Hydrometeoizdat, Leningrad, 1976, 288 pp.

THE INHO!<OGENEOUS FEATURES OF STRATIFORM CLOUD ECHO STRUCTURE AND PRECIPITATION IN MEI-YU FRONTAL CLOUD SYSTEM

Huang Mei-yuan Hong Yan-chao

Institute of Atmospheric Physics, Academia Sinica,
Beijing, China

During summertime the mei-yli frontal cloud system is an important precipitating system in the southern part of China. Therefore, we have observed mei-yli frontal cloud system by use of 711 type radar (3cm) and airplane at Tunxi, Province Anhui since 1979. It was found that the structure of stratiform cloud, especially the structure of its warm region appears to be inhomogeneous (Refs. 1,2)". This is a significant feature of cloud structure in mei-yli frontal cloud system. In this paper, we shall further analyse this inhomogeneous structure of. stratiform cloud and study its effect on the precipitation.

1. INHOMOGENEOUS STRUCTURE OF THE STRATIFORM CLOUD

In mei-yli frontal cloud system, there are complicated cloud types, such as various stratiform clouds, convective clouds, and coexistance of stratiform cloud and cumulonimbus with heavy rainfall. The inhoogeneous structure of stratiform cloud shows generally as follows.

1.1. Convective clouds embedded in the stratiform cloud

On PPI section, in large region of echo there are many stronger irregular spots and patches with horizontal size from 2.0 to 4.0 km. They are echoes from convective cells embedded in stratiform cloud. These tops are generally in the vicinity of the cl C isotherm. The reflectivity of conve.ctive cells is from 6.0 to 38.0 dbz. Usually, these cells do not produce thunder and lightning. Because convective cells "hide" in the stratiform cloud, it is difficult to find them from either satellite picture or visual observation on the ground. They may directly cause a horizontally inhomogeneous struc;ture in warm region of the stratiform cloud (see Fig,1),

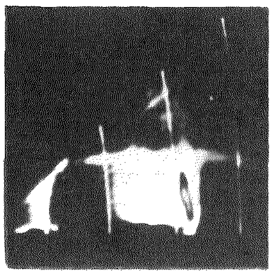

Fig.1. A convective cell embedded in stratiform cloud,

1.2. The downward extending echoes (DEE) in the warm region of stratiform cloud

Sometimes, we can see that echo structure of strati form cloud without convecti've cell (it is named pure stratiform cloud) is still inhomogenebus. In a widespread region of relatively uniform reflectivity; there are some- dot-like and mass-like higher reflectivity echoes as thoce of convective cells embedded in stratiform cloud (Fig. 2). They are downward ext_ension of precipitation or virga from the cores with strong reflectivity in the. bright band (CSR) (their reflectivity is at least 5 dbz more than the surrounding echo) in strati form cloud, We call them as DEE. DEE, as well as the convective cells, may cause inhomogeneous structure in the warm region.

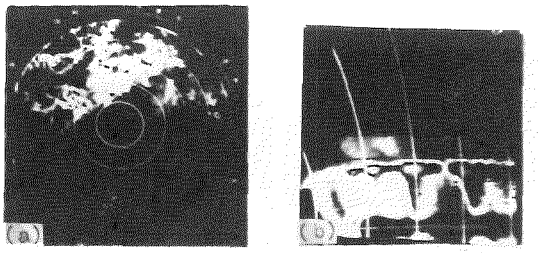

Fig.2. *CSR* in the bright band and corresponding DEE* (on 5 July 1980).
(a) 1825,5"elevation,(b) 1827,340° azimuth.

Description mentioned above shows that inhomogeneous structure in stratiform cloud may be caused either by convective ce_lls embedded in it which can't easily find on ground, or by DEE in the warm region. But according to the radar observation, the DEE can be observed frequently, even for the stratiform cloud containning convective cells, the DEE exist also in it. To-the author's best knowledge, there are no published papers on the similar structure in the frontal cloud syst m yet. It is probably an important feature of structure in stratiform cloud in mei-yli frontal cloud. system. The higher liquid water LOntent and higher temperature in warm region of stratiform cloud observed by the airplane (Ref.2) are likely relative-to the DEE.

*Echoes used in this paper are laminated , in 5 db intervals unless otherwise stated.

2. THE DEE IN THE STRi,TIFORM CLOUD

The feature of DEE from CSR are closely relative to those of the bright 'oand. As it has been pointed out that the structure of radar bright band in mei-yti frontal cloud ·system is usually inhomogeneous. There are several cores with stronger reflectivity, which uncontinually distributs in the bright band on RHI section (Fig.2b and Fig.3). The maximum intensity, horizontal size of the cores and distance between the cores in the bright band directly affect on corresponding parameters of DEE. The reflectivity factors of CSR vary from 6 dbz to 30dbz, but usually are 19 24 dbz. The thickness of CSR and distance between them are different as shown in F::.g. 2b and Fig.3; In generally, the CSR with high reflectivity corresponds to strong DEE, but the reflectivity of the DEE is about 5 dbz lower than the CSR. Intensity of the DEE reduces downward with height elow the C level (5 km). As consistent - ith this fact, horizo tal size of reflectivity contours of the DEE reduces downward as well, thus the DEE is shaped like a "funnel". Stat::.stical results for 102 CSR bhow that average values of horizontal size of CSR and DEE are 5. 4 km and 2. 7 km respectively, the average value of vertical rthickn.ess of CSR is 850 m. It indicates hat the radar bright band in mei-yli frontal cloud system is comparatively th ck.

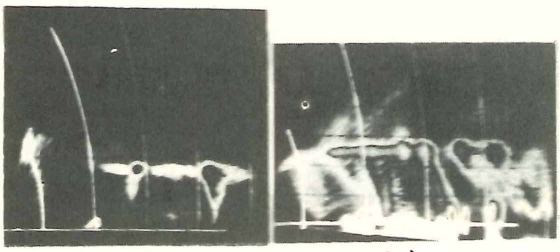

la) (b)

Fig.3. Inhomogeneous bright band in stratiform cloud.
(a) 1436, 18 JunE:<, 1980, 15° azimuth,
(b) 1151, 5 July,1980, 14° azimuth.

P-hysical process of the CSR formation is worthy of further study. According to the radar observation, the DEE results from the CSR. At first, echo spots are formed near below C level, then intensity of the spot increases gradually with the size, and eventually form cores of high reflectivity near C level, or the CSR. In the great majority of cases, the cores with a reflectivity larger than 14 dbz begin to extend downward and form the DEE. When there are many echo spots and the cores of high reflectivity have formed below 0 C level, the inhomogeneous bright band is omposed of the cores. In **view** of the position of reflectivity cQre which is near O' C level, it can be affirmed that it:s formation is related to the melting of ice cryptal and snowflake falling from upper level. Primary theoretical c,,lculaiion (ReL3) ·has shown that nonuniform structure of echo over bright band may be di.rectly results in CSR of the bright band. If in the upper part of bright band there are some generating cells which have large size· ice crystals of high concentrati6n and, intensity of the brigh b nd under these cells is high. Then-it will ·cause a horizontally inhomogeneous structure of bright band. Fr6 observation and analysis by Hobbs et al (Ref.4), there are ertainly generating cells over upper frontal zone in cold frontal and warm frontal cloud system in com-. pany with extratropical cyclones. Ice .crystall yieded and provided by generating cells play a role of the natural seeciing in the stratiform-cloud rainfall. In mei-yfr frontal cloud system, a wide runge oi precipitation from atratiform cloud occurs usually in the northern side of the stationa**ry** frontal zone. Whether there are also generating cells producting larger ice crystals over the upper frontal zone and the CSR results from melting of ice crystals as they fall from generating cells through o•c level to intensity reflection and scattering of electromagnetic w ves, this is only a presumption for formation of the CSR and the DEE. In addition, shape and size of the ice crystals and liquid water content in meltin'g zone, and others also have influenc on inhomogeneous structure in the bright band. An appropriate combination of these factors may form also the CSR and the DEE. Because of the large thickness of bright band in mei-yli frontal cloud system, the liquid water content can play an important role in formation of the CSR as a results of growth of melt1 g particles by coalescence.

3. PRECIPITATION FEATURES OF STRATIFORM CLOUD ·IN _MEI-YU FRONTAL CLOUD SYSTEM

In order to qu,mtitative analysis for precipitation features of stratiform clouds, we shall divide them into three classes named SI, S and SI. SI contains only a few convective cells. Its inhomqgeneous structure results principally from the DEE. There are many convective cells and not ·bright band in S L Slii.is a pure stratiform cloud with existence of bright band and DEE. We take respectively one precipitation process for SI and S and two precipitation µrecesses for S , and then find average rainfall intensity R in mm/hr within 10 min. from data of rain fal l ·amount at ea ch station, maximum rainfall i ten§ity' R""1', average rainfall intensity R, R =1R/n, maximum difference S =R.•,.R ••, and fluctuation amount > = 1J/R, in which d' i's dispersion. The parameter values listed in table 1 are average value for rainfall station (SI and **SJD** and values for individual stc,tion (.5.ii.). Some precipitation parameters of three thunder cloudsobserved in 1962 (Ref.5) are.also listed in t ble 1 for omparison with parameters of the stratiform cloud. Some features can be seen from tclble 1 as follows.

Precipitation pattern is nonuniform. The fluctuation amount for SI and S1 are -1.14 and 1. 17, ·respectively, it is e ual to 0.76 and 1.05 for s.m. . But they are 1. 12, 2.38 and 1.39 for thunderclouds. Obviously,

Table 1. Some parameters of precipitation fluctuation in stratiform cloud

	SI (5 July)	SII (6 July)	SII (18 June)	(5 July)	Thundercloud (1962)		
R''	29.1	15.8	1.8	7,8	44,5	133	47;6
R	4.5	3.8	o.6	1,7	9,0	12.9	9,9
S	20.1	15.8	1.8	7.8	43,3	133	47,1
σ	5.02	4,33	0.43	1.74	10.1	30;7	13,0
μ	1.14	1.17	0,76	1.05	1.12	2.38	1.39
n	26.3	25,0	22.0	21.0	16.0	17.0	13.0

* SI, S.II.and sI. were observed tn 1980.

some of for stratiform cloud are close to that of weak thundercloud.

Inhomogeneity of precipitation in stratiform cloud is related to inhomogeneous structure of the cloud, Because there are convective cells and strong DEE in SI and SII, μ. values are larger. In SI, which did not contain convective cells, μ-values for two precipitation processes are different, In case of strong inhomogeneous bright band and DEE, the μ value is larger, too. Thus, they have an effect on precipitation from stratiform cloud, For example, in stratiform clo.ud on 5 Ju],y 1980, stru.cture of the 'bright band is inhomogeneous, and its intensity is high (30dbz) , R." andμ. are respectively 7,B mm/hr and 1.05. These values are no better than those in SI, SI[and the thundercloud. It is seen from this that the convectiv•e cells and the DEE can cause larger fluctuations of rainfall intensity in stratiform cloud, and produce shower features.

The convective cells differ markedly from the DEE in rainfall intensity. I case of stratiform cloud with convective cells, R-. and R in two precipitation precesses are 20.1, 4,5 and 15.8, 3,8 mm/hr, respectively. They are much larger than those of pure stratiform cloud,

Now, further analysis are made for stratifdrm cloud precipitation on 5 July 1980. The rain at Rucun and Xucun station was from a wide spread stratiform cloud moving face east on that day. Fig,4 displaies partial PPI and RHI echo photographs. Of all the strong echoes, strong zone I with the intensity greater than 20 db is the largest in area (Fig,4a), RHI section at 1105 (Fig.4b) demonstrates that it is a DEE from CSR. It was moving at 40 km/hr sorth-east by east and reached to Rucun station (326' azimuth, 31 km distance) at about 1120. Th@ strong zone I. reached to the range between 20 and 30 km to the north of the radar et at 1145, The leading edge of zone I neared Xucun station (1f azimuth, 30 km distance}, Fig,4d shows a vertical RHI section along the. azimuth of 11' at 1148. It may be seen that in bright band there are three reflectivity cores from which DEE consist of a wide precipitation echo zone because of short ringe between the cores. Itl addition, there was a strong zone II. with largest area in range from 30 to 40 km behlnd strong one I. Its edge eached Rucun station. The zone X contains a convective cell (.see Fig,4f')', the remainder of zone]:. is DEE. At 1159 (Fig.1.jie), Rucun station was covered by the echo wi.th 20 db of the convective cell and the echo of. 30 db was moving to the station.

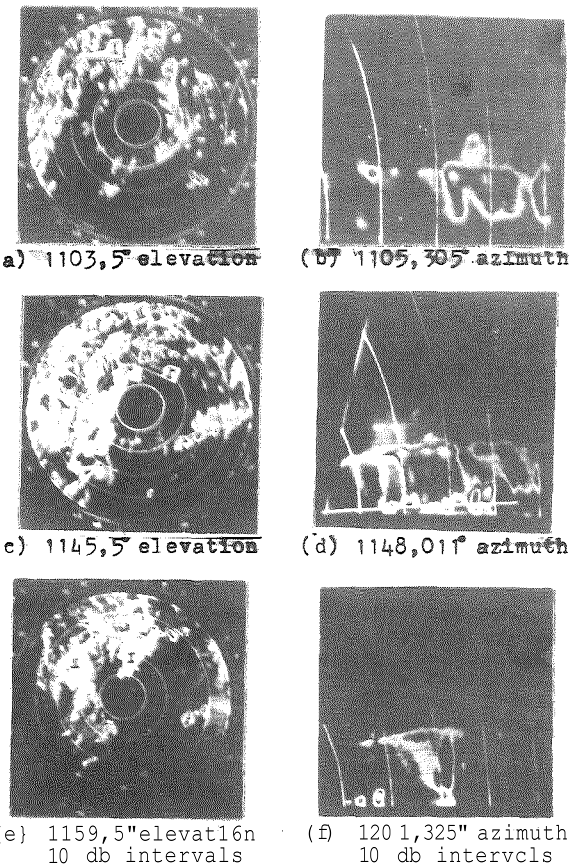

Fig.4, Some PPI and RHI echoes photographs of stratiform cloud which was moving east wardo on 5 July 1980.

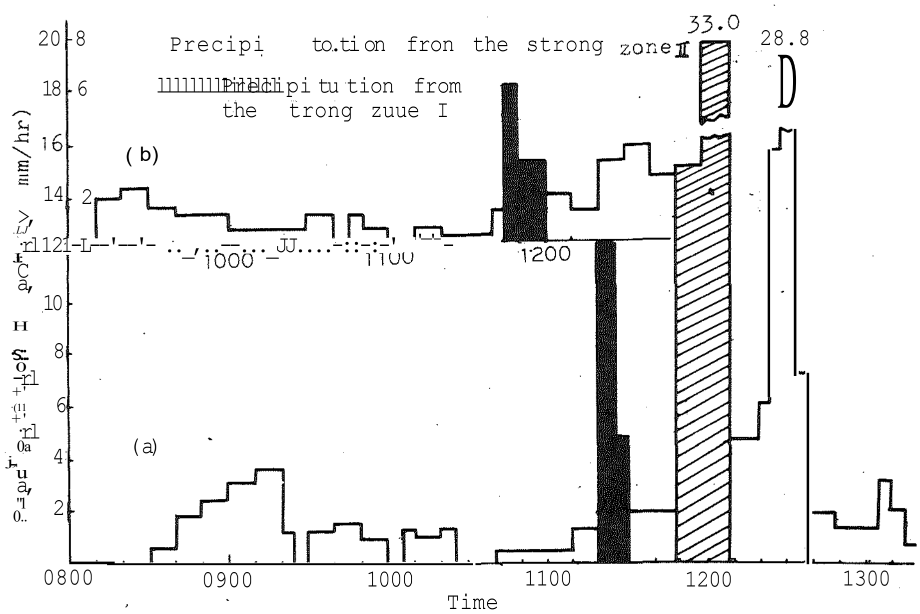

Fig,5, Precipitation intensity change with time in stratiform cloud rainfall at Rucun station (a) and Xucun station (b) on 5 Jul 1980.

Fig,5 illustrates rainfall rates change with time at Rucun station (Fig.5a) and Xucun station (Fig.5b). As mentioned above, strong zone I and II arrived at Rucun at 1120 and 1145, respectively. They are consistent in time with the rain observed at this station at 1120 to 1130 and around 1200, It is clear that the DEE corresponding to the CSR can yield rainfall of 5-12mm/hr in intensity (for example rain from strong zone I and II) but rainfall rates' around DEE is lower. Thercifore, shower rainfall is occured at somewhere as the DEE move through, The convective cells embedded in the stratiform cloud, although reflectivity and size are not as high and large as isolated cells, may produce rain with higher rate, Maximum rainfall rate was 33 mm/hr at Rucun station after stronger zone II pass through there. It was the time to rain in the highest rate when convective cell in stronger zone II reached Rucun (Fig. 4e). Consequently the rain with the highest rate lasted 10 min. was from the convective cell.

4, SUMMARY

The structure of stratiform cloud in mei-yli frontal cloud system is often inhomogeneous. Convective cells embedded in stratiform cloud, cores with high reflectivity and DEE from the bright band are major reasons for the inhomogeneous struture. The DEE which has a close ralation with inhomogeneity of the bright band is a significant feature of echo structure in mei-yli frontal cloud system. Either the convective cells or the DEE can cause nonuniform distribution in time and space of precipitation from stratiform cloud. The calculation indicates that average rainfall rate within 10 min, is 15-20 mm/hr and flucturation amount of rainfall rate (-1 1) is approximately equal to that of weak thunderclouf for stratiform cloud in which contains convective cells. [r pure stratiform cloud, the bright band with obvious inhomogeneous structure and strong DEE can also make the precipitation pattern inhomogetieous. Sometimes the rainfall rate is above 10 mm/hr-and fluctuation amount of rainfall rate can reach 1.05.

REFERENCES

1. Huang Mei-yuan, Hong Yan-chao and Wu Yu-xia 1981, Several features of radar echo in mei-yU frontal cloud system, Conf. on Cumulus Precipitation in The South of China, Changsha City.

2. He Zhen-zhen, Huang Mei-yuan and Shen Zhi-lai 1981, Some features of convective zone in warm stratiform cloud, Conf. on Cumulus Precipitation in The South of China, Changsha City.

3. Hong Yan-chao, Huang Mei-yuan and Wang Shou-ping 1983, A theoretical study on inhomogeneity of bright band in mei-yii front cloud system, Accepted for publication on Scientia Atmospherica Sinica.

4, Hobbs P V 1978, Rainbands precipitation cores and generating cells in a cyclonic storm, J. Atmos. Sci., 35, 230-241.

5, Zong Pei-ying and Xu Hua-ying 1965, The rainfall characteristics of thunderstorms and showerstorms, Studies on Microphysical Characteristics of Clouds and Precipitation in China, 62-68.

!1ESOSCALE DISTRIBUTION OF WATER VAPOR AND LIQUID WATER OBSERVED WITH A SCANNING MICROWAVE RADIOMETER

Alexis B. Long

Desert Research Institute

Reno, Nevada, U.S.A.

1. INTRODUCTION

Aircraft observations of cloud liquid water can be made with varying suc_cess depending on the kind of cloud. Orographic clouds pose particular observational problems •. The topography which leads to the clouds also prevents safe aircraft sampling of the clouds especially in their lower levels.

A remote sensing, radiometric technique of liquid water observation has been developed recently which allows rather complete observations of orographic clouds. The technique is briefly described here, and mesoscale observations of some winter orographic clouds in Utah are presented. Some observations of the water field are also presented.

2. RADIOMETRIC TECHNIQUE OF LIQUID WATER AND WATER VAPOR OBSERVATION

The dual-wavelength microwave radiometer used in the present work was designed and .built by the Wave Propagation Laborator of the United States N.O.A.A. Environmental Research Laboratories (Hogg, et al. (1983); Guiraud, et al. (1979); Westwater (1978); and Westwater andGuiraud (1980)). **The** radiometer remotely senses atmospheric microwave emission at frequencies of 20.6 GHz ($\lambda =$ 1.46 cm) and 31.6 GHz ($\lambda =$ 0.95 cm). Emission at the lower frequency is primarily from water vapor. Emission at the higher frequency is primarily from liquid water. Emissions received at these two frequencies are expressed in terms of black-body equivalent temperatures or values of atmospheric absorption. A linear statistical inversion scheme relates these temperatures or absorptions to the depth of water vapor and depth of liquid water integrated along the 2.5 degree beam of radiation sensed by the radiometer. Depth of'liquid water can be converted to average concentration of liquid water if the geometric distance along the beam containing liquid water is known. The• radiometer is sensitive only to liquid water. Ice crystals which are dry do not affect the data. If raindrops are present they may scatter radiation into the· beam and confound the measurements. Wet snowflakes have a similar effect." Rain or wet snow lying on the a tenna surfaces- will also affect the data. An electric fan is thus often used to blow precipitation away from these surfaces.

3. RADIOMETER OBSERVATIONS

The radiometer was located at the western base of the Tushar Mountains near the town of Beaver, Utah (Latitude 38° 17' North, Longitude 112° 35' West) during the time period 15 January to 15 March 1983. The Tushar Mountains are oriented north-south. The radiometer was at an elevation of 1875 m. The crest of the mountains is at about 3 00 m elevation and was approximately 20 km east of the radiometer.

The radiometer collected data on changes in atmospheric water vapor and liquid water in association with weather disturbances moving through the area. Of particular interest was the liquid water in clouds forming over the Tushar Mountains because of these disturbances.

The radiometer was operated in two modes. The radiometer was pointed toward the zenith some of the time in order to gather data on the atmosphere and clouds passing overhead. ·Most of the time the radiometer scanned 360° of azimuth at a 20° fixed elevation angle above the fiorizon. The time for a complete scan varied but averaged about 15 min. The azimuth-scan data provide information not only on the temporal ehavior of the water vapor and liquid water but also on their spatial distributions.

A cold front passed through the Beaver area from the .west at 13002 on 7 February 1983, and with it were observed a variety of changes in the water vapor and liquid water fields.

- Water vapor. Figure 1 shows the observed water vapor depth integrated along the radiometer beam or field of view. The depth is corrected for the slant path taken by the beam when the raqiometer is in the azimuth-scan mode. Water vapor depth was 0.6 -0.7 cm until about 21002 on 6 February. There was then a small increase in vapor to 0.9 cm, but vapor depth decreased back to 0.7 cm by 00002 on 7 February. A steady increase in vapor then commenced and the depth reached a maximum of about.1.3 cm at 13002 when the cold front passed through. Vapor dep_th then decreased to about 1.0 c.;.n.

The considerable temporal detail in Figure 1 could not have been detected with conventional rawinsondes launched every 12 hr. SpeciaJ. rawinsondes launched-every 3 hr .would show the main

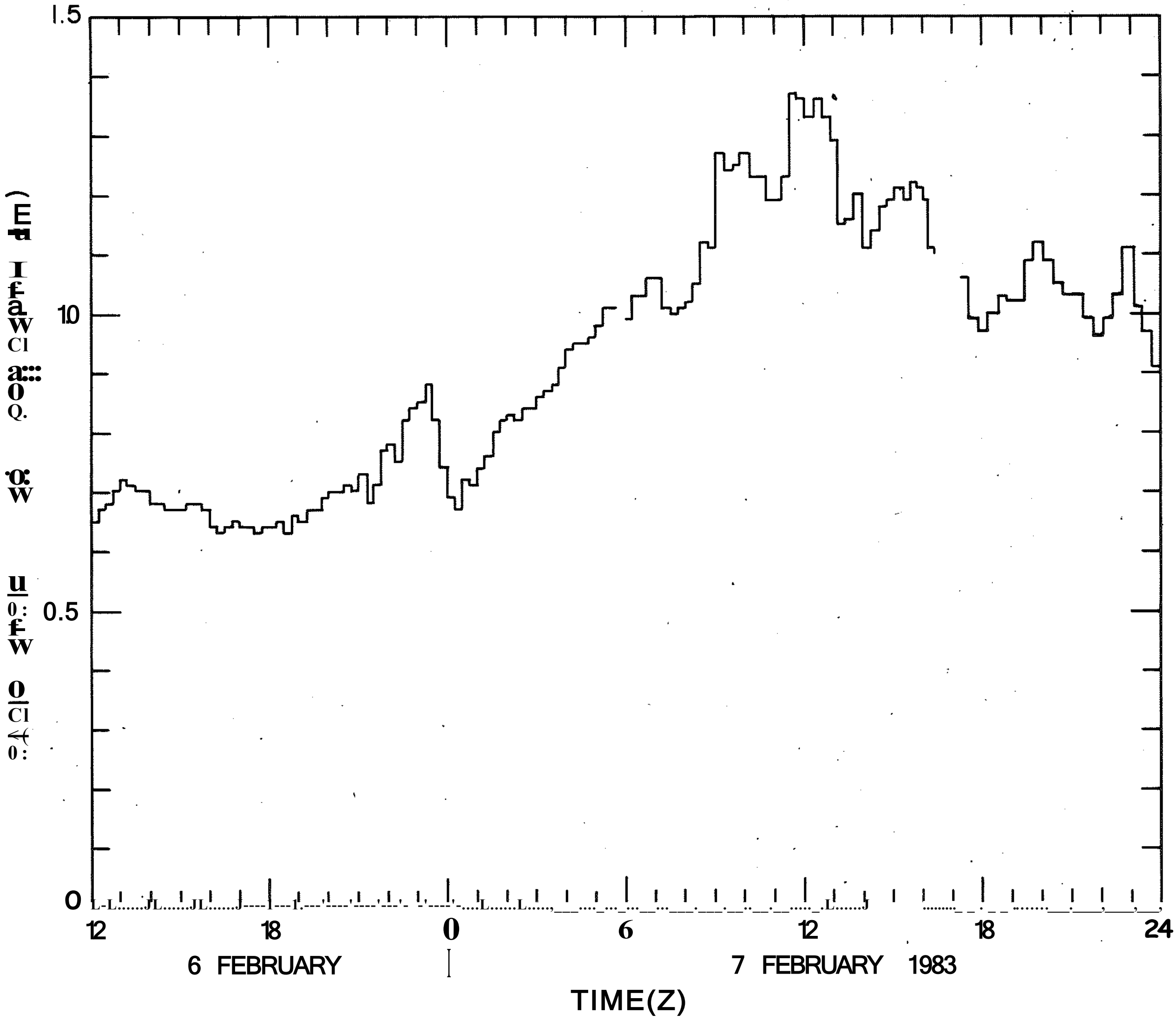

Figure 1. Radiometric precipitable water vapor depth (cm). The depth is integrated along the beam of radiation sensed by the radiometer. The depth is corrected for the slant path taken by the beam when the radiometer is in the azimuth-scan mode after 0600Z on 7 February and not pointing toward the zenith. Fifteen minute average data (zenith mode) and scan-average data (azimuth-scan mode) are presented.

features of Figure 1 but would not resolve the finer details of 1-2 hr time scale.

Associated with the changes in water vapor in Fig. 1 were significant changes in the cloudiness. Prior to 2100Z on 6 February there were a few scattered showers over the Tushar Mtns but clearing) elsewhere. Cloudiness then increased but by 0000Z on 7 February skies were again broken, and clear conditions were visible to the west. At about 0300Z on 7 February the leading edge of extensive cloud cover advected in from the west in advance of the approaching cold front. By 0530Z on 7 February a vertically-pointing K-band radar (λ = 1.79 cm) collocated with the radiometer showed echoes continuous from near the surface up to 4500 m above the surface. Convective or stratiform cloud was present to varying degrees from then until the end of the day.

The influx of water vapor seen in Fig. 1 was responsible for the overall increase in cloudiness on 7 February, but as shown next topography was responsible for any appreciable condensation of water within the clouds.

Liquid water. Figure 2 displays the depth of liquid water observed with the radiometer during the time it was operated in the azimuth-scan mode. A correction has again been made for the slant path of the beam. A prominent feature of Fig. 2 is the significantly greater depth of liquid water at azimuths near 90 degrees. It is in these directions from the radiometer that the Tushar Mtns lie.

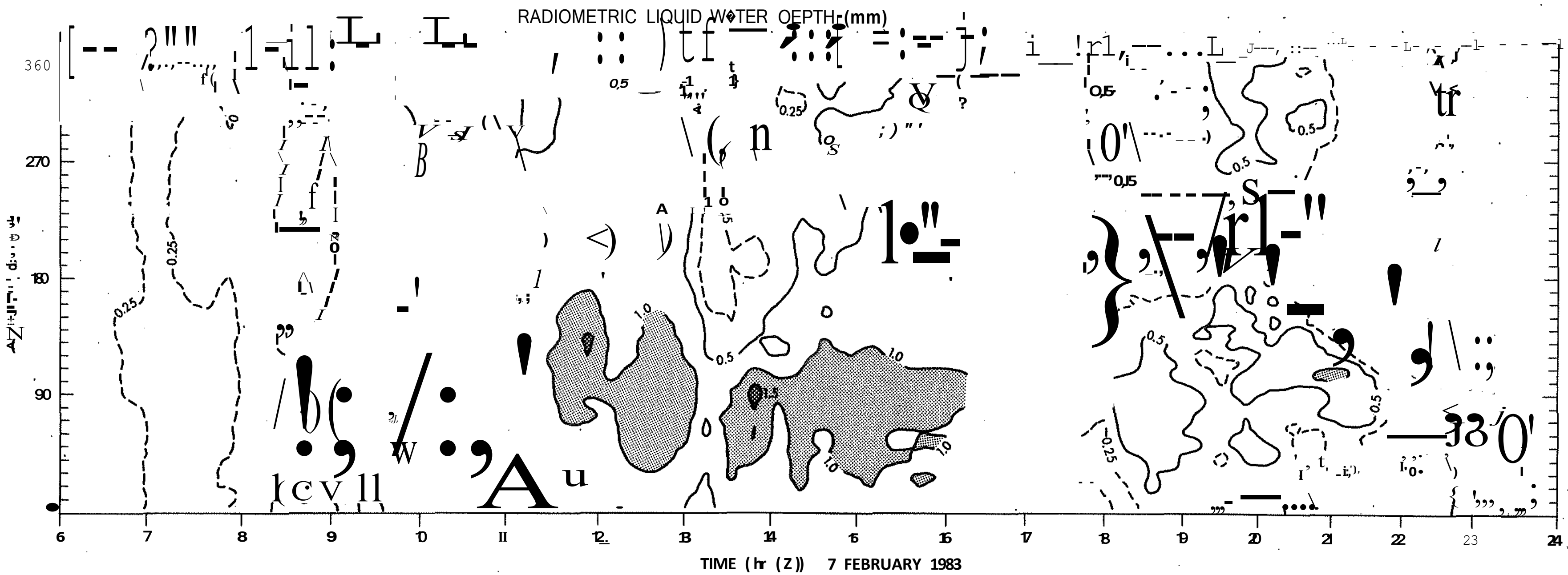

Figure 2. Radiometric liquid wat.er depth (mm) measured in the azimuth-scan mode. The depth is integrated along the beruli of radiation sensed by the radiometer and is corrected for the slant path taken by the beam. Data collected in .sixty ·azimuth-scans are contoured. Contours are at 0.25, 0,5, 1.0, and 1.5 nm. Depths gr ater than 1.0 Dill are shaded. No data were collected.from 1625Z to 1730Z. The time \$Cale is shorter after 1730Z when ·the-radiometer was scanning more rapidiy.

The depth of liquid water is approximately two cu three times greater over the r.,ountains than to the west.

The effect of the mountains on the condensation process may be even greater than shown in Fig. 2. Although cloud depth varied it was approximately 2-4 km according to the K -band radar. Thus the radiometer beam at 20 eleva ion angle would have intersected the main part of the cloud only about 6-12 km from the radiometer site. At this close distance to the mountains air even upwind will already be rising and orographically-induced condensatior, should already be occurring in the cloud. The depths of liquid water observed at westerly azimuths in Fig. 2 thus may be overe?timates of the amount of. water that would be condensed without any effect of topography. The true effect of topography .is thus likely greater than the factor of two or three increase seen in Fig. 2.

The topographic effect does not appear to depend on the kind of clouds. From 0830Z to 1300Z the clouds were mainly convective according to the K -band radar and from 1430Z to 2100Z they were inly stratiform.(The contour intervals in Fig.2 were selected to show the topographic effect on liquid water amounts and do not show this difference in cloud type.)

The radiometric depths of liquid water in Fig. 2 can be used to estimate average liquid water concentrations. In order to make the estimates information is required on the vertical depth of cloud containing most of the liquid water. The K -band radar collocated with the radiometer showea the high r cloud reflectivities were spread over a vertical depth of about 2 km. For· our purposes this approximate depth of the clouds at the base of the mountains is a sufficient estimate of the .depth of the clouds lying over the Tushar M ns themselves. We then find the 1.0 to 1.5 mm depths of liquid water in Fig. 2 convert to averag 3liquid water concentrations of 0.5 to 0.75 g m . These concentrations are in rough ag!3ement with the concenttations of 0.5 to 1.5 g m measured simultaneously with a supercooled water detector located near the crest of the Tushar Mtns. The agreement of surface and radiometric concentrations may suggest most of the liquid water was located in the lower parts of the clouds over the **mountains.**

4. CONCLUSIONS

Observations with a NOAA Wave Propagation Laboratory dual-wavelength azimuth-scanning radiometer have been made of the water vapor and liquid water integrated over the depth of the atmosphere. Data collected during passage of a cold front through Utah show an influx of water vapor preceding frontal passage and an associated increase in the general cloudiness. The detail of the radiometric water vapor record permits the identification of temporal changes of scales of 1-2 hr or shorter. The effect of topography on the amount of liquid water condensed in the clouds is prominent. In the case presented at least two to three times more water is present in clouds over the Tushar Mountain range than in clouds only 10-20 km upwind. This appears to be true regardless whether the clouds are convective ur stratiform.

Acknowledgements. Ms. Vatricia A. Walsh of DRI skillfully provided all computer processing and display of the radiometer data. This research was supported by a contract with the Utah Division of Water Resources as part of the NOAA/Utah cooperative weather modification program.

REFERENCES

Guiraud, F.O., J. Howard, and D.C. Hogg, 1979: A dual-channel microwave radiometer for measurement of precipitable water vapor and liquid. IEEE Tran . Geosci. Electron., GE-17, 129-136.

Hogg, D.C., F.O. Guiraud, J.B. Snider, M.T. Decker, and E.R. Westwater, 1983: A steerable dual-channel **microwave radiometer for measurement of water** vapor and liquid in the atmosphere. J. Clim. Meteor., 22, 789-806.

Westwater, E.R:, 1978: The accuracy of water vapor and cloud liquid determination by dual-frequency ground-based microwave radiometry. Radio *Sc{.*, 13, 677-685.

Westwater, E.R., and F.O. Guiraud, 1980: Ground-based microwave radiometric retrieval of precipitable water vapor in the presence of clouds with high liquid content. Radio Sci., 15, 947-957.

OBSERVATIOUAL MODEL OF THE STATISTIC.\.L STRUCTURE OF CU111JLUS FIELD FROLI THE GROUND- Alm SEA-BASED MEASUREI.IEIJTS OF RADIATION FLUX DENSITIES

L.B.Rudneva, R.G.Timanovskaya, D.F.Timanovsky

Voeikov Main GeophY.sical Observatory, Leningrad, USSR

To provide for an adequate model of the statistical structure of cumulus fields multiyear sainples of radiative data from field observations were used. To this end shortwaveradiation flux densities and atmospheric sky radiation.intensities in the 8-12111,1.l band measured under the presence of cumulus clouds were analyzed. Accumulation of data from systematic. observatio11s of variability of such features as characteristic dimensions of cumulus clouds and intercloud gaps and of mean cloud frequencies in dependence of cloud amount made it possible to acqlil.ire reliable, statistically adequate data on the structure of cumu-11;1s cloudiness fields. The samples are valid for the European territory of the USSR and the Equatorial Atlantics.

Experimental material which served as the basis for the model of structure of the cumulus cloudiness field consisted of continuous recordings of global.and direct solar radiation flux densities together with the data on the intensity of atmospheric sky radiation from the zenith zone in the 8-1Jny.i. pectral band.

The total land-based sample of data recordings is 195 hrs long, which corresponds to the linear dimensions of the cloudiness field of 7200 km. Measurements were taken at two sites of the European territory of the USSR in the regions of Leningrad and Rostov.

The total sea-baaed sample of observational da:ta obtained during the 1972-1976 cruises of research vessels in the Atlantics is JOO hrs long (z 7600 km).

Statistical proce.ssing of the measurement data recordings provided assessment of the probability density for linear dimensions of cumulus cloud cross-sections p(s), of cloud frequency, i.e. the number of clouds per_ unit length _of the cloud field croas- ecti n- The analyses techniques a;re outlined in referenced studies (Refs.1,J). he principal r sults are presented both. ·in these and elsewhere (Refs.1,3,5,6,9).,

Whil ·plotting the hystograms of the cloud cross sections' size distributions the initial data were grouped according to gradations of clbud amount: n = 0 + 0.29; 0.3 + 0.59; 0 6 + 0.9.

To obtain statistic lly valid estimates of the characteristics of cloud field the measurement data from various rc1.diation ensors were grouped into the above gradations of cloud_ amount. Averaging of the initial data was performed with the account of the corresponding weighting factors proportional to the volume of the sample.

In Figure 1 the hystograms of linear cros3-p,0ctio11s' ::listributions for cumulus c.1ouds retrieved from the data of land and p,ea-based measurements (the latter - for Eqatorial Atlantics) are presented.

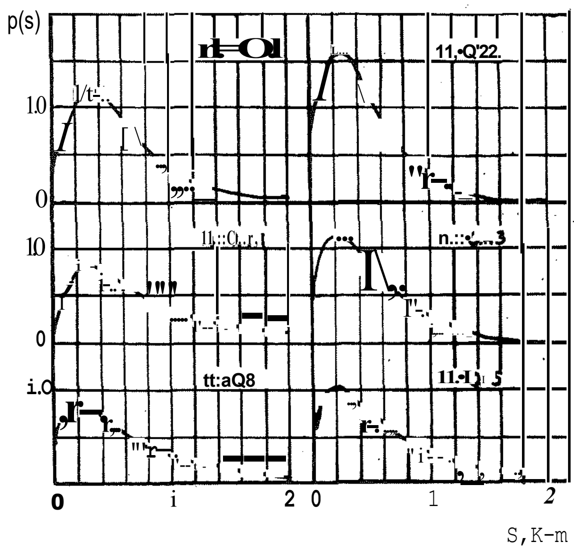

Figure 1. Probability density of the cLU1tUl-us clouds' cross-sections from the data of a) land-based measurements; b) sea-based measurements for various cloud amounts.

Temporal cross-sections were recalculated into spatial ones using the values from radiosonde measurements of wind speed at the cloud base at each observational site. It is known that cloud velocity constitutes 80-90% from the speed of wind .:n case the latter exceeds 4 m/s. About 70% of sampling over land was performed under the wind speeds of 8-13 m/s, therefore the spatial cross-sections are overestimated by 10-20%.

Observational Yalues of the probability density for cumulus clouds' cross-sections were approximated by the log-normal distribution:

$$p(S) = \frac{1}{\sqrt{2\pi}\,\sigma S} \exp\left[-\frac{1}{2\sigma^2}(\ln S - \ln S_o)^2\right] \quad (1)$$

where σ is the RMS deviation of the value $\ln S$. It should be noted that the mean value $\bar{S}$ and its RMS deviation constitute

$$\bar{S} = S_o \exp \tfrac{1}{2}\sigma^2 \quad (2)$$

$$6^2 :: S[(i/'-1].$$ (3)

The distribution p (S) includes two parameters So and 6' • These approximation p_arameters have the following values:

for n = 0.2 So = 0.54 D = 0.81

n = 0.44 So = 0.81 6 = 1.06

n = 0.8 So = 0.91 6 = 1.44

(over land),

for rt = 0.22 So = 0.47 6 = o.68

n = 0.43 So = 0.53 6 = 1.07

n = 0.75 So = o.65 6 = 1.19

(over the Equatorial Atlantics).

Para.meters and, depend on cloud .amount. Such dependences may e expressed with the help of the following formulas:

a) over land:

$5_o = 2,1'1 n - 2n^2$; 6'=-o,6+1,DS; 0,1:::n� o,9

b) over the Equatorial Atlantics:

So= OL{n., + a,32n; 6=3,nn-2,8'ffl,' ,qt n=o,

The problem of transition from the statistics of the cloud cross-sections. to the statistics of cloud uia.meters is treated in one of the referenced studies (Ref.2).

The dependence of mean llnear dimensicns S and, respectively, of cloud frequency elf:. on the amount of cloudiness 1't. **demonstrates** considerable variability of these c aracteristics from sample to ea.mple.

In Figure 2 the estimates are presented of- cloud frequencies and mean cross-sections of cwnulus clouds versus the amount of cloudiness.

The observational data on cloud frequency cf. in the zenith zone show that the dependence cf. (n.) is assymmetric .in respect of the median amount of cloudiness n = 0.5 both over land and over ocean.

It is of interest to compare the estimates of the average cross-sections of cumu.las clouds obtained with the help of different techniques. In Table 1 th estim- tes are presented of the value S in dependence of the amount of cloudiness. The volumes of respective initial samples are also indicated.

To assess the energetics of the cumulus cloudiness field the relative cloud cover of sky was used, that is the value

$$<Jt/ \quad 11./\int_0^{Smax} S^2 p(s)\,ds .$$

was calculated. The relative input of small clouds to the energetics of the field (of those occupying the P (**S**) mode cif the distribution) is negligible, therefore the probability density of the cloud size distribution may, to the first approximation, be expressed as an exponent:

P(S,A)== ;\exp->..s; 5?0, A 70 (4)

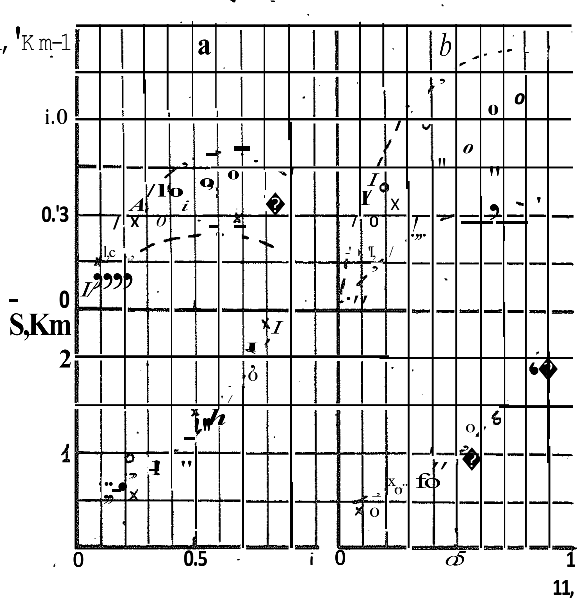

Figure 2. Dependence of the cloud frequency cf. and the average linear dimension of clouds on the amount of cloudiness from the dat.a of a:) land-based measurements; b) sea-bE ,d measurements. x - average values from the infrared radiometer; o - same from the actinom.etric data. Dashed lines show variability limits for ct'..(n.,), S (n..) for separate samples.

Table 1
Estimates of the average cross-sections of cumulus clouds

Values	Instrumentation		
	Actinometric		
rt	0.21	0.4·5	0.10
5	0.52	0.82	0.98
t,h	67	66	41
	Infrared radiometer		
Yt	0.22	0.41	0.72
S	0.58	0.98	1.20
[t,h	75	38	10

Joxperimental ass esment of the average value of the cross-sections makes it possible to retrieve the value of the parameter A =s-1, According to the land-based actinometric and infrared radiometric data we obtain the following estimates of parameter A versus the amount of cloud-i-n Js :ac conor;ietric data

for	n, =0.21	A=1.92
	n, =0 ,45	)ı =1•22
	n =0. 70	>=1.02

b) infra'red radiometric data

for	n =0,2i	;\=1, 72
	n =0,45	;\=1,02
	n, =0,70	;\=0, 83

Comparisons of the average cross-sections reveal systematic differences in values retrieved from different radiation sensors: estimates of S from the infrared radiometric data are 10 to 20% overestimated as compared to those retrieved from actinometric data.

Figures 3,4 present the averaged autocorrelation functions for direct solar radiation.They reflect the spatial-temporal variability of the cumulus cloudiness field in depe1idence of their amount.

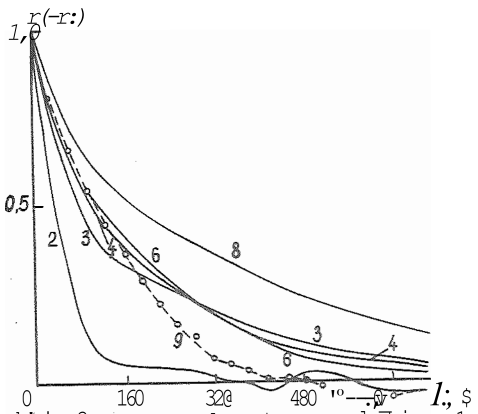

b':i.g,3, '·.remporal autocorrelation 1·unctions of direct solar radiation averaged by realizations (full amount of the data used is 190 realizations), Figures near the curves are cu.1JJulus amount (balls).

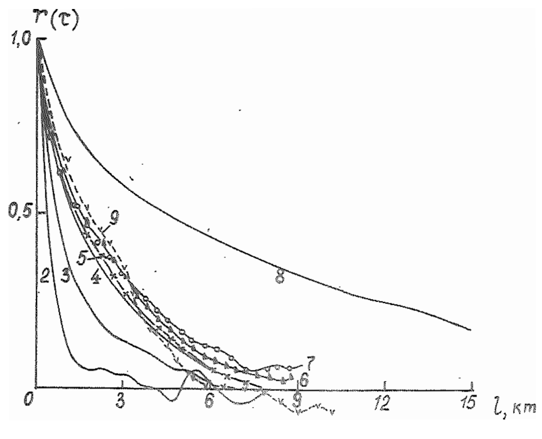

1.?ig1t40Spatial autocorrelation fu.nctio11...s of direct solar radiation averaged by realizations (full araounċ of che data used is 190 realizasiorlli).Figures near the curves are cumulus amount (balls).

The curves in .:?igure 3 were anprox2.matecl by means of the ::ollowing forr,rnl;s:

$$(., (r:) c e -cir ıı Jc- \quad (4)$$

$$\tau(\ell) \simeq e^{-ql1\ )ov} \quad (5),$$

where 7:"is expressed in seconds, ri. - in decimal points (balls) (n =1,2,J,..,9), v - the wind speed at the cloud level in mis¢

In Table 2 the values of °'- are given in dependence of n ,

Table 2

ıı	2	J	4-7	8	9
A,	1022	ıro30	0,64	0,37	0,55

Substitut tne data from Table 2 into the formula (4) we may assess the spectral density of the cumulus clouds temporal variability from th following expression:

$$s(w)==1hJ\ 11('C)Cos(wc:)cl'L \quad (6)$$

It appeared that within the 2-9 points range of cloud cover the maxi.mum values of spectral densities were observed at freouenci es i-i0-2 -o,5-10-2 s -i, respectively, while the mi11imu.m value is cut off at f=-i·i0-.1.s- (The latter corresponds to the cut-off frequency of the receiver-recorder system).

'fhe density versus frequency curve is linear in the:1-i0-!co,5,1d}'range. This part of the curve may fitted by the dependence of the following type: s(/),.... f(K) , where K approaches the value of 2. This result agrees quite **well** with the data from a referenced study(Ref,10), in which the values of SCw) were retrieved from the fluctuations of brightness of the cumulus clouds field. These were obtained from pictures of cumulu.ss clouds field taken from aircraft.

Variations in the intensity of direct solar radiation transmitted by Clliuulus clouds make it possible to distinguish opaque (op) cloud zones from semitransparent (sp) ones (Ref.7).

Respective amounts of cloudiness 11op and nsp are presented in 'l'able 3 in dependence of the total value n., =/11,op+ n 5p . 'fhese data were obtained in the region of l/ioscow.

Table J

i-lelationship between riop and n spat given YI,,

n	0,2	O,J	0,4	0,5
n_{op}	0	0,05	0,16	0,22
n_{sp}	0,2	0,25	0,24	0,28

1'able 3 (cont.)

n	0,6	0,7	0,b	0,4
nop	0,32	0,40	0,58	0,84
n5p	o,28	o,90	0,22	0,06

References

1. Kasatkina, O.r., Krasilshykov, L.B., Kropotkina, E.P. et al., 1972, On the task of objective retrieval of the characteristics of clou4iness (in Russian). Meteorologiya i Gidrologiya, N 8, P• 23-2 SJ.
2. Kuusk, A.E., 1978, Horizontal dimensions of trade-wind cumulus clouds (in Russian). In: Variability of cloudiness and radiation fields, Tartu, P• 70-80.
3. Gudimenko, A.V., Rudneva, L.B., Timanovskaya, R.G., Timanovsky, D.F., 1977, Linear demensions of cumulus clouds according. to the data from surface measurements (in Russian), Trudy Glav.Geofiz.Obs. 388, p.114-
4. Rudneva, L.B., 1976, Retrieval of the characteristics of cloudiness from the results of measurements of cloud radiation in the atmospheric transparency window 8-12 um, (in Russian), .Trudy Glav.Geofiz.Obs •• 363, p,44-50.
5. Rudneva, L.B., 1980, .(lssessment of cl0ud characteristics from the data of m•asurements of cloud radiation in the 8-12 um band in the Tropical At-lantic (in Russian), Trudy Olav.Geo-fiz.Obs •• 434, P•
6. Radiation in the cloudv atmosphere, 1981, Ed : Feigelson, E.M., Gidrometeoizdat, 280 P•
7. Timanovskaya, R.G., 1979, Optical density of cumulus clouds in the temperate latitudes. of the European territory of the USSR and the Tropical Atlantics (in Russian), Meteorologiya i Gidrologia. N 6, p.52-56.
8. Timanovskaya, R.G., Timanovsky, D.F., 1975, Determining the amount of cloudiness from continuous recordings of 'direct solar radiation (in Russian), Trudy Glav.Geofiz.Obs., 345, p.8-14,
9. Heat exchange in the atmosphere. 1972, Nauka, 152 P•
10. Istomina, L.G., 1966, On determining statistical characteristics of the spatial structure of cloudiness fields from air-borne photographs (in Russian), Izv.of the USSR Acad.of Sci. Phys. of the Atm. and Ocean, v.2, N 3, P• 31-33.

MICROSt;;ALE STRUCTURE OF CONVECTION IN STRATIFORM CLOUDS : AN OBSERVATIONAL AND NUMERICAL STUDY

Henri Sauvageot, Richard Auria and Bernard Campistron

Laboratoire d'Ae.rologie - Universite Paul Sabatier
.centre de Recherches Atmospheriques - 65300 Lannemezan - France

1. INTRODUCTION

The initiation of precipitations in clouds depends on the interaction between microphysical and dynamic processes. In order to study these interactions and to know accurately the precipitation initiation conditions, it is necessary to take into account the microscale structure of the field of motion because mean values are not representative for this purpose. To understand such processes is on of the main purose of the Precipitation Enhancement Project (PEP) sponsored py the WMO. This program aims at answering a maj r concern of the scientific community dealing with the possibility to modify the precipitation distribution in arid country from diverse kinds of clouds including stratiform species. This aim justified the use of the millimetric Doppler radar RABELAIS (35 GHz) (Ref. 1) in Spain during the selection site phase (SSP3) in 1981 (Ref. 2).

This paper describes some results from the study of a thin, low reflectivity altocumulus cloud. The RABELAIS radar was used to analyse the organization of the convective regions where precipitations are initiated. Reliable air motion measurements in the cloud were obtained from the observation of the non precipitating component of the scattering medium. Then the data on the observed field of air motion were introduced in a numerical simulation of the particle growth in the convective region. Simulated particle trajectories, radar reflectivity distributions and particle size spectra are presented and compared with the data.

2. REFLECTIVITY PATTERN

The data were collected on 21 Y.arch 1981 near Valladolid in Spain. Those presented are representative of the altocumulus cloud observed between 1400 and 2000 TU in an eastward flow associated with low pressure on the Atlantic ocean.

Fig. la shows a 10 mn period of the time-height distribution of the radar reflectivity factor (in dI!z) measured by the RABELAIS radar in vertical scan. The equivalent space scale indicated at the top of the figure is calculated for a horizontal velocity of 2Q ms- which is the average value measured by the radar in VAD scan.

The main features are a cellular structure in the upper part of the cloud above 6400-m. The cells are generating precipitation trails. Those are tilted by the vertical shear of the wind and merge in a layer with a more homogeneous reflectivity distribution-up to 4600 m. The temperatures -are -35 and -15 °C respectively at the top and at the bottom of the echo layer. The minimal reflectivity factor ob::;erv·ed in the echo layer is -18 dBZ and the maximal precipitation intensity is 0.1 mm-h-1.

3. DYNAMIC STRUCTURE

The RABELAIS radar is able to detect small hydrometeors with negligible terminal velocity. Then in clouds, vertical air velocity W is obtained-directly from the Doppler velocity of the smallest scatterers.

Knowing W and the mean Doppler velocity Vd it is possible to obtain the mean terminal velocity in still air V1 and then to calculate accurate V1-z relationships applicable locally (see for example Ref. 3). V1-z relationships are after used to calculate the air velocity in the precipitation region below the cloud, according to the equation :

$$\overline{W} = \overline{V_d} + \overline{V_1} \qquad (1)$$

Fig. lb shows the contoured time height cross. section of the air velocity obtained with the above mentionned method for the same cloud as in Fig. la. The largest W values (up to 1.6-2.0 ms-1) are-located at the generating cell level near the reflectivity maxima. The horizontal gradients of W are very sharp;. However it seems that the activity of the generating regions presents of the whole some perennity since the length of the trails implicates a generation time of more than about 1000 s. Fig. le shows the mean V1 values.

Fig. 2 represents the horizontal divergence **above** 6400 m calculated for a 5 mn period between 1913 and 1919 TU.from :

$$\text{div } V_h = -\frac{\Delta W}{\Delta z} \qquad \text{with } \Delta z = 75 \text{ m} \qquad (2)$$

In the generating region, absolute maximum values of divergence are about 10-2 s-1 ; negative values (convergence) are assoc-iated with updrafts, large reflectivity and large Doppler velocity variances and positive values cerrespond to the upper.part of the cells and to downdrafts and low reflectivity regions.

4. NUMERICAL SIMULATION

In order to analyse the connection between dynamic structures and distribution of reflectivity a numerical simulation has been stablished for the growth of particles put into the measured motion field. For the simulation it is necessary to have a complete descr.iption of the air motions including the horizontal component. Air motions had been calculated, assuming that in the middle vertical section parallel to the wind of a conve tive generatin cell, the circulation is approximately bidimensionnal. From the equation of continuity for an incompressible fluid, the horizontal component of the. air velocity is approximately :

$$u(x,z) + u_0(z) = -\int_{X_2}^{x_1} \frac{\partial W}{\partial z}(x,z)\, dx \qquad (3)$$

where uo(z) is the environmental wind.

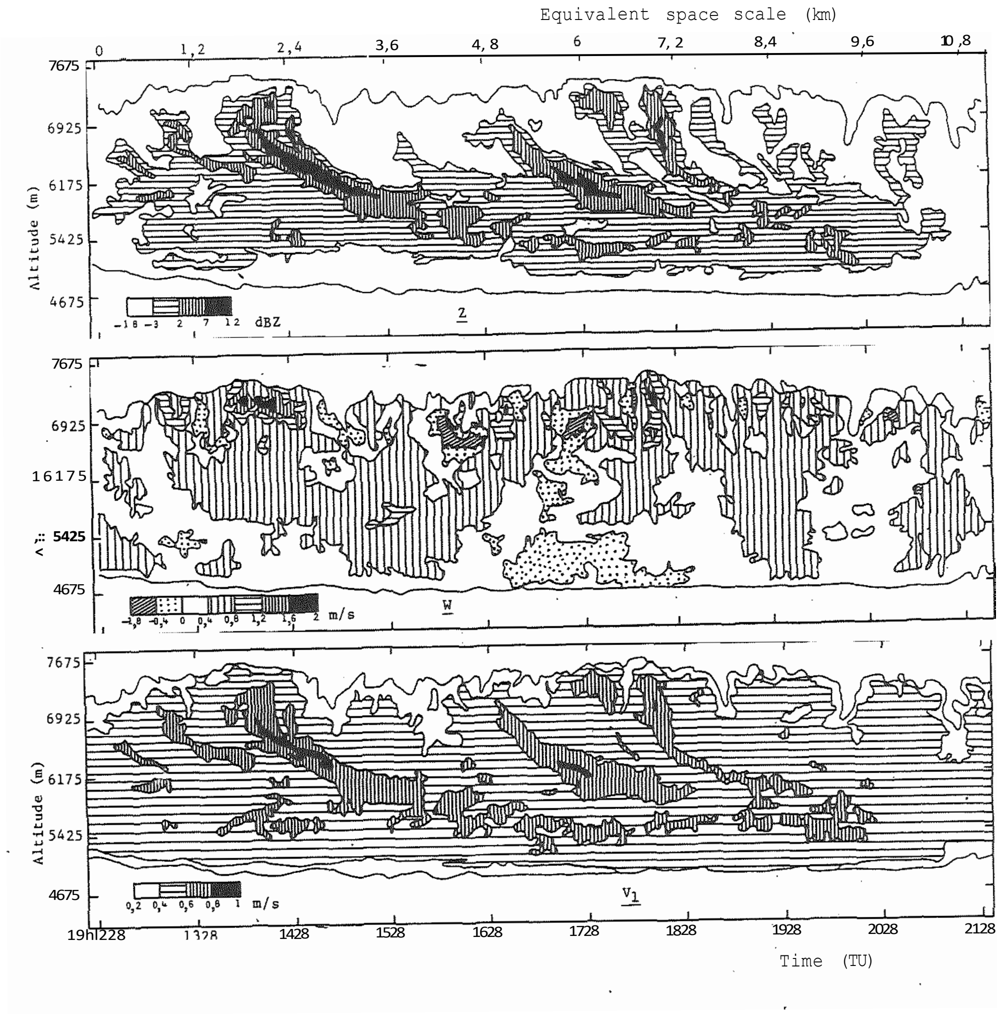

Figure 1. Contoured *time-height sections of (a) radar reflectivity factor, (b) vertical air velocity and (c) mean terminal velocity of hydrometeors on 21 March 1981.*

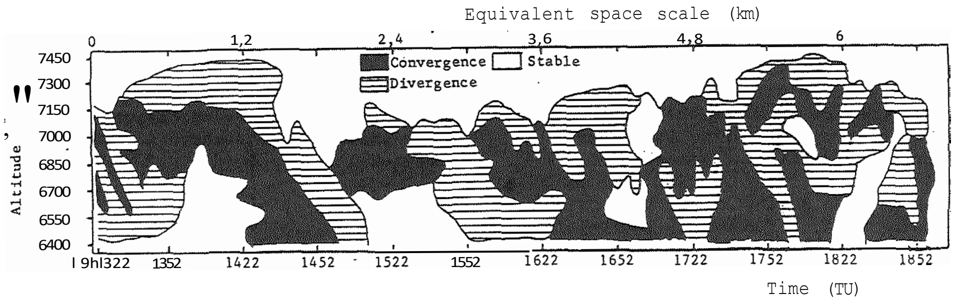

Figure 2. Horizontal divergence in the convective layer on 21 March 1981.

The u and W components are obtained after integration of Eq. 3 with a smoothing on 3 points, horizontally for W and vertically for u.

Fig. 3a shows the reflectivity distribution in one of the regions selected for the simulation. Fig. 3b represents the corresponding air motions calculated for an environmental wind profil constant with height.

In this case it can be assumed that the cloud particles are ice crystals growing by deposition of water vapor in excess in the upward air flow (on the model see Ref. 4).

The crystal trajectories are deduced from their velocities given by :

$$\vec{V}_c = \vec{W} + \vec{V}_1 \qquad (4)$$

Fig. 4 presents some examples of the crystal trajectories in the cell for diverse initial locations (x,z) of the embryos. We see that the particles undergo eventually several recycling in the updraft and that the growth takes place in the rising air between 191630 and 191650 TU whereas evaporation occurs in the downdraft between 191530 and 191610 TU. The particles leave the cell on the side of the updraft. These conclusions are in agreement with previous results (Refs 1 and 5).

Fig. 5 shows the distribution of the reflectivity factor Z given by the simulation for 2 values of N, the crystal concentration. The simulated contours agree well with the observed ones. Fig. 6 shows the corresponding particle size spectra through the cell. These spectra agree also with the experimental data (not presented).

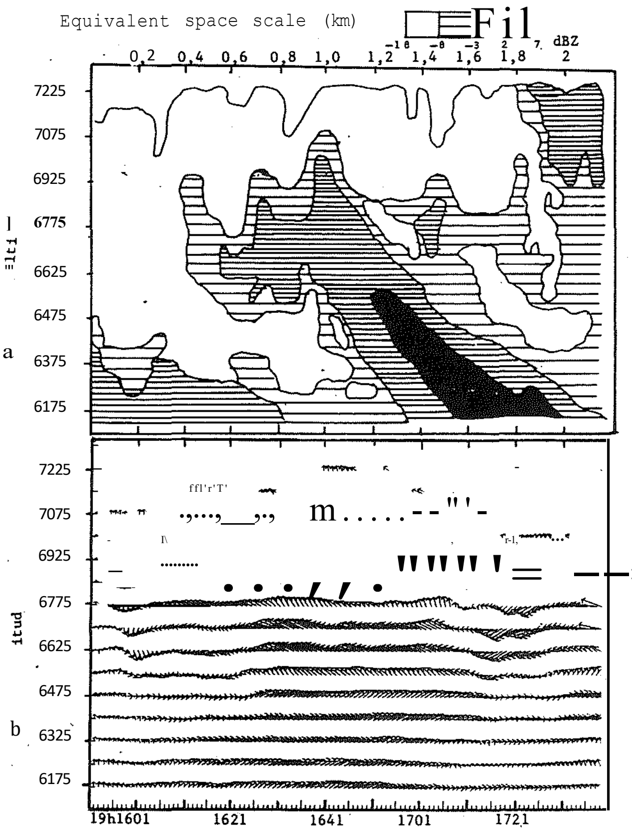

Figure 3. (a) Contoured time height section of a cell on 21 March 1981. (b) Air velocity vectors calculated for a bidimensional circulation in the cell of Fig. 3a.

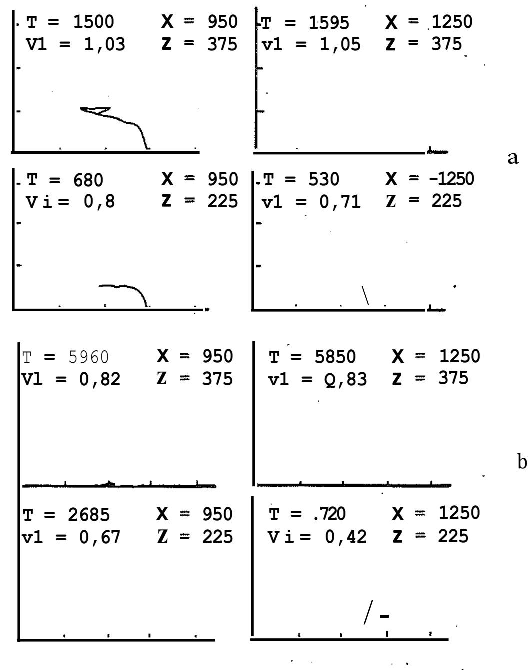

Figure 4. Examples of ice crystal trajectories in the cell of Fig. 3. T = time (s) for the total trajectory, V1 = terminal velocity at the ice crystal at the end of the trajectory, X and Z horizontal and vertical coordinates of the crystal at the beginning of growth.
(a) for 0.02 embryo cm-3
(b) for 0.2 embryo cm-3

5. CONCLUDING REMARKS

The partial results presented in this paper leave many unexplained points. They are a first approach on a particular case of the precipitation initiation study from Doppler radar observation of the microscale dynamic structure in precipitation generating clouds. The radar data show a structure which is not at all homogeneous but which has a strong organization with very sharp and correlated fluctuations in reflectivity and velocity. However, the length and continuity of the precipitation trails corresponding to cellular activity duration of more than 1000 s, partially justify the use of a velocity field measured at one time for the simulation of the precipitation particles growth. The simulated reflectivity patterns show caracteristics similar to the observed one with the main precipitation zone located on the upward part of the cell.

An uncertainty remains on the physical conditions prevailing in the cloud (presence of supercooled water). It can be noticed that the ideal tool to study such cloud structures is probably a millimetric Doppler radar with polarisation diversity on board of an instrumented aircraft ; such an instrument will be able to observe the dynamic and microphysical structure of generating cells during all their time life without degradation of the sensitivity and resolution of the data and with the possibility of some *in situ* measurements of thermodynamic and granulometric characteristics of the cloud.

a

b

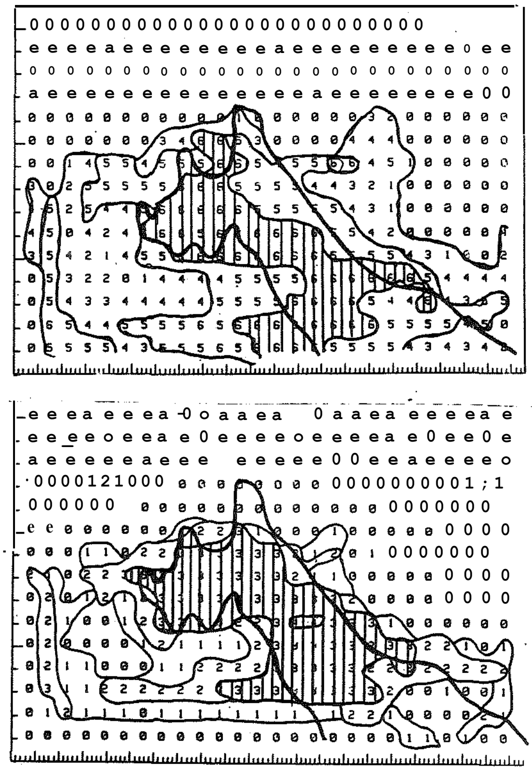

Figure 5. Simulated refle tivity factor contours for the air motions of Fig. Jb after 600 s (a) for N = 0.02·cm-3 and (b) for N = 0.2 cm-3• The numbers Dre Z V?lues by 5 dBZ step with 0 =- 30dB'Z, The thick line is the -3 dBZ measured contour.

a

b

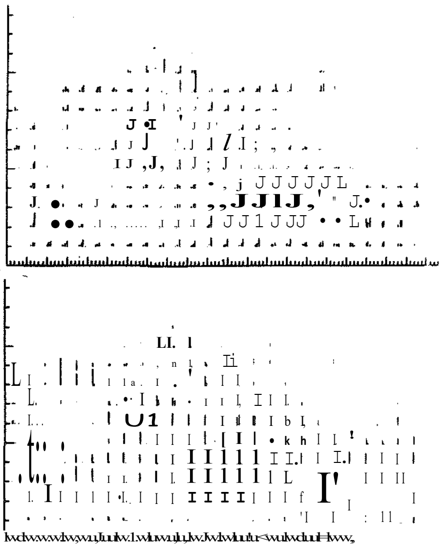

'Figw:,e 6. Simulated pa.rtiele size speetra through the eeZZ after 600 s (a) for N = 0. 02 em·5 and (b) for N = 0.2 em-5 for the same eeZZ as in Fig. 5, The speetra have 4 elasses between 20 a:n.d 5()0 t' m.

Acknowledgements. This work was supported by the Institut National d'Astr.onomie et de Geophysique, A.T.P. Recherches Atmospheriques under grant n°46-25.

6. REFERENCES

1. Sauvageot H, Auria Rand Campistron B 1982, Long-lasting precipitation cells in stratiform clouds, in ·cloud *Dynamics,* E.M. Agee and T. Asai Eds, D. Reidel Publishing Comp.any, 73-85.

2. World Meteorological Organization 1983, Studies based on data acquired by radar, *PEP Report* n°29, *Weather Modification Program,* WMO Geneva.

3. Sauvageot H 1982, *Radarmeteorologie,* Editions Eyrolles.

4. Auria R 1983, Etude par radar millimetrique Doppler de la·structure dynamique fine de la convection dans les nuages, *These de specialite* n°2807, Universite Paul Sabatier, Toulouse.

5. Sauvageot H 1973, On the fine scale structure of .precipitation generating cells, *J. Rech. Atmos.,* 8, 213-219.

SESSION IV

CLOUD DYNAMICS AND THERMODYNAMICS

Subsession IV-1

Stratiform clouds and cloud systems

BEHAVIOUR OF TEMPERATURE STRUCTURE PARAMETER IN CLOUD- AND CLEAR-AIR DURING THE SUMMER MONSOON :

P.C.S. Devara, A.Mary Selvam and Bh.V.Ramana Murty

Indian Institute of Tropical Meteorology, Pune 411 005, India.

1. INTRODUCTION

High resolution temperature observations were made in cloud-air and clear-air during aircraft horizontal level flights made at different heights in the lower atmosphere over the Deccan Plateau, India. Temperature fluctuations in the horizontal at different flight levels were studied by computing the temperature structure parameter ($C_T = \overline{(\Delta T)^2}/r^{2/3}$). These computations may be useful for the understanding of the dynamical characteristics of warm monsoon clouds as the C_T represents the turbulence characteristics of the eddies in the atmosphere. The results of the study are presented in the following.

2. DATA AND ANALYSIS

High resolution aircraft observations of dry-bulb temperature were made in cloud-air and clear-air environments in the lower atmosphere (10,000 ft ASL) over the Deccan Plateau India, during the summer monsoon season (June-September) of 1976. These observations were used for computing the C_T^2.

The details of the temperature sensor used for these measurements and its accuracy were published elsewhere (Refs. 1,2). The data were classified into two categories of days with active and weak monsoon conditions. This classification was based on the rainfall data recorded in the region of these observations and the associated synoptic conditions. The structure parameter (C_T) was computed using the temperature data for the consecutive levels of 500 ft intervals. The method of computation is based on that described by Wyngaard (Ref. 3) and the following equation was used for the computations.

$$C_T^2 = \overline{(\Delta T)^2}/r^{2/3}$$

where ΔT is the difference in temperatures between two successive points along the horizontal aircraft flight level separated by a distance of r (165 m).

3. RESULTS AND DISCUSSION

3.1 Active monsoon condition

The mean variation of C_T with height in cloud-air and in clear-air and the associated scatter diagrams for the active monsoon conditions are shown in Fig. 1. The large scatter in these plots may be due to the shorter averaging times (2-5 minutes) and the larger averaging heights (±250 ft) adopted in the present analysis. In cloud-air, the C_T^2 parameter slowly increased with height up to about 8750 ft level and thereafter decreased whereas in clear-air, it decreased up to about 5750 ft level and thereafter it increased. The variations in the mean temperature with height are shown in Fig. 2. The observed values of C_T^2 varied between 0.11 x 10^{-3} and 0.44 x 10^{-3} °C^2 $m^{-2/3}$ with an average value of 0.28 x 10^{-3} °C^2 $m^{-2/3}$ in cloud-air whereas it varies between 0.16 x 10^{-3} and 0.53 x 10^{-3} °C^2 $m^{-2/3}$ with an average value of 0.3 x 10^{-3} °C^2 $m^{-2/3}$ in clear-air environment. There appears to be an association in the variations of C_T^2 and the mean temperature particularly in the case of clear-air. The values of C_T and their variations in cloud-air are less compared to those in clear-air. This is consistent in view of the observations of temperatures in warm monsoon clouds reported by others (Ref. 2). The lapse rates of temperature in cloud-air were found to be less than those in the immediate environment particularly at the cloud-base levels.

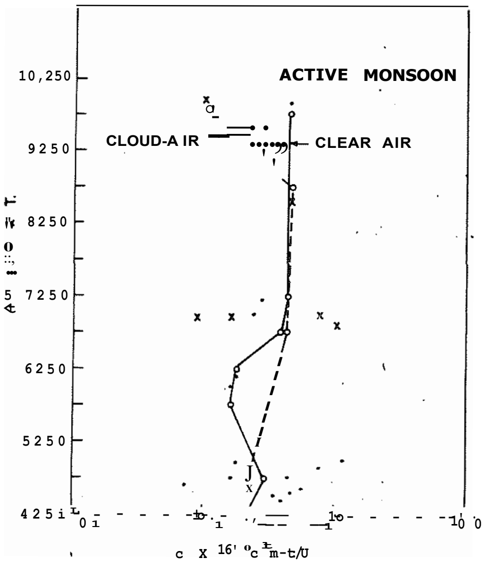

Figure 1. Variation of C_T with height in cloud-air and clear-air during active monsoon conditions.

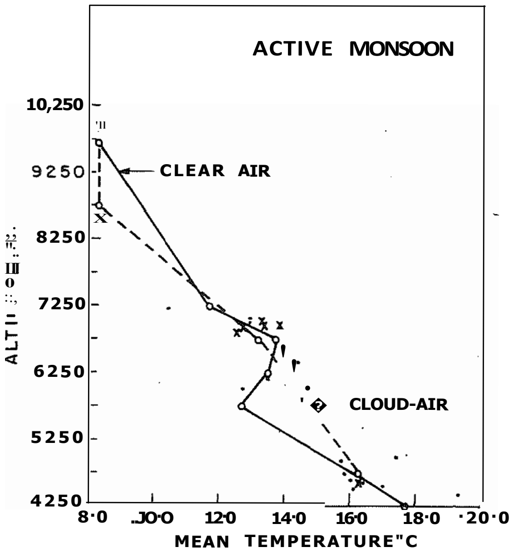

Figure 2. Variation of mean temperature with height in cloud-air and clear-air during active monsoon conditions.

3.2 Weak monsoon condition

The ,ean variation of c; with height in cloud-air and clear-air and she associated scatter diagrams for the weak monsoon condition#are shown in Fig. 3.. In the case of cloud-air the c; almost increased up to abocc 6750 ft and thereafter decreased with increase in height. The variations in mean temperature with height observed during weak monsoon conditions are displayed in Fig. 4. A close association can be seen between the variations of c; and mean temperature as in the case of active monsoon conditions. The observed values of C_T^2 ranged between 0.09 x 10 and o.66 x 10^{-3} $^oC^2$ $m^{-2/3}$ with an average v lue of 0.25 x 10^{-3} °C^2 $m^{-2/3}$ in cloud-air whereas it varied between 0.29 x 10^{-3} and 0.54 x 10^{-3} °C^2 $m^{-2/3}$ with an average value of 0.54 x 10^{-3} ^oC $m^{-2/3}$ in clear-air..

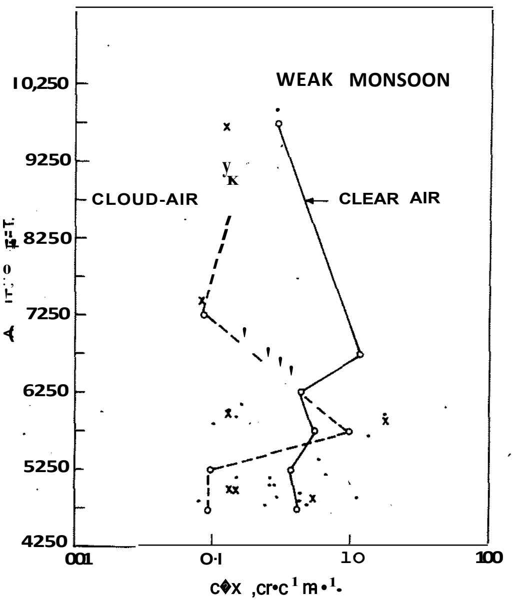

·igure 3. Same as Figure 1 during weak monsoon conditions.

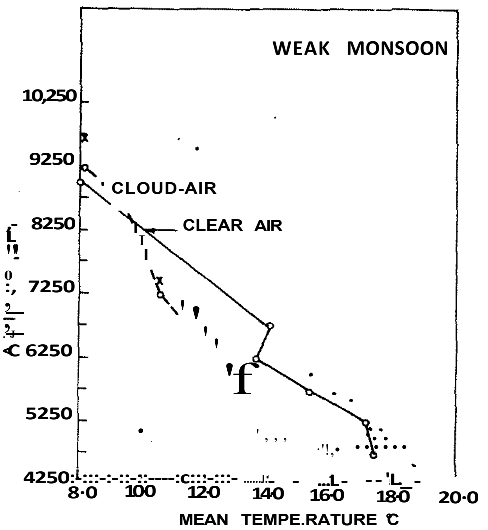

Figure 4. Same as Figure 2 during weak monsoon conditions.

The values of the· CT for the active and weak monsoon conditions are snown in Table 1.

Table 1

Values of temperature structure parameter (CT 10^{-3} °C^2 $m^{-2/3}$) in cloud-air and clear-air for the active and weak monsoon conditions.

Monsoon Condition	Cloud-air			Clear-air		
	Minimum	Maximum	Average	Minimum	Maximum	Average
Active	0.11	o.44	0.28	0.16	0.53	0.31
Weak	0.09	o.66	0.25	0.29	0..54	0.54

The values, during the active and weak monsoon conditions, are lower in cloud-air fhan those observe.d in clear-air. This is due to the difference in the lapse rates in temperature in cloud-air and its environment as explained earlier.

4. REFERENCES

1.. Vernekar KG and Brij Mohan, 1975, Temperature measurements from aircraft using vortex thermometer, Indian J Met. Hydrol. Geophys. 26, 253-258.

2. Mary Selvam A et al 1980, Some thermodynamical and microphysical aspects of monsoon clouds, Proc Indian 'Academy Sci, 89, 215-230.

3. Wyngard JC 1973, On Survace-layer Turbulence in Workshop on Micrometeorology, Haugen Ed American Meteorological Society, 392 pp.

CHARACTERISTICS OF TURBULENCE IN CLOUDS OF DIFFERENT TYPES

V.M. Ermakov, I.P. Mazin, S.M. Shmeter, V.I. Silayeva and li.A. Strunin
Central Aerological Observatory, Moscow, USSR

1. INTRODUCTION

Turbulence plays an important role in the entrainment of dry air into clouds of dif.ferent types and thus in cloud microstructure and precipitation formation. but inadequate amount of data on the structure of the turbulence field within clouds is still available. The main purpose of this study is to fill up the gap in these data. The paper summarizes the observations made in spring and autumn seasons, 1978-1980 within warm and cold frontal cloud systems over the European and F·ar-Eastern parts of the USSR. Fluctuations of the longitudinal (u') and vertical (w') components of air motion in the frequency range from 0.06 to 1 Hz were measured using a well instrumented aircraft Il-18D (flight speed 100-140 m/s). Instruments and measuring techniques are described in (Refs. 1, 2), where it is shown that the data on wind pulsations of spatial scales from 0.15 to 1.5 km are reliable. The sensitivity of the pneumoanemometer was not less than 0.1 m/s, the additional errors of measurements did not exceed 8 % for u and 7 % for w. The measurements have been performed at horizontal flight legs (runs).

2. TURBULENT ZONES (TZ) AND SOME CHARACTERISTICS OF WIND PULSATIONS WITHIN THEM

The part of runs witb standard deviation of pulsations σ_u and w not exceeding 0.1 m/s will be called hereafter calm (undisturbed) zones, whereas with σ_u, $\sigma_w > 0.1$ m/s turbulent (disturbed) zones. In Table 1 one can see the total length of the runs in different types of clouds (L) relative part of them (1/L) being occupied by TZ - may serve as a measure of turbulence. Intermittency of zones with $\sigma_{u,w} < 0.1$ m/s and with $\sigma_{u;w} > 0.1$ m/s is a common featu e of frontal layer clouds. The frequency of occurrence of different TZ length, met in the clouds of the given type, is presented in Fig. 1. TZ of high intensity ($\sigma_w > 0.2$ m/s), where according to aircraft cf6ud hysicist's conclusion embedded convection may occur, will be called convective zones (CZ) (Ref. 3). The horizontal dimensions of CZ quite frequently (20 % of cases) exceed 30 km. Horizontal dimensions of Cu, embedded in Ns-As (Cu emb.) seem to be comparatively large.

The components of wind pulsations in each TZ fairly fit the normal distribution of frequency. The deviat,ip n of mpiric distributions of ji = U J:YW11),J and '1.JJ. = = W•ji; (6"')j (i - being the numoer of th§ cloud, jw- the number of the zone, $\sigma_u^2 = \overline{u'^2}$, $\sigma_w^2 = \overline{w'^2}$) from normal distribution for every i,j does not exceed several per cent; According to Chebyshev criterion, the skewness of and - distributions Sk = M3/6, = o in 70-80 % of cases, and excess Ex = (f14/ 4) - 3 = O in 50 %.

The typical values of dissipation.rate of turbulent kinetic energy ε.cm²/s³ and mean values of σ_u and σ_w are presented in Table 1. The values of 50 % an 90 % quantile of - distribution are given in brackets. Here

6"" : 6' lA,m. t,..../ t,,, > Ow = Ow,m"m

and m runs over all numbers of-TZ in the clouds of the given type.

TABLE 1

The total length of flights (L) and relative part (1/L) and some characteristics of TZ in the clouds of different types

		Types of clouds								
		As-Cs	Ns-As	As	Cs	Ns-Sc	Sc	Ac	Conv. zones	Total
L (10³ km)		2.7	7.7	1.6	2.3	1.0	1.2	1.0	1.0	18.5
1/L		0.19	0.23	0.37	0.52	0.75	0.85	0.89	1.00	
$(\overline{u'^2})^{1/2}$	(m/s)	0.21	0.21	0.20	0.24	0.32	0.37	0.36	0.50	
$(\overline{w'^2})^{1/2}$	(m/s)	0.21	0.21	0.19	0.23	0.34	0.38	0.40	0.64	
ε_u	(cm²s⁻³)	1.5	3.2		2,9	7.7	13.4	11.4	29.0	
		(0.5-5.0)	(2.5-5.5)		(1.5-8.0)	(6.5-13.0)	(9.5-19.5)	(9.5-19.5)	(15.0-70.0)	
ε_w	(cm²s⁻³)	1.1	2.2		2.4	8.5	14.3	18.1	57.o	
		(0.5-2.5)	(1.0-4.5)		(1.0-6.0)	(4.0-22.0)	(8.0-40.0)	(8.0-40.0)	(24.0-150.0)	

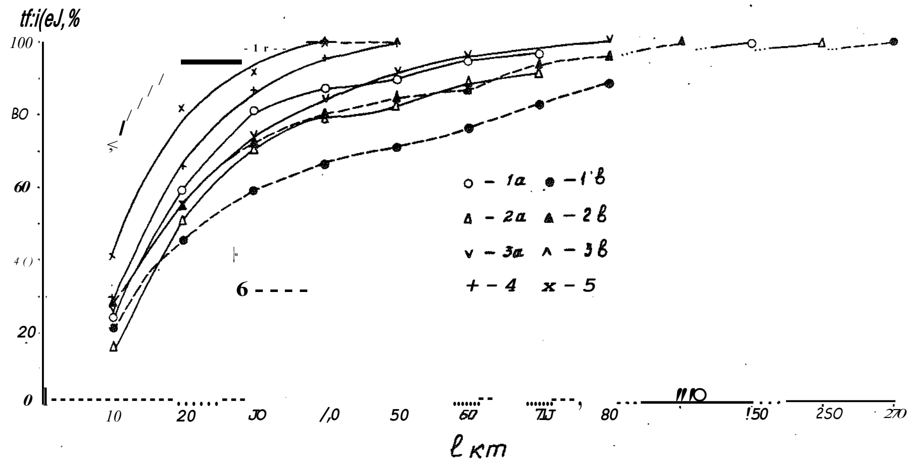

Figure 1. The empirical distribution of TZ length (a) and length of the undisturbed zones (b) in the clouds of different types 1-Ns-As, 2-Cs, 3-Sc, Ac, 4-Convective zones, 5-Cu emb.

3. SPECTRAL CHARACTERISTICS OF PULSATIONS

The spectral densities of horizontal $S_u(k)$ and vertical $S_w(k)$ wind speed pulsations were found by Fourier-transformation of autocorrelation function.

$$S_{u}(k) = 2\int_0^{\infty} R_u(\lambda) \cos k\lambda \, d\lambda$$

where k is a wave number in m-1.

As it is seen from Fig. 2 the averaged Su and Sw curves fit well enough the so-called "minus five-thirds" law in the wave length range from 150 to 1000 m.

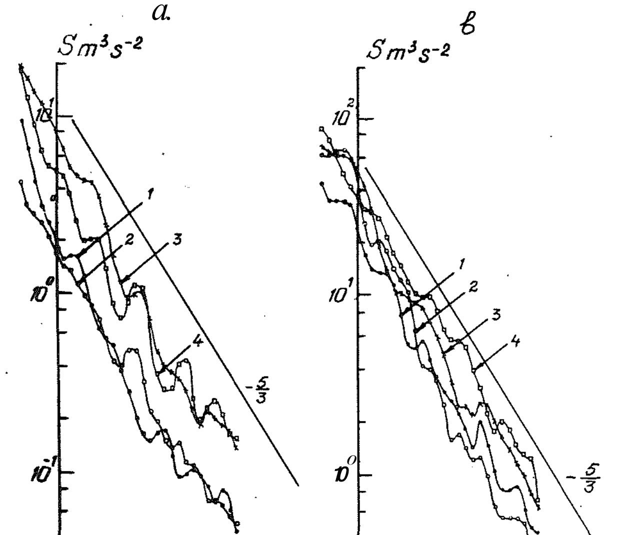

Figure 2. The typical curves of spectral density of vertical (1, 3) and horizontal (2, 4) pulsations.

a) 1, 2 - outside the clouds, December 5, 1978, flight level H = 1.8 km,
3, 4 - homogeneous Ns, November 26, 1979, H = 1.2 km
b) 1, 2 - Sc, April, 1979, H = 1.1 km,
3, 4 - Ns with convective cells, December 5, 1979, H = 1.2 km.

Energy spectra plotted in semilogarithmic coordinates (not presented here) show pronounced local maxima at λ 900 - 1000 m (Ref. 2), which imply the existence of turbulent energy-carrying interval of turbulence near such wave length. The secondary maxima of kS(k) in Ns with Cu emb are often observed at λ 600 m.

For every case dissipation rates ε were computed according to (Ref. 4).

$$\varepsilon_{u,w} = C_{u,w}\, k^{5/2}_{u,w} S^{3/2}_{u,w}$$

where

$C_u = 0.14$, $C_w = 0.19$

Distributions of ε_u and ε_w values in different cloud types are given in Fig. 3.

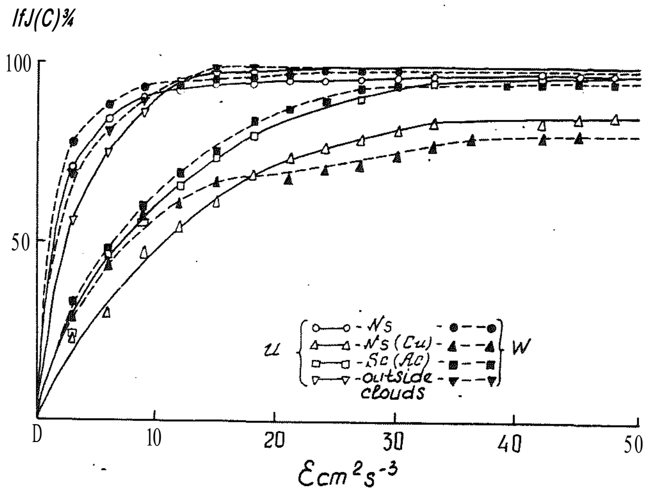

Figure 3. The empirical distributions of dissipation rates of turbulent energy ε for the clouds of different types and outside the clouds.

In calm Ns, As the values of ε are of the same order as in clear air and do not exceed several cm^2 s-3. In CZ ε reached 10 cm s-3, i.e. the values, typical for Cu Cong.

4. ANISOTROPY OF WIND SPEED PULSATIONS

In fact, the distributions of values of σ_u and $6'_w$ for TZ in As, Ns-As, As-Cs, i.e. ф ((fu) and ф (6'w) practically coincide. It means that on the average the e is no preferable direction of wind speed pulsations in the clouds of these types. For a separate TZ the values of $6'_u$ and $6'_w$ are usually not equal. Relation 6',,J6'w may serve as a measure of anisotropy. The distributions ф, (w/ ...) for layer, wave-like and Cu emb. clouds are presented in Fig. 4.

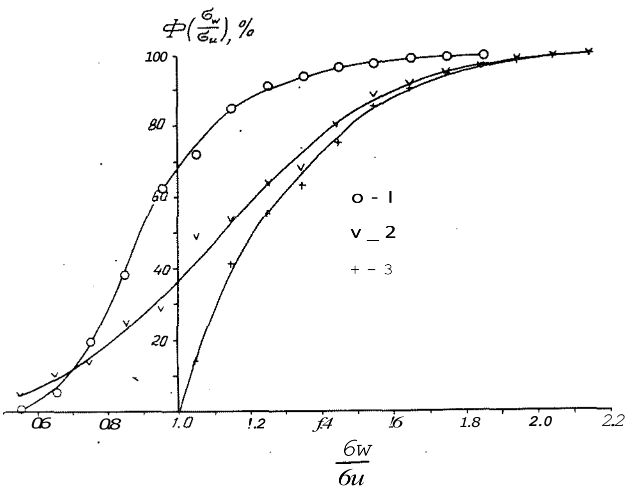

Figure 4. '.Ehe distributions of (fiw/6'...) values for clouds of different types. 1 - for layer clouds, 2 - for wave-like clouds, 3 - convective zones.

The fact that Ow /fi,, differs from unity is likely due to convection interfering with turbulence. Convection is more intensive and occurs more frequently in wave clouds and naturally, in Cu emb, where (Ow/ 6'...) > 1. Obviously in convective clouds ф(f5;) dpes not coincide with ф(6''w).

5. CONCLUSION

The collected data enable us to reveal statistica.l regularities of spatial inhomogeneity of turbulence in different types of-clouds. The uantitative peculiarities of intermittency of turbulence and the length of TZ lead to the conclusion that unlike cloud microstructure, they are markedly different in stratiform and wave clouds.

The conclusion about the normal distribution of wind pulsations is usually quite acceptable for various purposes. However, sometimes Ex > 0 and Sk ≠ 0 (Ref. 2), being indicative of small-scale intermittency, namely the presence of some heightened number of calm areas in TZ.

we think that in order to study the effect of turbulence on the development of cloud microstructure it is necessary to extend the spatial range of the measured wind pulsations by shifting the minimum scale to values less than phase scale '1p (Ref. 5), equal to several metres.

6. REFERENCES

1. Dmitriev, V.K. and Strunin, M,A., 1983. Aircraft measurements of the. vertical components of wind speed pulsations,. Trudy CAO, Issue 147, 39-51 (in Russian).
2. Strunin, M.A., 1983. Airborne pneumoanemometer for measuring pulsations of horizontal components of wind speed in clouds, Trudy CAO, Issue 147, 26-38, (in Russian) •
3. Mazin, I.P., Silayeva, V•I. and Strunin, M.A., 1984. Turbulent pulsations of horizontal and vertical components of wind speed in clouds of different forms, Izvestia Academii Nauk SSSR, Fizika Atllosfery i Okeana, No. 1, 10-18, (in Russian).
4. Ermakov, V.M., Silayeva, y.I., Strunin, M.A. and Shmeter, S.M. 1984. Turbulence in the atmosphere of frontal clouds, r-leteorologia i Gidrologia (in Russian).
5. Mazin, I.P. and Shmeter, S.M., 1983. Clouds, their structure and formation, Leningrad Gidrometeoizdat; 279 pp. (in Russian).

INVES'l'lGATIOiiTS OF CLOUD SYS'J:EMS AT THE PEP SITE IN SPAIN

B.P.Koloskov, Yu.V.Melnichuk and Yu.S.Sedunov

Central Aerological Observatory, Moscow, USSR

1• INTRGDUCTION

The success of solving of many scientific and practical tasks related with investigation of the processes of precipitation formation and cloud system development to a great Bxtent depends on quality and pl'.'Omptitude of obtaining information about microphysical characteristics of clouds and specifically, liquid water content (LWC). In view of the extremely important role of supercooled liquid water (SCLW) for processes of cloud and precipitation development, its distribution within cloud systems presents particular interest. One of the main objecti- ·,es of the PEP Site Selection Phase 3 (SSP-3) was to assess suitability of cloud systems in the Duero River Basin of Spain for seeding to increase amount of precipitation over the area. Essential element of such assessment is information about SCLW within the cloud systems in the area, their spatial distribution and temporal evolu ion.

The detection of the regions with SCLW within clouds and their investigation have been carried out mainly with specially instrumented aircraft. Along with the unquestionable advantages, sircraft observations of cloud microphysics have intrinsic limitations, such as spatial and time insufficiency-of data collection and the impossibility of simultaneous observation of clouds in large area. The latter is the more important, the larger is the experemental area and the greater is the horizontal extent of explored cloud systems. The analysis of PEP data showed that widespread cloud systems, defined by the PEP cloud classification as class A clouds (Ref.1), are the main rain-forming systems over the PEP area. Such systems give 70% of winter-spring (January-May) seasonal precipitation amount and due to this they are the most interesting object for seeding increase the amount of precipitation over the area.

The first investigasions of the class A clouds carried out during the 1979 season by the University of Wyoming (USA) Queen Air aircraft showed that the SCLW regions as a rule had small sizes and were randomly distributed with the cloud systems. Besides, SCLW regions were detected by the aircraft only for one in every six class A cloud systems (Ref.1). However, it is obvious that during such investigations one must -supplement the aircraft in-situ measurements by remote observations providing, in principle, data over the whole area. Unfortunately, it is necessary to ascertain the fast of the absence of remote methods for operative detection of the LWC zones.

Taking into account significance of information about liquid water in clouds and systems, task of the remote detecting SCLW in the different type of clouds was declared to be one of the main objects of the 1981 PEP field season (the meeting of the PEP principal investigators in Montreal, December 1980). During the season Soviet team suggested new radar technique of operative detecting SCLW regions in clouds and cloud systems, using data about wind field inhomogeneities in the boundary layer. The description of the proposed technique and results of investigations of the main rain-forming cloud systems over the PEP rea (class A) are presented below.

2. RAD.AR TECHN"IQUE OF DETECTING SCLW REGIONS IN CLOUD SYSTEMS

The method is based on the relationship of microphysical characteristics with cloud dynamic. It is known, that the characteristics such as liquid water content, cloud droplet size distributions, particle concentration and phase structure of clouds are to a great extent defined by the vertical drafts. In this connection,· spa tial structure of cloud microphysical parameters and, especially, LWC are defined by spatial structure of the vertical motions (Ref.2,3). In one's turn the vertiacal flows determining cloud-and rain-forming processes are related with horizontal motions in the atmospheric boundary layer where the flows are formed (Ref.4,5). If. there is such relationship the information about the horizontal motions in the atmospheric boundary layer may be used to evaluate the cloud microphysical characteristics and, especially, SCLWC.

To st dy this possibility it is necessary to carry out experimental investigations, including the A/C measurements of cloud microstructure and measurements of motions in the boundary layer. Program of SSP-3 field investigations provided realization of these experiments. The Soviet radar WU.-5 was equipped with the "Device or indication of turbulence" (DIT)(Ref. 6) ch allowed us to discover and depict on the radar indicators the zones of clouds and precipitation with difference of radial velocity components (& V) on the scale of 500 m exceeding a threshold value, i.e. to detect radial velocity inhomogeneity areas (RVIA). DIT was successfully used for sty typical air flow structures in Cb eRef. 6). The PEP field investigations in Spain were the firs! experimental utilization of DIT for st ng widespread cloud systems. In Fig. 1(b) and 1ld) the examples of RVIA distributions in horizontal and vertical planes, respectively, are presented for one of the class .A events observed over PEP area. "White" regions in the pictures correspond to zones with value LLV?1,6 ms-1. In Fig.1(a) and 1(c) radar reflectivity pictures, corresponding to the Fig. 1(b) and 1(d), are presented. Radial velocity differences 4 V measured with the anterw.a angular altitude less than 3-5° depend on smallscale turbulence

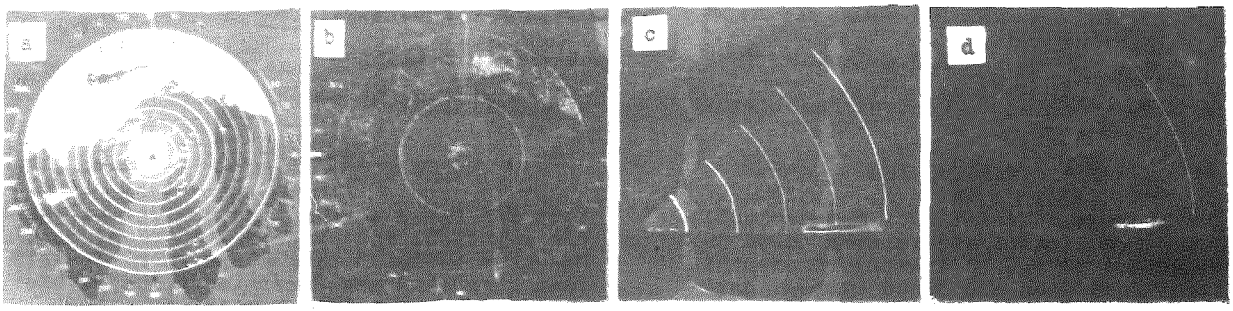

Fig.1. Photo rafphs of PPI (a,b) and BHI (c,d) displays with radar echoes (a,c) and RVIA tb,d) distributions. Range markers are 10 km (l'PI) and 20 km (BHI).

and mesoscale inhomogeneity of horizontal wind in the atmospheric boundary layer. The experimental evaluation of the component for RVIA shows that its level for class A cloud systems does not exceed 0,7÷1,0 ma-1. Hence the detection of RVIA with ΔV 1,3 ms-1 shows the presence of mesoscale divergence and/or convergence. If their vertical extention is higher 0,5-1,0 km they are quasiregular vertical drafts greater 0,5-1,0 ms-1. Doppler radar measurements of vertical velocities over RVIA show, that when ΔV 1,0-1,6 ms-1 a number of intermittent updrafts and downdrafts at the height 1-2 km are observed. Their velocities are up to 1-2 ms-1 and horizontal extention 0,5-2 km. Considering the relationship of updrafts with the amount of cloud condensed water we can expect higher water content in supercooled cloud portion over these zones in compe\rison with the zones without these strong movements.

3. EXPERIMENTAL STUDIES OF RELATIONSHIP OF RVIA WITH SCLW ZONES

The data obtained with the Soviet MRL-5 radar and microstructure characteristics collected by the .American "Queen Air" and kindly made available to the participants of SSP-3 by the head of the american group Dr. G.Vali were used. The presentation form of the aircraft data and A/C instruments were described in the PEP Report 15 (Ref.?).

The first comparison of radar and aircraft information showed a higher probability of finding SCLWC in flights over RVIA compared to that outside of these zones. However, in some cases QA encountered SCLW zones and at the same time RVIA were not detected. In Fig.2(a), part of QA track for 20 Kay 1981 is shown. Fig.2(a) shows that at the moment 1040Z-1055Z there was no RVIA with value ΔV 4'1,3 ms-1 in the flight area and at the same time the aircraft recorded SCLW with Q:0,1-0,4 gm-3 at altitude of 3,5 km (temperature -11°C).

The following analysis showed that when flighing at an altitude above 2-3 km the aircraft detects SCLW zone if RVIA with ΔV;,:,1,3 ms-1 llai:Ibeen en QW!1.t•Ni in the boundary layer 30-50 min before the moment of A/C penetration into the zone (Fig.2(b)

This time delay determines the time required for rising moist air from 200-300 m (the RVIA detection mean level) to aircraft level when updrafts over RVIA are 1-2 ms-1. Owing to this delay one should to compare A/C data with RVIA pattern, observed 30-50 min before the moment of flight. With this purpose tracks of he QA flights were drawn, using the vector of the radar echo movement i.e. tracks were f,lotted over each relatively "frozen" RVI.A 'image". Fig. 2 shows an example of the plotted track over RVIA "images" for 20 May 1981. At the moment when QA encountered SCLW, RVIA were lacking (Fig.2(a)). However, one can see in Fig.2(b) that RVIA with a ΔV ≥ 1,3 ms:-1 existed in this part of cloud system 40 min before. The zones of RVIA conditioned the formation of vertical drafts and as a result, the appearance of SCLW at the level of QA flight. Analysis showed that the aircraft recorded SCLWjust during flight over this RVIA "image" (Fig. 2(c)).

During the analysis it is necessary to keep in mind: a) inexact determination of A/C co-ordinates over radar pictures; b) inexact determination of RVIA "image" positions owing.to inevitable errors of defining vector of the zone movement. In this connection, comparison was made for the regions corresponding to RVIA "images" linear sizes of which were increased to 5,0 km (1,0 min time intervals of the aircraft flight), These regions are marked as RVIA1,

To estimate possibility of the employment of RVIA information for detection of SCLW zones in the cloud systems, all events (10 caces) of joint aircraft and radar investigations of widespread cloud systems in the 1981• season at the PEP area were analysed.

For every case the distributions of flight time when the LWC exceeded given levels were plotted, For every one minute interval both mean ($\bar{Q}$) and m (Qmax) values of SCLWC were determined. Q and Q ax. were calculated according to graphs or we along the track QA flight. The distributions were plotted for the flight legs when: 1) QA flew at altitudes with temperature range 0,. T.,.-15 C; 2) QA flew above the regions of radar echo, with observed angular altitude 0,3° i 3) aircraft detected liquid or ice cloud particles. These graphs show the probability of finding differe t values of SCLWC in rainy clouds.

Fig.3 gives the probability of finding SCLWC averaged over all the events of the observations for RV (PR) and for radar echo zones (Pp_R) without RVIA4.

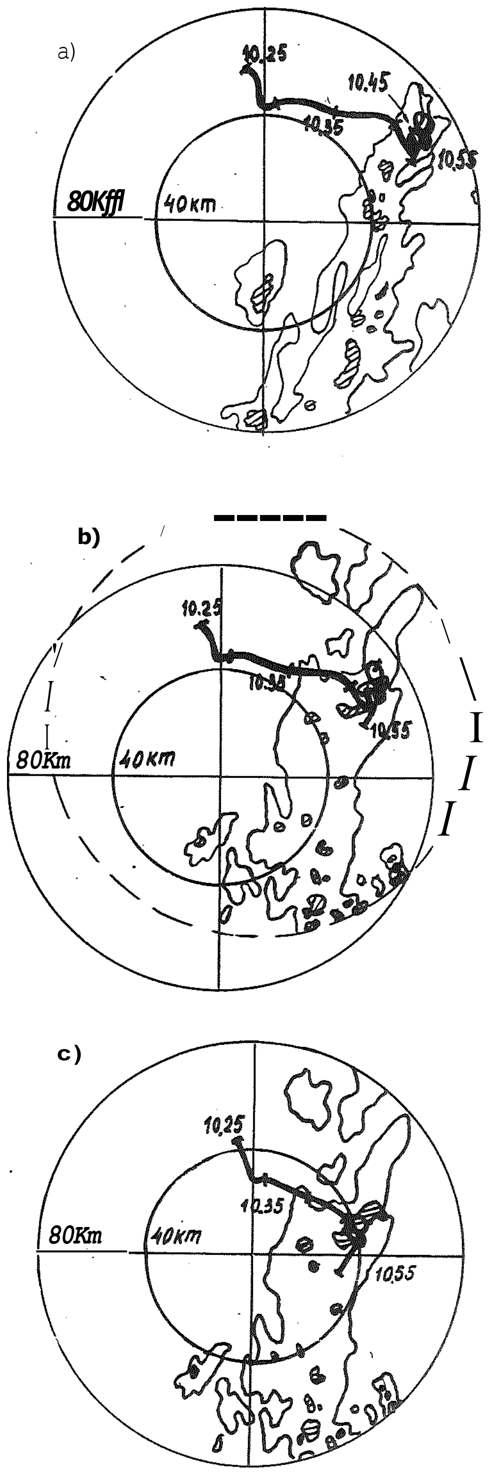

Fig.2. Flight track from 1025Z to 1055Z on 20 May 1981 and the position of the radar echo aud *RVIA* (shad regions) at 1048Z(a), 1010Z(b) and RVIA "images" at 1010Z(c).

The Fig.3 shows 1hat probability of finding3SCLW with Q and Qmaz from 0,02 to 0,1 gm- in cloud above RVJ.A1 is on the average 2,5-3 times greater, that when flying out of these zones.

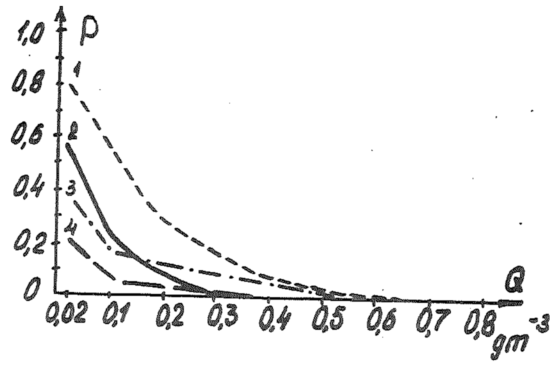

Fig.3. Probabi!ity distribution of detecting given mean (Q) (3 and 4) and maximum (Qmaz) (1 and 2) SCLWC in the class A clouds: 1 and 3-above RVl11 "images"; 2 and 4 - within the precipitating clouds without RVIA1.

Similar results have been obtained in the analysis of separate observational days, although there are variations. of . the probability of finding SCLW, due to distinctions in thennodynamical conditions of the atmosphere on different days. In particular, PR1 value for ti:a0,02 varies on different days from 0,33 to 1,0. (The observations on 26 February 1981 were as an exceptional case. On this day a very strong inversion was observed at the altitude 1,3 km with 1=-2°C and aircraft detected SCLW with Q 0,1 gm-3 only below this level). For all cases the probabilities of finding SCLW above RVIA1, as on the averr.3e, were 2-5 times greater than out of these zones.

The obtained probabilities were used for calculation of SCLWC values in different parts of cloud Gystems. These assessments show that the average SCLWC values above RVIA1 were always greater than out of these zones. Mean values are 0,057 and 0,019 gm-3 respectively, i.e. mean LWC value for zones of the increased motions is 3 times greater than out of these zonea

The obtained estimations of finding SCLW prove the relationship of RVIA "images" with zones of supercooled liquid water and indicate the possibility of using radar data for detection and even forecast of the zones in cloud systems.

4. SPATIAL AND TIME EVOLUTION OF SCLW ZONES .ACCORDING TO RVIA DATA

Owing to obtained relationship of RVIA "images" with the areas of SCLW, information about such characteristics,as relative coverage of precipitation area with RVIA, the typical size and lifetiD'e of these zones are of interest.

For all the days under consideration the diurnal variation of the overlap of precipitation area (Ar,) with RVIA (AR) was plotted. Fig.4 gives the mean ARIAp values f r different days with the range of values for the 1981 class A cloud systems and this give8 also mean Al-{/Ap values for RVIA1. Fig.4 shows that AR/Ap for RVIA with A V 1,3 ms-1 varies during a day and from day to day. But it is extremely important that these zones exist in all widespread cloud frontal systems and practically during the whole period of passing of these systems through the radar observational area. The mean daily values of AR/Ap vary from 2 to 18% with the mean value of 8% for all days. The overlap of precipitation area with RVIA1 on the average for all days is 46% that is 6 times greater than the RVIA.

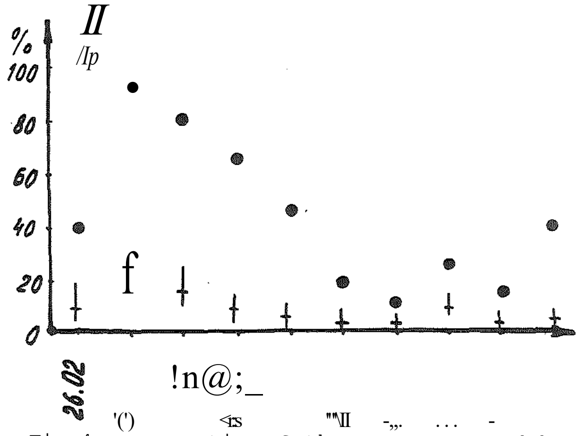

Fig.4. The ratio of the area covered by .RVIA **(+),** RVIA1 (e) to the total radar echo area at the lowest elevation angle for A-type cloud systems. Vertical lines denote the deviation of the values during day.

From the point of view of cloud and precipitation. development, it is very important to have information e.bout SCLW region lifetime. Taking into account the relationship of the RVIA "images" with the areas of SCLW zones an analysis has been for RVIA lifetime. Fig.5 gives the lifetime values versus the area of RVIA. It shows that lifetime is greater for the larger areas (RVIA dimensions). For RVIA of 10 km2 the lifetime is on the average 15-20 minutes and approahes 40-50 minutes for areas in order of 50 km.2.

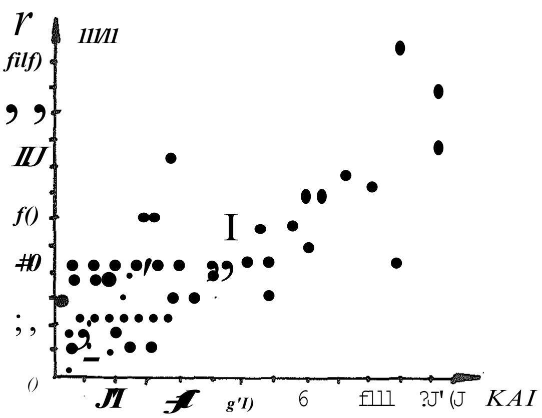

Fi7.5. RVIA lifetime values vs.their area

5. CONCLUSIONS

During the investigations of cloud systems over the PEP experimental area in Spain the radar technique of detection of the SCLW zones ln the cloud systems was developed and checked up. Radar technique based on an analysis of the information about in homogeneity wind field in the boundary layer of the atmosphere allows to distinguish in cloud and frontal systems the most "active" regions. These regions are apparently "embedded" convection zones where there are intensive inflow of water vapour from low altitudes and efficient involvment of the latter one in processes of cloud and precipitation forntation, The obtained relationship of RVIA "images" with SCLW zones allows us to assess some parameters of these zones from similar parameters of the RVIA. An analysis of the radar and aircraft data allowed the determination of the following characteristics of class A cloud systems for the 1981 season: mean SCLWC in raily clouds in the experimental PEP area; relative coverage of the experimental area with precipitation zones; mean LWC in rainy clouds over the RVIA and outside of it; dimensions of SCLW zones and their relative overlap of the precipitation area; lifetime of the SCLW zones of varions sizes. These parameters may be useful in numerical models of widespread cloud systems. This is essential when solving the problems of cloud seeding with the object of increasing the amount of precipitation over an area.

6. REFERENCES

1. PEP Report N 28, 1982, Preliminary assessment report of the site selection phase-3 of the precipitation enhancement project, Geneva, 168 p.
2. Heymsfield A,J., 1977, Precipitation development in stratiform ice clouds: A microphysical and dynamical study, J. Atm. Sci., v. 34, N2, p•.367-381,
3. Mazin I.P., 1983, On the phaze reconstruction of clouds, Meteorologiya i gidrologiya (in Russian), N7, p.34-44,
4. Chen C.H. and Orvill H.D., 1980, Effects of mesoscale convergence on cloud convection. J. Appl. Met., 3, p. 256-274,
5. Ulanski S.L. and Garstang M,, 1978, The role of surface divergence and vorticity in the life cycle of convective rainfall, Part I: Observation and analysis, J. Atm. Sci., v. 35, N 6, p. 1047-1062.
6. Chernikov A.A., Ivaaov A.A., Melnichuk Yu.V., 1975, The turbulence structure in cumulonimbus clouds, Proc. 16 Rad. Met. Conf., Houston, ·.:exas, p. 134-137.
7. PEP Report N 15, 1980, PEP Site Selection Phase-3, 1979 FIELD PROGRAMM-Overvisw and Data Catalogue, Geneva, 38 P.

COMPARISONS BETWEEN A MIXED LAYER MODEL AND HIGH RESOLUTION AIRCRAFT OBSERVATIONS OF STRATOCUMULUS

S.Nicholls

Cloud Physics Branch, Meteorological Office
Bracknell, Berks, UK

1. INTRODUCTION

The ability to predict the behaviour of layer cloud, and in particular stratocumulus, is of great importance to a wide range of meteorological activities e.g. the presence of extensive sheets of layer cloud and the accompanying changes in the radiation balance can markedly affect both short term forecasts of surface conditions and atmosphere-ocean interaction on timescales relevant to climate simulations. However, despite the recent increase in model studies (Refs. 1-3), the dynamics of such layers are surprisingly little understood and many of the assumptions implicit in these models have not been tested against observations. This paper presents results from an observational study using an instrumented aircraft which are interpreted within the framework of a mixed layer model, enabling the effectiveness of such models to be assessed. A full account of this work appears in Ref. 4.

2. MEASUREMENTS AND MODEL DESCRIPTION

The results were obtained in thick, horizontally uniform stratocumulus over the North Sea by the C130 aircraft of the Meteorological Research Flight on 22 July 1982. Measurements of cloud microphysics together with turbulent and radiative fluxes were made on horizontal (60 km) runs and during ascents and descents ('profiles'). The fast response turbulence instrumentation has been described in Refs. 4, 5. The cloud physics probes consisted of a noseboom-mounted Johnson-Williams liquid water content sensor and PMS probes located in the undisturbed airflow on underwing pods to count and size particles in the (radius) ranges 2-24 μm (ASSP) and 12.5-500 μm (OAP).

The cloud was located in the upper half of the boundary layer (Fig. 1), being about 450 m thick. Within the boundary layer, the conservative variables θ_e and q_T (see Appendix for nomenclature) were approximately constant with height, a sharp temperature inversion of 5°C at cloud top marking the upper boundary.

Within the cloud layer, the increase in q_l with height was accounted for by an increase in droplet size, r_v increasing to about 10 μm near cloud top, the total concentration remaining constant. This is apparent in Fig. 2 where the concentration of droplets larger than a particular size, r, increases with height if r < 20 μm. For larger drops, the opposite is true which suggests that droplet growth up to r ≈ 20 μm is dominated by condensation with coalescence important at larger radii. Note that significant concentrations of drops up to r ≤ 150 μm were observed both within cloud and beneath in drizzle.

The results shown in Figs. 1 and 2 suggested that a one dimensional mixed layer model, similar to those in Refs. 1-3 would, with some modification, adequately describe the main observed features.

The central assumption of this class of models is that internal mixing is sufficiently thorough that vertical gradients of conserved quantities are negligibly small. If horizontal advection may also be neglected, conservation laws for θ_e and q_T may be expressed as

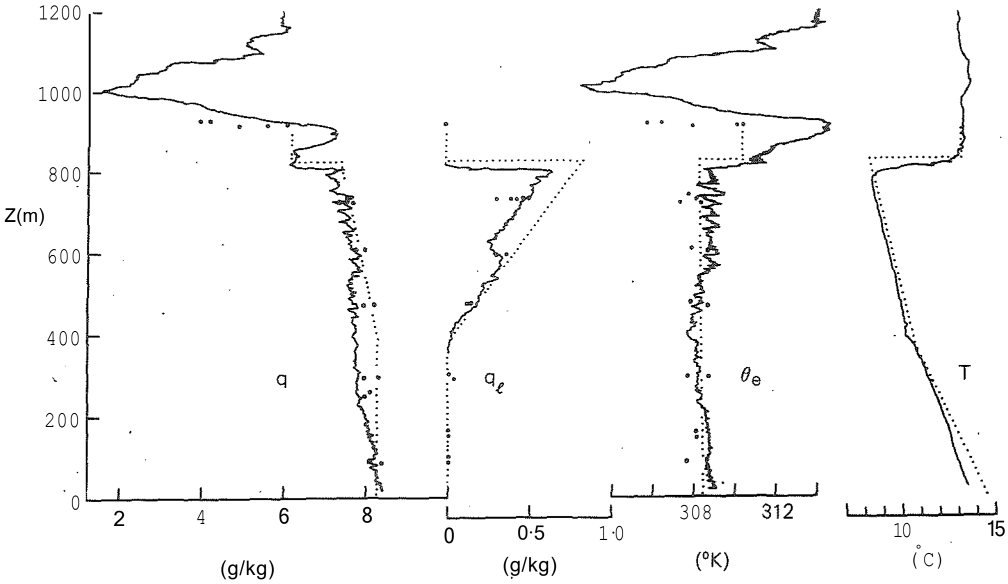

Fig. 1 Vertical structure measured on a slow descent at 1100GMT and horizontal run averaged data (•). The model initial conditions (defined using additional data) are shown dotted.

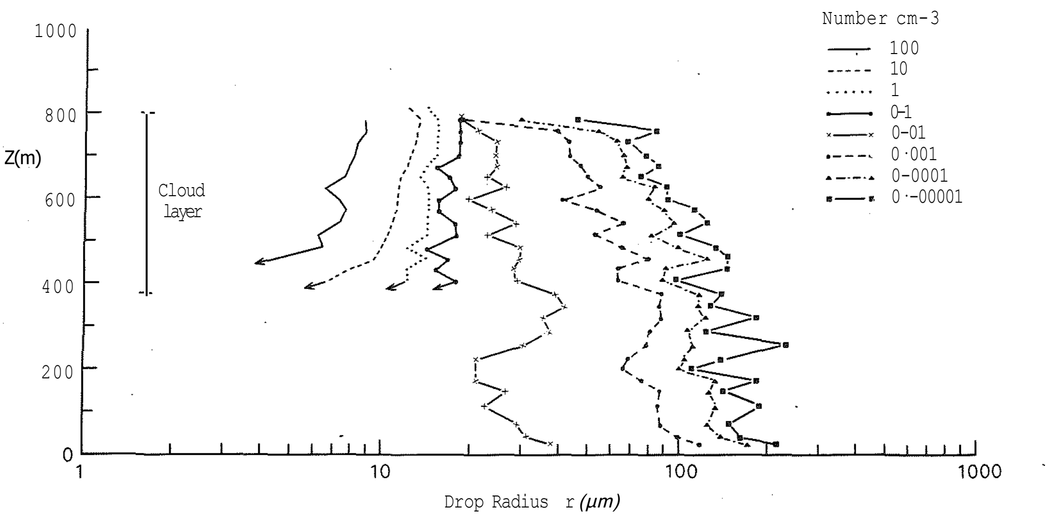

Fig 2 Contours of cumulative number distribution $N(r,z) = \int_r^\infty n(r,z)\,dr$ *from OAP and ASSP data on the 1100GMT descent. Each point is a 10s (1 Km) average.*

$$\frac{\partial \bar{q}_T}{\partial t} = -\frac{\partial}{\partial z}(\overline{w'q'_T}) \qquad (1)$$

$$\frac{\partial \bar{\theta}_e}{\partial t} = -\frac{\partial}{\partial z}(\overline{w'\theta_e'}) - \frac{\partial R}{\partial z} \qquad (2)$$

where the flux of total water is expanded to include transport by gravitational settling (or rainfall, denoted $\overline{w_T q_l}$ and defined in Fig. 4 below)

$$\overline{w'q'_T} = \overline{w'q'} + \overline{w'q'_l} + \overline{w_T q_l} \qquad (3)$$

(Note that $q_T = q + q_l$ remains a good approximation at all levels: the large drops make a large contribution to the water flux but carry a negligible fraction of the total water substance). By assumption the LHS of eqns. (1) and (2) are constant with height in the mixed layer, so integration across the depth of this layer yields the height variation of $\overline{w'q'_T}$ and $\overline{w'\theta_e'}$ given values at the boundaries and R and $\overline{w_T q_l}$ as a function of height.

At cloud top, the fluxes are related to the jumps $\Delta\theta_e$, Δq_T occurring at the upper boundary (eg. Ref. 6):

$$-\overline{w'\theta_e'} = w_e\Delta\theta_e \; ; \; -\overline{w'q'}_T = w_e\Delta q_T \qquad (4)$$

where w_e is the entrainment velocity. Furthermore by assuming that the cloud remains exactly saturated, equations may also be derived from which the vertical variation of the buoyancy flux $\overline{w'\theta_v'}$ and other components ($\overline{w'\theta'}$, $\overline{w'q'}$, $\overline{w'q_l'}$ etc.) can be obtained (Refs. 1, 4).

3. SPECIFICATION OF INITIAL AND BOUNDARY CONDITIONS

Initial profiles of θ_e and q_T were chosen to closely resemble the observations (Fig. 1).

The vertical variation of the net radiative flux, R, (Fig. 3) was calculated by theoretical methods described in Ref. 7 using the observed temperature, humidity and liquid water profiles together with the measured cloud droplet spectra. This approach was necessitated by the difficulty of making long wave radiation flux measurements in cloud and because the vertical spacing of the flight levels was insufficient to define the strong gradients near cloud top. However, the calculations agree with the available observations within the limits set by measurement error. The profile shown in Fig. 3 refers to the period around local noon when the measurements were made, during which time the short wave fluxes were quite steady (R changed by less than 7% in a 4 hour period). As in a previous study (Ref. ?), strong radiative cooling (i.e. $\partial R/\partial z$) is confined to the uppermost 30 m of cloud but warming by insolation occurs over a much greater depth. The net radiative flux divergence across the cloud layer is very small, but although this implies no overall heating such a distribution is strongly destabilizing and would be expected to generate turbulent mixing.

The definition and vertical variation of the rainfall rate, $\overline{w_T q_l}$, are shown in Fig. 4. The expression was evaluated using mean ASSP and OAP droplet spectra from each measurement level with terminal velocities from Ref. 8. In accordance with the data shown in Fig. 2, the contribution from the larger drops ($r > 24$ µm) increases downwards through the cloud layer while the smaller drops' contribution increases towards cloud top. Here the much larger concentration of the smaller drops compensates for their smaller fallspeeds.

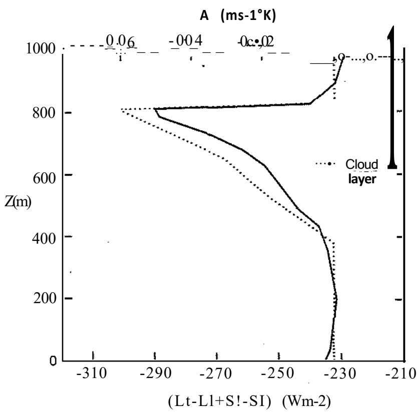

Fig.3 (Full curve): The calculated net radiative flux profile $R = (L\uparrow - L\downarrow + S\uparrow - S\downarrow)/\rho c_p$.
(Dotted curve): Model representation.

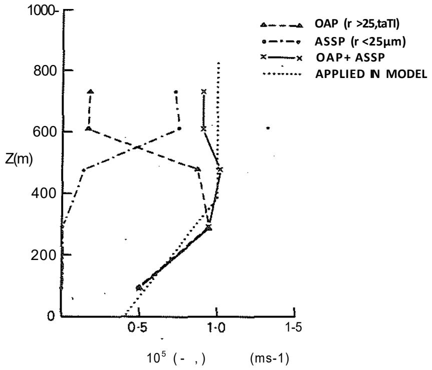

Fig. 4 Mean rainfall rates for each level calculated from the expression

w?i'; { TTpw/p J: wT(rJr^{3}n[r)dr

using the mean OAP and ASSP spectra.

Within cloud, the total flux, ¥ 1, is therefore nearly constant but beneath cloudoase only the larger drops make a significant contribution, decreasing downwards due to evaporation in the unsaturated subcloud layer. Although these values are small compared to conventional rainfall rates (10-5 ms-1 is equivalent to ~1 mm day-1), this is as large as the measured turbulent fluxes of vapour or liquid water (see below).

The surface fluxes were prescribed by comparison with near surface measurements and the entrainment rate, we; specified to give agreement with measurements of w'q'T near cloud top.

4. COMPARISON OF MODELLED AND MFASURED FLUX PROFILES

Given the initial and boundary conditions specified above, it is possible to use the model to predict the vertical variation of the turbulent fluxes necessary to maintain a well-mixed layer. Measurements of the corresponding quantities were made in conditions selected for horizontal uniformity and steady boundary conditions i.e. around local noon over the ocean. It is therefore reasonable to expect the turbulence to be in quasi-equilibrium with the slowly varying mean conditions so that the measurements and modelled values are directly comparable.

Fig; 5 shows some comparisons between two model solutions and corresponding measurements. The solutions display characteristics typical of this type of model (e.g. Refs. 1-3, 11): double jumps near cloud top and jumps in fluxes of non-conserved quantities at cloud base. These are caused by the sharply defined cloud boundaries in the simplified model geometry. In reality these boundaries are distributed over a range of heights and the observed gradients should cons quently be less extreme. At cloud top, the upper part of the double jump is related to entrainment while the lower part reflects the shape of the R-profile i.e. the strong cooling at cloud top. Only quantities directly related to *R* display this second jump. w'q' , which is not directly related, has only a single jump associated with entrainment. This lack of direct sensitivity to radiative effects makes observations of this quantity particularly useful as measurements made close to cloud top can be used .:!:2, j.irectly infer we using eqn. 4•. In both cases, w'q'T was set to 1.5 x 10-5 ms-1 at cloud top (i.e. we. 0.71 cms-1).

Near cloud top, radiative cooling outweighs the effects of entrainment giving rise to a positive maximum in w'0'. In this case, the entrainment instability criterion (Refs. 9, 10) is not satisfied so this source of positive buoyancy is generated by radiative cooling alone. The observations also display a similar positive maximum near cloud top in a region characterized by cold, negatively buoyant downdraughts.

The first model solution includes the assumption made by all previous models of this type: that the well-mixed layer extends from the surface to cloud top. This does not agree well with the rvations. In particular, w'q'T is not linear, w•q1 is poorly predicted and the large negative buoyancy flux below cloudbase is n01t observed. This solution shows that for the whole layer to remain well-mixed, the cloud layer must do work on the subcloud layer i.e. the latter mu t be stirred from the top. Physically, turbulence is set up by radiative destabilization which activates the entrainment of potentially less dense air into the cloud. With no net radiative cooling, the density of the cloud layer tends to decrease. Meanwhile, the weak surface heat flux cannot warm the subcloud layer at a similar rate which is also being cooled by the evaporation of precipitation. To maintain an equal rate of density increase in both layers i.e. to retain a well-mixed density profile, some mechanism is needed to maintain large negative buoyancy fluxes near cloudbase. The observations show that this does not happen; the main sources of turbulent kinetic energy near the surface and cloud

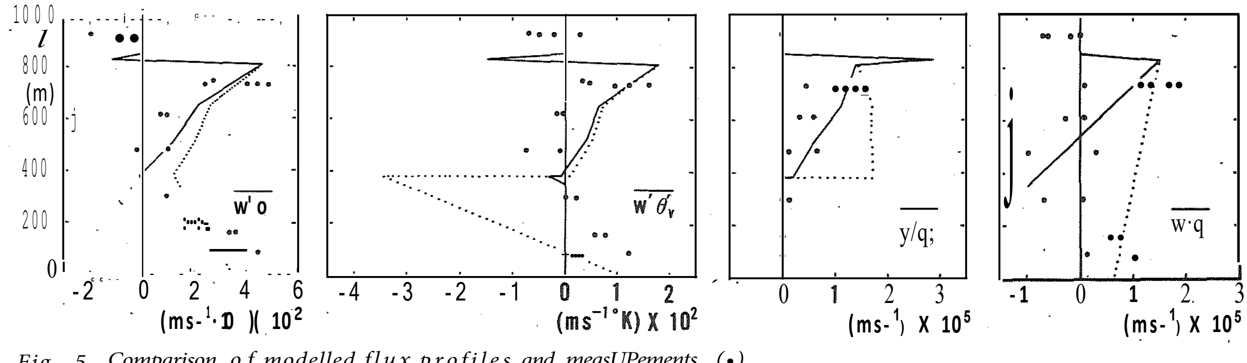

Fig. 5 Comparison of modelled flux profiles and measUPements (•).
Solution 1:....... assumes a mixed layer extending from the surface to aloud top.
Solution 2:-- assumes a mixed layer extending from aloud top down to 350m.
The extent of the aloud layer is shown by the vertical bar.

top cannot export sufficient energy to maintain such a large loss near cloudbase. Instead, the cloud and subcloud layers become decoupled and evolve as two separate mixed layers.

The second model solution shows the effect of this decoupling on the fluxes in the cloud layer by assuming that the cloudy mixed layer extends only from cloud top to just below cloudbase (350 m) where the fluxes are set to zero. This gives much closer agreement with the observations. Other measurements, e.g. minima in vertical velocity variance and dissipation rate estimates provide further evidence that the layers are decoupled.

Decoupling has a number of important consequences for the evolution of the cloud layer and the boundary layer as a whole:

i. The water supply to the cloud is effectively cut off, but radiative destabilization will still result in turbulence and entrainment. This may cause the cloud to thin quite rapidly, cloudbase rising quickly and leaving behind a layer stable to dry convection (θ_v increasing with height) thus strengthening the layers' separation.

ii. The layers may become potentially unstable (θ_e decreasing with height). The increased water vapour convergence in the lower layer might lower the lifting condensation level sufficiently for cumulus to form within it which could release the instability and rise up into the stratiform cloud, thereby reconnecting the layers. This could be sufficiently energetic to break up the stratiform cloud and might provide an alternative mechanism to entrainment instability for explaining the break up of subtropical stratocumulus into cumulus (Ref. 11).

The sensitivity of this decoupling process to changes in the boundary conditions can also be assessed using the model. Changing the radiative fluxes to nocturnal values by setting the shortwave components to zero results in a considerable increase in $\overline{w'\theta'_v}$ within cloud (for the same w) and the negative region beneath cloudbase almost disappears suggesting that a single well-mixed layer is more likely to occur at night. To achieve the same result with the daytime values requires a sevenfold increase in the surface heat flux. As such large surface heat fluxes are infrequent over the oceans, especially in conditions where stratocumulus exists, it seems likely that decoupling is a common occurrence during the day, especially at lower latitudes with increased insolation. Recent flights suggest this is the case and that the sensitivity of the model to the radiative fluxes is realistic, but further work is necessary to provide conclusive evidence.

5. CONCLUDING REMARKS

Observations made from an instrumented aircraft in stratocumulus and comparisons with a mixed layer model suggest:

i. Microphysical structure is an important factor in determining the behaviour of stratiform cloud, not only because of its interaction with the radiation field, but also because of precipitation growth. In the example considered, water transport by rainfall was as large as that by turbulent transfer. Evaporation of precipitation beneath cloud also tends to stabilize the subcloud layer.

ii. A combination of effects can cause the cloud and subcloud layers to become decoupled. This can lead to significantly different cloud and boundary layer evolution and is most likely to occur during the day with weak surface buoyancy fluxes. A strong sensitivity to the radiative fluxes is suggested.

Most present stratiform cloud models consider neither of these processes which probably severely limits the range of conditions under which they remain valid. Both decoupled layers and cumulus rising into an elevated stratiform layer are common occurrences and models should be constructed to permit these possibilities.

Acknowledgements: I would like to thank my colleagues within the Cloud Physics Branch and at the Meteorological Research Flight whose contributions have made this work possible, especially Mr J R Leighton.

6. APPENDIX - NOMENCLATURE

$L\uparrow, L\downarrow, L$	Hemispherically integrated up and downward broadband (4-45 µm) fluxes.
$n(r)$	Concentration of droplets in the radius interval r to r + dr.
q, q_l	Specific humidity, liquid water content.
q_T	Specific total water content = $q + q_l$.
r, r_v	Radius, mean volume radius.
R	Net radiative flux - See Fig. 3.
$S\uparrow, S\downarrow, S$	As $L\uparrow, L\downarrow$ except shortwave (0.3-3 µm)
w, w_T	Vertical air velocity, drop terminal velocity.
$\widetilde{w_T q_l}$	Rainfall rate (defined in Fig. 4).
θ_e	Equivalent potential temperature = $\theta + L_v q/c_p$.
ρ, ρ_w	Air and liquid water density.

7. REFERENCES

1. Deardorff J.W. 1976, On the entrainment rate of a stratocumulus topped mixed layer. Quart J. Roy Meteor. Soc. 102, 563-582.
2. Fravalo C, Fouquart Y. and Rasset R. 1981, The sensitivity of a model of low stratiform clouds to radiation, J. Atmos. Sci. 38, 1049-1062.
3. Stage S.A. and Businger J.A. 1981, A model for entrainment into a cloud topped marine boundary layer. Parts I and II. J. Atmos. Sci. 38, 2213-2242.
4. Nicholls S. 1984, The dynamics of stratocumulus: aircraft observations and comparisons with a mixed layer model, submitted to Quart J. Roy. Meteor. Soc.
5. Nicholls S, Shaw W. and Hauf T. 1983, An intercomparison of aircraft turbulence measurements during JASIN, J. Appl. Meteorol. 22, 1637-1648.
6. Lilly D.K. 1968, Models of cloud topped mixed layers under a strong inversion, Quart. J. Roy. Meteor. Soc. 94, 292-309.
7. Slingo A, Nicholls S. and Schmetz J. 1982, Aircraft observations of marine stratocumulus during JASIN, Quart. J. Roy. Meteor. Soc. 108, 833-856.
8. Beard K.V. 1976, Terminal velocity and shape of cloud and precipitation drops aloft, J. Atmos. Sci. 33, 851-864.
9. Randall D.A. 1980, Conditional instability of the first kind upside down, J. Atmos. Sci. 37, 125-130.
10. Deardorff J.W. 1980, Cloud top entrainment instability, J. Atmos. Sci. 37, 131-147.
11. Randall D.A. 1980, Entrainment into a stratocumulus layer with distributed radiative cooling, J. Atmos. Sci. 37, 148-159.

A NEW PHYSICAL HYPOTHESIS FOR VERTICAL MIXING IN CLOUDS

Mary Selvam, A. Ramachandra Murty, A.S. and Ramana Murty, Bh. V.
Indian Institute of Tropical Meteorology, Pune-411 005, India.

1. OBSERVATIONS IN MONSOON CLOUDS

Extensive aircraft- cloud physical observations have been made in a large number of isolated warm cumulus clouds'forming during the summer monsoon season (June-September) in a few regions in India (Ref. 1): Results of these observations obtained during the horizontal aircraft traverses made at different levels above the cloud-base suggest the following·.

The horizontal structure of the air flow inside the cloud has consistent variations with successiv positive and negative values of vertical velocity representative of ascending and descending air currents inside the cloud. The regions of ascending current are associated with higher liquid water content (LWC), and negative cloud ·drop.charges. The descending currents are associated with lower LWC and positive cloud drop charges. The width of the ascending and descending currents is about 100 metres.

The measured LWC (q) at the cloud-base levels is far smaller than the adiabatic value ( ) with q/qa = 0.60. The LWC increases with height from the base of the cloud and decreases towards the cloud-top-region. The cloud electrical activity is found to increase with the cloud LWC. The distribution of cloud drop spectra is unimodal near the cloud-base and multimodal at higher levels. The variations· in the mean volume diameter (MVD) are simiiar to those in·the LWC. The temperatures inside the cloud are colder than the environment. The lapse rates of the temperatures inside the cloud are less than the i=ediate environment. The environment lapse rates are nearly equal to the saturated adiabatic value. Positive increments in LWC are associated with the increments in temperatures inside the cloud. Positive increments in temperature are associated with the increments in temperature of the i=ediate environment at the same level or the level i=ediately above. The variances of in-cloud temperature and humidity are larger in the regions where the values of bWC are higher. The variances of temperature and humidity are larger in the clear air environment than in the cl-0ud air.

The dynamical and physical characteristics of monsoon clouds described above cannot be explained by simple entraining cloud models. This paper seeks to examine a new physical mechanism which can explain the observed cloud characteristics.

2. NEW MECHANISM FOR EDDY GROWTH IN THE ATMOSPHERIC PBL

The atmosplieric planetary boundary layer (PBL) is often organised into helical secondary circu-:j.ations aligned parallel to. the mean flow (Ref. 2). These secondary circulations are often·referred to as vortex rolls or large eddies. It is not known how the vortex rolls in the PBL are sustained without decay by the turbulence arQund them. The simulation experiments in laboratory wind. tunnels suggest on the contrary that turbulc ce causes decay of the vortex rolls. In a·recent paper (Ref.1) it has been shown that the buoyant production of energy by microscale-fractional condensation (MFC) in turbuient eddies is responsible fqr the sustenance and growth ·of large eddies. The turbulent eddies originating from surface friction exist all along the envelope of the large eddy (Fig. 1). MFC occurs in turbulent eddies even in an unsaturated environment. The energy gained by the turbulent eddies would contribute to the sustenance and growth of the large eddy as explained below.

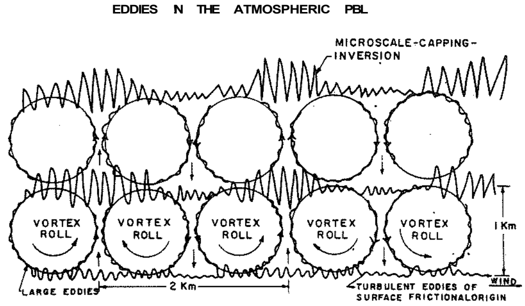

Fig. 1 : Schematic representation of the eddies in the Atmospheric Planetary Boundary Layer

The circulation speed of the large eddy is equal to the integrated mean circulation speed of the turbulent eddies. A net upward vertical velocity is imparted to the large eddy by the MFC processes in the turbulent eddies. Townsend (Ref.3) has shown that the circulation speed of the large eddy is ,elated to that of the turbulent eddy according to the following expression.

$$W^2 = \frac{2r}{\pi R} w^2 \tag{1}$$

where W = root mean square circulation speed of the large eddy

w = root mean square circulation speed of the turbulent eddy

r = radius of the dominant turbulent eddy

R = radius of the large eddy

From Equation (1) it follows that for a large eddy which is ten times bigger .in size than the turbulent eddy, the increase in circulation speed of the large eddy is 25 per cent of the increase in the circulation speed of the turbulent eddy i.e,, W - 0.25 *w*.

The buoyant production of turbulent energy by the MFC is maximum at the crest of the large eddies and results in the warming of the large eddy volume. The turbulent eddies at the crest of the large eddies are identifiable by a microscale-capping-inversion which rises upwards (Fi·g. 1) with the convective growth of the large eddy in the course of the day. This is seen as the rising inversien of the day time planetary boundary layer in the echosonde records.

The above theory of eddy growth in the PBL is also able to explain the observed spectrum of gravity waves and the evolution of larger scales of weather systems from the basic turbulence scale (Ref. 4).

3. VERTICAL MIXING

The dilution by environmental mixing of the large eddy volume by turbulent eddy fluctuations across unit cross-section of the large eddy surface is derived as follows.

The ratio of the upward mass flux of air in the turbulent eddy to that in the large eddy across unit ross-section per second= w* /dW

where

ω_* = increase in ve'rtical velocity per second of the turbulent eddy due to the MFC process and

dW = corresponding increase in vertical velocity of large eddy.

This fractional volume dilution of the large eddy occurs in the environment of the turbulent eddy. The fractional volume of the large eddy which is in the environment of the turbulent eddy where dilution occurs= r/R.

Therefore, the total f actional volume dilution k of the large eddy per second across unit cross sect.ion can be expressed as

$$k = \frac{\;}{dW}\,\frac{r}{R} \qquad (2)$$

The value of k = o.4 when R/r = 10 since dW = 0.25 w* (Equation 1).

3.1 Wind profile in the PBL

In Equation (2), dW is the increase in vertical velocity of the large eddy per second as a result of w*. The height interval in which this incremental change in the vertical velocity occurs is, d'lr,.which is equal t o r (Fig. 2).

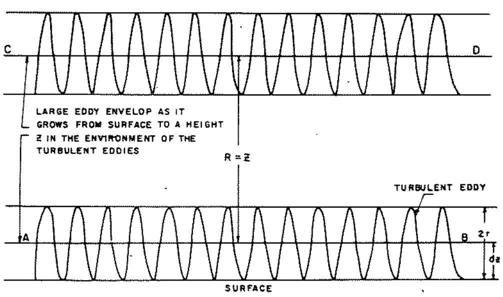

F,:i.g. 2. Growth of large eddy in the environment of the turbulent eddy.

Using the above expressions Equation (2) can be written as follows :

$$dW = \frac{\omega_*}{k}\,\frac{dZ}{Z} \qquad (3)$$

Integrating Equation (3) between the height interval r and R the following relation for W can be obtained

$$W = \int_r^R \frac{\omega_*}{k}\,\frac{dZ}{Z} = \frac{\;}{k}\ fo\,\frac{R}{r} \qquad (4)$$

In the above expression for W it is assumed that w* is constant for the height interval pf integration.

A normalised height z with reference to the turbulence scale r can be defined as

$$z = \frac{R}{r} \qquad (5)$$

Using the above expression Equation (4) can be written as, follows :

$$W = \frac{\omega_*}{k}\ 9.nz \qquad (6)$$

The value of k is constant for a fixed value of R/r. As defined earlier k represents the fractional volume dilution rate of the large eddy fluctuations across unit cross-section on its envelope and is constant for a fixed value of the scale ratio z.

It is well known from observations and from existing theory of eddy diffusion (Ref. 5) that the vertical wind profile in the atmospheric PBL follows the logarithmic law which is identical to the expression shown in Equation (6). The constant k for the observed wind profile is called the Von Karman constant. The value of k as determined from observations is equal to 0.4 and.has not been assigned any physical meaning i the literature.

The new theory relating to the eddy mixing in the PEL proposed in the present study enables to predict the observed logarithmic wind profile without involving any assumptions as in the case of existing t heories of eddy diffusion processes. Also, it is shown that the Von Karman constant is associated with a specific physical process. It is the fractional volume dilution rate of the large eddy by the turbulent scale eddies for the scale ratio of 10.

4. CUMULUS CLOUD MODEL

The mechanism of large eddy growth in the atmospheric PEL discussed earlier can be applied to the formulation of the governing equations for cumulus cloud growth. Based on the above theory equations were derived (Ref. 1) for the incloud vertical profiles of (i) ratio of .actual cloud liquid water content (q) to the adiabatic liquid water content (qa), (ii) vertical velocity, (iii) temperature excess, (iv) temp erature lapse rate, (v) total liquid water content, (vi) cloud growth time, (vii) cloud drop size spectrum and

(viii) rain-drop size spectrum. The equations were derived starting from the MFC process at cloud-base levels. This provides the basic energy input for the total cloud growth. There is agreement between the predicted and observed values of different cloud parameters. The salient features of the cloud model are discussed below.

4.1 Vertical Profile of q/qa

The observations of cloud liquid water content, q indicate th t the racio q/qa is less than one due to dilution by vertical mixing. The fractional volume nilution rate in the cloud updraft can be computed as follows.

The rate of the upward mass flux of air in the large eddy to that in the turbulent eddy across unit cross-section of the large eddy = W/W_*.

This fractional upward mass flux occurs across unit cross section in a volume r/R of the large eddy which is in the environment of the turbulent eddy fluctuations (see Fig. 2). Therefore the fractional upward mass flux of air f in the large eddy per unit volume across unit cross section is given as

$$f = \frac{W}{\omega_*}\frac{r}{R} = \frac{W}{\omega_*}\frac{1}{z} \tag{7}$$

Substituting for W and k we arrive at

$$f = \sqrt{\frac{2}{\pi z}}\ \ln z \tag{8}$$

In Equation (8), f represents the fraction of the airmass of surface origin which reaches the height z after dilution by vertical mixing caused by the turbulent eddy fluctuations.

Considering that the cloud base level is 1000 m the value of $z = \frac{R}{r} = \frac{1000\ \text{m}}{100\ \text{m}} = 10$. From the above it is **seen** that $f = 0.6$ for $z = 10$.

The value of q/qa at the cloud base level is also found to be about *0.6* (Fig. 3) by several investigators (Ref. 6).

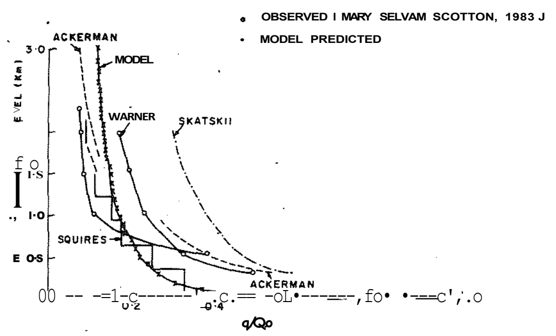

Fig. 3 : Observed vertical profiles of the ratio of cloud liquid water content to its adiabatic value (q/qa). Profile predicted by the present model for r = 1m is also given.

In Equation 8, f will also represent the ratio q/qa inside the cloud. The observed q/qa profile inside the cloud is seen to follow closely that predicted by the model for r = 1m (Fig. 3). It is therefore inferred that, inside the cloud the dominant turbulent eddy radius is 1m while below the cloud base the dominant turbulent eddy radius is 100 m. Observations of temperature spectra show that the dominant turbulent eddy radius is of the order of a few metres only above the lifting condensation level and also that the dominant turbulent eddy length is shorter in cloud air as compared to that in clear air conditions (Ref. 7). The decrease in the dominant turbulent eddy radius is thus directly related to the amount of moisture available for condensation.

The distribution will also represent the vertical profile of cloud drop number concentration since the cloud condensation nublei originate from surface levels. The observed vertical profile of cloud drop number concentration (Ref. 8) is found to resemble closely the f distribution at Fig.3.

4.2 Incloud vertical velocity profile

The logarithmic wind profile relationship (Equation 6) derived for the PBL in Section. 3.1 holds good inside a cloud because the same basic physical process, namely microscale-fractional-condensation, operates in both the cases. he value of vertical velocity inside a cloud will, however, be much larger, than in cloud-free air.

From Equation (6) the in-cloud vertical velocity W' profile can be expressed as

$$W' = \omega_*\, fz \tag{9}$$

The vertical velocity profile will follow the fz distribution assuming w* is constant at the cloud-base level during the cloud growth period (Ref.1). The total liquid water content profile also follows the fz distribution (Ref. 1).

4.3 In-cloud excess temperature perturbation profile

The relationship between temperature perturbation θ' and the corresponding vertical velocity perturbation is given as follows :

$$W' = -\frac{g}{\theta_0}\theta'$$

where g = accleration due to gravity

θ_0 = reference level potential temperature

By substituting for W' and taking θ* as the production of temperature perturbation at the cloud-base level by microscale-fractional-condensation, we arrive at the following expression

$$\theta' = \frac{\theta_*}{k}\ \ln z = \theta_*\, fz \tag{10}$$

Thus the in-cloud temperature perturbation profile also follows the fz distribution.

4.4 Incloud temperature lapse rate profile

The in-cloud temperature lapse rate Γ_s is expressed as

$$\Gamma_s = \Gamma - \frac{L}{C_p}\frac{dq}{dZ} \quad (11)$$

where Γ = dry adiabatic lapse rate
L = latent heat of condensation
C_p = specific heat of air at constant pressure
dq = liquid water condensed during parcel ascent in a height **interval** dZ.

Equation (11) can be expressed as

$$\Gamma_s = \Gamma - \ldots = \ldots - f = \ldots - \frac{8;}{f_z} \quad (12)$$

where ,d8 is the temperature perturbation 8' during parcel ascent d%. By concept d2\ is the dominant turbulent eddy radius r. (Fig. 2).

4.5 Cloud growth-time

Let W' be the vertical velocity of the cloud at height z. The time dt for the incremental cloud growth is expressed as follows;

$$dt = \frac{dZ}{dW'}$$

$$t = \frac{r}{\omega_*} \, I + \quad li \left(/";" \right)_1^z \quad (13)$$

where ti is the Soldner's integral or the logarithm integral. The cloud growth time t can be computed using Equation (13).

4.6 Cloud drop size spectrum

The evolution of cloud drop size spectrum is critically dependent on the water vapour available for condensation and the nuclei number concentration in the sub-cloud layer. Cloud drops form as water vapour condenses in the air parcel ascending from cloud-base levels. Vertical mixing during ascent reduces the volume of cloud-base air peaching higher levels to a fraction f of its initial volume. Thus the nuclei available for condensation i.e. the cloud drops number concentration also d creases with height according to the f distribution. The total cloud water content as mentioned earlier increases with height according to the f_z distribution. Thus bigger size cloud drops are formed on the lesser number of condensation nuclei available at higher levels in the cloud. Due to vertical mixing unsaturated conditions exist inside cloud. Water vapour condenses on fresh nuclei available at each level since, in the unsaturated in-cloud conditions (MFC) occurs preferentially on small condensation nuclei. Also, as the cloud growth progresses an appropriate fraction of the cloud drops formed at lower levels are carried in the updraft. These cloud drops do not grow appreciably during the ascent in the unsaturated conditions inside the cloud.

The cloud drop spectrum at any level will thus consist of (i) cloud drops transported from lower leyels and (ii) large size cloud drops formed on fresh nuclei at that level. On the basis of the above physical concept the cloud drop size spectrum was derived (Ref. 1). The model predicted spectra are in agreement with the observations.

5. REFERENCES

1. Mary Selvam A et al 1983, Some physical and dynamical aspects of warm monsoon clouds and their modification, Proc. Indian Academy of Sciences (s.ubmitted).

2. Brown RA 1980, Longitudial instabilities and secondary flows in the planetary boundary layer, Rev Geophy Space Phys 18, 683-697.

3. Townsend A A 1956, The Structure of Turbulent Shear Flow, Cambridge University Press, Cambridge, 113-130.

4. Mary Selvam A et al 1984, Role of frictional turbulence in the evolution of cloud systems, Proc. 9th International Cloud Physics Conference, Tallinn, USSR, 21-28 August 1984.

5. Holton JR 1979, An Introduction to Dynamic Meteorology, Academic Press, New York, 391.

6. Warner J 1970, The microstructure of cumulus clouds. Part III : The nature of updraft, J Atmos Sci 27, 682-688.

7. Mary Selvam A et al 1984, Characteristics of temperature spectra in warm monsoon clouds, Proc. 9th International Cloud Physics Conference, Tallinn, USSR, 21-28, August, 1984.

8. Mason BJ 1971; The Physics of Clouds, 2nd Ed. Clarendon Press, Oxford, 671 pp.

9. Mary Selvam A and Cotton WR 1983, Comparison of one dimensional cumulus cloud model predictions with observations in summer monsoon clouds in the Indian region, Proc. Indian Academy of Sciences (submitted)

ROLE OF FRICTIONAL TURBULENCE IN THE EVOLUTION OF CLOUD SYSTEMS

A Mary Selvam, A S Ramachandra Murty and Bh V Raman Murty
Indian Institute of Tropical Meteorology, Fune 411 005, India.

1. INTRODUCTION

Satellite cloud pictures show that synoptic **scale weather systems consist of mesoscalc convective** cloud clusters organised in a spiral cloud band around the low pressure centre. In the present paper it is shown theoretically that turbulent eddies of surface frictional origin are mainly responsible for the generation of the observed scales of eddy systems in the atmospheric planetary layer (PBL). The convective, meso-, synoptic and planetary scale eddies develop by mixing in successive decadic scale ranges starting originally from the turbulence scale. The quantitative relationships of the length, time and velocity scales of the convective, meso-, synoptic and planetary scale systems with those of the turbulence scale are discussed in this paper.

2. NEW PHYSICAL MECHANISM

The new mechanism for eddy growth in the atmospheric PBL is discussed in another paper (Ref. 1) of this Conference. Briefly, the new hypothesis envisages that large eddy growth occurs by micros.cale - fractional - condensation (MFC) in turbulent eddies (Fig. 1). The turbulent eddies originate from surface friction and are contained on the envelopes of the large eddies. Townsend (Ref. 2) has shown that the root mean square circulation speed of the large eddy is related to tha of the turbul nt eddy according to the following expression

$$W^2 = \frac{2}{\pi}\frac{2}{R}\,\omega^2 \qquad (1)$$

where W and w are respectively the root mean square circulation speeds of the large eddy and turbulent eddy. R and r denote the radii of the large eddy and turbulent eddy respectively.

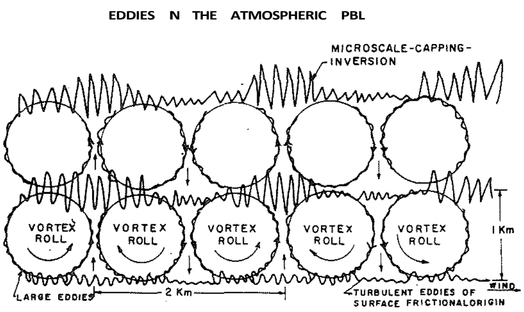

Fig. 1 : Schematic representation of the eddies in the Atmospheric Planetary Boundary Layer.

2.1 Eddy mixing and the Richardson number

The region of the turbulent eddy environment at the crest of the large eddy in the PBL can be identified by the microscale-capping-inversion (Fig. 1).

The Richardson number Ri (Ref. 3) which is used as an index of shear produced turbulence is defined as follows :

$$R_i = \frac{N_B^2}{(\text{wind shear})^2} \qquad (2)$$

Observations show that Ri 0.25 for-the region of turbulence in the atmosphere.

In the following it is shown that Ri 0.25 in the region of the microscale-capping-inversion for the scale ratio, z 10 (where z = R/r).

Substitution in Equation (2) for NB and assuming three dimensional similarity.

$$R_i = \left(\frac{g}{\theta_v}\frac{d\theta_v}{dz}\right) / \left(\frac{d\omega}{dz}\right)^2 \qquad (3)$$

$$\frac{g}{\theta_v}\,d\theta_v = \frac{g}{\theta_v}\,\theta' = w_* = dW$$

where ω_* = vertical velocity production in the turbulent eddy per second.

Using the above expression Equation (3) can be written as :

$$R_i = \left(\frac{dW}{dz}\right) / \left(\frac{d\omega}{dZ}\right)^2 = \frac{1}{(dw/dZ)} \qquad (4)$$

where dZ = upward ascent of the large eddy per second due to the energy supplied by the turbulent eddy.

Hence $Ri = \frac{dW}{dw}$

Frcm Equation (1) $\frac{dW}{dw} = 1/4$ for scale ratio, z =10.

Hence Ri = 1/4 = 0.25 for z = 10.

z = 10 is the lower limit for identifiable large eddy growth, as shown below.

For z < 10 the value of K > 0.5 i.e. the fractional volume dilution by the environmental vertical mixing becomes more than half. Thus identifiable large eddies in the atmospheric PBL have size ratio, z 10. The minimum size of the large eddy which can grow as an identifiable entity is Re = 10 r where Re is the convective scale radius.

Organised growth of large eddy occurs for scale ratios z 10 and in the microscale-capping-inversion layer at the crest of the large eddy the Richardson number, Ri ;; 0.25. Observations (Refs. 4,5) indicate onset of turbulence when Ri = 0.25 and it is consistent with the above theory.

In the context of the new theory of eddy growth in the atmospheric PBL proposed in the present study the Richardson number Ri actually corres onds to the ratio of the vertical velocity in the large eddy to that in the turbulent eddy in the region of the microscale-capping-inversion. Richardson number can be obtained directly, from Equation (1).

2. 2 Gravity waves in the PBL

The buoyant production of turbulent energy by the MFC process is maximum at the crest of the large eddies and results in the warming of the large eddy volume. The turbulent eddies at the crest of the large eddies are identifiable by a Microscale-Capping-Inversion (MCI) which rises upwards (Fig. 1) with the convective growth of the large eddy in the course of the day: This is seen as the rising inversion of the day time PBL in the echosonde records.

As the parcel of air corresponding to the large eddy rises in the stable environment of the MCI, Brunt Vaisala oscillation are generated. These oscillations generate gravity waves. The frequency of the Brunt-Vaisala oscillation is equal to

$$N_B^2 = \frac{g}{\theta_v} \frac{d\theta_v}{dz} \tag{5}$$

where g is the acceleration due to gravity, θ_v the virtual potential temperature and $d\theta_v/dz$ is the virtual potential temperature lapse rate in th MCI. Thus the rising large eddy generates a continuous spectrum of atmospheric gravity waves (Ref. 6).

2. 3 Wind, temperature and mixing ratio spectra in the PBL

The slopes of the turbulence spectra of wind, temperature and mixing ratio in the BPL can be computed as follows.

A logarithmic scale is generally used to plot the variance of the parameter with respect to the wave number. The slops S_w of the wind spectrum can be expressed as

$$S_w = \frac{\ln(E/E)}{\ln(K/k)} \tag{6}$$

In Equation (6), E is the kinetic energy of the large eddy at wave number K and can be expressed as follows

$$E = \frac{1}{2} \frac{4}{3} \pi R^3 \rho W^2 \tag{7}$$

where ρ = density of air and

E = kinetic energy of the dominant turbulent eddy at wave number k

$$= \frac{1}{2} \frac{4}{3} \pi r^3 \rho \omega^2 \tag{8}$$

Equation (6) can be written as

$$S_w = \frac{\ln\left(\frac{R^3}{r^3} \frac{W^2}{\omega^2}\right)}{\ln\left(\frac{K}{k}\right)} \tag{9}$$

From equation (1)

$$W^2 = \frac{2}{\pi} \frac{r}{R} w^2$$

Since the wave number is inversely proportional to the wave length

$$\frac{K}{k} = \frac{r}{R}$$

$$\text{Hence} \quad S_w = -2 + \frac{0.451285}{\ln(R/r)} \tag{10}$$

From Equation (10) we can obtain the following values for the slope of wind spectrum for different scale ratios

$$\left.\begin{array}{ll} S_w = -1.8 & \text{for } R/r = 10 \\ S_w = -1.935 & \text{for } R/r = 1000 \\ S_w = -2 & \text{for very larger values of } R/r \end{array}\right\} \tag{11}$$

The slope S_θ of the turbulence spectrum for temperature will also be the same as that for wind since there is a linear relationship (Equation 12) between the temperature perturbation θ' and vertical velocity perturbation W'.

$$W' = -g \frac{\theta'}{\theta_v} \tag{12}$$

Observations of turbulence spectra of wind and temperature in the atmospheric PBL (Refs. 4, 7-12) show that there is a continuous spectrum of waves in the atmosphere extending from the turbulen e scale to the meso- and larger scales. The slope of the turbulence spectrum in the wave region is approximately equal to -5/3. Actually, the slope is slightly steeper than -5/3 and it increases witb wavelength (Ref. 10). There is no satisfactory explanation for the observed characteristics of the turbulence spectra (Refs. 1, 8). Also, observations show that the wave region is separated from the turbulence region by a spectral gap (Refs. 8, 9). In the present study we now propose that the spectral gap is the region of separation of two different entities, namely, the turbulent eddies and the large eddies, the former sustaining the latter's growth. The predicted spectral slope of -1.8 (Equation 1) for the scale ratio $R/r = 10$, is close to the observed spectral slope which is slightly steeper than -5/3 (~ -1.67).

The slope S_q of the mixing ratio spectrum may similarly be derived as follows :

$$S_q = \frac{2\ln(M/m)}{\ln(K/k)} \qquad (13)$$

M = variance of moisture perturbation in the large eddy

$$= \frac{4}{3}\pi R^3 \rho Q^2$$

Q = moisture perturbation per unit mass of the large eddy

m = variance of moisture perturbation in the turbulent eddy

$$= \frac{4}{3}\pi r^3 \rho q^2$$

q = moisture perturbation in unit mass of the turbulent eddy

The moisture perturbation in the large eddy is governed by dilution process due to vertical mixing by turbulent eddy and it can be shown that (Ref. 1).

$$Q = 0.6\, q \text{ for scale ratio } \frac{R}{r} = 10$$

$$\left.\begin{aligned} S_q &= -3 - \frac{2\ln 0.6}{\ln R/r} \\ &= -2.5564 \text{ for } R/r = 10 \\ &= -3 \text{ for large values of } R/r. \end{aligned}\right\} \qquad (14)$$

3. SCALES OF EDDIES

3.1 Formation of different scales of weather systems

The theory of eddy mixing discussed in the previous section can also explain the generation mechanism for various scales of weather systems e.g. convective, meso-, synoptic- and planetary-scales.

The fractional volume dilution rate of the large eddy by the vertical mixing of environmental air by turbulent eddies is expressed as follows (Ref. 1).

$$k = \frac{w}{W}\,\frac{r}{R} = 0.4 \quad \text{for } z = 10$$

$$k > 0.5 \quad \text{for} \quad z < 10$$

Identifiable large eddies can grow only for scale ratios $z \geq 10$. The convective scale eddy of radius R_c evolves from the turbulent eddy of radius r for the size ratio (z), $R_c/r = 10$. This type of decadic scale range eddy mixing can be visualised to occur in successive decadic scale ranges generating the convective, meso-, synoptic-, and planetary scale eddies of radii, R_c, R_m, R_s, R_p where c,m,s and p represent respectively the convective, meso-, synoptic-, and planetary- scales respectively.

The R_c, R_m, R_s and R_p are related to the basic turbulent eddy radius, r as shown below.

$$\begin{aligned} & r : R_c : R_m : R_s : R_p \\ &= r : 10r : 10^2 r : 10^4 r \end{aligned} \qquad (15)$$

From Equation (15) dominant wavelength scale ranges for various weather systems can be written as follows. The value of r is taken as 100 m from observations.

Turbulence scale	200 m	- 2 km	(16)
Convective scale	2	- 20 km	
Meso-scale	20	- 200 km	
Synoptic scale	200	- 2000 km	
Planetary scale		> 2000 km	

The vertical velocities of different scale weather systems can be expressed as follows in terms of the vertical velocity of the turbulent eddy using Equation (1).

$$\begin{aligned} & \omega : W_c : W_m : W_s : W_p \\ &= \omega : 0.25\omega : 0.25^2\omega : 0.25^3\omega : 0.25^4\omega \end{aligned} \qquad (17)$$

The total time period of circulation, t, of the turbulent eddy is given by

$$t = \frac{2\pi r}{w} \qquad (18)$$

Similarly the time periods of circulation, T, of different scale weather systems can be expressed, in terms of the time period of circulation, t, of the turbulent eddy.

$$\begin{aligned} & t : T_c : T_m : T_s : T_p \\ &= t : 40t : 40^2 t : 40^3 t : 40^4 t \end{aligned} \qquad (19)$$

The turbulent kinetic energy E is given by

$$E = \frac{1}{2}\,\frac{4}{3}\,\pi r^3 \rho w^2 \qquad (20)$$

In the same manner, the kinetic energy E of the different scale weather systems can be computed and related to the kinetic energy of the turbulent eddy

$$\begin{aligned} & E : E_c : E_m : E_s : E_p \\ &= E : 62.5E : 62.5^2 E : 62.5^3 E : 62.5^4 E \end{aligned} \qquad (21)$$

Thus, the energy production in the turbulent eddy integrated over large space scales and time periods .results in organised large scale eddies with energy content several orders of magnitude larger.

The turbulent buoyant energy production by microscale-fractional-condensation in the atmospheric PBL is uasically equivalent to the conditional instability of the second kind (CISK) mechanism. The various decadic scales of eddies are always present in the atmosphere and the weat_her systems are produced with favourable energy supply from the CISK mechanism.

Also, it follow.s from the above discussion that the larger eddies contain inherently the smaller scale eddies. The planetary scale eddy thus consists of the synoptic, meso-, convective, and turrulence scale eddies. When the eddy length becomes large as in the case of the cyclonic system, it gives rise to the spiral cloud bands. Each one of these cyclonic cloud bands is found to consist of mesoscale convective cloud clusters.

3.2 Synoptic scale spiral cloud bands

It was shown in another paper (Ref. 1) of this Conference that the wind profile in the atmospheric PBL follows the logarithmic law. Thus, since eddy growth involves increase in radius simultaneous with angular displacement from origin the trajectory of airflow associated with the large eddies will follow a logarithmic spiral pattern both in the horizontal and vertical. Thus the convergence, divergence, ascent and desccent airflow of vortex rolls occurs along logarithmic spiral curves. In the extreme case of a tornado with decrease in turbulent eddy radius the large eddy radius is reduced sufficiently $uch that the ascent/d scent airflow spirals lmost overlap giving rise to the tornado funnel.

4. REFERhliCES

1. Mary Selvam A et al 1984, A new hypothesis for vertical mixing in clouds, Proc. 9th International Cloud Physics Conference, Tallinn, USSR, 21-28 August 1984.
2. Townsend, A A 1956, The structure of turbulent shear flow, Cambridge University Press, Cambridge, 113-130.
3: Holton, J R 1979, An introduction to dynamic meteorology, Academic Press, New York, 391.
4. Vinnichenko N K 1969, "Recent investigations of clear-air turbulence in the USSR in Clear Turbulence and its Detection, ed. Y H Rao and A Goldburg, Plenum Press, New York, 246-270.
5. Wallace J M and Hobbs P V 1977, Atmospheric science, an introductory survey, Academic Press, New York, 467.
6. Mary Selvam A et al 1983, Some physical and dynamical aspects of warm monsoon cloud and their modification, Proc Indi n Academy of Sciences, (submitted).
7. Dewan E M 1979, Stratospheric wave spectra resembling turbulence, Science, 204,832 835.
3. Weinstock J 1980, A theory of gaps in ttie turbulence spectra of stably stratified shear flow, J.Atmos.Sci.37,1542-1549.
9- Parasnis S S et al 1980, Temperature stratification of the atmospheric boundary layer over the Deccan Plateau, India during the **summer monsoon.** Boundary Layer Meteorology, 19, 165-175-
10. Van Zandt T E 1982, A uniyersal spectrum of buoJancy waves in the atmosphere, Geophysics Res. Letters, 9, 575-578.
11. Gage K S 1979, Evidence for a K-5/3 inertial range in mesoscale two dimensional turbulence, J. Atmos. Sci., 36, 1950-1954.
12. Carter D A and B B Balsley 1982. The summer wind field between 80 and 93 km observed by the MST Radar at Poker Flat Alaska (65.°N), J.Atmos. Sci., 39, 2905-2915-

SESSION IV

CLOUD DYNAMICS AND THERMODYNAMICS

Subsession IV-2

Convective clouds

RESULTS OF HAILSTORM STUDIES AND HAIL SUPPRESSION ACTIVITIES IN THE USSR

M.T. Abshaev, N.Sh. Bibilashvili, I.I. [illegible] L.M. Fedchenko,
V.G. Khorguani. High-Mountain Geophysical Institute,
Nalchik, USSR

The main purpose of hailstorm studies in the USSR is to learn the mechanism of hailstone generation and growth inside various clouds based on laboratory and theoretical modelling and composite studyins of hailstorms for scientific justification of hail suppression principles and of new methods of severe hailstorm modification.

A three-dimensional nonstationery numerical model of a hail cloud based on the thermohydrodynamical equations for cloud convection and kinetic equations for microphysical processes has been developed (Ref. 6). An algorithm based on a combination of splittering and projection methods is used for the numerical realization of the model. Effective applicability of the algorithm [illegible] the calculation of cloud processes is examplified by the solution of the test problems and a two-dimensional microphysical model of a hail cloud. A modified three-dimensional quasistationary model of a supercell hailstorm is proposed (Ref. 9). Here a transition is made from the averaged parameters or the cloud jet to their cross-section distribution using semiempirical relationships. During the calculation of cloud spectrum transformation the kinetic equation for a three-phased cloud is solved. Temporal variations of precipitation, and radar reflectivity are calculated on the basis of stationary thermodynamics. Stationary thermodynamics is valid for supercell clouds existing for a long time in their maximum development stage. Taking into account the supercell cloud features the regeneration movement velocity of a hail cloud as a function of atmosphere conditions relating to its continuous self-renewal at the front and breakdown at the rear as well as rotation effect of the upcraft around vertical axes are introduced into the model; besides, the feedback between liquid water content fields and precipitation intensity is considered. This model enables to calculate radar reflectivity fieldi and kinetic energy of hail and rain on the ground as for natural processes so at the crystallizing agent injection as well. On the basis of axisymnetrical nonstationary hail cloud model (Ref. 11) a set of numerical experiments on seeding by crystallizing and hydroscopic agent was performed. The effect of injected agents on the hail formation mechanism, the [illegible] and the size of falling hailstones was investigated, which helped to develop an optimal scheme of hail cloud seeding based on the norms, of agent consumption.

However, physical-mathematical modelling faces a set of difficulties relating to the necessity for accounting not only the processes of different scales, but also the interaction between the cloud and environment; in particular the process of cloud selfgeneration due to mesofront initiating during the spreading of a cold downdraft. Radar investigation of the structure, the evolution dynamics, [illegible] flow structure in clouds and in their vicinity was conducted by means of active, passive, coherent and noncoherent radars to develop empirical models of hail clouds (Refs. 1-5, 7). A severe hail process spectrum in the North Caucasus may be divided (Ref. 1) into three main types: singlecell, multicell, supercell, having similar main features with those in the other parts of the world. Besides, the classes of nonordered, weakly organized multicell processes and of intermediate or transitional types between the main three types were separated. Characteristic features in the structure and dynamics of hail clouds are exhibited during the maximum development of convection, but before this the frontal band of [illegible] cores of nonorganized [illegible] processes the supercell cloud [illegible] [illegible] multicell, [illegible] processes in the North Caucasus [illegible] average 20: 30, [illegible] processes occur in the days when wind direction changes sharply with height and its velocity is significant at all levels. Convective cells in these processes unlike [illegible] any part of the cloud system 2-10. have different directions and movement velocities. It is difficult to determine the place of formation [illegible] cells, to distinguish between "young" and "old" cells, while ordered processes [illegible] the right upwind flank where the [illegible] formation activity is found. [illegible] processes are observed 2-3 times rarer than the ordered ones, but they are intensive enough and may be accompanied by severe hailfalls. Weakly organized multicell processes develop in days when wind direction changes gradually with height and essential velocity at all levels in relatively dry air masses at surface layer is observed. Here the cloud system consists of a small number of convective cells and displaces along the leading flow or a little bit to the right. The majority of the convective cells generate and dissipate simultaneously, in contrast to the ordered processes, without replacement of one cell by another. Convective cells have relatively small cross sections, but considerable height (8-11 km) and curved form on RHI. They move [illegible] parallel to each other in one direction. [illegible] processes are relatively rare, weaker [illegible] mentioned above and do not [illegible] intensive hailfalls. Similar [illegible] conditions in absolutely different [illegible] conditions (Fergana Valley) confirm these results with [illegible] processes [illegible] not [illegible] cells and cloud systems have cross-sections 2-3 times larger than those in the [illegible] Caucasus, [illegible] hailstones fall rarely (Ref. 2). The studies of hail cloud microstructure with the help of three-wavelength radar and airflow structure by vertical Doppler radar and rocket sounding showed that the hall generated in the new convective cells, the first radar echo of which appeared above -6 -8 °C isotherm and in the frontal part of radar echo overhang of mature hail clouds at updraft velocities 2-5 m/s. Intensive hail growth is observed in the same zone at updraft velocity increasing in time and water content at -5 -25 °c. Maximum Wm updraft velocity is observed below the level of maximum hailstone size. It is supposed that this mechanism provides balance between some parts of hail embryos and later on of growing hailstones above the Wm level. Increasing win time makes it possible to keep them (long enough for hail growth) in high liquid water content zone. Continuous variations of Wi n hail growth processes in the vertical sounding regime show that the balance between the veloci-

e f a a ; : t n :te f t!; itvra f w 1i 1 s

between the velocity of hail growth and updraft velocity increase, i.e.

$$Wm = V_r + AV, \quad \text{where} \quad \Delta V < V_r,$$

$$dWm/dt \quad dVr/dt.$$

It is evident that at the balance disturbance hail emvry.os of growing hailstones will be either ejected upward from hail growth zone, or fall out of it not reaching large sizes. Such growth conditions obtained directly from experimental observations show that the process of hail growth is selective and not all hail embryos can grow to a large size. Small hailstones appearing late will be ejected upward, but early appeared and quickly growing embryos will not be kept by the updraft and fall out. The falling out of separate large drops from the radar echo overhang of supercells proves this observation. Large amount of these drops can prevent hail growth. I is noteworthy that Wm level increases in time and hail fall out process takes place at the moment when HWm becomes equal to Hdm. During the fallout hail continues to grow intensively and reaches the maximum size in the negative temperature region. Hail formation process may be conventionally divided into 4 stages: the formation of hail generation conditions, hail generation, hail growth, hailfall. We suppose that all 4 stages in axisymmetric cells of singlecell processes take place in the same spatial volume successive in time, but in nonsymmetric cells of supercell and multicell processes all 4 stages occur simultaneously in different parts of cells. So, the formation of hail generation conditions takes place in leader clouds in the front and at the boundary of the main cloud radar echo, hail formation - in the renewing part of the radar echo in the frontal right flank of the radar echo overhang, hail growth - in the radar echo overhang. The time of hail formation from the moment of the first radar echo (Ref. 3) is on an average 6-10 min, varying from 4 to 25 min. All.obtained results and the interpretation of dynamical, thermodynamical and radar structure of convective clouds allow to develop a preliminary empirical model of severe hail clouds, accounting for mesoscale circulation in hail clouds and the mechanism of cloud self-generation. The model expla1Qs pulsatory and continuous cloud development, resulting from mesoscale circulation nature (Ref. 7). Nowadays the equipment and techniques for microstructural, condensational and ice-forming properties of natural and artificial aerosols are developed for ground and airborne studies (Ref. 14). Numerous measurements of ice-forming nuclei concentration (IN) and giant aerosol particles were conducted. It is shown that the influence of the underlying surface is observed at the leveL of 1.5--2 km. As a rule, giant and supergiant (more than 30 m) aerosol particles are high temperature IN (active at -6 -S. °cJ. The concentration of IH in the atmosphere may change by 2-3 orders of magnitude and it depends on the underlying surface and different weather conditions. Besides, IN concentration has direct dependence on water vapour saturation. Special attention was paid to supergiant particles. It is due to their remarkable role in large drop formation and hailstone generation in clouds. The supergiant particle concentration changes from 1 to 10-1-1. Under the growing convective clouds their concentration increases approximately by an order of magnitude. The analysis of experimental data shows that there are two types of hail embryos (R f. 11): large drops and graupel. On the average graupel hail embryos are encount:ed more often. However, in some hailfalls one or another type of the embryo may prevail. The investigation of microphysical features and ice-forming properties of aerosol particles contained in hail embryos and their correlation with aircraft measurements and also the analysis of drop embryo bubble structure show that hail generates at the temperature above -10 °c. IN concentration - potential hail embryos - in the atmosphere by 2-3 orders higher than hailstone coneentration in clouds. Only high temperature giant and supergiant nuclei may convert into hailstones (Refs, 10, 11). Hailstone concentration in clouds is in inverse power law against mean-cubical hailstone diameter and varies from 10-1 to 102m-3. The fallout of hailstones- with 5--10 cm in diameter is characterized by the least hailstone concentration and that of small hailstones by the largest one.

In the USSR great attention is paid to the development of modification methods of hail processes. The well known hypothesis of modification are the following:

- development of enlarged hail embryo concentration, slowing down hail growth due to competition for liquid water;
- enlargement of drops with their subsequent freezing providing a-large amount of competitive nuclei;
- Cb dynamical failure by downdraft initiating;
- full crystallization.

The well known principle of competition is usually considered the most effective modification hypothesis. However, this hypothesis faces certain difficulties when interpreting its realization using new data on the mechanism of hail generation and growth. According to the second hypothesis which is.used in one of the hail suppression stations of the USSR more optimal conditions for effective competition are provided and therefore it has the same diffi-

Table 1

The results of hail suppression activities during 1976-1983

N	Hail suppression stations	1976		1977		1978		1979		1980		1981		1982		1983	
		TA	E	TA	E	TA	E	TA	E	TA	E	TA	E	TA	E	TA	E
1.	North-Caucasus	484	46	631	60	660	84	600	92	625	23	660	90	662	37.6	702	33.3
2.	Krasnodar	485	87	575	50	625	59	635	73	635	83	655	87	645	33.0	750	33.7
3.	Azerbaijan	737	89	737	97	752	99	822	97	902	95	962	92	1022	97.3	1022	75.0
4.	Armenia	911	95	911	99	920	99	920	99	920	97	950	95.	1010	99.2	1030	95.8
5.	Tadjikistan	450	79	520	91	550	89	550	71	620	88	650	86	660	66.4	660	97.2
6.	Uzbekistan	300	89	400	98	410	80	500	97	500	100	580	72	590	98.6	670	96.8
7.	Georgia	350	95	350	98	380	97	400	94	405	84	415	91	415	75.0	415	34.0
8.	Moldavia	730	89	810	91	910	73	1000	96	1180	95	1325	97	1430	98.1	1670	96.2
9.	Crimea	275	89	275	88	390	99	390	99	500	93	430	100	430	93.0	430	73.4
10.	Odessa											120	98	125	97.0	205	96.1
		4695	84	5209	86	5537	87	5817	91	6387	87	6747	91	7010	82.3	7565	73.1

TA - total target area; thousand ha; E - efficiency8 ".

culties.as the competition hypothesis.

In 1978 one more hail process modification hypothesis was proposed, the so-called hypothesis of precipitation formation acceleration in the condition formation zone for hail generation (Ref. 3) which suggested washing-out of this zone by prematurely stimulated precipitation befor'e hail formation. On the basis of this hypothesis and on the results of the investigations of the structure, evolution dynamics of hail clouds o'f various types and hail formation process a differentiated modification method of singlecell, multicell and supercell hail processes is developed (Ref. 3).

In all. types of hail processes the injection of the agent is supposed in the weak updraft. region, where cloud volume overheat is negligible. Such seeding is considered to be the most effective from the point of view of competition hypothesis either.

The analysis of the results of hail process modification showed that the fulfilment of this modific tion method requirements provides successful suppression and hail damage prevention. As the modification strategy of hail processes including the choice of place and time of agent injection, seeding volume and so on is determined by the structure, evolution dyriamics and hail process intensity the more detailed hail forecast is required for operational work and qualified planning of the experiments on seeding principle and method verification. That is why, together with the improvement of an alternative hail forecast we develop-the following methods of forecast:

- of hail cloud evolution mesoregion;
- of intensity,- structure and type of the hail processes.

This development is conducted on the basis of complex researches of aerosynoptical and thermodynamical evolution conditions for hail clouds of various types and intensity, the interaction between circulational.factors of different scales, the eftect of relief on hail process localization.

Graphical method of intensive hail process forecast based on consideration of the peculiarities of thermodynamical con ditions of low and middle troposphere as well as circulational factors providing a different degree of realization of air mass potential instability budget in this or that region (Ref. 3) is proposed. The forecast method of mesoregion of intensive hail process development based on the potential atmosphere instability, the structure of the thermobaric fields of upper and middle troposphere and surface distribution of pseudopotential wet-bulb temperature char acterizing thermodynamical peculiar ty of air mass is worked out (Ref. 8). The type of hail process at the given favourable conditions is determined by the wind structure in the atmosphere (Ref. -10). As applied to hail suppression activities further improvement of hail suppression method and means is carried out which includes:

- development and improvement of methods and equipment for distant hail detection;
- searching of new crystallizing agents - substitutes for AgI and PbI, development of compositions with low AgI and PbI content, optimization of the method of their dispersion with the purpose of increasing the effective ice-forming particle output from 1 g of composition and 1 g of agent;
- development of new and improvement of the existing means of agent delivery;
- development of optimal technology of hail process modification and the automatization of hail suppression activities.

Operational work on hail damage protection of agricultural crops in the USSR is conducted with the help of artillery and rocket hail suppression complexes on the territory of more than 7 million ha.-The regions of the most valuable crops (grape), cotton, gardens, etc.) which are more often subjected to hail damage, are taken under protection.

Table 1 shows the results of hail suppression activities in the USSR from 1976 to 1 83. The analysis of the results of hail suppression shows that in all regions and all hail suppression stations the stable positive result is obtained. On the average in all hail suppression stations during this period hail damage area is reduced by 4-5 times in comparison with the averaged data for many years.

REFERENCES

1. Abshaev, M.T., Atabiev, M.D., Malbakhova, N.M., 1976. Radar investigations of hail formation in cumulonimbus. Trudy VGI, No. 39, 7-32.
2. Absha v, M.T., Imamdzhanov, Kh.A., 1976. The structure and evolution of multicell storms in Fergana Valley. Trudy VGI, No. 39, 100-114.
3. Abshaev, M.T., Zhubo·ev, M.M., 1978. The principles of modification of single-cell, multicell and supercell hail processes. Trudy VGI, No. 39, 106-129.
4. Abshaev , M.T. , 1981. Complex radar investigations on structure and evolution dynamics of hail processes. Trudy V All-Unj on Conference on Radar Meteorology, M., 94-101,
5. Abshae.v, M.T., 1982. Structure and evolution dynamics of thunder-hail processes in the North Caucasus. Trudy VGI, No. 53, 70-89.
6. Ashabokov, B.A., Kalashokov, Kh. Kh., 1984. Nonstationary three-dimensional numerical model of a hail cloud with an allowance for microphysical processes. Trudy Intern. Conference on Cloud Physics, Tallinn.
7. Bibilashvili, N.Sh., Kovalchuk, A.N., Terskova, T.N., 1982. Empirical model of a severe hail cloud and some aspects of hail generation and growth. Trudy Intern. Conference on Hail suppression, Sofia.
8. Goral, V.G., Gorokhova, V.L., Chepovskaya, 9.I., 1982. On the detection of the mesoregion of· severe hail process development in the North Caucasus. Trudy VGI, No. 53.
9. Kachurin L.G., Bekrya_ev; V.I., 1982. Numerical model of a supercell hailstorm. Trudy Intern. Conference on Hail Suppression, Sofia.
10. Malbakhova, N.M., Belentzova, V.A., 1982. The effect of synoptical situation, wind regime, thermodynamical state of troposphere on the types of hail processes in the central regions of the North Caucasus. Trudy VGI, No. 51, 100-107.
11. Nadibaidze, G.A., Sulakvelidze, G.K., 1984. On the active modification on hail clouds using crystallizing agents. Trudy VGI, No. 59, 11.
12. Tlisov, M.I., Khorguani, V.G., 1982. On the condition of hail embryo generation in clouds. Izv. Acad. Scie., USSR, Atmospheric and Oceanic ?hysics, 18, No. 3, 256-261.
13. Fedchenko, L.M., Belentzova, V.A., 1982. Severe hail process forecast in the•North Caucasus. Trudy VGI, No. 50.
14. Khorguani, V.G., 1982. Microphysical investigations on hail generation and growth. Meteorology and Hydrology, No. 8, 118-125.

SEVERE HAILSTORM INVESTIGATIONS IN THE NORTH CAUCASUS

M.T. Abshaev, A.Kh. Adzhiev, V.A. Belentzova, V.S. Makitov, B.Kh. Tkhamokov, L.M. Fedchenko, V.G. Khorguani, M.M. Chernyak, Ya.A. Ecba

High Mountain Geophysical Institute, Nalchik, USSR

1. EXPERIMENT

In-order to receive detailed insight into hail processes a complex experiment on the development of hail cloud model and hail formation mechanism investigation was conducted at High Mountain Geophysical Institute. This experiment was based on the studies of:

- thermodynamical and aerosynoptical conditions of hail cloud generation and development;
- spatial structure and dynamics of hail cloud and their classification;
- itructure and evolution of hail cores;
- condensation and the role of ice-forming nuclei in hail formation;
- hail embryo nature, region and time of formation and growing hailstone trajectories;
- hail cloud microstructure and hail growth mechanism due to liquid and mixed fractions;
- airflow structure and metebelernent (ME) fields in h il clouds and environment by different methods;
- thunderstorm activity and prethunder radiation of hail clouds.

various numerical cloud models are used to interprete available experimental data. The experimental polygon 200x100 km in the North Caucasus at the foothills of the Main Caucasus Range where high hail activity combines with all main types of hail processes was used. The equipment used:

- apparatus for frequent radio and rocket sounding of atmosphere and clouds;
- precipitation gauge network on 50 x 50 km^2 area; 1 apparatus per 100 km^2, ground network for air sampling;
- apparatus for obtaining satellite and synoptical information;
- apparatus on 20 X 100 km^2 with 1 apparatus per 9-10 km2;
- two MRL-5 dual-wavelength radars with a device for receiving the reflectivity isolines;
- three-wavelength radar;
- MRL-2 polarization radar;
- decimeter Doppler radar with 6 m antenna of vertical sounding and 0.86 cm radar and triple Doppler radars with an electronic **computer;**
- radar-radiometric station with two receiving channels of hail cloud thermal ra diationf
- experimental complex "Spectrum" to obtain thunder radiation at 10 frequencies (from 4 kHz to 3000 MHz);
- decimeter radar for lightning discharge channel detection;
- thunder detector-range finder for lightning discharge recording;
- aircraft laboratory with equipment for air sampling, aerosol particle dispersion and conductivity analysis, microstructural and thermodynamical measurement of atmospheric and cloud characteristics;
- mobile laboratory with an apparatus. for air sampling and hail spectrum determination;
- thermodiffusion chambers.

Each complex is provided with an apparatus for first treatment and information recording. Complex experiment was started in 1983 though investigations of separate parts of the program were conducted since 1975. In this work the results of the investigation of three hail pr'ocesse_s observed on June 15, 17, 20 are given.

2. CIRCULATIVE CHARACTERISTICS AND PRECIPITATION DATA OF THE ANALY_SED PERIOD

Studies showed (Refs.5, 8, 9) that for formation of certain types of hail processes tre following conditions re necessary:

- high enough humidity in the low tropospheric layer;
- existence of strong wet and convective instability layer above condensation level and optimal temperature range in hail growth region;

Table 1. Circulative characteristics and precipitation data of analysed period

Data	14.6.83	15.6.83	16.6.83	17.6.83.	18.6	19. 6.	20.6.	21. 6.
Synoptic. situation	Cold front from north at night	Second cold front from north at 5 a.m.	Low pressure non-gradient field					
Front T 0C	4	2	-	-	-	4	4	4
Front V (km/h)	20	20		-2.3 mb	-	30	40	30
Observed events	Dry thunder	Squall, hail	Small hail	Squall thunde:c-storm, intense shower	Weak shower, rain	Intense hailfall d≤ 2 cm	Intense hailfall d"" 5 cm	Hail
Precip. maximum (mm)	-	15	17	6.8	70	69	40	30

- some dynamical mechanisms leading to the development of convective movements in low tropospheric layer and realization of middle troposphere instability;
- particular wind structure leading to formation of mesoscale convective system of corresponding type.

The period from June 14 to 23, 1983, when actually every day the development of the convective systam with precipitation occurred was chosen for analysis. Weather conditions on the polygon territory during this period were determined by two natural synoptical periods (NSP). The first period (June 9-16) was characterized by a deep cyclone in the region of Dickson island and latitudinal orientation of interfaces displacing from the north to the target area. Second NSP (June 17-21) was characterized by the existence of a blocking anticyclone in the region of Nizhnee Povolzhye, by the movement of cyclonical disturbances from the south to the polygon territory and meridional interface orientation. Table 1 shows the main circulative characteristics of the analysed period. As seen from the Table the most favourable circulation conditions for intensive hail process generation in the Central North Caucasus (Ref. 5) are observed on June 14-15 (passage of interfaces with latitudinal orientation). However, thermodynamical characteristics of low and middls troposphere do not promote the realization of these processes (s = 300 J, wm = 10 15 m/s) (Fig. 1). Optimal combinations of thermodynamical and circulating characteristics were observed on June 19-20 (Fig. 1, Table 1). Thermodynamical and synoptical characteristics were practically the same on June 19-20 with the only difference in wind structure in heights. On June 19 the considerable negative wind shear at 1.5-3.0 km level was observed, which was not true for June 20. So, the most favourable conditions for initiation and maintaining for a long time of organized convection in all troposphere layers were observed on June 20.

Airborne investigations showed that at the development of hail processes during the specified period the mean ice-forming nuclei (IN) concentration in the atmospheric layer up to 3-4 km increases several times (Fig. 1). In subcloud layer of severe convective clouds during their development the concentration of high-temperature IN increases more than by an order of magnitude and at -10 °c is more than 1 i-1. At the same time the concentration of falling hailstones is by several orders lower. From this follows that there is IN excess in atmosphere; these nuclei are considered as potential hailstone embryos. This shows that selective formation of hail particles takes place at which only high-temperature IN convert into hailstones (Ref. 6).

3. HAILSTORM ON JUNE 15, 1983

Rawinsonding data showed that weak south-eastern wind was observed in surface layer up to 1,5 km at 13.00, but at higher atmospheric layers - south-western wind with velocity increasing in height (Fig. 1). Such wind structure is favourable for the development of ordered multicell processes or intermediate processes between ordered multicell and supercell hailstorms (Refs. 1, 8). Fig. 2 shows the spatial structure and dynamics of hail process development. According to Fig. 2 cloud system at 16.21 consists of a strong hail convective cell (N1), on the left flank there is one dissipating cell and on the right there is a new generating convective cell (N2} at the height of 8-10 km. Intensive development of cell N2 is observed later. In 46 min cell N2 became dominant and cell N1 dissipated gradually. At 17.20 the hailfall from it finished; in 8 min it almost completely dissipated. This dynamics of the development characterizes the ordered multicell process. Cell N3 and several new cells quickly reaching hail stage and so quickly dissipating generate ahead along the direction of hail process movement. Radar echo on RHI is characterized by the fact that at 16.41 cell N1 has overhang of intensive radar echo in the rear part of which hail growth is observed. Spatial overhang orientation deviates from the direction of cell movement to the right, that is typical of many intensive hail cells of llRllticell and supercell processes. At the development stage the cell N2 is observed along the direction of radar echo overhang. In this cell there is a local hail core and overhang of radar echo is forming at the same time. During the development of the cell N2 precipitation from it actually completely cove+s the region of cell N1 ordered updrafts and causes its dissipation. Hail streaks of cells N1 and N2 merge and are practically the continuation of each other (Fig. 2). Hail cores displace to the right upwind flank of a convective cell. Maximum hail size (5 cm) and maximum total kinetic energy (6.10 Jm-2) were reported in the central part of hail streaks and decreased to periphery according to the data of surface hail indicator network. The length of hail streaks N1, N2, N3 was 32, 50, 38 km, respectively, total length being 120 km. Convective cells moved at the angle of 10-15° \to the right) in the direction of the leading flow and had velocities of 1.5--2 times smaller than that of the leading flow. Maximum activity of thundercloud system was observed in the rear of the more intensive convective cell. In ME fields at the ground surface the mesofront corresponding to the period of maximum development, is clearly seen. (Fig. 2).

4. HAILSTORM ON JUNE 20, 1983

Circulative and thermodynamical characteristics of the atmosphere facilitate the formation and development of intensive hail processes (Ref. 5, Fig. 1). Wind in surface layer was easterly 3 5 m/s, at 3.1 km-southerly and above this level - south-eastern with increasing velocity in height. As is seen from Fig. 3 cloud system from 13.49 to 15.55 consisted of one intensive asymmetric convective cell with the structure and features of a supercell of moderate (for the North Caucasus} intensity. Supercell life time was a little more than 2 hours including development stage from 13.45 to 14.00, dissipation stage from 15.30 to and quasisteady stage from 14.00 to 15.30. At 14.00 n the right flank of the supercell the development of a new convective cell is observed as in multicell processes. But this cell did not develop and dissipat-

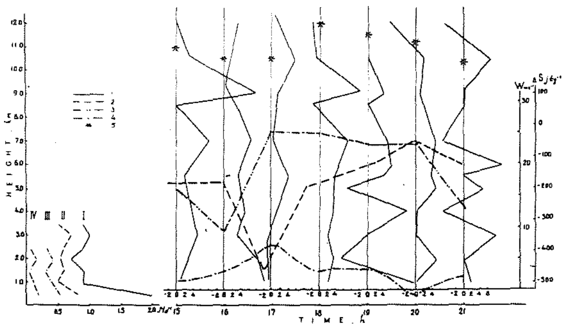

Fig. 1. Circulative and thermodynamical characteristics and vertical profiles of ice-forming nuclei concentrations. 1-wind shear; 2-j$; 3-Wm; 4, 5-heights of condensation and convection levels, respectively; I, II-IN concentration on June 15 at -20 °C and -10 °C, III, IV-the same on June 9.

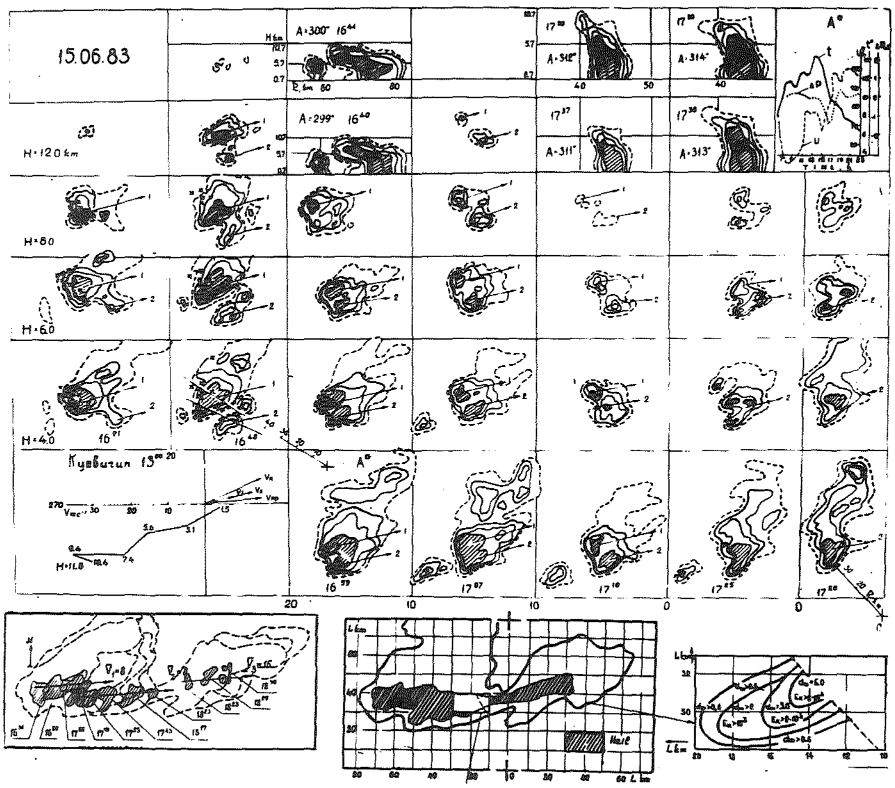

Fig. 2. Radar echo structure of ordered multicell of hail process on June 15, 1983 on PPI an RHI is shown by reflectivity isolines at = 10 cm with 10 dB intervals. The first dashed profile corresponds to 10 = 10-12 cm-1 (lg Ze = 15 dB). Hail cores obtained by dual-wavelength method are shown by shaded areas, crosses indicate lightning discharge bearings. In the low left corner the wind hodograph before the beginning of the process is shown. Hail streaks and kinetic energy isolines are given at the bottom of the picture, the variations of the temperature t, pressure P and relative humidity U are in the upper right corner.

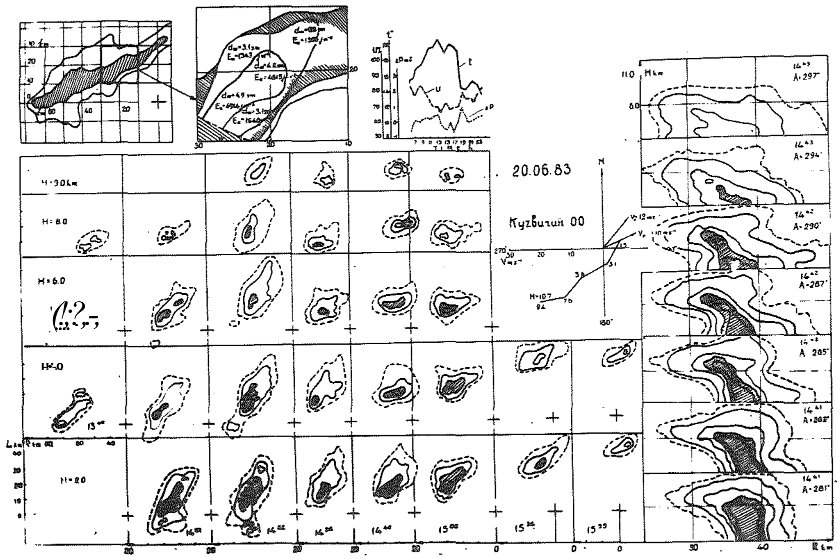

Fig. 3. Supercell hail cloud radar structure on June 20, 1983 on PPI and RHI. The symbols are the same as in Fig. 2. Reflectivity isoline is not given on PPI display 11. 1o = 10-10cm-1 (35 dB).

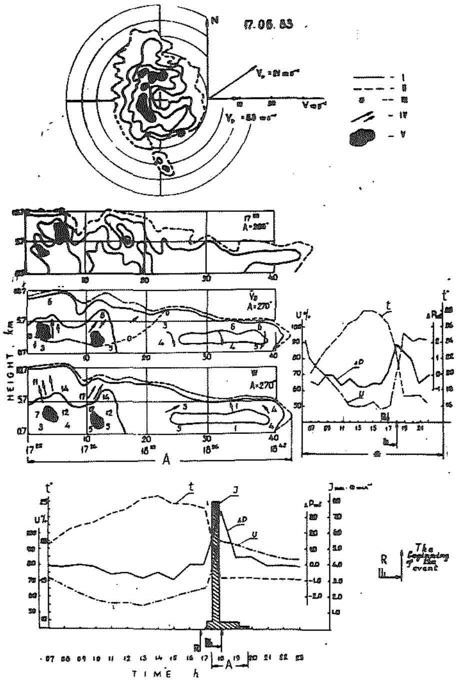

Fig. 4. Horizontal (a) and vertical (b) cross-sections and height-temporal distribution of vertical motions of hydrometeors (c) and air (d) in one of the cells of random multicell process on June 17, 1983. Arrows show direction, numerals - motio velocity, fVP high reflectivity zoneyt 10-9cm- ! ,A= 11 cmi.

ed at 14.25. At the development and dissipation stages supercell moved. along the leading edge to the north-east and at the quasi-steady stage to the right of the leading flow direction with 36 km/h which is 1.2 times less than the leading flow velocity. Radar and ground observations show continuous hailfall streaks (Fig. 3). In - the central part of the hailfall streaks and near the right flank the largest hailstones are observed (<l? 5 cm, E = 4800 J/ /m^2). Radar data. on hailfall region, dimension and kinetic energy agree well with hail indicator network data. Fig. 3 shows ME trajectories near ground surface. Airflow structure investigation in 1983 was conducted with the help of Doppler radar of vertical sounding. Hailstorm on June 15, 20 passed to the north of the Doppler sounding limit, that is why it was not possible to get information on vertical motion in hail clouds. Fig. 4 shows high-temporal picture of vertical flow distribution in one of the nonhail convective cells of a random multicell process observed on June 17, 1983. It is obvious that maximum updraft velocities (W = 16-17 m/s) are accounted in the mi dle part of the radar echo overhang at 4-5.5 km a.s.l. that is on 0.5-1.15 km higher o0 isotherm. In the case of hail cloud maximum updraft velocity is met above. From radar echo overhang the fall-out Gf separate large drops is observed which leads to radar echo overhang propagation with weak· echo region practically.up to the ground surface. In the rear weak updrafts about 1 3 m/s are observed, near the rear edge they increase up to 4 m/s. ME trajectories in two regions shown on PPI justify the existence of mesofront, accompanied by intense precipitation from·17.30 to 17.50, which agrees with radar data.

5. DISCUSSION OF THE RESULTS

The results of complex investigations of hail processes and radar studies of more than 200 hail processes during 1975-1982 (Ref. 1) show that severe hail process spectra in the North Caucasus may be devided into three main types (Ref. 2): single cell, multicell, supercell, which have the same structural features and dynamics as hail processes in other regions of the world. Besides, the types of random and multicell processes with weak organi·zation and the intermediate type between the first three are determined.

Charac·teristic features of structure and dynamics of hail processes are observed during maximum convective development. Frontal cores usually precede the appearance of supercell and organized multicell process development, as a rule, on the right flank of frontal, cloud system in the form of a new cell generating in high levels with the development of which frontal cores dissipate and at the mature .stage there are no other convective cells. Here, hailfall intens'ity in the middle troposphere is d_etermined (Ref. 5) by convective instability budget and conditions of "wet" growth regime, in the low troposphere by sufficient moisture supply and possibilities of thermal and convective _dynamical mechanism realization. Orography greatly influences increase and decrease of hailfall in certain mesoregions due to interaction with large-scale circulation; wind structure variations in height at given conditions determine mesoscale convective system organization. Repetition of hail processes of different types in the North Caucasus is the following:

single cell 20 %
random multicell 25 %
organized multicell 30 %
intermediate (transitiona] type 15 %
supercell 10 %.

The analysis of inner hailstone structure shows that in the whole hailfall two types of embryos, that is large drops and grauple are observed simultaneously. However in some hailfalls one type of embryos dominates the other and vice versa. For example, in hailfall on May 4, 1983 80 % of the embryos were drops, but on May 5, 1983 they were only 15 %. On the whole the prevalence of grauple embryos is observed (Ref. 7). The analysis of bubble structure of drop embryos, microstructural, condensational and ice-forming features of aerosol particles in hailstone embryos shows that a hailstone particle generates at the temperature above -10 °C. Transition of large supercooled drops into hailstone embryos is due to heterogeneous ice nucleation. Hail cloud characteristics calculations on'the basis of stream model (Ref. 4) show a good correlation with experimental.observa ion data.

6. REFERENCES

1. Abshaev, M.T., 1981. Complex radar investigations of structure and dynamics of hail clouds. Trudy V All-Union Conf. on Radar Meteor. M., 94-100.
2. Abshaev, M. T. , Burtzev, I. I. , et al. , 1980. Manual on radar MRL-4, MRL-5, MRL-6 application in the system of hai suppression., L., Hydrometeoizdat, 231 pp.
3. Abshaev, M.T., Belyavski, A.B., Tkhamokov, B.Kh., 1981. Doppler radar investigation of hydrometeor movement and vertical flow in thunderclouds. Trndy V All-Union Conf. on Radar Meteor., M., 46-50.
4. Kachurin, L.G., 1978. Physical basis of atmospheric process modification. L., Hydrometeoizdat, 455 pp.
5. Fedchenko, L.M., Belentzova, V.A.·, Berova, M.A., 1983. Severe hail process forecast in the North Caucasus. Trudy VGI, No. 8.
6. Khorguani, V.G., 1982. Microphysical investigations of hail generation and- growth. Meteorology and Hydrology, No. 118-125.
7. Khorguani,V.G., Tlisov, M.I., 1982. On conditions of hail embryo generation in clouds. Izv. Acad. Sci. USSR, Physics o Atmosphere.and Oceans, vol. 18, No. 2, 256-261.
8. Hail report No. 3. The dynamics of hailstorms and related uncertainties of suppression. Geneva, 1981, 22 pp.
9. N1=wton, C.W., 1-63. Dynamics·and severe convective· storms. Met. Monogr., No. ·27, 33-58.

THE MORPHOLOGY OF MERGING CLOUDS

B. Ackerman and N. E. Westcott
Illinois St2te Water Survey, Champaign, IL, U.S.A.

1. INTRODUCTION

.The aggregation of individual clouds or the joining of smaller clouds with larger ones is a common feature of the evolution of convective rainstorms. It is possible to propose a number of **scenarios aS to how and where individual convective elements joiq, with the nature of the union** ran_,·ng from a true blending of vertical drafts to expansion of decaying cloud masses without any significant dynamic interaction. Cloµds may simply grow together as they individually expand; new cloud, triggered by ·downdraft-induced convergence, can bridge two older storms; detrained or decaying cloud material from two systems may join aloft, providing **a better environment for expansion of the original** clouds or the development of new ones between, or large convective storms may so modify the environ**ment so as to cause new clouds to form nearby and to** be drawn into the existing cloud mass.

Examples of some of these scenarios are presented in this short note. These selected cases occurred in the early stages of cloud lines on two summer days in Illinois, in central U.S.A. a midlatitude continental region with relatively simple topography. The study was based on digital reflectivity data obtained with a high-power, narrow beam **(1°) 10** cm radar. The merger events occurred over a high-density surface network of wind and precipitation sensors, with ·spatial resolution of about 6.5 and 5 km resp. and smoothea temporal resolution of 5 **min (Ref. 1).**

The full 3-dimensional volumetric radar data (temporal resolution, 4 min) have been objectively analyzed for all reflectivities > 10 dbz using an 8 point interpolation scheme to provide horizontal and vertical slices through the cloud systems. Cloud areas·are considered to have merged if separation between echoes with boundaries defined by the minimum level of 10 dbz, was greater than the spatial resolution of the radar data. This threshhold for merging is considerably less than that used n most ·published studies dealing with precipitation "cells" or with cloud histories (most of which have been for heavy rain or severe storms). In Fig. 1 are shown curves of.drop concentration and liquid water content as a function of drop size for a monodisperse drop spectrum. As can be seen, IO dbz represents very thin cloud matter.

2. SEMI-ISOLATED CLOUD DEVELOPMENT

Two of the merger events are related tq the development of a semi-isolated multi-cellular shower cloud, which was an early member of an E-W line of clouds extending for nearly -200 km. The first cell (A in Fig. 2) appeared as an echo at 4 km at 1511 local· time and· increased rapidly' in vertical and horizontal extent and in intensity. Within 5 minutes, a few scattered small, weak, short-lived echoes developed at 2-3 km to the SE of A. As A grew and intensified, 2 or 3 of these •smalI echoes clustered and became one. Both A and this new cell (B in Fig. 2) expanded, and by 1528 had merged.

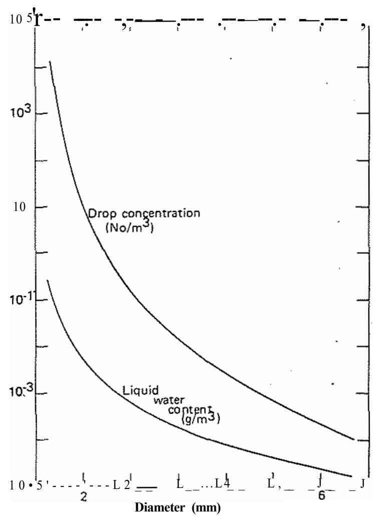

Figure 1. Drop concentration and liquid water content at 10 dbz, as a function of drop size.

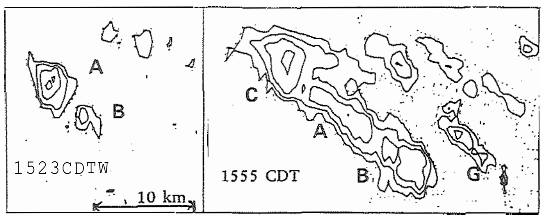

Fif,ure 2. The evolution of the radar echoes of the cloud complez discussed in Cases I and II. Contour interval is 10 dbz, with the 10 dbz threshold shown dotted.

The cloud continued to grow as a complex of 3 cells, elongated in a NW-SE direction, through development of a third area on the NW side of A. These three cloud sectors remained identifiable at upper altitudes and in reflectivity for over an hour, persisting not as single reflectivity cores but through the dev-elopment and decay of new reflectivity cores of much shorter duration and smaller areal extent.

Around 1544 a few small scattered echoes developed several km east of cell B. These clustered and fused and the resulting cloud (G in Fig. 2) grew and intensified rapidly. Cloud G rem ined independent for 20 min., finally joi·ning cell B of the complex to the west after it had reached heighrs of 9 km and intensities of nearly 50 dbz.

The manners in which the mergers cell B to cell A and cloud G to cell B occurred were quite different. In the first of these (Case I) the echoes expanded in the lowest levels until they joined. The level of reflectivity at which this "bridge" first occurred was over 20 dbz (Fig. 3). The two echoes had reached about equal heights f7.5 to 8 km) with the older slightly taller. Cell A h d reached a reflectivity of nearly 50 dbz and the level of the maximum was descending, whereas the younger cell B was still increasing in height and intensity and the maximum reflectivity core was aloft. The first small shower at the surface began at about the time f the merger (from Cell A) but the surface wind. field (which had been weakly convergent in the area for an hour or more) did not indicate any noticeable hange due to outflow.

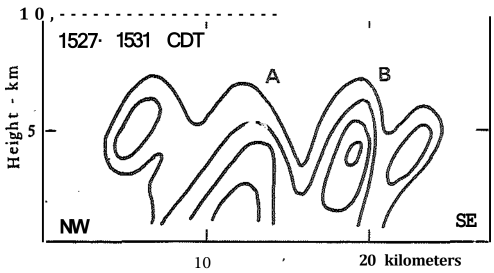

Figure 3. Vertical slices throu9:h the echo discussed in Case I. Contour interv l is 10 dbz, with 10 dbz minimum.

In the second case (II) both individuals of the union were larger and older and reflectivities were higher. Whereas area expansion of both A and B had been greatest in the lower levels, cloud G expanded in area with height to :hP middle levels with iµcrease primarily t0 the west thus producing a "shelf" at altitudes of 6 to 7 km which extended over the eastern edge o cell B. It is in this area that the first tenuous connection between Band G occurred at 1603. This connection grew through a greater depth within the next few minutes but remained aloft. At the same time the top of cloud G grew rapidly from 9 to 13 km and maximum reflectivity increased by 10 dbz, to nearly 60 dbz. Quite a separate bridge formed between the two echoes in t next 4 minutes (Fig.). A narrow hand of echo with reflectivity levels reaching near 20 dbz joined the two cloud area from 1 to 3 km, while about 3 km north the two were distinctly separated at the lower levels but "merged" around 8 to 9 km as the top of B met the westward shelf of G. Throughout this period B was decreasing in intensity while maximum reflectivity remained near 60 dbz in G. Brief showers fell from cloud G started at about 1600 but the most intense rain shower at the surface did not occur until 15 or 20 min later.

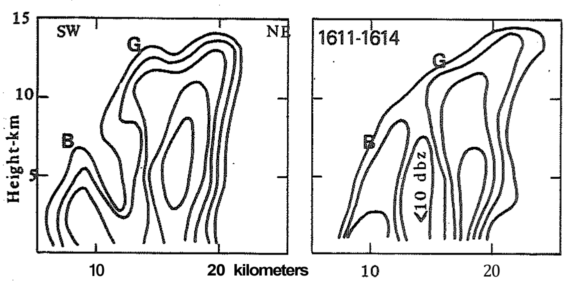

Figure 4. Two vertical slices through the e ho. disctissed in Case II. The section on the right is about 4 km northwest of the one on the left. Contours as in Figure 3.

3. PREFRONTAL SQUALL LINE CLOUD

The following three merger cases (III-V) are related to the evolution of a large cloud complex in the leading line of two pre-frontal squall lines. Starting first as a merger of several individual clouds (A-C in Fig: 5), an eastern arm was added by union with cloud (D), a northern extension when cloud F linked up and a western arm when cloud G joined the complex. The complex produced some very **intense rainshowers.**

Clouds A and B, although larger than those of Case I, joined in much the same way by expanding as they grew taller and stronger until their echoes merged, first at the lower levels and then through greater depths. The merger of B to C was of the same type.

Case IIi deals with the development of the eastern arm. Cloud D first appeared as a well defined small echo 12 km to the east.of A. It grew rapidly in height and breadth, principaliy on the west so that its separation from A decreased. By 1753 (18 minut s after D first appeared), the gap had narrowed to 5 km. Both echo areas were producing significant showers (8-9 mm in 10 minutes) although of limited areal extent, as were Band C. They had reached heights of 10 km and intensities in the rang!= of 50-55 dbz..

The clouds were on the southern limits of the wind network so data are sparse. However there is some evidence of modification of the southerly surface winds due to outflow.

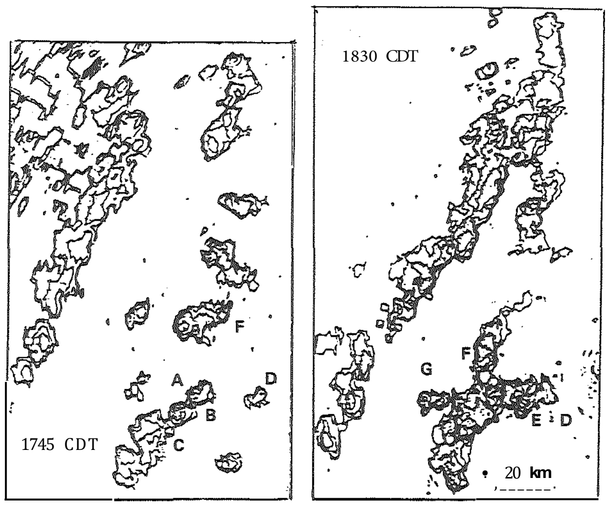

Figure 5. The evolution of the radar echoes of the cloud complex discussed in Cases III to V. Contour interval is 10 dbz with 10 dbz minimum.

At 1756 a small, well-defined echo (E) appeared between A and D, separ ted by about 2 km from each of them, and extending from 1 to 4 km, with max reflectivity about 25 dbz (Fig.6). By 1800 some weak cloud matter had formed to join this new small cloud to A in the lowest 3 km, and 4 min later, as E grew in dimensions, it joined cloud D. The latter bond was the stronger of the two for the next 10-12 min in the sense of greater depth and intensity of the "bonding" cloud. However about 1818 cloud D

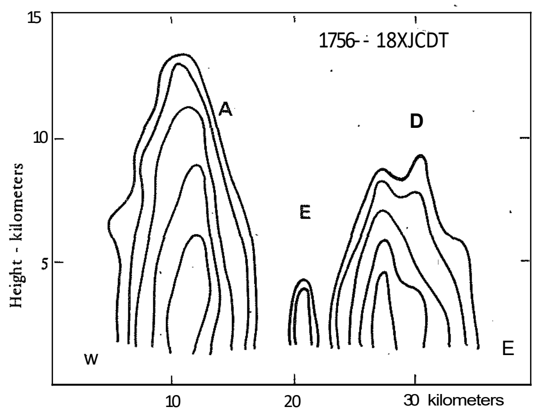

Figure 6. Vertical section through echo discussed in Case · III. Contours as in Fi f;U re ,3.

began to decline, and the union of E and A became more complete, although they remained as individual reflectivity cores above 20 dbz. By this time the A-C complex had become as one at 30 dbz at the lower· levels, and A-B were definable as separate cores only at reflectivities above 40 dbz. This part of the complex reached 13 km, but the northern edge had begun to decrease in reflectivity, particularly above 2-3 km.

Case IV deals with the "bridging" between cloud F and the north end of the A-E complex. Cloud F was a long lived cloud mass which had produced significant rain at the surface as early as 1700 local time and continued to provide rain at the surface for an hour before it joined the cloud to the south. Some of the showers were heavy (rates to 6 cm/hr) but of short duration. Outflow from this storm was pronounced and caused a sizable area of convergence at the surface with central values over 5 x 10-4 s-1 to its south, where the outflow had direction opposite that of the ambient air. The convergent flows spanned the space between the two cloud masses, which were 10 km apart. The magnitude of the convergence varied during the first half hour but persisted at 4 to 6 x 10-4 s-1 (areal resolution of 100 km^2) from 1740.

Starting at about 1800, small weak fibrous-appearing echoes occasionally appeared at altitudes Qf around 6 km. However these were transitory and the first persistent echo between the two clouds did not appear until 1815. This expanded and moved northward, feeding into the main reflectivity core of cloud F, narrowing the gap between the two cloud masses to about 2 km. The low reflectivity(< 30 dbz) echo aloft continued and co.nsolidated as ***a*** "shelf" between 6 and 8 km, on the north and west s_ide of complex A-E (main activity was on the S edge of cloud). By 1823 this shelf had extended sufficiently far orthward at 6 km to bridge the gap in a narrow band. Subsequently the bridge becanie broader, althougb reflectivities remained at 20-30 dbz. The two cloud masses joined in the lower levels at about 1830 as the new cell in cloud F bulged southward. The jun.cture points at low levels (below 5 km) were to the west of those between 6 and 8 km (Fig. 7) so for at least 10 min the merger was not complete through the entire depth. Rain from the new development in F was observed as early-as 1825 but the rain intensity increased dramatically at 1835, when rain rates of about 10 cm/hr occurred for a period of 15 min.

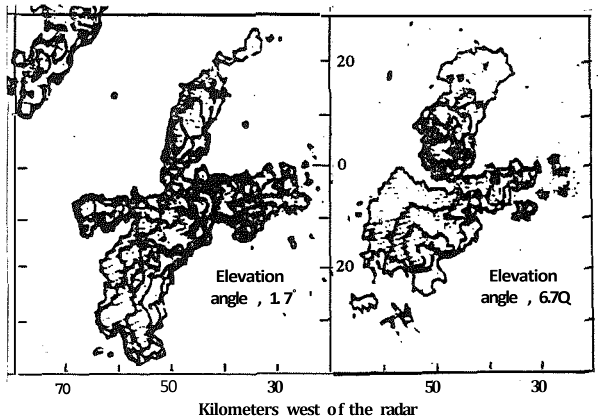

Figure 7. PPI views of the radar echo discussed in Case IV, at two elevation angles. The altitudes of the bridges between the northern and southern echoes are approximately 1.5 and 5.5 **km** ,resp., for left and right views.

The final event (Case V) started in a manner not unlike that in Case III, i.e., as the formation of an independent cloud adjacent to·, but some· distance from, the complex A-E. Cloud G fir.st appeared on the radar at altitudes from 2 to 6 km, about 7 km west of complex A-E, at 1812. (By this time the complex had developed its ea.stern "arm".) The echo grew and intensified as an independent echo for about 10 min. Areal expansion occurred through the development of a new small core on the east side, thus narrowing the separation to the larger cloud to the east. This small cell first appeared at 1818 as a shallow weak echo at 2 km, and grew to 4 km in the next 4 minutes. By this time the middle level "shelf" on the west side of the A-E complex (mentioned above in the discussion of Case IV) had E:<P,anded to the extent that it overhung this new reflectivity core at 7 and 8 km (Fig. 8).

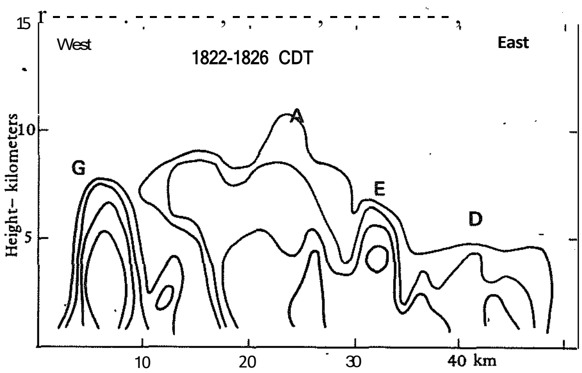

Figure 8. Vertical section through echo discussed in Case V. C ntours as in Figure 3.

The main cell of cloud G persisted s a well-defined entity and, though its vertical extent remained below 9 km, reflectivities reached 50 dbz, and a small rainshower was produced. The eastern core of G remained a low-level phenomenon, never exceeding 5 km in height, but acting as a bridge between G and th main cloud to the east. The bridge which exceeded 20 dbz, first formed at about 3.5 mat 1830 and grew vertically in both directions so that by 1836 it extended from about 1 km to 5 km. The shelf from A-E continued to extend over this lower bridge.

4. SUMMARY COMMENTS

A recent review of literature dealing with the aggregation of convective elements (Ref. 2) has demonstrated the importance of this phenomenon to the development of significant precipitation. The encouragement of cloud mergers has also been proposed as an intermediate goal of cloud modification for dynamic enhancement of convective rainstorms, ultimately leading to increased precipitation (Ref.3). In this short note,we have illustrated some of the ways in which the physical substance from two clouds, i.e. the cloud particles, may join. We have also attempted to indicate, within the limitations of space, how the consequences of such mergers may vary, both with regard to the evolution of the storms and to the precipitation that they yield.

This study was based on cloud detection by radar, as have the majority of other studies of convective clouds. Although we used a threshold of 10 dbz as the criterion for merger, the radar echo reached 20 dbz almost simultaneously in the connecting area. Thus our definition is comparable to that used in many other studies in the literature.

The examples presented here point out, once again, the complexity of convective storm development. Although clouds A-B-C of the semi-isolated cloud discussed in Section 2 and of the prefrontal etorm discussed in Section 3 merged in a similar manner the degree.to which their reflectivity patterns became one was much greater in the latter than in the former. Case III is an example of the mechanism proposed in Ref. 4, by which two cloud masses are "bridged" by a new -elQ-ud.which. has heen triggered by outflow-induced convergence. However strong convergence associated with out flow produced only a small feeder cloud into one of the storms in Case IV, and then after a relatively long time. In this case (IV) evidence of evaporating middle level "shelves" from both storms was noted for some minutes before.they were joined, suggesting modification of the air at these levels as a factor in the formation of the bridge betweem them. In Cases V and II cloud shelves with reflectivities of less than 25 or 30 dbz extended from the stronger of the two clouds, over the gap between them before the union of the two cloud masses. It is hypothesized that :hl these two cases, as in Case IV, the overhanging.shelves often observed from convective clouds in the area of this study and evaporating cloud matter at mid-levels may be important factors in inducing cloud unions, by seeding lower clouds with the large water drops or ice particles in their virga-and/or by evaporative cooling in these levels, thus acting toward destabilization of the air in the lower few kilometers.

Aoknowled.gments This work was supported by the State of Illinois as part of PACE, a State-Fed·eral cooperative program to study weather modification in the U. S. Corn Belt.

5. REFERENCES

1. Ackern:an, B., Scott, R. W., and Westcott, N.E., 1983': *Swmmary of the VIN Field Program: Summer* 1979. Tech. Rpt. 1, NSF Grant ATM-78-08865. Illinois State Water Survey, Contract Rpt. 323.

2. Westcott, N. E., 1984: A historical perspective on cloud mergers, *Bulletin Amerioan MeteorZogioal Soaiety*, (in press1 ..

3. Simpson, J., and W. L. Woodley, 1971: Seeding Cumulus in Florida: New 1970 Results, *Saienae*,. 172, 117-126.

4. Simpson, J., Westcott; N. E., Clerman, R. J., and Pielke, R. A., 1980 : On cumulus mergers, *Arah. Met. Geoph Biokl* Ser A 29, 1-40.

BOUNDARY LAYER THERMODYNAMICS OF A HIGH PLAINS SEVERE STORM

Alan K. Betts

West Pawlet, Vermont 05775, USA

1. INTRODUCTION

This paper analyses the bulk thermodynamics in the lowest few hundred millibars. A relatively new analysis technique using air parcel saturation point (Ref. 1-3) will be used to simplify the thermodynamic analysis in terms of conserved parameters, and simultaneously compact data from surface and aircraft (sampled at different levels) into comparable form. This paper also draws on the conceptual analysis of downdrafts in terms of mixing and evaporative processes suggested by Ref. 4.

The data used comes from the 1981 Cooperative Convective Precipitation Experiment (CCOPE). This experiment was designed to study convective clouds and storms over a network near Miles City, Montana, using a dense surface mesonetwork, upper air soundings from 5 stations, fourteen research aircraft and seven Doppler radars (Ref. 5). The mesoscale thermodynamic structure associated with a severe storm which passed through the research area on August 1, 1981, is analysed. The environment of High Plains thunderstorms is complex; with large horizontal gradients of moisture at the surface and large gradients in the vertical. On August 1, 1981, conditions occurred favorable for severe weather with a deep mixed layer of high θ and low θ ('continental tropical air') overlying a slightl cooler mixed layer of moister air (Refs. 6-8);

In part this paper is simply using a new presentation for the thermodynamic environment common to most storms. However, the saturation point method has several advantages as an analysis tool in the study of thunderstorm and boundary layer thermodynamics:

i) The method simplifies the analyses of data collected by horizontal and vertical spatial sampling and single station time series by different systems: aircraft, upper air soundings and the surface mesonet.

ii) It compacts the cloud and mesoscale thunderstorm thermodynamics into two basic branches on a saturation point diagram (Ref.1): a mixing line and an evaporation line. This permits a clear physical separation between the different processes of vertical mixing and the evaporation of precipitation. The slope of the mixing line is related directly to the vertical gradient of virtual potential temperature, so that the changes in stability associated with advection and the conditioning of the pre-storm boundary layer are readily visible.

2. GENERAL SITUATION ON AUGUST 1

Fig. 1 shows a schematic of the radar echoes (> 30 dBZ) (composited from the Bureau of Reclamation Skywater radar and the NCAR CP-2 radar) and the storm outflow boundary as it crossed the surface mesonet. The coordinate origin is at Miles City, Montana. The pentagonal outline marks the location of five of the Doppler radars. The major severe storm developed to the north and propagated towards the southeast. A smaller system grew in the east of the dashed pentagon (1600 MDT) and then decayed. A new cumulonimbus grew at 1800 MDT within the pentagon and merged with the major system by 1900 MDT. Fig. 2 (which will be discussed further later) shows an example of the surface fields as the gust front crosses the dense surface mesonet, which has the scale of the pentagonal area in Fig. 1. Southerly surface winds (region A) are bringing in moist air beneath an unstable sounding aloft (see Fig. 3).

3. DATA SOURCES

3.1. Surface Mesonet Data

Fig. 1 shows the area of the surface mesonetwork, which was a mixture of two systems.

The Portable Remote Observation of the Environment (PROBE) system, developed by the Bureau of Reclamation and operated by the Montana State Department of Natural Resources, collected five-minute-average data, which were transmitted to a satellite every hour (and retrievable within an hour) from 96 surface stations spaced within the area shown in Fig. 1.

The Portable Automated Mesonet (PAM) on NCAR's Field Observing Facility consisted of 27 stations that collected one-minute-average data, telemetered every minute to the PAM base, where they were immediately accessible. The PAM stations were located within the pentagonal area to give a smaller but dense mesonet centred on the Doppler radars (Fig. 2).

3.2. Aircraft Data

We shall use aircraft data primarily from two CCOPE aircraft: the Wyoming King Air and the NCAR Queen Air N306D. The location of aircraft observations or soundings will be expressed in km using the (x,y) coordinates shown in Fig. 1.

3.3. Sounding Data

The principal sounding network was not operating on this day and only three soundings (at 0600, 1400 and 1700 MDT) of low vertical resolution (significant levels) are available from Miles City.

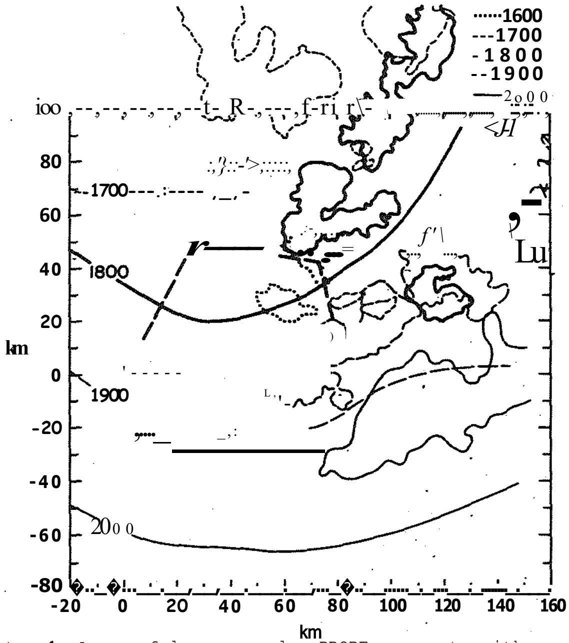

Fig. 1 Area of larger scale PROBE mesonet, with radar echoes (>30 dBZ) shown at hourly intervals and position of surface gust front as it crosses the network.

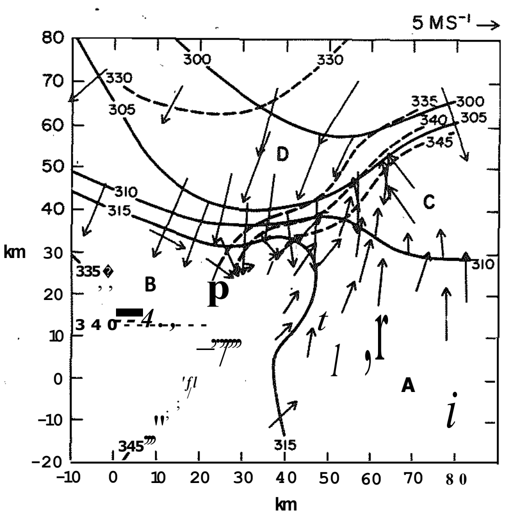

Fig. 2 Analysis of θ, θ_E fields (in °K) of dense mesonet at 1745 MDT, with superimposed wind vectors.

4. THERMODYNAMIC STRUCTURE BEFORE PRECIPITATION

4.1. Vertical sounding structure

Fig. 3 shows two soundings made by the Wyoming King Air over the dense mesonet in the inflow region to the storm system. The first (heavy line - solid circles) is near 1440 MDT with approximate co-ordinates (+30, +10 km), the second near 1610 MDT at a similar location (light lines, open circles). The circles denote the SP's for representative sounding levels. The heavy dashed line is the mixing line drawn between an SP of (10.1 C, 706 mb) corresponding to subcloud air and (-17.7°C, 473 mb): corresponding to the SP's of air in the upper nearly adiabatic layer between 650 and 550 mb. All the sounding SP's lie close to this mixing line. The Miles City sounding at 1700 MDT is west of the surface dry line and has a drier mixed layer, but its SP's (symbol M) still lie on the same mixing line.

The dotted line is the virtual potential temperature isopleth for unsaturated air θ_{vu} = 315K (Ref.1) through the cloud-base SP. The mixing line lies above it, as is necessary for the atmosphere to be stable to dry overturning (Ref.1), but not much above it, indicating the extreme instability of the atmosphere to moist convection. The evaporation of cumulus towers which have not precipitated their liquid water content will produce temperatures **on this mixing line, and these mixtures can sink** towards the stable layer at cloud-base (710 mb), but not into the subcloud layer. However, the evaporation of a little precipitation into the dry layer will easily lower θ_v so as to produce downdrafts to the surface. The θ_E = 325K line is drawn to indicate this. The evaporation of only 0.67 g/kg liquid water into air with SP on the ML will move its SP down the 325K θ_E isopleth and lower θ_{vu} to 315K, sufficient to penetrate the stable layer near cloud-base and produce downward mixing into the subcloud layer.

4.2. Structure below cloud-base

The NCAR Queen Air (N306D) made two flights covering the time period from 1400 to 2030 MDT mostly at a flight level just below cloud-base in the storm inflow region, followed by soundings through the storm gust front in the final half-hour. This long

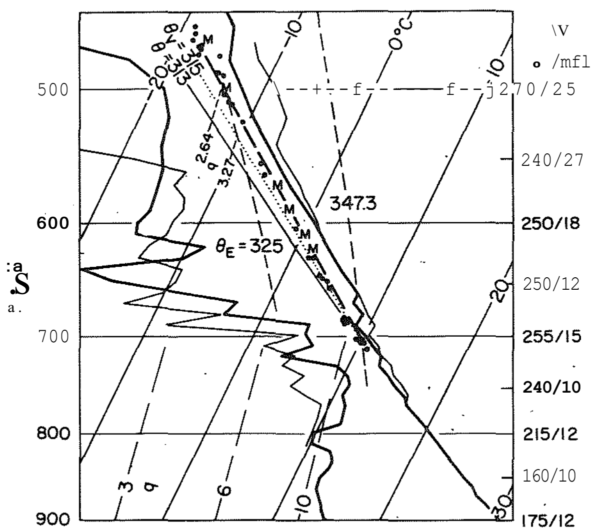

Fig. 3 Soundings by Wyoming King Air on a skew-T, log-p diagram at 1435-1450 MDT (showing T, TD as heavy lines and SP's as solid circles) and 1605-1616 MDT (light lines and open circles). Heavy dashed line is mixing line between subcloud layer and drier air (550-650 mb) aloft. M denotes SP's of Miles City sounding at 1700 MDT.

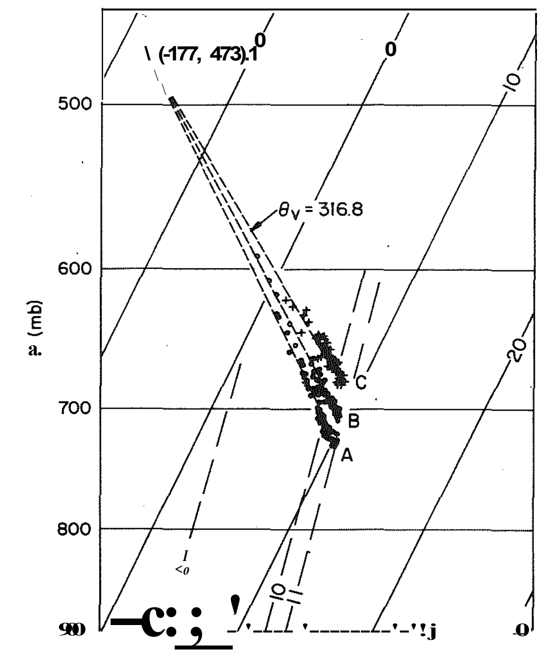

Fig. 4 Saturation points (SP's) of air just below cloud-base corresponding to three time periods: 1430-1530 MDT (solid), 1530-1630 (open circles), and 1845-1945 (crosses), showing change of mixing line structure with time.

time-series near cloud-base shows the evolution of the thermodynamics of the inflow region and is shown in Fig. 4. While flying at one pressure altitude, the plane samples air from the subcloud layer interspersed with pockets of warmer, drier, lower θ_E air which have descended dry adiabatically from above cloud-base. On an SP diagram, the flight level data thus give a similar mixing line structure to a vertical sounding. Fig. 4 shows the time· evolution of this mixing line (ML) through the afternoon. The stratification of all the data along a well. ¢lec!rined mixing line indicates that only mixing betwee the subcloud layer and the cumulus layer above has taken place (Ref.l) in this air. Fig. 4 shows several important features:

(i) For each time period, the aircraft data stratifies along a well-defined ML, which is shifting ±n time (see iii).

(ii) The change of cloud-base SP, and of the mixed layer with time can be estimated from the lower right end of the ML's, as.the vector ABC.

(iii) ML's constructed from the points A,B,C rnd the early SP of the layer above (see Fig• .3) are shown as dashed lines. They fit the data very well, indicating that the dominant process during this time period is probably the change of subcloud SP A to c. There may also be smaller changes of the SP of the upper dry layer, but they are not well-defined by the i;ircraft soundings. Thus it appears that by 1915 MDT the ML is parallel to ev; 316.SK. This suggests that the initial stabilization above cloud-base has been eliminated, and the inflow atmosphere may have approached the marginal instability conditio·n for dry overturning.

5. THERMODYNAMIC STRUCTURE PRODUCED BY EVAPORATION OF PRECIP.ITATION

Before the onset of precipitation, the thermodynamic data are scattered along a well-defined mixing line. However, with the onset of precipitation, and its evaporation into unsaturated air (which. drives downdrafts), a new characteristic evaporation line (EL) appears in the scatter of the SP's. Evaporation lines.are parallel to moist adiabats and rPprPsent SP's that result from different amounts of evaporation. Evaporation produces cooling, a lower 0v and the downward transport of air in and from above the subcloud layer, until a complete restratification of the atmosphere results.. Cold air of lower 0E from cloud-scale downdrafts **spreads over the surface, beneath mesoscale regions** which have also been modified by precipitation and downdrafts.

5.1. Surface mesonet analysis

Fig. 2 shows an analysis of 5 min averages of surface wind at 1715 MDT as the surface gust front covers nearly half the dense network. Four regions are lab lled with distinct properties. Region A is the southerly inflow of moist air with (0, 0E) of about (314, 347K), region C is the same air modified by evaporation of showers (see evaporation line on Fig. 5)., region B is warm dry air west of the.dry line with ·(0, 0E) of (316, 335K), while region D is the major storm outflow of low (0, 0E) of typically (302, 333K).

Fig.Sa shows the mesonet data at 1700 MDT (near onset of first shower). The surface SP's **scatter about two lines. One, AB, is a nuxing line** (light dashes) parallel to that (heavy dashes) of the mean sountling in Fig. 3 (the surface data, being in the superadiabatic layer, have a higher 0 and q). The drier SP's (towards B) correspond to drier surface air to the west. The fact that the ML structure is· essentially similar to that below cloud-base in the storm inflow air (Fig.4) and that of the vertical soundings (Fig. 3) implies that the dry continental air to the west at the surface is thermodynamically similar to the dry air overlying **the moister inflow air. The second line,** Ac, **is an** evaporation line. The SP's of air modified by precipitation (a cell towards the northeast of the

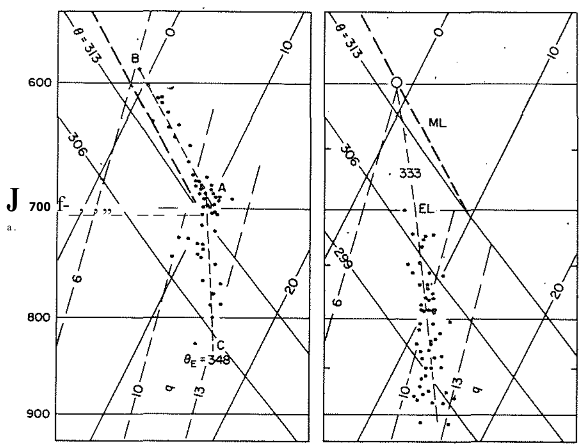

Fig. Sa,b. SP plot of dense surface mesonet data at 1700, 1900 MDT, showing scatter along mixing and evaporation lines.

network; region C in Fig. 2. The 0E values of these SP's are characteristic of the surface and subcloud values in the undisturbed inflow air (344-351K). These correspond. to e aporation of precipitatibn in!1 subcloud layer air in amounts from 1 to 3 g kg . Only a few SP's have lower 0E values su gesting an origin near cloud-base. This early storm downdraft thermodynamics differs markedly from Fig, Sb. Fig. Sb shows the plot of the surface mesonet SP's at 1900 MDT. No unmodified surface air remains (the gust front has crossed the dense mesanet (Fig. 1), and the downdraft air SP's are scattered along an evaporation :).ine with. 0E - 333.1 ±2-.6K. The spread along the 0E moist ad abat corresponds· to evaporation of from about 3 to 6 g kg-1, into air with initial SP where the EL and ML intersect (-1°c, 600 mb). Although there is a wide spread ill the evaporation that has occurred into ·the downdraft air, the spread in 0E is rather small considering the range initially present between the two airstreams. Comparison with the King Air soundings in Fig. 3, shows that these thermodynamic properties (0E) do not correspond either to the subcloud moist air or the dry air above, but rather to the transition between them just above cloud-base. The downdraft outflow air probably originates either from some mixture of the two characteristic airstreams of high and low 0E. The spread in evaporation corresponds to a spread in 0 from about 306 to 299K. This is highly structured spacially. The air close behind the spreading gust front has 0-306K, but 0 decreases to below 299K 50 km behind the surface gust front (Fig. 2).

5.2. Single station time-sequence

Fig. 6 shqws the time-series of SP from a single PAM station. The data are minute averages: values are plotted every 10 mins from 1400-1700 MDT and 1750-2300 MDT, and every minute from 1700-1745 as the gust front approaches, and passes the station. This one station shows the features of many of the· preceding diagrams. From 1400-1700 MDT the surface SP has a trend towards higher 0, lower q similar to that shown by the subcloud aircraft data· (Fig. 4). Thirty minutes before the gust front, the surface wind turns towards the southwest and (0E, q) drop rapidly. '!'he SP path approximately traces the mixing line of Figs. 3, and Sa. This drier air is probably advected in from the west, ·although it could also descend from above ahead of the gust frcnt, since the SP structure shows constant 0v; 316.SK (dashed line).

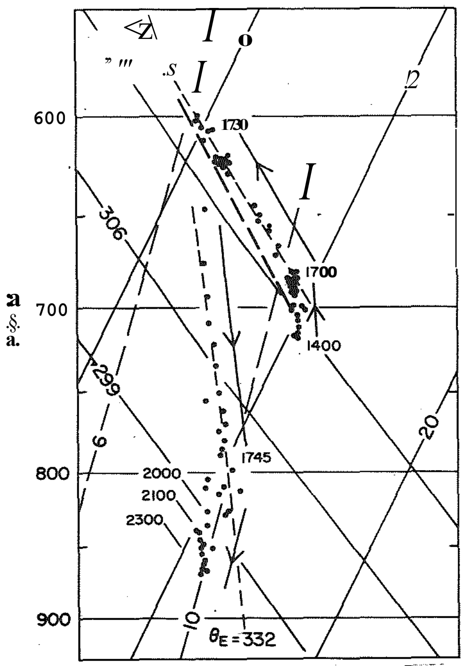

Fig. 6 Time sequence (from 1400 MDT to 2300 MDT) of surface SP from PAM station 8.

5.3. Aircraft gust front traverses

The NCAR Queerr Air N306D ma.de gust front traverses while making soundings just before landing. Fig. 7 shows the three soundings on an SP diagram, starting at 1945 MDT. Ahead of the gust front, the ML structure corresponding to the final time on Fig.4 appears (d-a,shed) . The aircraft then enters air of ΘE -333K (dashed) and lower Θv, modified by the evaporation of rain. The heavy dots show SP in the first descent sounding from 690 mb to 912 mb (coordinates near (60,0 km) at 1957 MDT), the open circles the following ascent from 910 to 822 mb, and the crosses the dPscent into landing at Miles City from 822 mb. The symbols S denote surface values from the mesonet stations nearest to the aircraft at the bottom of its soundings. The general SP structure following an evaporation line o f - 333K is very similar to that shown in Figs. Sb, 6. The dotted line (a virtual potential temperature isopleth for cloudy air) also fits the data wel .

6. CONCLUSIONS

This paper has studied the boundary layer thermodynamics of the inflow to and outflow from a severe thunderstorm which passed through the CCOPE network near Miles City, Montana. The analysis technique used air parcel saturation point to compact and compare different data sets. The SP analysis method facilitates the comparison of horizontal and vertica:l spacial and time sampling by different systems: airfraft, upper air soundings and the surface mesonet. The cloud and mesoscale thunderstorm thermodynamics involve two basic physical processes, which can be seen as distinct branches on a saturation point diagram: a mixing line and an evaporation line.

7. ACKNOWLEDGMENTS

This work was supported by the National Science Foundation, partly through the Convective Storms Division of the National Center .for Atmospheric Research and partly bv the Global Atmospheric Research Program under Grant ATM-8120444.

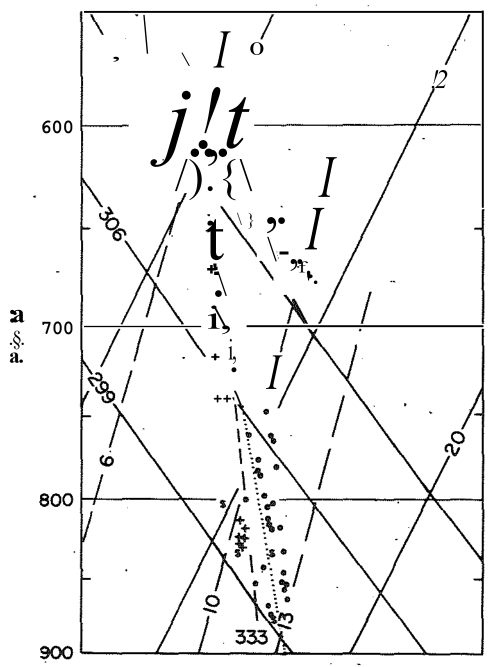

Fig. 7 SP structure from three aircraft soundings through or behind the surface gust front. The ΘE = 333K evaporation line and the mixing line through C on Fig. 4 are shown dashed. The dotted line is the θ_{ESV} = 340K isopleth

7. REFERENCES

1. Betts, A.K., 1 82a, Saturation point analysis of moist convective overturning. *J. Atmos. Sci.* 39, 1484-1505.
2. Betts, A.K., 1982b, Cloud tlhermodynamic models in saturation point coordinates. *J. Atmos. Sci.* 39, 2182-219.1.
3. Betts, A.K., 1983, Thermodyn cs of mixed stratocumulus layers: Saturation point budgets. *J. Atiros. Sci.* 40, (Nov.)
4. Betts, A.K., 1976b, The thermodynamic transformation of the tropical subcloud layer by precipitation and downdrafts. *J. Atiros. Sci.* 33, 1008-1020.
5. Knight, C.A., 1982, The Cooperative Convective Precipitation Experiment (CCOPE) 18 May- 7 Aug. 1981. *Bull. Amer. Meteor. Soc.* 63, 386-398.
6. Knight, C.A., and P. Squires, 1982, Hailstorms of the Central High Plains. The National Hail Research Experiment (C.A. Knight and P. Squires, Eds.), Vol. 1, *Colorado Associated University Press, Boulder. Colorado,* 282 pp.
7. Ludlam, F.H., 1963, Severe Local Storms: A Review *Meteor. Monogr.,* 5, No.27, *Amer. Met. Soc. Boston*
8. Ludlam, F.H., 1980, Cloud and Storms. *Penn State Univ. Press,* 405 pp.

STRUCTURE AND EVOLUTION OF MESOSCALE CONVECTIVE SYSTEMS

N. Bibilashvili, T. Terskova, A. Kovalchuk

Transcaucasian Regional Research Institute, High Mountain Geophysical Institute, C imean Hail Suppression Service

1. AMBIENT WIND REGIME EFFECTS ON STRUCTURE AND EVOLUTION OF MESOSCALE HAIL CONVECTIVE SYSTEMS (MHCS)

Relation o'f hail cell structure and evolution to circulation and thermodynamic prehail environmental conditions of the inflow is identified on the basis of a detailed analysis of data from frequent soundings (529, including over 300 soundings into hail clouds). Ambient wind regime on days with MHCS development, wind field disturbances and quantitative criteria typical of MHCS fo:i:;mation and development (160 cases) are determined. Experimental results for intense (type 1) and weak to moderate (type 2) MHCS are shown in Table 1. It is found that the direction of the mean ambient wind in the cloud layer initially changes the day before the development of HCS. The shift to the left up to 40° is observed with a slight increase of the wind speed (V). A twofold increase of V is observed on the day of the MHCS development Nith the shift of the wind slightly to the left towards a more southerly component. The ambient wind distribution in the undisturbed atmosphere determines the structure of convective cells in their initial stage. Low and middle level flows in the environment determine the structure of airflows in mature .Cb due to transport and conservation of a horizontaL momentum from the inflow regions. The middle level momentum (W, SW, S, SE) is transported in pri mary downdrafts and secondary updrafts and the low-level easterly momentum is transported in primary updrafts of Cb (Ref. 1). The inflow directional difference at low and middle levels for different cell types is essentially important for the dynamics of airflows in Cb determining their subsequent structure and intensity of mesofronts. 'l'he mean wina has a more southerly component for (1) as compareu to that for (2). The mean wind on days with weak convective growth or without it is 2390, 11 m s-1. A well-defined turning with height and increase in V is typical of an undisturbed atmosphere on hail days. Mean wind speed at middle levels (VML) usual y-exceeds VLL for low levels by a factor of 3, an.9: $\overline{V}$uL for upper levels is twice larger than VML. Fig.1 shows mean ambient wind hodographs for both types of MHCS. Mean hodographs with common, low- and upper-level veering are typical of (1). Mean hodographs for (2) are close to linear with the wind turning to the left at low-levels. The average angle between the wind direction at low and upper levels is 1800 for (1) and 130° for (2), which may be considered as differentiating criterion.

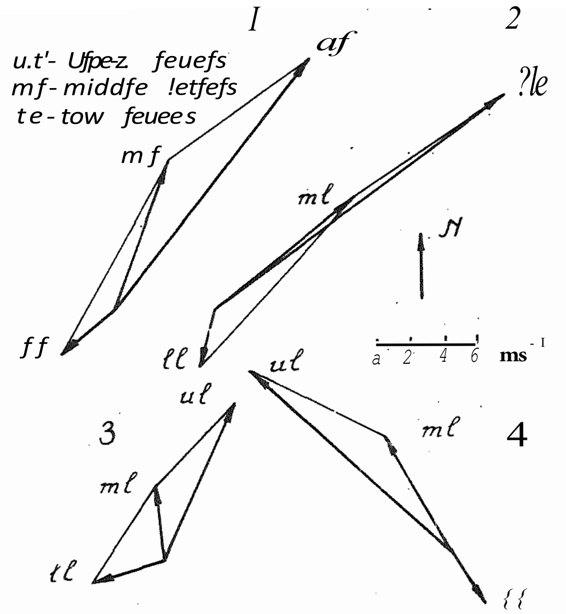

Figure 1. Mean ambient wind hodographs with developing hailstorms of various intensity. 1-intensive; 2-weak to moderate; 3-for right-moving cell; 4-for left-moving cell.

Table 1

Ambient wind distribution during MHCS development
(1-intense; 2-weak to moderate; height - in km AGL)

		Z_u / Z_1	Direction degr.	V ms^{-1}	ILJ (ULJ) Z	Direction degr.	V ms^{-1}	Turning Angle degr.	Direction	Z1	Z/4
Low levels	1	2.0	49	4.0	0.30	55	8.6	181	right	0.65	2.3
	2	1.9	12	4.1	0.25	16	10.2	154	left	0.55	1.8
								Mean wind Direction degr.	V ms-1	Mean wind shear x 10-3. s-1	
Middle levels	1	-	201	10.6							
	2		232	11.3							
Upper levels	1	8.5	219	20.4	10.2	222	31.0	198	13.0	3.2	
	2	8.2	234	22.5	9.6	237	32.0	234	13.6	3.0	

Direction and value of the turning vary also with height at low levels for (1) and (2): stronger turning of wind above 180°, which is. ~30° in excess of that for (2), has been observed for (1). The minimum turning angle for (1) is always over 100°, but for (2) it can be very small.

In right-(lef -) moving cells the inflow toward the cloud base is from S, SE (N, NW), making an angle of 0-90° (90-180°) with the mean ambient wind direction. Right (left) turning with height has been noted for the subcloud layer (Figs .1. 3-1. 4, respectively) .

The mean wind at the low levels has a more easterly component for (1) and at the middle and upper levels a more southerly component (by 30°) of the wind vector has been observed for (1) as compared to that for (2). The variation range of wind direction at low and middle levels, in the low-level jet (LLJ), 'upper level jet (ULJ) for (1) turns out to be more narrow. There is a rise by 500-1000 m for the mean height of low- and upper-level jets (ZLLJ, ZuLJ), and for low-level upper boundary (Zu) and upper-level low boundary (ZL).

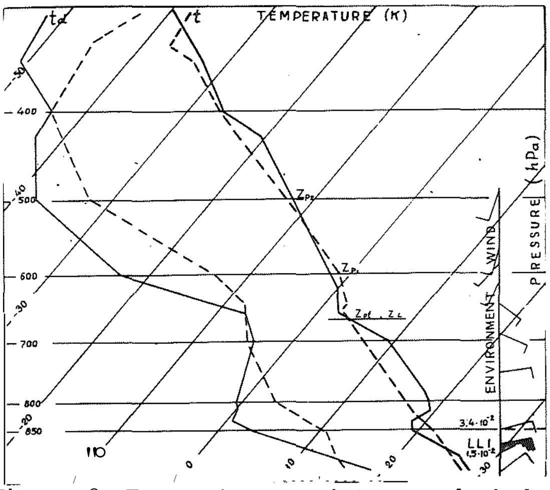

Figure 2. Temperature, moisture and wind rawinsonde data prior to the development of the intense MHCS of June 8, 1975. Solid lines - for 1342, dashed lines - for 1504LST.

MHCS deve·lops in the environment.with the mean value of the cloud-layer wind shear equal to > 3.0 x 10-3s-1. There is little difference in mean and extreme values of the wind shear for (1) and (2). Wind shear vertical gradient is observed in the environment for (1) (Fig. 2).

The layers with a shearing gradient are often singled out: at upper levels under the ULJ axis in a layer "' 1 km high with the possible wind shear over 11 x 10-3s-1 and in the low troposphere (~5 x 1o-3s^{-1}), where another 2 layers of maximum shear are found not more than "' 500 m high. The first layer is close to LLJ, the second is close to the upper boundary of the potentially unstable layer (PUL) at middle levels (Z2). n intermediate layer in the vicinity of the upper boundary of the latent instability layer (Zr) (Ref. 2) is a layer of the air inflow into the hailcloud base and is characterized by a flow, which is uniform in speed and direction, separating layers with strong veering. The .above parameters of the wind regime are typical of the MHCS environment and may be indicative of their future structure, evolution and intensity.

2. RELATION OF ENVIRONMENTAL THERMODYNAMIC CONDITIONS TO MHCS STRUCTURE AND EVOLUTION

Based on the understanding of the dynamic and thermodynamic structure of hail clouds and the environmental conditions obtained from experimental studies (Refs. 1, 3-6), a relation of thermodynamic parameters of the environment to major hail-cloud characteristics and the governing role of the above parameters in the organization of the hail-cloud structure and evolution are established. According to an empirical hail-cloud model (Refs,1, 5) there are 3 layers in mature Cb. The layer boundary height largely determines the internal structure of the cell. It is found that the upper bounda:cy of layers 1, 2, 3 coincides and is physically determined by zL, Zp and by the low boundary of the latent instability layer for downdrafts (Z), respectively (Ref. 2). Table 2 presents mean values of the layer boundary heights and temperatures at these boundaries. Table 3 gives mean values and variation range for thermodynamic parameters of the environment prior to the development of hailstorms

Table 2

Thermodynamic parameters of the environment and hail clouds (mean values) • Height is given in km MSL

z cond			ZL			Zp			.z*		
hPa	km	t°C	hPa	km	tOC	hPa	km	t°C	hPa	km	tOC
817	1. 8	12.6	705	3.0	3.9	533	5.2	-11 .0	402	7.4	-25,8

Table 3

Environmental thermodynamic parameters on hail days (variation range and mean values). Height is given in km MSL

	Z hPa	Z km	.t°C	q g kg^{-1}	Est K	Q_W °C	I_E K
Low levels	877-796 832	1.3-2.1 1•7	12.0-23.0 17. 5	8.1 -12 .6 9·.8	315-335 326	16.1-21.0 18.4	-6.9 - -17.8 -10.2
Z_p	692-466 551	3.2-6.2 4.8	.o - -19.0 -8.9	0.9-4.5 2.2	309-321 316.5	12 .0-17 .o 15 .0	

typical of the Cb inflows into the downdraf and updraft at Z and low levels: temperature (tO), speci¥ic humidity (q), pseudo-potential wetbulb temperature (Owl, static energy (Estl and energy index (JE) equal to (Estzp - EstLL1 (Ref. 6). It has been found experimentally that before the development of MHCS environmental potentially cold air is located around Zp, flowing into the region of the downdraft formation in a mature hail cloud, and determining its thermodynamic parameters and intensity. The upper limit of the low-level layer is identified through the analysis of the patterns of meteorological elements (ME) as the upper limit of warm and moist PUL air flowing into the hail cloud. The entire air mass of the above layer rises and flows into the Cb base. Mean and maximum values of the thermodynamic parameters of this layer determine similar parameters of the cloud updraft. Mean values represented in Tables 2-3 can be used as criteria for optimum parameters of the environment, which represent conditions of the MHCS development for nowcasting. But since the aJ:,ove parameters ,9ive the most complete picture of the air flow dynamics and thermodynamics in hail clouds in physical cases for the build-up of their energy reserves, they can be used for estimating the Cb internal structure and intensity.

3. CHANGES IN THE CHARACTERISTICS OF THE METEOELEMENT FIELDS DURING THE DEVELOPMENT OF MHCS

Relation of the MHCS evolution to disturbances of tne ME fields is considered. Dependence between amplitude and disturJ:,-ance gradient values for the ME fields and MHCS intensification is found out. Mesostructure of the ME fields is seen from the analysis of the trend of isopleths. Nonuniform amplitude changes, dissimilar and asynchronous in height were found to occur in the ME patterns on a hail day. Periods with the sign alteration and sharp changes of the ME gradient values, which determine the value and direction of the advective and vertical transport are marked out. Detailed analysis of the ME distribution on a severe hail day (Fig. 3) is presented. The first period (Oq00-1400 LST) presents undisturbed environmental conditions prior to the development.of active convection up to 100 km in radius and specifies major conditions of circulation and thermodynamics on days with intense MHCS. The second period (1 00-1 00 LST) is characterized by the largest vertical redistribution of moisture. Most of the moisture content in the-troposphere is concentrated in the surface layer. The dry layer and the zone of major vertical gradients of q ('t) descend to almost 1 km. By the end of the period Qq,,,AX (1.5 g kg-1/100 m) is observed in.the lower 0.5 km. The driest air zone forms in a 1-12 km layer starting from the upper levels which is probably related to the beginning of the active convection development at ~ 70 km from the observation site.

The largest moisture advection is observed at ~ 1 km (Fig. 4). The q ridge, observed in the surface layer at the beginning of the period, feeds the updraft of a future hail cloud, originating above the surface convergence line (CL). The third period (1 00-1 00 LS 1 is determined by t

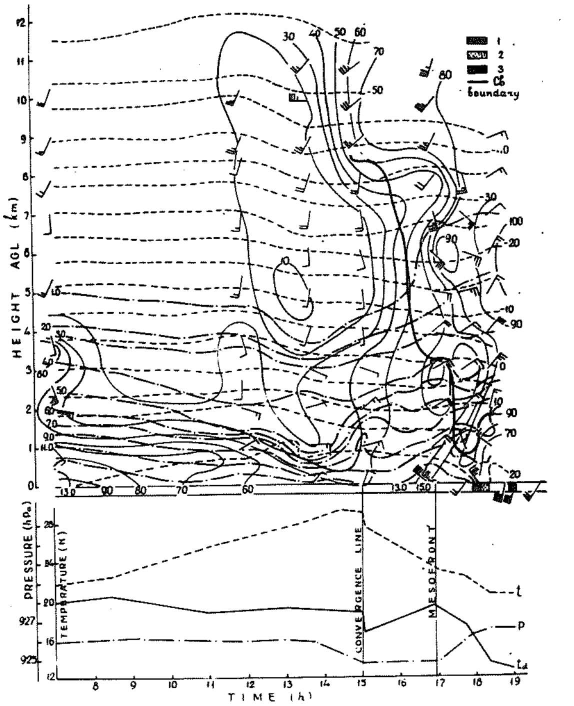

Figure 3. ME distribution near the surface (bottom) and aloft (top) for June 8, 1975. Solid lines - isolines of relative humidity and new point temperature; dash lines - isotherms, dot and dash lines - isolines of specific humidity (top) and pressure isolines (bottom); 1-rain; 2-light rain; 3-hail.

strongest disturbances of the ME fields ~ 40-70 km from the actively developing MCS, by crucial changes in the thermodynamical structure of the environment and by the formation of most favourable conditions for hail cell development: build-up of a single thick PUL, rising of Zp (Fig. 2), and ZL up to optimum values. The above regularities are illustrated in Table 4 showing that the greatest changes in the stratification of the atmosphere occur directly within 1-3 h before the hailstorm development.

Table 4
Environmental thermodynamic parameters prior to the MHCS development

Date	Time (LST)	ΔZ_L km	hPa	ΔZ_p km	hPa
16.05.1975	12.01 13.34	1.38	168	0.00	0
29.05.1975	12.26 14.19	2.34	217	1.27	90
30.05.1975	12.38 14.54	1.67	151	0.00	0
31.05.1975	12.11 13.56	1.71	167	0.62	52
08.06.1975	13.42 15.04	-0.67	-55	L4o	100
09.07.1975	13.12 14.33	-0.80	-70	0.00	0
13.06.1977	11.35 15.17	0.85	80	0.84	60
12.Q].1977	12.01 13.22	1.31	110	-0.18	-11

In order to form a severe MHCS the thickness of the latent in-:tability layer should be over 200-250 hPa and p around 500 hPa. The largest heat and moisture advection was observed near the low boundaries of the inversion layers. Position of 2 major conveyor belts of the potentially warm air (PWA) was identified and is supposed to play a crucial role in the change of the atmospheric stratification. The first belt is located between LLJ and the frontal inversion and advects the air from the NE out of the prefrontal band ~30 km away. The above belt causes the distruction of the low inversion layer and the rise of ZL to a maximum. The second southerly conveyor belt at 3-5 km advects PWA from Cb and plays a major role in the breakdown of the subsidence inversion and in rising Zp by ~100 hPa. It forms with the divergence development at the Cb middle levels in the mesohigh (Ref. 1) and extends to 5-15 km ahead from the cloud boundaries. The above factors increase latent and potential instability of the atmosphere and result in its release. At the beginning of the per'iod y- -increases by more than a factor of five (0.7) (Fig. 4) in the surface layer, indicating the entrance into the inflow toward the updraft to a future hail cloud ~30 km from the CL (the warm front of the surface mesoflow), occuring at the end of the period. The entire troposphere begins to reveal disturbances of the pressure (p) field (Fig. 4). The updraft and negative pressure anomaly (p< 0) regions are bounded by a PUL (Zp) . Values Lip< O increase with height and f.p ""• O (> 3.0 hPa) is observed in the layer 2, where I_p is also maximum (~1.0 hPa/10 km) (Ref. 10). Within this period the NE flow, uniform in velocity and direction, forms in the boundary layer with an increase in V and forms conditions typicai of the severe MHCS development. The fourth period (15 30-17.30 LST) is represented by considerable disturbances of the ME field and is identified by the passage of the mesolow warm sector, which is the most active updraft development zone. A sharp increase of q is observed throughout the troposphere with maximum positive dewpoint temperature anomaly (Fig. 4) at about 2.0-2.5 km and moisture flux from MHCS toward the updraft. Surface t h (-0.9) sometimes increases twofold against the third period, indicating further growth of the inflow toward the updraft core of the developing cell and its intensification. In the surface layer both sources of moisture supply are ~30 km (~10-15 km for weaker MHCS) away from the updraft core. The updraft is fed by the air from 2 ridges of q (Fig. 3) formed by the moist air tongues extending out of Cb due to low- and middle level Cb divergence in mesohigh regions, thus resulting in moisture reuse and considerable enhancement of MHCS. Negative pressure anomaly is observed throughout the troposphere. Its value equals ~0.5 hPa in the low-level mesolow and sharply grows to maximum of ~ 10 hPa (Ref. 5) at 2.0-3.5 km, which determines a mesolow location around the Cb. low boundary. Maximum I_p ~1.0 hPa km-1) is found here, too. Existence of the above perturbations of the p field causes considerable disturbances of the wind field. The value of VLL increases twice resulting in a respective intensification of the inflow into Cb. The centre of .dp < O is biased from the mesolow centre along the CL to the right or left according to the cell type. It lies around the occlusion point which is the se t of the new cell formation in multicell storms and indicates the supercell propagation direction.

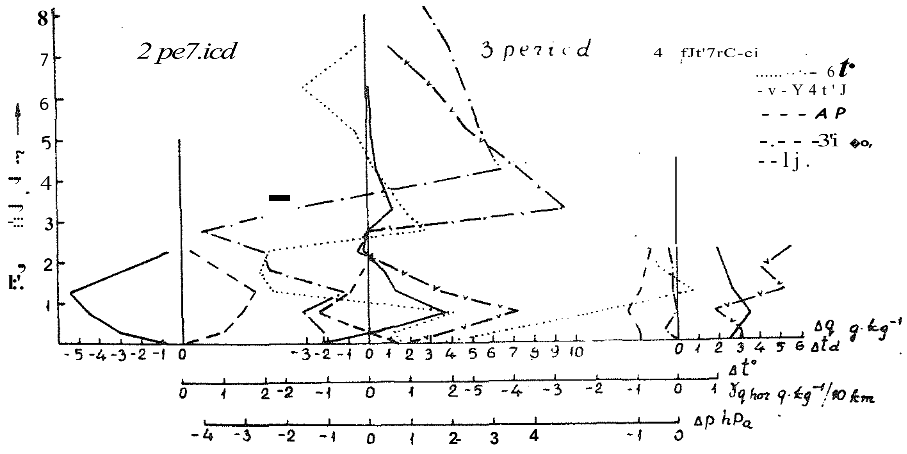

Figure 4. Variation of temperature, dew-point temperature, specific humidity, pressure and horizontal gradient of specific humidity

4. REFERENCES

1. Bibilashvili, N., Kovalchuk, A., Terskova, T., 1983. Dynamics and thermodynamic structure of a supercell hailstorm, (in Russian), Trudy VGI, 50, 3-8.
2. Normand, C.W.B., 1938. On instability from water vapour, Quart. J. Roy. Met. soc., 64, 47-69.
3. Bibilashvili, N., Terskova, T., 1974. An investigation of the dynamics of airflow in a cumulonimbus, (in Russian), Trudy VGI, 28, 85-99.
4. Bibilashvili, N., Terskova, T., 1976. Profiles of vertical velocities and thermodynamic features of updrafts in intense hailstorms, (in Russian), Trudy VGI, 34, 3-957.
5. Bibilashvili, N., Kovalchuk, A., Terskova, T., 1983. Pressure field disturbance associated with the development of deep convection, (in Russian), Trudy VGI, 50, 36-50.
6. Belentsova, V., Goral, G., Terskova, T. et al. 1982. Aerosynoptical and thermodynamic features of formation and development of intense hailstorms and squalls in the North Caucasus, (in Russian), Trudy VGI, 51, 88-99.

RAINING AND NON-RAINING CUMULI - THE INFLUENCE OF CLOUD PROPERTIES AND ENVIRONJ.IENTAL CONDITIONS

C.E. Coulman
Cloud Physics Laboratory,
Division of Atmospheric Research,
CSIRO, ?Ydney, Australia

1, SYMBOLS USED

z vertical coordinate, altitude
zs cloud top ai'titude
zb cloud base altitude.

$S = \frac{}{z_s - z_b}$ normalized height in cloud

8 potential temperature
q water vapour mixing ratio
q_5 saturation mixing ratio
qL liquid water mixing·ratio
qT total w.ater mixing ratio
N droplet concentration
o standard deviation of droplet spectrum
dm mean droplet diameter
\- overbar denotes an average.

2. INTRODUCTION

Not all cumulus clouds produce rain; prediction of rain from such clouds in a particular area and a particular time interval may be facilitated if certain properties of cloud and environment can be measured. Observational data are examined for indications of which parameters appear to be useful diagnostic tools for this purpose. Implicit in such investigations are questions of cause and effect but in this short paper we concentrate on the diagnostic aspect.

3. OBSERVATION'S

Most of the data were obtained with an instrumented aircraft (Ref. 1) during an expedition in February 1981 over land but near the east coast of Australia in the vi inity of Lat. 29°45'S, Long. 152°50'E. Vertical soundings were made in the air between clouds and horizontal passes through cloud were made at numerous heights; before entry, and after exit from cloud, the aircraft remained in the clear air for long enough to make valid measurements of the properties of cloud environment. Lifetimes of clouds were sufficient for at least 5, and sometimes more, traverses.

\- Several wet and dry-periods were experienced as shown by a pluviograph record in Figure 1. On days such as 3, 4 and 5 February a high proportion of.the clouds observed produced rain whereas in a period such as 10, 11, 12 very few of the cumuli produced even a light shower. Typically, the-cumulus cloud cover was greater than 5/8 with some altostratus during the high rainfall periods and about 3/8 cumulus during the low rainfall days. The presence of a range of hills and low mountains (maximum 1200 m a.m.s.l.) running parallel to the coast implies that orographic influence on cloud growth may often have been significant.

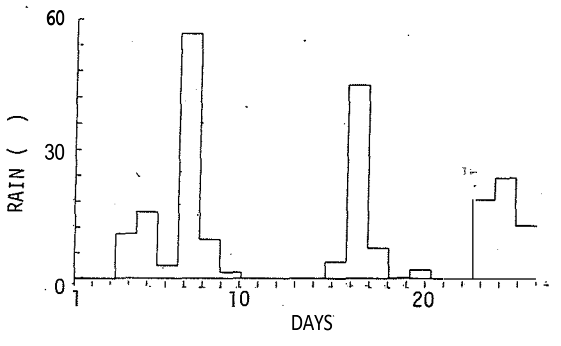

Fig. 1 - Rainfall at a station in the area where airborne observations were made in February 1981. Note successive wet and dry periods each of several days duration.

4. RESULTS - ENVIRONMENTAL PROPERTIES

In Figure 2 typical midday soundings of potential temperature and wind velocity are shown for the high- and low-rainfall periods of the expedition; corresponding moisture soundings are shown in Figure 3. There are clearly very marked differences between soundings which typify periods with very different rain production.

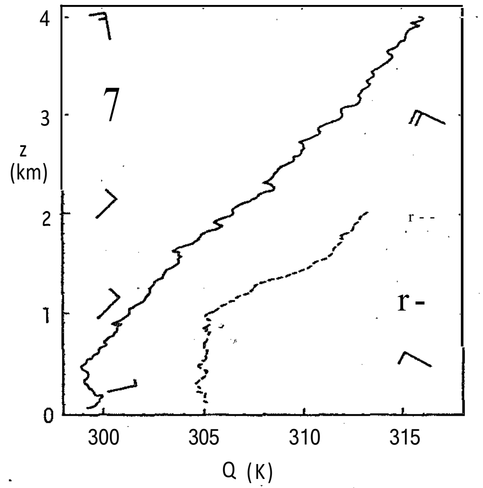

Fig. 2 - Potential temperature profiles for wet and (solid line) and dry periods (broken line) of Figure 1. Corresponding wind profiles shown adjacent to 6-profiles; convention is north at top, sho t feather denotes 0-2 m s-1, long denotes 2-5 m s-1.

During 'the low-rainfall period, in winds which were predominantly off the land (i.e. westerly), a convectively well-mixed boundary layer, of depth about 1 km, developed. Notwithstanding the high moisture content of this layer, cloud growth was inhibited by the inversion across which intense drying existed (Fig. 3). Over level land cloud base was usually around 1 km altitude with cloud tops about 1.5 km. Where orographic effects were significant cloud base was about 0.8 km above terrain and cloud tops occasionally reached 3 km.

The rainy periods are characterized by a very shallow, often unstable, lower layer surmounted by a moderately stable, moist atmosphere with air flo'V!'-ing from the ocean at all heights to 4 km and above.'

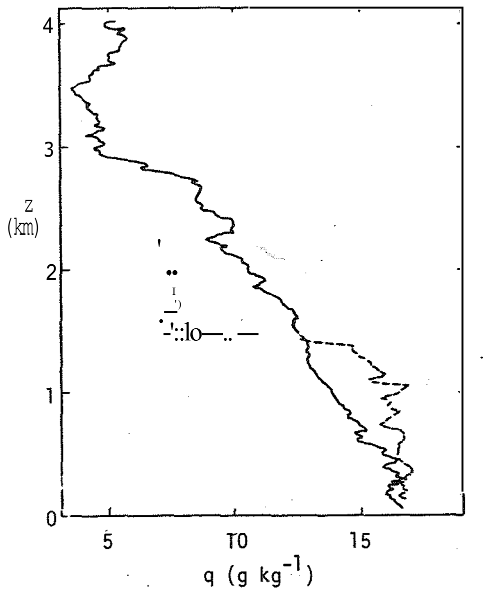

Fig. 3 - Humidity profiles corresponding to the 8-profiles of Figure 2. Note inversion and dry layer at about 1.4 km for the broken line.

Cloud base was usually less than 0.5 km above any terrain and cloud tops usually between 3.5 and 4.3 km. The temperature at cloud tops (4 km) was often about +1.-5°C so that this was an essentially warm cumulus regime.

Simple inspection of these soundings of the cloud environment suffices to diagnose the difference between such low- and high-rainfall situations but when the distinction is more subtle it may well be necessary to calculate the potential energy available to rising cloud parcels. For example, the available potential energy E(µ) may be calculated for a range of entrainment rates µ between cloud and environment as

$$E(\mu) = \int_{zb} [illegible] \qquad (1)$$

The behaviour of E(µ) may then indicate whether or not conditions are favourable to moist, deep convection, and hence to rain production as suggested by Betts (Ref. 2).

5. RESULTS - PROPERTIES WITHIN CLOUD

Appreciable evolution of cumulus clouds occurs in minutes rather than hours (Ref. 3) and so it is necessary to economise in the flying time required to obtain data at a number of altitudes. A vertical stack of horizontal passes through cloud, connected by helical climb or descent paths, suffices for thermodynamic and microphysical observations whereas more time is required to set up the aircraft attitude carefully for measurements of the velocity field. Here we concentrate on the former type of data.

Records of water substance variables are shown for a typical pass through a large orographic cumulus in Figure 4. Liquid water and total water mixing ratios are measured directly (Refs 4, 5) but qs has been calculated from wet bulb temperature; within cloud this value of qs is a reasonable measure of vapour saturation mixing ratio. It can be seen that,

$$q_L \simeq q_T - q_S \, , \qquad (2)$$

to a high degree of approximation in the cloudy region in Figure 4 if we consider instantaneous values at corresponding points in the three traces. To eliminate possible effects of differing instrument response time these data have been numerically filtered with a low-pass filter of maximum frequency 0.5 Hz, which corresponds to a spatial wavelength of about 150 m at 75 m s-1 airspeed.

The average properties of cloud at any height are usually more useful than instantaneous values for discussion of cloud characteristics. However, the probability distribution functions (PDF) for such variables in turbulent conditions are not generally known and so an average, ql for example, cannot easily be specified. Manton (Ref. 6) suggested that the behaviour of qL might be modelled by a binary switching process such that,

$$q_L = \max(0, q_T - q_s) \, . \qquad (3)$$

He cited some experimental evidence to show that a uniform, peak value of qL was often found in cloud; the alternative value being observed to be near zero.

Inspection of the present data, of which Figure 4 is typical, does not suggest this strongly. When PDFs for qL are calculated it is found that the shape of such histograms depends critically on which segment of a passage through cloud is selected. Our observations were often made in large cumuli or aggregates of cumuli, many of which rained; the observations mentioned in Ref. 6 referred mainly to small, separate cumulus clouds.

It does appear from our records however, that qs varies rather smoothly in cloud and that its fluctuations are small compared with ql so that, approximately, Equation 3 becomes,

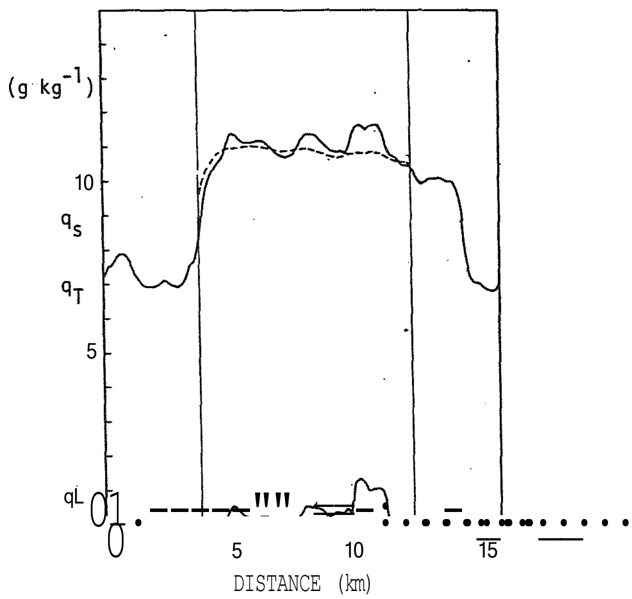

Fig. 4 - Typical data obtained in a horizontal pass through a large cumulus which rained at a later time. Total water qT in cloud closely approximates the sum of liquid qL and saturation vapour qs, denoted by broken line.

$$q_L = \max(0, q_T - \bar{q}_s) \quad . \qquad (4)$$

Furthermore, qs is a suitable parameter with which to normalize the other measures of water substance in cloud.

On the basis of the assumption that qL has a step-function-shaped PDF (Eq. 3) a relationship between the averages of liquid water and total water content was proposed in Ref. 6. The data from our observations in Figure 5 are not inconsistent with that result but there is a great deal of scatter and some suggestion that the points relating to raining and non-raining clouds are grouped separately.

The variation of qL with height in cloud might also be thought to be a useful diagnostic relationship. In Figure 6 the ob?erved value of qL has been normalized by the value it would have in undiluted, adiabatic ascent from cloud base qLA; ·it is shoWP. against normalized height in clouds- Again, we see a weak grouping of points which suggests that in raining clouds qL/q_{LA} tends to have a higher value than at the same height in non-raining cumuli.

Microphysical data were obtained on cloud droplets in the range 3 to 45 µm diameter with the aid of a Particle Measuring Systems FSSP instrument. This, of course, is a very limited segment of the full range of particle sizes. encountered in a rain-

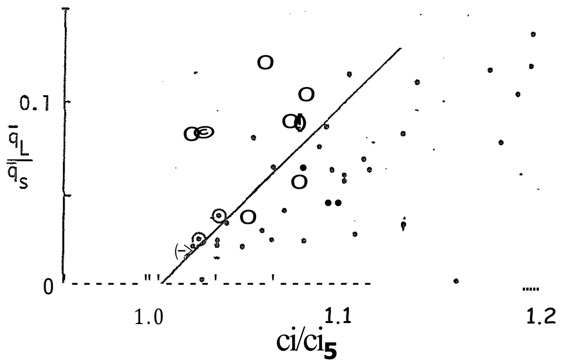

Fig. 5 - These observations suggest that the relationship between qL and qT (normalized by qs) may be different in raining clouds (circled points) from that in non-raining clouds (thus ·).

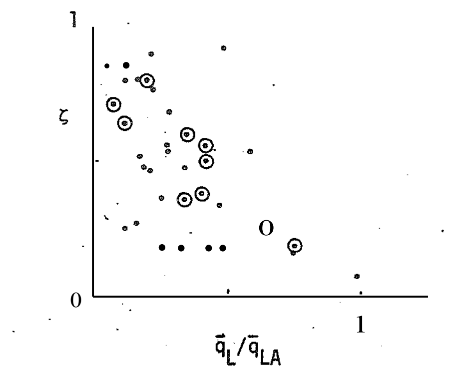

Fig. 6 - Profile of normalized liquid water as function of normalized height in clouds shuws only weak separation of data-from raining (circled points) and non-raining clouds.

producing cloud but, nevertheless, the results are interesting when taken in conjunction with other physical results already quoted.

Number concentration of droplets is shown in the upper part of Figure 7 and mean diameter in the lower part; in both graphs the variation with normalized heights is considered. In raining clouds N decreases with height more noticeably than it does in non-raining conditions. This is consistent with the hypothesis that an effective coalescence process exists and that comparatively moist air is available for entrainment from the environment into cloud, even at cloud top. Most of the clouds whi h were observed to rain did so after they had been in existence, and in an actively growing condition, for a considerable time. Furthermore, most of the observations were made during that time period and rain shafts were seldom intercepted. Hence, it is not surprising that evidence of small droplet depletion in the lower part of cloud by the sweeping effect of falling rain drops is absent from these data.

Both raining and non-raining clouds a e essentially coastal in nature as shown by the relatively low values of N. However, the generally higher N-values in non-raining conditions are consistent with the winds (seen in Fig. 2), which were blowing from the continental direction during the low-rainfall period.

In Figure 8 the ratio o/dm, often called the dispersion of the droplet spectrum (Ref. 7), shows neither a variation with height nor any evident grouping according to raining or non-raining conditions. When dm is plotted against o, in the lower part of Figure 8, there is, likewise, no clear segregation of raining and non-raining observations.

6. SUMMARY

The overall aim of this research is to document and account for differences between raining and non-raining cumulus clouds with a view to improving the forecasting of rain over a short range in time nd over areas of meso-scale dimensions. In this preliminary analysis of a limited sample of the observational data available we have sought to identify some of the parameters which appear to be useful to diagnose whether or not conditions favour rain production by cumulus clouds.

The environmental conditions in which clouds grow is shown to be of dominating importance and inspection of the soundings for temperature and humidity can provide a valuable guide to the expectation for rain; at a near-coastal site wind direction is lso very significant.

Probably as a result of the environmental properties, there appears to be a characteristic difference between the relationship of liquid- to total-water mixing ratio found in clouds which rain and those which do not. Furthermore, these relationships provide some support for recent theoretical models of the probability distribution function for liquid water in clouds.

The small-droplet end of the cloud particle spectrum provides only a weak test to diagnose the robability of rain production and therefore extension of the size-range of measurements will be required to ascertain the real value of microphysical measurements for this purpose.

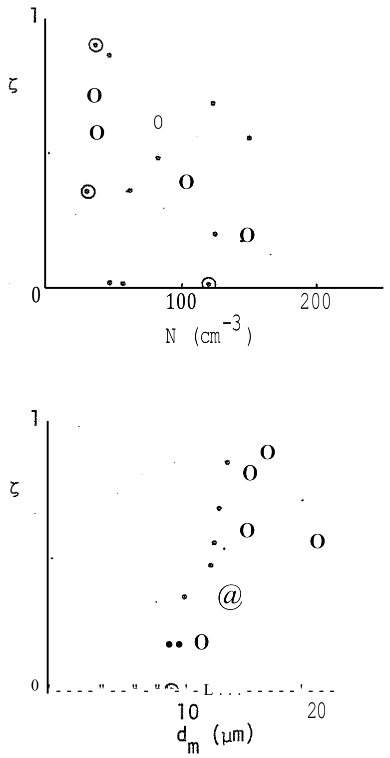

Fig. 7 - Numbel concentration N of small droplets in rain_ing clouds (circled points) decreases with height more noticeably than in non-raining conditions (upper graph). Mean diameter of droplets tends to be slightly greater in raining clouds (lower graph).

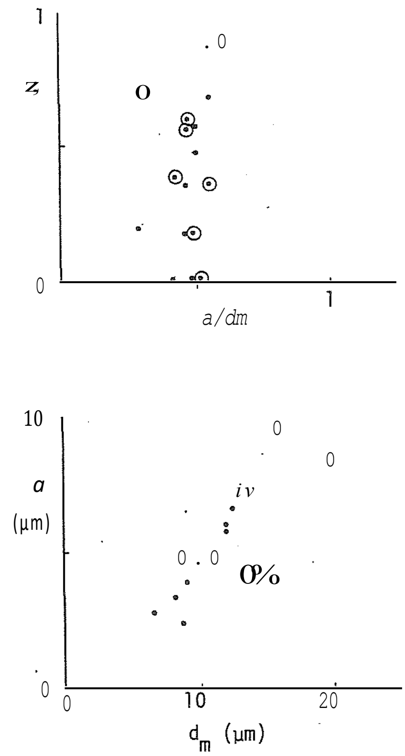

Fig. 8 - Dispersion of small droplet spectrum is sensibly constant with normalized height in both raining and non-raining clouds (upper graph). Droplet spectra show a roughly linear relationship between a and dm in both raining and non-raining clouds.

7. ACKNOWLEDGEMENT

I wish to thank Professor R.G. Soulage for the opportunity to work in his laboratory at Clermont-Ferrand, France at his invitation; my stay there gave me an opportunity to evaluate the data referred to above.

8. REFERENCES

1. Coulman C E and varr Dijk 1981, Features of the research aircraft and intercomparison of aircraft and rawinsonde data, Tech Rep 46, Bur of Meteorol, Melbourne, Australia.

2. Betts A K 1974, Thermodynamic classification of tropical convective soundings, *Mon Wea Rev,* 102, 760-764.

3. Coulman C E 1980, Observations of the scale and duration of cumulus cloud initiation, 8th Int Conf on Cloud Phys, 541-545, Clermont-Ferrand, France.

4. King W D, Parkin D A and Handsworth R J 1978, A hot-wire liquid water device having fully calculable response characteristics, *J AppZ Meteorol,* 17, 1809-1813.

5. Coulman C E and Parker M A 1982, On the calibration and performance of an instrument for measuring total water mixing ratio in cloud, *J AppZ MeteoroZ,* 21, 695-702.

6. Manton M J 1978, A finite element model of a moist atmospheric boundary layer: Part I - Model equations, *TeZZus,* 30, 219-228.

7. Twomey S 1966, Computations of rain formed by coalescence, *J Atmos Sci,* 23, 405-411.

INFLUENCE OF GUST FRONTS ON THE PROPAGATION OF STORMS

G. Brant Foote

National Center for Atmospheric Research*
Boulder, Colorado 80307 USA

1. INTRODUCTION

It has become apparent from radar observations over the last several decades that most thunderstorms consist of a succession of individual cells or groups of cells. The motion of these storms over the ground is comprised of the motion of individual cells, as well as a propagation component that arises when new cells form in preferred locations with respect to the parent storm, as is usually the case. The conventional explanation for the preferred location of new cell development is in terms of enhanced convergence below cloud base as the inflowing air runs up against the outflow boundary caused by downdrafts striking the surface and spreading horizontally. The inflow is forced to rise over the denser air behind the gust front, and new cells are thereby expected to appear preferentially on the inflow side of the storm.

Discussions of the possible importance of gust fronts for maintaining the inflow into thunderstorms and for triggering the development of new convective cells date to at least Espy (1841). Humphreys (1940) gave a lucid account of the phenomenon that is not qualitatively different from or. present understanding, and Byers and Braham (1949) made the first comprehensive measurements. In more recent times there have be n numerous field studies of both the structure of gust fronts (e.g., Colmer, 1971; Charba, 1974; Goff, 1976; Wakimoto, 1982) and the effect of gust fro ts on storms (e.g., Foote and Fankhauser, 1973;- Ellrod and Marwitz, 1976; Miller and Betts, 1977; Barnes, 1978; Ulanski and Garstang, 1978; Wade and Foote, 1982; Weaver and Nelson, 1982; Miller and Fankhauser, 1983). Important laboratory and theoretical investigations of density currents have also given valuable insights into the dynamical structure of established storm outflows (e.g., Simpson, 1969; Benjamin, 1968). The role of storm outflows in maintaining as well as modifying stvrm structure has been emphasized in a number of numerical simulations (e.g., Hane, 1973; Orville and Kopp, 1977; Miller, 1978; Thorpe and Miller, 1978; Weisman and Klempfr.,j982; Wilhelmson and Chen, 1982). An import-ant role. for ou_tflows in setting off or intensifying convection has also been inferred from satellite observations (Purdom, 1976).

While certain of the studies just cited have noted- correlations of gust front position with that of new cell development, the evidence for cause and effect is largely circumstantial. Also, until the study of Wilhelmson and Chen (1982) the numerical simulations have not had sufficient resolution to treat the vertical motions accurately near the gust front and have probably overestimated the effect of its presence. The detailed numerical solution of Mitchell and Hovermale (1977) is clearly s-trongly influenced, particularly in the middle and upper part of the domain, by the rigid lateral boundaries of the model. Thus, despite the extensive literature that- exists, it appears that more can be learned about the detailed mechanisms taking place, and there is some justification for a further consideration of the problem.

*The National Center for Atmospheric Research is sponsored by the National Science Foundation.

2. LIFTING EXPECTED FROM THE GUST FRONT.

The significance of the gust front to storm evolution is linked to its ability to force air upward. In this respect the important question is how much lifting is produced and what is its effect. In laboratory experiments Simpson (1969) found that in the important forward region of the front the flow was in. good agreement with that of an ideal fluid over an obstacle of such a shape. Following this idea estimates have been made here of the lifting to be expected from flow over two-dimensional obstacles approximated by the upper half of cylinders of ellipsoidal cross section, for which analytic solutions exist. Examples of the results are shown by the two dashed curves in Fig 1. The curves are for cylinders with vertical-to-horizontal axial ratios of 0.5 (upper curve) and 2 (lower curve). The amount of lifting realized by air passing over such an obstacle (the ordinate in Fig 1) is a function of the initial height of the air parcel some large distance upstream (plotted on the abscissa). Air initially at the surface is lifted exactly the obstacle height, 1.5. Ian as assumed in this calculation (1,5 Ian may be considered a typical depth for the gust front). Air at an initially higher altitude is lifted correspondingly less. At 2 Ian above the ground, for example, air is lifted only 1 Ian or so.

These estimates are, of course, fairly rough. As shown by the shaded area in the figure, the amount of lifting depends to some extent on the shape of the obstacle assumed (though considering that it is the-head of the outflow that produces the lifting, the range of shapes shown here may be adequate). Since real gust fronts are three-dimensional, the lifting is probably overestimated somewhat. Waki,noto's analysis, on the other hand, indicates that two-dimensional considerations should be sufficient. The use of potential flow is justified here on the basis that the inflow is often near neutral stratification. If there was very strong stratification, then the launching of gravity waves by the gust front could produce stronger effects, particularly at heights greater than the obstacle height. However, this will not generally be the case. It should be noted that dashed curves for the frontal lifting, L, are scaled by the barrier height. If one wants to consider other barri'l!r heights, b, then the ordinate and abscissa of Fig 1 can be scaled by b/1.5 Ian.

Since the gust front is generally below the base of the cloud, it is apparent from Fig 1 that air near the surface will not generally be lifted all the way to cloud base by forcing from the gust front alone.

We next consider another lifting distance before continuing the discussion of gust front effects.

3. LIFTING TO THE LEVEL OF FREE CONVECTION (LFC)

Let us denote by H the amount of lifting required to bring an air parcel at some initial height z in the atmosphere to its level of free convection. 13rowning and Foote (1976) pointed out in a study of the Fleming supercell storm that all the environmental air in the sub-cloud region of that storm had an H greater than 2.5 km or so, a rather large distance. They felt that this situation was significant in preserving the single isolated updraft of the storm by preventing a succession of new updrafts from breaking out, as in multi-cell storms.

In fact, H is in general also a function of height, like L of the previous section. The upper solid curve in Fig 1 shows behavior similar to that described for the Fleming storm. Here H is derived from a sounding from Miles City, Montana. The sounding was taken about 100 km to the southeast of a very large supercell storm that produced giant hail. As shown in the figure, H is about 3 km for air near the ground. It decreases slightly at higher altitudes reaching a minimum near 1.4 km, and then rises sharply due to a sharp reduction in moisture in the upper part of the boundary layer. Above 1,9 km the humidity is low enough that air cannot exceed the environmental temperature and experience free convection no matter how far it is lifted. H becomes essentially infinite.

It is now important to contrast this curve with the amount of lifting to be expected from the gust front, L (the shaded part of the figure). One sees that there are no heights for which lifting by the gust front will bring an air parcel to its LFC; that is, $H(z) > L(z)$ for all z, In such a situation one expects a more minor role for the gust front. It may help push inflowing air through the slightly stable boundary layer, a process usually thought of as being accomplished by non-hydrostatic pressure gradients. However, it cannot in itself trigger new convection.

The lower solid curve shows H derived from a sounding at Knowlton about 1,5 h later than the Miles City sounding. The Knowlton sounding was taken at a similar distance from the storm, about 80 km in this case, but in contrast to the Miles City sounding, it was released within a zone of convergent low-level winds along which the storm was moving, Within this zone the convergence had produced a deep moist layer, Mixing ratios of 12-13 g kg^{-1} extended through the whole depth of the subcloud region. In this situation, with nearly constant potential temperature and mixing ratio below cloud base, the lower H-curve displays a nearly linear decrease with height, in sharp contrast to the Miles City curve. Using the Knowlton data, L is greater than H for heights above about 2 km. One then expects that any air at these altitudes that passes over the gust front will initiate new convection.

4. DISCUSSION

It is apparent from the foregoing that one cannot automatically assume that gust fronts can initiate convection. Their ability to do so depends on the compatibility of two important lifting distances L and H, both of which are functions of height, For the common severe storm sounding in which the moisture is confined primarily to a shallow layer near the surface, H remains large at all altitudes. In this case it appears to be impossible for the gust front itself to trigger the development of cumulus clouds. The example of the Montana storm shows, on the other hand, that in situations in which there is a fairly deep moist layer, H can decrease to effectively zero in the upper part of the boundary layer, This situation of finding one type of H-profile in the inflow sector ahead of the storm and another stable (large H) regime in other sectors around the storm has also been found in three other published cases that have been reexamined in this way (Chalan, et al., 1976; Foote and Wade, 1982; Miller and Fankhauser, 1983). In each case there appears to have been a deepening of the moist layer just ahead of the storm resulting from localized horizontal convergence. There is a question of whether this coincidence in the position of storms and narrow convergence zones results from storms preferentially forming and moving along such pre-existing moist convergence zones, or whether, in fact, the presence of a large storm itself sets up the convergence ahead of it. Of the four storm cases considered here, two appear to be of the former category. Examples of the latter categorr will be harder to identify.

Of course, it is not necessary a priori to have storms satisfy the relation $L > H$ so that gust fronts can play an important role. However, the fact that the four storms examined had a moisture distribution in the inflow sector that allowed this relation to be satisfied deserves some explanation. For each of these storms there was also a proximity sounding that would not have satisfied the $L > H$ condition at any height.

One wonders whether there is in fact a distinction in the L-H regimes between multi-cell and supercell storm environments as claimed by Browning and Foote (1976), and hence, a different role for the gu t front in the two situations. The present evidence is that there probably is no strong distinction (the Montana storms was a classical supercell). It is possible that if measurements had been made in the appropriate region ahead of the Fleming storm, a modified sounding with more moisture throughout the lower levels could have been constructed. However, further work is necessary to verify these ideas.

As noted in the previous section, when L is greater than H it is for heights greater than some critical height where the two curves cross. Thus the initial roots of new convection: spawned by gust fronts should be in the upper part of the boundary layer, rather than near the surface, This result seems to show up in the numerical simulation of Wilhelmson and Chen (1982) in which the authors model the forcing of new convection by gust fronts,

5, SUMMARY

The present analysis has supported the idea that in certain situations, gust fronts can have an important role in the structure and evolution of convection. However, it has been found that there are two important lifting distances that are involved in the problem and which do not appear to have been previously considered, The condition $L > H$ appears to be necessary in order for gust fronts to play a significant role. In the feur cases that have been examined, this condition is only satisfied when the upper part of the boundary layer is considerably more moist than is typically found on storm proximity soundings, and then it is only satisfied for heights above a critical level- This deepening of the moist layer is apparently the result of localized zones of low-level convergence,

Further work is needed to determine how often storms experience this deepening of the moist layer in front of them, to examine the horizontal scale of phenomenon, and to determine the cause,

Consideration of these lifting distance is of importance to numerical modeling work that attempts to clarify the factors controlling storm structur and evolution,

6. REFERENCES

Barnes, S, L,, 1978: Oklahoma thunderstorms on 29-30 April 1970, Part I: Morphology of a tornadic storm, Mon, Weather Rev, 106, 673-684.

Benjamin, T. B,, 1968: Gravity currents and related phenomena. J. Fluid Mech, 31, 209-248,

Browning, K. A., and G, B, Foote, 1976: Airflow and hail growth in supercell storms and some implications for hail suppression. Q,J,R, Meterol. Soc., 102, 499-533.

Chalon, J.P., "T.C." Fankhauser, and P.J. Eccles, 1976: Structure of an evolving hailstorm, Part I: General characteristics and cellular structure, Mon. Wea. Rev., 104, 564-575,

Charba, J., 1974: Application ofgravity current model to. analysis of squall-line gust front. Mon. Weather Rev. 102, 140-156,

Colmer, M, J., .1971: the character of thunderstorm gust fronts. Royal Aircraft Establishment, Bedford, England, 11 pp.

Ellrod, G. P,; and J. D. Marwitz, 1976: Structure and interaction in the subcloud region of thunderstorms. J. Appl, Meteorol. 10, 1083-1091.

Espy, J.P. 1841: The Philosophy of Storms. Little and Brown Co., 347 pp.

Foote, G. B., and J. C; Fankhauser, 1973: Airflow and moisture budget beneath a northeast Colorado hailstorm. J. Appl, Met orol. g, 1330-1353,

------, and C.G. Wade, 1982: Case Study of a hailstorm in 'Colorado. Part I: Radar echo structure and evolution. J. Atmos. Sci., . 2828-2846.

Goff, R. c., 1976: Vertical structure- of thunderstorm outflows. Mon, Weather Rev, 104, 1429-1440.

Hane:-C. E., 1973: The squall line thunderstorm: numerical experimentation, J. Atmos, Sci, 30, 1672-1690,

Humphreys, w. J., 1940: Physics of the Air. McGraw-Hill, New York, N.Y., 676 PP• (Also reprinted by Dover Publications, New York, N,Y,, 1964).

Miller, L.J., and J.C. Fankhauser, 1983: Radar echo structure, air motion and hail formation in a large stationary multicellular thunderstorm. J,Atmos, Sci., 2399-2418

Miller, M. J., 1978: The Hampstead storm: numerical simulation of a quasi-stationary cumulonimbus system, Q. J. R. Meteorol. Soc. 104, 413-427,

-----=-:--and A. K. Betts, 1977: Traveling conv ctive storms over Venezuela. Mon. Weather Rev. 105, 833-848,

Mitchell, K. E., and J. B. Hovermale, 1977: A numerical investigation of the severe thunderstorm gust front. Mon. Weather Rev, 105, 657-675.

Orville, H. D., and F. J. Kopp, 1977: Numerical simulation of the life history of a hailstorm. J. Atmos, Sci. 34, 1596-1618.

Purdom, J. F, W., 1973: Meso-highs and satellite imagery. Mon. Weather Rev. 101, 180-181.

Simpson, J. E,--;--1969: A comparison between laboratory and atmospheric density currents. Q. J. R. Meteorol. Soc. 95, 758-765,

Thorpe, A, J., and M. J. Miller, 1978: Numerical simulations showing the role ot the downdraught in cumulonimbua motion and splitting. Q. J. R. Meteorol. Soc. 104, 873-893.

Ulanski, s. L,, and M. Garstang, 1978: The role of surface divergence and vorticity in the.life cycle of convective rainfall: Part I. Observations and analysis. J. Atmos, Sci, 35, 1047-1062,

Wade:-c.G., and G,B. Foote, 1982: The 22 July 1976 case study: Low-level airflow and mesoscale influences. Hailstorms of the Central High Plains., Vol. 2, Colorado Associated University Press, Boulder, 115-130,

Wakimoto, R.M., 1982: The life cycle of thunderstorm gust fronts as viewed with Doppler radar and rawinsonde data. Mon. Wea. Rev., **110,** 1060-1082.

Weaver, J.F., and S.P, Nelson, 1982: Multi scale aspects of thunderstorm gust fronts and their effects on subsequent storm development. Hon. Wea. Rev., 110, 707-718.

Weiaman, M.I:", and J.B. Klemp, 1982: The dependence of numerically simulated convective storms on vertical wind shear and buoyancy. Mon, Wea. Rev., 110, 504-520.

Wilhelmson-;---il.B., and c.s. Chen, 1982: A simulation of the development of successive cells along a cold outflow boundary•. J. Atmos. Sci,, 39, 1466-1483.

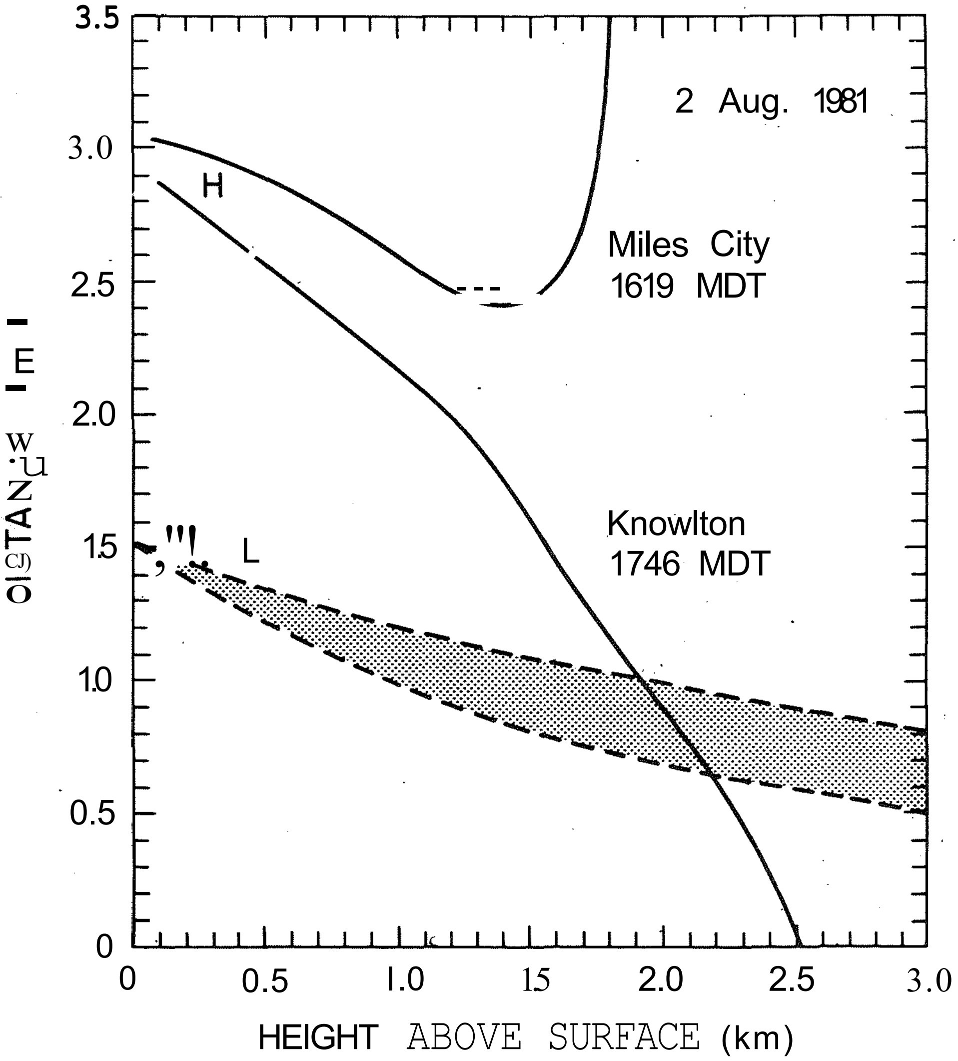

Figure 1. Plot of lifting distances versus height above the surface. The two solid curves show the variation with height of H, the lifting required to bring an air parcel at some initial height to its level of free convection. The dashed curves show estimates of the amount of lifting, L, that might be produced by a gust front of depth 1.5 km. L is estimated from the potential flow over the upper half of two dimensional cylinders of elliptical cross section. The upper dashed curve is for a cylinder **with** vertical-to-horizontal axi-al ratio of one half. The lower curve is for an axial ratio of two.

PRECIPITATION DEVELOPMENT JN CUMULUS CLOUDS IN SOUTHERN AFRICA

D.R. Hudak and R.E. Stewart

University of Toronto
Toronto, Canada

L. INTRODUCTION

The Bethlehem Precipitation Research Project is testing the feasibility of summertime precipitation enhancement in southern Africa. The project area, located in the eastern portion of the interior plateau of southern Africa, encompasses an area of radius 100 km centred on Bethlehem (28°S, 28°E, elevation 1681 m). The region lies along the path of the subtropical high which in summer has its strongest cell at approximately Bethlehem's latitude but over the Indian Ocean. This circulation provides the moisture lacking in winter so that 85% of the area's annual precipitation of 580 to 680 mm occurs during the summer.

Studies, begun in 1977 of weather over the project area from October to March, illustrate that most summer weather is convective. Sixty-seven percent of the days over this period were convective (days with convective clouds with tops coJder than -s°c and producing some precipitation), 8% were days with widespread rain, and 25% were fair weather with no cumu"ius development.

The purpose of th present study is to examine the precipitation processes, both natural and artificially induced, occurring during convective situations. In this paper two case studies will be used to illustrate precipitation deveiopment in different air-masses and in response to different triggering mechanisms.

2. DATA

These clouds were viewed by several platforms. Two cloud physics aircraft, one at -10°c and one at -1S°c, made concurrent penetrations. On each aircraft, liquid water was measured by a Johnson-Williams probe, and particle spectra were measured to 309 µmat -1soc and to 800 µmat -10°c using Particle Measuring Systems Inc. (PMS) 1D and 2D cloud probes, respectively. The aircraft at -1ooc aiso had an optical ice particle counter (Ref. 5). A hird aircraft, used for seeding on a randomized basis., flew at -1s°c and made penetrations irrespective of the seeding decision. Another aircraft near cloud base measured droplet spectra up to 47 µmusing a PMS Forward Scattering Spectrometer Probe (FSSP). A 5. cm wavelength radar at Bethlehem was operated in a yolume scanning mode. A mesonetwork of some 40 weather stations measuring surface parameters and an upper air station at Bethlehem provided further data.

3. FEBRUARY 5, 1981

A tropical airmass was passing over the area from the north and this resulted in moist unstable conditions over the project area. Synoptically there was strong convergence below 40 kPa giving a 20 cm s-1 vertical velocity at 40 kPa, as determined from continutty considerations using surrounding rawinsonde stations (Ref. 2). On the mesoscale, surface convergence values of 2 x 10-4_ s-1 were found· in the vIcInIty of the clouds studied by the aircraft. There were 55 radar echoes observed with 80% having their first echo temperatures between -s°c and -20°c. Of these, 40 showed significant upward growth. The spectrum of echo top temperatures of these 40 echoes illustrated that 70% occurred between -20°c and -40°c, although a few complexes existed with tops as cold as -70°C.

A typical small convective cloud was first penetrated. It had a relatively weak echo (maximum reflectivity between 25 and 35 dBZe), its fi:r:st echo temperature was -Jsdc, it did not grow appreciably, and it lasted 30 rllin (Fig. 1). Cloud base was at +6°C and initial loud diameter at -10°c was 3.6 km. Aircraft observations at both -1soc and -10°c indicated abundant quantities of liquid water on all penetrations, even as the cell was collapsing below their respective flight levels. At -10°c on the initial penetration the average liquid water content was 0.8 g m-3 with a 1-km maximum of 1.3 g m-3 (Table 1). On penetration 5 (at t = 17 min; times relativ to the initial penetration of the seeding aircraft) the average was 1.2 g m-3. Particle concentrations as determined by the optical ice particle counter at -10°c (no cloud probe d ta were available) and by the PMS 1D cloud probe at -1s°c were sl i-1.

Numerical simulation of this cloud was conducted using a one dimensional time dependent microphysically detailed model (Ref. 1). A seasonal average cloud'condensation nuclei spectra was ass'llln.r ed. The model confirmed the essential aspects of the observations. These included cloud top, first echo height, and maximum reflectivity at -s°c. The maximum reflectivity was due to the accretion of water drops by the few ice particles present.

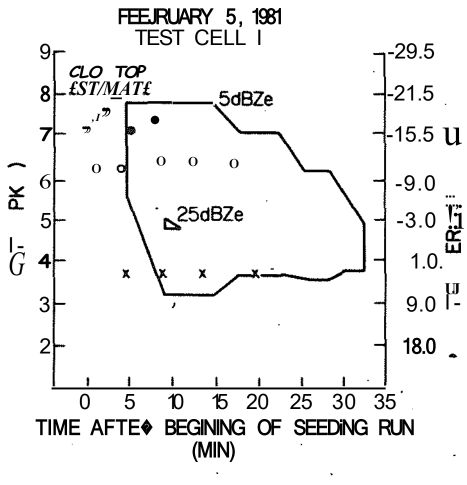

Figure 1. Time-height radar cross section for first cloud (unseeded) examined on February 5, 1981. Closed circles, open circles and crosses indicate the time and height of aircraft penetrations.

Table 1

Summary of data taken by the aircraft making penetrations at approximately -10°C on February 5, 1981 (time refers to the midpoint of the penetration relative to start of seeding run).

Time	Length (km)	Temperature (OC)	Liquid Water Content 1-km Max (g m-3)	Pen Avg	Ice Particle Content 1-km LWC Max (R^{-1})	Pen Avg
:24	3.6	-10.9	1.3	0.8	1.6	1.1
3:54	5.2	-9.8	1.5	0.6	1."0	0.6
8:37	3.3	-12.0	1.6	0.9	0.2	0.2
12:21	2.3	-11.8	0.7	0.5	0.7	0.7
17:05	1.4	-12.1	1.2	1.2	0.1	0.1
1:39	4.1	-10.5	2.6	1.5	0.1	0.1
8:30	6.9	-11.9	1.6	1.8	0.1	0.4
16:04	8.9	-10.1	3.4	2.5	2.6	2.3
20:59	8.4	-10.2	0.8	0.3	9.6	7.0
27:39	8.4	10.3	0.4	0.2	4.7	3.1
.32:49	9.0	-10.6	0.1	0.1	2.7	2.2
38:22	5.4	-10.3	0.1	0.1	7.4	4.5
43:23	12.7	-9.4	0.4	0.1	0.2	0.5

Liquid water values at -10°c for drops <SO µm were 1.6 g m-3 and for drops >50 µm 0.03 g m-3 initially and. 1.4 g m-3 and 0.05 g m-3, respectively, after 17 min. Ice concentrations remained <l i-1 and precipitation efficiency (defined as the ratio of the integrated amount of precipitation at cloud base to the total condensate of the cloud) was 0.1%.

Both observational and modelling evidence suggests that the accretion process was inefficient due to a lack of ice crystals. The model further suggests that coalescence was also inefficient in producing larger sized water drops.

A second cloud was chosen 20 min after studies of the first were completed. This cloud was seeded heavily at -1s°c with silver iodide (40 ejectable 50 g flares). It had a relatively warm first echo at -7°C, a cold echo top around -39°C, and one of the highest echo ascent rates (7.9 m s-1) observed (Fig. 2). Maximum reflectivity was between 35 and 45 dBZe. Cloud base was at +6°C and initial cloud diameter at -10°c was 4 km. During the first 16 min after seeding both aircraft noted high liquid water readings of 1.5 g m-3 to 2.5 g m-3 (Table 1 and Fig. 3). Ice particle concentrations, low initially (<l i-1), increased by more than an order of magnitude between t = 8 min and t = 20 min (Table 1, Fig. 3). It was during this time that the radar echo experienced its high growth rate and the diameter of the cloud increased, at -10°c, from 4 km to 8 km. This was followed by a dramatic decrease in liquid water readings and the development of the most intense radar reflectivity.

Numerical simulations were run using the same initial conditions as in the first case except for the addition of seeding effects. In general agreement with observations the model predicted a more intense radar echo (to 50 dBZe) and a higher precipitation efficiency (16.0%). It demonstrated a 2 order of magnitude difference in millimetre sized ice particle concentrations in the seeded case over the non-seeded case. These larger particles resulted in a higher precipitation efficiency.

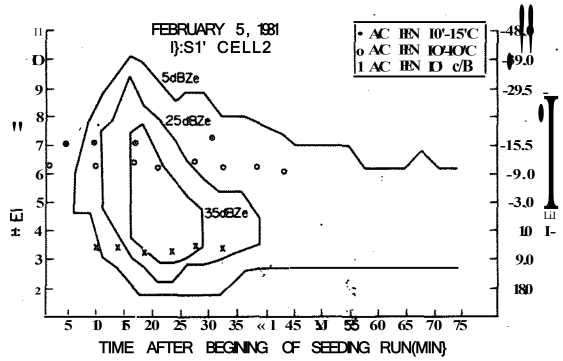

Figure 2. Time-height radar cross section for the second cloud (seeded) examined on February 5, 1981.

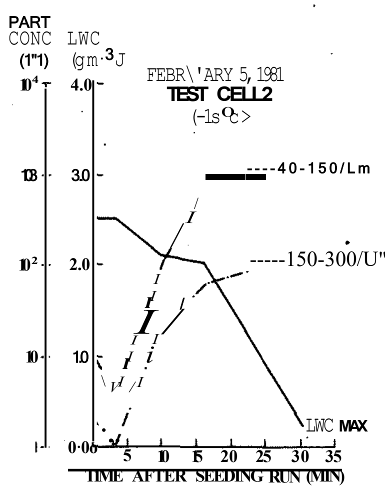

Figure 3. Time evolution of maximum observed liquid water content and penetration averaged particle concentrations at -1s°c for the second cloud (seeded) on February 5, 1981.

4. FEBRUARY 19, 1982

The situation this day was post-cold frontal. Mid-latitude air moist in the low levels but dry aloft had moved into the area the previous night. During the c!.il the frQDt....weakened and surface heating was able to trigger convection where the influx of cooler air was shallow. Despite the weakening of the front, droplet spectra measurements with a FSSP tak n just above cloud base in updraughts showed a maritime-like profile with concentrations >l cm-3 of droplets as large as 30 µm. Only five radar echoes developed in this mid latitude air. All but one had first echo temperatures between -10°c and -12°c, echo tops ranged from -15°C to -3o°c, and maximum reflectivities were between 35 and 45 dBZe.

The numerical simu'iation in this case used a cloud condensation nuclei spectra based on the droplet spectra measuremen.ts. It gave reasonable first echo temperature and maximum reflectivity information. However the model predicted at -1ooc liquid water values would be -2 g m-3 for more than 10 min. This is not consistent with the observation that clouds glaciated very quickly. Precipitation efficiency was calculated to be 2.3%:

It appears th t coalescence was tonverting some of the smaller drops to intermediate size. The accret-on process was also taking place, aided by the increased collision efficiency due to the larger drops, and was responsible for the maximum radar reflectivities, which observations and model calcul-ations indicated to be between 35 dBZe and 45 dBZe. One possible explanation for the discrepancy between observed rapid glaciation and the model's more slow-ly depleting liquid water content values is that ice splinter production; a process not modelled was taking place (Ref. 6). The coalescence pro;ess ould, according to the model, produce drops >25 µm in concentrations in excess of 1 cm-3 which in the presence of the rimed ice crystals could possibly generate large concentrations of ice particles. These in turn could grow and begin riming and in this way rapidly deplete the liquid water and glac-iate the cloud. Inadequate modell'ing of the en-trainment of the very dry mid-level air could also be a source of discrepancy. The result is that a lack of supercooled water, not lack of ice crystals, was the limiting factor in the precipitation devel-opment in clouds with tops colder than -15°C.

The one cell examined by aircraft was seeded with dry ice (1 kg km-1) at -15°c. Cloud base tempera-ture was +9°C and at -10°c its diameter was 3.6 km. Fig. 4 indicates the abundant liquid water before seeding and its rapid decay with time after seeding and the dramatic increase in ice particle concen-t:ation, first in the small sizes then the larger sizes, after seeding. However, no radar echo was observed. In this case .there seemed to be an over-abundance of ice crystals compared to the available liquid.water for an efficient accretion process. y tel2 min when significant concentrations of part-icles were approaching precip itation size the liquid water was depleted and further growth by accretion was prohibited.

The numerical simulation of seeding supports these general observations and predicted a precipitation efficiency of phly 2.1%.

5. DISCUSSION

The fi rst day discussed (February 5, 1981) had a tropical airmass characterized by moist conditions to great heights and a continental CCN spectra in which low level convergence was triggering the con-vective activity. Clouds with maximum tops around -20°C (the smaller convec tive clouds on this day) produced relatively weak echoes. Both observationau and modelling studies sugges:!= that substantial

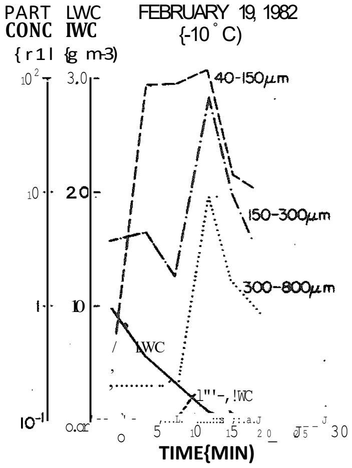

Figure 4. Time evolution of observed penetration averaged liquid water content and parti-cle concen-trations in cloud (seeded) examined on February 19, 1982. Ice water content was derived from 2-D imag-ery.

liquid water amounts persisted throughout the life-time of the clouds. However the continentality of the CCN spectra and relatively high cloud base pre-ven ed an effective coalesceuce process from being activ, and lack of natural ice crystals inhibited the ccretion process. The result was a microphys-ical inefficient cloud and only a weak radar echo.

The results of the addition of nuclei through seed-ing support this .. The observed seeded cloud produc-ed a much more intense radar echo and the modelled seeded cloud a more intense radar echo and higher precipitation efficiency.

The second day(February 19, 1982) had a mid-latitude airmass characterized as moist in the low levels but dry in the mid levels with a maritime-like CCN spec-tra. Surface heating triggered the convection in this case giving echo tops from -15°c to -3o°c and radar reflectivities between 35 dBZe and 45 dBZe, but of relatively short duration. Observations and modelling efforts suggest intermediate sized drops may have been produced through coalescence. These interacted with the natural ice crystals to give a reasonably efficient accretion process. However the supercooled water was depleted quickly, due either to the entrainment of the dry mid-level air or a large increase in ice concentration due to ice multiplication. Seeding studies again support this. The observed seeded cloud produced no echo as there was insufficient liquid water to support the growth to precipitation size of the large number of ice crystals introduced and the modelled seeded cloud gave a lower precipitation efficiency.

The three clouds discussed had initial characterist ics which were comparable to those of the clouds used in the High Plains Experiment (Ref. 3). The average conditions of the IPLEX-1 clouds were cloud base temperature of 5.9°c, horizontal size of 3.1 km, 1-km average liquid water content of 1.05 g m-3, and 1-km average ice concentration of 0.2 1-1. Cloud top temperature and depth of cloud for the African cases do, however, lie at the extremes of the HIPLEX-1 clouds at -17.9°C and 3.7 km, respectively. The tjme history of the liquid water content and ice water content (Fog. 4) of the cloud examined in the mid-latitude airmass follow very similar-trends to those of the HIPLEX-1 seeded clouds (Ref. 3,4). The corresponding time histories for the clouds studied in the tropical airmass differ drastic lly.

In summary, some aspects of the southern African convective clouds have been presented. Precipitation production almost always involves the ice phase but the role of coalescence can be jmportant in certain instances. The result is that on different days convective clouds of comparable physical size (horizontal diameter, vertical depth) can have precipitation mechanisms which differ considerably; many of tJ·,ese differences can be related to airmass characteristics and perhaps triggering mechanisms.

Acknowledgements: The South African Weather Bureau and Water Research Commission, as well as the Cloud Physics Research Division of the Atmospheric Environment Service of Canada are gratefully acknowledged for their support and co-operation.

6. REFERENCES

1. Nelson L D 1979, Observations and numerical simulations of precipitation mechanisms in natural and seeded convective clouds, Technical Note No. 54, Dept. of Geophysical Sciences, University of Chicago, 186 pp.

2. O'Brien J J 1970, Alternative solutions to the classical vertical velocity problem, J Appl Meteor 9, 197-203.

3. Cooper W A 1981, Characteristics of seeded and unseeded .HIPLEX-1 clouds, Preprints Eighth Conf on Inadvertent and Planned Wea Modif, Reno, Amer Meteor Soc 120-121.

4. Lawson R P 1981, The ice/water budget in seeded HIPLEX-1 c',uds, Preprints Eighth Con£ on Inadvertent and Planned Wea Modif, Reno, Amer Meteor Soc 110-111.

S. Turner F M and Radke L F 1973, The design and evaluation of an airborne optical ice particle counter, J Appl Meteor 12, 1309-1318.

6. Hallett J and Mossop S C 197:, Production of secondary ice particles during the riming process, Nature 249, 26-28.

MIXING IN SMALL MARITIME CUMULUS CLOUDS

K A Knight and S Nicholls

Meteorological Office
Bracknell, United Kingdom

1. INTRODUCTION

The structure and development of small, warm cumulus clouds has been studied extensively in recent years and the idea originally suggested by Squires (Ref 1), that most environmental air is entrained through the cloud top has been supported by both observational and theoret.ical work (for example Refs 2, 3). The mechanism of entrainment and the origin of the entrained air have obvious effects on the dynamical and microphysical structure of the clouds, and heuce their ability to produce precipitation. Some observations fro flights with an instrumented aircraft in small maritime cumulus clouds around the coasts of Britain are presented, in particular those relatin vertical velocity structure and droplet size distributions.

2. INSTRUMENTATION AND DATA ACQUISITION

The Meteorological Research Flight (MRF) Hercules C-130 aircraft was used on all flights. Details of its instrumentation are given in Ref 4. in addition, PMS ASSP and/or FSSP instruments were fitted to measure cloud droplet size spectra (see Ref 5 for a description of the FSSP instrument).

A series of straight and level runs was flown through isolated growing cumulus clouds at various levels, usually commencing at cloud top. Profiles of the environmental air in which the clouds were developing were also obtained.

3. RESULTS AND DISCUSSION

Figure 1 shows the clear air sounding obtained off the South-west Coast of England on 11 February 1982 during flight H496. The cumuli which developed on this day were mostly around 1000 metres deep and were not precipitating. Vertical velocity data (sampled at 4oHz) for runs through clcud on this flight were examined and distinct regions of updraught and downdraught identified. The width of these.regions as a percentage of cloud width were calculated together with the average values of vert cal velo ity and other parameters. Averaging the data-from different

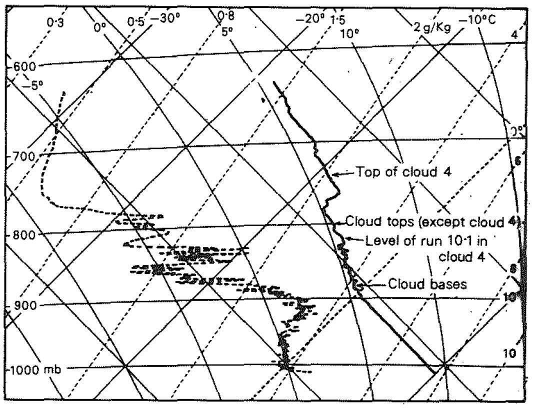

Fig. 1 Tephigram for flight H496 showing approximate heights of cloud bases and tops.

clouds means that the data is also averaged, to some extent, with respect to cloud age. However only growing clouds were selected for investigation so the initial growth, and usually the final decay, stages were excluded. The cloud penetrations were made relative to cloud top and baste thereby partially compensating for variations in cloud depth.

Table 1 shows the averaged vertical velocity data and updraught/downdraught sizes from flight H496 together with the buoyancy of these regions as indicated by the difference in virtual potential temperature inside and outside the cloud. It is clear that downdraughts are most frequently encountered at cloud top and that on average the maximum updraught and downdraught velocities are found at around the mid-height of the cloud. These observations are consistent with cloud top entrainment causing downdraughts to penetrate into the body of the cloud. This negatively buoyant air is probably produced by evaporative cooling after environmental air is entrained y turbulent motions at cloud top as discussed by Deardorff (Ref 6). The maximum negative buoyancy in down-draught regions at cloud top yields maximum downward

TABLE 1

LEVEL	**TOP**		MID-HEIGHT		BASE	
Updraught (+)/Downdraught (-)	+	-	+	-	+	-
Updraught/Downdraught as a % of cloud width	36	46	42	41	59	22
Average width of Updraught/Downdraught (m)	390	460	510	380	700	.300
Average velocity of Updraught/Downdraught (m/s)	+1.1	-0.8	+1.2	-1.0	+1.1	-0.5
(θ_v) in cloud - (θ_v) outside cloud (deg C)	-0.4	-0.7	+0.1	-0.1	+0.1	+0.1
θ_v = Virtual potential temperature						
Droplet concentration (cm-3)	37	24	26	18	25	11
Mean radius (μm)	9.7	9-9	9.3	9-5	6.6	6.7
Liquid wate content ($g\,m^{-3}$)	0.19	o. 14	0.13	0.09	0.04	0.01
Dispersion of droplet spectra (%)	37.5	37.0	35.9	34.8	29.8	28.0

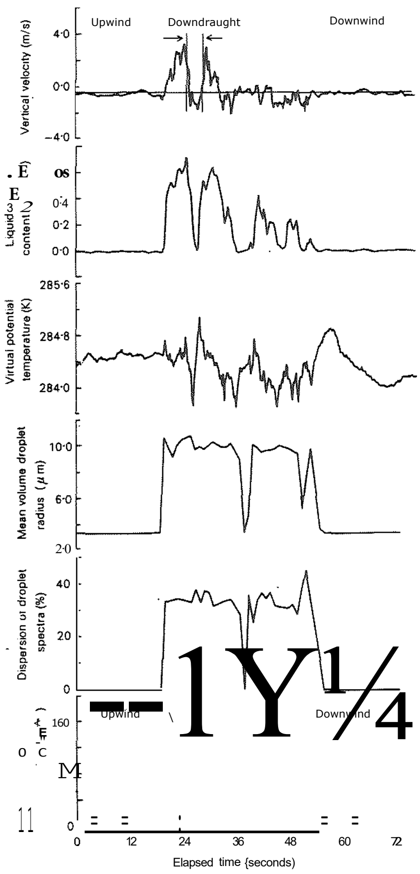

Fig. 2. Time history plots of various parameters during a run through the top of a cumulus cloud. Numbers on concentration trace refer to droplet spectra in Figure 3.

velocities at around mid-level. The average width of updraughts in the cloud decreases steadily towards cloud top as they are diluted by entrained air and their momentum is transferred to downdraughts. The downdraughts, however, do not appear to grow in size as they descend, although data from other flights does show some increase in downdraught width. This may suggest that many of the downdraughts do not penetrate deeply into the cloud as a whole, but are split up into smaller regions by the ascending air. Cooper and Rodi (Ref 7) suggest that downdraughts are forced to the edges of clouds, after entrainment at cloud top. This is confirmed in data for the moat vigorous clouds sampled, presented below, but for most clouds, downdraughts are present in the centre of clouds, at and below mid-height.

Cloud drople data from flight H496 were averaged in a similar way and the values of microphysical parameters in updraught and downdraught regions are also presented in Table 1. The mean radius, integrate·d liquid water content and dispersion increase with height above cloud base as expected. However, there is little variation in either mean radius or dispersion between updraught u d downdraught regions at any level despite significant reductions in liquid water content and droplet concentration in the descending air. This is an indication of the inhomogeneous nature of the majority of tne mixing procesoes occurring in the dowr.draughts as described by Latham and Reed (Ref 8). No evidence, however, of a significant broadening of the spectra due to mixing as suggested by Baker and Latham (Ref 9) is indicated.

These results are typical of the clouds studied on all our flights conducted in small cumuli •

3.1 Detailed Structure of Clo d Top

Data from a cl.oud penetration made at about 150 metres below the top of a devel ing cumulus cloud of approximately 600 metres in height will be examined in some detail. It is typical of many runs made near the tops of growing cumulus. Figure. 2 is a series of time history plots for this run showing vertical velocity, Johnson-Williams liquid water content, virtual potential temperature, and mean volume droplet radius, dispersion and droplet concentration. The first 3 parameters are plotted at 5Hz (equivalent to 20m between data points) and the lower 3 at 1Hz (equivalent to 100m between data points).

A region of descending air embedded in a strong updraught can be clearly observed. It coincides with a very large reduction in liquid water content and a marked decrease in temperature. The air in the downdraught is still strongly negatively buoyant. 'fhis is probably due to the mixing in of air from above cloud top which could have produced a maximum temperature decrease of about 1 deg C in this case, slightly more than -that recorded in the downdraught. Evaporation has significantly reduced the droplet concentration within this region, by approximately a factor of 10, but despjte this the mean volume radius, and dispersion of the spectra, are practically unchanged. Figure 3 shows droplet spectra for 1 second (100 a) suples for a section of this run around the downdraught region as indicated by tr. numbers on the droplet concentration plot of figure 2. The shape of the droplet spectra is largely unchanged in this downdraught and it is not pushed towards smaller droplet sizes implying that the mixing processes are mainly inhomogeneous, i.e. that dry environmental air compietely evaporates a number of droplets of all sizes before mixing into the cloud (Ref 8).

Figure 4 shows the air flow around the cloud, relative to the mean wind, measured on this run. The cloud was penetrated from the upwind and upshear aide. The main updraught is on the upwind edge of the cloud with rather chaotic, mostly descending motion on the downwind side. The

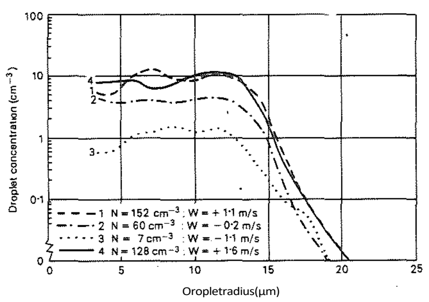

Fig. 3. Cloud droplet spectra (averaged o•er 1 second) around downdraught ·region in top of cumulus cloud. The droplet concentration (N) and vertical locity {W} are also shown.

growth of cumulus clouds on their upshear side - Aeems to be a common characteristic of clouds growing in a sheared environment. Telford and Wagner (Ref 10) report similar observations with tne cloud effectively moving through the air in the upshear direction. Another feature of interest is the near reversal of the horizontal wind field with respect to the mean wind from the front to the r!!ar of the cloud. This was observed on many runs tr.rough small cumulus at all levels. It is consistent with the idea proposed by Heymsfield et al. (Ref 11), that the environmental air is forced to flow around the cloud core producing a turbulent wake, where mixing is enhanced. Figure 2 also suggests that mixing is more pronounced on the downwind side of the cloud where the liquid water content and droplet concentration are both very variable and reduced considerably from the values in the updraught core on:the upwind side.

3.2 The Effect of the Environment on Cloud Structure

Data relating to clouds of various sizes from flights on days under different conditions have been examined. The data presented above are typical of fairly small cumulus of about 750-1000 metres in vertical extent. The vertical velocity structure at the mid-height of clouds however, seems to depend on the size and vigour of the cloud. On many runs downanrng .t., were aetectea deep inside the cloud at mid-level but in some of the more vigorous clouds, downdraughtA were observed only st the edges. Descending air was most frequently encountered on the edges of clouds at all .levels. These observation,:i agree with data presented by Cooper and Rodi (Ref 7) who suggest that the descending air on the edges-of clouds is caused by weak downdraughts a.t cloud top being pushed aside by vigorous updraughts. Where the ascending airflow ie not particularly.strong, however, downdraughts can penetrate the core of the cloud. Examples of the airflow in and around clouds in two contrasting cases are shown ill Figure' 5. The top diagram ia for a run (10.1) at mid-level in a vigorous cloud (cloud 4) of about, 1500 metres depth studied during flight H496. The lower diagram is a similar plot for a much weaker and shallower cumulus cloud, of about 600 metres in vertical extent, on a flight when the environment was more stable. Both clouds had strong downdraughts and rather weak updraughts at cloud top. The vigorous cloud had penetrated the inversion and was larger than most of the cumulus that developed on that day (see Figure 1). The difference in vertical velocity structure between the two clouds is clear, with downdraughts from cloud top unable to penetrate the strong adiabatic updraught region at the centre of the vigorous cloud forcing the descending air to the edge of the cloud, whereas

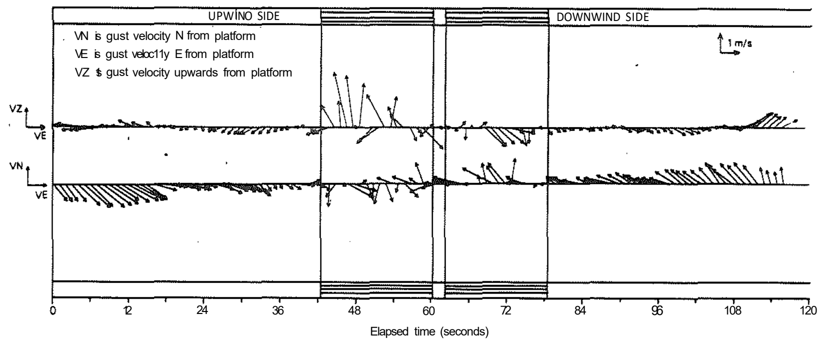

Fig. 4. Fluctuations in gust velocity vectors about the mean wind in top of cumulus cloud. Shaded areas denote presence of cloud.

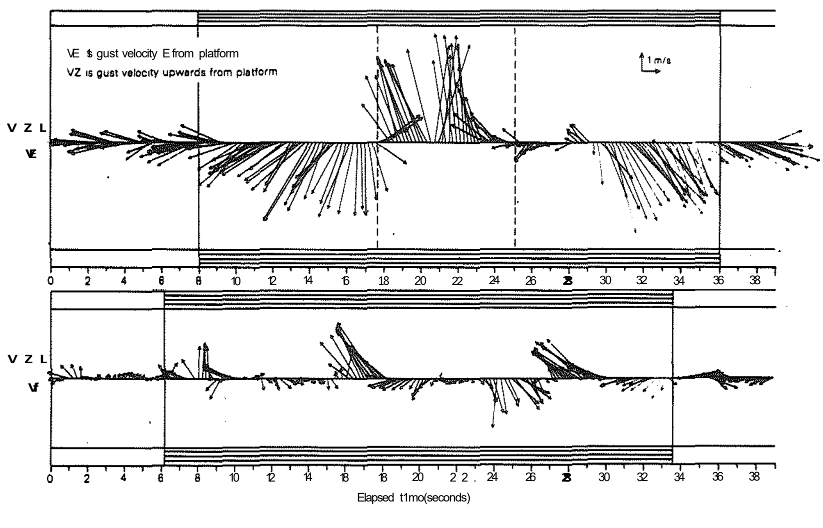

Fig. 5. nuctuations in gust velocity vectors about the mean wind for runs at mid-height in a vigorous cumulus cloud (top) and weak cumulus cloud (bo.ttom). Shaded areas denote presence of cloud and dashed line indicates region of updraught core.

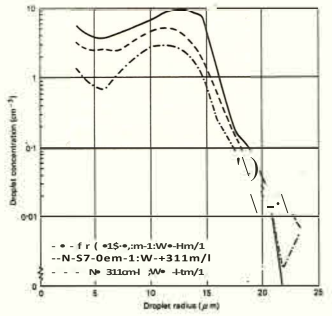

Fig. 6. Cloud droplet spectra (averaged over 1 second) measured at mid-level of vigorous cumulus cloud in updraug t and downdraught regions as shown in Figure 5 (top). Droplet concentration (N) and vertical velocity **(W)** are also shown.

in the weaker cloud updraughts and downdraughts alternate across the cloud width. It should be noted, however, that structures similar to that in the top half of Figure 5 were only found in the most vigorous clouds, usually ones that t ,d managed to break through the inversion. The majority of clouds investigated had a structure similar to that in the.lower section of Figure 5.

The effect on the droplet spectra of these different vertical velocity structures may be significant. Figure 6 shows average droplet spectra for the :wo edge downdraught regions and the central updraught region for the mid-level run in the vigorous cloud. The droplet concentration in the descendi g edges is reduced but the spectral.shape is little changed. It is of interest though that droplets larger than 21;tun are absent from the updraught but are present in the peripheral downdraughts. The vertical velocity structure suggests that these droplets have been brought down from nearer cloud top **where** significant numbers of droplets of this size were observed. If this negatively buoyant air containing large droplets is then mixed into the rising core as suggested by Cooper and Rodi (Ref 7), enhanced growth rates of droplets could be achieved. Similar processes in clouds where downdraights break up the updraught core would not be as effective.

4. CONCLUDING REMARKS

The-development of the droplet spectra in cumulus clouds, in particular the rapid growth of some large droplets, and the effect of the mixing in of dry environmental air has been studied for **some** time. Many different mechanismo which allow droplets to be recycled, or remain in the supersaturated regions of the cloud have been proposed and various models built around these ideas, (for example Refs 9, 12, 13). However, observations such as those presented here suggest that the internal turbulent structure of the cloud effectively controls the microphysical structure. **This** is only considered in the most rudimentary fashion by simple models like those listed above, whose conclusions must therefore have a very limited scope.

From the data analysed so far, it seems clear that pene• ative downdraughts originating at cloud top are an important mechanism by which environmental air is mixed into the cloud. This **mixing** process appears to be mainly inhomogeneous, with the spectral shape and mean radius almost unaltered, which.allows some larger droplets to be retained in the descending parcel of air and carried down to lower levels. If these droplets can then be forced to rise again, the increased supersaturation will promote further growth. This is most easily achieved in a vigorous cloud with an adiabatic core and strong updraught.

The environmental profile of temperature and wind also seem to play an important role i the dynamical and physical structure of cumulus clouds and ultimately their ability to precipitate. Further work is being carried out on this data looking at the thermodynamical properties of the clouds in particular, making use of humidity data from a fast response microwave refractometer.

5. ACKNOWLEDGEMENTS

We would like to. thank the staff ,and aircrew of the: Meteorological•Research flight at Farnborough and those members of the Cloud Physics branch of the Meteoro ₀ical Office at Bracknell whose help and co-operation made this work possible.

6. REFERENCES

1. Squires P 1958, Penetrative downdraughts in cumuli, Tellus 10, 381-389.
2. Paluch IR1979, The entrainment mechanism in Colorado cumuli. J Atmos Sci 36, 2467-2478.
3. Emanuel KA 1981, A similarity theory for unsaturated downdraughts-within clouds. J Atmos Sci 38, 1541-1557.
4. Nicholls S 1978, Measurements of turbulence by an instrumented aircraft in:a convecti e atmosphere boundary layer av.er the sea. Quart JR Met Soc 104, 653-676.
5. Pinnick R G, Garvey D M & Duncan L D 1981, Calibration of f<nollenberg FSSP light scattering counters for measurements of cloud drops, J Appl Met 20, 1049-1057.
6. Deardorff J W 1980, Cloud top entrainment instability, J Atmos Sci 37, 131-147.
7. Cooper WA & Rodi AR 1982, Cloud droplet spectra in summertime cumulus clouds, Preprints AMS Conf on Cloud Physics, Chicago, 147-160.
8. Latham J & Reed R L 1977, Laboratory studies of the effect of mixing on the evolution of the cloud dropl t spectra, Quart JR Met Soc 103, 297-306.
9. Baker MB & Latham J 1982, A diffusive model of turbulent mixing of dry and cloudy air, Quart JR Met Soc 108, 871-898.
10. Telford J W & Wagner PB 1974, The measurement or horizontal air motion near clouds from aircraft, J Atmos Sci 31, 2066-2080.
11. Heymsfield A J, Johnson P N & Dye J E 1978, Observations of moist adiabatic ascent in NE Colorado cumulus congestus clouds, J Atmos Sci 35, 1689-1703.
12. Mason BJ & Jonas PR 1974, The evolution of droplet spectra and large droplets by conden-sation in cumulus clouds, Quart JR Met Soc 100, 23-38.
13. Telford J W & (,nai S K 1980, A n..,. aspect of condensation theory, Pure Appl Geophys 118, 720-742.

PUCIPITATING CONVECUVE CLOUD DOWNDRAFT STRUCTURE - A SYNTIIESIS OF OBSFRVATIONS AND MODELING

Kevin R. Knupp and William R. Cotton
Dept. of Atmospheric Science
Colorado State University
Fort Collins, Colorado 80523
U.S.A.

1 • INTRODUCTION

DowLdrafts are a fundamental CO"'JJOnent of all convective cfouds and mesoscale. convective systems. They contribute not only to cloud mixing processet, but also to vertical tran ports of mass, momentum and moist static energy. Moreover, there is gro - ing evidence that downdrafts in mature precipitat- ing convective clouds influence cloud regeneration, propagation and general structure.

A thorough review of the literature (Ref. 1) reveals that convective cloud downdrafts exhibit a wide range of magnitudes and spacial/ temporal scales. Direct observations indicate that down- draft speeds and sizes range from several meters per second and several hundred meters in nonprecip- itating cumulus cong-estus (Cu con) to several :•m and 10-2o·m s-1 in inten e cumulonimbi (Cb), Down- draft structu e tends toward uniformity and lar&e scales within precipitation at low levels. · Con- trastingly, downdraft structure exhibits smaller scales and greater.inhomogeneity in nonprecipitat- ing Cu con nd in upper regions of precipitating Cu con and Cb. Isolated single-celled clouds often display mVlevel downdrafts along Qloud edges, with a preference within the downshear flank."

Based on a composite of observations and cloud model results, Fig. **1** and Table **1** categorize down- drafts according to their location and prol,able thermodynamical and dynamical characteristics. Small scale penetrative downdrafts which may dom- inate at mid- to upper cloud levels appear to be driven·by evaporation of cloud associated with discrece entrainment processes. Such entrainment may occur at cloud top or along lateral edges as depicted in Fig. **1**. Observations and modeling results indicate that larger scale downdrafts, dis- tinct from penetrative downdrafts, have preferred locations along cloud edges at mid- to upper levels. These downdrafts are probably also forced by evaporational-cooling of cloud and precipita- tion. in addition to pressure forces produced by interactions of cloud vertical mo'tion with shear flow and updraft mass flux compensation. There is very little evidence that the penetrative and cloud edge downdrafts extend to .he surface in any organ- ized fashion.

The low level precipitation downdraft, the subj ec·t of this paper, differs from the other down- draft types in that it transports significant mass, momentum and moi t static energy to the surface. These transports thus provide mechan.isms by which mature Cb propagate, regenerate and tr· ~sform the boundary layer. The precipitation do draft as depicted in Fig. 1 may consist of two branches. **An** inflow branch (a) originates from the updraft inflow sector (on the downshear flank in this case), an another branch (b) lies along the upshear flank where air with lower moist static energy is immediately accessible.

The following sections present **some observa-** tions on the structure• and characteristics of pre- cipitation downdrafts for 3 contrasting cases. Following this, 2-D numerical experiments arP sum- marized to help clarify the observations and further examine the role of melting in producing and maintaining the low level downdraft.

2. RESOURCF.S

The observational analyses presented in **Sec-** tion 3 utilize data from two field experiments, **the** 1977 South Park Area Cumulus Experiment (SPACE) conducted in Colorado, and the 1981 Cooperative Convective Precipitation Experiment (CCOPE) con- ducted in southeastern Montana. Each progra included rawinsonde, surface mesonet and multiple Doppler radar observational platforms, the **charac-**

TABLE 1. Features of Convective Cloud Downdraft Types

	Typical values			
Downdraft tne	speed	width 1ml	depth 1ml	level•
precipitation (PR)	1-15	1-10	1-5	l,m
penetrative (P)	1-20	(1.0	1/2 to 1D	m,u
regional compensating (R)	4-5	5-25	1-5	m,u
cloud/updraft edge (L)	1-15	1-10	1-5	mu
overshoot in§ (o)	1-40	1/2 - 5	1-3	u

•relative cloud level: 1 - lo,r, m - middle, u - nppr

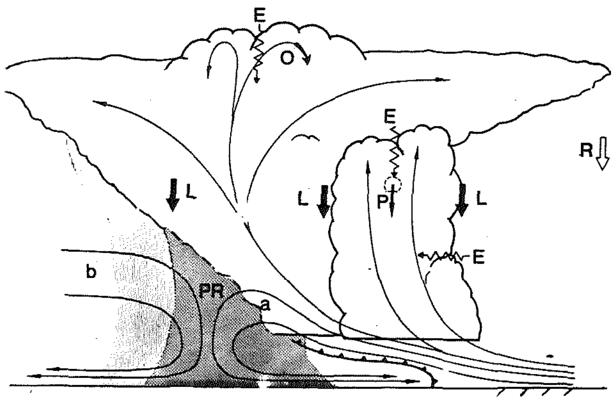

Fig. **1.** Schematic of **updraft,** &owndraft and entrainment flows within a typical Cb,. based on a **composite** of observational studies, numerical model st dies and research by the authors. All flows are storm relative. E denotes entr inment. Other sy _ols label downdraft circulations which are defined in Table 1.

teristics of which are descrioed in Ref. 2 for SPACE and in Ref. 3 for CCOPE.

Doppler radar data reduction and analysis utilizes standard procedures of interpolation of radial velocity and reflectivity to a Cartesian arid where synthesis of horizontal velocity components is performed. Vertical air motion was obtained by integrating the anelastic mass continuity equation downward from echo top where a zero boundary condition was assumed. In all cases downdraft• appear to be well depicted in the analylil, and the pattern, are.oonliltent with observed storm evolution and aurfact data anllylil.

Cloud model results in Section 4 were generated by the CSU cloud/mesoscale model described in Refs, 4, 5 and 6. This model contains a full set of dynamical/thermodynamical equations and a number of microphyaical parameterizations which predict ice and water phase precipitation.

3. OBSERVATIONS

Multiple Doppler radar analyses described below exemplify the variability in structure and properties of the low-level precipitation downdraft.

3.1 The SPACE Caae of 26 July 1977

In this oaae a meaoacale cluster of moderately intense Cb developed over South park and adjacent areas. Doppler analyses of several storms displayed similar downdraft structure, in which downdraft magnitude and areal extent were greatest at levels below the melting level (~ 2 km AGL over South Park). Fig. 2 illustrates the pat"terns in a cloud at 2354 GMT (subtract 7 hr for local time). A precipitation downdraft (labeled PR) having peak speeds of 5 m • 1 at the lowest grid level (~ 0.5 km AGL) is present along the upahear flank, and a weaker midlevel downdraft (labeled L) exhibiting speeds of 3-4 m •-1 exists on the downshear flank. The downshear inflow branch to downdraft PR is dominant at this time (see branch a in Fig. 1).

Doppler analyses at 2338 and 0003 GMT indicate that downdraft PR formed within newly fallen precipitation il the lowest 2]qn, This circulation then intensified and grew upwards over the next 25 min, obtaining a maximum height of 5 km AGL. By 0003 GllT the dominant downdraft inflow was from upshear, as in branch b of.Fig. 1. Concurrent with this downdraft deepening and intensification was a relative shift in downdraft location from the reflectivity core at 2338 to the upshear gradient of the reflectivity field at 0003 GMT, The surface analylil in the plane of Fig. 2 indicates that lowest-valued θ_0 air occurred on the upshear flank of the dowadraft.

Fig. 3 show, vertical profile• (averal•• over three time period,) of man flux within downdrafts PR and L. Difference, in pr file shapes indicate physical diferences between downdraft• PR and L. For example, th• aharp inoreaae in downdraft PR mall fluz lullllt1 that aignifioant downward forcing aot1 over the lowest 2 km. We believe that such forcing ia provided by the combined effects of precipitation loading, evaporation and especially meltins in the lowest 2 km. Downdraft L, whose maximum occur, at midlevels within weaker reflectivity, ia probably forced by vertical gradients of perturbatioa-,rellure and evaporation of precipitation.

3.2 The SPACE oaae of 4 August 1977

. This multicell storm was characterized by updraft, and downdraft& of 10-12 m •-1 peak magnitude,. At 1950 GMT a broad downdraft circulation (Fis, 4) exhibited well defined inflow branches

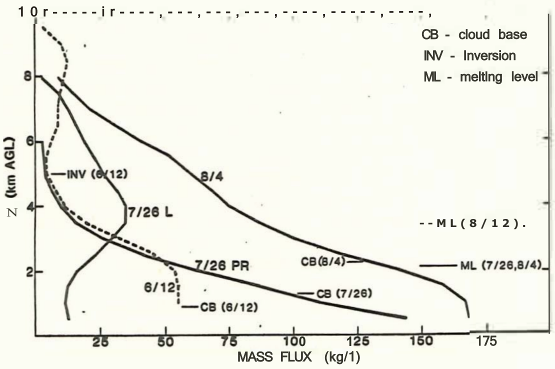

Fig. 3. Vertical profiles of downdraft mall flux composited for 3 time periods in downdrafts PR and L (Fig. 2) on 26 July 1977 (7/26). Other profiles through the downdraft core on 4 Aug 1977 (8/4) in Fig. 4, and through dowil.drafts I and II (Fig, 5) on 12 June 1981 (6/12) are also shown.

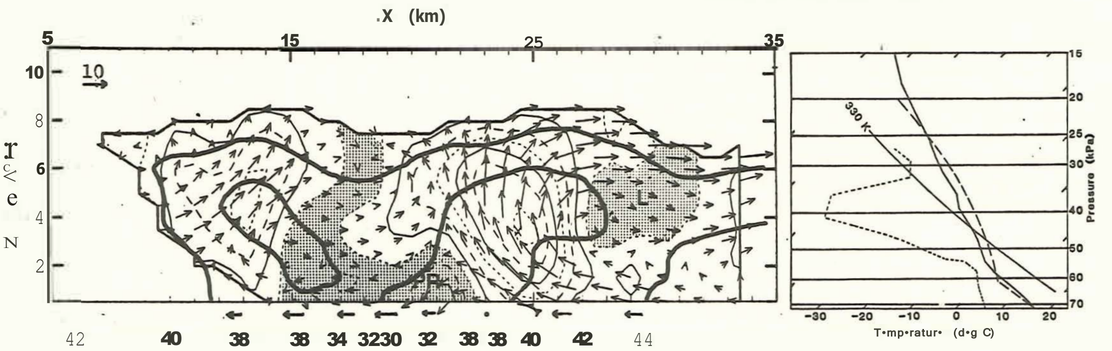

Fis. 2. Triple Doppler radar analylil at 2354 GllT 26 July 1977. The vertical section lhowinl storm relative flow cuts through the core of a low-level downdraft (PR). Light dashed and solid lines are vertical motion analyzed every 2 m s-1, negative values are stippled. Heavy line, are reflectivity factor contoured at 20 and 40 dBZ. A representative sounding having the same vertical scale is plotted on a akew T 101 p diagram on the rilht. Heights are lcm above sround (add 3 km for height above ISL). Wind, and equivalent potential temperature (300 subtracted) from mesonet analyse, are included on the bottom.

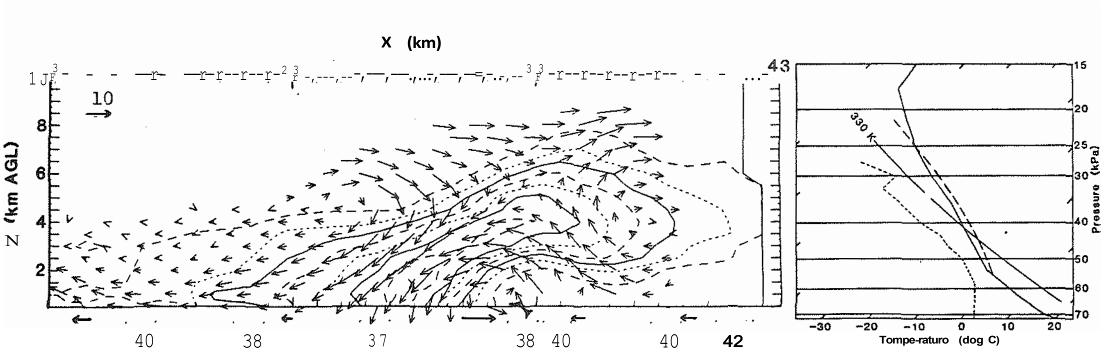

Fig. 4. Same as Fig. 2, except for 1950 GMT 4 Aug 1977. Analyzed co tours are reflectivity factor drawn every 5 dBZ, beginning at 15 dBZ.

from the downshear sector at low levels and from the upshear sector at high levels. The transient upper level branch was associated with a collapsing echo top. This downdraft apparently formed as a consequence of cloud and precipitation loading, and was perhaps also aided by pressure forces produced in the lower levels by the process described in Section 3.1. Because the air at upper levels was statically stable, the upper portions of this downdraft would be expected to gain buoyancy and thus weaken, as was indeed analyzed 8 1/2 min later.

The lower portions of the downdraft in Fig. 4 are more intense than in the case of Section 3.1 because of several possible factors: (1) a deeper and drier b.oundary layer in the 4 Aug. case; (2) less buoyant updraft air parcels in the 4 Aug. case, which would increase relative effects of loading; (3) wealter updrafts producing smeller precipitation particles in the 4 Aug. case, which would permit greater rates of melting and evaporation in downdrafts. Because of these physical differences, downdraft mass flux (Fig. 3) exhibited greater magnitudes, peak values at higher levels, and deeper downdrafts than the case of Section 3.1. As in the previous case, mass flux divergence was greatest at and above the melting level.

3.3 The CCOPE Case of 12 J.. e 1981

Environmental characteristics for this case differ from the previous two in that greater potential instability a d much greater wind shear were present. However, downdrafts were confined to relatively small magnitudes and areas. Fig. 5 illustrates flow patterns in a horizontal plane at 3 km AGL and shows a pair of updraft/downdraft couplets, in which downdrafts (I and IT) are located downshear of updrafts. These .relative patterns, typical for this case, are opposite those found in the previous low shear cases. The mass flux profile for downdraft I (Fig. 3) reveals a relatively deep downdraft whose maximum height was apparently limited by an inversion near the 5 km AGL level.

We infer that two mechanisms acted together to produce a 5 km deep downdraft. In the lowest 3 km, the region below the melting level, precipitation effects (melting, evaporation, loading) dominated, while above 3 km dynamic entrainment effects augmented precipitatior, loading. Organized entrainment into the downshear flank of updrafts, where pressure perturbations are low, often occurs (e.g. Refs. 4,7) and was evident .n all Doppler analyses of this case. We hypothesize that downdrafts did not attain strong magnitudes because a 1.S km deep moist adiabatic layer existed at and above cloud base. Such a profile dampens downdrafts since only weak downdrafts are possible in moist adiabatic atmospheres (e.g. Ref. 8).

4. SUMMARY OF 2-D CLOUD 1\lODEL SENSITIVITY RESULTS

A series of sensitivity tests were run on the 26 July 1977 sonnding shown in Fig. 2 to further examine the role of precipitation in downdraft forcing. With tho aid of Table 2, we briefly

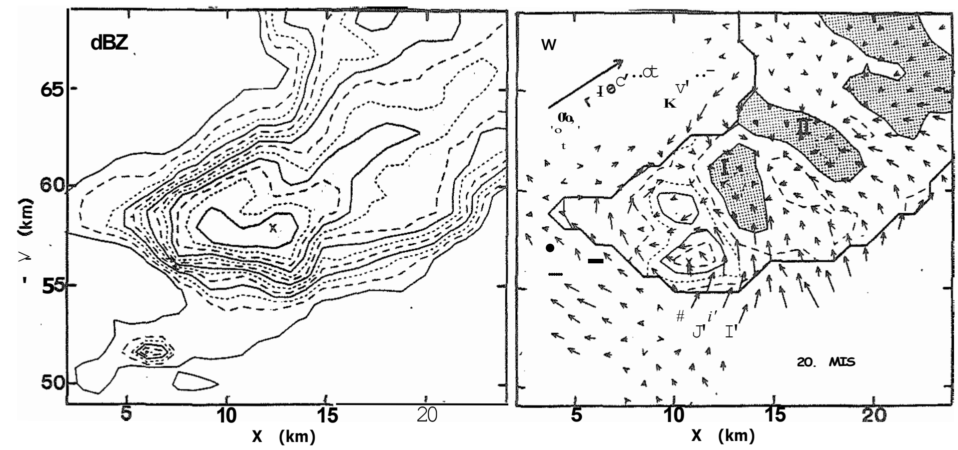

Fig. 5. Relative horizontal airflow patterns from a four Doppler radar analysis at 3.8 km above 1\lSL (3 km AGL), 2320 GMT 12 Jnne 1981. Reflectivity factor on the left is analyzed every S dBZ beginning at O dBZ. Vertical motion, contoured every 4 m s-1, is analyzed in the right panel. DOWlldrafts are shaded. The shear vector was calc lated from cloud top and clond. base environmental winds.

TABLE 2. Summary of Low Level Downdraft Chracteristics from 2-D Cloud Model Experiments

Experiment	min. w	height of min. w	minimum T'	downdraft depth
control	-10 m s^{-1}	0.9 km	-7 °C	2.7 km
rain only	-5	1.6	-4.5	2.9
no ice melting	-5	0.7	-4.5	1.4
1/4 precip. size	-12	0.9	-11	3.5

describe here comparisons of the control case having ice microphysics with runs having the following variations: (a) water phase only, (b) ice phase but no melting, and (c) ice phase with the characteristic precipitation size reduced by one quarter.

In all experiments downdrafts formed at mid- to upper levels near cloud and updraft edges, and at low levels within precipitation. Low level downdraft formation is associated with recipitation arrival into the lowest layers, ana low-level downdraft intensity variations closely parallel chances in precipitation rates. In another experiment with the precipitation process deleted, low level downdrafts were absent. Examination of individual runs reveals that downdrafts rapidly build upward from the. 1 km level.

A summary of the model results in Table 2 demonstrates a striking sensitivity of downdraft characteristics to precipitation microphysics. Downdraft strength and total cool-ing are significantly greater when the ice phase is activated. Moreover, downdraft characteristics are highly sensitive to assumed particle size distributions. Decreasing ch racteristic raindroi and graupel diameters by a factoT of 4 result in more energetic downdraft circulations. In the no melting case, cooling results from evaporation of rain water which is shed from graupel 1rowin1 by accretion of cloud water in the lower cloud layers.

In all cases downdraft activity is most significant within the c nditionally unstable region in the lowest 2 km, consistent with the observations in Section 3.1. These results confirm that downdraft forcing is strong in the lower levels and that melting effects significantly infhence downdraft properties. Further experimentation in three dimensions will further examine downdraft initiation and dynamics.

5. DISCUSSION AND SUMMARY

The observations and model results indicate that l w level downdrafts are driven by precipi•ation effects, and that cooling produced by melting of ice phase precipitation is significant when compare1 to precipitation loading and evaporation. Because the atmosphere usually exhibits greatest static instability in the lowest 1-4. km where melting is ac7ive, downdraft• can be expected to be most active in these layers, as the analyses and model results herein indicate. We anticipate that total low-level downdraft mass flux is a function of the areal extent and intensity of precipitat·Jn, details of ,recipitation ,roperties such as phase •nd cha acteristic size, and the depth and dryness f the lowest 2-4 km. Observational eviaence indicates t at low level downdraft properties are influenced by stable layers, as in the 12 une 1981 case. Indeed, the maximum of height of the low level precipitation downdraft is probably limited by conditio..ally stable layers.

Based on tke observations, we envision that tke followia1 hypothetical process occurs. Provided that updraft inflow air is sufficiently buoyant to support cloud and precipitation weight, the low level downdraft forms first at low levels where greater static instability exists. Downward accelerations, provided by loading, evaporation and melting, are sufficiently strong to dynamically induce low pressure perturbations which are greatest in value just above the level of.strongest downdraft accelerations. In response to lowering pressure, downdraft circulations may build to greater heights and incorporate dry environmental midlevel air having low θe values. This inferred pressure reduction thus provides a mechanism in which midlevel air systematically enters the low level downdraft. If updraft inflow air becom·s less buoyant through anvil shadowing effects or relative advection of less unstable air, precipitation loading becomes more significant and downdrafts may begin at higher levels as in the 4 August 1977 case:

Additional analyses of observations and 3-D model results will examine more cl sely the charac teristics of p essure fields associated with developing and mature downdraft•, t e role of entrainment in downdraft developme t, and the significance of meltina in initiating and maintaining low level downdrafts.

6. ACINOWLEDGEIIENTS

The authors thank Ms. Brenda Thompson for preparing the manuscript. This research was sponsored by the National Science Foundation under Grant ATM-8312077.

7. REFERENCES

1. Knupp K R and Cotton W R 1984, Convective cloud downdraft structure -··,;.n interpretive survey, to be submitted to Rev. Space Phys. Geophys.

2. Cotton W R et al 1982, An intense q asi-steady thunderstorm ever mountainous terrain. Part I: Evolution of the storm-initiating mesoscale circulation, J. Atmos. Sci. 39 (3), 328-342.

3. Knight C A 1982, The Cooperative Convective Precipitation Experiment (CCOPE) 18 May - 7 August 1981, Bull. Amer. Meteor. Soc. 63 (4), 386-398.

4. Tripoli G J and Cotton W R 1980, A numerical investigation of several factors leading to he observed variable intensity of deep convecrion over South Florida, J. Appl. Meteor. 19 (9), 1037-1063.

5. Tripoli G J and Cotton W R 1982, The Colorado State University three-dimensional cloud/mesoscale model - 1982. Part II: General theoretical framework and sensitivity e periments, J. Rech. Ataos. 16 (3), 185-219.

6. Cotton W R et al 1912, The Colorado State University three-dimensional cloud/mesoscale model - 1982. Part II: An ice phase parameterization, J. Rech. Atmos·. 16 14), 295-320.

7. Heymsfield A J et al 1978, Observations of moist adiabat', ascent in northeast Colorado cumulus congestus clo ds, J. Atmos. Sci. 35 (9), 1689-1703.

8. Kamburova P L and Ludlam F H 1966, Rainfall evaporation in thunderstorm downdrafts, Quart. J. Roy. Meteor. Soc. 107 (3), 510-518.

THE HYBRID MULTICELLULAR - SUPERCELLULAR STORM: AN EFFICIENT HAIL PRODUCER

Stephan P. Nelson* and Nancy C. Knight**

*National Severe Storms Laboratory, NOAA
Norman, Oklahoma 73069

**National Center for Atmospheric Research[1]
Boulder, Colorado 80307

1. Introduction

The concepts of multicellular and supercellular storms are well known and descriptions can be found, for example, in Browning (1977). Application of these classical characteristics to a population of storms quickly reveals that many storms do not fit our idealizations (WMO, 1981).

In studying the most severe hailstorms in Central Oklahoma, one's attention is often drawn to storms that we have named "hybrid" hailstorms because they exhibit features common to both the classical multicellular and supercellular storm structures. These hybrid storms typically produce not only very large hail (typically >5 cm in diameter), but also very wide (>20 km) and long (>100 km) hailswaths.

In the following we briefly describe the structure and formation mechanisms of hybrid hailstorms and how they relate to what Foote and Frank (1983) have termed the "weakly evolving" hailstorm.

2. STRUCTURAL CHARACTERISTICS OF THE HYBRID HAILSTORM

On broad spatial and temporal scales, the hybrid hailstorm displays all the characteristics of the classical supercell storm. The factors that distinguish the hybrid storm are unusually large bounded weak echo regions (BWER) typically extending to heights >8 km; multiple BWR centers which are presumably indicative of multiple updrafts; disposition towards long "pendant" rather than "hook" echoes (see explanation below); and a tendency towards being non-tornadic or, if tornadic, to producing only funnel clouds or minor tornadoes.

Figure 1 shows the reflectivity structure of a well documented tornadic supercell (8 June 1974) and a hybrid hailstorm (17 May 1980). The presence in the storm on 8 une of an intense mesocyclone a,.d the production of three major tornadoes has been reported by Brandes (1977). Ground surveys revealed a few reports of large hail (maximum diameter 5.0 cm), but the hailfall was fairly localized.

The hailswath from the 17 May storm was over 300 km long and at one point 40 km wide with maximum reported hailsto e diameter of 7.5 cm. No known tornadic activity was reported with this storm.

The most striking feature in Fig. 1 is the comparative horizontal and vertical extents of weak echo regions in the hybrid hailstorm and tornadic storm. For example, the bounded weak echo region at mid-levels of the 17 May storm is almost as wide as the entire 8 June storm and the hybrid hail storm's bounded weak echo region extends to >8 km. Due to the lack of multiple-Doppler data on these storms little is known about the updraft characteristics. Nelson (1983) presents vertical velocities for the 8 June storm at a time about 1 h after th t shown in Fig. 1. At the later time there was only one strong updraft (max velocity ~50 m s^{-1}), but the 5 km level of Fig. 1 indicates two possible BWERs separated by a distance of 3 to 4 km. Based on the separation between the minima in the BWER shown in Fig. 1 and other times not shown, the updraft separation of the 17 May storm is estimated to be 5 to 8 km, or twice that of the 8 June storm.

Another significant difference between the storms lies in the configuration of their low level reflectivity fields. The terms "hook" and "pendant" echoes have typically been used somewhat interchangeably in the literature. We propose an explanation for the structural differences between the 17 May "pendant" and the 8 June "hook". It is easily imagined that at 1 km the weak reflectivity indentation to the southwest of the 8 June storm's high reflectivity core and the southward extending high reflectivity to the west of the indentation are both caused mainly by the horizontal advection of precipitation particles. To the contrary, however, the presence of multiple and extensive bounded weak echo regions in the 17 May storm suggests that tha southward extension of the pendant echo from the main storm body at 1 km is not due advection but rather to significant convection along an intense gust front.

3. FORMATION MECHANISM OF HYBRID HAILSTORMS

Data collected from a storm that occurred on 25 May 1974 indicates that its transition from multicellular to hybrid structure was coincident with the formati n of an intense downdraft and the accompanying gust front.

The storm's hailfall characteristics were well measured with a maximum hailswath width of about 20 km and a swath length >100 km. Maximum hailstone diameter was 6.4 cm and there was one report of a possible funn,l.

For two hours the storm exhibited multicellular structure with seven distinctive dominant cells. These behaved in a classical manner in that each new cell formed within 10 km of the old dominant cell at regular intervals (19.5 ±4 min) and moved toward the northeast as it first intensified and then decayed.

First indications of a change in the storm's basic structure occurred in the reflectivity field near 1205. In Fig. 2 note that the reflectivity gradient on the storm's west side steepens substantially from 1205 to 1224. This sharp gradient is even more distinctive when viewed in the vertical,

[1] NCAR is sponsored the. National Science Foundation.

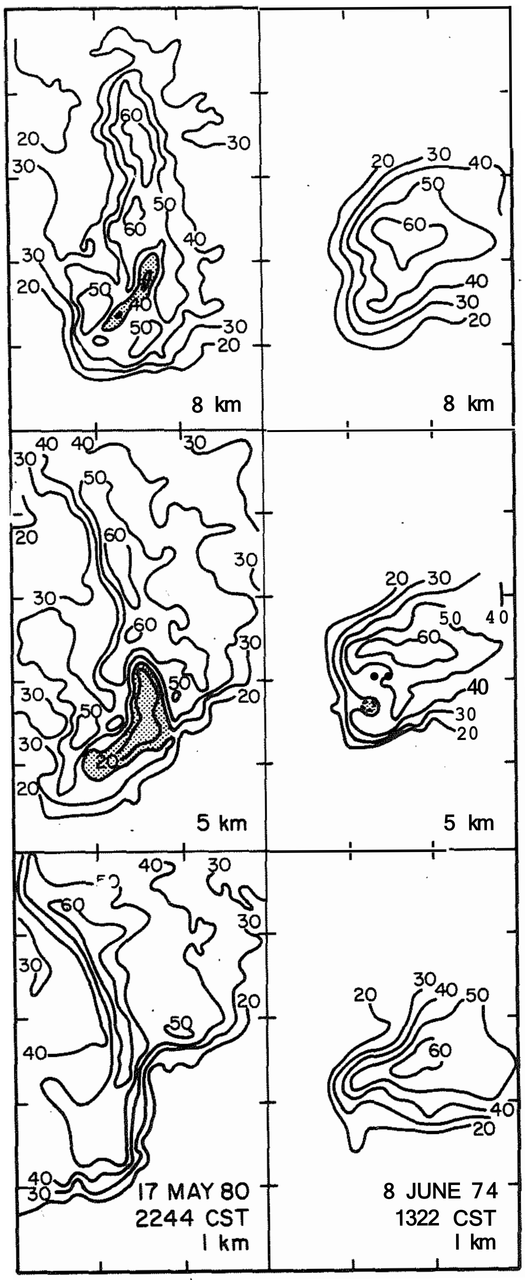

FigUJ:>e 1. Reflectivity (dBZJ structUJ:>e of the storms on 17 May 1980 and 8 June 1974 at three selected levels. Weak echo regions are shaded. Tick marks are at 10 km intervals.

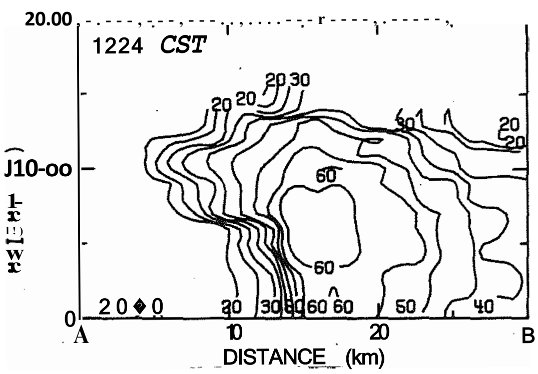

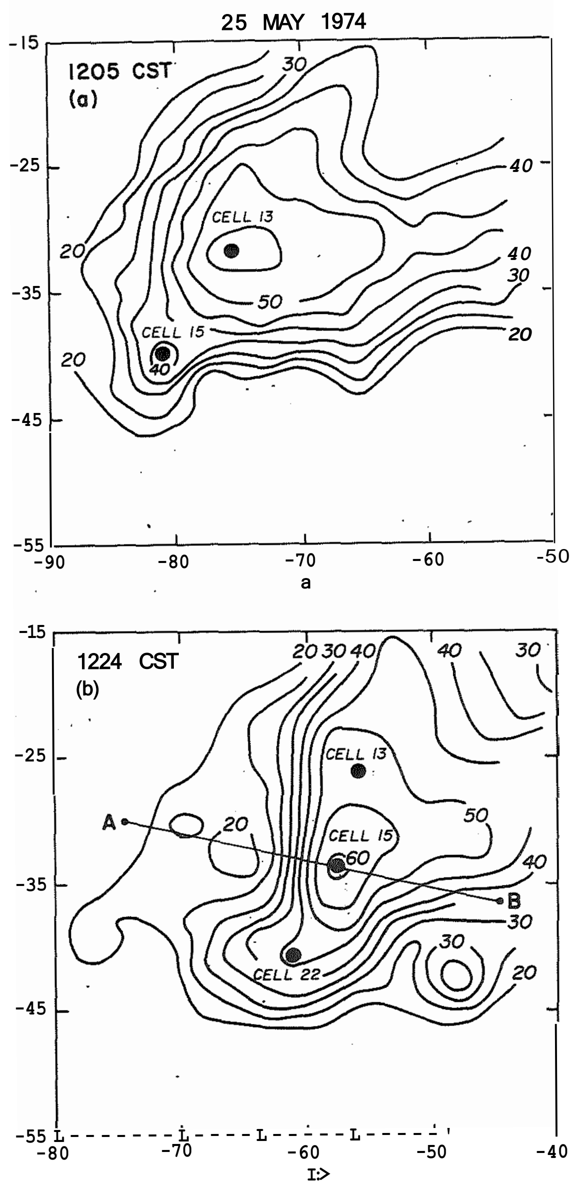

FigUJ:>e 2. Zero degree tilt reflectivity structure of 25 May 1974 storm at 5 dBZ intervals. Individual cells are indicated by solid dots. Distanees on the abseissa and ordinate are in kilometers e st and north of the radar. a) 1205 CST; b) 1224 CST. The $\overline{AB}$ vertieal seetion is gtven in Fig. 3.

Fig=e 3. Vert1:eal eross-section of re fleetivity at 5 dBZ intervals. See Fig. 2, 1224 CST for orientation.

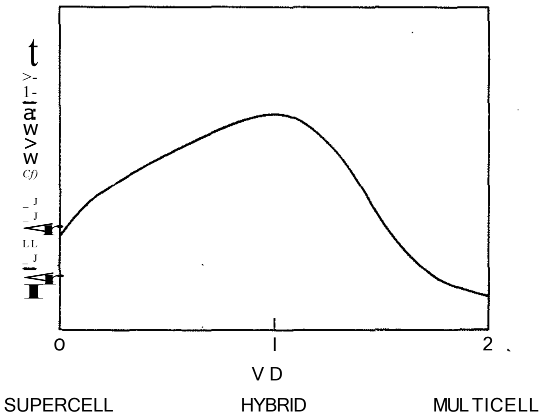

Figure 4. Hypothetical variation of a storm's hailfall intensity with its structure. D - updraft diameter; t - distance between updrafts. See text for further explanation.

Fig. 3. There is obvious erosion of the reflectivity field at and below 7 km on the storm's west side. This area is associated with the phenomenon described in the literature as the "rear flank downdraft" (RFD) (e.g., Lemon and Doswell, 1979). The RFD spawns a gust front on which new convection forms transforming the storm from a classical multicellular structure to more of a hybrid. This transformation is followed by a rightward deviation in the storm motion, strong surface winds (maximum gust of 21 mi-1), and both an increase in the hailswath width and maximum hailstone sizes.

4. DISCUSSION

The most severe hailfall events in central Oklahoma are caused by storms with hybrid or mixed characteristics. The reasons for enhanced hail growth are not well known, but Nelson (1963) showed that an extensive area of moderate updraft is necessary for a major hailfall and the large and multiple BWER's of these storms certainly imply large and strong updrafts. Another possibility is that closely spaced updrafts facilitate embryo transfer between cells.

Foote and Frank (1983) systematized the various gradations of structures between the multicellular and supercellulur extremes through consideration of the relationship between a storm's updraft diameter (D) to the spacing between old and newly forming updrafts (2.). The 1/D ratio is O for classical supercells and >l for classical multicellular storms. When e=D Foote and Frank termed this a "weakly evolving" storm and such an evolutionary pattern with new cells growing along a strong gust front would produce a hybrid structure. We envision hailfall severity varying with the R/D ratio as shown in Fig. 4 with a maximum occurring for storms with a hybrid structure. If this figure has validity then it suggests a dynamically oriented technique for suppressing hail in those relatively rare storms that are the most damaging and apparently the least amenable to modification (Abshaev et al., 1980). If one could increase the dominance (2.g., by dynamic seeding; Woodley, 1970) of every other cell along the hybrid storm's gust front, then the 9/D ratio would increase and the hailfall might be mitigated. While this is highly speculative, we believe that these storms are of sufficient importance to warrant further investigation.

5. REFERENCES

1. Browning K A 1977, The structure and motion of hailstorms, Meteor. Monogr. 38, 1-39.

2. WMO 1981, The dynamics of hailstorms and related uncertainties of hail suppression, World Meteorological Organization Hail-Suppression Research Report No. 3, Geneva, 25 pp.

3. Foote G B and Frank H W 1983, Case study of a hailstorm in Colorado. Part III: Airflow from triple-Doppler measurements, J. Atmos. Sci., 40, 686-707.

4. Nelson S P 1983, The influence of storm flow structure on hail growth, J. Atmos. Sci. 40, 1965-1983.

5. Brandes E A 1977, Gust front evolution and tornado genesis as viewed by Doppler radar, J. Appl. Meteor. 16, 333-338.

6. Lemon L R and Doswell C A 1979, Severe thunderstorm evolution and mesocyclone structure as related to tornadogenesis, Mon. Wea. Rev. 107(9), 1184-1197.

7. Abshaev M T et al 1980, On the possibility of hail suppression in supercell convective storms. 3rd WMO Conf. on Wea. Mod., Clermont-Ferrand, 649-653.

8. Woodley W L 1970, Precipitation from a pyrotechnique cumulus seeding experiment, J. Appl. Meteor. 9, 242-257.

CHARACTERISTICS OF-TEMPERATURE SPECTRA IN WARM MONSOON CLOUDS

A.Mary Selvam, P.C.S.Devara, S.S.Parasnis, S.K.Paul,
A.S.R.Murty and Bh.V.Ramana Murty
Indian Institute of Tropic.al Meteorology, Pune-411 005, India

1. INTRODUCTION

Observations of in-cloud temperature spectra are scanty (Refs. 1,'2). Extensive aircraft high resolution temperature observations and other micro-physical observations have been made in isolated warm cumulus clouds forming during the summer monsoon season (June-September) in the Pune (18° 37'N, 73° 51'E, 559 m ASL) region. The temperature observations obtained in horizontal flights at different levers in the lower atmosphere (10,000 ft ASL) are utilized for studying the differences in the spectral characteristics of temperature in cloud-air and cloud-free-air. The differences in temperature spectral characteristics are used to study the dynamical characteristics of warm monsoon clouds apd their interaction with the environments.

2. MEASUREMENTS

High resolution temperature observations in cloud-air and cloud-free-air were obtained from a DC-3 aircraft using vortex thermometer (Ref. 3) in the Pune region durinf the summer monsoon of 1976. Temperature values were extracted at 3 sec intervals (150 m resolution) from **the** continuous recordings and subjected to power spectral analysis (Ref. 4).

The temperature data were not corrected for compressive heating of the air due to aircraft speed (Ref. 5) since the speed,of the DC-3 aircraft is slow (about 55 m sec-1). The estimated maximum error due to compressive heating is about ±0.15°c (Ref. 6). Also, as the lower atmosphere in the regions of the observation is nearly saturated during the summer monsoon (relative humidity exceeds 80 per cent), the error from wetting the thermometer and subsequent evaporative cooling will be negligible.

3. COMPUTAT_IONS

The high resolution temperature spectra was fitted.with a quadratic equation to eliminate trend. The trend eliminated temperature perturbations 8' were then determined for the N aata points along the aircraft traverse length. The following statistical parameters were then computed.

Variance =

Standard deviation = $\sqrt{\text{variance}}$ = σ

Normalised skewness = $\overline{8^1} / \sigma^{3/2}$ = s

Normalised kurtosis = $\overline{8^1} \; \sigma^{2}$ = K

Standard error of S = $\sqrt{6/N}$

Standard error of K = $\sqrt{24/N}$

3.1 Test for normality

The temperature distribution follows normal distribution characteristics if the normalised skewness and kurtosis are less than twice their respective standard errors.

3.2 Significance of the statistical para.rr,eters for interpretation of the dynamics of air motions in cloud-free-air and cloud-air.

The variance is a measure of the intensity of turbulent transport of temperature while skewness is a measure of the nett warming/cooling.accompanying the turbulent transport and kurtosis gives a measure of the intermittency of the turbulent transport processes.

4. RESULTS

Temperature spectra in cloud-free-air and cloud-air are shown in Figures land 2 respectively. The mean, standard deviation, skewness an:d kurtosis of the temperature observations relating to cloud-free-air and cloud-air are given in Tables land 2 respectiv ly. The characteristics of the temperature distribution are also given in the Tables. The following results are arrived at from the spectra shown in Figures 1 and 2.

The slope of the temperature spectra at levels below cloud-base levels (<5500 ft asl) closely ollow the -5/3 power law.

The temperature s::,ectra above **cloud-base** leve-! have steeper slopes particularly towards the longer wavelength regions. The cloud-air spectral slopes are slightly steeper than the cloud-free-air spectral slopes. A maximum spectral slope of -3 was recorded in several cases.

The temperature spectra in the region of cloud-top heights exhibit a spectral slope close to -5/3.

An examination of the standard deviation, skewness and kurtosis of the temperature distribution in cloud-air and cloud-free-air !Tables 1 and 2) indicates the follqwing dynamical processes operating in the clouds.

The intensity of ttifb len9e is slightly larger in cloud-free-air as compared to cloud-air.

Turbulent transports result in cooling of cloud-air as compared to cloud-free-air.

The intermittency of turbulence is slightly more in cloud-air than in cloud-free-air.

Table 1

Results of 2omputat.iJns of **temperature** observations in cloud-free-air.

Sr. ;,a.	Date 1976	Time IST	Height (in ft.)	Mean oC	Standard deviation oC	Skewness	Kurtosis	Distribution
1	1 July	1452	3700	20.17	0.18	0.14	2.36	Normal.
2	1 July	1525	5200	17 .24	0.17	0.05	3.24	Normal
3	19 August	1528	5000	17.11	0.15	0.37	2.67	Normal
4	20 August	1455	4900	17.12	0.08	-0.08	2.02	Normal
5	1 July	1529	5200	17.67	0.24	0.31	2.87	Normal
6	23 July	1527	6000	15 .49	0.18	-0.39	3.43	Normal
7	16 Au ust	1457	6')00	12. 75	0.17	0.16	2.?7	Normal
8	16 August	1516	6100	13.54	0.19	-0.18	3.24	Normal
9	23 July	1520	6000	14.62	0.21	-0.18	1.62	Normal
10	1 July	1557	5400	16.00	0.21	2.68	13.94	Leptukurtic
11	20 September	1!531	8000	6.06	0.26	-0.26	2. 07	Normal
12	26 August	1618	10000	8.25	0.17	0.52	2.95	Normal
13	20 September	1536	8100	5.08	0.57	-0.04	1.63	Normal

Table 2

Results of computations of cloud microphysical and temperature observat ons in cloud-air

Sr. No.	Date 1976	Time (IST)	Height (in ft)	LWC gm m-•	Mean oC	Standard Deviat1on oC	Skewness	Kurtosis	Distributio:1
1	1 July	1555	5400	0.03	16.10	0.19	-0.21	1.97	Normal
2	2 July	1550	6000	0.08	16.33	0.10	-0.85	3.62	Normal
3	28 June	1516	6250	0.05	14.81	0.21	0.79	3.34	Normal
4	24 August	1515	64oc	-	13.15	0.19	0.04	2.56	Normal
5	28 At>gust	1510	6100	0.18	14.65	0.12	0.36	2.26	Normal
6	1 July	1547	5700	-	16.18	0.32	-0.12	2.60	Normal
7	16 August	1503	6100	0.32	12.63	0.10	-0.93	3.72	Normal
8	4 July	1549	5900	O.C)	15.47	o.41	-2.28	12 .45	Leptokurtic
9	26 August	1524	7000	0.89	12.60	0.22	-1.12	4.88	Leptokurtic
10	18 September	1506	7300	0.50	10.10	0.16	0.57	2.66	Normal
11	18 September	1514	7000	0.30	10.10	o.49	0.::,2	4.05	Normal
12	18 September	1554	7300	0.20	9.57	0.14	0.31	3.14	Normal
13	Hl September	1540	7200	0.50	9.82	0.27	O.Ol	2-37	Normal
14	20 Septem.Ge	1S29	8100	0.90	4.97	0.15	0.14	2.60	Normal

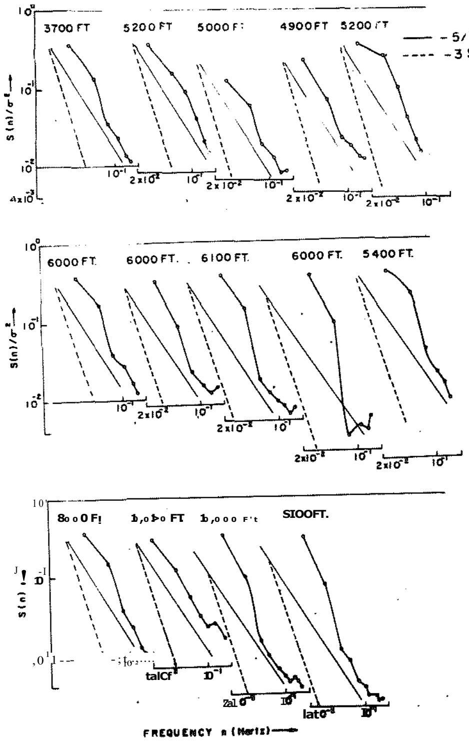

Figure 1 : Temperature spectra in cloud-free air.

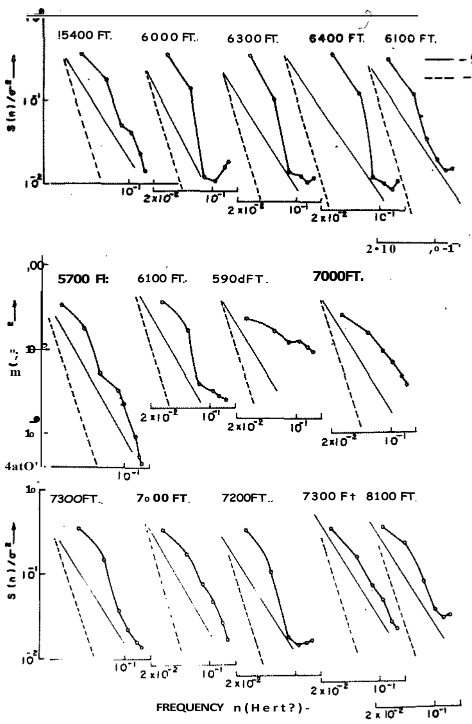

Figure 2 : Temperature spectra in cloud-air.

5. CONCLUSIONS

The observed spectral slops of -5/3(-1.67) in the sub-cloud and in the regions above the cloud-top level is equal to the predicted spectral slope of - 1.8 (Ref. 7) for a decadic scale range of eddies starting from the turbulence scale. The temperature perturbation θ' is directly related to the vertical velocity perturbation (W') in the sub-cloud and in the regions above the cloud-top level where the moisture content is less.

Inside the cloud layer, the temperature perturbation (θ') is governed by the moisture transport processes and is thus directly related to the moisture perturbation q' since $\theta' = Lq'/Cp$ where L is the latent heat of vaporisation and Cp is the specific heat of air at constant pressure. The slope of the temperature spectrum ($S\theta$) will be the same as the slope of the mixing ratio (q) spectrum (Sq) which is shown (Ref. 7) to have the following values

$$Sq = -2.5564 \text{ for } \frac{R}{r} = 10$$

$$Sq = -3. \text{ for large values of } \frac{R}{r}$$

where R and r are respectively the radii of the large and turbulent eddies.

The observed in-cloud temperature spectrum appears to follow more closely the -3 power law. It is thus inferred that cloud growth occurs mainly by microscale-fractional-condensation in turbulent eddies of dominant radius equal to a few meters.

The above conclusion is supported further by the observed profile of Q/Qa which agrees with cloud model predicted values for turbulent eddy radius size equal to 1 m (Ref. 8).

The multimodal cloud dropsize spectrum inside the clouds may be attributed to the transport downwards of large size cloud drops from higher levels to lower levels by the cloud-top gravity oscillations (Ref. 9). These oscillations originate from surface frictional turbulence and are mainly responsible for the cloud growth processes.

The temperature distribution both in cloud-air and cloud-free-air follows normal distribution characteristics (Tables 1 and 2) since the turbulent eddy mixing process in the planetary boundary layer which gives rise to the observed temperature distribution is basically random in nature.

6. REFERENCES

1. Almeida P C D 1979, The collisional problem of cloud droplets moving in a turbulent environment. Part II. Turbulent collision efficiencies. J. Atmos. Sci. 36, 1564-1576.

2. Parasnis S S et al 1982, Dynamic Responses of warm monsoon clouds to salt seeding, J. Weather Mod. 14, 35-39

3- Veruekar K G and Mohan B 1975, Temperature measurement from aircraft using vortex thermometer. Indian J. Meteor. Hydrol. Geophys. 26, 253-258.

4. Parasnis S S et al 1980, Temperature stratification of the atmospheric boundary layer over the Deccan Plateau, India, during the summer monsoon. Boundary Layer Meteorol. 19, 165-174.

5- Ruskin R E and Scott W D 1974, Weather modification instruments and their use. Weather and Climate Modification, W.N.Hess Ed., John Wiley and Sons, New York, 136-205.

6. Mary Selvam A. et al 1980, Some thermodynamical and microphysical aspects of monsoon clouds, Proc. Indian Academy Sci. 69, 215-230.

7- Mary Selvam A et al 1984, Role of frictional turbulence in the evolution of cloud systems, Proc. 9th International Cloud Physics Conference, Tallinn, USSR, 21-28 August,1984.

8. Mary Selvam A et al 1984, A new physical hypothesis for vertical mixing in clouds, Proc. 9th International Cloud Physics Conference, Tallinn, USSR, 21-28 August,1984.

9- Mary Selvam A et al 1982, Evidence for cloud top entrainment in the summer monsoon warm stratocumulus clouds. Preprint volume Conference on Cloud Physics, 15-18 November, 1982, Chicago, USA, 151-154.

WIND SHEAR EFFECTS ON WARM RAIN DEVELOPMENT

Tsutomu Takahashi

Cloud Physics Observatory
Department of Meteorology
University of Hawaii
Hilo, Hawaii 96720

ABSTRACT

Extensive aircraft observational data on warm clouds in Hawaii were analysed to study the rain formation process. Three parameters were studied: cloud top height, potentially available excess in-cloud water (P-value), and wind shear. Clouds were classified into single-cell clouds, band clouds and multi-cell clouds. It is necessary to exceed the critical P-value to produce rain. Rain formation is greater in band clouds than in single-cell clouds; this is probably due to the transport of drizzle from areas of maximum updraft.to the boundary between the updraft and downdraft. There, even small drizzle may grow by collection. The much higher rate of rain formation in multi-cell clouds m.::.ybe due to the growth of large cloud drops through cell-cell circulation in the upper part of clouds.

Shower duration is longer from band clouds than from isolated clouds in a Poiseuille-type wind flow. Rain showers are briefer when strong winds blow at lower levels. In a Couette-type.flow, the shower duration b comes briefer with. increasing wind shear. A three-dimensional microphysi al numerical model was first tested by comparison with observational data and then used to interpret the observations.

1. INTRODUCTION

Aircraft data (1976-1980) on warm clouds in Hawaii previously were analysed for rain initiation (Ref. 4). The modal size of cloud droplets must reach **30** µm in diameter during upward motion for drop broadening to occur. Near the cloud top, drizzle and raindrops form in close association with the motion of the cloud top cell. The formation of raindrops near the cloud top is necessary for precipitation to occur at the cloud base. The amount and duration of rain at the cloud base, however, differs greatly with the cloud type. Further analysis was done to elucidate the difference in rain formation arr0ng-different cloud systems.

2. AIRCRAFT DATA ANALYSIS

The aircra t carried a number of instruments: a cloud droplet sampler, drizzle sampler, raindrop sampler, rainwater collector, variometer, temperature (back-flow type) and humidity (Lyman-) probes. The aircraft fiew into the cloud at about 100 m above the cloud base and sampled cloud droplets. After this sampling, the plane ascended to the cloud top and flew across the developing cloud cell at about **200** m below the cloud top. Both drizzle and cloud droplets were measured. The plane made several successive flights across the same cloud cell until the cell dissipated. As the top cloud cell began to descend, the aircraft quickly descended to the cloud base and made successive traverses beneath the cloud base to measure the a,aount of rainwater and to record the raindrop size.

The maximum rain amount and rain shower duration beneath the cloud base were chosen to characterize the rain formation process in various clouds. Many parameters may be important in determining the rain formation process. These include the temperature, humidity, wind profile, cloud nuclei concentration and cloud size. The temperature lapse rate remains almost constant in Hawaii-and the number concentration of cloud droplets is 50 to 100 cm 3 (unless northerly winds blow) , suggesting a rather uniform cloud nuclei concentration around the island of Hawaii.

The amount of condensed water in the cloud probably is proportional to the difference between the saturation mixing ratio of water vapor at the cloud base and the corresponding ratio at various heights. At the same time, however, the water amount is inversely proportional to the difference between the saturation and the environmental mixing ratios of water vapor. The ratio calculated within the cloud region is newly called the P-value.

The cloud top height also is important in determining rain formation since cloud droplets must grow large enough to exhibit drop broadening during upward motion. Wind profiles appear to affect not only the maximum rain amount but also the duration of rainfall.

Cloud systems were classified with reference to the updraft profile near the cloud top and to cloud appearance as single-cell clouds, multi-cell clouds, and band clouds.

3. ANALYSIS RESULTS

3.1. Rain Amount

In order to detect rain at. the cloud base, it appears necessary for the cloud to attain certain P-values. Taller clouds require smaller P-values to produce rain. Rain formation.is more efficient in band clouds than in single-cell clouds (Fig. 1). Considerable rain is observed in multi-cell clouds. However, rain becomes weaker in single-cell under conditions of strong wind shear (shown in solid circle). When the wind direction changes radically in band clouds, the rain also became.weaker (shown in solid triangles).

A detailed analysis suggests the foll wing explanation for the variety of rain activity in

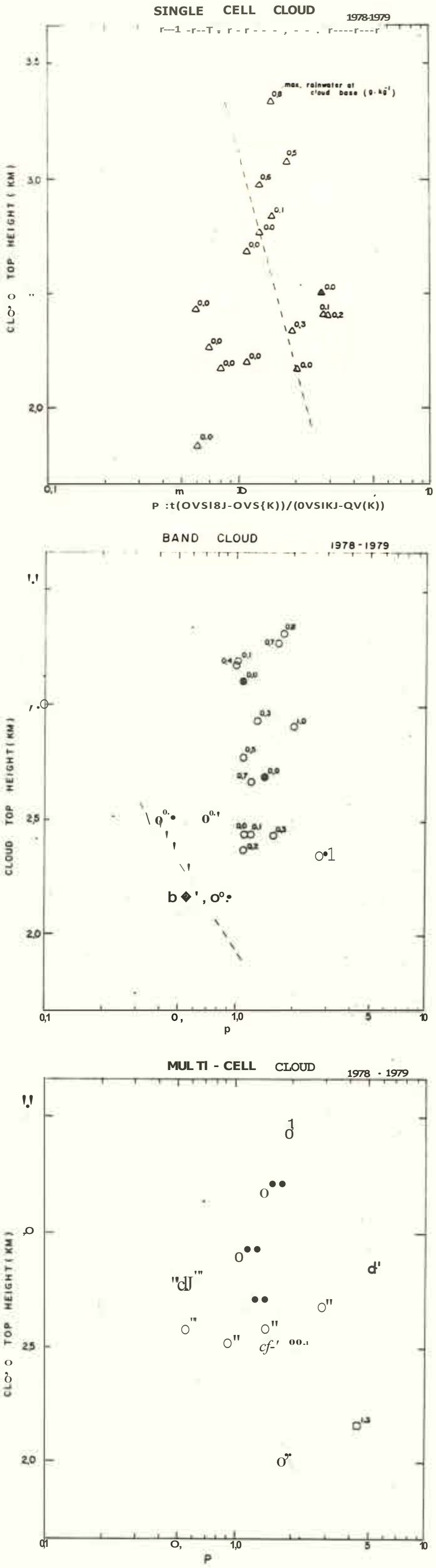

Figure 1. Maximum rainwater amount beneath the cloud base compared with cloud top height and P-value (see test for definition). Top: single-cell clouds, Middle: band clouds, Bottom: multi-cell clouds.

different cloud systems.

In band clouds, wind shear helps to transport upper level drizzle from the center of the upward motion to the boundary between the updraft and downdraft. Drizzle grow by collection. In single-cell clouds, drizzle are size sorted during upward motion. Relatively large drizzle fell within the updraft region but the growth rate was slow due to small cloud droplets with small P-values. Smaller drizzle, carried outward, evaporated. In multi-cell cloud droplets, grow during cell-to-cell circulation near the cloud top, thus accelerating rain formation.

3.2. Rain Duration

With a Poiseuille-type wind profile in the trade wind layer, rain lasts about 30 min in band clouds, and about 18 min in single-cell, isolated clouds (Fig. 2A). Reducing the location of the maximum wind speed seems to shorten the rain duration. Under weak wind shear conditions, rain lasts about 20 minutes, but strong wind shear in a Couette-type flow also shortens the rain duration (Fig. 2B).

In band clouds, drizzle is transported from the cloud center to the boundary between the updraft and downdraft so that the upper cloud cell has a longer life span. In Single-cell clouds, the accumulation of precipitation particles in the cloud center may shorten the cloud cell life; thus, rain formation may occur for only brief periods of time.

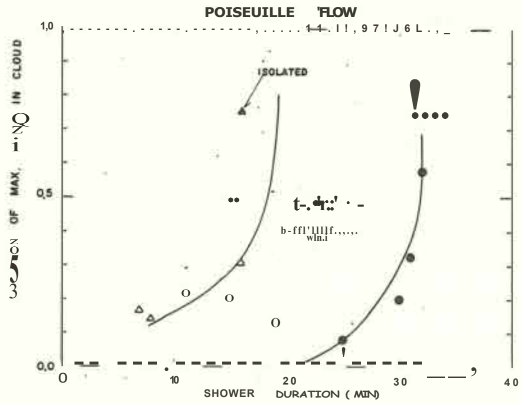

Figure 2A. Shower duration ($> 0.05\ gm^{-3}$) beneath the cloud base in band clouds (circles) and in isolated clouds (triangles) under Poiseuille-type wind flow. Open circles (triangles) show a strong wind flow at the cloud top while circles (triangles) with crosses indicate situations when the direction changed radically with height.

4. CLOUD MODEL

A three-dimensional microphysical numerical cloud model is used to help interpret the results of the analysis. Dynamic equations are shallow-anelastic; the diffusion coefficient is determined by solving the prognostic equation of the turbulence energy, as in Klemp and Wilhelmson (Ref. 1). Drop condensation and collection processes are calculated by the methods of Kovetz-Olund (Ref. 2) and Soong (Ref. 3). Drops are classified into 30 groups. Supersaturation is calculated at a forward time step but modified to include warming of the air by condensation. The grid size is 200 m in each direction. An initial disturbance is given to the potential temperature over 1.2 km x 1.2 km in th!: x-y plane at the lower level (Ref. 5).

The March 19, 1979 case was used to test the model. On that day, the wind shear was weak and the cloud was single-cell and isolated. As initial conditions for the model, the temperature and humidity profiles and the cloud droplet size distribution at the 100 m level above cloud base were specified. The cloud nuclei concentration was assumed to be so·cm-3, based upon observed cloud droplet concentrations. Predicted values were cloud size, maximum up4raft, maximum cloud water content near the cloud top, maximum rainwater at cloud base and the peak raindrop size at the cloud base (Fig. 3). Since the model agreed with observations reasonably well, model calculations were extended to study rain formation processes in various clouds within a wind shear enviTonment.

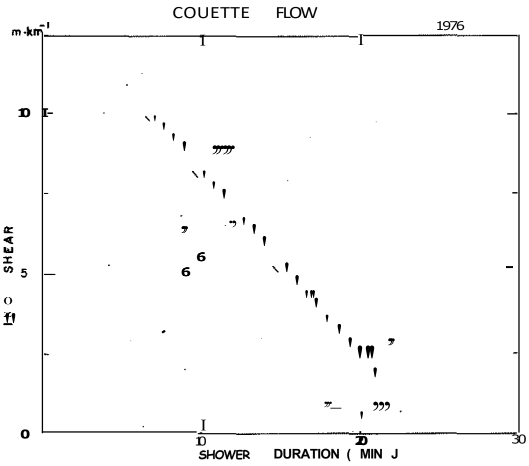

Figure 2B. Shower duration beneath the cloud base with Couette-type wind flow.

	CLOUD SIZE	[illegible]	[illegible]	MAX. RAINWATER AT CLOUD BASE	[illegible] (D)
[illegible] [illegible] 19, [illegible]	CLOUD TOP HEIGHT H_T = 2.2 km CLOUD DIAMETER C_D = 2 km CLOUD BASE HEIGHT H_B = 0.6 km	[illegible]	1.25 g kg^{-1}	0.46gkg-1	1.1 mm
PREDICTED	H_T = 2.3 km at 15 min C_D = 2 km H_B = 0.5 km	[illegible]	[illegible]	0.47gkg-1	1.3 mm

Figure 3. Comparison of model predictions with observations.

In the single-cell model cloud without wind shear, the maximum cloud droplet water content (1.0 g kg-1).was calculated at H=1.7 km and T=12 min. Drizzle (2.03 g kg-1) was formed at higher levils (H=2.1 km) at T=18 min and ater raindrops (0:57 g kg-1) developed at low levels (H=1.5 km) at T=:z6 min (Fig. 4A, 5A, 6A).

When a relatively strong·wind blew at lower levels in a Poiseuille flow, wind inhibited the transport of low level moist air in the cloud. The cloud droplet growth rate was slow so. that drizzle and raindrop formation was performed poorly (Fig. 4B, 5!, 6B). Maximum.cloud droplet water content was 0. 80 g kg-1. at H=1. 7 km at T=14 min. Drizzle (0.85 g kg-1) was formed at .H=2.1 km and T=22 min.

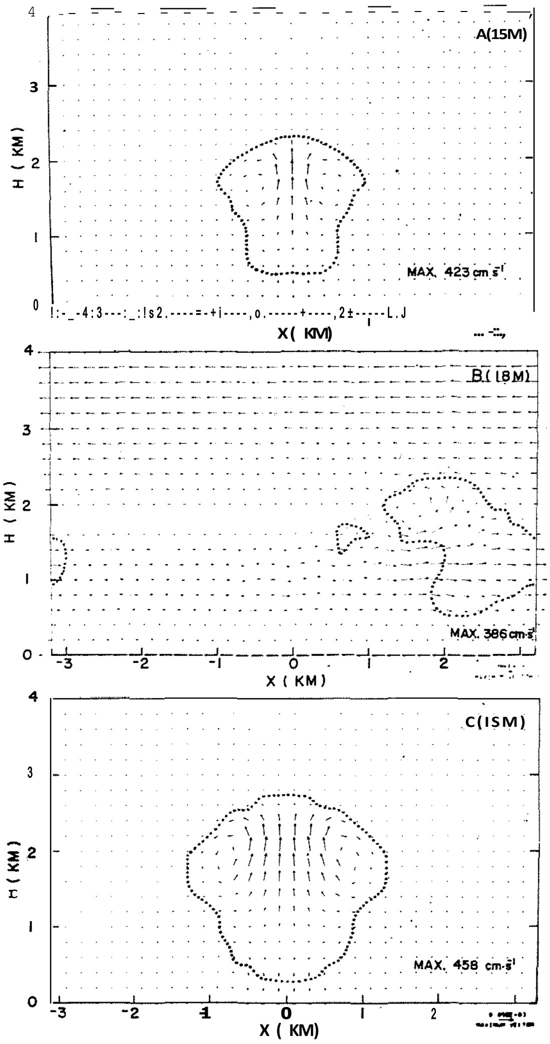

Figure 4. Airflow in the x-z cross section across cloud center as calculated in single cell, A (top), in single cell with low level Poiseuille flow, B (middle) and in double cells, C(bottom). Cloud boundary(> 0.001 g kg-1) was shown by dotted line.

Raindrops (0.068 g kg-1) developed at H=1.5 la, and T=32 min. The raindrop size range did not show a peak size and rainfall intensity at the surface was also weak.

Multi-cell c,louds were simulated to give double dist·urbances initially. The maximum cloud droplet water content (1.0 g kg-1) was calculated at H=1.7km and T=12 min, A large drizzle content (2.48 g kg-1) was calculated at H=1.9 km and T=16 min and raindrops (3.19 g kg-1) developed at H=1.5 km and T=22 min (Fig. 4C, 5C, 6C). The very effective raindrop formation process in the double dlilturbance cells was due to the supply of large drops through circulation from the upper part of the ·cloud into the main updraft region. When the cloud was small and single-celled, large cloud drops evaporated during circulation so that drop circulation.did not' aid in drizzle formation. Rainfall was intense from double disturbance cells (Fig. 7). ·Model results appear to support the interpretation derived from the analysis of aircraft observations.

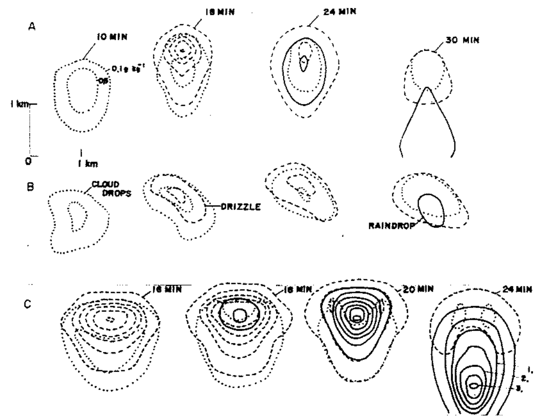

Figure 5. Mixing ratio of cloud droplets (dotted lines), drizzle (dashed lines) and raindrops (solid lines) in the x-z cross section across cloud center at various times.

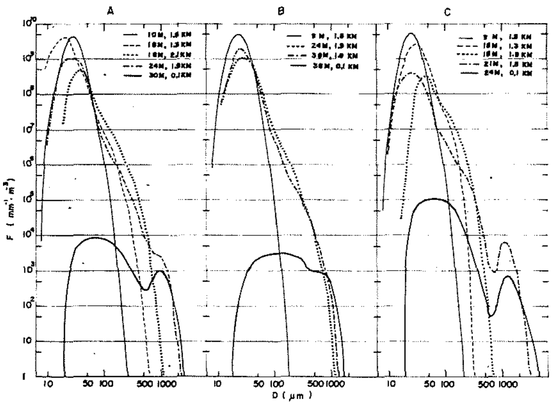

Figure 6. Drop number concentration (llllil-lm-2) calculated various heights in the cloud center.

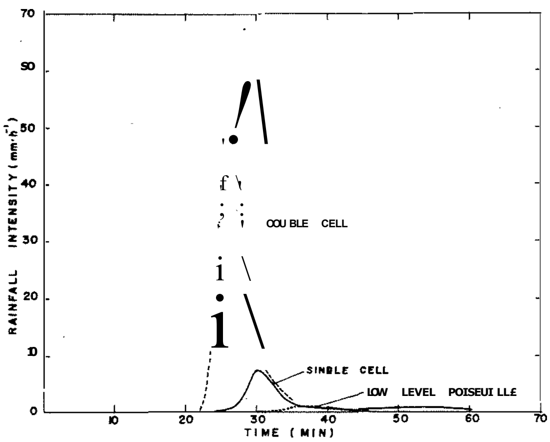

Figure 7. Rainfall intensity resulting from a single-cell disturbance, single-cell disturbance with low-level Poiseuille-type wind flow, and a double-disturbance cloud.

5. REFERENCES

1. Klemp J B and Wilhelmsen R B 1978, The simulation of three-dimensional convective storm dynamics, J *Atmos Sci* 35, 1070-1096.

2. Kovetz A and Olund B 1969, The effect of coalescence and condensation on rain formation in a cloud of finite vertical extent, J *Atmos Sci* 26, 1060-1065.

3. Soong S T 1974, Numerical simulation of warm rain development in an axi-symmetric cloud model, J *Atmos Sci* 31, 1262-1285.

4. Takahashi T 1981a, Warm rain study in Hawaii - rain initiation, J *Atmos Sci* 38, 347-369.

5. Takahashi T 1981b, Warm rain development in a three-dimensional cloud model, J *Atmos Sci* 38, 1991-2013.

SOME NEW PHENOMENA ON THE STUDIES OF SEVERE STORMS

Ang Sheng Wang and Nai Zhang Xu

Institute of Atmospheric Physics, Academia Sinica
Beijing, The People's Republic of China

ABSTRACT

Some new phenomena of severe storms in northern China are presented in this paper. They had been found during recent 4 years. We will introduce some new phenomena as following: some severe hailstorms which had an overhang echo, weak echo region and echo wall fall small hailstones on the ground; a new kind of hailcloud - dot-source hailcloud; severe windstorms and their characteristics; and one kind of rainstorm - accumulational rainstorm.

Keywords: Severe storm, Thunderstorm; Hailstorm, Windstorm, Rainstorm, Radar echo.

1. INTRODUCTION

Severe storms are a very important meteorological phenomenon. They include thunderstorm, hailstorm, windstorm, rainstorm, snowstorm and tornado etc. damaging phenomena. During recent about 20 years, many scientists studied a lot of severe storms in our country, specially thunderstorm (or lightning - storm), hailstorm, windstorm and rainstorm etc. (Shi Yan Tao et. al, 1980, Ref. 1; Mei Yuan Huang and Ang Sheng Wang, 1980, Ref. 2; Institute of Atmospheric Physics, 1976, Ref. 3, etc.). Before four years, we already studied physical processes of hailcloud (Ang Sheng Wang, Nai Zhang Xu and Mei yuan Huang, 1980, Ref. 4), lightning research (Ang sheng Wang, Mei Yuan Huang et. al, 1976, Ref. 5), vertical airflow (Ang Sheng Wang et. al, 1972, Ref. 6, and Ang Sheng Wang, Jia Mo Fu, Wen Quan Shi et. al, 1983, Ref. 7), hailcloud category (Ang Sheng Wang et. al, Ref. 8), "wind-sall" mechanism (Ang Sheng Wang, Yan Chao Hong et.al, 1983, Ref. 9), and the merger of cells (Ang Sheng Wang, Xiao Ning Zhao, Nai Zhang Xu, 1983, Ref, 10) etc. problems. Now, we will introduce some new phenomena as follows.

2. SOME SUPERCELL HAILCLOUD FALL SMALL HAILSTONES

During recent about 20 years, many scientists found that the supercell hailcloud fall heavy hailstones and cause severe damages (Mei Yuan Huang and Ang Sheng Wang, 1980, Ref. 2). But it is an interesting thing to find a supercell hailcloud falls small hailstones. One case of above phenomenon had been found in our country on June 20, 1980 (Ang Sheng Wang and Nai Zhang Xu, 1983, Ref. 11). As you see, Fleming hailstorm was a very famous hailstorm in U. S. A, (K. A. Browning and G. B. Foote, 1975, Ref. 12), it passed through about 450 km, its lifecycle

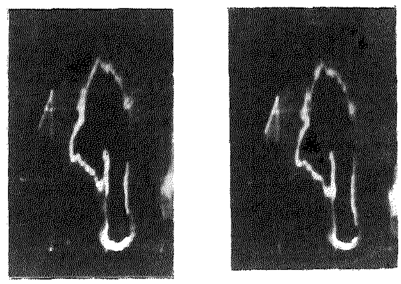

Fig. 1 Typical RHI data of Beijing hailstorm on June 20, 1980.
Azimuth angle: Left-323°, Right-324°,

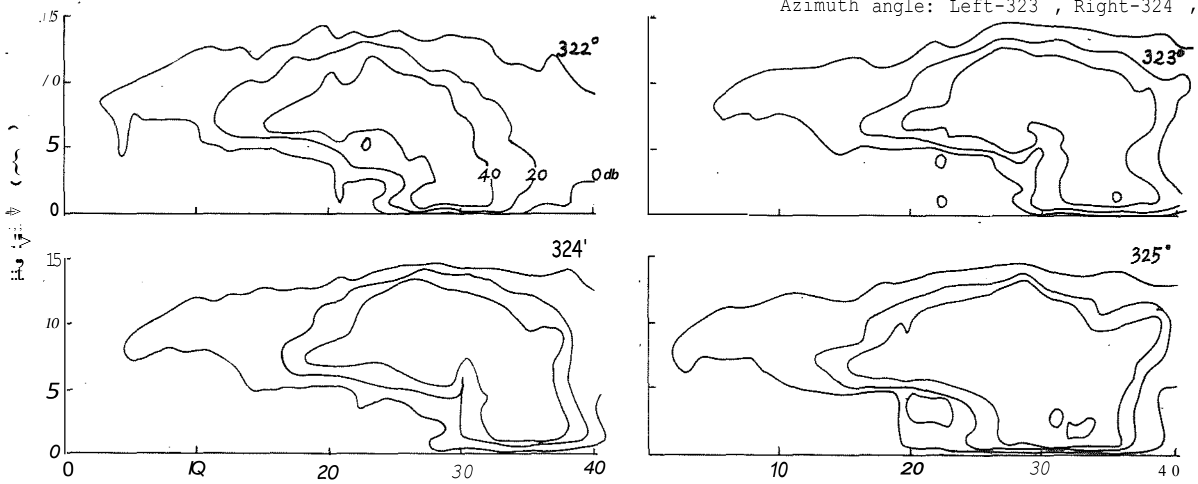

Distance (Km.)

Fig. 2 Radar echo structure of supercell hailstorm at about 16:00, on June 20, 1980. Their azimuth angles are: 322°, 323°, 324° and 325° respectively, was about 9 hours, it fell hailstones during about 6 hours, the biggest hailstone was abouc golf ball. The typical echo structure of Fleming hailstonn had been given in :Browning's :paper (Ref. 12)•

In Beijing on June 20, 1980, we probed a supercell hailstonn which was like Fleming stonn very much on radar echo structure, Two typucal RHI photoes of the Beijing storm has been shown in Fig. 1. They were shot at 16:00, and their azimuth angles are 323° (Fig, 1, left) and 324° (Fig. 1, right) respectively, Four vertical profiles of the stonn radar echo has been drawn in Fig. 2. In Fig. 2, the horizontal scale is equal one of vertical, so we see their characteristics of echo structure easy. They wer shot at about same time (2 to 6 min.). Their azimuth angles are 322°, 323°, 324° and 325° respectively as same as Fig. 2.

From Fig. 1 and Fig. 2 and another detail data, we pointed out that although :Beijing supercell hailsto:cm had a typical overhang echo, weak echo region and echo wall etc. radar structure of supercell storm,and it was like Fleming storm on the size, form, height etc; then they were different each other on hailfall and damage. :Beijing supercell ·hailstorm fell smali hailstones on the ground only, the biggest hailstone was about· 1-2 cm, and no damage happened on the ground.

According to this phenomenon, we checked about 30 supercell hailstorms which happened in China, England, U.S.A., U. s.s.R., and Canada etc. countries (Ang Sheng Wang and Nai Zhang Xu, Ref. 13)• Preliminary studies show that there are 27 supercell storms, including 19 hailstorms which have the boundary of weak echoregion (EWER), and 8 hailstorms which haven't the boundary of WER (NBWER)• In 27 ;upercell hailstorms, 11 stonns caused heavy damages and 16 storms caused light damages only, That means some supercell hailclouds which have an overhang echo, weak echo region and echo wall only fell small hailstones and didn't cause heavy damages. In studies of BWER supercell hailstonn, we found that·when the vault of storm was bigger and the top of vault was higher, the damage was heavy. In our sta.tistcs, the volume of mean vault is about 84 km³ for heavy damage storm of BWER, and their mean top height of storm vault is about 7 km; but the data of light damage storm of BWER are 12 km³ or 5 km respectively. So they are different each other. Above phenomena are relative closely with the updraft.

As above mentioned, our data show that some supercell hailstorms fall small hailstones which cause weak damage on the ground. That is a new phenomenon. We will study it deeply in near future.

3, DOT-SOURCE HAILCLOUD

A new type hailcloud -- dot-source_hailcloud has been found i. our coun.ry (Ang Sheng Wang and Wen Quan Shi et. al, 1983, Ref. 14). Although we already studied four classifications of hailclouds (Ang Sheng Wang et. al, 1980, Ref. 4), the characteristics of dot e hailcloud a.re different from fonner. Dot-source hailcloud consists of two or more than two cells. Their cells emerge in same source and one of cells fall hailstone, so we call it dot-source hailcloud.

One case of dot-source hailcloud has been given in Fig. 3. That was a hailcloud on August 23, 1977 in west of Xinjiang. In Fig. 3A (top), we can see there are five cells in radar PPI; cell 1 already decays, cell 5 emerges just, and all cells move a.long f-f' line. The profile of two dimensions radar echo along f-f' has been given in Fig. 3B (bottom). There a.re four cells in the profile; cell 1 already decays; cell 2 is very strong and fall hailstones, its center of radar echo is about 50 dbz. Then cell 5 emerges just, another cells develop. According to our data, every cell of this storm emerges at same source near the point of cell 5 in Fig. 3A, then they move along same direction (close f-f'). At same time, new cell 5 emerges, cell 4 or 3 develops, cell 2 falls hailstones, and cell 1 decays; that means they have different stages of lifecycle.

We studied several dot-source hailstorms, and got the model of this lcind of hailcloud as showing in Fig. 4. From Fig.4A, we can see clearly that all cells (A, B, c. D.) emerge in same source. When cell B emerges, cellA develops; when cell C emerges, precipitation happens in cell A, and cell B develops and so on. At same time, we can see different cell stays different stageofits lifecycle. And they change their stages gradually (Ang Shen&: Wan£, W"n

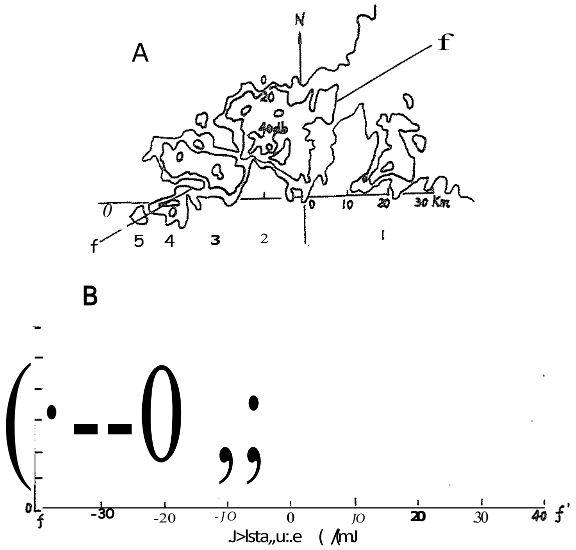

Fig. 3 The dot-source hailcloud on August 23.
A. PPI(8°) radar echo at 18:20.
B. Radar echo profile along f-f'.

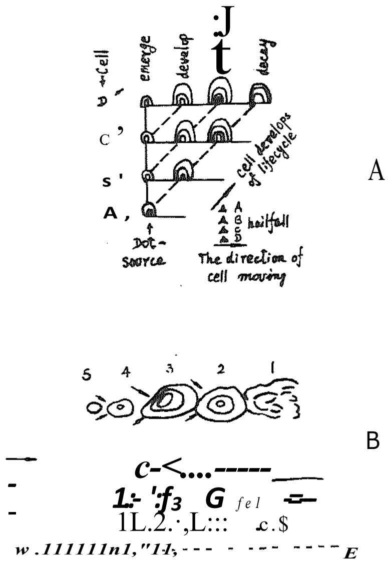

Fig, 4 The model·or dot-source hailcloud.
A. The model of cell change.
B, Rorizontal(top) and vertical(bottom) profile of model,

Quan Shi et.al, 1983, Ref. 14). This is special feature which is different from another kinds of hailcloud. The horizontal and vertical profiles of dot-source hailcloud model have been -shown in iig• 4B. According to our cases, most dot-source hail-clouds emerge over the foot of a mountain,

4. SEVERE WINDSTORM

The gust wind of thunderstorm can cause heavy wind damage at some· time. According to our data, although the gust wind of thunderstorm generally is stronger, but it has a heavy wind damage only in a few case. So we specially call the thunderstorm after severe windstorm. Now, we hope to lcnow its feature,

A heavy wind damdge happened in Beijing on June 20, 1980. In the day, when-windstorm passthrough southern part of Beijing, the strongest gust wind was stronger than 22.7 m/s (the mem wind during 10 min.in Xiang He county). When the storm passes, some buildings were broken, a lot of trees were blown down out. From 1973 to 1980, we studied about one hundred thunderstorms; there are three kinds of storm in our cases. One is rapid moving storm, the mean velocity is about 30 km/hour; one is slow moving storm, the mean velocity is about slower than 10 km/h; and another is meddle velocity (about 10 - 30 km/h)• Then there are only two storms whi-ch moved very rapidly, their moving velocity of radar echo were about 60 km/h. They were the storm on August 11, 1977 in Xiyang, and the storm on.June 20, 1980 in Beijing. And only in these two days, when thunderstorms passed through the county, the strongest gust wind happeRed (20-25 m/s) and caused heavy wind damages. So we think that the rapid moving storm is a cause of Wind damage (Ang Sheng Wang, Yan Chao Hong et. al, 1983, Ref. 9).

When the storm pass through Tong county, we got the data as Fig, 5, i.e. Wind (the mean Wind during 10 min,} velocity (V), Precipitation (Pre.) (shadom region), Temperature. (T) and Humidity (R) plotted as a function of time, It is clear, when thunderstorm come to Tong county, 'I, R, V **and** Pre. changed rapidly. As same a.s this ee, in several ca.sea we found that the strongest gust Wind is relative with falling rain. ·That means rapid falling rain or hail is another cause of gust wind probably.

5, AN ACCUMIJLATIONAL RAINSTORM

From 3 to 4 July 1981, a rainstorm passed through Beijing. The maxillIUII value of precipitation was 178 mm/day, **and** the region in where precipita ion value was more than 100 mm/day was about 160 km.

We are interested that how did the heavy rain form ? As you see, there are several causes which. can fo:cm it. let us to analyse the case.·

In that day, there were several precipitation processes passed through Beijing, In the southern part of Beijing, when every precipitation **radar** echo passed, rain fell in some stations always. As Fig. 6 showing, an accumulational heavy rain llll.Bbeen fomed by four precipitations. That means the accumulation of rain is an important use of heavy rain.

Acco::i:ding to our radar date., we found that the cloud system was s. wide strs.tifom cloud: system, and there were some stronger convective cells in the Wide stra.tiform cloud system. And we found the tops ofrain value in Fig. 6 just respond stronger convective cells. So we believe the precipits. ion mechanism. of convective cloud and the supporting me-

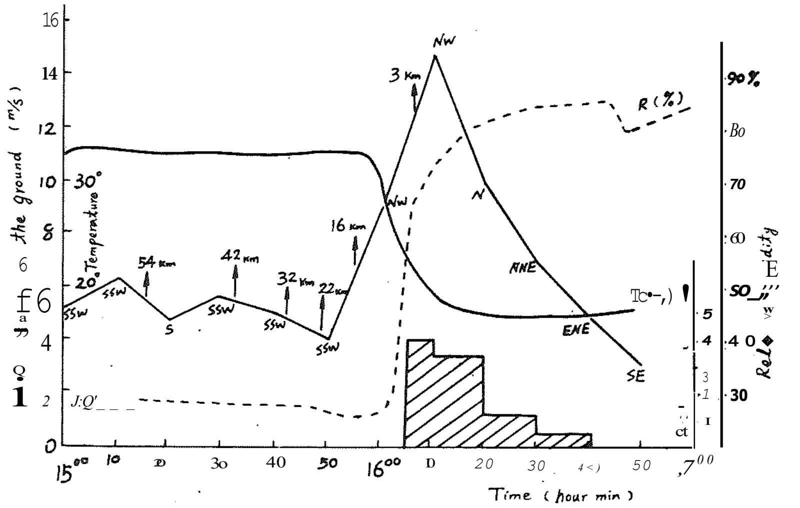

Fig. 5 V, T, Rand Pre. plotted ass. function of time on June 20, 1980 in Tong county,

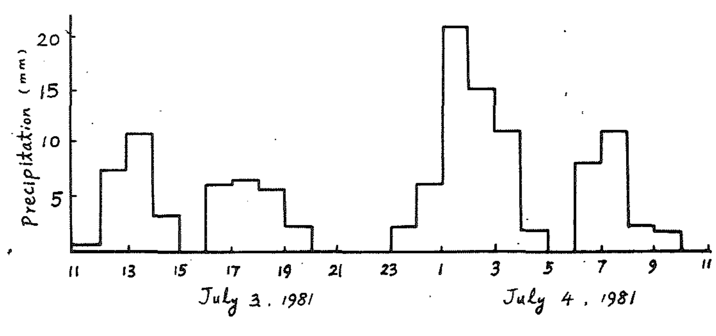

Fig. 6 An accu.mulational heavy rain was been.formed by four precipitations in Beijing, from 3 to 4 July 1981.

cba.nism of stra.tiform cloud are another important ca.use of heavy rain.

As mentioned above, we already gave some new phenomena of severe storms, but we only presented them. Then we will do more work to study deeply them. We hope to get more useful results in near future.

6. REFERENCES

1. Tao Shi Yan et. al, 1980: Chinese Heavy Rain. Science Press. Beijing. 225.

2. Huang Mei Yuan and Wang Ang Sheng, 1980: The Introduction of Hail Suppression. Science Press. Beijing. 204.

3. Institute of Atmospheric Physics, 1976: The sounding of thunderstorm and. the studies of thunder - lightning physics. Science Press. Beijing. 84.

4. Wang Ang Sheng, Xu Nai Zhang and. Huang Mei Yuan, 1980: On the characteristics of the physical processes of ha.ilcloud. 8th International Con!. on Cloud **Physics**. Clermont-Ferrand, France. July 15-19, 1980. 519-522.

5. ______ anii Huang Mei Yuan et. al, 1976: Lightning observation of the ideiitTIT"ca.tion of hailcloud and. thundercloud in hail suppression, **Science** Bulletin. 1976, No. 12, 546-549.

6. ______ st. al, 1972: On the characteristics of uplUll,f't !n thundercloud. Papers Presented st tlie **National** Conf. on Rain Enhancement a.nd Hail **Suppression**. No. 2, 169-179, Changsha of China.

7. Wang Ang Sheng, Fu Jia Mo, Shi Wen Quan et. al 1983: Clo d a.nd vertical airflow sounding by use of two radars. 21 st Conf. on Radar Meteorology. AMS. Sept. 19-23, 1983. Edmonton, Alta, Canada.

a. ______ et. al, 1982: Some research on the developent "oTlia:i.lcloud. Annual Report, Institute of Atmosphsric Physics, Academia Sinica.. Vol. 1• Science Press, Beijimg; Gordon and Breach Science Publishers, Inc. New ork. 110-114,

9. ______, Hong Yan Chao et. al, 1983: Primary !UISlysis on severe" windstorm"• The studies of hail and hail suppression, Science Press. Beijing, 111-120.

10. , Zhao Xiao Ning and Xu Nai Zhang, 1983: Tiie"iiierger of cells promotes the formations of hailcloud. 13th Conf. on Severe Local Storms. AMS. Tulsa, Okla. Oct. 17-20, 1983,

11. ______ and Xu Nai Zhang, 1983: Beijing hailstorm probing by using 5 cm radar. 21st Con!. on Radar Meteorology. AMS, Sept; 19-23, 1983, Edmonton, Alta, Ganada.

12. Browning, K. A, and Foote, G, B., 1975: Airflow and hail growth in supercell storm and come implications for hail suppression. NHRE Tech, Report. No. 75/1, 75.

13. Wang Ang Sheng and Xu Nai Zhang: The studies of supercell hailstorms. (Submitted for publication)•

14. and Shi 'wen Quari et. al, 1983: The research on dot-source hailcloud, Scientia Atmospherica Sinica. 7, 319-327.

STORfl KHIEMATICS FROM REFLECTIVITY MEASUREMENTS

-I. Zawadzki
Universite du Quebec 11 tlontreal, Canada H3C 3P8.

1. INTRODUCTION

Conservation equations for water substance in storms (rain and cloud) had been used (Ref. 1) to study the distribution in time and space of water assuming a parabolic vertical velocity profile. For the same purpose those equations are also used in some moist convection mode-ls. In this case, the two additional equations of the model introduce two new variables: rain and cloud water con tents. The other variables in the conservation equations are the three components of the wind derived from the model. In fact one can, in principle, invert the use of these equations and diagnose the wind field if one velocity component and the mass density of precipitation are measured (as with a single Doppler radar) and the continuity equa tion for air is added to the system. This possibility is being presently explored.

In this paper the conservation equations for precipitation, cloud and air are considered with some symplifying assumptions to deduce a number of kinematic properties of convection using some general characteristics of radar measurements of precipitation within clouds. An application of these ideas to actual adar measurements leads to results consistent with other ob ervations.

2. BASIC EQUATIONS

Following Kessler (Ref 1), continuity equations describing distribution of rain and cloud water within a precipitating system are written as:

$$\frac{\partial M}{\partial t} + \vec{v}_H \cdot \vec{\nabla}_H M + w\{\frac{\partial M}{\partial z} + kM\} - \frac{\partial}{\partial z}(MV) = S \qquad (1)$$

$$\frac{\partial n}{\partial t} + \vec{v}_H \cdot \vec{\nabla}_H n + w\{\frac{\partial n}{\partial z} + kn\} = wG - S \qquad (2)$$

In the above, M is defined as the precipitation content of a unit volume of air and is always positive or zero. The quantity n is interpreted as the cloud content when positive and when negative, as the 3mount of moist re requiered to satu:ate the air. The symbols vH and w refer t? horizontal and vertical velocities of air respectively, $k=-\partial(\ln\rho)/\partial z=10^{-4}m^{-1}$ is the air compressibility and V is the velocity of M relative to the moving air. The function $G=-\rho(\partial r_s/\partial z)$, where rs is the saturation mixing ratio, gives the amount ?f co - densed water for a reversible saturated adiaba ic expansion and can be evaluated from an upper air sounding. All the microphysical processes characteristics of transfer between different water substances within the system, are symbolized by the letters. The term wG in (2) represents the rate at which cloud appears (disappears) in saturated updrafts (downdrafts).

We assume that air motions obey the following continuity equation:

$$\vec{\nabla}_H \cdot \vec{v}_H + \frac{\partial w}{\partial z} = kw \qquad (3)$$

To make explicit here that M(x, y, z, t) is considered as a known function (given by radar measurements), let us define the following parameters.

$$p = \frac{\partial \ln M}{\partial t} ; \quad q = \frac{\partial \ln M}{\partial z} ; \quad \vec{g} = \vec{\nabla}_H \ln M \qquad (4)$$

For typical warm moist convection $G\sim10^{-3}-10^{-4}$ and t ,o-2 ,o 1gm-3. Vertical profiles of radar reflectivity, (Ref 2) show that vertical gradient ot ln(M) could be as high as $5 \times 10^{-4}m^{-1}$. The high y transcient nature of convective storms make possible $|p| \sim 10^{-2}s^{-1}$.

On the other hand, the effective fallsp d of the median diameter particle for an exponential drop-size distribution, is given in Ref. 1 as:

$$V(M,z) = cM^a \exp\{kz/2\} \qquad (5)$$

where $c = 5.2ms^{-1}$ and $a = 0.125$ if the fall speed V(D) of drops of diameter D is proportional to $D^{1/2}$. With (4) and (5), continuity equation (1) becomes.

$$\frac{p}{V} + \frac{\vec{v}_H \cdot \vec{g}}{V} + \frac{w}{V}(q+k) - (\alpha+1)q - \frac{k}{2} = \frac{S}{MV} \qquad (6)$$

All the microphysical processes were co tained so far in the terms S. A number of descriptions of these processes were given, Ref. 3 for example. For our purpose it is sufficient to retain the more simple parametrization given in Ref. 1. Thus we separate S in terms of cloud auto-conversion, AC, cloud collection by rain, CC, and evaporation of rain E. We have:

$$S = AC + CC - E$$

Where AC, CC and E can be approximated by (Ref. 1):

$$\{AC = k_1(n-a); \ CC = k_2 Mn; \ E = k_3 n M^{0.65}$$

$$\text{with } k_1 = 10^{-3}s^{-1}; \ k_2 = 5.2\exp\{\tfrac{kz}{2}\}; \ k_3 = 5.4\times10^{-4}$$

$$a = 0.5gm^{-3}\} \qquad (7)$$

The system of equations (2), (3) and (6), with an explicit expression for S represents three iquations with four unknown: the two component of v , w and n. A number of simplyfing assumptions, some of which permit the closure of these equations will now be considered:

2.1. Cloud-free model

Solutions of (1) and (2) as given in Ref. 1 demonstrate that in well developed precipitation areas, n is generally much smaller than M. This is not surprising given the high efficiency of scavenging of cloud droplets by precipitation. Thus, if we add together (1) and (2) and neglect n with respect to M we get:

$$\frac{p}{V} + \frac{\vec{V}_H \cdot \vec{g}}{V} + \frac{w}{V}(q+k) - (a+1)q - \frac{k}{2} = \frac{wG}{VM} \qquad (8)$$

where (4) has been used. Comparing (6) and (8) one must conclude: $S = wG$ (9)

This indicates that equilibrium conditions could be approximated by a balance between the rate of condensation and generation of precipitation. An obvious implication of (9) is that in updrafts, all newly condensed water (above a certain equilibrium value wich may change with time) is instantly transformed into precipitation, while in downdrafts water substance evaporates at the rate wG. It is clear, that in this case (8) is independant of the cloud water density, and when considered simultaneously with the continuity equation for the **air**, provides a system of 2 equations with the three carthesian component of the wind as unknowns.

It can be shown that in weak and slowly varying storms ($wv^{-1} \sim 0.1$; $p \sim 0$) the equilibrium condition $S = wG$ holds as well, athough in this case M and n are of the same order of magnitude.

2.2. Non-advective and symmetrical models

In weak and wide spread precipitation, horizontal gradients as well as horizontal advection terms in continuity for water substances could be neglected as a first approximation. Thus, these equations constitute now a closed system for the two unknowns w and n and can be solved providing suitable initial and boundary conditions are specified. However, this is not normally the case and these equations are of interest only in combination with other assumptions or additional measurements.

In those special cases where the precipitation field exhibits a synmetry about a vertical axis, or is slab-symmetrical it is easily seen that our basic system is closed for the horizontally symmetric component of the wind field, w and n. Even if this formulation could be applicable to some specific atmospheric situations (e.g. axisymmetrical cells or rainbands structure) no furthur attention will be given to it here.

3. SIMPLE CASES

We will consider several situations at the center of the core of a precipitating cell where $g = 0$.

3.1. Under cloud base

In a steady state case and in absence of evaporation the vertical gradient of M should reflect exactly the effect of air compressibility. That is, $q = -10^{-4}$, which represents a decrease of reflectivity with height of 0.76 dBZ/km (for M-P drop-size distribution). However, in moderate to heavy rain it is quite frequent to observe no vertical gradient or a small increase of reflectivity with height under cloud base; this is indicative of evaporation. Thus, in general under cloud base $S = -E$ and

$$\frac{w}{V} = \frac{(a+1)q + \frac{k}{2} - \left(\frac{p}{V} + \frac{E}{VM}\right)}{q+k} \qquad (10)$$

At a temperature of ~ 10 °C, pressure of 850 mb and a relative humidity of 90% the saturation deficit n ~ 1 g m^{-3}. Thus $E(Mv)^{-1} > 5\times10^{-5}$ for $M < 5$ g m^{-3} (equivalent rain rate of 110 mm h^{-1}). Therefore (10) indicates that, for a steady state precipitation and for $q \sim 0$, downdraft is prevailing in most situations. A temporal increase of M is indicative of an even stronger downdraft. Fig. 1 represents (10) with q as a parameter.

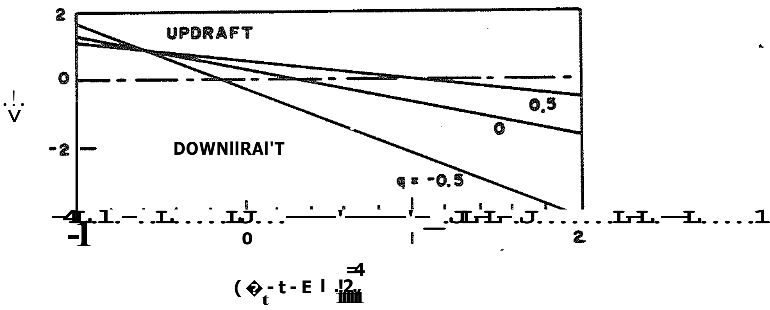

Fig. 1. Vertical velocity at the center of the precipitation under cloud base. The vertical gradient is shown as a parameter (in $(10^4 m)^{-1}$).

3.2 Equilibrium between condensation and precipitation production

When g = 0 equation (8) yields the following expression for w:

$$\frac{w}{V} = \frac{(a+1)q + k/2 - p/V}{q + k - G/M} \qquad (11)$$

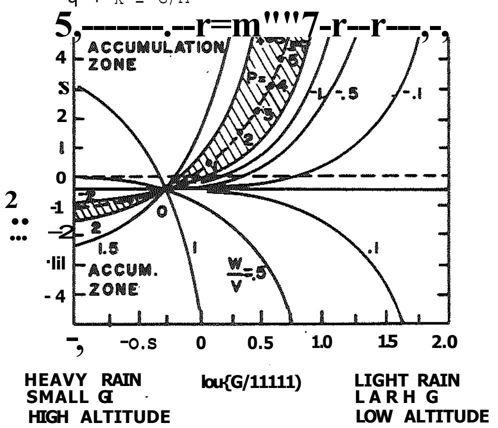

Fig. 2.1.- Isolines of wV^{-1} as function of GM^{-1} and q, for a steady state situation and assuming S = wG. The dashed line represents the singularity line of (11). The dots on this line show the position of the singularity point for different time variations of lnM in units of 10^{-4}.

Equation (11) is represented in Fig. 2.1 for a = 0.125 and p = 0 (steady state). It is clear that our assumptions cannot be valid everywhere: for example, w tends to infinity on the singularity line q = G/M-k (dashed line in Fig. 2.1). When the distribution of M is such that very strong vertical velocities are obtained, (as for example, within the shaded area in figure 2.1) our postulated balance between condensation rate and precipitation no longer holds; microphysical processes are unlikely to proceed fast enough to balance the large condensation rate. In these cases, most of the condensate may remain in the form of cloud-sized droplets; echo-weak regions observed in intense convection are an example.

The point of indetermination O of (11) is located at:

$$G/M = \frac{k(a+0.5) + p/V}{a+1} \qquad (12)$$

$$q = \frac{p/V - k/2}{a+1}$$

As p varies, this point moves on the singularity line $GM^{-1} = q+k$. For example, as indicated in Fig. 2.1, when p increases O moves toward higher values of q. We note that since all isolines of w converge toward the point of indetermination, the relative surface of the shaded zone increases as O moves out of the domain. For P/V ;,,$k(a+½)$ the point of indetermination does not exists for positive G. During the growing period of a storm (p positive) O and the line w = O shift toward hither values of q. Thus, a point (G,q) indicative of downdraft in a steady state profile of M could correspond to ascending air when M is increasing in time. Similar arguments can be invoked during the decay period (p < O).

The regions characterized by $GM^{-1} > q + k$ imply intensification of the vertical velocity when p > 0 and a decrease of w when p < 0. However, when q > G/M - k increasing p is the signature of weakening upward motion (for example, regions of the domain corresponding to an accumulation zone in the steady state situation could be transformed to do•ndraft regions for suffisent large p > 0) while decreasing p is indicative of stronger upward motion. The former could correspond to a region below an accumulation zone where an increase in M due to descending precipitation is indictative of weakening updraft.

The line w = 0 separates the regions of upward and downward motion of air. For a steady state situation this separation occurs at $q = 0.4 \times 10^{-4}$, a vertical gradient which in weak convection is rarely present outside the region near the could base. Although values of $q < (p/V - k/2)/(a+1)$ are always indicative of updrafts the inverse is not true. In particular a profile of M locally increasing with height, such as under an "accumulation zone", is indicative of updraft when it happens at high elevation (where G is small), while it could be a signature of dow draft at low elevations.

Although (11) indicates that w depends on M, on its time and space variation ar. independently on height (through G) we can consider the more broader question as to wether larger values of M indicate stronger convection for a given configuration of M in time and space. For this, from (11) we obtain

$$\left(\frac{\partial \frac{w}{V}}{\partial M}\right)_{q,p,z} = \frac{\frac{w}{V}G}{M^2(\frac{G}{M} - q-k)}$$

or

$$\left(\frac{\partial \ln w}{\partial \ln M}\right)_{q,p,z} - \left(\frac{\partial \ln V}{\partial \ln M}\right)_z = \frac{G/M}{G/M - q - k}$$

since

$$\left(\frac{\partial \ln V}{\partial M}\right)_z = \frac{a}{M}$$

$$\left(\frac{\partial w}{\partial \ln M}\right)_{q,p,z} = w\left(a + \frac{G/M}{G/M - (q+k)}\right) \qquad (13)$$

Thus, if G/M > (q + k), a condition valid in weak to moderate convection

$w > 0 + \left(\frac{\partial w}{\partial \ln M}\right)_{p,q,z} > 0$: stronger updraft with higher values of M

$w < 0 + \left(\frac{\partial w}{\partial \ln M}\right)_{p,q,z} < 0$: stronger downdraft with higher values of M

An analysis of (13) for G/M < (q + k) leads to the same results outside the shaded areas of Fig 2.1, thus, in a general sense stronger radar echoes are, indicative of stronger convention. Fig. 2.2 ummarises the conclusions just described.

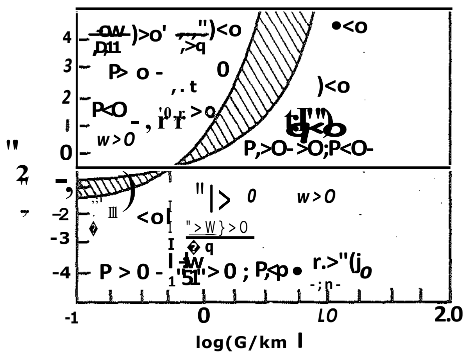

Fig. 2.2. SwnmM.y 06 k..lnel'la.ti.cc/uvr.ae,tVU,6,t.i.<Y.06 mo,ú.,t: convec,t.i.on,i.n t:he vo.M.ow., dma.,i.lv.,06 t:he pa.M.met:e.M $[q - G(kM)^{-1}]$. The pa.Jr.tia.ldvuva.uvv., ,i.mp,/'.y:ha.t: ut:heA (p,q,z) on (p,/.f,z) Me held COl'1/2-t:a.nt:.

3.3 Average vertical motion

Under the assumption of S = wG we can apply (8) and take the average over a horizontal surface containing the entire radar echo:

$$\langle w \rangle = \left\langle \frac{V_H \cdot q}{G - (q+1)} \right\rangle - \left\langle \frac{p - [(a+1)q + ½]}{G - (q+1)} \right\rangle \qquad (14)$$

If the advection of precipitation is statistically independent of $[G - (q+1)]$ then

$$\left\langle \frac{V_H \cdot q}{G - (q+1)} \right\rangle = \frac{\langle \vec{V}_H \cdot \vec{q} \rangle}{\langle G - (q+k) \rangle}$$

In the coordinates of the storm system the average advection is nil, thus

$$\langle w \rangle = -\left\langle \frac{p - V[(a+1)q + k/2]}{G - (q+k)} \right\rangle \qquad (15)$$

which can be obtain.ed from radar measurements and surface e (to determine G). A similar expression is derive for the mean vertical velocity under cloud base, where S = - E :

$$\langle w \rangle = \left\langle \frac{[(a+1)q + k/2] - [p + E]}{q + k} \right\rangle \qquad (16)$$

In a weak to moderate precipitation, where (15) may apply, the vertical gradients of reflectivity tend to be strongly negative, such that q < - k. Thus from (15) we see that in steady state ⟨w⟩ is positive, as expected. Even at the decreasing stage Eqn. (15) indicates an average upward motion (of a decreasing intensity) as long as q < - k. Although these results are not surprising our derivations present them in an elegant way.

4. APPLICATIONS TO RADAR DATA

The ideas developed in the previous sections where applied to actual radar data by Tremblay (Ref. 4). Some of his results will be reporduced here.

First, let us consider the mean core profile of reflectivity factor Z given in Ref. 2 and assume steady state and S = wG. In Fig. 3 is shown the profile of M (obtained from $M=3.8\mathrm{x}10^{-3}Z^{0.57}$ which corresponds to a M-P drop-size distribution) toghether with the profiles of vertical velocity calculated with the aid of (11) for two pseudoadiabatic ascends (characterised by two values of the wet bulb potential temperature, ewl- Note that a warmer parcel will be slower in its ascent in order to be compatible with the given profile of M. The profile of n was calculated for $\theta_w = 20^\circ C$ from S = wG. This result is consistent with the assumption of the cloud free model since Fig. 3 shows that n is an order of magnitude smaller than M.

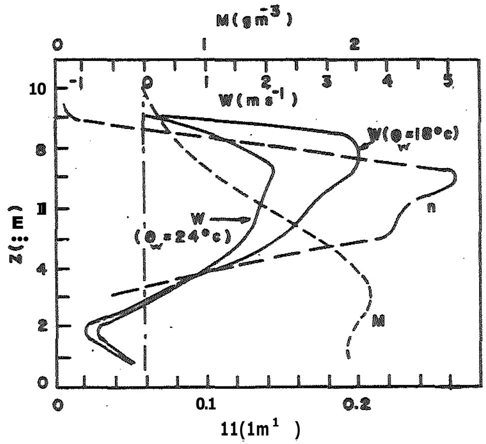

.Elg. 3. VeJr;Ucai. pttoo,U.e. 06 M 6Mm Re.6. 2 t:oghe:the.Jt w-Uh t:he. ptto6,U.e/.>06 w ob.ta..ln.e,d6JWm (11) oOJt. p = o a.nd t:he. c.lou.d pti.06,U.e 6Mm S = *wG*.

Two hours of radar data from the GATE experiment corresponding to.a weak (but deep) · and wide spread convective system (day 261, 18/09/74) were analysed. The equilibrium between the rate of condensation and generation of preclpitation was assumed. The horizontal advection was neglected with respect to the vertical advection as well. Both approximations seem to· be reasonable given the low and slowly varying values of Mand weak horizontal gradients. The rad r pattern of reflectivity at 2 k;n height is shown in Fig. 4. Only mean values of M, n and w will be shown here (Fig. 5).

The values of n and w obtained through theequations of conservation of water substance are very reasonable for this type of system. The maximum core vertical velocity, 0.24 m/s compares very well with the mean GATE value as reported in Ref. 5 (~0.27 m/s).

5. DISCUSSION

The conservation equations for water substance were used to infer kinematic properties of precipitating systems using some general characteristics of the distribution of precipitation as revealed by radar. This method leads to conclusions consistent with observations and represents a simple and didactic method of presentation.

When applied to actual time evolving radar data the conservation equations appear to be a useful diagnostic tool, for the storm kinematics. Work is under way to evaluate the potential of t ese equations in conjunction with a single Doppler radar measurements of reflectivity and radial velocity.

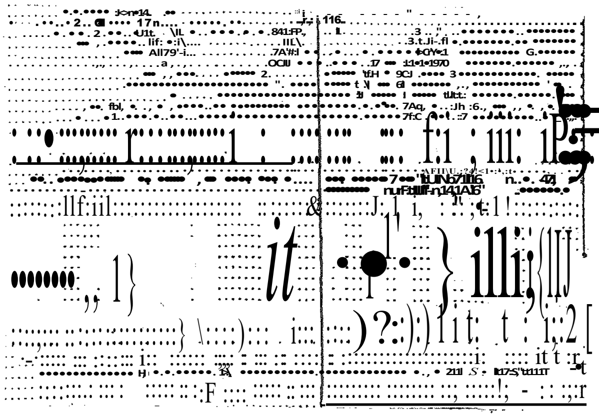

F-i.g. 4. Pti.e.clp,Ua:tlonpa.tte/U1 6.1!.omJr.a.d.aJIolu.eh.ua.t:lon6 ori t:he. 18/9/14 ,i;n GATE. The. .1!.e.c:tangt.e6hOW6 t:he, a.na.ly-o_e.dti.eg..lo.

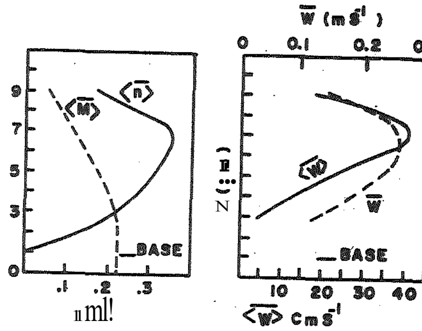

Fig. 5. Lent:: .t-i..mea.nd <lpa.c.e,a.veJLa.ge 06 pti.eclp,Ua.t:lon wa.t:e,1l.a.nd c.loud wa.t:e.ti. (6Mm S = *wG*) .ln :the 6rJ,ot:em <1hown .ln F-i.g. 4•. !Ught:: .t-i..me,and <lpa.c.e a.veJLa.ge 06 veJr;Ucai. ve.loe,i;ty.ln t:he .6!J-ot:em (60.Ud .Une) a.nd .t-i..mea.ve.Jta.ge.06 ,t:he,ma.umum updti.a.6-t: (da.ohe.d Un.el.

6. REFERENCES

1. Kessler E 1969, On the distribution and continuity of water substance in atmospheric circulation, Me.t:eoti.Monogti., No 32, Amer. Meteor. Soc., 84 pp.

2. Konrad. T G, 1980, Statistical models of summer rainshowers derived from fine-scale radar observations, *J* Appl Me.t:e.oti., 17, 171-188.

3. Clark T L 1973, Numerical modeling of the dynamics and microphysics of warm cumulus convection, *J* Atmo-6 Scl, 30, 857-878.

4. Tremblay A 1980, Etu.de. d'u.n -o!J-6.t e ptteclp.l-t:a.nt: c.onvecti.6 it pMt:,iJr. de!> donnee/.> de. GATE, Th se de maltrise, Universit du Qu bec a Montr!:!al.

5. Zipser E J t: LeMone M' A 1980, Cumulonimbus **ver**tical velocity events in GATE, Part II: Synthesis and mr.del core structure, J Atm06 Sci., 37, 2458-2469.

SESSION IV

CLOUD DYNAMICS AND THERMODYNAMICS

Subsession IV-3

Impact on cloud microstructure

WATER BUDGET OF A TROPICAL SQUALL-LINE OBSERVED DURING "COP: 81" EXPERIMENT

Michel CHONG, Daniele HAUSER, Paul AMAYENC.

CENTRE DE RECHERCHES EN PHYSIQUE DE L'ENVIRONNEMENT TERRESTRE ET PLANETAIRE (CNET-CNRS)
38-40 rue du General Leclerc
92131 ISSY LES MOULINEAUX
FRANCE

1. INTRODUCTION

Tropical squall lines are long-lived propagating chsturbances characterized by int.ense convective rain region (or c-region) followed by an extended area of stratiforrn rain (ors-region), sustained by organized rnesoscale downdraft and updraft (e.g. Ref. 1). Garnache and Houze (Ref. 2, hereafter noted GH) proposed a etailed analysis of the water budget of a GATE squall line (12 September 1974 event). They found that the c- (respectively S-) region contributed to 47% (respectively 53%) of the total precipitated rain mass. These authors used radar-derived rainfall estimates and air dynamics deduced from rawinsonde data to compute the different terms of the water budget.

The present paper deals with the water budget analysis of a tropical squall line (22 June 1981 event) observed during the COPT81 experiment, using the three-dimensional wind structure deduced from Doppler radars data. Tt:e COPT81 experiment (Ref. 3) was devoted to the study of tropical deep convection in the Northern part of Ivory Coast, near Korhogo (5°37' W, 9°25• N). Main features of the involved squall line are recalled in Section 2. Section 3 deals with a global approach of the water budget of the system in a way similar to that of GH. Section 4 presents a detailed analysis of precipitation efficiency in the convective part of the system.

2. THE 22 JUNE 1981 SQUALL LINE

The detailed meteorological and radar observations were previously describ d in Ref. 4. Fig. 1 displays the reflectivity pattern deduced from one of the two Doppler radars, Rl, scanning at 0547 GMT (or local tilpe). The frontal part of the system (West of Rl) is characterized by an intense precipitation zone (up to 55 dBZ) associated with a 50km width convective line, extending from south to North. It is followed by a large region of roughly stratiform precipitations (30-40 dBZ). The system preserved its main structures while it moved towards south-West along a direction close to the radars baseline Rl-R2 at a constant speed of 20 m s-i. This allowed to interpret the Doppler radars observations obtained at different times as being typical of different parts (Fig. 1) of the squall iine. Dual-Doppler radar measurements were performed in the c-region using the coplane methodology (Refs. 5-7) to obtain the 3D wind and reflectivity fields, while VAD analysis with single radar were used to derive mean height profiles of wind at the mesoscale.

Fig. 2a represents the relative airflow at low level(i km) associated to the c-region. Surface meteorological observations and radiosoundings indicate that the westerly flow is associated with unstable warm air, while the easterly flow is associated with cold air, A vertical cross section(along AA' axis) of the relative airflow is shown in Fig. 2b. The strong ascent(up to 6 km) of the westerly warm flow is forced by the low level easterly cold flow coming

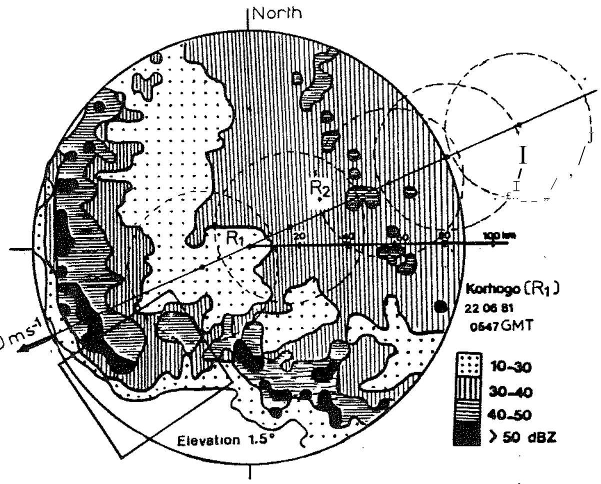

Figure 1: Reflectivity pattern **(dBZ)** of the 22 Jun 1981 squall-line at 0547 GMT. Rl and R2 show the location of the two radars. The direction of motion is symbolized by the **arrow. The different regions observed** by **radar are indicated: rectangle for the c-region and circles for the S-region.**

from the rear of the system. The dynamical structure in the c-region reveals a quasi two-dimensional character of the flow with abscence of strong convective downdrafts. Fig. 3 represents a vertical cross-section of the airflow, derived from VAD analysis in the s-region, in a plane parallel to the direction of motion of the system. This figure clearly snows that the low level cold air pool is induced in the s-region by an extended mesoscale downdraft (reaching 30 cm/s) below the 4 km level. In the c-region the structure of the reflectivity pattern (Fig. 2b) and of the precipitation trajectories(Fig. 2c) indicates that the extent of the flow lines relative to the heaVY precipitation do not exceed the -10°C isotherm level. Then it is likely that precipitations grow mainly by warm micropnysical processes. on the contrary, in the S-region, radar data reveal a well-defined bright band pointing out ice region above the 0°c isotherm level (4.2 km).

3. THE WATER BUD ET: A GLOBAL APPROACH.

The water budget is investigated by calculating the various terms defined by SH, in order to facilitate comparisons with their results. These terms(see Fig.4) contribute to the balance equation as follows:

$$R_c = C_u - E_{cd} - E_{ce} - C_A \quad (1)$$

$$R_m = C_{mu} - E_{md} - E_{me} + C_A \quad (2)$$

where Re (or Rm) is the total mass of convective (or stratiform) rain at ground level, C_u (or CmJ is the mass of water condensed in convective (or mesoscale) updraft, Ecd(or Em4) is the mass of water evaporated in convective(or mesoscale) downdraft, Ec (or Emelis the mass of cloud water evaporated by miXing with the unsaturated pre-squall air inflow (or flowing out of the s-region at the rear of the

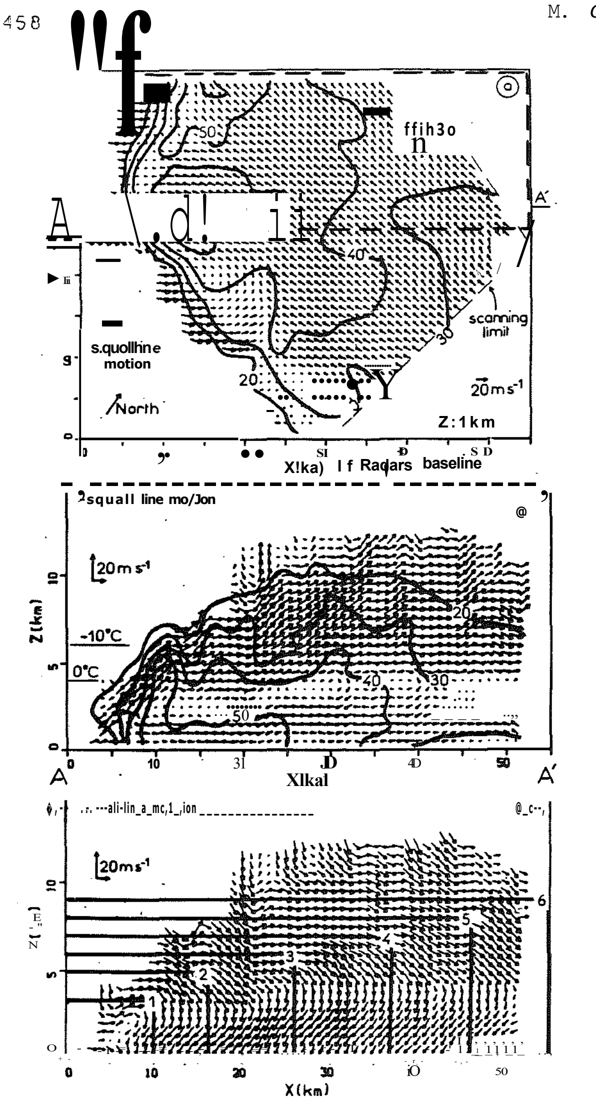

Figure 2: a - Horizontal section of the relative airflow at 1kll and reflectivity contours {dBZ) at .Skm,in the C-region. **X-axis is** parallel to the RlR2 radar baseline which is very **close to the direction of motion. The heavy dashed contour encloses the** North **part** of the -C-region.

b - Vertical cross-section along AA' axis of Fig. 2a,of the relative airflow and of the reflectivity contours {dBZ).

c - ame as in b but for the precipitation trajectories. The slx rectangle& (1 to 6) show the vertical cross-sections of the n.. domains (see text) .

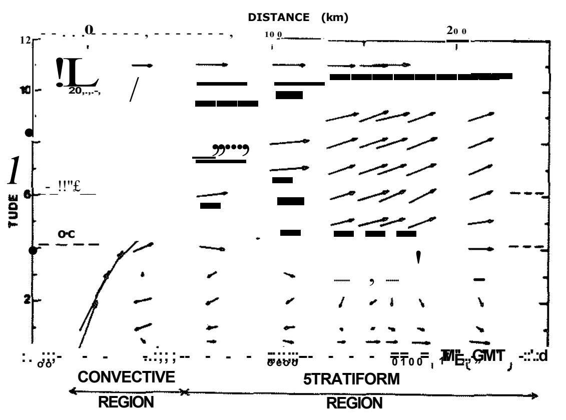

Figure 3: Vertical L.oss-section of the relative airflow along the direction of motion ,for the c- ands-regions. Correspondance time-distance is indicated.

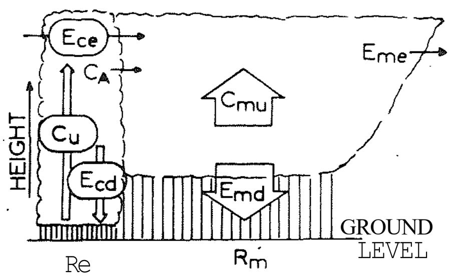

Figure 4: Water budget tenüii in the c- and S-regions (after Ref. 2) •

Convective region	Re	Cu	Ecd	Ece	CA
22June 1981	.69	1.44	.06	.0„	.63
GH	.17	1.62	-	.23	.78

Stratiform region	Rm	Cmu	Emd	Em•	-CA
22June 1981	.31	.61	.65	.37	.72
GH	.53	.26	.23	.15	.65

Table 1: Water budget of the 22 june 1981 COPTSl squall-Hne compared to the 12 September 197& GATE squall line water budget of Gamache and Houze{Ref.2).

system). C_A is the mass of water transferred from the c-region to the s-region.

we used Doppler radar data(3D wind structure),radiosoundings relative to the pre- and post- squall line pass (thermodynamical characteristics of air) and surface network data (mass of rain observed at Jround level) to calculate the different terms of Eqs. land 2 except CA which was evaluated as residual in both cases. Surface measurements indicate that convective rai n and stratiform rain fell respectively during 35 and 175 minutes. This corresponds respectively to 42 and 210 km along the direction of motion of the system. Then the total masses of convective rain Re(respectively stratiform rain R_m) fallen over a typical area Sc= 50x42 km^1 (respectively s = 50x210 knt),during the total period of observation (-c=210 min) are:

Re = 1.42 10^{H} kg and R_m = 0.65 10'1 kg

All the water budget terms are computed using Sc, S ,and -c as reference values. Vertical air motions derived from radar observations within both c- and s-regions are used to calculate condensation (C and c...) and evaporation (E_cd and E_mJ) terms using the water mass continuity equation with the assumptions that:(i}the air remains saturated; (ii) the squall line structure is in a steady state;(iii) the entrainment effects are negligible. For example the condensation (or evaporation) rate of cloud water per unit volume, at altitude z, is:

$$c(z)= \rho(z)\, w(z)\ (\partial r_s / \partial z) \qquad (3)$$

where is the air density, w is the vertical air velocity, and r_5 is the water vapor mixing ratio of an air parcel moving up (or down) along moist adiabats. It is likely that the term E„d repi:esents evaporation of precipitation in unsaturated air rather than that of cloud ater in saturated air. Thus the calculated EmJ. is thought to give a maximum es-.timate of evaporation. The term Ece is evaluated by using the inflow of unsaturated air in front of the squall line. The term E,.,,is determined from the horizontal outflow of condensate at the rear of the system.

The computed water budget terms in the c- and s-regions are summarized in Table 1. They are expressed with respect to the total amount of rain $R = R_c + R_m$ and compared with the values obtained by GH (Ref. 2). The convective rain (Rc) and stratiform rain (Rm) both contribute significantly to the total rainwater mass even though in our case the ratio R_c/R_m is higher (2.2 instead of .9). The major contribution of water production comes from condensate in the c-region. Both estimates of C_A in our case are in rather good agreement and reveal that a large amount of cloud water is transferred from the s region. The main differences between the two sets of results are that our case evidences lower relative values of evaporation terms in the c-region (small convective downdrafts) and higher relative values of evaporation and condensation terms in the s-region (due to higher values of mesoscale updrafts and downdrafts).

The water budget of the convective part shows that 48 % (Re/ c) of the condensed water falls in this region and about 50 % (C / Cu) is transferred to the s-region, while evaporation of cloud water is almost negligible. Then the rather low value of the local precipitation efficiency $E_c = R_c/C_u$ is primarily due to the outflow of condensed water. Note that when referred to the net condensation rate (c - Ec&) the precipitation efficiency becomes E'c = 51 %. In the S-region the local precipitation efficiency Em = R.,l(Cmu.+CA) is only 20 %. Although the total available cloud water (Cmu.+ C_A) is large (comparable to C_), the precipitation efficiency is very low because evaporation of cloud water within mesascale downdraft (Emd) and transfer into the large scale environment (Eme) are both important, accounting respectively for 55 % and 25 % of the total available condensate (Cmu.+CA) in this region. Then it is clear that cloud water transferred from the convective region and local condensate due to the mesascale updraft are both essential to maintain the stratiform rain region at the rear of the squall line. Finally the global precipitation efficiency of the system combining c- and s-regions is **E=** (R_0+ R)/ (C + c ..)= 44 %, the remaining part of the total condensate being eittler evaporated in the stratiform region or blown away at the rear of the system.

4. THE WATER BUDGET: A DETAILED ANALYSIS IN THE CONVECTIVE PART

An other approach to investigate the water bud et is to use the observed reflectivity and three-dimensional wind fields to evalua .e the net production of precipitating and of condensed water. This was done for the observations relative to the c-region where data are available at cartesian grid points of volume elements (1x1x.5 km^3) in the total volume (55,45,12 km^3). The condensation rate is computed from Eq. 3. The rate of precipitating water production p is derived from the steady-state continuity equation for the precipitating water content M:

$$p = \operatorname{div} M\,(\bar{V} + \bar{V}_T) \qquad (4)$$

where V is the air velocity vector (u,v,w) and V_T is the mean intrinsic fall speed of raindrops. The use of a spectropluviometer (Ref. 8) measuring size and velocity distributions of drops at ground level allowed to determine relationships involving the reflectivity factor Z, relative to the COPT81 experiment:

$$Z = 3.19\ 10^4 M^{"'3} \quad (5) \qquad \text{and} \qquad V_T = 3.28\ Z^{'.on} \quad (6)$$

V_T is corrected for air density decrease effect in altitude when used in Eq. 4. A positive production rate p indicates a local source of precipitation resulting from accretion and/or collection processes while a negative production rate is interpreted as a local sink of precipitation due to evaporation. Diffusion terms are neglected.

Integrating Eq. 4 within a given volume leads to:

$$P = T - E^P = F^P \qquad (7)$$

where the net production rate P is the difrerence between the integrated source terms T and sink terms E^P. P is balanced by the net outflow of precipitating water F^P which is also the sum of the net vertical outflow through tht lowest level (1 km) F crt., and of the net outflo F t through the other sides of the domain. The complete liquid water budget equation in a given volume is obtained by combining the rain water and the integrated cloud water continuity equations:

$$P + E^P + F^C_{lat} = C \qquad (8)$$

or

$$F^P_{m0} + F^P_{lat} + E^P + F^C_{lat} = C \qquad (9)$$

where C is the net integrated condensed water, and F^C_{lat} is the net outflow pf condensed water through all side of the domain.

Two parameters E_1 and E_2 can be defined to characterize the precipitation efficiency:

$$\varepsilon_1 = P / C \qquad (10) \qquad \text{and} \qquad E_2 = F^P_{crt} / C \qquad (11)$$

E_1 and E_2 represent respectively the percentage of condensed water that is converted to precipitable water mass or precipitated at the lowest level. Table 2 indicates the results obtained for c, p, E_1, E_2, in the n t volume. E_1 amounts to 54 % and E_2 to 55 % • The 1 % difference is due to a weak lateral flow Fe t of precipitating water entering the volume. These results are in good agreement with the value of E'c (E'c 51 %) obtained by the method proposed in section 3, for the same region.

The dynamical structure analysis of the convective region (see section 2) indicates that the wind field has two-dimensional features. However Fig. 2a shows that this characteristic is best evidenced in the North part of the convective region (first 19 kms in the North). Therefore it was chosen to restrict the water budget study to this part, by considering then domain ,-'1=55,19x12 km^3 (se Fig. 2a). Table 2 indicates that in this domain the efficiency (E_1= 73 %) is much higher. Then it is interesting to investigate in details the water budget in this region.

DOMAIN (km^3)	C (10^7 kg s^{-1})	P (10^7 kg s^{-1})	E_1 (%)	E_2 (%)
(55x45x12)	1.73	.93	54	55
0 (55x19x12)	.80	.58	73	84

Table 2: Values of the parameters C,P,f ,E in the two domains fl\. and n (see text).

Fig. 5 shows the variation with height of C, P, T, E integrated within horizontal slices of .5 km thickness. P and T reach a pronounced maximum at 3.5 km. E^P is small when compared to T except at the lowest altitude (1 km). This is likely a result of evaporation of raindrops in the low level cold air. Though the water condensed above 5 km is significant, maximum of precipitation production rate occurs near

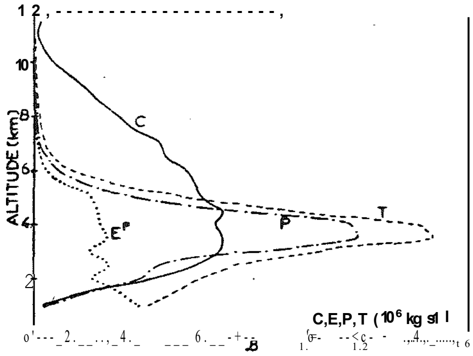

Figure 5: Rates of condensation (C), rates of precipitation production (T), evaporation (E^P), and net pr ction (sT-E) as a function of altitude. All these quantities are integrated values within horizontal slices of ss 19 0.s km¹ (North part of the c-region).

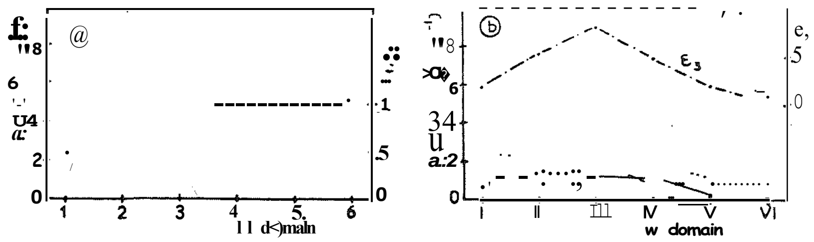

Figure 6: a - Rates of condensation (C), and of the net precipitation production (P), precipitation efficiencies E_1 and E_a, in each subdomain (rt to n,) shovn in Fig; 2c (see text for more details.
b - Same as in a for C and P but for each differential domain w (see text). In each case, also drawn are the total available condensed water (C+f) and the precipitation efficiency (E3•P/(C+f)).

3.5 km. **These** results suggest to seek for possible local variations of the precipitation efficiency inside the .n. ·domain.

For that purpose subdomains included within the fl domain. are defined by varying simultaneously the altitude and the horizontal extent (Fig. 2c). These dimensions are chosen for each subdomain in order to best enclose thE precipitation trajectories, i.e. in order to minimize the lateral outflow of precipitation Fi:t· This allows to interpret t, as a local efficiency of conversion of condensed water. Fig. 6a indicates the values of P, C, E_1, E_1 as a function of the considered sUbdomain (!1, to .n.,). The difference between e, and E_1 is nearly constant and denotes that only 15 to 20 % of the water fallen through the lowest level comes from the outside. The production rate and the efficiency increase rapidly in the first three domains, then stabilize at nearly constant values. It is -interesting to note that the region of rapid increase in the efficiency corresponds to a vertical extent of the intense precipitation not exceeding 6 km, i.e. the -10°c isotherm level. so it is clear that the precipitation efficiency depends on the space extent of the considered precipitation flow.

This suggests to compute a precipitation efficiency relative to precipitation stream "tUbes". A simple approach for this purpose consists in considering "differential• domains (""•to w,) enclosing the differential volumes between two consecutive n SUbdomains. In that case, the total available condensed water is.considered to compute the efficiency

$$\varepsilon_3 = P/(C+f) \qquad (12)$$

where f is the inflow of condensed water entering t e domain, deduced from the computed outflows F_t,t (Eq. 9) relative to the adjacent domains. Fig. 6b shows tha E_3 regularly increases up to the third differential domain where it reaches a pronounced maximum value. so. the maximum of efficiency (80%) is obtained for a precipitation stream tUbe entering the 5 to 6 km levels and falling down to the zone of the most intense precipitations (Z>50 dBZ). Abov.a 6 km, the decrease of the efficiency i= likely due to changes in the microphysical processes which involve the presence of ice phase in the growth of precipitations. Indeed, such processes would certainly require larger residence time of the particles along their trajectories to convert more efficiently the condensed water into precipitations.

5. REFERENCES

1. **Zipser E J 1977: Mesoscale and convective-scale downdrafts as distinct components of squall-line circulation,** Month Weath Rev 105, 1568-1589.

2. Gamache J F and Houze R A Jr 1981: The water budget of a **tropical squall-line system, Preprints 20th Conf on Radar Meteor, Boston, Amer Meteor Soc, 346-352.**

3. Sommeria G and Testud J 1983: COPT81, a field experiment **designed for the study of dynamics and electrical activity of deep convection in continental tropical regions,** (to appear in Bull Amer.Meteor Soc).

4. Roux F, Testud J, Pinty Band Chalon JP 1982: Dual-**Doppler radar and surface network observations of a west-•african squall line during the COPT81 experiment, Conf on Cloud Physics, Chicago, Amer Meteor Soc, 547-550.**

5. Testud J and Chong M 1983: Three-dimensional wind field **analysis from dual-Doppler radar data. Part I: Filtering, i.nterpolating, and differentiating the raw data, J Cli**mate Appl Meteor 22, 1204-1215.

6. Chong M, Testud J and Roux I' 1983: ________ **Part II: Minimizing the error due to temporal variat·ion,** J Climate Appl Meteor 22, 121,-1226.

7. Chong M and Testud J 1983: ________ **Part III- The boundary condition: an optimum determination based on a variational concept, J Climate Appl Me**teor 22, 1227-1241.

8. Jiutten B, Bauser D, Alllayenc P and lialdteufel p 1981: An improved optical spectropluviometer: Technical description end first results, Prepri s 20th Conf. on Radar Meteor., Boston, Amer. Met. Soc., 232-238.

FIELD STUDIES OF THE INTERACTION OF TURBULENT ENTRAINMENT AND CLOUD DROPLET EVOLUTION IN A MOUNTAIN CAP CLOUD

T W Choularton, I E Consterdine, B A Gardiner, M J Gay, M K Hill and I M Stromberg
Physics Department, UMIST
Manchester M60 1QD, England

1. INTRODUCTION

In this paper we describe two case stucties of the evolution of the cloud droplet spectrum in cap clouds enveloping the UMIST field station on Great Dun Fell (GDF).

The measurements were performed on 24th March (Case 1) and 6 April (Case 2) 1982. The major difference between this and earlier studies, e.g. Ref.1, are i) measurements of the cloud microphysical properties were made at two sites at different altitude on the mountain side and ii) higher rate microphysical data was available facilitating a more detailed study of the effect of dry air entrainment on the cloud.

The results are interpreted with the aid of a numerical model of a cap cloud (Ref. 2) in order to understand the contribution of various physical processes in affecting the evolution of the droplet spectrum.

2. THE FIELD MEASUREMENTS

Table 1 lists the instrumentation at each of the measurement sites.

Measurements of cloud condensation nuclei concentrations were made continuously, at Wharleycroft, using a Mee Industries CCN counter. This information plus standard meteorological parameters (wet and dry bulb temperatures and wind speed and direction) were logged on magnetic tape. Hourly observations of cloud conditions and visibility were also made. This is especially important in assessing total cloud cover. Tests were conducted to ascertain whether it was acceptable to make measurements of CCN concentrations at this site rather than at cloud-base. The Mee counter was run alternately at Wharleycroft and at the Silverband mine site on a cloudless day with steady south-westerly winds. No significant variation in activity spectra was found. Care has to be taken, however, to ensure that no blocking of the air in the valley floor is occurring on the day under study.

Measurements of cloud-base temperatures, wind speed and height were made regularly using a Land Rover. These parameters provid an important input into any cloud growth model.

The instrumented van was sited just above cloud base, and directly down wind of the top station about 200m lower down the hill. The cloud droplet spectra were measured using a Knollenberg FSSP probe. From these spectra, values of cloud liquid water content and droplet concentration could be obtained. Spectra were measured every second and the probe was operated on Range 1 (15 size channels from 2-32μm diameter). Standard meteorological parameters, at a height of 2m, were recorded at 1Hz. These were supplemented every half an hour by hand measurements - to provide a calibration and observations of visibility.

2.1 Great Dun Fell Summit

A sturdy platform 4m above ground level was used to mount the various instruments at the summit of Great Dun Fell. Generally these consisted of a Knollenberg FSSP and a met. pole (dry and wet bulb, wind speed and direction). Additional meteorological measurements were obtained from a 10m mast. A Barnes transmissometer with a 15m path-length at a right angle to the airflow, measured extinction coefficients for the cloud at a wave-length of 10.6μm to provide a separate measure of liquid water content. An acoustic sounder was situated 40m from the other instruments, and provided information on mixing-scales and cloud-top height. The FSSP spectra were recorded at a data rate of 1Hz, and occasionally at 10Hz.

2.2 Case Study 1

The case study was in an isolated cap cloud over the mountain. The satellite photograph shows that the sky above the cap cloud was largely free of cloud, some cirrus was present. Winds were from the southwest and around 30 knots on the GDF summit.

A major feature of the data is that when the van-site was near cloud base very large fluctuations occurrred in the liquid water content, number concentration. These rapidly dissappeared as cloud base lowered. These may be attributed to small scale (tens of metres) fluctuations in the humidity of the airstream entering cloud base. This has the effect o broadening the droplet spectrum at the Silverband and it is suggested in Ref.2 that this staggering of the condensation process may slightly increase the size of the largest droplets. Figures 1a and b show the effect of growing the observed van spectrum adiabatically to the summit site a) when large liquid water content fluctuations are occurring at the Silverband, b) a period with much smaller amplitude fluctuations. It is apparent that enhanced growth of the largest droplets in the spectra is occurring ana that this is greater in (al than (b). As no change occurs in other parameters between these two times it seems likely that the difference between these two results is representative of the contribution of the cloud base patchiness to the enhanced growth.

Other major features whicl1 arise from a comparison of the observed and grown -spectra are
1l the width of the observed spectrum is only slightly greater than the adiabatic model suggesting that activation of new drops following the effects of dry air entrainment is insignificant in this case;
2) an enhanced growth of the largest drops is observed which is additional to that produced by the cloud base patchiness. This does not occur in Case 2 when higher cloud layers were present. The largest drops are always found in the regions of highest (nearly adiabatic) water content. Further, as the magnitude of the effect is consistent with that predicted for the effect of radiative cooling from cloud top in Ref.2, we suggest this is the likely source.

If the "droplet spectra are averaged over the highest 10% liquid water contentrations and the lowest 10% it is apparent (Figure 1) that fluctuations occur which may be attributed to dry air entrainment at the.cloud top. Conditions were generally too windy for the sounder but there is some evidence that the capping inversion is about 600m above the mountain top. In this case the liquid water changes are largely produced by changes in the spectral shape consistent with uniform evaporation.

Small scale structure in the droplet .number concentration is evident consistent with droplet loss to ground.

2.3 Case Study 2
Throughout the period the area was in light south-westerly winds. Northern England was covered by 4/8 to 7/8 stratocumulus with base at about 1km. The Aughton radiosonde ascent showed that the cloud was capped by an inversion about 1200m above sea-level. The acoustic sounder record (Figure 2) shows this about 300m above the mountain summit. Considerable small scale structure is evident in this layer indicating that dry air from above this ivnersion is being entrained into the cloud.

The cloud divides into two periods.

Early in the case study, water contents at the summit are on average only slightly sub-adiabatic. Growing a droplet spectrum from the Silverband site to the mountain summit (Figure 3) shows that a slight enhancement of growth of the largest drops; however, the effect is smaller than Case 1 and may be attributed to the patchiness at cloud base.

Later the entrainment effects were dominated by frequent smaller scale fluctuations in liquid water content which were associated with both fluctuations in mean radius and number concentration. now-ever, the magnitude of the number concentrations increases on smaller cales. The average liquid water content is much more sub-adiabatic during this period. Figure 4 shows a spectrum grown adiabatically from the Silverband site compared to the average 10% highest and 10% lowest liquid water content spectra at the summit. It is evident that the dry air entrainment has resulted in considerable spectral broadening due to the addition of many more small droplets; however, the concentration of large droplets has fallen to or below the adiabatic values.

3. CONCLUSIONS

It is apparent that a certain amount of enhancement in the growth of the largest drops in the spectrum is observed. This woul.d seem to be due to two effects:
1l A staggering of the activation of droplets in the vicinity of cloud base;
2) Radiative cooling from cloud top.
Process (1l is unlikely to be important in deeper clouds as the effect rapidly disappears with increasing distance above cloud base. Process (2) may, however, be important in initiating coalescence in some clouds: this is pursued in Ref.3.

The pattern of evaporation observed during the later part of Case 2 with liquid water changes being produced by changes in mean droplet radius on large scales but with fluctuations of increasing magnitude of number concentration on smaller scales is consistent with the process describeq by Ref.4.

REFERENCES

1. Baker MB, Blyth AM, Carruthers DJ, Caughey SJ, Choularton T W, Conway, BJ, Fullarton G, Gay M J, Latham J, Mill CS, Smith M H & Stromberg I .M 1982 Field studies of the effect of entrainment on the structure of cl.cuds at Great Dun Fell. Quart J Roy Met Soc, 108, 899-916
2. Carruthers DJ and Choularton T W 1984 A model of a mountain cap cloud. Proc. Int Cloud Physics Conf, Estonia
3. Hill TA and Choularton T W, 1984 The effect of radiative cooling on the evolution of cloud droplet spectra and the generation of rain. ibid
4. Baker MB, Breidenthal RE, Cnoularton T W and Latham J 1984 The effects of turbulent mixing in clouds. J Atmos Sci (in press)

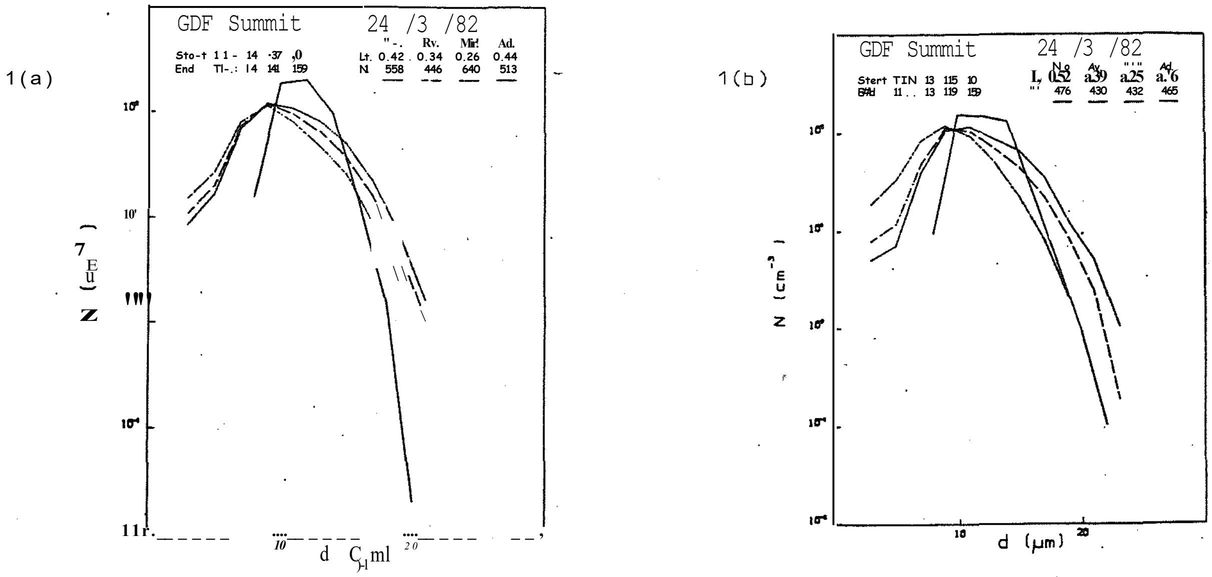

Figure 1a Cloud droplet spectra observed at the summit station for Case 1 showing 10% highest liquid water content regions, average and 10% lowest water content regions and adiabatic spectrum grown from the Silverband site. Liquid water contents are in gm and number concentration in cm-.

(a) When large liquid water fluctuations are occurring at the van site.

(b) In the absence of fluctuations at the van site

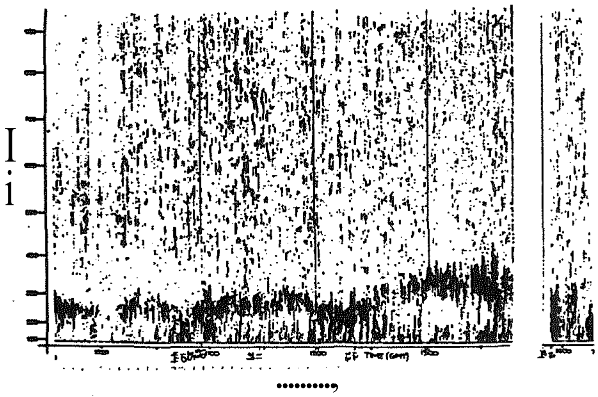

Figure 2 Acoustic sounder trace obtained during Case 2.

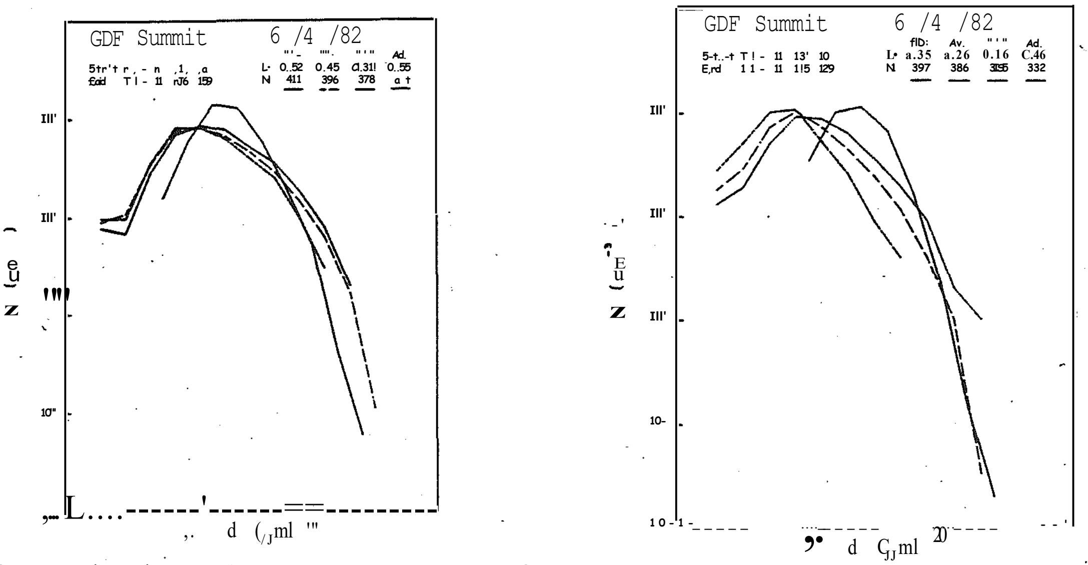

Figure 3. As in Figure 1, but for Case study 2.

TABLE 1
Station Position 54°40'N, 2°25'W

Site	Wharleycroft	Cloud Base	Silverband Mine	GDF Summit
Height (Metres ASL)	205	Variable	686	847
Instrumentation	Mee CCN counter Dry Bulb Temp. Wet Bulb Temp. Wind Speed Wind Direction	Dry Bulb Temp. Wet Bulb Temp. Wind Speed Wind Direction Altimeter	PMS FSSP Probe Dry Bulb Temp. Wet Bulb Temp. Wind Speed Wind Direction	PMS FSSP Probe PMS OAP Probe* Optical LWC Device* Humidity Probe* Barnes Transmissometer Acoustic Sounder Dry Bulb Temp. Wet Bulb Temp. Wind Speed at 5m Wind Direction at 5m Wind Speed at 10m Wind Direction at 10m
Additional Measurements	Visual observations of cloud type and visibility	Visual observations of cloud type and visibility and cloud height	Observations of visibility Hand held temperature and measurements	Observations of visibility. Handheld temperature and wind measurements

*Not always operational

OBSERVATIONS OF THE EVOLUTION OF THE MICROPHYSICAL AND THERMO-DYNAMICAL CHARACTFRISTICS OF THUNDERSTORM ANVILS

Andrew J. Heymsfield and Andrew Detwiler

National Center for Atmospheric Research
Boulder, Colorado 80307, U.S.A.

1. INTRODUCTION

Thunderstorm anvils are thought to play important roles in the overall dynamics, water budget, and possibly microphysics of thunderstorm cells, yet little is known about their internal composition, level of importance, or the processes by which particles evolve within them. In an attempt to fill some of the gaps in our knowledge of processes operative within thunderstorms, the present study examines the internal composition of thunderstorm anvils associated with storms on two different days and discusses growth processes in the anvils which may be important in the development of precipitation from these storms.

The storms were sampled by the National Center for Atmospheric Research (NCAR) Sabreliner jet aircraft in association with the Cooperative Convective Precipitation Experiment (CCOPE) in northeast Montana, U.S.A., during the summer of 1981. One of the storms investigated, which occurred on 12 June 1981, was multicellular in nature and was also characterized by moderate reflectivities (up to 55 or 60 dBZ) and little or no reported hail. The other storm investigated, which occurred on 1 August 1981, was multicellular to supercellular in nature and was characterized by high reflectivities (up to 65 dBZ) and reports of large hail (up to 10 cm) in copious quantities.

The sampling aircraft was equipped with intrumentation to measure the three dimensional winds and turbulence levels (from an inertial navigational system), the air and dew point temperatures, and the liquid water content. Measurements of particle concentrations and shapes were made using a Particle Measuring Systems (PMS) two-dimensional (2-D) imaging probes covering the size range from about 25 µm to > 800 µm (2D-C probe) and 200 µm to >6.4 mm (2D-P Probe). Unfortunately, the 2D-C probe was not operational for the 1 August case, The 2D probe data was reduced according to the procedures outlined in HeymsfieJ.d and Parrish (1979).

2, DATA fRESENTATION

2.1. Case of 12 June 1981

Radar data relating to three of the seven penetrations into the anvil on 12 June 1981 appear in Figs. lA-C. Figure 1A shows CAPPI presentations at the aircraft altitude (Z), where the outer contours represent 0 dBZ and increments in contours represent 10 dBZ, The CAPPI's are rotated in space so as to facilitate presentation of RHI and aircraft data along the same coordinates. The penetrations (solid lines, Fig, 1A) were made along a nearly perpendicular line through the anvil and near its upwind edge. Reflectivities of 20 to 30 dBZ were penetrated, RHI's taken along lines B1-B2 in Fig. lA parallel to the anvil axis and through the reflectivity core are presented for each penetration in Fig. 1B; reflectivity contours are as in Fig. lA. Solid circles show the posifion of the aircraft as it crossed lines B1-B2, From "cells" located along the upward edge of the storm, the anvil appeared to decay slowly over a relatively long distance. RHI's taken along lines Cl-C2 in Fig. lA perpendicular to the anvil axis and along the aircraft track appear in Fig. lC. The reflectivities appear to be nearly symmetrically distributed abo t the center of the cells. The aircraft appears to have penetrated fairly uniform regions of the storm.

Measurements of the potential tenperature, 8 , and the vertical velocity appear in Fig. 1D; virtually no liquid water was measured during these penetrations. rhe horizontal scales in the plots in Figs. lD-E are expanded from those in Fig. lC to facilitate plotting of the data, Comparisons of 8 at different positions in the anvil are also likely to reflect differences in the equivalent potential temperature, 0 becau.se the mixing ratio within the anvil was likely to be approximately the same at all positions. The data indicates that 8 was fairly constant across the anvil, but a minimum was noted near the end of each penetration. The trends would suggest that mixing was uniform throughout the anvil except along the northern edge where additional mixing was apparently occurring. Vertical velocities derived from an inertial navigational system and gust probes are shown in increments of 3 m s^{-1} to reflect an uncertainty of about those magnitudes. Regions where no vertical velocitie& are shown ranged from -3 to +3 m s-1. Vertical velocities were usually weak throughout these penetrations, but several distinct updraft regions were penetrated, particularly during Pen. 7. Downdraft regions were also observed.

Hydrometeor measurements using a 2D-C and 2D-P probe appear in Fig. lE. Predominant particle habits as shown, using the following nomenclature: AG: aggregates; CL: columr.; GR: graupel; and SP: spatial crystals (.bullet rosettes, spatial dendrites, etc.), Graupel and spatial crystals predominated for the penetrations. Graupel were found mostly in association with updrafts> 3 m s-1 and in the downdrafts while the spatial crystals were observed in the quiescent regions. Ice particle concentrations exceeded 100 Q^{-1} at many locations, and concent.rations >1 mm averaged about 1 9,-l. The largest particles, up to 5 or 6 mm sizes, were observed in connection with the reflectivity maxima (Fig, lC) and in regions mostly associated with updrafts.

2.2. Case of 1 August 1981

Radar data relating to three of the six penetrations into the anvil on 1 August 1981 appear in Figs. 2A-D, Figure 2A shows a CAPPI presentation at the aircraft level; reflectivity contours are as in Fig, 1A. One of the CAPPI's was rotated to facilitate comparison with the aircraft measurements. Two major "cells" or reflectivity centers were noted along the upwind (western) portion of the storm, particularly during the first two penetrations. This storm was much larger than the storm penetrated on 12 June. The aircraft penetrations (dark, solid lines, Fig. 2A) were made at positions from 50 to 80 km from the upwind portion of the storm, at an orientation about 30° from the perpendicular to the axes of these anvils, Pen. 5 was made near the limit of available radar data, RHI's taken along lines B1-B2 in Fig, 2A parallel

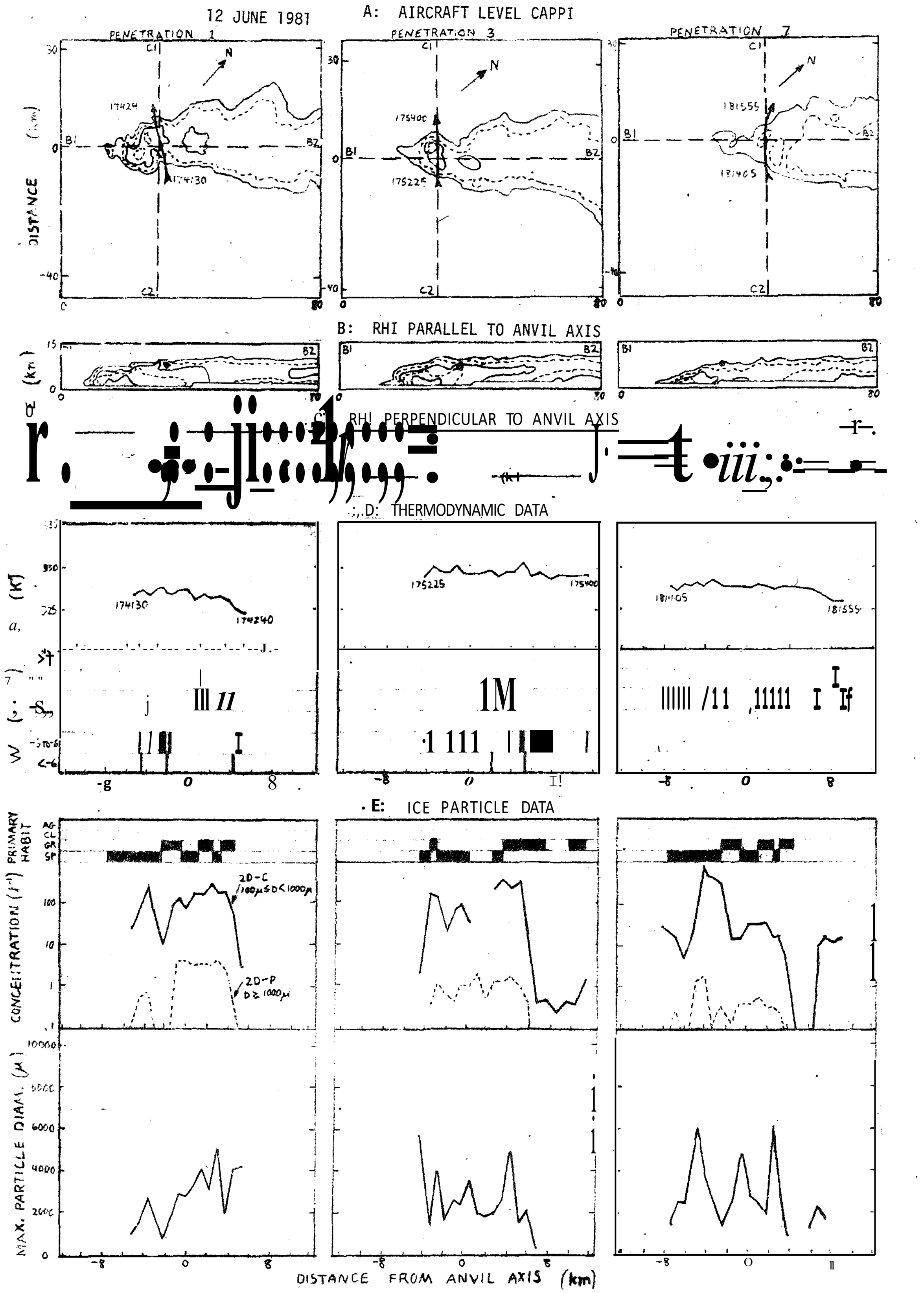

Fig. 1. Summary of the data for 3 penetrations on 12 June 1981. A description of the data is given in the text.

to the anvil axis and through the reflectivity core of the most intense (southwestern) cell are presented for each penetration in Fig. 2B. Solid circles show the positions of the aircraft penetrations when the aircraft crossed. the positions of these RHI's. Strong reflectivity cores were noted along the upwind edge of the storm; storm tops > 15 km were impressive. A very gradual decrease in the reflectivities from the reflectivity cores outward to the edge of the available reflectivity data was noted. RHI's taken along lines Cl-C2 and D1-D2 in Fig, 2A perpendicular to the anvil axis bounding the aircraft track appear in Figs. 2C and 2D, respectively, The i111111ense size of this storm can be seen along these perpendicular sections. lteflectivities appear to be higher near the position marked C2 in Fig. 2C during Pen, 2 when the ail:craft penetrated close to the cell located near the nor hwestern portion of the storm. Another reflectivity core, although less marked, appeared to be located near position Cl and Dl in Figs. 2C-D, respectively, during Pen. 2.

Measurements of the potential temperature and the vertical velocity appear in Fig. 2E, using the same. plotting.scheme for vertical velocity as discussed for Fig, 1D; very little liquid water was found. Values of 0 gradually increased from the southern to northern edges of the anvil, perhaps indicating that mixing was p.refereritially taking place on the southern portion of the anvil. Downdrafts were mostly found in the anvil, although a few updrafts were found along the southern portion of the anvil during Pena. 1 and 1.

Hydrometeor measurements obtained with a 2D-P probe appear in Fig. 2F. The predominant particles were graupel during Pens. 1 and 2; these particles apparently developed in conjunction with the updrafts sampled during tho e penetrations. Some spatial crystals, particularly spatial dendrites, were also observed. Particles were mostly spatial crystals and aggregates during Pen. 5, Concentrations of these particles are considerably lower than those for 12 June, because data was not available for sizes< 300 μm. Concentrations nevertheless ranged up to 100 t^{-1}. Maximum particle diameters ranged up to 1 cm. These large particles were aggregates.

3, CONCLUSIONS

Th data presented here is intended to provide.a first look at the microphysical and thermodynamical characteristics of the two thunderstorm anvils investigated. D velopment of particles in the two anvils sampled appeared to differ markedly. For the 12 June case, the data suggests that most growth took place in the updrafts and that the anvil was a region containing cloud debris, Conversely, the anvil for the 1 August case appeared to be a region of active particle gr-0wth, The particles of 5 111111to 1 cm size observed during the penetrations of positions far downwind of the intense updraft centers where they probably originated would indicate that continued growth had taken place at positions within the anvil. We are now using the data in conjunction with particle growth models and measured three-dimensional windfields for these cases to infer the processes of particle growth, Some of these calculations will be shown at the conference.

4. ACDOWLEDGEMENTS

The authors wish to thank Joanne Parrish ana Bob Bawn for their help in data analysis. Typing of the manuscript by Frances Ruth is apprec ated. Data collection by the NCAR Research Aviation Facility (RAF) is greatly appreciated.

5• REFERENCES

L Reymsfield, A. J. and J. L. Parrish, 1979: Techniques employed in the processing of particle size spectra and state parameter data obtained with the T-28 aircraft platform. NCAR Tech. Note (NCAB./TN-137+1A), 78 pp• Boulder, Colorado, U.S,A.

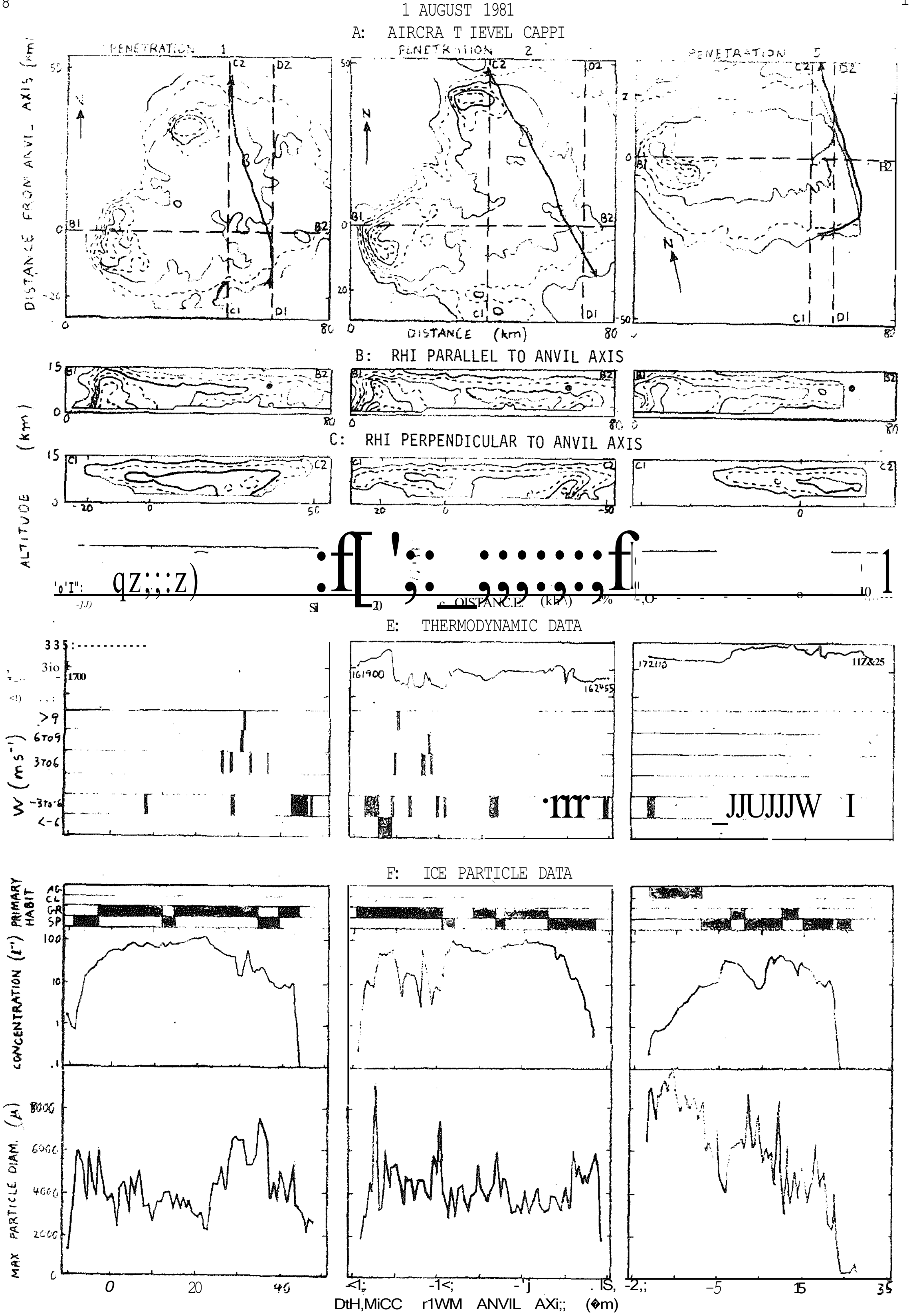

Fig. 2. Summary of the data for 3 penetrations on 1 August 1981.

SJ'UDIES OF DROPLET CONTIUENTAL AHD W,ARITIMB CUMULUS C:LOUD3: FI2LD EXPZRII.IEI'TT AHD IilODBL

N.V. Klepikova, G.I. Skhirtladze
The Institute of Experimental Hetcoroloc;y
Obninsk, USSR

The studies of vra.m convective clouds development have made a possibility to find some important dependences, but it is impossible still now to say hat the processes in convective clouds a.re understood well enough. The Institute of Experimental IIcteorology performs field experiments and numericalrrodeling of cumulu::; clouds. Uodern instrumentation and developments of computers allow to make a detailed analysis of cumulus cloud microphysics and dynamics, to obtain addi,-tional data and verify the resultP found t=a.rlier. The paper giv.es experimental and numerical results for cumulus cloud microphysics. Some parameters of a numerically simulated cloud are compared vrith the experimental data.

The experiments were carried out with the instrumented aircraft IL-14. Cloud drops vmre counted with a photoelectric counter (FEC) (Ref.1). Drop radius range from 0.7 to 40Jtm is divided into 31 channels;their width is proportional to drop sizes. The2 measurement volu, e cross-section S=O.J m. In he automati5 regime at cloud drop concmtration of 10 cm-3 the counter is capable to obtain· statistically representative samples of drops with :r "'-15 .,Mn on the fl:ight-paths 20 - JO m with the same interval between the samples·. When averaging scales are increased large drops are sampled. Then on the basis of the data registe ed on a pinched tape the computer calculates drop spectra, drop mean radius, concentration, relative dispersion and liquid water content. As f= as cumulus cloud microstructure depends on convection motion (Refs.2, 3) the above parameters may be considered separately for regions inside and outside the convective updrafts. Identification of convective updrafts of both zones of increa,sed temperature (Ref. J) and optical thickness (Ref. 4) horizontally more than 100 m was made with a quiclc-response airborne thermometer (τ ~ O.OJ s)and with an optical thickness meter (τ ~ o. 01 s). The records were synchronized with the FEC. Drop spectra were measured in continental Cu in southern.regions of the Ukraine and Moldavia as well as in Iu-U'itime Cu in the Far East of the USSR near the Sea of Olchotsk and Salchalin.

Fig. 1 shows Cu microstructure parameters variation with height within updrafts in continental and maritime clouds. For comparison measurement results obtained in the thickest '(2-4 km) clouds lilte Cu congestus. Cloud heights in Fig. 1 are calculated from their bases. In maritime clouds measurements were made only in the middle and upper parts of Cu clouds.

From Fig. 1 it can be seen that maritime cloud microstructure considerably differs from that of continental clouds. Cloud drop concentration in maritime Cu clouds is several times smaller and mean drop radii larger than in continental clouds. These facts are not unknown in general (Ref. 5), where Squires has shown that these differences are caused by vc1.riations-bet.reen condensation nuclei concert ations. The results obtained are confirmed by the present paper. Drop spectra in maritime clouds are wider as compared to continental clouds. The value of drop spectrum relative disnersion 6/r in continental clouds varied in- the range uf 0.2 - 0.4 and, in maritime clouds -vr.i.-thin O.J - o.6. High values of o/:r in maritime Cu clouds depend on a greater number of both large (r,.. 10 .Mm) ani' fine (:r<J m) drops in these clouds (Fig.2).

The value of O/r if averaged over the clouds is practically constant with increasing the height above the cloud base both in continental and maritime clouds (Fig. 1). In some continental clouds is observed· a significant decrease of o/:r with height over drop spectra within updrafts (Fig.J) (see Ref.4). A slight decrease of tr/:rwith height corresponds to numerical data according to the theory of regular condensation in view. of salinity and drop surface curvature effect on condensation drop growth (Ref. 6). Calculated drop spectra in shape and parameters are in rather a good agreement with the experimental data (see Fig. 2). But the results do not confirm the assumption about increasing relative dispersion of drop spectra with height for maritime clouds (Ref.7). Such a discrepancy may be expluined by the fact that the given paper concerns experimental drop spectra within an updraft and in (Ref.7) the drop spectra are considered for a whole cloud. In "(Ref. 4) it is shown that the relative drop spectra dispersion outside the updrafts may increase with he:ight. In continental clouds local drop spectra were generally (65 :·i) unimodal. Within the updrafts the spectra were mostly unimodal. There were few multimodal spectra in continental clouds observed mainly in2the regions of small-scale (less than 10 m) temperature variations, most probably, in mixing zones. In maritime, on the contrary, more than a half of all the spectra were multimodal even within updrafts (Fig. 2). But the analysis has shown that local maxima in the multimodal spectra occupy in width one channel of the FEC analyser and only in 2 % of cases - two channels. In the amplitude they do not exceed the ranges of drop concentration measurement accuracy in several channels. Besides at increasing the dnp sampling time or at averaging local dTop samples with multimodal spectra in temperature inhomogeneous cloud portion (within an updraft) a mean drop spectrum obtained tend:! to a unimodal one (Fig. 4). At last, not a single drop spectrum, at drop sampling during a flight through a whole cloud, was multimodal. /\.tsuch measurements only unimodal spectra were observed as in continental clouds. On the basis of the results obtained one may conclude that the drop spectra multimodality in maritime Cu clouds is caused not by peculiarities of the clouds but insufficient statistics when obtaining local samples due to a smaller drop concentration as compared to continental clouds. For studying the structure of mesoscale convective fluxes and formation and evolution of warm Cu clouds a three-dimensional physical-mathematical model of moist convection has been constructed. With this model an attempt is made to compare some parameters of numerical and experimental resu ts. The following basic equations and assumptions are used:

dzt.. ftt = CPVolJ i ii fl+a (80 +0.5f n/- ') 'l1tUtJ'+ 1' (1)

iELJ ox. -0, (2)

de att = B+-KM s² -E + f'1;, (3)

1=-;e (1+ æ.ies1 8l1l -;;C Ja:r3) , (4)

KM =∞ e E ,12, (5)

diii dt =Mq; +P<P (6)

where d dt = a at + u tt; aar/ ... J1= 4,Po, r = c w,

<P={ +@: ... 9-(J,9zj,

Here zeros denote the variables describing environmental atmospheric conditions and are the functions of height only, dashed variables mean deviations of the data fro the reference values and are the functions of coordinates and time. We shall give only a short explanation of these equations, the notations for them are standard. The motion equations (1) describing moist convection with the Bllussinesq, and turbulent transport, buoyancy forces with account for drop drag ant pressure forces. It is assumed that the reference pressure satisfies the static state equation. Local variations of r density in time in the continuity equation (2) are neglected. The equation for pressure deviations is obtained by spatial differentiation from the motion equation (1) and by using the continuity equation (2). The equation of turbulence kinetic energy balance (3) is described with account for buoyancy effects (B), shear stress (S^2), dissipation (e) and diffusion ( ) of turbulent energy. An average space scale of fluctuations is given as in (Ref. 8) in the form of (4). The turbulent exchange coefficient as in (Ref. 9) in the form of (5). For describing phase transitions of water and corresponding heat fluxes Kessler's parametrization scheme (Ref. 10) is used. It is assumed that water supersaturation doe not exist and any its surplus condenses a-mediately causing cloud drops formation h specific liquid water constant c. Large drops (z :,,100I'm), so-called "precipitation drops", have specific liquid water, The laws of conservation of energy, water vapor mass and liquid water give the equati n like (.6) where describes turbulent mixing, M - processes connected with crol physical effects: condensation rate (, the rate of coagulation (Az) of those drops with each other turning into precipita.tion ones, the coagulation rat ol PZ"ef cipitation drops with cloud drops \.cz), evaporation rate (£11) and drop sedimentation (Vz). On the er and lower boundaries of the calculation volume stated are rigid and free-slip boundary conditions with zero heat and moisture fluxes. For the lateral surfaces heat, moisture and tangential velocity components have zero horizontal gradients. Normal to the boundaries momentum fluxes through the lateral surfaces may change with time.

To numerically realize the model the finite-difference methods were used with standard spatially staggered mesh. The momentum advective terms in (1, 3) are approximated conservatively (Ref. 11). In (6) a monotonous conservative scheme with upstream differences is used. For calculating time differenc.es the leapfrog scheme with Robert's integration (Ref. 13) was used. A direct method (Ref. 14) is used to solve the equation for pressure deviations. The **scheme uses** spatial grid intervals :r,= 4.:S=300 m, the time steps JI= 5 s, the number of grid nods is 28x28x20.

Initial conditions in the model were stated on the basis of radio and aircraft sounding data for days when the measurements in Cu clouds were performed. The profiles of liquid water content heating in a cloud, its height were found by averaging the measurement results of different clouds at sounding the Cu cloud field. The initialization of convection in the model is simulated by introducing a temperature perturbation.

A comparison of simulated and "averaged" experimental cloud has shown that the height of the simulated cloud base is smaller than that of the experimental one for~200 m. This difference may be considered reasonable as it can be compared with the accuracy of determining the lower cloud boundary in the experiment. The coincidence of cloud top heights is satisfactory (within 100 m). Fig5 gives the results of comparison of some model parameters with the experimental data. Vertical profiles of heating and liquid water content in a cloud (as modeled) are given for the central cloud axis and for 300m from it. The data are compared with the experimental results obtained in the updrafts with the horizontal dimensions of 400+200 m. The discrepancy of experimental data for heating holds between two model profiles. The agreement in liquid water content is worse. The difference of the model data along the cloud axis with the experimental results in heating is 32 % and in liquid water content 50 %. Several reasons of such discrepancies in numerical and experimental results may be found. This can be imperfection of microphysics parametrization according to Kessler overestimating the liquid water content in the model; nonaccount of large drop contribution into liquid water content- calculated over local s ectra in the experiment (is about 80 %); impossibility to guide an aircraft into the zone of maxi mum liquid water content in a cloud, etc., Thus, possibly, can be explained a better agreement of experimental and simulated profiles of liquid water content taken at some distance from the cloud (maximum liquid water content zone).

The intensity of turbulence during the experiments can be estimated on the base of a r-craft overloading and during the experime ts with tracer diffusion. The numerical eddy diffusivity coefficients /(under the cloud are about 20 $m^2 s^{-1}$, at the central axis of the cloud in its lower third they are 40 m s^{-1} and in the upper third they are 100 m s^{-1}. At the lateral boundaries of a cloud the eddy diffusivity coefficient is greater than in the cloud center. This situation corresponds qualitatively to overloading observed on board the instrumented aircraft. The values of K_M obtained with the model are in a good agreement with the experimental data on a tracer (admixtures) diffusion in cumulus clouds (Ref. 15).

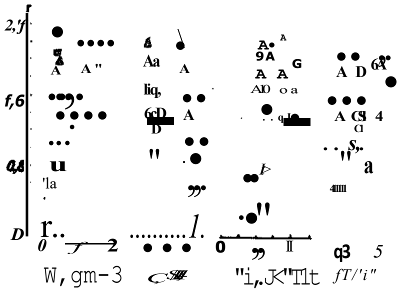

Fig. 1. Vertical trend of microstructure parameters in cumulus clouds (experiment). • - 5.09.77; • - 1.09.77 -(1 case); A - 7.09.77 (2nd case) for continental clouds. o - 2.09.82; D - 3.09.82; 4 - 11.09.82 measurements in maritime clouds).

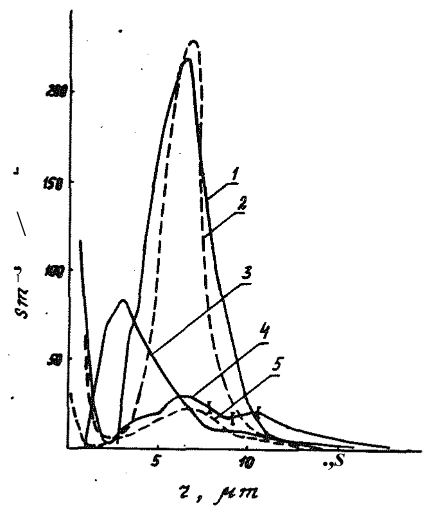

Fig. 2. Local cloud drop spectra within updrafts in cumulus clouds. 1 -measurements in a cumulus cloud, 5.09.77. h - 1.8 km; 2 and 5 - calculated spectra of a continental and a maritime clouds obtained with the theory of regular condensation; 3 and 4 measurements in maritime clouds, 11.09.82 d 3.09.82, h = 2.2 and 1.5 km; I - measurement uncertainty.

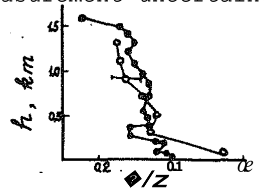

fig 3. Vertical trend 6/z spectra within updrafts of some continental cumulus clouds. o - 2.07.76; • - 17.09.77; I - dispersion of 0/i: •

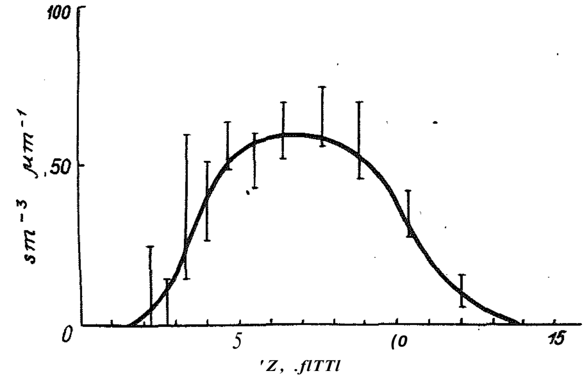

Fig. 4. Cloud drop spectrum averaged over samples within a maritime cumulus cloud. 2.09.82, h - 1.2 km; I - dispersion over local spectra.

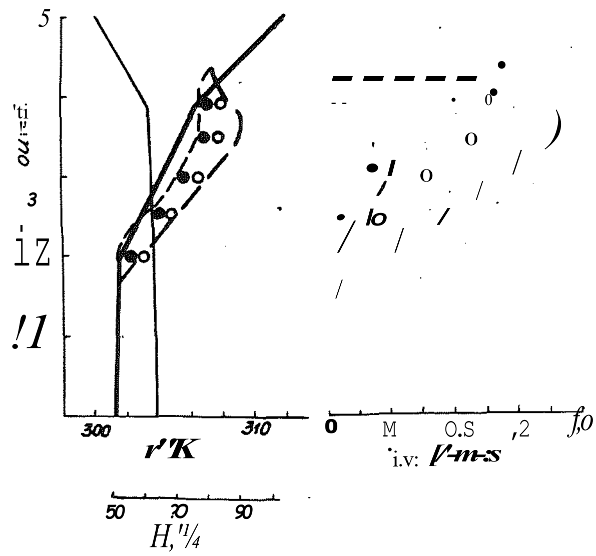

Fig. 5. Comparison of simulated cloud parameters with the experimental data (measurements carried out on 5.09.77, Moldavia). ---and ---- parameter profiles on the cloud axis and at the distance of 300 m from the axis; o and • - are maximum and mean experimentally obtained parameters within updrafts; --- and -- - profiles of potential temperature and relative humidity (radioacoustic sounding).

REFERENCES

1. Alexandrov E.L., Lachikhin A.M., 1978, Airborne photoelectric device for measuring cloud drops. Trudy IEM, 19(72), P. 71-82.

2. Vulfson,H.I., Laldionov,A.G., 1970, Studies of cumulus cloud structure, Trudy VIII All-Union Conference on Cloud pnysics and weather modification, Leningrad, Gidrometeoizdat, P• 22-30.
3. Vulfson,N.I., 1961, Investigation of convective motions in free atmosphere, 522 PP•
4. Skhirtladze1 G. I. , 1980, }.Ieasurement results for drop spectra in cumulus clouds.,Izv. Acad. Sci. USSR, Atmospheric and Oceanic Physics, 16, No. 1, p. 65-72.
5. Squires, P. , 1958, The microstructure and colloidal stability of vm:rm clouds. Parts I and II.Tellus, 10, p.256-271.
6. Alexandrov,E.L., Klepikova,N.V., Sedunov, Yu.s. Some results of cloud droplet spectrum formation modeling,1976,Trudy IE! ,12 (31), p. 19-53.
7. Warner, J. The microstructure of cumulus clouds. Part I. General features of the droplet spectrum, 1969, J.Atmos.Sci., 26, No. 6, P• 1049-1059.
S. Vager;B.G., Nadezhdina,E.D., 1979, Atmospheric boundary layer under horizontal inhomogeneity, Leningrad, Gidrometeoizdat, 136 PP•
9. Mo:nin,A.s., Yaglom,A.M. , 1965, Statistical hydromechanics. Turbulence mechanics, Part I., Moscow, "Nauka", 640 pp.
10. Kessler,E., 1969, On the distribution and continuity of water substance in atmospheric circulation, Meteorol.1':lonography, No. 32, 84 pp.
11. Piacsek, S.A., Williams,C.P., 1970,,i. ComBut. Phys., 6, No. 2, P• 392-405.
12. 198 , Computational Hydrodynamics, l':1oRcow, "MIR" , 61 6 pp.
13. Robert,A.J., 1966, The integration of a low order spectral form of the primitive meteorological equations., J.lcleteorolo ical Soc. Japan, 44, No. 22, p. 23 -245.
14. Williams1G.P., 1969, Numerical integration of the three-dimensional Navier-Stokes equations for incompressible flow, J. Fluid hlech.,Xl, Ho. 4, p. 727-750.
15. Skhirtladze, G. I., Yurchak, B. s., 1979, Measurements of eddy diffusivity horizontal coefficient in cumulus clouds with a raaar, Izv. Acad. Sci.USSR, Atmoslheric and Oceanic Physics, 15, To.2, p. 46-153.

IKTERIOR CHARACTERISTICS OF SOUTI:!EAST MONTANA THUNDERSTORMS

Dennis J. Musil and Regina A. Deola

Institute of Atmospheric Sciences
South Dakota School of Mines and Technology
Rapid City, South Dakota 57701

1. INTRODUCTION

During the spring and sUlll!Der of 1981, the field phase of the Cooperative Convective Precipitation Experiment CCCOPE) was conducted in southeastern Montana. CCOPE is a collaborative effort involving more than 20 organizations and more than 100 scientists throughout the United States and the world. The overall objective of CCOPE is to develop an increased understanding of the precipitation mechanisms in convective clouds of the northern High Plains of the United States. The field experiment resulted in nUlllerous observations from many storms over a wide range of convective scales.

One of the aircraft involved ill these studies was an a:rmored T-28 (Ref. 1) ,, which was used to make numerow; observations of the internal characteristics of thunderstorms. The purpose of this paper is to describe some of the in situ observations ude by the T-28 while participating in CCOPE.

2. DESCRIPTION OF THE DATA S.ET

The T-28 (Fig. 1) has been a valuable platform for making measurements in thunderstorms and hailstorll!S. Systematic storm penetrations have been 11111.de in various projects since 1972, resulting in nearly 500 penetrations. The microphysical instrumentation permits detailed observations and characterization of hydrometeors throughout the entire size spectrum. Other quantities observed include temperature, vertical air 1110tiens, liquid.water concentrations, and turbulence. For this study, observations from 9 days were used, which re$Ultecl in a total of 27 storm penetrations by the T-78.

An arbitrary selection criteria was used to select vertical velocity regions in each .penetration. Updrafts and downdrafts selected for. anal.ysJ:s. haui to occur continuously for at least 5 sec and had to have a peak value exceeding +S .m s-1., respectively, within the draft regions. Thus, we.are

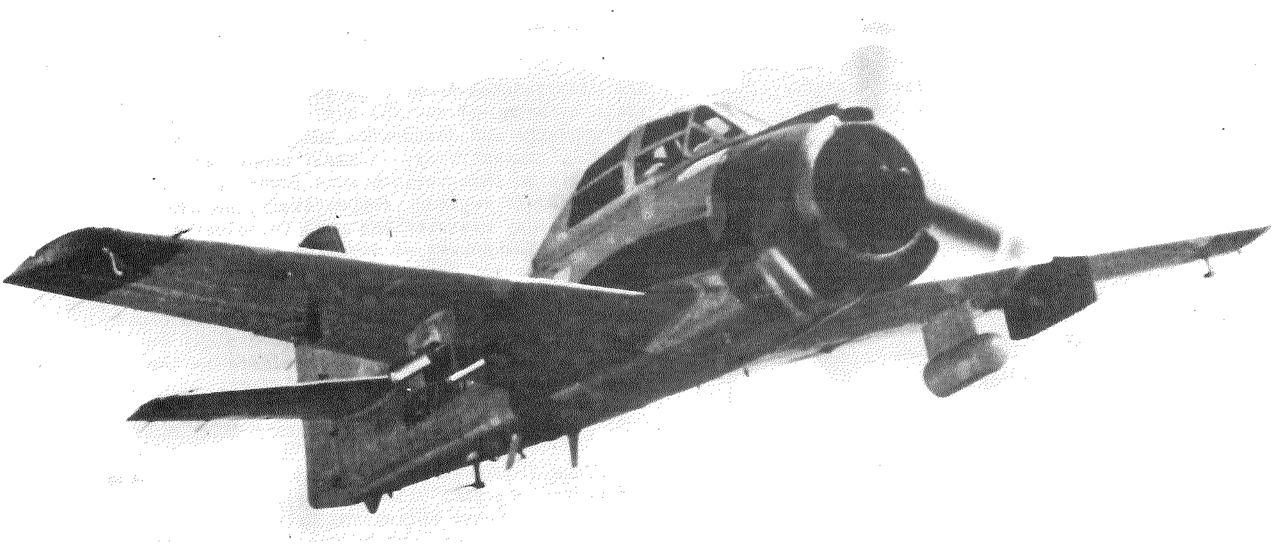

Figure 1. View of af1llored T-28 aircraft in flight. Gamm camera device comisting of 1,/b.ite pod hwing film tZal118port, rotating lllirror and control eZ8ctronica, and black fla$h 1ly8lll U sholin on the aircraft's left wing. The revarse flow temptilratuzoe device (with ezlaU.IJt por,ts) is outboard from the Gamm ca]111hr. The FSSP and flD Particle Meas=ing Systems probes aze s/w,m on the pyZOn of the :ri.ght wing, with the ff>iZ impactor Zocated been the probes. Outboard flom thea,s. instruments are the-angZe-of-attack and the Joh:nson-WZZiams liquid water devices. [Phou by Roger RoulZe - AOPA Pilot lfagazineJ

considering only draft scale Yertical JJlotions with the T-28, as this selection process eliJllinated the small pockets of weak up- or downdrafts. No attempt is made to describe rapid short-te:rm gusts described by several investigators (I{ef. 2}. Considering all the complicated factors inherent in the calculation of vertical velocities, the values discussed in this paper are felt to be within about 10% of true draft velocities.

In this study, a description of the identified vertical velocity regions will be given, as well as the observations cf liquid water concentrations, turbulence, and hail encountered in those regions.

3. DISCUSSION OF -·sSULTS

An analysis of the data gathered in southeastern Mo1.lana by the T-28 has been made. The most important findings are outlined below, although a more detailed discussion of these a. d other aspects of the investigation can be found in a study by Deola !,Ref. 3).

3.1 Storm enviroDlllents

The storms investigated were all mature thunderstorms/hailstonns. Table 1 shows pertinent parameters taken from radiosondes which were selected so as to have been in the inflow regions of the storms penetrated.

The storms exhibited a wide range of instability, ranging between about 0 and -10. The storm on 2 August was particularly unstable and contained some of the largest vertical velocities and liquid water concentrations ever observed with the T-28 system. The storm on 2 August also forms the basis for a detailed investigation of hail growth processes and.is found elsewhere in these conference proceedings (Ref. 4). The other variables show in Table 1 are quite typical for northern !:!igh Plains thunderstorms in the U.S.

3.2 Distribution of vertical velocities

A CUl!lulative frequency distribution of the vertical velocities observed in each identi.f"ied updraft/doimdraft zone for the entire field season is shown in Fig. 2.

TABLE 1: CCOPE sounding characteristics from storm inflow regions.

Date	Temp Cb (°C)	CbMR (g/kg)	Precip ..§E__ (inches)	eE	Stability Index
Jul 12	11.9	12.2	1.41	352.0	-2.6
Jul 13	9.2	10.8	1.27	349.3	-3.7
Jul 19	3.0	7.2	0,84	332.5	-2.0
Jul 21	-4.0	4.9	0.70	328.0	O.O
Jul 22	-1.8	S.4	0.68	329.;0	-1.8
Jul 23	5.7	8,9	0.95	341.0	-5.1
Jul 29	5.5	9.0	1.02	346.0	-5.9
Aug 1	8.3	10.0	0,70	342.S	-8.8
Aug 2	11.7	12.9	1.06	3S4.0	-9.7

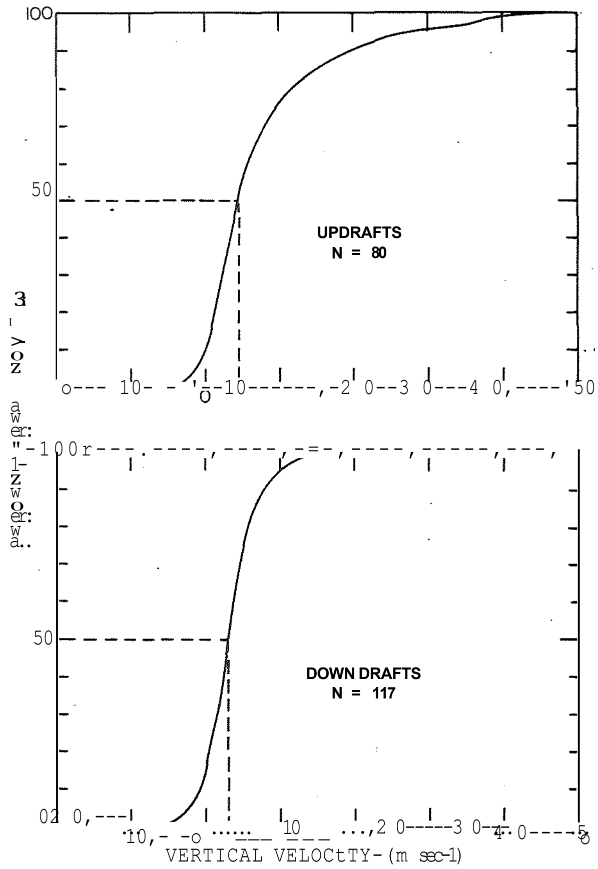

Figure 2. Frequency distribution. of updrafts and downdrafts in id.nt,ified vertical. velocity :regwns for data coZZected with the T-28 syaten, during the CCOPE fu Zd season. The ordinau shows the percent of obsel'Uaticne <vertical-velocities shown on the abscissa.

The distribution shows that the vertical velocities range between -24 and +52 Jlls-1, with the medians for updrafts and downdrafts being. about 4 and 3 Jlls-1, respectively. A small number.of negative and positive observations were found in updraft and downdraft.regions, respectively, because of the arbitrary restrictions used to select the regions. The number of negative observations in the updrafts and positive observations in.the domdrafts represent about 10% of the total observations in each case. Accordingly, the absolute value of the l!ledians shown in Fig. 2 might be viewed as being a slight underestimate in the case of the updrafts and the downdrafts.

3.3 ic..cons.iderations

The cloud liquid water concentration (LWC) in the identified vertical velocity regions was characterized by extrElllle variations between.0.mtd near adiabatic. A comparison between adiabatic and the maxilllllm:.Gbserved LWC in. each region (Fig. 3) shows that l!IOSt LWC observations were well below adiabatic, except for a few updraft regions which were Sall!pled on 1 and 2.August. Most vertical velocity regions hali.negligible obse:r:vations of cloud liquid and are not included.in Fig. 3. The reasons for the low cloud liquid water coDcentrations :may be due to a combination of instrument

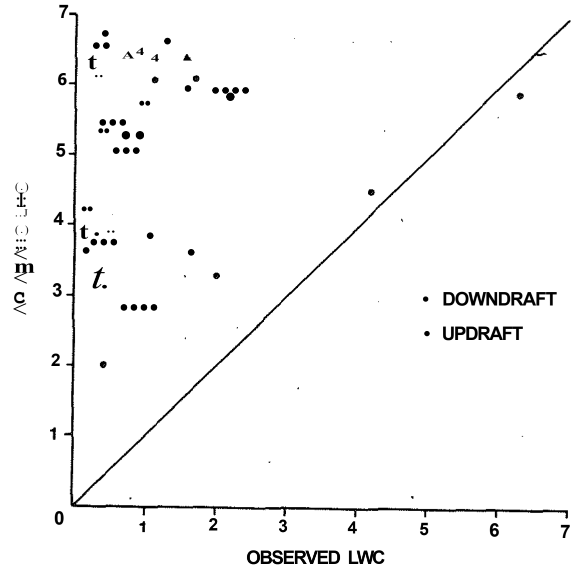

e . . Adiabatic vs. nia:x:imw,z ob,sU'Ved Uquid water concentration for each vertical- vel-ocity region that ccnta:iTU!d cl-oud Ziquid. Regions with negUgible LWC are not pl-otted.

error, mixing, or depletion by larger particles. Continued in.vestigations of these aspects are still underway.

3.4 Turbulence

Observations of turbulence in these storms range from 111Oderate to extreme accordi g to values of the turbulent energy dissipation rate {cm$^{2/3}$ s-^{1}1. Figure. 4 shololS the relationship betllleen maximum vertical velocity and peak turbulence in each vertical velocity region. As might be expected, there is a strong indication that larger storms are associated with more severe turbulence because the larger velocities are .found in larger storms. The correlation coefficients for updrafts and downdrafts were 0.75 and 0.71, respectively. Well organized storms were more turbulent along the edges o£ the larger updraft.regions, while being much less turbulent in the interior regions, which is in agreement with other observations (Ref. 5.). Beyond this general feature, any categorization of turbulence according to its location in a draft region or intensity was all .but impossible because of the extreme variations of turbulence values.

3.5 Presence of hail

A summary of the regions in which hail was observed is given in Table 2. A larger percentage of the updraft regions than dollr.2draft regions contained hail; however, there were substantial amounts of hail located in regions of weak vertical velocities (quiescent) that did not qualify for selection as updraft/downdrrlt regions. .The reason. for this is lmknown, but may be related to the fact that thunderstorm cells are penetrated at various .stages of development. Thus, it is difficult to relate the presence (or size) of hail to such variables as vertical velocity because so many conditions can be present in a given thunderstorm at any given time, and an aircraft is only able to sample .a very small portion of it. As expected, the larger hail was **associated with** the larger storms; hence, larger and **stronger** up- and aowndraft regions.

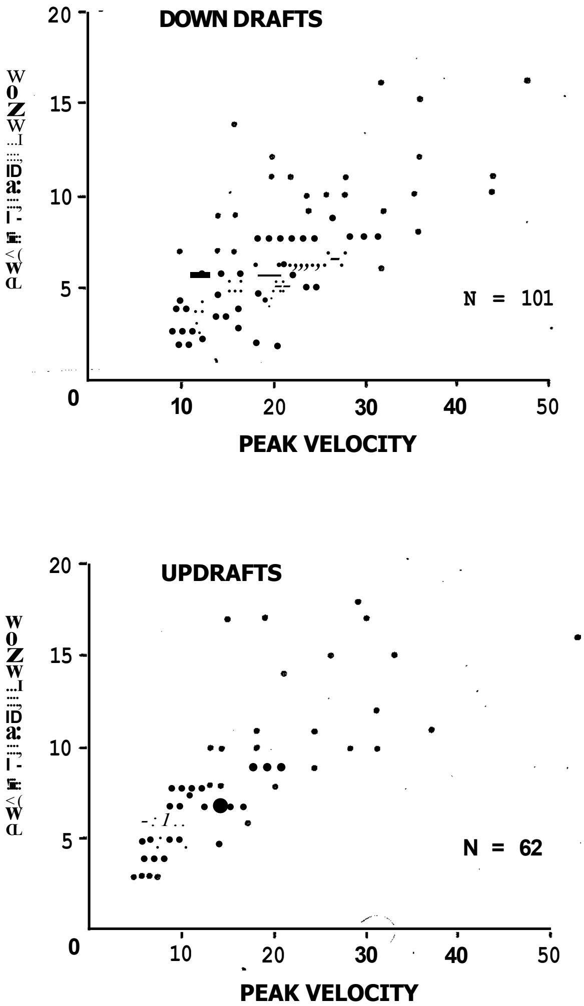

Figure 4. Peak vertical, vel-ocity and aslDX:iated peak tuz,l7u.Zence values for 160 regione of CCOPE ilrr.ta.

4. CONCLUSIONS

Based upon the observations presented in this paper, the following conclusions are given:

1) In general, the Observations in south-eastern Montana.ue quite similar to those obtained in other High Plains thunderstorms observed with the T-28. The sizes and intensities of the vertical velocity regions are quite similar to those found-in other places.

21 Observations of cloud liquid **were** ctremely low, except in two.ye:cy- large, and intense stoz:ms.

.31 A rather strong correlation between vertical velocity and turbulence was found, indicating that at least in a general sense,-1110re extreme values of turbulence can be associated with larger 11102'e intense storms.

4) The presence of hai! was rather random according to the method used to identify vertical velocity regions in this paper•. The technique did not allow for the examination of hail in updraft/. downdraft. COllplets.

TABLE 2: Swmnary of regions in which hail was observed.

!Flight	tl'otal No. Updrafts	No. With Hail	Total No. Dmm.drafts	No. With Hail	No. IOuiescent	No. With Hail
Aug 2	14	**11**	18	12	**0**	
Aug 1	2	1	3	1	0	
Jul 2	16	**11**	27	14	7	4
Jul 2[illegible]	5	5	5	4	3	3
Jul 2[illegible]	5	2	10	6	5	4
Jul 21	7	0	12	1	2	0
Jul [illegible]	**9**	3	16	3	3	2
Jul [illegible]	15	*8*	16	7	8	4
Jul 12	**8**	3	10	3	**2**	1
Totals	80	44	117	51	30	18
% with Hail	55%		**44%**		60%	

Acknowledgment. The research reported here was carried out with the support from the Division of Atmospheric Sciences, National Science Foundation, under Grant No. A'IM-8311145.

5. REFERENCES

1. Johnson G N and Smith P L 1980, Meteorological instrumentation system on the T-28 thunderstorm research aircraft, BuZZ Amer Meteor Soc 61, 972-979.

2. Telford J W, Wagner P B and Vaziri A 1977, The measurement of air motion from aircraft, J AppZ Meteor 16, 156-166.

3. Deola R A 1984, Internal characteristics of southeastern Montana thunderstorms, M S Th£sis, Dept of Meteorology, S D School of Mines and Technology, Rapid City, SD.

4. **Musil** D J, Heymsfield A J, Miller L J and Smith P L 1984, The evolution and transfer of hail in a **severe** Montana thunderstorm, (accepted for presentation at the 9th IntnZ CZoud Physics Conference, Tallinn, USSR, August 1984).

5. **Musil** D J, Heymsfield A J and Smith P L 1982, Characteristics of the weak echo region in an intense High Plains thunderstorm as determined by a penetrating aircraft, Preprints Conf on CZoud Physics, Chicago, IL, Af!er Meteer Soc, 535-538.

EXPERil\llENTAL AND THEORETICAL STUDIES OF THE DYNAMICS AND MICROPHYSICS---OF CONVECTIVE CLOUDS

Vorobjev B.M., Gromova T.N., Dovgalyuk Yu.A., Zinchenko A.v., Klingo v.v., Nikand.rov V.Ya., Orenburgskaya E.V., Sinkevich A.A.

Main Geophysical Observatory
Leningrad, USf''t

During a number of years combined theoretical, laboratory and field studies on the processes of natural and artificial precipitation formation in convective clouds have been made at the Main Geophysical Observatory. Prof. N.S. Shishkin was the head of these studies for more than twenty years. As a result of theoretical studies the fundamentals of the theory of showers have been developed, the regularities of the growth of rain drops and hailstones, as well as artificial precipiration particles, have been studied, the optimal conditions of precipitation formation have been found out /Ref .1/.

At present, to study the process ș of cloud and precipitation formation, steady--state and time-dependent models have been developed and are used in which a convective cloud is cons.idered as axis-symmetrical turbulent jet}Reta . 2-5{.Reynolds stresses were expressed through the characteristics of average motion with the aid of PJ;"an.dlf0rmula for the turbulence coefficient in jet stream. Investrgations were also carried out on specifying the type of turbulent diffusion coefficient using the equation of turbulent energy balance.

The parameters of convective clouds in oceanic tropical regions (GATE area) were studied with the help of the steady-state model. The rawinsonde data: from ships participated in the expedition were used as the initial ones. The results of aircraft and radar observations of clouds were used in the analysis of calculation results. The ranges of typical values of cloud parameters for different circulation zones were found out as a result of the calcuJ.ations. Thus, duxing observation period I inside the developed :rrcz clouds more than 9 km thick prevailed (78%), the mean vertical velocities in 96% of the cases varied from 3 to 7 m/sec. ·Outsid the ITCZ cloud thickness-did not exceed 3 km in 93%, and the mean vertical velocities in 94% were up to 5 m/sec,

Figure 1 presents.the results of calculating the vertical extent of clouds which developed on 6--10 July 1974 over the GATE area•. At that period the passage of synoptic disturbance (easterly wave) was observed. When analyzing the calculation results there were used satellite data, the results of radar and radio sounding from two Soviet shiis .("Professor Vize" and "Professor Zubov") and Canadian ship ("Quad.ra"). In the period under consideration the ITCZ was accompanied by the thick convective clouds and shifted greatly in latitude (see Figure la). Figure la shows that successive crossings of the :rroz a. is took place over the

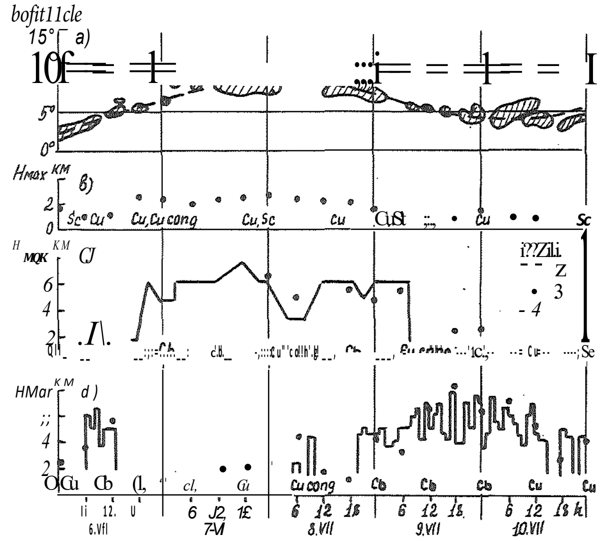

Figure 1. Latitudinal shift with time of the ITCZ position for the longitude of the GATE .area centre - a)and comparison of the calculated and observed heights of convective cloud tops H for the positions of shil;s "Professor fffe" (latitude 9"0O'N) - b); Quad.ra" (latitude 9"15'N) - c); ••Professor Zubov"-(latitude 5"N) - d}
1 - cloudiness according to data obtained by meteorological fixed satellite; 2 - ITCZ a.Jl:is; 3 --calculated data; 4 - radar data.

points of ship positions, the ITCZ passage caused the corresponding increase in convective cloud development in these regions. Figure lb,c,d shows the time variation of convective cloudiness upper boundary that was calculated from radio sounding data (diagnostic calculation) and observed. The ship "Professor Vize" was in the most northern position and, according to the data in Figure la, was only covered by the edge of the cloud field related with the ITCZ, The convective clouds in that area did not reach the stage of precipitation formation and their vertical thick:n ss was not higher than 2 km. This result agrees with calculation results. Figures le and ld show the temporal variation (solid lines) of the height of convective cloudiness upper boundary from radar data. Figure le presents one maximum in the calculated and observed variation of the cloud top height: 7 to 8 July, and Figure ld gives two maxima: 6 July and 9 to 10 July. These maxima coincide in time with the periods of ITCZ passage over the points of corresponding ship moo:r·ings (Figure la is compared with Fugures le and ld). The absence of calculation points in Figure 1c for 6 and 7 July is explained by gaps in the radio soundin5 data for these days, The example shown in the Figure as well as some similar calculations for other periods allow us to conclude that the use of the jet model enables a sufficiently accurate description of qualitative and quantitative properties of convective clouds in tropics.

Using the slice method, the intensity coefficient of the cloud convection Cc) /Ref.5'was estimated in the area under study. It was obtained that at E ;;:,,-l in the tropical sea areas precipitation-forming clouds evolution is observed, while at E.<i cloud develop which do not give precipitation. It is suggested to use, along with t, the microphysical index of convection rate equal to the ratio of cloud water content q, mean in height to the value of q,ci= :2 g/;/J , Its preliminary estimations t•rere made.

Considering that the development of cloud ensembles is typical of the sea tropical areas, the problem has been examined on the cescription of evolution of the ensemble of non-interacting clouds. The scheme has been developed for calculating the parameters of function of cloud size distribution obtained by Plank.

The steady-state jet model was also used to analyse convective cloud evolution in Leningrad area. Figure 2 shows the relationship, obtained from calculation, between the maximum speed of updraft in the cloud· and the cloud vertical thickness,

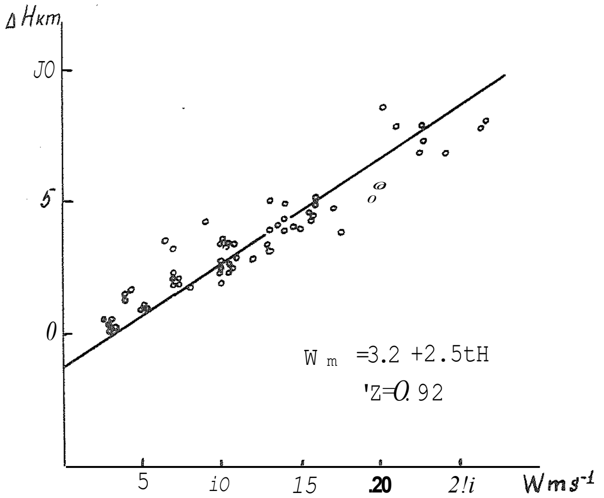

Figure 2. Relationship between the maximum up-current velocity and the vertical cloud thickness.

At present the time-dependent one-and-a--half-dimensional axis-symmetrical model has been developed for a precipitation-forming convective cloud which includes its interaction with the environment due to the lateral turbulent mixing and ordered influx; the precipitation formation process is described in the model in the parameterized form. With the help of this model the study was made of the effect of environment characteristics and the initial overheating of underlying surface on loud evolution jRef.21.Calculation results are given in Table 1. It is seen that the overheating value substantially affects convective cloud characteristics. In particular, an especially sharp change in cloud parameters is observed wnen T increases from 0 to 3°c and wnen R = 1,5km.

The results of the numerical experiments show that the given model can be successfully used both as an instrument for studying convective cloud evolution and for the purposes of forecasting and weather modification.

The experimental studies of convective clouds included studies of the cloud thermal regime using their-radiometer operating in the band of water vapour absorption with the centre 6.3 microns/Ref.6/.The measurements made from the aircraft-laboratory IL-14 have shown that developing cumulus clouds of weak vertical evolution are warmer than the· surrounding air by 0.3-0.4°0 and thick cumulus clouds by 0.5-0.8°0. Breaking thick cumulus clouds are cooler than the surrounding air by 0.2-0.3°0.

To include the microphysical and electrical characteristics into the numerical model of clouds, it is necessary to study the elementary processes of ph.ase and microstructural transformations of cloud elements ahd the accompanying electrical processes in laboratory /Refs, 7, 8/.

To study the behaviour of single water drops, old cooling thermal and baric microchambers were modified and new ones were created having the volume 0.1-1 , the design and volume of which were determined in each case by the problem stated. The study of freezing of water drops and the solutions of matters included in the composition of condensation nuclei which was made in small chambers has shown that the character of drop freezing depends on temperature, pressure, the environment humidity ·and the presence of admixture in it, The intensive evaporation of cloud particles under the conditions of low pressures and high humidity deficits occurring, for example, at the boundary of a convective cloud with the environment leads to their freezing even at positive air temperatures {Ref.81The freezing is accompanied by escape of ice particles or deformation and subsequent break of drops; in this case water drops acquire the charge equal to (2-5)• .•10-14coul. The separation of fragments in the process of freezing results in the increase of charge by an order of magnitude. The experiments have shown that water drops are charged mostly negat.ively when freezing, while the drops of the solutions of all matters studied (NaCl, KCl and others) positively; in this case the values of charges appearing in the process of water drops freesing are always higher than in the case when solution drops freezern. t.7/,The absolute value of the negative charge increases .with the decrease of the solution concentration and at some value of the concentration (10- -10--tl) it becomes higher than the ab-

Table 1

Maximum values of macrocharacteristics of the clouds as a function of the heat source power T with different cluud radius.

R :	T ∞	t min											
		20				40				60			
km		W m/s	H km	TV grad	°/00	W m/s	H km	TV grad	°/00	W m/s	H km	TV grad	"/00
	0	3.9	0.4-	0.77	0.56	4.7	1.0	0.39	1.04-	5.2	1.4	0.95	1.31
	1	6.0	0.6	1.27	0.35	7.3	1.6	1.37	1.58	7.8	2.4-	1.36	1.99
0.5	3	8.2	0.8	1.76	1.07	9.7	2.2	1.79	2.01	9.7	3.4	1.79	2-?.7
	5	9.8	1.0	2.n	1.24	11.0	2,6	2.11	2.20	11.0	4.o	2.11	2.31
	0	5.0	0.6	1.09	0.87	7.3	1.6	1.46	1.76	9,4	2,8	L52	2.62
	1	7,8	1.0	1.77	1.24	11.6	2.6	2.15	2,61	13.5	4,4	2.13	3.56
1.5	3	10,6	1.0	2,46	1..51	15,8	3.4	2.75	3.34	16.7	5.4-	2.75	4,02
	5	12.2	1.0	2.88	1.50	18.1	3.8	3.20	3.56	18,9	5.6	3.20	4,14
	0	5.4-	0.6	1.19	0.92	8.6	1.8	1.74	2.07	12.0	3.6	1.83	3.36
	1	8,4	0.8	1.,97	1.32	14.3	3.0	2,58	3.22	17.6	5.4-	2.56	4.85
5.0	3	11.5	1.0	2.73	1.62	19,8	4.0	3.30	4,18	22.2	6.0	3.30	5.37
	5	1L!-.7	1.6	3.4-4	2.09	24.7	5.0	3.34	5.0	25.3	6.2	3.84	5.64

solute value of the positive charge, approaching the values typical of freezing distilled water drops. Corona charges increase the ionization intensity by 2-3 orders of magnitude as compared with the ordinary process related to the effect of radioactivity of air and cosmic rays. Drop freezing in the corona discharge field occurs at much higher temperature (-3 •••-4 °0) than in the absence of corona discharge field (-15 •••-17 °0). The effect of corona discharge on the temperature of solution drops freezing is smaller•.

Along with experimental and theoretical studies of the dynamics and microphysics of convective clouds, since 1975 the Main Geophysical Observatory has carried out studies on estimating resource clouds in different areas of the USSR/tfei:-;.9/.The aim of these studies is to determine regions which are most promising for artificial rain stimulation for the national economy (forest fire extinction, agriculture fields irrigation etc.). The ground meteorological observations.of clouds and rain are the initial data for estimating. As a result of the analysis the data have been obtained on the space and time distribution of resource convective clouds over the J:IBFSR regions with extended forests, as well as in some regions with moisture deficit, The areas most promising for artificial rain stimulation have been determined.

REFERENCE

1. Shishkin-,N_0S. et al 1982, Theoretical studies'of processes of the natu.raf::-ana artificial formation of precipitation, Proc of the 5th All-Union Meteorol Congress. Leningrad, Gidrometeoizdat, 4.

2. Baranov,V. G, and Dovgalyuk,Yu,A, 1983, Preliminary results of the numerical modelling of non-stationary cloud convection. Trudy GGO 469, 12-21.

3. Bekryayev, V, I., Dovgalyuk, Yu.A, and Zinchenko, A. V, 1978. Determination of some properties of a convective clouds ensemble using aerological sounding data. Trudy GGO 405, 3-9.

4. Zinchenko,A,V, 1981. A model for shower and hail development in the .single-cell cumulonimbus cloud. Dep VNIIGMI-WDC 95, D-81, 25.

5. Dovgalyuk Yu.A, Kuchinskaya T,F. and Orenburgskaya,E.V. 1979. dn the estimation of cloud convection intensity in the Eastern part of the Tropical Atlantic, Trudy GGO 420, 33-38.

6. Sinkevich,A,A. 1981. On the problem of temperature distribution in the thick cumulus clouds turned into cumulonimbus clouds. Trudy GGO 439, 102-109.

7. Nikandrov, V.Ya. 1981. A meteorological aspect of electrification of a co:iwective cloud. Leningrad, Gidrometeoizdat, 42.

8. Burchuladze, N, N., Gromova, T. N., Nik:androv, V. Ya., Pershina, T, .A., ShishkinJ N, S, 1982. Experimental studies of the role played by freezing and destruction of cloud elements in electrification of a convective cloud, Trudy GGO 457, 141-148.

9. ZamiralovaiV.l, Orenburgskaya,B,V., Uglanova,T,L, 98;,. On the frequency of conditions favourable for artificial inducement of precipitation in fire-dangerous regions of Yakutia and Kamchatka, Trud;}r GGO 468, 94-101.

480
IV-3

SESSION V

NUMERICAL SIMULATION OF CLO.UD FORMATION PROCESSES

THE INTERNATIONAL CLOUD MODELING WORKSHOP - RESULTS OF THE PLANNING SESSION

B. A. Silvennan
�ureau of Reclamation
Denver, Colorado, 80225 USA

L. R. Koenig
World Meteorological Organization
Geneva, Switzerland

and

G. B. Foote and T. L. Clark
National Center for Atmospheric Research
Boulder, Colorado, 80307 USA

ABSTRACT

The World Meteorological Organization is conducting an international cloud modeling workshop to promote constructive interaction between scientists wo·rking on theory and those working with observations, and thus to encourage the development and use of cloud models in research and application roles, especially as related to weather modification. The planning session was held October 3-7, 1983, in Colorado, U.S.A. and the workshop itself will be held in Europe in 1985. The results of the pla_nning session and plans for the workshop are discussed.

Keywords: Weather . Modification, Cloud Mode1s, Microphysical Parameterizations, Model Verification, Model Sensitivity.

1. INTRODUCTION

During December 8-12, 1980 the WMO (World Meteoro1ogica1 Organization) convened a pane1 of experts to consider the uses· of numerical models in weather modification research and operations (Ref. 1). One of the recommendations of the panel was that the WMO conduct an international cloud modeling workshop as part of its weather modification programme. A primary goal of the workshop s_hould be to promote constructive interaction between scientists working on theory and those working with observations and thus to encourage the development and use of cloud models in research and application roles, . especially as related to weather modification. The workshop should feature intercomparison of models and, on the -basis of selected sets of data, comparisons between model predictions and verifying observations. The Bureau of Reclamation, U. S. Department of the Interior had conducted a similar workshop in• 1976 (Ref. 2) for a set of models in .existence at that time, primarily one-dimensional and two-dimensional cloud models. Therefore, in 1982 the senior author was asked to assist the WMO in organizing and conducting the international workshop.

At the outset it was p1anned that the international cloud modeling workshop would be conducted in two phases, a planning session and the workshop itself. During the planning session, which was conducted from October 3-7, 1983 in Aspen, Colorado, U.S.A., potential participants in the workshop met to define the scope, content and procedures for the model experiments. During the workshop, which will be conducted in Europe during the Summer 1985, the resulf� of these model experiments and their ramifications will be discussed. The workshop will consider cloud models of all dimensions and scales that are capable of simulating precipitation processes (wann and/or cold) or predicting precipitation amounts.

The present paper discusses the results of. the planning session and the plans for the workshop.

2. THE PLANNING SESSION

The planning session was conducted in two pq.rts. The first part focused on a review of current knowledge of natural and artificially modified precipitation development from both an observational and modeling perspective. General themes of the discussion included ice evolution and hydrometeor development, entrainment and mixing, nuclei and seeding agents, and mathematical frameworks and parameterizations. Invited observtionalists who have been associated with recent field investigations summarized the basic characteristics and properties of the clouds they investigated and presented their view of the state of knowledge on the above topics. Then the mode1ers summarized the purposes and results of their on-going model investigations including information on the characteristics of their models, model strengths, weaknesses and problems and their views on the state of knowledge on the above topics. Finally, modelers and observationalists interacted in the second part and discussed mutual needs for advancing the science, identifying several areas of model experimentation that would further the development and use of models in research and application roles.

A total of 39 scientists representing 23 organizations from 9 countries participated in the planning session. Observationalists discussed the results of field studies conducted in Spain, 2 areas in Australia, and 5 areas in the United States. Modelers discussed their investigations with 1-D, 2-D and 3-D cloud models and other studies ,;ncluding parameterization schemes, grid nesting, advection schemes and new mathematical frameworks. Finally, a set of model experiments for the.workshop was identified.

3. RESULTS OF THE PLANNING SESSION

The discussions of the current research dealing with cloud and meso-scale atmospheric phenomena exposed ,nore questions than could be effectively addressed by the planning session. A sub-set of issues were identified and grouped into the following three categories:

(a) Model verification against observations
(b) Sensitivity tests
(c) Application of models to increase physical understanding

3.1 Model Verification Against Observations

Models are commonly constructed with the purpose of simulating certain characteristics of the atmosphere. The confidence one places on the predictions (the "output") of these models commonly is proportional to the ability of the model to match nature. Generally, the greater the fidelity of the model with regard to the greater number of cloud and environmental parameters, the greater is the confidence in model outputs. Therefore, examination will be made of how well the various models simulate nature. The primary test quantity will be the prediction of the amount and rate of precipitation. ·This, plus other cloud parameters will be ·compared against observations of nature and against other model outputs with the view to determining reasons causing variations in models. This exercise will provide an opportunity to test the model's response to both natural and seeded conditions and the breadth of the differences between natural and seeded conditions should provide some indication of the consistency of the models with regard to the prediction of changes in precipitation brought about by seeding. The experiments should also contribute to development of the tools for quantitative precipitation forecasts. Experiments dealing with convective and orographic clouds were recommended.

3.1.1 Experimental Approach. Both open (confirmation information supplied) and closed (blind) data sets were recommended. Open sets would permit examination of how well a model could be forced to simulate nature. Closed data sets wou1d permit examination of the ability of the model to predict nature.

Open data sets, i.e., those which contain the observations to verify the fidelity of the model, will be used to change adjustable parameters within the models to optimize them so that the model replicates the observed conditions as closely as possible. This exercise will permit comparisons of the model outputs under ideal circumstances. Through these comparisons and knowledge of the nature of the optimization needed, information on the critical and sensitive aspects of the models should be obtained.

Closed dota sets, i.e., those which contain the· initial conditions necessary to run the model but not the observations to verify their output, should provide information on how we11 the models predict cloud characteristics. It was recommended that the closed data set be from the same area and season as the open data set. This would justify the use of the optimized adjustments from the open set with the closed (blind) set.

In order to examine the response of various models to a given starting perturbation, it was considered useful to specify a sta·ndard pulse for use on each data set.

3.1.2. Model Experiments. Four convective situations were proposed for one experiment:

(a) all warm cloud with rain
(b) maritime (mixed phase precipitation process)
(c) continental (all ice precipitation process)
(d) hai1

The number of cases wi11 be reduced in order to maintain a focus that will permit useful intercomparison of models in a few data sets. In addition, at least one case involving cloud seeding will be included.

The second experiment would be primarily to test the ability of a model to simulate the evolution of the microphysical properties of a cloud. The emphasis would be on ice-phase microphysics and an orographic situation is recommended in which the flow field is dominated by forced rather than convective lifting. Flow fields will be provided either from field data or from the output of an appropriate model.

3.2. Sensitivity Tests.

Sensitivity tests provide information on the dependence of the model to changes in input values or in the ways in which the model is internally constructed. The sensitivity of a perfect model would mirror the sensitivity of the atmosphere to the change made. Two types of sensitivity studies were proposed: (a) fluid dynamics, and (b) topics related to the mathematica1 architecture of the models. In all these experiments open data sets are recommended. Comparison of model behaviours would be carried out at the workshop.

3.2.1. Fluid Dynamics Tests. The first series of these experiments deal with the effect of the initialization technique on the outcome of the simulation. Many models of convective clouds impose a somewhat arbitrary energy perturbation to initiate convection. Experience has shown that the evolution of the simulated cloud is initially dependent on the perturbation. In some cases this memory of the perturbation remains throughout the simulati.on, in other cases, the characteristics of the initiating perturbation. The purpose of this experiment, is to examine the effects of the perturbations of various sizes. The sensitivity of a given model to a range of perturbations should be established. These sensitivities could then be used as a basis for inter-model comparisons. It would be particularly useful to examine the performances of several models initialized in identica1 manners.

Three situations were proposed: (a) initialization by boundary layer convergence (forced lifting; the assumed reference), (b) bubble in the form of energy or its equivalent (heat, moisture, momentum, etc.), (c) a combination of (a) and (b).

The second experiment in this series deals with information that becomes available if a finer resolution grid were employed. Commonly, numerical models need large passive domains and have low resolution within the cloud itself. The entire idth of the, cloud may occupy at most five grid inte.rva1s. Finer reso1ution (about 30 grid interva1s) should permit greater fidelity in the model, but at greater cost of computer resources. Additional studies are also possible using finer resolution. Two studies were proposed: (a) the sensitivity of dynamics to the formulation of the microphysics; and (b) processes of entrainment/ detrainment at the cloud boundary and internal mixing.

The sensitivity of the dynamical properties of the cloud to the microphysical characteristics is directly related to the question of the degree to which the dynamics of a cloud can be manipulated by changes in the microphysica1 processes. Dynamical properties are believed to play the dominant role in cloud and precipitation development. If the dynamics are influenced by 11\lcrophysics, this may be an effective way to effect changes in precipitation. Sensitivity tests should include systematic changes in the rate of conversion from c1oud (non-precipitating liquid) to precipitating drops, the rate of conversion of liquid to ice and changes in the treatment of the fall of hydrometeors. Accounting for the gravitationa1 separation of hydrometeors has proven difficult and the last topic should provide information on model sensitivity to this formulation. It should also provide information on effects of changes brought about by seeding for substantial differences in fall velocities of liquid and ice hydrometeors commonly exist.

Debate continues concerning the location at which clear air from the environment is e.xtrained within clouds. The substantially uniform ("top hat") composition of clouds in their early growing stage is not well matched by many cloud models, apparently due to the coarse resolution employed and inadequate replication of the internal mixing within clouds. The finer resolution experiments are recommended to study the effects of different gtid intervals on the simulation, the importance of the resolution of different scales of motion, and in particular to explore the possibility that the finer resolution will lead to new insight on the entrainment and mixing processes.

3.2.2. Model Architecture Tests. The second type of sensitivity experiments concerned the mathematical architecture. of the model, these might include:

(a} variations in numerical schemes (for example: Smolarkiewicz's scheme)

(b) formulation of equations (for example: entropy formulation, filtering methods, anelastic vs. non-anelastic, etc)

(c) focusing techniques, (for example: stretched or nested grids).

3.2.3. Experimental Afproach. The value of the sensitivity tests wi1l be increased if the input data are common to another experiment being carried out for the workshop. Some of these tests require substantial computer resources and it is likely that relatively few participants would carry out these experiments. However, with input data common to other aspects of the workshop, it will be possible to gain much more benefit than if a unique data set were used.

Data sets for the sensitivity tests will be from days in which cumulus congestus or small thunderstorms develop. The experiment on the retention of the memory of the perturbation shotild include two sets, one in which the outcome is strongly dependent on the perturbation and another where it is not. The finer reso1ution studies requires only on2 input data set. However, tests from simiJar n;,tural and seeded situations might shed light on tne effects of seeding. The experiment on the mathematical a.'chitecture requires only one input data set.

3.3. Applications of Models To Increase Understanding

An ultimate goal in creating cloud models is to use them as a tool in the analysis of field data. They should serve to help formulate and evaluate concepts. The objective .of this cat-egory of experiments is to examine a given domain by the combined use of analyses of both observations and model output to assemble a comprehensive description of air motions, cloud and precipitation. The models are to be combined and compared with observations and will augment them. Two field data sets were recommended. One from a convective situation that produced 1arge cumulus congestus, another from a nimbo stratus situation.

Interaction between field observers and modelers will be necessary to reach the objectives of this series of experiments. If this occurs, one of the major objectives of the modeling workshop will be achieved.

4. WORKSHOP PLANS

Following the planning session, specific data sets were identified for all the recommended model experiments. Data sets from the GATE, HIPLEX, CCOPE, NHRE, FACE, SCPP, COSE and Canary Islands Program were selected. Not al1 data sets are complete with respect to initialization and verification information as specified at the planning session but all should serve the purposes of the model experiments. The data sets have been incorporated into a data cata1og which wi11 be made available to prospective participants of the wor.kshop.

The workshop wil1 be conducted during the Summer of 1985 in Europe. Anyone wishing to participate can obtain a copy of the data catalog by writing to Dr. Bernard A. Silverman, Bureau of Reclamation, Code D-1200, PO Box 25007, Denver CO 80225 USA. It is not necessary to have attended the planning session to be eligible to participate in the workshop.

Copies of the WMO report on the planning session and informal copies of the extended summaries of the presentations by the observationalists and modelers at the planning session can be obtained by writing to the WMO Secretariat.

Acknowledgments. All that is described in this paper resulted from the hard work and stimulating constructive discussions by the participants of the planning session. Credit for all the material comprising this summary goes to all participants. A special thanks goes to Renate Colloton, Bureau of Reclamation for her handling of the workshop correspondence and announcements, to Vonda Giesey, NCAR Conference Coordinator for her handling of the logistic arrangements for the planning session and to Carol Brown, NCAR for her efforts as workshop assistant. A special thanks also goes to the National Scientific Foundation for their financial support of the planning session.

5. REFERENCES

1. World Meteorological Organization 1981, The uses of numerical models in weather modification: research and operations, Precipitation Enhancement Project Report No. 24,

2, Silvennan, BA et al 1976, Comparisons of cloud model predictions: A case study analysis of one and two - dimensional models, Proc. International Conf on Cloud Physics, Boulder, Colorado July 1976, 343 - 348.

SESSION V

NUMERICAL SIMULATION OF CLOUD FORMATION PROCESSES

Subsession V-1

Sirnulation of microphysical processes

THE !-:.OE OF LOW DE!liSITY RINI!liG GROWT!:i IK HAIL PRODUCTION

Richard D. Farley

Institute of Atmospheric Sciences
South Dakota School of Mines and Technology
Rapid City, South Dakota 57701

1. INTRODUCTION

One aspect of the hailstone growth problem which has received increased attention in recent years is assessing the mportan e 0£ low density rIl!Ung growth in the production of hail, particularly in the generation of hailstone embryos. It has become quite evident that the general assumption of high particle density is not valid for much of the growth history of an ice particle, particularly for those continental clouds which produce precipitation primarily through ice processes without undergoing a significant collision-coalescence process.

In his classic treatise, Ludlam (Ref: 1) assired the rime density deposit a value of 0. 3 g cm- during dry growth. This value was based on a number of studies, chief among them being the observations taken at Mt. Washington (Ref. 2). These studies showed a wide variation in rime density ranging from O. for clear ice to 0.2 for feathery ice, the variation being dependent on the ambient temperature, air speed, liquid water content, and sizes of the droplet and ice particle. Ludlam[1]s model was not particularly sensitive to the treatment of dry growth, since wet growth dominated the particle growth history due to the high water contents assumed.

Ti,e laboratory work of Macklin (Ref. 3) has shollll IL,t the density of the rime deposit can be expressed as a power law involving certain growth parameters. According to Macklin's formula, the riming density increases with increasing cloud droplet size, ice particle surface telllperature, and impact velocity. In spite of tnese studies, and perhaps influenced by the dominance of wet growth in Ludlam's study, much of the modeling work -Of the 1960's and 1970's abandone<l the role of low density rime deposits and generally assumed a ·uniform high density.

The work of Pflaum and Pruppacher (Ref. 4) provided verification of Macklin's basic functional form for the density of the rime deposit, although the low density por ion of the relationship was refined to reflect their data as well as other experimental findings (Ref. 5). As has been pointed out by P£1= (Ref. 6), allowing variations in particle density, in turn, allows for variability in terminal velocity and cross-sectional area per equivalent mass, which can be of crucial importance relative to particle growth history and growth times, especially for storms without a significant collision-coalescence process. The va:iable riming density may also be important in the development of such radar observed features as weak echo regions and vaults.

This paper reports the results of a cloud :modeling study which incorporates the physical factors controlling the riming density in a dynlllllic cloud :model with discretiz.ed·treatment of the graupel/hail size distribution. Comparisons are made between cases in which the .mass-diameter relationship is fixed, based on assumed particle densities rui.d cases in which the mass diameter relationship is allowed to vary in accordance with current growth environ:ment and past growth history.

2, MODEL DESCRIPTION

The theoretical framework for this study is a two-dimensional, time-dependent, slab-symmetric cloud model which covers a domain of 20 x 20 km in both x and z directions with 200 m grid intervals. This model has been used previously to simulate long lasting clouds, to compare simulated hail characteristics with actual data, and to test hail suppression concepts (Refs. 7-9). A density-weighted stream function has been used to extend the model to deep convection. Atmospheric motion, potential temperature, water vapor, and the various classes of hydrometeors are the primary dependent variables in the set of nonlinear partial differential equations which constitute the model. Details of the hydrodynamic equations for this deep convection model can be found in Chen and Orville (Ref. 10), whereas derivation of some of the cloud physics equations can be found in (Refs. 11-12).

For this model, the rain, cloud water, and cloud ice are treated by bulk water parameterization techniques, while the precipitating ice field is discretized as 20 size categories. Production of cloud water, cloud ice, rain, and precipitating ice are simulated in the water conservation equations. Cloud liquid and cloud ice travel with the airflow, while rain falls out with mass weighte terminal velocities. Precipitating ice particles may be generated by the probabilistic freez.ing of raindrops and/or via a crude parameterization of the Bergeron-Findeisen process which converts cloud liquid to precipitating ice (Ref. 12). Evaporation of all forms of cloud particles can occur and the melting of frozen particles is simulated.

Growth of the precipitating ice particles is based on wet and dry growth concepts applied to the continuous accretion process (Ref. 1). Determina.tion of the proper growth mo e is based on the equilibrium temperature of the ice particle SlfXface (Ref. 13). This equilibriUE te:mperature allows no heat storage within the ice particle so that the heat gains and losses from the conduction/convection, sublimation/evaporation, latent heat, and sensible heating terms must be exactly in balance.

The model treats a distrib11tion of ice particles evolving in, and interacting with, a time dependent· dynmc framework. For our purposes, the growth rate is used to determine changes in the number ,'ensity of the ice particles per category, per grid point, instead of tracing the history and traj ectcry of 2..1,individual **g:rowing** particle, It srould be empi1asized that the precipitating ice categories co not interact as is the case, £or exrutple, in the modeling of stochastic coalescence, Rather, discretL,ation of t!le spectra is employed here to allo'AC differential transport, generation, and growth of the ice spectra,

This study employs 20 logarithmically-spaced :mass size categories to represent the precipitating ice particle spectra at any grid point, but cowpares cases in which the mass-diameter relationship is fixed based on a priori assumed partic:e densities, as in earlier work (Refs, 7-9), to cases in which the Eass diameter relationship is allowed to float, varying in accordance with the mean particle density per category deduced from past growth history and the density of the current growth deposit, For the fixed density (FD) scheme, the sizes range from approximately 100 J1l1lto 4.5 cm diruneter, with the first six categories **allowing** the density to increase from 0,35 to 0,85 g —3 with larger particles having a density of 0.9 g c:a:-3.

The variable density (VD) scheme is **i1llplemented** by carrying an additional discretize field variable, the mean particle density per category. This scheme requires the mxing of populations of particles of dissimilar densities, the calculation of the density of the newly collected deposit frcm differeut sources, and the calculation of the nei, me2..1, density fol::.owing growth and interpolation back to the fixed system of mass spectral points. All of these combining operations employ the **mass-weighted** mean of.the sum of the individual contributions.

l:uring dry growth, the density of the dep,osit created within a time **step** is taken as the mass growth rate weighted mean of **the** sum of the individual mass contributions arising from the collection of other types of hydrometeors and the mass contributed by the vapor transfer term. The density of the deposit contributed by cloud **liquid** is calculated wSing Macklin's formula (.Ref, 3), assuming that the impact velocity (a **complexly varying** quantity) c,m be represented by the **terminal velocity.** Collection of rain is assumed to result in a high density deposit (0,9 g cm-3). The vapor diffusion tel7-1 is assumed to act at the current particle density, and the deuosit due to cloud ice is assumed to be that appropriate for .:randomly packed ice crystals (Ref. 14).

The weighting schemes used to calculai:e the density of the total deposit and the particle density following **2rowth** are essentially the same as used by others (Refs. 1 and 13). Ice particle fall speeds are **computed** in the manner of **Xu (Ref**, 13), **although** this procedure (based on data for smooth rigid spheres) **may** overestimate **the** fall speed (underestimate **the** drag) for **low** ctensi·ty pa:r-cicles.

The low density ice deposit formed in the dry growth regime provides a porous structure which may retain some of the excess water encountered in **the wet** growth regime. This provides a means for increasing the particle density, as well as allmdng increased growth beyond the strict wet **growth** amount, As implemented within the model for the VD scheme, the growth rate actually applied in the wet growth regime is **dependent** on the particle densitr, with the density of the deposit **being** 0.9 **g** cm-j in all situations, If the current ice particle density is greater than 0.8 g C1lJ-3, the strict **wet** growth rate is applied, whereas for particle densities less than Q,5 g cm-3, the dry growth rate is aDDlied. In the interiill range, the actual growth r;te assu.med varies between the strict wet gro.,wth rate and the dry growth rate, depending on the trajectory of **the** particle and an estimate of the tiille available for £reezing compared to the time required to accomplish the freezing (Ref. 15).

ivielting is assumed to result in no chaz1ge in particle density, although realistically, this regime should also allow for redensification of the particle due to retention of some of the melt water within the porous ice structure. The odel in its current fonn does not al lo;,t for mixed phase particles

3. RESULTS

The **model** simulations conducted for 1:nis study have concentrated on a particular supercell hailstorm from the National Hail Research Experiment (NHRE), this being the Fleming storm of 21 June 1972 (Ref. 16). Earlier studies with the FD form of 1:he model (Ref. 8) **compared** model results and observations, **indicating** :many areas of ·agreement, although several importru.tt features were not properly simulated. **Among** the major areas of agreeTcent **between** the **model** results and observations were the characteristic sloping updra£t and moving gust front, the rounded dowe cloud top, the radar overhang and the intense precipitation cascade, ar,d the therwodynamic structure of the subcloud region. Characteristic interrelationships of updraft, liquid water, and precipitation content consistent witn measurements from penetrating aircraft were also predicted, The model s·mulations also produced pedestal 2..1,dshelf type clouo:s, although these were transitory rather than persistent ,,atures. The maj o:r observed features which were L ,dequately simulated were the persistent bounded **weak** echo region, the high concentratiorr of giant hail and; in association with this, the iligh radar reflectivity values (model generally 5-10 dBz **low)**.

The current study involves four basic cases, the fixed (FD) a.nd 1;ariable density (VD) schemes applied to both rain active (RA) 2..1,drain inhibited (RI) sinmlations cf the Fleming storm. The R.A. cases al2.ow all potential :rain production terms; whereas the RI cases were n m with the para.ueterization of the collision-coalescence (autoconversion) process suppressed and by assuming that excess "tfate:r not retained. during wel: growth is shed as small cloud droplets rather tha.'1 as precipi-cation-sized drops. The RP. :..:ases require more time to develop the severe star.ill couplet ch.aracteristic of the Flelilng storm simulations; this is due to th.e ea::lier development adci f21 l.out of precipitation (mainly rain) I12 the developing stage of the storm, The larger scale features are very si..milar for the FD atld VD cases, although the VD cases generally **produce** more rain and hail reaching the ground **and** produce clouds with sligl:tly more active dynamic clia.racteristics, including maximum updraft strength, cloud top height, and speed of movement of the gust front, Figure 1 illustrates the strong similarity in **the** larger scale features for the FD and VD schemes applied to the R1 cases, which are considered 1:0 **be** more representative of precipitation development in the litlFE clouds than the RA cases.

Domain-tille integrals of the various production terms are quite similar for the FD and VD schemes. Accretional growth is the domnant growth mechanism for precipitating ice accounting for 92-9£% of the

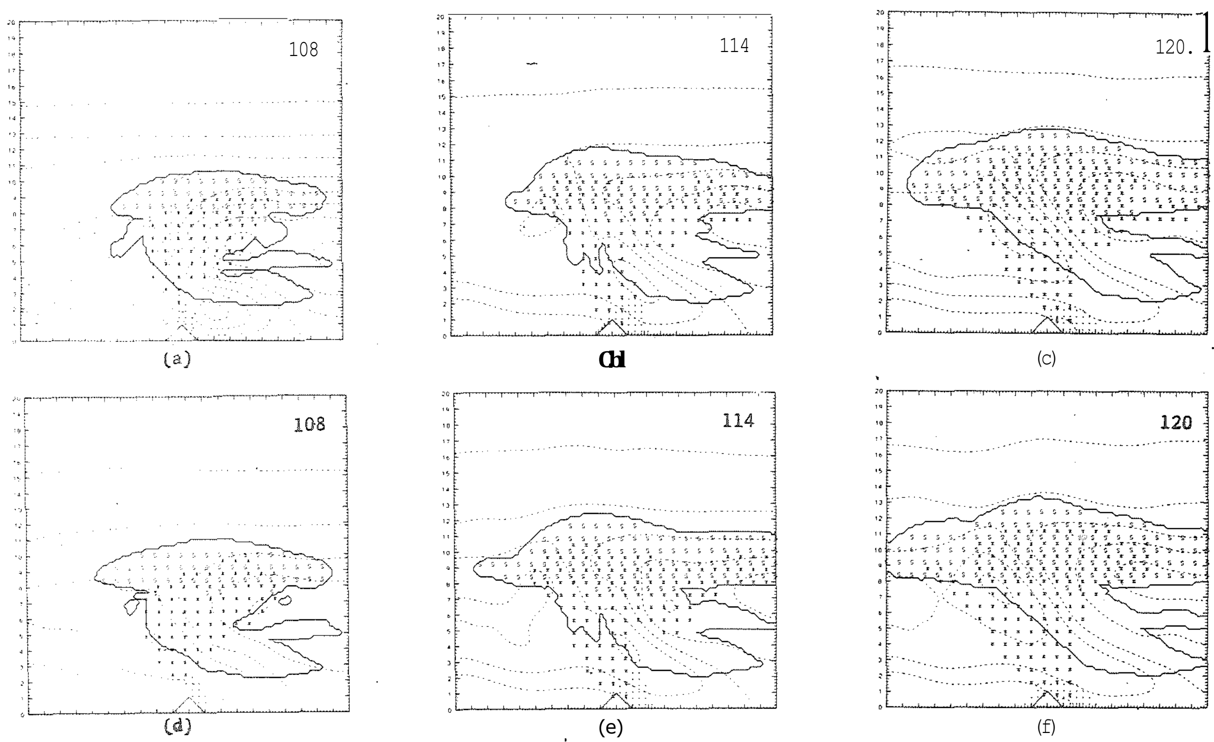

Figure 1. Results of i:he hail aai:egO'P/:f model. at :1.08, 114, 120 min of simul-at;ed time for the fi:,;ed density (la-c) and variabl.e density (ld-f) schemes. Cloud areas (1OOZ relative humidity) are outZined by the soZid line, and dashed lines represent the streamZines. SrraZZ soZid circles and asterisks indicate rain and precipitating ic greater than 1 g kg^{-1}, respectively, and the S's indicate cZoud ice .greater than 0.2 g kg^{-1}• The S's and asterisks are at half the density of the ciroles. The contour interval for the stream function is 1.0×10^4 kg m^{-1} s^{-1} except in 1a, which uses ha7.f of the normal value.

ice mass in the RI cases and 86-89% for the RA cases. Melting is the dominant mechanism for the production of rain accounting for 96-98% in the RI cases and 77-86% in the RA cases. The VD cases indicate slightly earlier formation (2-3 min). This is due to the fact that for equivalent masses, the lower density particles have enhanced capture volume and ventilation effects, even though fall speeds are reduced. The VD cases indicate a 10-15% increase in accretional growth and a 5-10% increase in melting, with this effect being stronger in the early stages.

The less dominant production terms are changed more dramatically. Wet growth is increased by a factor of 2 in the VD cases, but is still less than 10% of the total accretional growth, being largest in the RA cases. Diffusional growth processes also tend to be greater in the VD scheme. The ice generation mechanisms are also affected, but in different ways. Frozen drops account for <5% of the mass produced by generation mechanisms in the RI cases and about 30% (more in the early stages) in the RA cases. The VD scheme indicates enhanced production of frozen drops throughout the life of the storm, whereas particles of ice origin are suppressed in the early stages but enhanced during the mature storm stage in the RI cases. The VD scheme in the RA case suppresses the generation of particles of ice origin, whereas frozen drops are suppressed early but enhanced in the early mature storm phase.

Comparison of ice particle spectra between FD and VD schemes indicate changes not te be expected from the strong similarities in the domain-time integrals and dynamic characteristics. Figure 2, which displays the percentage of total spectral growth rate per category at selected points and times, illustrates s=e of these differences between FD and JD solutions £or the RI cases. The most proO nounced effect is noted to the rear of the sloping updraft near the precipitation cascade, mainly for sizes >5 llllll (Fig. 2a). These changes can be traced back to the embryo curtain region with increased concentrations of the larger siz.ed embryos in the inner regions (Fig. 2b}, although the extreme forward edge of the embryo curtain indicates increased. concentrations of inter.mediate sizes in the FD scheme. The rear of the sloping updraft near the precipitation cascade shows markedly increased mass concentrations of hail size particles for the VD scheme. The VD scheme indicates as :much as 90% of the total ice spectral :mass in sizes greater than 5 :mm with 70% being the mllillru:m for the FD scheme. Fer izes greather than 1 and 2 cm, the VD scheme produces :maxima of 65% and 20%, respectively, compared to 20% and 2% for the FD cases. Spectral ai£ferences £or the RI cases are :more pronounced than for the RA cases.

The major gzowth of the ice particles occurs in the high liquid water regions between -5 .and -30°C, with the :ma::ciJmml growth usually occurring a:reund -15°C, although s0llletimes as high as -20°C. The major growth region in the RA cases tends to extend to slightly warmer regions, being associated with active rain fomation regions just above the 0°C level. Major growth of particles less than 1 lll!ll occurs in a curved region e.:xtending from near the top of the major updraft into the lower portions of the forward overhang and down into the embryo curt'ain.

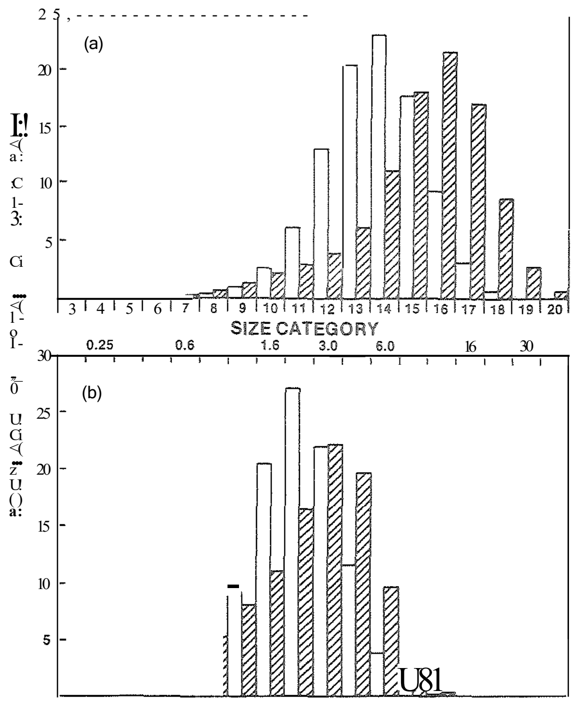

Fig=e 2. Comparison of aontributions tc total groi.!th :r>ate by size aategory for the fixed d£nsity ana variable aensity sahemes for the rain inhibited oases. The open aolwmuJ give the FD results, whereas the shaded aoZumns depict the VD results. The top p=l presents the results at 117 min at an aUitv.de of 6 km (AGL) and 9 km from the left-hand boundary. Th• bottom ., =l is at 108 min, altitude of 6 km (AGL) and 12 km from the left-hand boundary. The inegular scale at the top of the lower panel gives the app:roxiamte mean diameter in MM (for the FD scheme) for seZ.ected categories,

The VD scheme indicates Jllean particle densities in the range 0.2-0.3 in this region. Milli eter sized particles grow predominantly in the embryo curtain and leading edge of the updraft core, being in the 0.4 to 0,7 density range in the VD scheme. Larger particles grow mainly in the region between the updraft core and precipitation cascade, falling in the 0.7-0.8 density range in the VD cases.

4. CONCLUSIONS

Conclusions from this study are tenuous owing to the use of only one storm sounding and to same of the inherent difficulties in adequately modeling wet growth and melting in the variable uensity scheme. Nevertheless, the following tentative conclusions are offered:

1. Low density riming growth shortens the gro h time to embryo sizes, giving increased concentrations of the larger mass embryo sizes.

2. The increased concentrations of larger embryos in the forward overhang and embryo curtain lead to more effective hail growth in the major updraft regions and increased amounts of large hail in the precipitation cascade.

3. Low density riming growth is apparently more important in storms without an effective c0llision-coalescence mechanism. This is because Ji!Ore embryos and .Jllajor growth are at higher densities i.llRi. cases.

/;cknowl-edgJJ1ents. 1nanks and appreciation are e:i:pressed to Shu-:ing Kuo for her contribution to this work, and to Joie Robinson for typing the :manuscript. This material is based upon work supported .by the National Science Foundation under Grants No. ATM-7916147 and ATM-8311548. The computations were perfomed at the National Center for Atmospheric Research, which is sponsored by the National Science Foundation,

5. REFERENCES

1. Ludlam F H 1958, The hail problem, *Nuhila* 1, 12-95.

2. Clark V 1948, Icing nomenclature: Harvard-Mount Washington Icing Research Report 1946-47. USAF Tech Rep No. 5676, 415 pp .

3. Macklin W C 1962, The density and structure of ice fomed by accretion, *Quart J Roy Meteor Soc* 88, 30-50.

4, Pflaum J C and Pruppacher H R 1979, A wind tw-nnel investigation of the growth of graupel initiated from frozen drops, *J Atmos Sci* 36, 680-689.

5. Buser O and Aufdermaur A N 1973, The density or rime on cylinders. *Quart J Roy Met:,or Soc* 99, 388-391.

6. Pflaum J C 1980, Hail formation via microphysical recycling, *J Atmos Sci* 37, 160-173.

7. Farley R D, hopp F J, (.hen C S, and Orville H D 1976, Use of cloud lDodels to test hail scppression concepts. *Preprints 2nd WMOScientific· Conf Wia Modif,* \'MO l\o. 443, *IAl"»* and AMS, Boulder, CO, 349-556.

b. Farley R lJ and Orville H L 1982, Cloud modeling i, two spatial dimensions, Chapter 9 in *Hail-* stolwuS *of the Cent:ral High Plains, F The National Hail Reseach Experiment,* C. A. Knight and P. Squires, ed. Colorado Associated Univ. Press, Boulder, CO, 282 pp.

9. Farley R D and Orville H D 1982, The numerical modeling of hailstorms and cloud seeding effects. *Second IntnZ Workshop/Conf on Hailstorms and Hail Prevention*, WMO, Sofia, Bulgaria, 20-24 Sep 1982.

10. Chen C-H and Orville H D 1980, Effects of mesoscale convergence on cloud convection. *J Appl Meteor* 19, 256-274.

11. Wisner C, Orville H D, and Myers C G, 1972, A numerical model of a hail-bearing.cloud, *J Atmos Sci* 29. 1160-1181.

12. Orville H D and Kopp F J 1977, Numerical simulation of the life history of a hailstorm, *J Atmos Sci* 34, 1596-1618,

13, Xu J-L 1983, Hail growth in a three-dimensional cloud model, *J Atmos Sci* 40, 185-203.

14. Pruppacher H R and Klett J D 1978, *Microphysics of Clouds and PEecipitation,. Chapter 16,* D Reidel Publishing Co, Inc, Hingham, MA, 714 pp.

15. Plooster M N 1971, Freezing of spongy ice spheres, *J Atmos Sci* 28, 1299-1301,

16. Browning K A and Foote G B 1976, Airflow and hail growth in supercell storms and some implications for hail suppression, *Quart J Roy Meteor Soa* 102, 499-533,

A NUMERICAL M::JDEL OF HAIISTCNE GROvfill

Geresdi, I , Zoltan, ci, Szekely, Cs , M:::ilnar,K and Stoyanov, s

1pplied Cloud Physics Centre, Meteorological Service of the Hungarian People's Republic, 7601 Pees, Pf. 353. H'.mgary

i!ydraneteorological Service, blvd. Lenin 66. Sofia, Bulgaria

I. INTRODUCTim

The growth of individual hailstones was studiea using a one-dinensional steady-state @odel of thundercloud.

The dimension of the cloud model was extended supposing that the horizontal profile of the vertical updraft velocity is /Ref. 1/:

$$W(r,z) = \frac{3}{2}\overline{W}(z)\left(1-\left(\frac{r}{R(z)}\right)^2\right)^{1/2} , \qquad /1/$$

where Z is the height and r' is the distance frc:m the axis of the jet. Rczhs the jet radius,W(z> is the nean vertical velocity a::,nponent of the jet at a given level and they were calculated by the cloud model. One part of the horizontal velocity ccmp::ment can be derived fron the continuity equaticn. The other part which is the oonsequence of the.horizontal wind shear, the cloud ter.perature, the liquid and solid water oontent, the nean volume radius of the.frozen and the liquid water droplets were given. by the cloud rrodel. These parameters were supposed to be oonstant at a given level. Out of the cloud the terrperature, the wind and vapour pressure were given by the sounding.

The growth and rrotion of the hailstones were calculated in this three dimensional space.

2. '1'HE Ex;iUATICNS OF M'.JrICN AND GRJWI'H OF HAIISTCNE

'.!.'he equations were determined by the following conditions:

1. The frozen and liquid water droplets rrove with the updraft velocity.
2. The oollision effeciencies for hailstone colliding with frozen droplets / -/ and with liquid water droplets /f=..,I are given by LarJ.grnuir's expression in potential flow.
3. The coalesoence efficiency for hailstone colliding with liquid water droplets is equal to 1. The =alesence efficiency for h2ilstone colliding with frozen. droplets c$_{qF}$8rl on the temperature of the hailstone /T$_0$ /, /Ref. 2. /:

$$E_i' = \begin{cases} \dfrac{T_h - 268K}{5K} & \text{if } T_h \geq 268K \\ 0 & \text{if } T_h < 268K \end{cases} \qquad /2/$$

4. Ilhen E = *O*, the average rrarentum given by the co>lliding frozen droplet to the hailstone *is* m lo! / m *is* the nass of the frozen droplet and ,U *is* the velocity difference between the stone and the droplet/.
5. The interaction between the hailstone and the shedding water *is* neglected.
6. The m::mentur,1 of the hailstone is changed by the force of gravity and the drag force, too.
7. The terrperature of the droplets is equal to the terrperature of the cloud.
8. The inside terrperature of the hailstone is equal to its sur ace temperature.
9. The hailstone is spherical.

On the basis of these assurrption the acceleration of the hailstone is:

$$\frac{dv}{dt} = \frac{1}{M}\left[Mg + F_d + (w - v)\frac{dm_c}{dt}\right] , \qquad /3/$$

where M a n d Y are the mass and tjie velocity of the hailstone, respectjvely, **g** is the gravitational acceleration and **.f$_d$** is the drag force. The drag coefficient C, is given by /Ref. 3/:

$$c = 3.92 \cdot Re^{-0.1689} \qquad /4/$$

The ITass of the liquid water droplet dm-und that of the frozend droplets df'llc. oolliding in tine d-1: is c,iven by:

d $_{l'r\: vt}$ **='1.^{2} Eve,**1T /li'-J{ / *N*$_{,,}$ **d.f** /5/

clmc.: **=r:E,:T** *IW-xl dt* .

:where N $_v$ and *Ni* are the conoentrations of the liquid and frozend droplets /mass/volurre/, respectively and r$_1$ is the radius of the hailstone. The sum of dm $_{qt}$ and dmc;. is dm $_c$ •

The mass of the oollected droplets is:

$$dm = dm_c + E: dm_c \qquad /6/$$

Macklin's /Ref. 4/ empirical fonnula was used to calculate the density of the accreated ice:

$$\rho = \begin{cases} 900\ \mathrm{kg\,m^{-3}} & \text{if } T_h \geq 268K \\ 110\left(\dfrac{r_w u}{273 - T_h}\right)^{0.76} & \text{if } 253 \leq T_h < 268K \\ 10\cdot(r_w u)^{0.76} & \text{if } T_h < 253K \end{cases} \qquad /7/$$

where **r.**, is the nean volurre r, :lius of the liquid wat§f droplets /}'ID/ and U is the :impact velocity *lms* *l*.

We supposed that one part of the collected supercooled droplets freezes onto the surface of the hailstone and terrperatures of the frozen and liquid parts will be OOC irmediately after the collision. The mass of the frozen part is given by:

$$dm''_{cw} = \frac{c_w\, dm_{cw}\,(273-T)}{(L_f + c_i(273-T))} \quad , \qquad /8/$$

where Cir, and C. are the specific heats of water and ice, respectively, L_f is the heat of fusion of water and T is the temperature in the cloud.

In addition to the accretional growth, there is also a diffusional change of rrass. The rate of heat transfer due to this diffusion is given by:

$$\frac{dQ_D}{dt} = 4\pi r_h f_D\,(\rho_{ve} - \rho_{vs}) \cdot D L_s \quad , \qquad /9/$$

where f_D is the ventillation coefficient /Fef. 5/, ρ_{vs} anci ρ_{ve} are the water vapour density at the hailstone surface and its environment, L_s is the latent heat of sublimation and D is the coefficient of diffusion of water vapour in air.

The rate of heat transfer due to ocnduction and ventillation is:

$$\frac{dQ_c}{dt} = 4\pi r_h K f_h\,(T_h - T) \qquad /10/$$

where K is the thennal conductivity of air and f_h is the ventillation coefficient for heat /Ref. 5 .

2.1. Dry growth range

D:r:y growth oocurs when the temperature of the hailstone is lower than oC:C. The release of latent heat of freezing process does not raise the temperature of hailstone to 0^oC. In this range the temperature of the hailstone is given by:

$$T_h = \frac{-(dQ_D + dQ_c) + L_f\, dm'' - dm'_w}{c_i(M + dm + dm)} \qquad /11/$$

$$\therefore \frac{c_i(dm_g \cdot 273 + M\ldots + dm' T)}{c_i(M + dm_{cw} + d\ldots)}$$

2.2. Wet srowtll range

After collisions the terrperature of hailstone is equal to ooe. The pores formed during the dry growth range fill with water.

3. CALCUIATION OF HAILSTONE TRA'.JECTORIES

The differential equations were solved by the Eulerian numerical method. The initial conditions were the followings:

1/ The hailstone is a frczeild drop of 1 nm radius /Fef. 6/ and its density is 900 kgm-3.
2/ The velocity of the hailstone is equal to its tenninal velocity.
3/ 'l'he terrperature of the hailstone is equal to th terrperature of its environment.

For the calculation of hailstone trajectories .ie chose such a day /21.05.1982/ men heavy hailstorms formed in hornogenious air-rrass in the west part of Hungary. The sounding of Zagreb 21.05.1982 00 G':-llwas used to canpute the cloud rrodel, because the general orientation of the winds were south-"west /Fig. 1/. The largest hailstone diameters are 17.5-20.0 nm aocording to the hailpad measurement.

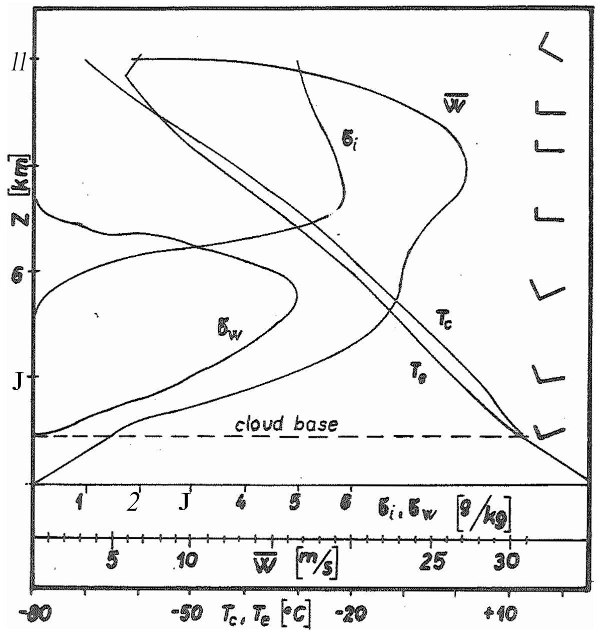

Figure 1. Characteristic parameters of the cloud: the mean vertical velocit yW , liquid water mixing ratio σ_w , ice mixing ratio σ_i, and the terrperature T_c. T_e is the temperature cf the environment, flags indicate the direction and velocity of the wind. /Half flag means 2-3 m/s, flag rreans 4-6 m/s. /

The hailstones were started from different points of the cloud at heights of 4, 5, 6 and 7 km. Only a small fraction of them reached the ground, the rrajority of them melt during their fall. /Fig.2/.

The hailstones.which completly melt during their fall rrove along two types of trajectories. In the first case the hailstones go out of the cloud and the wind does not blow back them into the cloud and they melt and do not reach the ground because of their small size.

In the other case /at windward side of the cloud/ the wind blows these small hailstones back into the cloud, but the entry point is under the ITElting level and they melt.

Only a few hailstones starting fran a small volume of the cloud reach the ground. These hailstones move along two types of trajectories /Fig. 3 and Fig. 4/.

a/ The hailstones start at the leeward side of the cloud, between 4 and 5 km and near the cloud boundary. These hailstones =oss once the region of large liquid water miYing ratio and spend lcng time in it. i'Jhen the hailstones leave the cloud their sizes are large enough to reach the ground. In the calculated cases their final radii are 3-7 nm and duration of motions is between 10-15 min.

b/ The other part of hailstones move along recycling trajectories. In this case the hailstones spend longer time in the region of large liquid water mixing ratio than in the case a/, because the wind blows back the hailstones into this regicn. In the calculated cases the radii of these hailstones are between 15 and 25 nm and they reach the ground between 30 and 40 min. after the starting.

In sorre cases the hailstones move rrore than 50 min. and remain srrall. These types of trajectories are called endless cyclical.

We suppose that the too large hailstone sizes in case b/ and the endless cyclical trajectories are due to the steady state cloud model. Under real conditions, except sl.T,:ercell, this state generally does not last for over 30 min. /Pef. 7/.

In dry growth range and in wet growth range different ice lay"rs form. Fig. 3 and Fig. 4 show these calculated layers in a hailstone. Fig. 3 shows that layered structure can also form in hail-stone moving along simple trajectories. The calcu-lated average aensity of hailstones were about 900 kg m-3 or a little more. The last case is caused.by pores filled up with water.

Finally an intercorrparison is done between the rreasured and calculated hailstreak / ig. 5/. Two separate hailstreaks were measured by hailpad net-work. According to the radar data the hailstreaks belong to a storm cell moving at a speed of about 3 ms-1. The distribution of the large hailstones in the hailstreak 1. seems to be similar to our calcu-lated results i.e. the largest stones are in the south-west part of the hailstreak.

It must be noted that these results were ob-tained fran only one case and our cloud model and the calculation of the flow are very simplified. We suppose that using a one-dimensional, time de-pendent cloud model, the sizes of hailstones moving along recycling trajectories become smaller and the difference between the measured and the calculated sizes will be smaller.

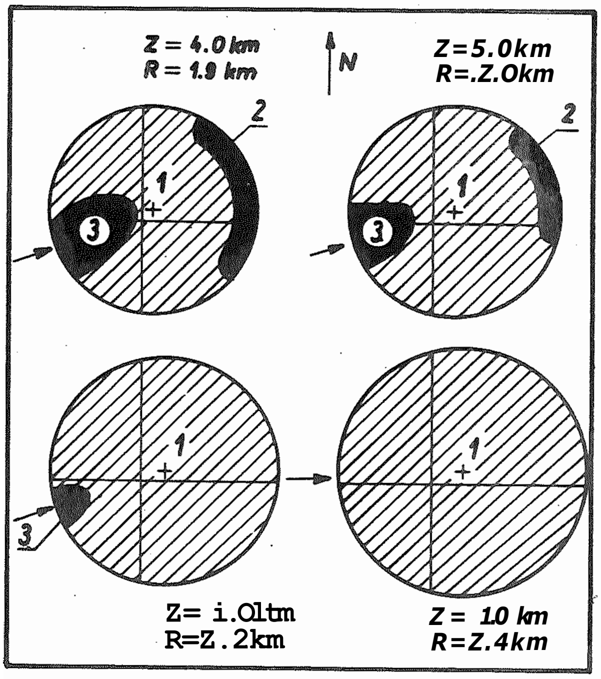

'h.. .e 2. The hailstones starting from region 1 do not reach the ground. The hailstones starting from region 2 fall onto the ground with radius of 3-7 mn '.and rrove. alona simple traiectories. The "hailsta.,es starting fran region 3 becane l e /15-25 mm/ and m:ive along recycling trajectories. "The arrows indicate the direction of the wind, the cloud axis is marked by + and R is the cloud radious at height.% . The co-ordinates of the cloud axis change because of the wind.

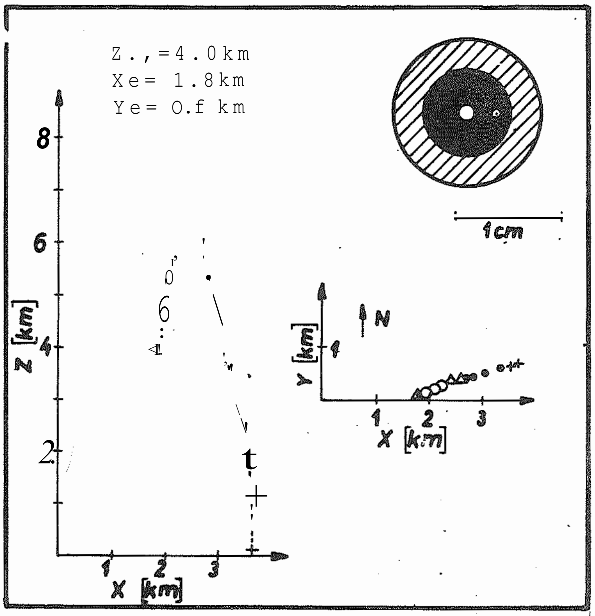

Figure 3. Two projections / x-z and X-Y plane ; of a typical hailstone trajectop starting fran regiDI; 2. The different s ls roar the different wa: s or growth: 4 starting point, △ dry growth rang e; o wet growth range, + rtelting range, "no growth. The syrrools are placed every minute; L X@ and t give the initial point of the hailstone. The calcu-lated ice layers of the hailstrne can be seen in the top riht hand corner. The black area indicates the J..ayers forining in wet growth range, the shaded area ti.r.dicates the layers forming in dry growth range and the white circle at the centre indicates the ,initial h }- 5ltone.

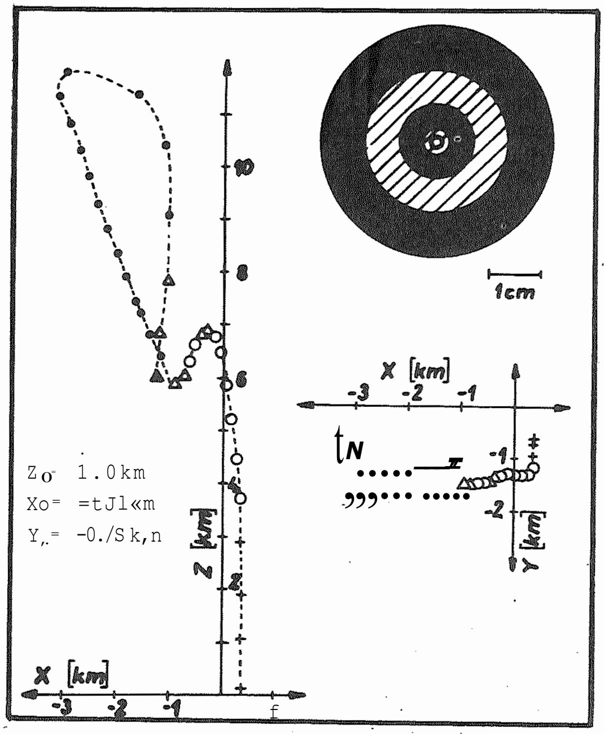

FigUre 4; Typical hailstrne trajecto:i:x starting fran region 3, the syrrools are as in Fig. 3.

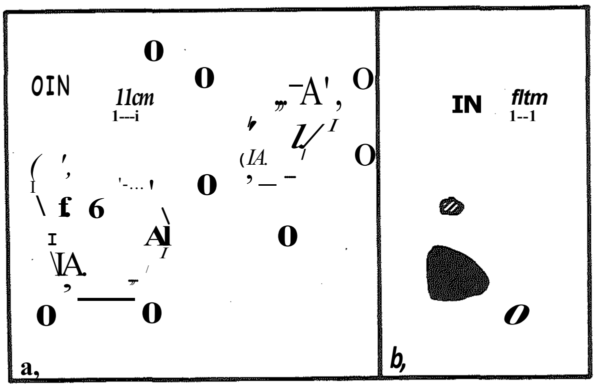

'Figure 5. The rreasured /a/ and calculated /b/ hailstone size distributions on the ground. The black triangles indicate the hailpads hit by large hailstones /d ;;;;15 mm/, the enpty triangles indicate the hailpads hit by smaller hailstones and the circles indicate the hailpads without hail. In calculated cases the larger hailstones /15-25 mm/ fell onto the black region, the smaller hailstones /3-7 mm/ fell onto the shaded regions.

4. REFERENCES

1. Bek:ryaev V I and Zinchenko A B 1973, Osesinnetricheskaya stacionarnaya m::xl.el rroshnovo kuchevovo oblaka, •..: 'GCD 302; 42-54.
2. Pflaum J C et al 19¥Hail Growth St-udies within a Doppler-Radar !€a:mstructed Supercell, Conference-Workshop on Hailstorms and Hail Prevention, Sofia 1982
3. Matson R and Huggins A W 1979, Field observation of the kinematics of hailstone, NCAR/TN-139 STR
4. Macklin W C 1961, The density and structure of ice fonred by accretion, QUart.; J; Rey; Meteor. Soc. 88, 30-50
5. Pruppacher H R and Klett J D 1978, Microphysics of-Cloud and Precipitation, Dodrecht, D. Reidel Publ. Co.
6. Paluch I R 1978, Size Sorting of Hail in a Three-Dinensional Updraft and Irrplications for Hail Suppression, J; Appl. teor. 17, 763-777
7. Byers H R and Braham R R 1949, The 'Thlinderstonnl us. Govt. Print. Office Washington D. C.

THE PARAMETERIZATION OF WARM RAIN PROCESSES

William D. Hall and Te.ry L. Clark

National Center for Atmospheric Research*
BouldLr, Colorado 80307 USA

INTRODUCTION

In the past the treatment of cloud microphysical processes within multidimensional cloud models has often been highly parameterized. These parameterization schemes typically partition each hydrometeor phase into various categories according to concepts introduced by Kessler (1969) such as cloud water and rain water or snow crystals, graupel, and hail. The principle reason for such parameterizations have been employed is that detailed microphysical treatments have proven cumbersome requiring large .amounts of computer storage and central processing time. In the detailed models the hydrometeor spectra are divided into a large number of categories in which the governing microphysical equations are cast into finite difference form and established numerical methods are applied. Thus the detailed model provides a straightforward solution to the physical equations. The accuracy of the solutions can be tested by increasing the size category resolution to provide guidelines and bench mark solution for testing proposed parameterization schemes.

In the present paper the recent coalescence parameterization method of Clark and Hall (1983) is modified to include the additional processes of nucleation and condensation. The method fir..t aasumes that the solution of the physical equations describing the spect_ral evolution of the liquid phase is represented by a short series of distribution functions. A system of equa:tions. describing the time tendencies of the distribution function variables are derived using a variational procedure that minimizes by least squares with a general weighting function the spectral time tendencies using Lagrangian multipliers to guarantee that the number and mass concentration obey the physcal equations precisely.

In the present paper we assume the distribution function is represented by a short series of log-normal functions of the form

$$f(\ln r) = \sum_{i=1}^{Nd} f_i(\ln r) \tag{1}$$

$$f_i(\ln r) = \frac{N_i}{\sqrt{2\pi}\sigma_i} \exp\frac{-(\ln r - \mu_i)^2}{2\sigma_i^2}$$

At a given time and special location within the model, the time tendencies at the parameters for all of f_i are determined by minimizing the following function Λ under constra nts

$$\Lambda = \frac{1}{S_f} \int_{-\infty}^{\infty} w(r) \cdot \left(\frac{\partial}{\partial t}(f(\ln r) - G(r))\right)^2 \times d\ln r + \sum_{k=1}^{K} \lambda_k C_k \tag{2}$$

where S_f is a chosen scale factor, $w(r)$ a weighting function, G the tendency determined from the governing equations, $C_k = 0$ is the kth constraint, and λ_k is the kth Lagrange multiplier, The precise form of each of these expressions have been presented by Clark and Hall (1983).

Defining the time tendencies at the parameters as

$$x_i = \frac{\partial \ln N_i}{\partial t}$$

$$y_i = \frac{\partial \mu_i}{\partial t} \tag{3}$$

$$z_i = \frac{\partial \sigma_i}{\partial t}$$

A general set of matrix equations is derived from (2) by solving

$$\frac{\partial \Lambda}{\partial x_i} = \frac{\partial \Lambda}{\partial y_i} = \frac{\partial \Lambda}{\partial z_i} = 0 \quad \text{for } i = 1, \cdots nd$$

and (4)

$$\frac{\partial \Lambda}{\partial \lambda_k} = 0 \qquad \text{for } k = 0,3$$

Here the two constraints k = 0, 3 represent number and mass concentration.

This results in a matrix equation in the form

$$AX = F \tag{5}$$

where A is of order 3Nd + k and

$$X^t = (x_1, y_1, z_1, x_2, y_2, z_2, \cdots x_n, y_n, z_n, \lambda_0, \lambda_3)$$

F, the right hand side of the matrix equation involves integrals at the form

$$\int_{-\infty}^{\infty} w(r) \{ f_i(\ln r)\, G(\ln r)\, d\ln r \tag{6}$$

for p = 0, and i = 1, •••nd

and constraint integrals at the form

$$\int_{-\infty}^{\infty} r^k G(\ln r)\, d\ln r \qquad \text{for } k = 0,3 \tag{7}$$

where *G* is the complete distribution tendency given by the physical equations.

MODEL PHYSICAL EQUATIONS

1. Nucleation of Droplets

The activation of dro_plets from cloud condensation nuclei follows an emperical activation spectra of the form

$$\eta_1 = C_1 S^{C_2} \tag{8}$$

where S is the cloud supersaturatJon (%) defined as

*The National Center for Atmospheric Research is sponsored by the Nat.:l..O.naLSdenre l:onndation.

$$S = \left(\frac{qv}{qv,sat} - 1\right) 100$$

where qv, and qv sat are the water vapor mixing and saturation mix'ing ratios. The constants C, and C_2 will vary according to the atmospheric aerosol characteristics of interest.

The first few attempts to include nucleation directly into the above system were not successful. The problem was that sudden decreases of ln (Ni) either through truncation errors or matrix ill conditioning lead to unstable results. An independent method was used successfully which was developed by Clark (1974) referred to here as three moment closure system where three different moment tendencies of the distribution, k = 0, 3, 6, are solved for exactly and the distribution parameter tendencies are then derived yielding

$$x_i = P_0$$
$$y_i = -(3P_3 - 4P_0 \quad P_0) / 6 \qquad (9)$$
$$z_i = (P_6 - 2P_3 + P_0) / 9$$

where Pn represents the nth logarithmic moment tendency.

2. Growth by Vapor Diffusion

The physical equation governing vapor growth by diffusion is given by

$$G = -\sum_{i=1}^{Nd} \frac{a}{a\ln r} \left(\frac{D\ln r}{Dt} f_i\right) \qquad (10)$$

where Dlnr/Dt represent the growth rate for an individual droplet. This growth rate is given by

$$\frac{D\ln r}{Dt} = \frac{1}{r^2}(a_0 + a_1 \ln r + a_2 \ln r^2 + a_3 \ln r^3 + a_4 \ln r^4)$$

where the coefficients a_0, a_1, ...a_4 have been determined by cure fits of the general physical equations which include both kinetical and ventilation terms. This procedure allows for the right hand side terms to be determined analytically.

The following section will discuss three important considerations of the model: 1) the use of large time steps; 2) analytic inverse during wide separation conditions; and 3) use of artificial diffusion to match the detailed model with computational dispersion.

The ideal parameterizaton will be one where the time stepping will match the time step at the multi dimensional cloud model in which it is incorporated. This can be as large as 25 sec. Twelve different updating procedures have been tested. The most effective updating schemes were a two-step process with the second step being an adjustment to insure that the constraints of number and mass concentration were preserved. The following will describe the best overall procedure. The first step of the updating procedure was to let

$$N^{*} + 1 = N (1 + x_{oi} \Delta t)$$
$$\mu_i^{*} = \mu_i^{t} + y_{oi} \Delta t / (1 + x_{oi} \Delta t) \qquad (11)$$
$$\sigma_i^{2*} = \sigma_i^{2t} + z_{oi} \Delta t / (1 + x_{oi} \Delta t)$$

Thus yeilding the pth moment tendency of the form

$$\frac{\overline{NR_i^P}^{t} - \overline{NR_i^P}^{t}}{\Delta t} = \overline{N_i R^P}^{t} \left((1+\Delta t x_{oi}) \exp\left(\frac{p y_{oi} \Delta t + \frac{p^2}{2} z_{oi} \Delta t}{1 + x_{oi} \Delta t}\right) - 1\right) \qquad (12)$$

Here the subscript ( )o1 represents the analytical solution for distribution i from the matrix equation which satisfies the physical constraints exactly only when the time step Δt approaches zero.

The adjustment procedure is first to let

$$y_{fi} = y_{oi} + y_i'$$
$$z_{fi} = z_{oi} + z_i' \qquad (13)$$

where the subscript ( )fi represents the final tendency. The adjustment tendencies are normalized as

$$y_i' = \left(\left|y_{oi}\right| + \varepsilon_y\right)\left(y_i^{\nu} + \delta y_i\right)$$
$$z_i' = \left(\left|z_{oi}\right| + \varepsilon_z\right)\left(z_i^{\nu} + \delta z_i\right) \qquad (14)$$

and determined by successive iteration and minimizing Λ with respect to δy_i and δz_i (15)

$$\Lambda = \sum_i^{N_d} \left((y_i^{\nu} + \delta y_i)^2 + (z_i^{\nu} + \delta z_i)^2\right) + \lambda\left(\sum \frac{\Delta \overline{NR_i^3}}{\Delta t} - F_3\right)$$

here the superscript ( )v represents the vth iteration.

The third important consideration is that if the distribution is not overlapping, many of the terms in the matrix A approach zero and simple analytical solutions are possible.

Beginning with the general matrix equation under wide separation

$$AX = F \qquad (16)$$

using a general weighti g factor

$$w(r) = a + \beta t^n \qquad (17)$$

by performing Gaussian elimination the matrix's A and F can be put into the form

$$(a+\ ) x_i + A1_i \ldots + A2_i A3 = R_{i1}$$
$$d/\ (2erf(a+\ ) y_i + B1_i \ldots + B2 \ldots = R_{i2} \qquad (18)$$
$$(a +\ ) c / (16 erid) z_1 + c1_1 \ldots + c2_i \ldots = R_{i3}$$

where

$$c = \{2(a + \ )^2 + a\beta \ln^{2} erf(3 + \ldots)\}$$
$$d = (a + \ )^2 + a\beta \ln^{2} erf \ldots$$

The remaining terms A_1, A_2, B_1, B_2, C_1, C_2, and R_1, R2, and R3 are available from the authors.

Once the matrix has been reduced to the above simplified form, the value of the Lagrangian multipliers and the tendencies of the distribution parameters is easily derived.

Clark and Hall 1983 showed this parameterization method compared well with detailed parcel calculations of the coalescence equations. For the present case where condensational growth is occurring, the distribution functions often became very narrow (i.e. σ •05) and the resolution of the detailed model became inadequate. An artificial diffusion term was then added to the parameterization such that it could match the detailed model at a specific resolution. The term is at the form

$$G = \sum \frac{\partial}{\partial \ln r}\left(D_i \frac{\partial}{\partial \ln r}(f_i \ln r)\right)$$

where

$$D_i = \gamma \sigma_o^2 \left| \frac{|\ 2}{|\ 2 \ |\ \ |\ 2} \right|^4 \quad (19)$$

where

$$\sigma_o^2 = .0025$$

γ depends upon the resolution

In Figure 1 is shown a comparison between the present parameterized model with decreasing artificial diffusion and the detailed model with increasing spectra resolution. The detailed model is a logarithmically spaced grid lattice with the resolution parameter J_{rs} defining the number of categories of a mass doubling interval. The parameterized model is shown with a solid line and the detailed model a dashed line. For the results on Figure 1 only one distribution function was used. The model run is of a parcel of vertical velocity of 5m/sec with the initial conditions N = 200 / cm^3, $\mu = 3_{\mu n}$, and α = .4, and only condensational growth occurring. Plotted in Figure 1 (a) is the initial mass weighted spectra as a function of radius. The vertical scale of each at the spectra plots is not the same in order to show the specific details at the calculation. Figures 1 (b), 1 (c), and 1 (d) are the results for the detailed model with resolutions J_{rs} = 2, 4, 6 respectively and the parameterization with artificial diffusion.

$$\gamma = 4/(J_{rs})^2$$

In Figure 2 is shown results where nucleation, condensational growth and stochastic coalescence were occurring. The detailed model resolution is J_{rs} = 4 and an activation cloud condensation nuclei spectrum, $\mathrm{T1} = 300\ s^{.5}$, and vertical velocity, 4 meters/sec. In Figure 2 are plotted model times at 4, 8, 12, and 15 minutes. These results show good comparisons between both models.

In the present parameterization appears to be a practical method for the treatment of microphysical processes within cloud models. Progress in incorporating the above parameterization onto two and three dimensional cloud models will be reported.

Figure 1

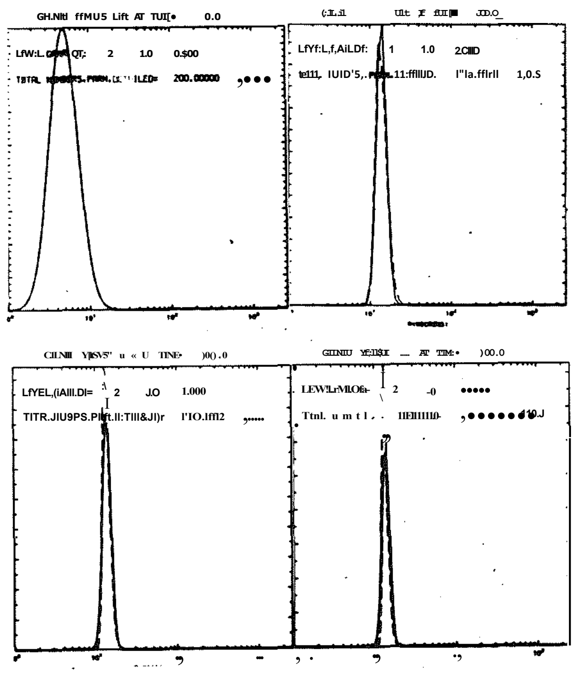

Figure 2

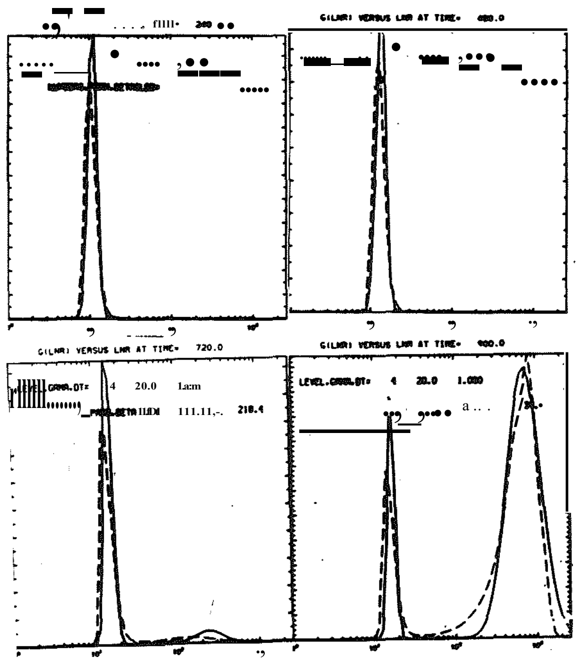

REFERENCES

Clark, T.L., 1974: One modelling nucleation and condensation theory in Eulerian spatial domain. J. Atmos. Sci., 31, 2099-2117.

Clark, T.L., and W.D. Hall, 1983: A cloud physical parameterization using movable basis functions: stochastic coalescence parcel calculations. J. Atmos. Sci., 40, 1709-1728.

Kessler, E., 1969: On the distribution and continuity of water substance in atmospheric circulation. Met. Monographs, 10, 84pp.

A PARAMETERIZATION SCHEME OF CLOUD MICROPHYSICAL PROCESSES

Hartmut Höller

Deutsche Forschungs- und Versuchsanstalt für Luft- und Raumfahrt
Oberpfaffenhofen
Institut für Physik der Atmosphäre
D-8031 Weßling, FRG

1. INTRODUCTION

Numerical modeling of the dynamics and microphysics of clouds requires an enormous amount of computational speed and storage capacity. Therefore it is desirable, especially in three-dimensional cloud models, to represent cloud microphysics in parameterized form. Instead of a spectral resolution of the different particle distributions, the use of only a few distribution moments can reduce computational amount.

Kessler (Ref. 1) used a one-parameter model for simulating liquid phase microphysics. The drops are classified as cloud droplets and raindrops and the corresponding liquid water contents were chosen as model variables. Raindrops were distributed according to a Marshall-Palmer spectrum, a cloud droplet distribution was not specified. Autoconversion and accretion were recognized as the processes responsible for the formation and increase of raindrop content.

Berry and Reinhardt (Ref. 2-5) could verify the basic concept of Kessler by numerical integration of the stochastic coalescence equation. Additionary, large hydrometeor self-collection was shown to be the efficient raindrop growth mechanism. Rate equations were derived for accretion and self-collection, using mean mass and predominant mass as parameters. These equations can be evaluated on the basis of the collection kernel rather than by arbitrary coefficients as in Kessler's scheme.

Clark (Refs. 6,7) and Clark and Hall (Ref. 8) assumed, that the drop spectrum may be approximated by a series of known functions (Gamma or log-normal distributions) which remain self-similar for all time. The parameters of these functions were used as prognostic variables. A matrix equation had to be solved for obtaining the tendencies of these parameters. Condensation and coalescence could be simulated by this kind of parameterization.

The present study also makes use of self-similar distributions. All particle spectra are represented by log-normal laws. Number density, water content and predominant radius are chosen as model variables whose time dependence is described by separate tendency equations. These equations are derived as polynomial approximations of the numerical values obtained from a detailed numerical treatment. So the parameterization scheme is more simple than that of Clark. Moreover, not only liquid phase but also ice phase processes are treated.

2. THE PARAMERERIZATION SCHEME

2.1. Distribution Functions

Numerical calculations of drop growth by stochastic coalescence have shown (Refs. 2,3) that typically a bimodal droplet distribution develops. The two maxima, corresponding to cloud droplets and raindrops, are separated by a minimum at around 38 μm droplet radius, which is regarded as the boundary between the two kinds of drops. The total spectrum may be approximated by two log-normal distributions. This kind of approximation is only valid in the initial stages of raindrop development. In the later stages breakup processes become essential and a Marshall-Palmer type of spectrum can develop.

Furthermore, it is assumed that log-normal distributions also fit the different kinds of ice particle spectra. Frozen drops, plate-like ice crystals and graupels are considered in this paper.

The general form of the i'th log-normal distribution is given by

$$f_i(\ln m) = \frac{N_i}{\sigma_i\sqrt{2\pi}} \exp\left[-\frac{(\ln m - \mu_i)^2}{2\sigma_i^2}\right] \qquad (1)$$

where

- m - particle mass
- N - number concentration of particles
- σ^2 - variance of $f(\ln m)$
- μ - mean value of $f(\ln m)$.

For convenience, the dependence of time and position has been omitted in the above notation. i refers to the kind of particle

1 - cloud droplets
2 - raindrops
3 - frozen drops
4 - rimed ice particles, **graupels.**

f_i depends on the three parameters N_i, μ_i and σ_i. These may be expressed as functions of the distribution moments M_i^n of order n

$$M_i^0 = N_i = \int_0^\infty f_i(m)\,dm \quad \text{- number density}$$

$$M_i^1 = L_i = \int_0^\infty m f_i(m)\,dm \quad \text{- water content}$$

$$M_i^2 = Z_i = \int_0^\infty m^2 f_i(m)\,dm \quad \text{- radar reflectivity}$$

or as functions of the mean masses $\bar{m}$ and the 'predominant masses' m_i,

$$m_{f_t} = \frac{L_t}{N_t} \quad , \quad m_t = \frac{Z_t}{L_t} \qquad (2)$$

so that

$$\mu_t = \frac{1}{;} \ln \frac{m/}{t_m ;} \quad , \quad \sigma_t = \ln \frac{m}{t^m i} \; .$$

The two moments Nt and L, and the predominant mass m (for numerical reasons) were chosen as the model variables.

2.2. Parameterization of the Microphysical Processes

2.2.1. Diffusional Growth. The diffusional growth rates of cloud particles may be represented by

$$\dot{m}_t = a_i m^{b_i} \qquad (3)$$

where we assume $b_t \approx 0.5$. a_i may be computed as a function of pressure, temperature and supersaturation or, inside the cloud, by saturation adjustment methods.

Now the change of moment M_t^n by water vapor diffusion (D) can be computed from

$$\frac{dM_t^n}{dt}\Big|_D = \int_0^\infty n\, m^{n-1} f_t\, \dot{m}_t \, dm \quad , \quad i=(1, \ldots ,4) \qquad (4)$$

The exact solution of Eq. 4 can be obtained by insertion of Eqs. 1 and 3 (see Table 1).

2.2.2. Freezing Nucleation. Following Vali (Ref. 9) the differential concentration of freezing nuclei may be expressed as

$$k^F(\theta) = a_F \exp(b_F \theta) \qquad (5)$$

where $\theta = T_0 - T$ is supercooling. The tendency equations follow from

$$\frac{dM_i^n}{dt}\Big|_F = \int_0^\infty m^n k \cdot V f_t \dot{T} \, dm \quad , \quad i=(1,2) \qquad (6)$$

where V is the volume of a drop of mass m. Substituting ft from Eq. 1 gives the results summarized in Table 1, where m_{ht} is defined as

$$m_{hi} = \frac{H_t}{Z_t} = \frac{m_{..}^2}{m}$$

for the log-normal distribution with $H_t = M_i'$.

2.2.3. Collectional Growth of Water Drops. Collectional growth can be parameterized by introdudng the following processes

1. Autocollection or self-collection (SC) of cloud droplets (collection of cloud droplets by cloud droplets). The result may be either a cloud droplet again (type conserving self-collection (TCSC)) or a raindrop (autoconversion (AUT)). The latter process is defined to occur whenever the radius of the resulting drop is larger than $r_{max,c} = 38\ \mu m$.
2. Autocollection or self-collection (SC) of raindrops (collection of raindrops by raindrops). The result is a raindrop again.
3. Accretion (ACC) (collection of cloud droplets by raindrops).

Now we assume that those drops passing through the r_{max}-boundary during cloud droplet self-collection contribute to the autoconversion rate. Then the moment tendencies can be written as

$$\frac{dM_2^n}{dt}\Big|_{AUT} = \int_{m_{max}}^\infty m^n \sigma_1^c \, dm = N_1^2 I_{AUT}^{M_2^n} (m_{f_1}, m_{g_1}) \qquad (7)$$

where $m_{max,c}$ is the mass of a droplet with radius r_{max} and σ_c is the spectral source term for cloud droplets by coilection (C). σ_1^c is described by the stochastic collection equation (SCE)

$$\sigma_1^c = \int_0^{m/2} f_1(m-m') f_1(m') K_{c}(m-m',m') \, dm' - f_1(m) \int_0^\infty f_1(m') K_{c}(m,m') \, dm' \; . \qquad (8)$$

K_c is the collection kernel for water drops.

Self-collection of cloud droplets (TCSC + AUT) can be computed from

$$\frac{dM_1^n}{dt}\Big|_{SC} = \int_0^{m_{max}} m^n \sigma_1^c \, dm = N_1^2 I_{SC}^{M_1^n} (m_{f_1}, m_{g_1}) \qquad (9)$$

Similary, self-collection of raindrops is given by

$$\frac{dM_2^n}{dt}\Big|_{SC} = \int_0^\infty m^n \sigma_2^c \, dm = N_2^2 I_{SC}^{M_2^n} (m_{f_2}, m_{g_2}) \qquad (10)$$

ft from Eq. 1 was inserted into Eq. 8 and then Eqs. 7, 9 and 10 were integrated numerically using the Berry-Reinhardt scheme (Ref. 2). The values of the integrals I depend on the two parameters m_{f_i} and mt which were used subsequently as variables for a polynomial approximation $A!(r_{f_i}, r_{g_i})$ of $I!(m_{f_i}, m_{g_i})$.

Accretion rates depend on four variables

$$\frac{dM_1^n}{dt}\Big|_{ACC} = \int_0^\infty m^n \sigma_{12}^{c,ACC} \, dm = N_1 N_2 I_{ACC}^{M_1^n} (m_{f_1}, m_{g_1}, m_{f_2}, m_{g_2})$$

$$\frac{dM_2^n}{dt}\Big|_{ACC} = \int_0^\infty m^n \sigma_{21}^{c,ACC} \, dm = N_1 N_2 I_{ACC}^{M_2^n} (m_{f_1}, m_{g_1}, m_{f_2}, m_{g_2}) \qquad (11)$$

where

$$\sigma_{12}^{c,ACC} = - f_1(m) \int_0^\infty f_2(m') K_c(m,m') \, dm'$$

$$\sigma_{21}^{c,ACC} = \int_0^{m/2} f_2(m-m') f_1(m') K_c(m-m',m') \, dm' - f_2(m) \int_0^\infty f_1(m') K_c(m,m') \, dm' \; . \qquad (12)$$

The number of independent variables was reduced by assuming that the following linear relations give fairly good results of accretion rates

$$m_{f_i} = c_i m_{g_i} \qquad i=(1,2) \qquad (13)$$

The coefficients c_i were determined by comparison with detailed model calculations. As in the case of self-collection, accretion can now be approximated by polynomials in r_{f_i} and r_{g_i}.

2.2.4. Riming of Ice Particles. Riming (R) of ice particles is described similar to accretional growth of raindrops, so that the corresponding transfer rates can be obtained from

$$\left.\frac{dM_1^n}{dt}\right|_R = \int_0^\infty m^n \sigma_{14}^R \, dm = N_1 N_4 I_R^{M_1^n}(m_{f1}, m_{f4})$$

$$\left.\frac{dM_4^n}{dt}\right|_R = \int_0^\infty m^n \sigma_{41}^R \, dm = N_1 N_4 I_R^{M_4^n}(m_{f1}, m_{f4}) \qquad (14)$$

where

$$\sigma_{14}^R = - f_1(m) \int_0^\infty f_4(m') \, K_{IW}(m',m) \, dm'$$

$$\sigma_{41}^R = \int_0^m f_4(m-m') f_1(m') \, K_{IW}(m-m',m') \, dm' - f_4(m) \int_0^\infty f_1(m') \, K_{IW}(m,m') \, dm' \qquad (15)$$

K_{IW} is the collection kernel for ice particles and water drops. The numerical values were computed for hexagonal plates using terminal velocities according to Zikmunda and Vali (Ref. 10), the mass-size relationship from Nakaya and Terada (Ref. 11) and collision efficiencies from Pitter (Ref. 12).

Again the relation

$$m_{gi} = c_i m_{fi} \qquad i=(1,4) \qquad (16)$$

was used to approximate the predominant masses.

2.2.5. Summary of the Parameterization Scheme and Initiation. The tendency equations of the parameterization scheme are summarized in Table 1. Special formulations were used for the initial growth of the particles. The raindrop spectrum was initiated by

$$m_{f2} = m_{f2,0} + a_f m_{f1}^4 \quad , \quad m_{g2} = 2\, m_{f2} \quad .$$

with

$$m_{f2,0} = 0.19 \cdot 10^{-6} \text{ g}$$

$$a_f = 0.108215 \cdot 10^{23} \text{ g}$$

for raindrop mixing ratios $Q_1 < 3 \cdot 10^{-3}$.

Observations of ice crystals in natural clouds have shown (Ref. 13), that riming can start after 2-4 minutes of crystal growth. So diffusional growth of ice crystals was prescribed by

$$m_{f4} = m_R \frac{t_G}{180} \quad , \quad m_{g4} = 1.5\, m_{f4} \quad .$$

Process	Parameterization			Parameter
	L	N	m_f	
Vapor Diffusion (D)	$\left.\frac{dL_i}{dt}\right\|_D =$ [illegible] $a_i N_i m_{fi}^{(3-b_i)}$ [illegible] $m_{fi}^{(b_i-1)}$	$= 0$	[illegible]	r_f, r_g, $i=(1,\ldots,4)$
Cloud Droplet Self-Collection (SC)	$\left.\frac{dL_1}{dt}\right\|_{SC} = \left.\frac{dL_1}{dt}\right\|_{AUT}$ [illegible]	$\left.\frac{dN_1}{dt}\right\|_{SC} = K \cdot N_1 A$ [illegible]	[illegible]	r_f, r_g
Autoconversion (AUT)	[illegible]	[illegible]	[illegible]	r_f, r_g
Raindrop Self-Collection (SC)	$\left.\frac{dL_2}{dt}\right\|_{SC} = 0$	[illegible]	[illegible]	r_f, r_g
Accretion (ACC)	[illegible] $\left.\frac{dL_2}{dt}\right\|_{ACC} = N_1 N_2 A$ [illegible]	[illegible] $\left.\frac{dN_2}{dt}\right\|_{ACC} = 0$	[illegible]	r_f, r_g
Riming (R)	$\left.\frac{dL_1}{dt}\right\|_R = -\left.\frac{dL_4}{dt}\right\|_R$; $\left.\frac{dL_4}{dt}\right\|_R = N_1 N_4 A_R^L$	$\left.\frac{dN_1}{dt}\right\|_R = N_1 N_4 A_R^N$; $\left.\frac{dN_4}{dt}\right\|_R = 0$	[illegible]	r_f, r_g, $i=(3,4)$
Freezing (F)	$\left.\frac{dL_3}{dt}\right\|_F =$ [illegible]; $\left.\frac{dL_3}{dt}\right\|_F = -\left[\left.\frac{dL_1}{dt}\right\|_F + \left.\frac{dL_2}{dt}\right\|_F\right]$	[illegible]	[illegible]	r_f, r_g, $i=(1,2)$, r_f, r_g

Table 1 : Tendency equations of the parameterization scheme

where t_g is the growth time (in s) and mR is the minimum mass of an ice crystal required for riming. mR was chosen as

$$m_R = 2.43 \cdot 10^{-6} \text{ g}$$

corresponding to a plate-like ice crystal of 150 µm radius.

The apparance of frozen droplets was coupled to the droplet spectra

$$m_{f_3} = m_{f_i} \qquad i=(1,2)$$
$$m_{g_3} = m_{g_i}$$

2.3. Approximation of the Collection Integrals

The collection integrals r.f were approximated by second order polynomials A_i^j. The large range of values which had to be covered made it necessary to choose a double-logarithmic representation

$$\ln\left[\pm A_i^j (r_K, r_\ell)\right] = \sum_{n,m=0}^{2} a_{i,n,m}^{j}\, x^n y^m \qquad (17)$$

where

$$x = \ln r \qquad\qquad x = \ln(\ln r_k)$$
$$\text{or}$$
$$y = \ln r_\ell \qquad\qquad y = \ln(\ln r_\ell) .$$

The coefficients $a_{i,n,m}^{j}$ were determined by least square fit. Their values are given in Ref. 15.

3. COMPARISON WITH A DETAILED MICROPHYSICAL SCHEME

A one-dimensional, stationary model of a cumulus cloud (Ref. 14) was used for comparing the results of the parameterization scheme with those of a detailed microphysical scheme (Ref. 15). The Berry-Reinhardt scheme (Refs **2,3**) was adopted for the collection computations, riming was treated as in Beheng (Ref. **16**).

The main differences of the two model versions are:

1. **During the initial phase** of **raindrop development the -ent tendencies** for **collection** in **the two models differ from each other, so that correction factors were used to fit the tendencies:**

$$k = 3 \;, \cdot k = 0.6 \;, \; k_{sc}^{m_{g1}} = 0$$

2. The parameterized model produces raindrop distributions which are slightly broader than those of the detailed model.

3. The freezing process is more slowly in the parameterized model.

4. The parameterization of the riming process overestimates the growth rate of predominant mass m . The results were fitted to the detailed calculations by

k;'1't= 0.2

In general we can say that the parameterized model is able to reproduce the results of a detailed model sufficiently well, especially concerning the integral parameters rather than the particle spectra in detail. Computation time could be reduced up to a factor of 10.

4. REFERENCES

1. Kessler E 1969, On the distribution and continuity of water substance in atmospheric circulations, Meteor Monogr 10, No 32, 1-84.

2. Berry EX, Reinhardt R L 1974, An analysis of cloud drop growth by collection: Part I. Double di tributions, J Atmos Sci 31, 1814-1824.

3. Berry EX, Reinhardt R L 1974, An analysis of cloud drop growth by collection: Part II. Single initial distributions, J Atmos Sci 31, 1825-1831.

4. Berry E X, Reinhardt R L 1974, An analysis of cloud drop growth by collection: Part III. Accretion and self-collection, J Atmos Sci 31? 2118-2126.

5. Berry E X, Reinhardt R L 1974, An analysis of cloud drop growth by collection: Part IV. A new parameterization, J Atmos Sci 31, 2127-2135.

6. Clark TL 1974, A study in cloud phase parameterization using the Gamma distribution, J Atmos Sci 31', 142-155.

7. Clark TL 1976, Use of log-normal distributions for numerical calculations of condensation and collection, J Atmos Sci 33, 810-821.

8. Clark T L, Hall W D 1983, A cloud physical parameterization method using movable basis functions: stochastic coalescence parcel calculations, J Atmos Sci 40, 1709-1739.

9. Vali G 1971, Quantitative evaluation of experimental results on the heterogeneous freezing nucleation of supercooled liquids, J Atmos Sci 28, 402-409.

10. Zikmunda J, Vali G 1972, Fall patterns and fall velocities of rimed ice crystals, J Atmos Sci 29, 1334-1347.

11. Nakaya U, Terada T 1935, Simultaneous observations of mass, fall velocity and form of individual snow crystals, J Fae Sci Hokkaido Univ., Ser II, 1, 191-201.

12. Pitter R L 1977, A reexamination of riming on thin ice plates, J Atmos Sci 34, 684-685.

13. Reinking RF 1979, The onset and early growth of snow crystals by accretion of droplets, J Atmos Sci 36, 870-881.

14. Hirsch J H 1971, Computer modeling of cumulus clouds during project cloud catcher, Rept 71-7, Inst of Atmos Sci, South Dakota School of Mines and Technology.

15. Holler H 1982, Detaillierte und parametrisierte Modellierung der Wolken-Mikrophysik in einem stationaren Wolkenmodell, Mitteilungen aus dem Institut für Geophysik und Meteorologie der Universitat zu Koln, Heft 36, 120 pp.

16. Beheng K D 1978, Numerical simulation of graupel development, J Atmos Sci 35, 683-689.

NUMERICAL SIMULATION OF HAIL EMBRYO GROWTH

Laura·Levi* - Luisa Lubart - Maria Victoria Carrilho
Servicio Meteorol6gico Nacional - * Comisi6n Nacional de Energla At6mica
Buenos Aires - R.Argentina

1. INTRODUCTION

Several works have been devoted to the study of the structure of hailstone embryos and classifications of these embryos, in accordance with their crystallographic structure, have been proposed (Refs 1-3). However, the characteristics of the accretion process during the initial stage of hailstone formation have been scarcely studied, either theoretically or experimentally. We may consider as a basic work on this subject a study, by Pflaum and Pruppacher (Ref 4), on the growth by riming of freely suspended frozen drops in an icing wind tunnel. These authors proposed a simple model of particle growth, which allows for the variations of surface temperature and of the corresponding ice density.

In the present work, an embryo growth model is developed, based on that of Ref 4, intended for such con:-ditions as might be expected in storms that give rise to large hailstones (R 2 cm). Our model is somewath like Heymsfield's (Ref 5), but more directly - oriented to the possibility of relating the growth conditions with the graupel structure that results from the analysis of hailstone sections. The phenomenon is discussed by taking into account the conditions prevailing in typical Argentine severe storms, as they are revealed by structural features of many hailstone samples and by the application of a modified Hirsch cloud model (Ref 6) to the sounding data These storms are usually characterized by a warm cloud base (T 10°C), large thickness (on about 15 Km) and a relatively high liquid water content (3-4 g/m³) The graupels are assumed to grow as spherical particles by the riming of frozen drops with different initial radio. In fact, frozen drops were almost always found at the tip of graupels grown in clouds with warm base and large thickness (Ref 7). The rarameters used in the gro•Hth model, such as the collection efficiency E, the drag ·coefficient Co, the - relation between rime density ρ_r and graupe·l-droplet impact speed Vi, etc., have been derived from the literature by assuming a droplet spectrum of mean radius r= 10 μm.

2. RESULTS

2.1. Graupel growth at constant Ta and w.

Calculations were carried out over the temperature and liquid water content ranges -25 ≤ Ta ≤ -5°C and 1 ≤ w ≤ 4 g/m³. Runs were stopped at the wet growth limit (Ts = 0°C), since wet growth transparent ice layers, frequently found about a graupel, are usually considered a first subsequent accretion layer and not part of the embryo itself.

The model gives the evolution, as a function of time, of different parameters which characterize the process, such as the particle surface temperature Ts, the rime and mean ice densities ρ_r and ρ the radius R and the terminal fall speed V.

2.1.1. Graupel growth versus time and the effects of R_o -. Some examples for Ta = -15°C, w = 2 g/cm3 and R_o= 0.1, 0.3, 1 mm are shown in Fig. 1. It can be seen that the wet growth limit is reached at a time -varying from 16 to 31 min for different R_o - However, the corresponding limit values of the parameters, ρ ≈ 0.85 g/cm³, R ≈ 9mm and V 27 m/s are nearly independent of R_o. This is due to the fact that the low density first accretion layers affect slightly ρ, on account of their relatively small radius. A minimum ρ value is observed, in all cases, within a

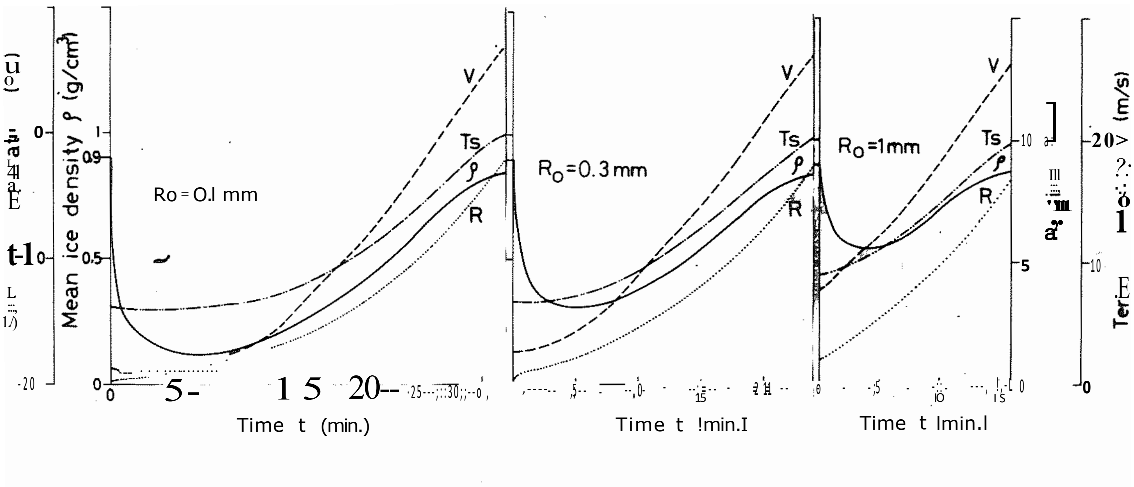

Fig.I. Growth embryo parameters versus time for Ta= - 15°C and w = 2 g/m³ few minutes of the beginning of the process. This is more pronounced for smaller R_o being $\rho = 0.13$ g/m^3 for $R_o = 0.1$ mm and $\rho = 0.31$ g/m^3 for $R_o = 1$ mm. Calculations for $R_o = 0.05$ mm gave minimum riming densities smaller than 0.01 g/cm^3, for $T < -5°C$. Graupel evolution on such small frozen droplets was therefore not considered, in the present study.

2.1.2. <u>Effects of Ta on the process.</u> Calculations at different Ta and fixed R_o show that the radius R_t attained after a given growth time depends slightly on Ta. The curves for R in Fig. 1, calculated for Ta = -15°C, are thus valid for any Ta in the considered range, if w = 2 g/cm3. However, the relation between ρ and R depends markedly on Ta; this is shown in Fig. 2, where ρ is plotted against Ta for $R_o = 3$ mm, w = 2 g/m3 and for different values of R. These results partially disagree with Heymsfield's (Ref 5), who found that both R and ρ vary slightly with Ta. However, it must be nnted that the initial particles used by this autor were mainly aggregates and planar crystals, instead of frozen drops. The different nature of these particles may modify the evolution of the phenomenon.

As it may be expected, also R_t and V depend on Ta, their value increasing when Ta decreases, as shown by the curves of R_t versus Ta, plotted in Fig. 3 for w = 1, 2 and 4 g/m^3. These curves, obtained for $R_o = 0.3$ mm, are approximately valid for any R_o.

2.1.3. <u>Effect of w on the process.</u> As shown in Fig. 3, the transition to wet growth occurs at smaller R for larger values of w, due to a faster increase of the riming density which reaches sooner the value of 0.9 g/m3. This effect is more pronounced for lower Ta. On the other hand, as noted by Heymsfield, the time needed to reach a given R varies aproximately as the inverse of w, i.e., $t_{w_2}(R) = (w_1/w_2)\, t_{w_1}(R)$.

2.1.4. <u>Radial variation of the embryo structure related to Ts(R).</u> When hailstone sections are analysed, direct relations can be found between the structure of a layer and its radial distance from the growth center. As crystal size and ice density depend on Ts, curves of Ts (R) for w = 2 g/m^3 and different values of Ta, were obtained. The curves in Fig. 4 correspond to $R_o = 0.3$ mm. In the figure, the line Ts = -10°C has been drawn, to separate the coordinate plane in a lower region (Ts<-10°c), where ice is opaque and crystals are small and an upper region, where the ice transparence and the crystal size increase with Ts. The curves are approximately parallel so that, for a given R, a variation of Ta determines a similar variation of Ts.

In Fig. 5, Ts(R) is plotted for different values of w, at Ta = -20°C. The curves show that a graupel of R = 5 mm, grown at this Ta, should be completely opaque for w ≤ 2 g/m^3 while it might exhibit an increasingly transparent external ice layer for w > 2 g/m3. The parallelism of the Ts(R) curves in Fig. 4, implies that Fig. 5 can be used to obtain similar families of curves for different values of Ta. Calculations for $R_o = 1$ mm, show similar behaviour when R > 2 mm.

As for the crystal size, evaluations for each Ta, Ts pair could be obtained, on the basis of previous results about the crystal size in accreted ice. These evaluations will not be carried out in detail in the present work. We will just remark that crystals larger than 1 mm may only be expected for Ta > -18°C, Ts > -10°C. For lower values of Ta, crystal dimensions would remain below this size, even if Ts ≈ 0°C.

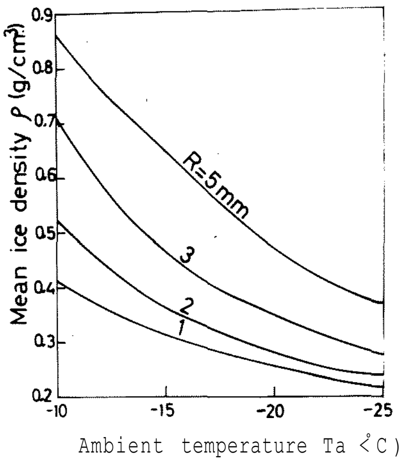

Fig. 2. ρ versus Ta for different R

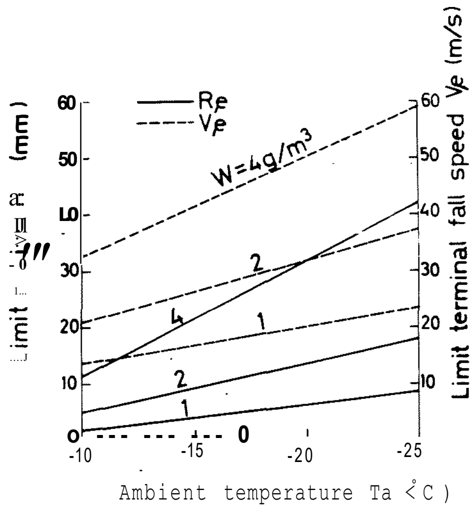

Fig. 3. R_ℓ and V_ℓ versus Ta for different w

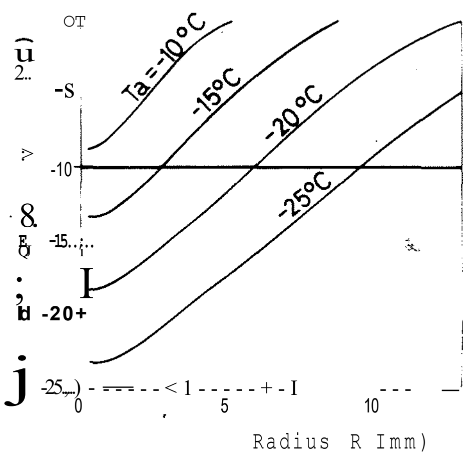

Fig. 4. Ts versus radial distance for different Ta, $R_o = 0.3$ mm. w = 2 g/m3.

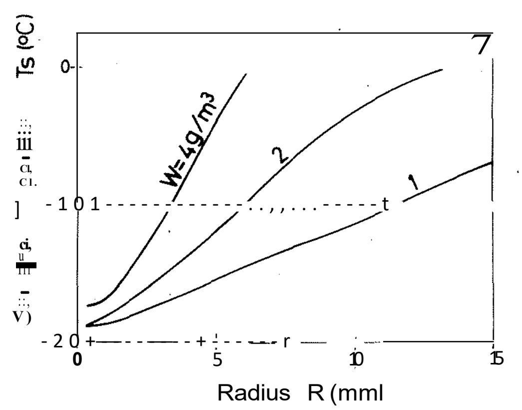

Fig. 5. Ts versus adial distance for different w. $R_o = 0.3$ mm. Ta = -20°C.

2.2. Graupel growth in an updraft profile.

Following Heymsfield, a simple unidimensional cloud model is used to analyse the growth process for embryos with different initial size, inyected at different levels inside an updraft. With this purpose, a "leader" embryo with a given R_o was selected and an updraft profile, capable of lifting the growing particle at low speed (2 m/s) to a level where the updraft is assumed to be maximum, was calculated. Above this level, placed at Ta = -20 or -15°C, the updraft sharply decreases, vanishing at Ta = -25 or -20°C, respectively. The vertical temperature gradient, of about 7°C/km, used to establish the relation between heiaht and Ta, is derived from the scunding data of a typical hailstorm day for Mendoza. Considering that, in the cloud region of embryo growth, the liquid water content should be somewhat lower than that calculated for the main updraft (Ref 6), a value of w = 2 g/m^3 was assumed.

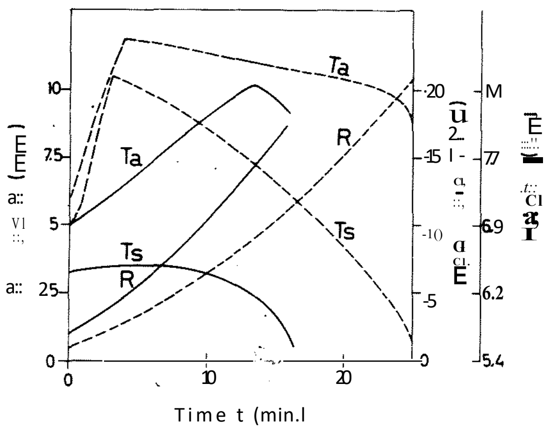

Fig. 6. Ta, Ts and R versus time in an updraft profile with maximum updraft at Ta = -15°C. -Leader embryo of $R_o = 1$ mm.---Embryo of $R_o = 0.5$ mm.

The updraft profile, used to draw the curves in Fig.6, was calculated by releasing a leader embryo of $R_o = 1$ mm at the Ta = -10°C, h = 6.95 km level. The maximum updraft set at Ta = -20°C, resulted 24 m/s. Most growth occurred at Ta>- 20°C, Ts -7 °C. The particle spent a few minutes near the -20°C level, reaching wet limit (Rt = 9 mm) after 16 min growth. The rime density (not given in the figure) was always Pr)0.6 g/cm^3. Under these conditions, the rime surro nding the frozen drop would progressively change from slightly opaque to transparent, whereas the crystals would be large throughout the whole structure. In this profile, particles with various R_o were placed at different levels, and their trayectory and development were computed. The results are exemplified by the curves in Fig.6 for $R_o = 0.5$ mm. The Ta curve indicates that; in this case, the particle is rapidly lifted over the -20°C level while, only for R>6 mm, does Ts increase above -10°C. Thus, an embryo of this type mainly develops in the low temperature region of the cloud and its structure consists of opaque ice and small crystals. The wet growth limit (RL= 10 mm) is attainea after 25 min. The growth times taken by either particle to reach Rt agree with the results in section 2.1. and they are compatible with the life time of a cloud cell (Ref 5). Embryos of R_o) 1 mm were placed in the same updraft. In this case, they rapidly fell dawn if located at the same level of the leader embryo; if injected higher than a critical level, they were rapidly carried over the -20°C level, remaining most of the time at low Ta.

Comparing the curves drawn for embryos of various R_o, placed in an updraft with maximum value at Ta = -20°C, it may be concluded that, for the critical value Re of the leader embryo,growth occurs mostly in the region of the cloud where Ta)-20°C. Such an embryo is mainly formed by transparent or slightly opaque ice and large crystals. For any other value of R_o,most of the graupel growth should occur in the region of the cloud over the maximum updraft. These embryos would be mainly formed by opaque ice and small crystals. Thus, in these conditions, hailstones with this type of embryos should prevail.

Since hailstone analysis from a given storm has shown that graupel embryos formed by large crystals often prevail (Ref 8) an updraft profile with a maximum at Ta = -15°C was also calculated. In this case, a 0.3 mm leader embryo was placed at the

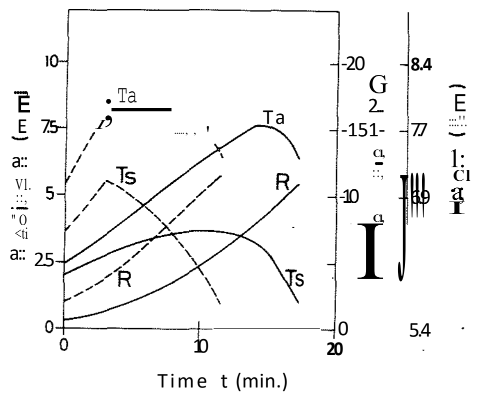

Fig. 7. Same as in Fig.6 but with maximum updraft at Ta = -15°C. -Leader embryo of $R_o = 0.3$ mm --- Embryo of $R_o = 1$ mm.

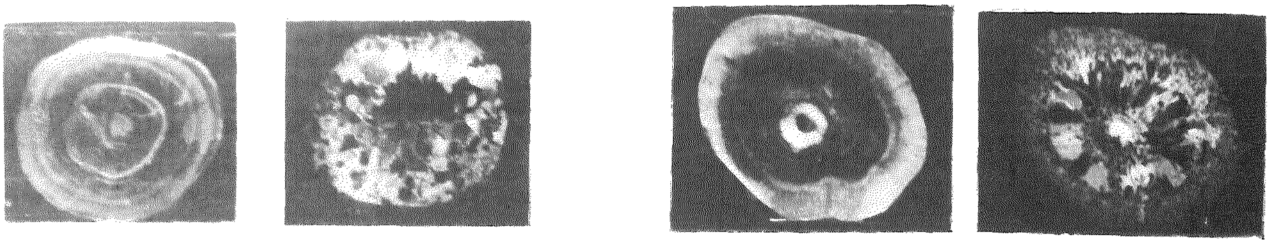

8 (o.) 9 (b)

Fig. 8. Hailstone section in natural and polarized light

la= -5°C, h = 6.15 km level. The curves in Fig. 7 are quite similar to those in Fig. 6, yet they indicate that the embryo develops most at Ta) -15°C, Ts"' -7°C. Consequently, graupels formed in these conditions should consist of large crystals though relatively opaque ice. For the same updraft profile, an embryo of R_o=1 mm was injected at the Ta=-11°C, h=7 km level. Under these conditions, most growth occul'l'ed at -15 TaL17°C, while Ts only decreased below -10°C for just a few minutes. The resulting rime structure would be quite similar to that of the 0.3 mm embryo. Thus, these updraft conditions would favour the development of graupels formed by large crystals, regardless of R_o.

2.3. Natural Hailstones

Fig. 8 shows two typical examples of hailstone sections with embryos grown about center units of different size: In Fig. 8(a), the initial unit is too smail to be revelead in the section. The slightly opaque embryo is surrounded by a layer which shows clear evidence of wet growth, being the radius at the graupel limit prnbably coincident with rv2 mm (w,..,2g/m3, Ta"'-2°C, according to Fig. 4). The water in excess of the wet layer has probably penetrated the low density initial zone, reducing its opacity. Large crystals, that begin in the embryo, are observed to continue in the subsequent zone. All these features suggest that growth has occuired in an updraft such as that of Fig. 7.

On the other hand, the growth unit in Fig. 8 (b) is a frozen drop of Ro=1.5 mm surrounded by an opaque ice layer. The latter is formed by small crystals which may have grown at Ta -20°C. In this case, the embryo is likely to have grown in an updraft of the kind shown in Fig. 6 and the trajectory should be similar to that corresponding to R_o 1 mm.

3. CONCLUSIONS

The results of the present work may be used to estimate the growth conditions for graupel embryos which exhibit a specific structure. Though they are strictly valid for embryos grown about frozen droplets, they may be easely adapted to simulate embryo growth about initial particles of lower density such as aggregates or small graupels (Ref 5).

It is shown that, when frozen droplets are injected in a given updraft profile with a fixed value of w, only particles with R_o=R_C may grow substantially, during their ascent, before reaching the upper cloud region where the updraft decreases. Frozen drops of Ro,Rc could only spend in the cloud a time large enough to attain the observed graupel dimensions, if injected at a high enough level to arrive ·Jpidly to the considered cloud region; frozen drops of R_o<R would get at high speed this region, indepenaently of the injection level. It would result that, since there is a low probability for an embryo to have the initial radius Re, a large particle fraction would mostly grow in the region above the maximum updraft. Thus, the embryo structure could inform about the temperature range in this region, which should be below -zo•cwhen the prevailing embryos are opaque and formed by small crystals but, mostly above this temperature when such embryos are transparent or slightly opaque and formed by large crystals.

When the embryo shows a transition to wet growth the evaluation of Ta, derived from the structure, and that of R may be used to also estimate the cloud liquid water content.

Acknowledgments: The authors are indebted to Dr. F.Requena for helpful discussions and to the Consejo Nacional de Investigaciones Cientificas y Tecnicas for economic support.

4. REFERENCES

1. Federer B et al 1978, Hailstone Trayectories Determined from Crystallography, Deuterium Content and Radar Backscattering. Pageoph. 116, 112-129.
2. Knight Ch A & NC Knight 1970, Hailstone Embryos, J.Atmos.Sci., 27, 659-666.
3. Knight Ch A & NC Knight 1976, Hail Embryo Studies. Proc.Int.Cloud Phys.Conf, Boulder, Colorado, 222-226.
4. Pflaum J C & HR Pruppacher 1979, A Wind Tunnel Investigation of the Growth of Graupel Initiated from Frozen Drops, J.Atmos.Sci., 34, 6-S0-689.
5. Heymsfield A J 1982, A Comparative Study of the Rates of Development of Potential Graupel and Hail Embryos in High Plair.s Storms. J.Atmos.Sci 39, 2867-2897.
6. Hurtis MG & ME Saluzzi 1980, Estudio de un modelo parametrizado de nube convectiva a traves de su aplicaci6n a casos reales de convecci6n severa. Com. Nae. Inv. Espaciales.
7. Harimaya T 1980, Graupel Embryos. Proc. Int.Cloud Phys.Conf., Clermont-Ferrand, 245-248.
8. Lubart Let al 1979, Estudio comparativo de la estructura de granizos. Geoacta, 10, 41-49.

SESSION V

NUMERICAL SIMULATION OF CLOUD FORMATION PROCESSES

Supsession V-2

Convective clouds. Sqall lines

NONSTATIONARY THREE-DIMENSIONAL NUMERICAL MODEL OF HAIL 1.IOUDS WITH AN ALLOWANCE FOR MICROPHYSICAL PROCESSES

B.A. Ashabokov and Kh.Kh. Kalazhokov

High Mountain Geophysical Institute, Naltchik, 360030, USSR

Mathematical description of thermohydrodynamical processes in clouds adequate to their p-lysical nature is an extremely_ difficult problem of mathematical physics and comoutational mathematics.

Complexity of this problem is associated with the fact that a cloud is a multiphase thermohydrodynamical and microphysical system with a number of reverse relations, degrees of freedom and scales of events, determining its state (Ref. 1).

In cloud orocess modelling there are two tendencies The works belonging to the first one (Ref. 2), give detailed description of thermohydrodynarnical processes with the help of physical process parameterization. The other works (Ref. 3) investigate cloud processes on the basis of detailed mi.crophysical processes through kinetic equations for cloud particle size distribution and simplified description of thermohydrodynamical processes. Interaction of these processes is complex and for detailed description of cloud formation. and development it is necessary to investigate and work out their numerical model including thermohydrodynamical and microphysical processes.

In this work the preliminary results of the development of nonstationary three-dimensional nURlerical equations of liquid and solid cloud particle distributions are presented.

To realize the model o an electronic computer computational algorithm is used, which is based on the splittering and Bubnov-Galerkin methods.

1. FORMULATION OF THE PROBLEM

Let (x, y, z) be a Cartesian system of coordinates (the beginning of which is on the ground surface; x, y - directed horizontally, z - vertically upward). Now let us consider the following domain:

G = {(x_y,z):O<-x<. LxJO<y<.Ly JO<z<LIJ

which is limited by the planes:

x,,O,Lx j y=o,Ly 1 = O,L i: 1

and

Gt:Gx{od:, <oo} Gt,rn:::Gtt{O<m<oo}

It is suppcsed that therrnohydrodyna ical characteristics in the doma;n of their determination Gt are continuous and have continuous derivatives of the first order with resoect to time and of the second order with resoect to spatial coordinates whereas microphysical characteristics in the domain Gt,m are continuous with continuous derivatives of the first order with respect to time and particle mass and of the second order with respect to spatial coordinates. We discussed mathematical formulation of a nonstationary three-dimensional model of mixed clouds, which is based on the system of equations :or cloud thermohydrodynamics ,nd microphysics with common and well known assumptions:

the equations of thermohydrodynamical processes in the domain Gt:

$$\frac{du}{dt} = -\frac{\partial \pi'}{\partial x} + \tilde{\Delta} u,$$

$$\frac{dv}{dt} = -\frac{\partial \pi'}{\partial y} + \tilde{\Delta} v,$$

$$\frac{dw}{dt} = -\frac{\partial \pi'}{\partial z} + g\left(\frac{\vartheta'}{\theta_0} + 0.61 q' - Q_s\right) + \tilde{\Delta} w,$$

a(,(,+o'lY+ ow=6"w-, / Jx oy a (1)

dJ} / dt = J / (C_p T) (SM / Le,8t + L oMs / s 8f. + L 8Mi) / 7..ot) +/J. >

= - oMc / St − 8Ms / 8t + ia_v,

$\pi = \Pi_0 + \pi'$, {} = e₀ + V'} q = Qo+ci,',

the equations of microphysical processes in the domain Gt,m=

$$\frac{df_1}{dt} = w_s^{(1)} \frac{\partial f_1}{\partial z} - \left[\frac{\partial f_1}{\partial t}\right]_c - \left[\frac{\partial f_1}{\partial t}\right]_z + \left[\frac{\partial f_1}{\partial t}\right]_{col} + \left[\frac{\partial f_1}{\partial t}\right]_{fr} + \tilde{\Delta} f_1 + I_1$$

$$\frac{df_2}{dt} = w_s^{(2)} \frac{\partial f_2}{\partial z} - \left[\frac{\partial f_2}{\partial t}\right]_s + \left[\frac{\partial f_2}{\partial t}\right]_z + \left[\frac{\partial f_2}{\partial t}\right]_{col} + \tilde{\Delta} f_2 + I_2 \quad (2)$$

initial-edge conditions:

-IA.,, uo 1 "",, ,,.. ° I w- = i.r o , V= ,..?:

t=<t⁰ 1 l1 = f/ , fi, :: J; at t=O,

f₁ =-fz=W-=11£.:: 0,.. / az = olJ / al. = =0 / a at =0,

= / a:z ah / h. =-1.v=11 / az -=-a / a" = c)V / a = / ol.. =O at z=l

l1 = f,:::au / OX =a,...:: / oJ:: d / ox = a / ox = / cx =0 at?t=O,L

-{-,.. au. / ay _ ov / ay _ ow / ay _ d1' / ay _ _0 / ay at y=O,L

Symbols and auxiliary relationships:

d / dt = I / at + u 0 / ax + ... 0 / a + ... 0 / d

A = 0 / ax + ... a / ax + ... a / a, a / a a / a d / ai.

$$K = K_0 + cL_T^2\left[\left(\frac{\partial u}{\partial x}\right)^2+\left(\frac{\partial u}{\partial y}\right)^2+\left(\frac{\partial u}{\partial z}\right)^2+\left(\frac{\partial v}{\partial x}\right)^2+\left(\frac{\partial v}{\partial y}\right)^2+\right.$$
$$\left.+\left(\frac{\partial v}{\partial z}\right)^2+\left(\frac{\partial w}{\partial x}\right)^2+\left(\frac{\partial w}{\partial y}\right)^2+\left(\frac{\partial w}{\partial z}\right)^2\right]^{1/2},$$

$$\pi = \frac{c_p\bar{\Theta}_0}{A}\left(\frac{P}{1000}\right)^{\frac{AR}{c_p}}, \qquad \Pi_0 = \frac{c_p \Theta_0}{A\Theta_0} T,$$

$$Q_s = \int_0^\infty m\,(f_1+f_2)\,dm,$$

$$\sigma = -\frac{d\ln\rho_0}{dz},$$

$$\frac{\delta M_c}{\delta t} = \int_0^\infty m\left[\frac{\partial f_1}{\partial t}\right]_c dm,$$

$$\frac{\delta M_s}{\delta t} = \int_0^\infty m\left[\frac{\partial f_2}{\partial t}\right]_s dm,$$

$$\frac{\delta M_z}{\delta t} = \int_0^\infty m\left[\frac{\partial f_1}{\partial t}\right]_z dm,$$

$$\left[\frac{\partial f_1}{\partial t}\right]_c = \frac{\partial}{\partial m}\left(f_1\left[\frac{dm}{dt}\right]_c\right)$$

$$\left[\frac{\partial f_1}{\partial t}\right]_z = A_f\, m \exp\left(B_f\,(273{,}16-T)\right)\cdot f_1$$

$$\left[\frac{\partial f_1}{\partial t}\right]_{cot} = -f_1\int K_{11}(m,m')\, f_1(m',x,y,z,t)\,dm' +$$
$$+\frac{1}{2}\int_0^m K_{11}(m-m',m')\, f_1(m-m',x,y,z,t)\, f_1(m',x,y,z,t)\,dm' -$$
$$- f_1\int_0^\infty K_{12}(m,m')\, f_2(m',x,y,z,t)\,dm',$$

$$\left[\frac{\partial f_1}{\partial t}\right]_{fr} = -P(m)\cdot f_1 + \int_m^\infty P(m')\,Q(m,m')\,f_1(m',x,y,z,t)\,dm',$$

$$P(m) = 2.9\cdot 10^{-7} \exp(3\cdot [illegible]),$$

$$Q(m, m') = [illegible] \exp\left(-7\,\frac{m}{m'}\right)$$

$$\left[\frac{\partial f_2}{\partial t}\right]_s = \frac{\partial}{\partial m}\left(f_2\left[\frac{dm}{dt}\right]_s\right),$$

$$\left[\frac{\partial f_2}{\partial t}\right]_{cot} = f_1\int_0^\infty K_{12}(m,m')\, f_1(m',x,y,z,t)\,dm' +$$
$$+\int_0^m K_{12}(m-m',m')\, f_1(m-m',x,y,z,t)\, f_2(m',x,y,z,t)\,dm',$$

Here t - time; u, v, w - wind vector velocity components along the axes x, y, z, respectively; T - absolute air temperature; Θ - potential temperature; q - specific humidity; Θ', q', ρ' - deviation of the respective values from their initial meanings; g - gravitation accelerating force; Q_s - total relationship of liquid and solid particle mixture; c_p - air heat capacity at constant pressure; L_e, L_s, L_z - specific heat of condensation, sublimation, freezing, respectively; A - thermoequivalent of work; $\delta M_c/\delta t$, $\delta M_s/\delta t$ - water vapour masses condensing on liquid and solid particles in unit time; $\delta M_z/\delta t$ - water mass frozen in unit time; T_0, Θ_0, q_0, Π_0 - background values of the respective parameters; $\bar{\Theta}_0$ - average potential temperature; f_1, f_2 - functions of liquid and solid particle mass distribution, respectively; v_1, v_2 - fixed fall velocities of liquid and solid particles, respectively; $(\delta f_1/\delta t)_c$, $(\delta f_1/\delta t)_z$, $(\delta f_1/\delta t)_{cot}$, $(\delta f_1/\delta t)_{fr}$ etc.-functional variations of liquid particle distribution due to condensation, fraction, coagulation processes, respectively; $(\delta f_2/\delta t)_s$, $(\delta f_2/\delta t)_z$, $(\delta f_2/\delta t)_{cot}$ - variations of functions of solid particle distributions due to sublimation, freezing, coagulation, respectively; I_1, I_2 - velocities of liquid and solid particle formation due to atmospheric aerosol activation, respectively; K - turbulence coefficient; $K_0 = 0{,}2\cdot 10^{-4/3}\cdot L_T^{4/3}$, $c = 1$, $L_T = 250$ m - constant values; A_f, B_f - constant parameters; K_{11}, K_{12} - collision probabilities of liquid and liquid-solid particles, respectively; $Q(m, m')$ - probabilities of m mass drop formation at splittering of m' mass drops; $P(m)$ - probability of m mass drop splittering in unit time; $(dm/dt)_c$, $(dm/dt)_s$ - growth velocities of some liquid and solid particles due to condensation and sublimation, respectively; ρ_w - water density. The equations solved in cloud process model (1) - (3) describe three-dimensional motion of cloud environment with an allowance for nonstationary, turbulent, dynamical and thermal interactions of gas components with liquid and solid cloud particles; mass conservation law with an allowance for air density decrease with hight; heat and moisture transfer taking into account water vapour phases and liquid cloud particles; liquid and solid cloud particle transfer with an allowance for gravitational fall, condensation, crystallization processes as well as the processes of liquid particle coagulation and fractioning, cloud particle formation due to atmospheric nuclei activation. Not considering all possible formulations of initial data one may say that in common case it is very difficult to choose and correlate initial fields for cloud process calculation due to significant scale differences of thermohydrodynamical and microphysical characteristics of the time of formation. There are several ways of formulation of edge conditions of cloud process computational problem. If equations of cloud processes account for turbulence as in (1), (2) then one may specify as edge conditions the values along the boundary of problem decision domain, as being equal to the background values. The demand for disturbance smoothness in the vicinity of the domain boundary is one of the possibilities of edge condition specification. The other way is the specification of the required values on one part of the domain boundary and the necessity of disturbance smoothness on the other part of it. If these equations do not consider turbulence, edge conditions are predetermined on the part of the domain boundary in the points where vector velocity is directed inward the domain. For the sake of simplicity, we assume that all input and output data of the problem (1) - (3) satisfy all the necessary conditions for smoothness.

2. NUMERICAL ALGORITHM OF CLOUD PROCESS EQUATION SOLUTION

The computational problem of cloud processes (1) - (3) is related to complex nonstationary polymeric problem of mathematical physics, numerical decision which meets great computational difficulties due to limited poss.ibilities of computer facilities (Refs. 4-6). Therefore, it is important to develop economic numerical algoritru s for computations. In our work an algorithm based on the splittering and Bubnov-Galerkin's methods is used.

The main stages of numerical algorithm are:

1. Formulation of computational problem of cloud processes (1) - (3) in dimensionless va],ues.
2. Division of the task by components (1) - (3) in each time step $\Delta t = t_{i+1} - t_i$ into the following more simple problems:
   2.1. advective and turbulent cloud transfer;
   2.2. processes based on phase transition;
   2.3. coagulation;
   2.4. drop splittering and liquid and solid particles formation in clouds;
   2.5. velocity field adaptation to pressure field;
3. Spectral formulation of the computational task of cloud processes on the basis of Bubnov-Galerkin method for the fractioned formulation of the problem.
4. Coordinate function choice.
   4.1. for decomposition of the thermohydrodynamical characteristics-eigenfunctions of some auxiliary problems for Laplacian operator with the domain of determination
   $G = \{ (x, y, z) ; 0 < x, y, z < 1\}$
   4.2. Ior decomposition of microphysical characteristics-eigenfunctions of Laplacian operator and orthogonal exponential functions (Ref. 9);
5. Unknown decomposition coefficient calcu4 lation on the basis of numerical decision of Koshi problem at each fractional step for common differential equation system.
6. Thermohydrodynamical and microphysical c'haracteristics of cloud processes.
   We underline some important peculiarities of the discussed algorithm. It is apparent that the module principle used allows to adopt the given numerical algorithm for various problems of cloud physics without significant changes of problem soft-ware. As Bubnov-Galerkin's method used in m1merical algorithm is an effective tool for the compression of large bulk of information, the volume of computations needed for problem realization on electronic computer substantially decreases.

3. RESULTS OF PRELIMINARY CALCULATIONS

Let us consider calculational results of the cloud processes with methodical character obtained for:

1. understanding applicabilities of numerical algorithm based on the combination of splittering and Bubnov-Galerkin's methods for calculation of thermohxdrodynamical and microphysical processes in mixed clouds.
2. determination of some qualitative and quantitative characteristics of computational problems.
3. obtaining preliminary numerical information on thermohydrodynamics and microphysics of clouds and its qualitative analysis.

The choice of concrete forms of initial-edge conditions of the problem depends on methodical character of calculations. Calculations were made at the following values of input data:

1. The domain of dimensionless spatial coordinate variations.

$$G = \{ (x, y, z) : 0 < x < 1, \ 0 < y < 1, \ 0 < z < 1 \}$$

2. The initial values of thermohydrodynamical and microphysical characteristics of cloud processes:

$$u^0 (x,y,z) = 0.1 \cdot \mathrm{Cos}\, \pi x/2 \cdot \mathrm{Cos}\, \pi y \cdot \mathrm{Cos}\, \pi z;$$

$$v^0 (x,y,z) = w^0 (x,y,z) = 0;$$

$$\vartheta^0 (x,y,z) = 1{\cdot}1 \cos x/2 \cdot \mathrm{Cos}\, \pi y/2 \cdot \mathrm{Cos}\, z/z;$$

$$q^0 (x,y,z) = 2 \cdot \cos \pi x/2 \cdot \mathrm{Cos}\, y/2 \cdot \mathrm{Cos}\, z/2;$$

$$f^0_1 (x,y,z,m) = \exp(-0.5m) \cdot \mathrm{Sin}\, x \cdot \mathrm{Sin}\, \pi y \cdot \mathrm{Cos}\, \pi z/2;$$

$$f^0_2 (x,y,z,m) = 0$$

The dimension type of the task is transferred to the dimensionless on the basis of the following characteristic values: velocity - V = 10 m/s, length - Lh = = 20 km, hight - H = 10 km, time - T_h = = 10^3 sec, temperature - Qh = 27$3^\circ$, water content qh= 0.1.13 g/kg,,mass - mo= = 0. 113 g, distriburion functions '.f= = $m0/N_0$ (N_0 = 1 kg-). The development of the convection in the region with un stable stratification due to thermal pulses is considered.

4. The parameters of numerical algorith. are given below:
   splittering step = 0,05 that is each of the tasks (2.1) - (2.5) was solved at fractional step Δt = 10 s;
   a number of items corresponding to each independent variable (x, y, z, m) in Bubnov-Galerkin's method, N = 3;
   Koshi task for Fourier coefficient determination was solved by Runge-Kutte method with automatical choice of steps1

The results of preliminary calculations are given in Figs. 1-3 in dimensionless values.

These preliminary results are in qualitative agreement with experimental data on the character of given cloud characteristics changes.

Qualitative analysis of numerical information shows that numerical algorithm based on both splittering and projectional methods may be useful when calculating thermohydrodynamical and micr9physical characteristics of mixed clouds. It takes about 6-7 hours of computer EC-1022 time to calculate one minute of cloud processes development in real time.

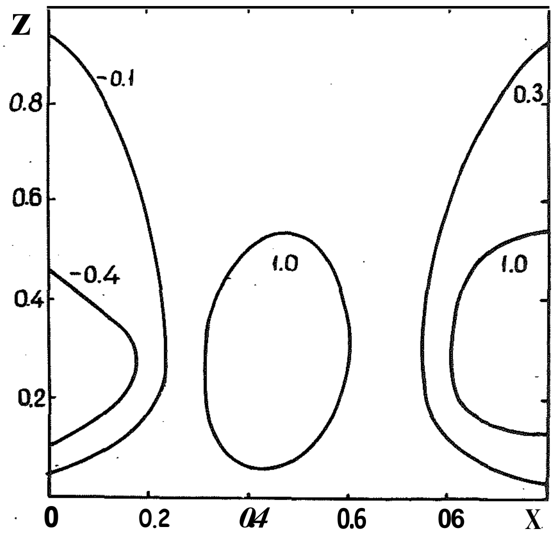

Figure 1. Isolines of vertica velocity component w in the planes (x; 0.5; z) at the moment "t = 0.3.

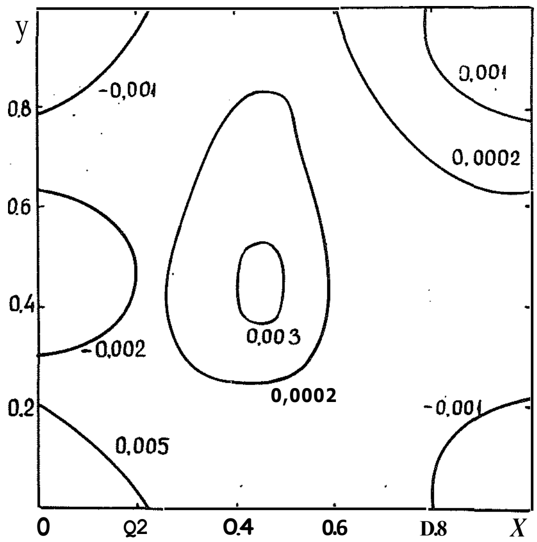

Figure 2. Isolines of horizontal velocity component u in the planes (x; y; 0.5) at the moment 'I:= 0.3.

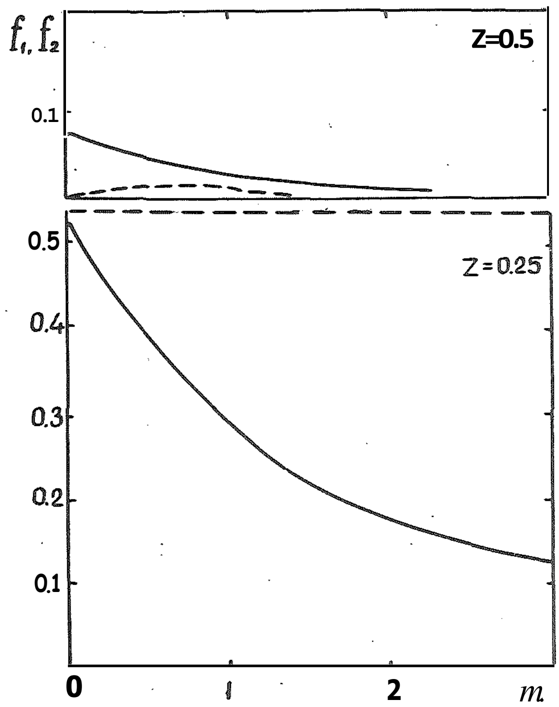

Figure 3. Functions of liquid f1 (solid line) and f2 solid (dashed line) particle distributions in the vicinity (0,5; 0,5; 0,25) and (0,5; 0,5; 0,5) points at the moment 't= 0. 3.

5. REFERENCES

1. Shmeter, S.M., 1972. Physics of convective clouds. L., Hydrometizdat, 231 pp.
2. Koryakov, C.A., Lebedev, T.M., 1983. Threedimensional numerical model of a single convective cloud. (Preliminary results). Trudy IPG, iss. 45, 2-20.
3. Kogan, E.L:, 1978. Three-dimensional numerical model of droplet cumulus clouds taking into account microphysical processes. Proc. Acad. Sci. USSR, Physics of Atmos. and Oceans, 14, 8, 876-886.
4. Yanenko, N.N., 1967. Method of fractional step to solve multidimensional prob, lems of mathematical physics. Novosibirsk, "Nauka", 236 pp.
5. Marchuk, G.I., 1977. Methods of computational mathematics. M., "Nauka", 456 pp.
6. Samarski, A.A., 1977. Introduction in the theory of difference schemes. 552 pp.
7. Ashabokov, B.A., Kalazhokov, Kh.Kh. 1983. On approximate solution of coagulation equations by splittering and Bubnov-Galerkins methods. Trudy VGI, iss. 55.
8. Ashabokov, B.A., Gaeva, Z.S., 1983. On the algorithm of numerical modelling of microphysical processes in clouds. Trudy VGI, iss. 61.
9. Dmitriev, D.A., 1983. Orthogonal exponential functions in hydrometeorology. L., Hydrometizdat, 119 pp.

A NUMERICAL STUDY OF THE lNITIATION OF MOUNTAIN CUMULI

Robert M. Banta

Air For,·, Geophysics Laboratory: AFGL/LYC
Hanscom AFB, MA 01731 .S.A.

1. INTRODUCTION

An accurate representation of the processes by which clouds are initiated is a problem which cloud modelers have had to address since they have attempted finite-difference simulations of moist convection. Ogura (Ref. 6) for example, started his clouds with bubbles that were 1C or 3C warmer at their maximum values thal, the environment. This kind of initiation process is likely to be very unrealistic, however, and the next section describes some difficulties which arise from using it or similar. processes. What seems more reasonable is to accurately model a continuous process such as mountain upslope flow which is known to lead to cumulus cloud formation, and then let the clouds form "naturally" from the evolving flow field, The present study us·es this example of mountain upslope flow to investigate the lnitiation of mou tain cumuli.

2. .THE PROBLEM OF MODEL CLOUD INITIATION

Clark(Ref. 3) and Tripoli and Cotton (Refs, il,12) discuss the problem of getting a cloud started n a numerical model, They cite studies in which th ,nitial field contains warm bubbles, moist bubbles eat sources, or vertical velocity impulses. Variou problems arise by introducing such perturbations, powever. Warm· or moist bubbles, for example, intro- /iuce spurious energy, which may he unrealistically large, into the system, and Clark points out that he size an<l intensity of these perturbations affect l:he selection of length scale and updraft intensity, t least in che early stages of the storm evolution, rripoli and Cotton contend that warm or moist perturbations generally have equivalent potential temperatures (0e 's) higher than anywhere else in he domain, and thus probably higher than observed i ature. As a result, the initial vertical impulse quickly deintensifies,·as lower 0e air is dynamically entrained (i.e. entrained by resolved-scale eddies) nto the base:-of the bubble; This often produces a ::pinching off" of the cloud and leads to its ultimat tlestruction.

Clark (Ref. 3) initiated his own simulated cloub ith a warm bubble and demonstrated that bubble- or mpulse-type i itiation procedures tend to produce torm-splitting. This occurs in the first fully-' eveloped cumulonimbus clouds as the downwind side of he main updraft entrains lower 0e air; a wedge- aped downdraft forms in the middle of the updraft, viding.it in two, The fact that the ultimate source he downdraft - and therefore of the storm split- ing - is the cloud initiation procedure and not atural cloud processes (such as precipitation loading or vorticity dynamics, exposes a problem to all these kinds of schemes. Clark's choice of case tudies further illustrates this difficuJ,ty.; i:he storm he attempted to simulate was not observed to split, but his simulation did produce storm-splftting by the mechanism just described,

Tripoli and Cotton (Ref 11) started their cumuli with a moist (saturated) bubble, but added a ..focused convergence .. scheme to sfmulate observe d mesoscale convergence and to help produce long-lived thunderstorms. They found that the magnitude of the mean convergence over the simulation domain had a dramatic effect on storm kinetic energy and total rainfall as expected, but also that the size and intensity of the focusing of the convergence within the domain had a significa*t ffect as well, Tripoli and Cot"ton (Ref 12) present' nother technique for cloud initiation, a gust-front echnique. In this scheme, they introduced a cooling function in the center of the domain to simulate rain pvaporation, and storms form along the ·inflow boundary bf the cold air.

Other realistic ways of initiating clouds in lufe introducing random asymmetries in an otherwise horizontally-homogeneous boundary layer. Hill (Ref t) n Sommeria (Ref 10) did this by adding a random oponent to their specification of the surface potential) temperature in their shallow cumulus odels.

Orville (Ref 7) recognized the importance of mountains in producing cloud-initiating convergence which lasted for long times, In this and other papefs (e.g. Refs 5,7-9) he studied in 2-D the development of clouds over triangular, heated ridges with rather steep slopes of 45°. In this paper (Ref 7), however) which considered cloud growth in the aeaence of flow aloft, he found little difference between clouds generated by a hill with a slope of 45° nd one with; a slope of 26.5°. He also investigated shallow clou s in the presence of flow aloft (Ref 8) and shallow clouds which precipitate (Ref 5). Orville and Sloan (Ref 9) found that this cloud initiation scheme coull produce thunderstorm-sized clouds, but their 2-D storm killed themselves by precipitating into their own updrafts. In addition, he has used this initiation scheme in many more-recent studies of thunderstorms.

3. CONVECTIVE CLOUDS FORCED BY MOUNTAIN LEESIDE CONVERGENCE

The heated triangu ar-hill initiating mechanism pf Orville has many desirable properties, since it provides a continuous convergence forcing (except for shadow effects) and the clouds arise from the errain-generated flow field. In studies which emphasize the details of the initiation process, owever, the steep slope may not properly produce th ynamic and thermodynamic properties of air entering! floud base, Banta (Ref 1) simulated dry upslope flow forced by surface heating using the Tripoli-Cotton cloud/ mesoscale model (Ref 12). These 2-D simulations used ridges with more realistic slopes, and, in agreement **with observations, they generated a persistent zone** of convergence to the lee of the ridge (Fig 1). Banta noted that aerodynamic effects of the flow over the hill seem to be important even for small hills, **and that these effects increase as the size of the hill increases.**

These simulations were based on observations of daytime upslope flow generation in a wide mountain valley (Refs 1,2). The observational analyses found **a zone of convergence on the lee side of mountain** ridges, formed where surface upslope flow meets convectively-mixed surface winds blowing down from the ridgetops, similar to the model-generated cross section in Fig 1. This zone is both a region of **persistent low-level convergence and a region where** high low-level moisture is advected in by the upslope. Therefore, it should be ideal for cloud initiation.

Fig 1 thus represents a successful simulation of the dry circulations. In the simulations to be presented, we have augmented the model by adding moisture to the dry case study days, to investigate the initiation 6r shallow cumuli. These studies test the sensitivity of tha effects of various values of moisture and mean low-level convergence on properties of the shallow clouds which form, These properties include both gross cloud features and the thermodynamic, dynamic, and turbulent properties of the air ascending through cloud base.

Acknowledgements: The portions of this paper on cloud initiation have benefitted greatly from. discussions with Greg Tripoli, Dr. Terry Clark, and Dr. Bili Cotton. Computations were performed on the Cray-1 computer at the Air Force Weapons Laboratory, Kirtland AFB, NM (USA).

4. REFERENCES

1. Banta, R.M., 1982: An observational and numerical study of mountain boundary-layer flow. Ph. D. Dissertation; Atmos. Sci. Paper No, 350, Colorado State Univ. Dept. of Atmos. Sci., Ft. Collins 80523 USA.

2. ____ , 1984: Daytime boundary-layer evolution over mountainous terrain. Part I: Observations of the dry circulations. Mon. Wea. Rev., 112, (in press).

3. Clark, T.L., 1979: Numerical simulations with a three-dimensional cloud model: Lateral boundarv condition experiments and multicellular severe storms. J. Atmos. Sci., : 2191-2215.

4. Hill, G.E., 1974: Factors controlling the size and spacing of cumulus clouds as revealed by numerical experiments. ci: Atmos. Sci, : 646-673.

5. Liu, J.Y., and H,D. Orville, 1969: Numerical modeling of precipitation and cloud shadow effec s on mountain-induced cumuli. ci: Atmos. Sci., 26: 1283-1298.

6. Ogura, Y., 1963: The evolution of a moist convective element in a shallow, conditionally unstable atmosphere: A numerical calculation. ci: Atmos. Sci., 20: 407-424.

7. Orville, H.D., 1965: A numerical study of the initiation of cumulus cl.Q tlds o mounta:!..rul.us terrain, ci: Atmos. Sci., : 684-699.

8. ____ , 1968:. Ambient wind effects on the initiation and development of cumulus clouds over mountains. ci: Atmos. Sci.,£' 385-403.

9. _______, and L.J. Sloan, 1970: A numerical simulation of the life history of a rainstorm. J. Atmos. Sci, "!:!.: 1148-1159.

10. Sommeria, G., 1976: Three-dimensional simulation of turbulent processes in an undisturbed trade wind boundary layer. J. Atmos. Sci., 33: 216-241,

11. Tripoli, G.J., and W.R. Cotton, 1980: A numerical investigation of several factors contributing to the observed variable intensity of deep convection over South Florida. ci: Appl. Meteor.,.!.'.!. : 1037-1063.

12. _______ and _____ , 1982: The Colorado State University three-dimensional cloud/mesoscale model - 1982. Part I: General theoretical framework and sensitivity experiments. J. Rech. Atmos., 16: 185-219.

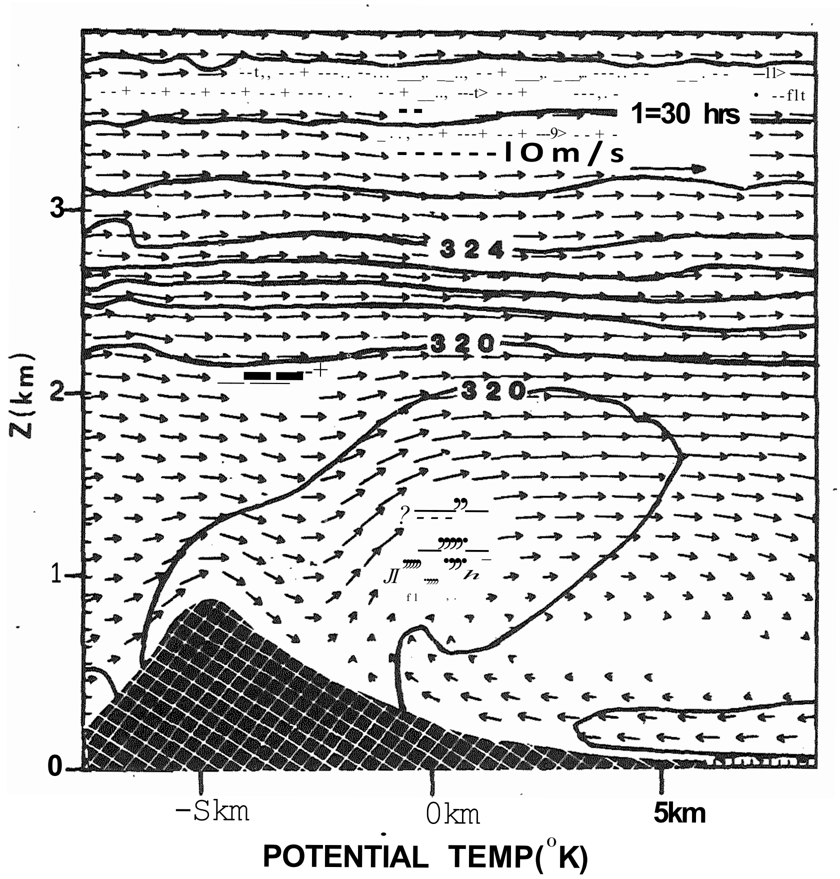

FIGURE 1: PotentiaL-temperature cross section of mountain upslope flow after 1 hr of simulated time, generatea by a two-dimensional numerical model. On *the lee slope (i.e. to the right) of the ridge top, thermally-forced upslope flow in the lower elevations meets well-mixed downslope flow* near *the surface in higher elevations, producing* a zone. *of convergence* near *x = -2 km (Ref 1).*

518

SORTING OF SOLID HYDROMETEORS AND ITS APPLICATION TO THE ANALYSIS OF PRECIPITATION FORMATION IN MIXED CUMULONIMBUS CLOUDS

M.V. Buikov, S.V. Nosar and N.N. Talerko

Ukrainian Scientific Research Institute, Kiev, USSR

1. INTRODUCTION

The observations of the structure of cumulonimbus clouds show that three-dimensional character of air motion may strongly influence precipitation formation (Refs.1, 6). One-dimensional cloud models cannot in principle simulate such processes and it is difficult to expect that two or three-dimensional models can "automatically", i.e. without special suggestions, explain all features of precipitation formation, because we do not know now which properties of atmosphere are responsible for those peculiarities of cloud dynamics that in their turn determine size spectrum of precipitation.

It is of great importance to elucidate the relative role of cloud microphysics and dynamics in converting cloud liquid water content into precipitation. It is evident that cloud microphysics and thermodynamics are necessary conditions to form precipitation, but we do not know what features of cloud dynamics are sufficient conditions. Some progress in this direction may be achieved by the investigation of growth and motion of hydrometeors in the given fields of updraft and liquid water content (Refs, 2, 5. 10).

The possibility of particle recycling and size sorting may be considered to be useful for understanding the growth mechanism of large hailstones (Refs. 1, 10).

The problem of hydrometeor sorting may be formulated as follows: for the given fields of air motion and liquid water content to explore all possible trajectories and to determine such regions of initial points that hydrometeors moving along the trajectories beginning at these regions can reach size large enough to be considered as precipitation particles. To analyse hydrometeor sorting two approaches may be used: 1) to explore the possible hydrometeor trajectories for the observed fields of velocity and liquid water content (Refs,2, 9, 10); 2) to analyse those for a conceptual cloud model which takes into account main features responsible for precipitation formation. The advantage of the second approach is the possibility to use the methods of the qualitative theory of differential equations that is the case in this paper.

It is worthwhile to note that in all investigations of precipitation formation in cumulus clouds it is implicitly suggested that the amount and size spectrum of precipitation is a function or a functional of stable and observable cloud parameters which may be simulated in numerical models and be predicted for a given state of atmosphere. But we cannot give up the possibility that precipitation is determined by some casual, changeable and small scale cloud parameters that are difficult to measure in real clouds and to simulate in models. To shed some light on this problem the influence of small variation of cloud parameters on precipitation must be investigated.

2. CONCEPTUAL CLOUD MODEL AND BASIC EQUATIONS

We take that a cloud is an updraft steady-state axisymmetrical jet of air with a known distribution of velocity and liquid water content, convergent (divergent) in lower (upper) part and approximately stable in intermediate part (trapezoidal or in particular triangular vertical profile):

$$w(s,z) = f(s)\begin{cases} 0, & z<z_1; \\ w_0+(w_m-w_0)\,z/z_2, & \\ w_m(z_3-z)/(z_3-z_2), & z_2<z<z_3, \end{cases} \qquad (1)$$

where $w(s,z)$ is updraft velocity; s,z are horizontal and vertical coordinates; $f(s)$ is the horizontal profile of updraft which may be taken from the observation; horizontal velocity $u(s,z)$ may be derived from the continuity equation with air density and rotation speed being constant.

The motion of solid precipitation particle growing in dry regime due to the capture of supercooled cloud droplets can be described by the following equations:

$$\frac{dz}{dt} = w(s,z) - v(R); \qquad (2)$$

$$\frac{ds}{dt} = u(s,z); \qquad (3)$$

$$\frac{dR}{dt} = \frac{E\, q_l v(R)}{4}, \qquad (4)$$

where $v(R)$ is the velocity of particle falling under gravity ($v(R) = b R^{1/2}$, a = 1, 2); E is the collision efficiency taken to be constant, is ice density, q_l is liquid water content.

When the theory of particle sorting is under consideration, these equations must be regarded not as the tool for computation of some trajectories but as the one to explore the properties of the whole field of possible trajectories. The surfaces of stationary points Zs, where $dz/dR = 0$ and that of bend points, where $d^2z/dR^2 = 0$ play important role in this analysis. In the phase space (z, s, R) the trajectories rise inside the zs surface and sink outside. It may be shown that there is the region on the zs surface in the convergent part of cloud jet where trajectories possess minima.

These facts allow to divide the whole variety of possible trajectories beginning inside the Zs - surface into three classes: 1) the trajectories intersecting the zs surface and reaching cloud base (quasi-one-dimensional ones); 2) the trajectories intersecting the Zs surface and reaching the region of minima of this surface (recycling ones); 3) the trajectories intersecting lateral boundary of cloud jet in its divergent part (the ones thrown off to anvil); hydrometeors moving along the last trajectories may be consi ered to be lost for EJrecipitation.

In order to calculate the number of the trajectories of each class it was assumed that the embryos of precipitation particles with the concentration which does not depend on horizontal coordinates appear at isome height z_0 •

The analysis of Eqs,2-4 shows that hydrometeor sorting and precipitation formation are determined by the dimensionless parameter which may be expressed as the ratio of two characteristic times:

$$p = tm/tg; \quad tm = (z2-z1)/wm;$$

$$tg = 49wm^{a-1}/Eq1 \, b^{a}, \qquad (5)$$

where tm is the time which a particle spends inside the growth region and tq is the time needed for a particle to grow to the size when v(R) = Wm· Conditions for precipitation formation are poor, if p« 1 (tg»).

The results of the investigation of -precipitation formation based on the particle sorting theory are presented below; it was suggested that initial size of embryo (R_0) is equal to 10-4 m as a rule. The details of the calculations may be found elsewhere.

3. SUPERCELL CLOUDS

Supercell may live during some hours and are considered to be in steady-state. The size of '3."recycling" particle, as a rule, is laiger than that of a partic le moving along quasi-one-dimensional trajectory and therefore the number of recycling trajectories may be considered to be the indication of cloud ability to form hail. Because of this the estimation of the recirculation possibility is of scme interest for these clouds.

The dependence of particle sorting on the horizonta·1 profile of updraft and instability energy was investigated in Refs. 3, 4. It was shown that if embryos appear at the upper boundary of the zone of convergence (z_0 = z1), then one critical value of the parameter (pc) exists: the trajectories of the first type are absent at p <Pc· The relative portions of one-dimensional (Mo), recycling (Mrl and anvil (Mal trajectories depend noticeably on the horizontal profile and p. The smaller is p, the smaller is M and the weaker is cloud ability to precipitate (M_0 + MR:).

The increase of the amount of instability energy in the atmosphere results in increasing the contribution of recirculation to precipitation.

3.1. Sorting dependence on the height of embryo appearance

If embryos appear at some height z_0 in the middle of a cloud, then the parameter p decreases:

$$p' = p(z_2 - z_0)/(z_2 - z_1). \qquad (6)$$

In this case there are two critical values of P'instead of one: at p' .(p 1, M_0 = O; at p' > Pc2' MR = 0; at P2c <p' (Pc1 both quantities are not equal to zero. The interval narrows, if z -+z2.

The integration over z_0 with regard to the activity spectrum of embryos give the estimation of the whole portion of embryos taking part in precipitation formation. It depends on cloud top temperature and in some cases it may be equal to 5-10 %.

3.2. Sorting in a sloping cloud

Sloping of a cloud jet is favourable for precipitation formation: the values of Ma and MR decrease due to the slope. It was shown that there is the critical value of the angle α_c between the vertical and cloud axis so that at d..>αc.M_a = MR = O (d.c~6o^0).

3.3. The evaluation of particle sorting for some real storms

The analysis Qf trajectcries sorting was carried out for the Fleming storm (Ref. 1) using two approximations of updraft from Ref. 8. As shown in Figure 1 the embryos appearing inside the polygon ABEF (the approximation c) or ACDF (the approximation d) belong to the third type. For c-approximation there is no recirculation; i.e. the small enough variation of air motion can lead to the essential change of precipitation size spectrum. In reality the trajectories in Figure 1 arc three-dimensional, if the rotation of air is taken into account and then the region below the line GC and further along a-trajectory may be considered to be the weak echo region.

Every trajectory in Figure 1 is the representative of the bunch of the trajectories which begin in some small volume. Because of this the divergence of trajectories at z >7 km can result in local intensification of radar reflectivity which may be interpreted as the radar streaks observed in Ref. 7.

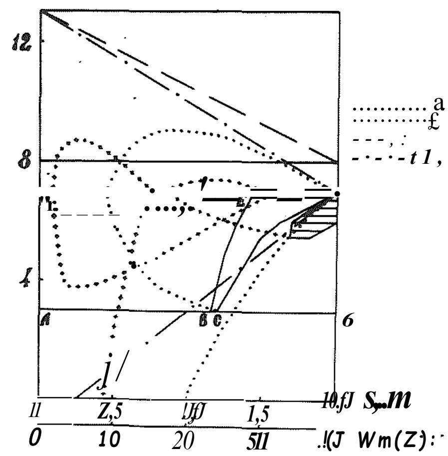

Figure 1. The results of the calculations for the Fleming storm. c, d are two approximations of updraft; at z (7 km both approximations coincide. The region of the origin of recycling trajectories for the cased is dashed. a(b) is the example of one-dimensional (recycling) trajectory for the case d.

The analysis of particle sorting in the storm described in Ref. 5 shows that there is high efficiency of the conversion of cloud water into rain: Ma= 7 %; = O.

4. ONE-CELL CLOUDS

4.1. Mixed clouds

The life-time of one-cell clouds is not very long and it may be suggested that recirculation trajectories do not play appreciable role in precipitation formation. In this case the whole sorting of trajectories takes place only in the upper divergent part of a cloud and is determined by two parameters p and $\lambda_m = w_m/v\,(R_0)$. Some simplifications of the analysis are brought by this and it is possible to obtain the formulas for intensity (j) and particle mean radius (R) of precipitation:

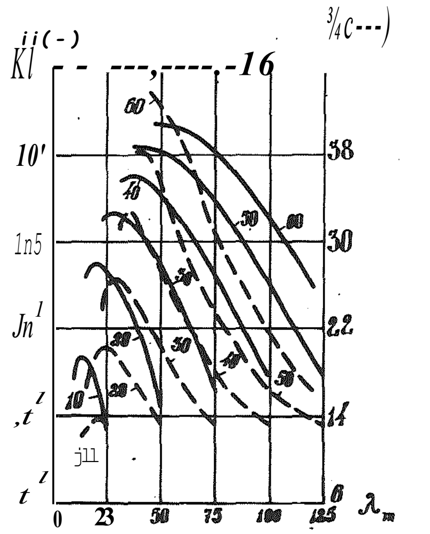

Figure 2. Dimensionless precipitation intensity and mean radius as the functions of the parameters p_0, λ_m. The numbers of the curves are p_0 - values.

$$j = \frac{4\pi\, S R_0^3\, w_m N \eta_t}{3\,(m+1)}\, \Pi_1 (p, \lambda_m), \tag{7}$$

$$R = R_0 \Pi_2 (p, \lambda_m), \tag{8}$$

where S is the area of cloud cross-section, N is the concentration of embryos at cloud top temperature; $\eta_t = (z_3-z_t)/(z_3-z_1)$; $T(z_t) = T_t$; T_t is threshold temperature of embryo activation; when deriving Eqs. 7,8 power activity spectrum of ice nuclei with the exponent m and triangle profile of $w(z_1 = z_2)$ were used.

It was shown that precipitation formation is hardly probable, if $p < 0.4$. There is the value of λ_m ($\lambda_{\infty} > \lambda_m$) at which precipitation intensity and mean radius are maximum, when the parameter $p_0 = E q_1 (z_3-z_1)/4 q R_0$ is constant.

4.2. The influence of the crystallized part of a cloud

The absence of liquid water in the upper cloud part may reduce cloud ability to precipitate. Hydrometeors obtain the main mass increase when falling through updraft but the particles entering crystallized part of a cloud may not return again to the mixed one and will lose the opportunity to reach the size large enough. In a cloud with crystallized part sorting is determined by three parameters: p, λ_m, $\eta_c = 1-(z_c - z_1)/(z_3 - z_1)$ (z_c is the Lower boundary of the crystallized part.

If the crystallized part is thick enough, precipitation intensity may possess two maxima (Figure 3). This is explained by the gradual displacement of the zone of intensive precipitation growth from the central part of a cloud to its lateral boundary.

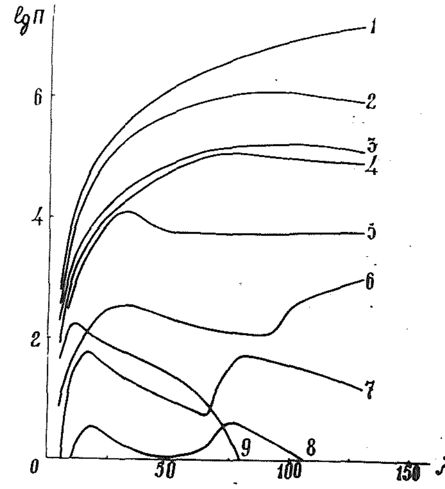

Figure 3. Dimensionless precipitation intensity as the function of the parameters p, λ_m, η_c:
1 - p = 1.9; η_c = 0.4, 2 - p = 1.2; η_c = 0.3,
3 - p = 1.9; η_c = 0.6, 4 - p = 0.6; η_c = 0.1,
5 - p = 0.6; η_c = 0.2, 6 - p = 1.9; η_c = 0.8,
7 - p = 1.2; η_c = 0.8, 8 - p = 1.9; η_c = 0.9,
9 - p = 0.6; η_c = 0.5.

Figure 4 shows the possibility of rain or hail formation on the p, η_c-plane. For given p the increase of the thickness of crystallized part results in the transition from hail to rain and to the absence of precipitation.

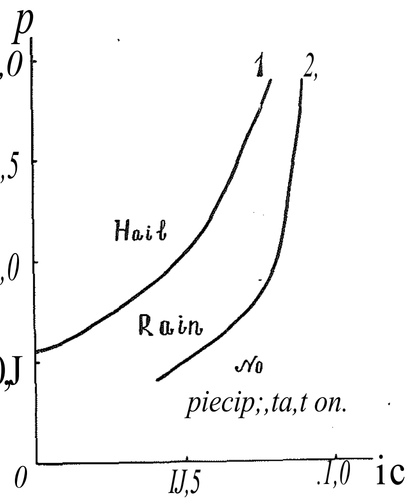

Figure 4. The regions of the values of the parameters p and η_c for which hail or rain is possible.

4.3. The comparison of the sorting theory with observational data and numerical model

To test the results of the sorting theory 88 clouds were observed and using one-dimensional lagrangian cloud model which ;considers entrainment on the basis of these ;data the values of p were calculated. For 'all clouds it was obtained that p) 0.4. The stratification of the data by the parameter p allows to gather clouds with different amount of precipitation w thin one p-category and to obtain for every category the regression equation:

$$\lg j = A + B\,\mathrm{wm}. \qquad (9)$$

The values of embryo rad;us ($R \sim 1\text{-}4 \cdot 10^{-4}$m) and concentration ($N \sim 10 - 10^3\ 1/m^3$) were also determined.

The comparison of the sorting theory with the simulation of precipitation formation using one-dimensional microphysical time-dependent numerical model of a mixed cloud shows that in a cloud with the thickness 4-5 km precipitation formation is approximately one-dimensional and particle sorting is of no importance; this inference is not true for thicker clouds.

5. CONCLUSIONS

It is worthwhile to mention the most interesting results obtained:

1. Cloud dynamics may play an important role in precipitation formation determining the spectrum and the amount of precipitation.
2. The greater is horizontal gradient of updraft, the laFger number of embryos turns to precipitation particles.
3. Small variations of vertical or horizontal profiles of updraft may result in a noticeable change of particle size distribution.
4. The experimental data confirm the conclusion that precipitation intensity depends on two dimensionless parameters.
5. The results obtained may be applied to develop methods of precipitation forecast, to parametrize microphysical processes in numerical models and to carry out theoretical evaluation of cloud seeding effect.

6. REFERENCES

1. Browning, K.A., Foote, G.B., 1976: Air flow and hail growth in supercell storms and some implications for hail suppression. Quart. J. Roy. Met. Soc., v. 102, 499-533.
2. Buikov, M.V., Kuzmenko, A.G., 1978: On the growth of hail in supercell hail clouds (In Russian). Meteorology and Hydrology, No. 11, 60-69.
3. Buikov, M.V., 1981: About two mechanisms of growth of precipitation particles in cumulonimbus clouds (In Russian). Trudy of Ukrainian Regional Res. Inst., No. 185, 3-25.
4. Buikov, M.V., Talerko, N.N., 1982: The influence of updraft profile on precipitation particle sorting in cumulonimbus clouds. Trudy of Ukrainian Regional Res. Inst., No. 187, 55-63.
5. Kropfli, R.A., Miller, L.J., 1976: Kinematic structure and flux quantities in a convective storm from dual-Doppler radar observations. J. Atmos. Sci., 33, 520-529.
6. Marwitz, J.D., 1972: The Structure and Motion of Severe Hail Storms. Part I, Supercell Storms. J. Appl. Meteor., 11, 166-179.
7. Marwitz, J.D., 1978: Vertical streaks in radar echoes from convective clouds. Proc. of the 18th Conf. on Radar Meteor. Atlanta, Georgia, 260-265.
8. Musil et al. 1976: Numerical simulation of hailstorm modification by competing embryos. Rep. 75-5 Inst. Atmos. Sci. s. Dakota School of Mines and Technology, 56 pp.
9. Paluch, I.R., 1978: Size sorting of hail in a three-dimensional updraft and implications for hail suppression. J. Appl. Meteor., 17, 763-777.
10. Sartor, J.D., Cannon, T.W., 1977: The observed and computed microstructure of hail producing clouds in Northeastern Colorado. J. Appl. Meteor., 16, 708-715.

AN EXAfUNATION OF THE PENETRATIVE DOWNDRAFT MECHANISM IN CUMULUS CLOUDS

Terry L. Clark and Gary P. Klaassen

National Center for Atmospheric Research*
Boulder, Colorado 80307 USA

1. INTRODUCTION

The concept of cwnulus· entrainment and mixing was first introduced by Stammel (1947). fo.ircraft observations of cwnulus clouds showed that the liquid water content qc within the clouds was typically much smaller than the value qca expected for saturated parcels of air which had ascended pseudo-adiabatica],ly from cloud base. Stammel suggested that the observed dilution of liquid cloud water could be explained .by the entrainment of unsaturated environmental air from the sides of the growing cumuli and the subsequent mixing.of the entrained air with the saturated air rising from cloud base. If this proposal were correct, one would expect the ratio qc/qca at a given level would be larger in the middle of the cloud and smaller near the boundaries. However, later observations of cumulus clouds have shown no systematic horizontal variations in this ratio.

Squires (1958) suggested an alternative explanation which would account for both the dilution of qc below the pseudo-adiabatic value as well as the lack of systematic horizontal variations. He suggested that parcels of unsaturated environmental air at the cloud top could penetrate downward into the cloud interior by mixing with saturated air and evaporating cloud water to enhance their negative buoyancy: This interpretation of environmental entrainment into cwnuli has the further advantage of explaining observations of downdrafts within cwnulus clouds.

Observations of cwnuli in the NHRE experiment analysed by Paluch (1979) showed that parcels of air. deep within the clouds were composed of a mixture of unsaturated air from the cloud top and saturated air from the cloud base. Telford (1975) applied the concept developed by Squires (1958) to show that realistic profiles of liquid water content could be obtained if unsaturated overlying air was allowed to mix down through the cloud. Emmanuel (1981) generalized the similarity theory for turbulent plumes and used it to predict the properties of penetrative downdrafts forming in cumulus clouds. It should be noted that observations have also shown that some cumuli have protected cores where qc is very nearly equal to the wet adiabatic value. Therefore, a comprehensive model of cloud entrainment must be able to differentiate between cases where claud-top entrainment is very active and affects a large portion of the cloud to cases where entrainment is rath r weak and affects only the immediate cloud boundary regions.

It is the purpose of this paper to investigate the mechanism of cloud entrainment employing two-dimensional numerical simulations of cumulus clouds• Three dimensional simulations are currently being performed and will be described in future publications. To model the .details of entrainment one requires very high spatial and temporal resolution. The large i'rregular structures at the top of growing cumuli are observed to range in scale from 100-200 m. Tc· accurately simulate such features one might require as much as 10 m spatial resolution in the vicinity of the actual entrainment. Such resolution has been achieved in the current study through the nesting of two· interactive model domains. The outer model provides coarse resolution over a large domain, while the inner model provides high resolution over a limited region. Thus, the outer model is used to simulate the cloud environment and boundary layer forcing and to supply appropriate boundary conditions to the inner model. The inner model is used to simulate the cloud and its immediate environment.

*N.C.A.R. is sponsored by the N.S.F.

2. MODEL DESCRIPTION

The numerical model described by Clark and Farley (1984) is employed for the current simulations. The model is non-hydrostatic and anelastic 1such that all acoustic waves have been filtered from the equations. Second-order numerical finite-difference operators are used for the fields of velocity, potential temperature, and water vapor mixing ratio (qv)· The qc field is treated with the hybrid scheme presented in Clark (1979) in order that positive definiteness be maintained. The model has the facility to treat up to three different interactive domains in a given simulation and calculations may be performed in either two or in three spatial dimensions. For further details of the model and the interactive nesting procedure, the reader is referred to Clark and Farley (1984) and ciark (1977).

The stress tensor is parametrized using the first order mixing theory of Smagorinski (1963) and Lilly (1962). The read r should bear in mind that one of the purposes of these· experiments is. to obtain sufficiently high spatial resolution so that the detailed form of K,n is of only minor importance. Hopefully the utility of higher order closure models or other first -order formulations can be assessed through future analy i.s of the present results.

The parametrization of the cloud microphysics. is described in .Clark (1979). The condensation• .rate, Cd, is determined so that 100 percent humidity is maintained within the cloud, i.e., qv -.. qv8 if qc > 0. The formation of rain is not permitted in these experiments. For the small. clouds under consideration here, this is a justifiable, constraint. The time available for warm rain production is rather small, 10-15 minutes, and the maximum liquid water mixing ratios are also small, being typically around 1.0 gr/kg. Furthermore, rain formation would make it difficult to assess the source of the depletion of cloud liquid water content.

Cyclic boundary conditions werE! specified in they direction for the outermost domain of the computations. The boundary conditions at the upper and lower surface of the outer model are given by

$$\frac{\partial}{\partial z}(v, qv, qc) \cdot w = \frac{\partial^2}{\partial z^2}\theta = 0 \qquad \text{at } z = H.$$

$$\theta\ (v, qv, qc, \theta) = w = 0 \qquad \text{at } z = 0.$$

3. CLOUD ENVIRONMENT AND FORCING

The environment was purposely chosen to represent the simplest of realizable atmospheric conditions that could be expect d to support cumulus clouds. The complications of shear have been avoided by assuming ambient conditions, Fig 1 shows ,he profiles of e and qv which were employed in all the experiments to be described here, We ha,ve imposed an initial. boundary layer with a slightly stable potential temperature gradient (0.36 K/km) and a mixing ratio profile which decreases slowly ,with height. The depth or this layer is 1.4 km.

Between z = 1.4 km and 1.8 km we have specified a stable layer with a potential temperature gradient of about 4 K/km. The relative humidity decreases from 91% at z = 1.4 km to a value of 39% at z = 1.8 km. Above z = 1.8 km the potential temperature gradient is 4.5 K/km, while the relative humidity decreases to 23% at z = 3.0 km and decreases only slowly thereafter. The clouds are initialized by heating the atmosphere in the boundary layer. The surface heat flux, Fs, is set equal to a Gaussian distribution

$$F_{s(x,y)} = f_0 \exp(-y'^2/\alpha^2)$$

where fo = 150 watts per m^2 and α = .7 km. The distance y' is measured from the center of the domain. The width of this heating function, 2α, was set equal to the depth of the boundary layer, since it was found that this was the preferred nonlinear scale of the resulting convection rolls. An attenuation length of 300 m was chosen so that at any level in the model the heat flux is given as

$$F(x,y,z) = F_s(x,y) \exp(-z/300m).$$

This procedure distributes the heating over a fixed depth of the model and generates a rising thermal which is well-resolved even for the coarsest resolution (50m) we employ. The type of forcing described provides the model with a controlled, smooth initialization of clouds at the top of the boundary layer. This method of initialization is considerably smoother and more realistic than the "buoyant-bubble" initializations employed in previous numerical simulations.

4. TWO-DIMENSIONAL CLOUD SIMULATIONS

In the first numerical experiment to be considered here, we employed a single computational domain with resolution $\Delta y = \Delta z$ = 50m. The convective circulation grew for some thirty minutes before the rising thermal penetrated the top of the boundary layer and initiated condensation. The lifting condensation level was found to be about z = 1.5km, in good agreement with parcel stability analyses. The cloud that formed had a flat cloud base which was approximately 900m across. Although there were 18 grid points across this cloud, at about t = 40 min the onset of small scale motions caused the cloud to break up into parcels with characteristic dimensions of about 100m. These parcels rose rapidly to the maximum level of conditional instability, evaporating as they rose.

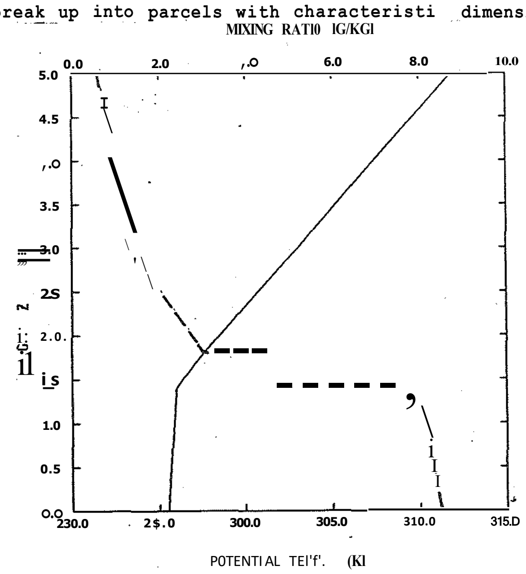

Fig 1. Environmental profiles of θ (solid) and qv **(dashed)**

Clearly, higher resolution experiments were required. In order to avoid excessive computational costs, we used the interpolation schemes described by Clark and Farley (1984) to "spawn" a fine-resolution inner domain from the fields of experiment 1 at t = 30 minutes. The domain of the inner model was chosen to cover the region in which condensation was expected to occur (z = 1.2 to 2.4km and y = 2 to 3 km). The experiment was then resumed at t = 30 minutes with two interacting domains. Throughout the remainder of the simulation, the coarse mesh (CM) outer model supplied the boundary conditions to the fine mesh (FM) inner model. In this paper we will describe simulations in which the inner FM model had resolutions of $\Delta y = \Delta z$ = 25m (Exp 2), $\Delta y = \Delta z$ = 10m (Exp 3). An experiment with an inner model resolution of 5m (which would provide 180 grid points across the cloud) will be performed in the immediate future.

In experiment 2 (25m resolution), condensation began at the same time and height as in Exp 1. However, the cloud in Exp 2 did not break up. Indentations or nodes appeared on the upper surface of the cloud at t = 44 min, and rapidly grew in amplitude until the cloud boundary became highly irregular. Fig 2 shows four times of the qc field for Exp 2. The cloud rose rapidly to the top of the inner domain and continued to rise in the CM domain until the level of conditional stability was attained. The liquid water content within this cloud corresponds well to that which would be predicted on the basis of the pseudo-adiabatic ascent of a saturated air parcel from cloud base. Although the early cloud history (i.e. before t = 45 minutes) in Exp 3 (10m resolution) is very similar to that in Exp 2, the later cloud histort is distinctly different. Initially, the cloud top in Exp 3 rises at the same rate as in Exp 2. However, at t = 46 minutes (shortly after the nodes appear on the cloud top surface), the rate of cloud top ascent begins to decrease in Exp 3. The cloud top in this experiment never exceeds z = 2.2km, which happens to be very near the level of maximum conditional instability. It is worth mentioning at this point that earlier numerical modeling attempts produced clouds that usually rose through the layer of conditional instability, whereas observations of cumulus clouds show that such clouds frequently cease to grow long before the maximum level of conditional stability is attained. Our results imply that, under certain conditions, a low resolution cloud simulation may produce a spurious result which would not be obtained using higher spatial resolution.

In Figure 3 we show a sequence of contour plots of the qc field for Exp 3. At t = 43.17 min, nodes appear on the previously smooth upper surface of the cloud. These nodes are about half the width of the nodes that appear on the cloud top in Exp 2. At t = 45.83 min we observe the formation of two distinct rising turrets on either side of the center of the cloud top. Up to this time, the cloud water content is nearly adiabatic. At t = 47.83 min, these turrets begin to turn in towards the center of the cloud, entraining unsaturated air as they do. At t = 48.83 min we see that the unsaturated air has begun to mix with the saturated cloud air. Fig 4, which contains the vertical velocity field at t = 48.83 min, clearly shows the formation of a downdraft in the entraining region. Later times show this downdraft penetrating into the cloud and modifying the liquid water content through mixing, e.g., see Fig 4(e) and (f).

S. CONCLUSIONS

We have performed a sequence of two-dimensional cloud simulations that differ only in spatial and temporal resolution. It is apparent that the formation of a penetrative downdraft in !'.he high resolution Exp 3 severely curtailed the growth of the cloud and was responsible for the reduction of cloud liquid water content below the pseudo-adiabatic value. Lower resolution experiments failed to resolve this feature .of the dynamics, and produced rapidly rising clouds with liquid water contents near the pseudo-adiabatic values. This illustrates the importance of achieving sufficient resolution (90 points across the cloud in the present case) when attempting to simulate the dynamics of cumulus clouds. Although there are well known differences between two and three dimensional dynamics, it appears that the cloud top instability is realizable in two spatial dimension. This is not surprising since this instability seems to be closely related to the classic Rayleigh-Taylor instability.

6. REFERENCES

Clark, T.L., 1q77, J. Comp. Phys. 24, 186-215
Clark, T.L., 1979: J. Atmos. Sci., 36, 2191-2215
Clark, 7.L. and R.D. Farley, 1984: J. Atmos. Sci., (in press).
Emanuel, K.A. 1981: J. Atmos. Sci., 38, 1541-1557.
Lilly, D. K., 1962: Tellus, 14, 148-172.
Paluch, I.R. 1979: J . Sci., 36, 2467-2478
Smagorinski, J., 1963: Mon. Wea. Rev. 91, 99-164.
·squires, P,, 1 58: Tellus, 10, 381-389 -
Stommel, H., 1947: eor":-;- 4, 91-94
·Telford, J,W., 1975: P.A. Geophy., . 1067-1084.

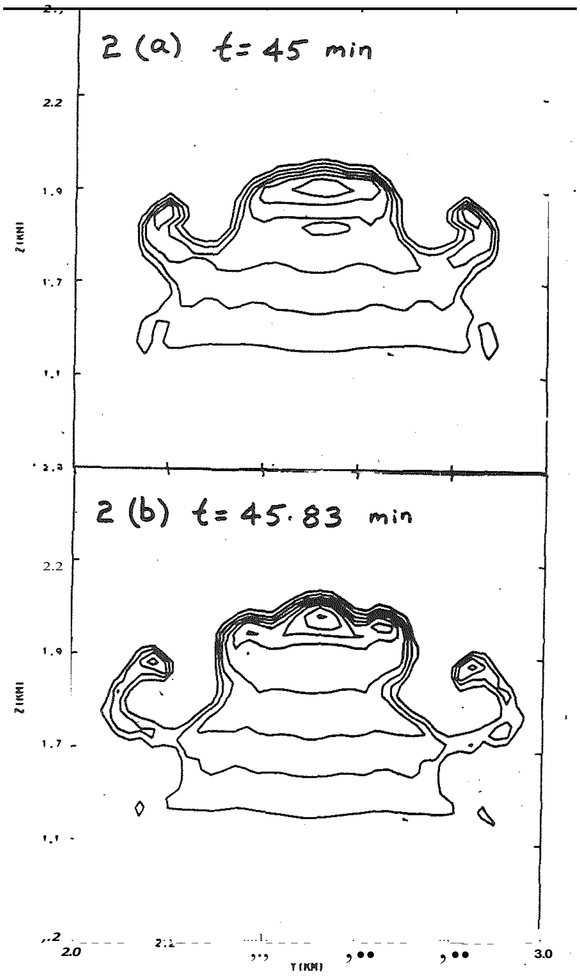

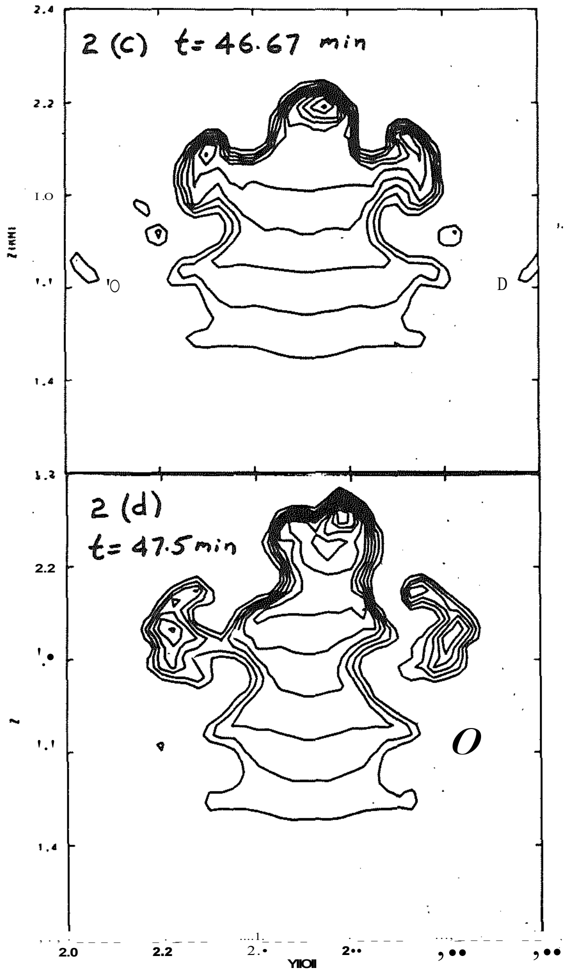

Fig 2. qc plots with contour interval of .2gr.kg-l for Exp 2. Times are (a)45, (b)45.83, (c)46.67, (d)47.5 min.

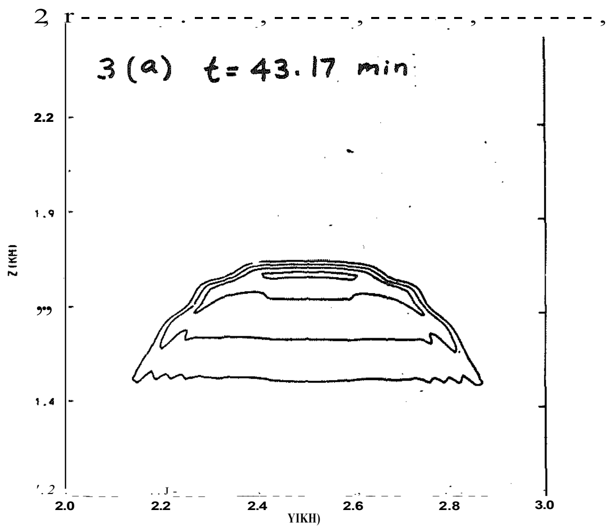

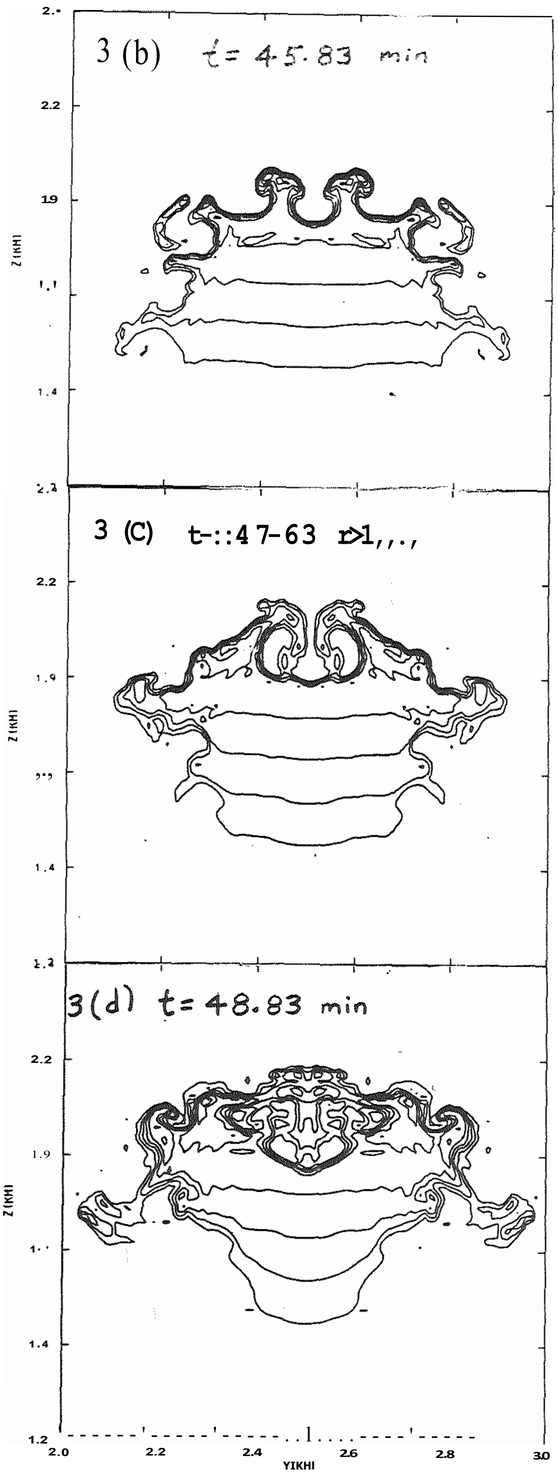

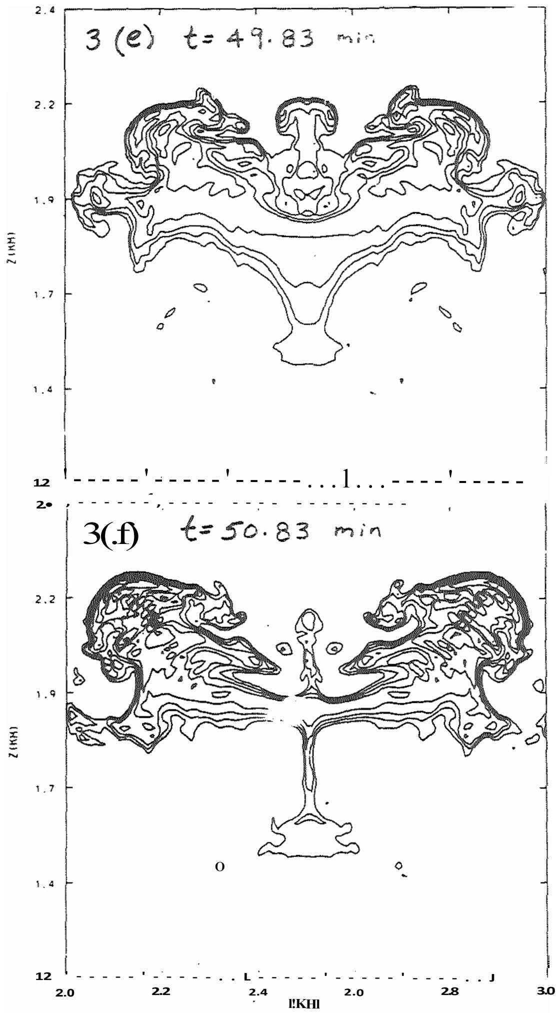

Fig 3. Same as Fig 2 except for Exp 3. Times are (a)43.17, (b)45.83, (c)47.83, (d)48.83, (e)49.83, (f)50.83 min

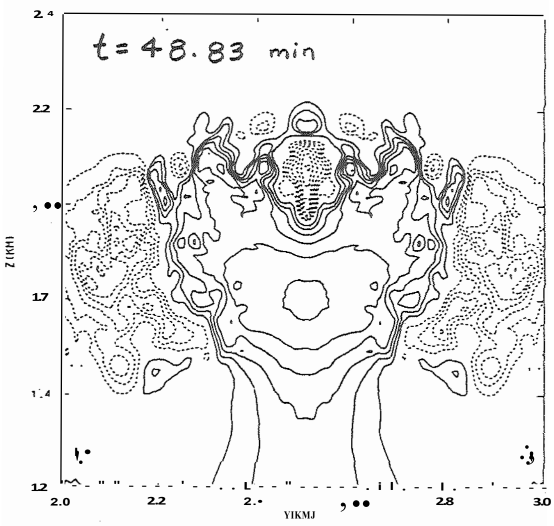

Fig 4. w plots with contour interval of .5ms^{-1}. Solid indicates positive and dashed indicates negative values. Time is the same as Fig 2 (d).

FOR,,,i,TlO:J oc DO\vNDRAFTS IN ,:;ut-lULUS CLOUDS

Krzysztbf E. Haman and Szymon P. Malinowski

Institute of Geophysics, University of Warsaw
Pasteura 7, 02-093 Warsaw, Poland

1. INTRODUCTION

xistence of downdrafts in various stages of developement of convective clouds has been recognized allready a long time ago, but their exact mechanisms and roles they play in the life cycle of a cloud are still a matter of discussion. Byers and Braham in their famous •Thunderstorm Project• (Ref.1) found them **mainly** in mature and dissipation stages of **this** cycle, and noted that the lateral entrainment of environmental dry air may help in **keeping** them negatively **buoyant** over long **portions** of the cloud. Downdrafts were **later** found to be an extremly important factor in dynamics of Cu ulonimbus clouds and their systems; there is a fairly extensive literature concerning their properties, **dynamic•** and effects. **But** it seems **that downdrafts** are important'also in the life cycle of smaller convective clouds. **Squires** (Refs2, 3) found, that **penetrative downdrafts** developing from **the tops** of convective clouds may play an **essential** role as an entrainment mechanism; later this point of **view** has been reiterated by Telford lRef.4) who noticed, that this **way** of entrain■ent (top entrainment) can **explain** some observational facts, which **hardly** could be explained **by hypothesis of lateral** entrainment. **Paluch (Ref.5) preaented** some observational evidence **strongly suggesting,** that the air found at the **middle levels of** at least some wall developed Cu clouds in Colorado, is a mixture of subcloud air with ambient air from above **rather** than below the observation level; this also **supports** the top entrainment **hypotheais. Si■ilar** results were recently **obtained by Boatman** and Auer (Rlilf.6).

Davelop■e■t ef penetrative **downdrafte** beco•e **1■tereeti■g** also for **weather** modification **research,** since some Soviet and American teams **(Ref.7,8)** announced cases of sucessful **dissipation of** Cu clouds **by** means of various **Mechanical i■pulees** supposed to initiate such **downdrafts.**

All this indicates, that **understanding** the nature and mechanisms of downdrafts **is** essential for the **knowledge** on convective clouds. **Unfortunately** the **theory** of penetrative downdrafts is **far** from **being** complete. Squires (Ref.3) calculated **the■** under tacit **assu■ption** that the surrouding cloud is in **hydroatatic equilibrium** with environment, **disregarding thus** entrainment of opposite **buoyancy. Similar** limitations concern later papers **by** Vulfson and Levin (Ref.7) and Emanuel (Ref.9}. Telford (Ref.4) try to substantiate this approach, arguing that major parts of convective clouds are dynamically dead and close to such an equilibrium, but it is not clear how these parts are formed, if penetrative downdrafts (assumed to be the main mixing mechanism), would require them as a prerequisite of developement. Paluch (Ref.5) tried %0 show that such downdrafts can sometimes penetrate into an active adibatic updraft, but her calculations refer to case studies and hardly permit wider generalization, while in similar computations in Ref.6, the impact of updraft velocity has been simply disregarded.

The aim of the present paper is to investigated this problem more detaily and with greater precision.

The interaction between updraft and downdraft with exchange of mass, water buoyancy and momentum has been detaily investigated by Haman (Ref.10) and Haman and Niewiadomski (Ref.11) and aplied to steady state Cumulonimbus; here a similar approach with some modifications is aplied to penetrative buoyant downdrafts in Cumulus.

2. THE MODEL

The model is intended to simulate a downdraft developing within en updraft from a blob of environmental air,encompassed by the top of developin Cumulus tower. The tower is simulated by an Eulerian steady, saturated buoyant plume within a hydrostatic environment; lateral entrainment and virtual mass coefficient as a substitute for nonbuoyant pressure forces,can be introduced in various forms. Physical parameters of the plume at a given level are assumed to represent the properties of the cloud top when reaching this level and the properties of the cloud when the top is allready above it.

The downdraft is simulated by a Lagrangian buoyant, spherical thermal with entrainment of updraft and eventually environmental air, and detraiment, both parametrized by means of Taylor hypothesis (entraiment/detrainment rates proportional to the relative vertical velocity). Nonbuoyant effects are simulated by aerodynamic drag and virtual mass coefficient. Only small droplet cloud water (no ice nor big particles mooving with respect to the air) is allowed. The downdraft starts at a selp,cted level with certain initial radius r_o, zero vertical velocity and environmental pressur, temps ra tu re and hu;;iidi ty.

External Dtratifioation is introduced by assuming certain hydrostatic distribution of temperature, humidity and pr-ssure.

,e equations express the conservation of momentum, enthalpy and total water, derjved carefully under assumptions of the model with only minor simpl fioations. Following sfmbols are used t - time, z - altitude, h - height of the cloud cop, p - pressure, T - temperature, - air density, q - specific hu idity, Q - q at saturation, V - specific liquid water content, r - radius of the thermal, R, C - gas cons:ant and constant pressure spe8ific heat for dry air C - specific heat for liquid water, L - la ten¥ heat of condenstation; r:,,r;.,**r** - dry adiabatic, **wet** adiabatic and environmental temperature lapse rates; fa.,,.JA,e- enrainment coefficients fro updraft and environment respectively; fa. - detrainment coefficient, C - aerodyna ic drag coefficient; - virtual mass coefficient, g - gravity acceleration, ,>,r,d - entrainment constants to be specifid for various runs of the model. 1'- ref**ere** to the up-.-draft, + refers to the downdraft, e - refers to environ ent, 0 - refers to the initial state of the run.

Integrations were made by **eans** of the 4th order Runge-Kutta ethod on the CDC 6600 computer.

2.1. Equations for the updraft

: ;l±,y}(.f.1.if4"- (1)

dT^t/dz = (c_p + e;Vt-- t,IQ)- .f(,i - It do^t ;d / dP li +

+Jt " (1;.-T) +JJ.l(L. - L^toD (2)

ci ::ll- 3 0' / T dL - '.!S / ,P &z. -+u (qe-rJ-'/) (3)

; . pe• iRTt(,!-1- 0.61Q (4)

dht"' / cft t,/ (ht} (5)

2.2. **Equations** for **the downdraft**

$$\frac{dw^{\downarrow}}{dt}=g\left(\frac{\varrho_e-\varrho^{\downarrow}}{\varrho^{\downarrow}}-V^{\downarrow}\right)\left(1+\varepsilon^{\downarrow}\right)^{-1}+\mu_u^{\downarrow}\left(w^{\uparrow}-w^{\downarrow}\right)+$$

$$-\mu_e w^{\downarrow}+\frac{C}{r}\left|w^{\uparrow}-w^{\downarrow}\right|\left(w^{\uparrow}-w^{\downarrow}\right) \qquad (6)$$

$$\frac{dT^{\downarrow}}{dt}=\left(c_p+c_w V^{\downarrow}+L^{\downarrow}\frac{\partial Q^{\downarrow}}{\partial T}\right)^{-1}\left[\left(\frac{A}{\varrho^{\downarrow}}-L^{\downarrow}\frac{\partial Q^{\downarrow}}{\partial p}\right)\frac{dp}{dz}w^{\downarrow}+\right.$$

$$+\mu_e^{\downarrow}c_p\left(T_e-T^{\downarrow}\right)+\mu_u^{\downarrow}\left(c_p+c_w V^{\downarrow}\right)\left(T^{\uparrow}-T^{\downarrow}\right)+$$

+JA.! (ItQ^t - IAQ•) ,Jd (Li ,iJ - L·d()) (7)

if q.i,,v^i > c^1

jt ·! [it/yt (.M "4) (T^t-T)+ k 1)+

- L,� v , L+ d"�i/ at (8)

$$\frac{d(q^{\downarrow}+V^{\downarrow})}{dz}=\mu_u^{\downarrow}\left(q^{\uparrow}+V^{\uparrow}-q^{\downarrow}-V^{\downarrow}\right)+\mu_e\left(q_e-q^{\downarrow}-V^{\downarrow}\right) \qquad (9)$$

$$q^{\downarrow}+V^{\downarrow}>Q^{\downarrow}\Rightarrow q^{\downarrow}=Q^{\downarrow};\quad q^{\downarrow}+V^{\downarrow}\leqslant Q^{\downarrow}\Rightarrow V^{\downarrow}=0 \qquad (10)$$

$$\frac{dr^{\downarrow}}{dt}=\frac{r^{\downarrow}}{3}\left(\mu_u^{\downarrow}+\mu_e^{\downarrow}-\mu_d^{\downarrow}\right) \qquad (11)$$

$$\mu_u^{\downarrow}=\frac{\alpha\left|w^{\uparrow}-w^{\downarrow}\right|}{r^{\downarrow}};\quad \mu_e=\frac{\beta\left|w^{\downarrow}\right|}{r^{\downarrow}} \qquad (12)$$

$$\mu_d=\frac{\gamma\left|w^{\uparrow}-w^{\downarrow}\right|+\delta\left|w^{\downarrow}\right|}{r^{\downarrow}} \qquad (13)$$

$$p^{\downarrow}=p_e=\varrho^{\downarrow}RT^{\downarrow}\left(1+0.62\,q^{\downarrow}\right) \qquad (14)$$

$$\frac{dz^{\downarrow}}{dt}=w^{\downarrow} \qquad (15)$$

3, **NUMERICAL** EXPERIMENTS AND THEIR RESULTS

The model, **though fairly** sophisticated is **obviousl y yet too crude for** realistic si**mulation of** the **downdraft developaent,** but **performing •i ulations over sufficiently wids** range of its free **paramat•rs,** initial conditions **end** a bient stratifications, **one ■ay** roughly **estimate poasible** bulk properties of the doftndrafts (such **as** their spe&d, **size** or dapth af penetration) even **accounting for inaccuracy of** Taylor entra**inment hypothesie (Ref.4).** Several hundreds of such **a simulations** have been perfor ed: eight axa■pl■s of typical runs **are presented** on Figs 1-3.

or **all these runs the** cloud **base** is at 1000 m with w!a 1 11/a; T+ = T ,q" = Q^t and v^t = 0 aesumed. Environ ental reiativ3 hu■idity is 50% (height indepedent) and te■psrature stratification is given by means of a para eter K • (r-rwV(r_c-rw) Its values as well as values of other constants of the wpdraft are shown in the part ai of each figure together with varticel distributions of updreft **pereaaters.** For **each updreft** tap **height** of **the** cloud (heavy **lina) and para■atars** of 4 downdrafts as function of time **are presanred** in **the** p51rts b/ and c/. For all calule and **C are** zero; **other constants** are **indicated in** the Figs. **Dashed** nd **dotted** lines correspond to **varioua starting height• z0•**

4. CONCLUS!,JNS

Inspection of the **aodel outpwt yields** a nu b•r of interesting and **ao■et ■es** un-

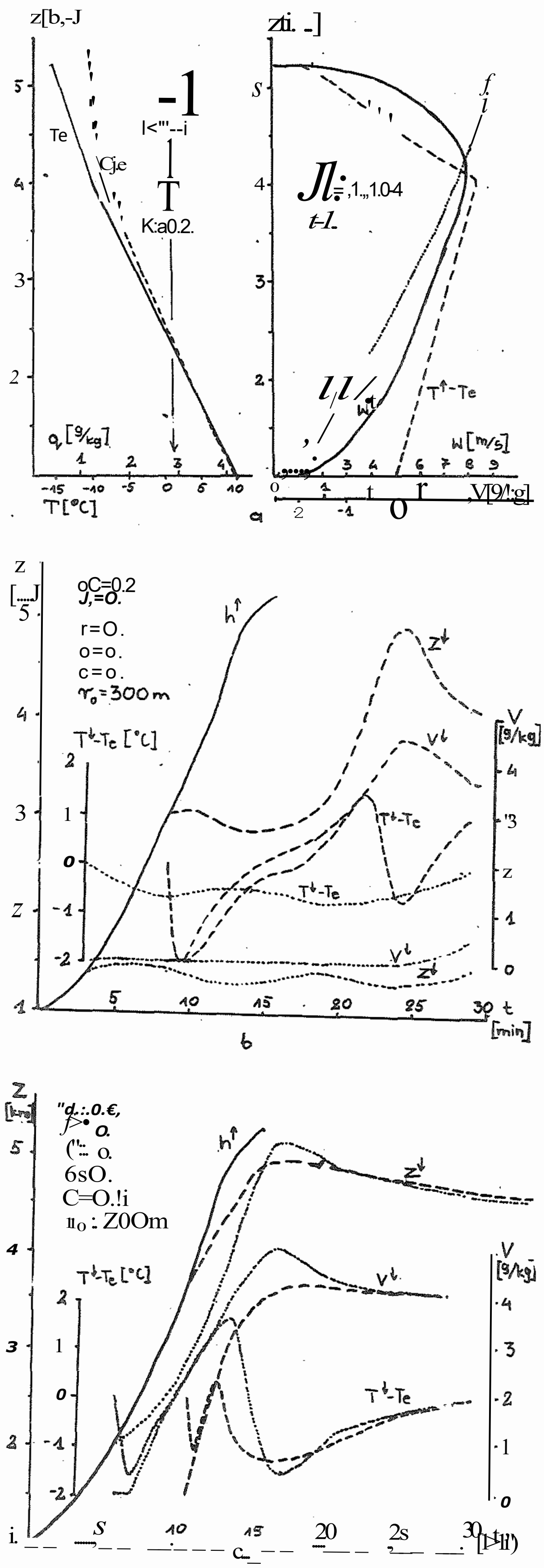
Te
q [g/kg]
T [°C]
$T^\uparrow - T_e$
W [m/s]
$h^\uparrow$
$z^\downarrow$
$V^\downarrow$
$T^\downarrow - T_e$ [°C]
$T^\downarrow - T_e$
V [g/kg]
t [min]
$r_0 = 300$ m

Fig. 1

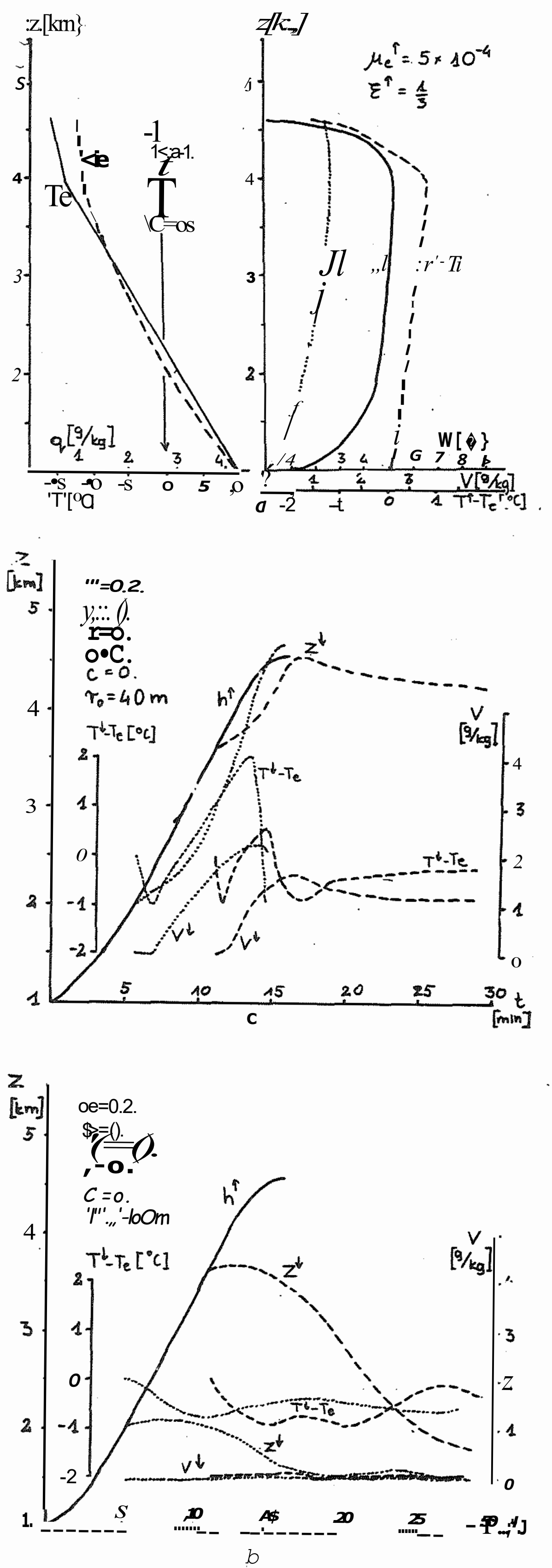
z [km]
Te
q [g/kg]
$\mu_e^\uparrow = 5 \times 10^{-4}$
$\varepsilon^\uparrow = \frac{1}{3}$
W
V [g/kg]
$T^\uparrow - T_e$ [°C]
$h^\uparrow$
$z^\downarrow$
$V^\downarrow$
$T^\downarrow - T_e$ [°C]
$T^\downarrow - T_e$
t [min]
$r_0 = 40$ m

Fig. 2

expecteu c c usions and suggestions. The most portant seeLl .. be the following ones:

A. Even weak updraft is a strong inhibitor for developffient cf downdrafts unless their initial diameters are very large (for typical entraiment constants - a kilometer or more). Even then strong damping of the updraft by nonbuoyant effects may be necessary in order to permit development of a reasonable downdraft. able to penetrate few hundreds meters downwards. Smaller bubles of environmental air are very soon turned to updrafts, sometimes even more vigo ous than the average clouc a ound them • Even in the upper , negatively buoyant-part of the cloud, small parcels (diameter less than 100 m) hardly can move against a moderate updraft (Figs 1c,2c).

This suggests that small spontanous downdrafts hardly can play any essential role in entrainment except a relatively thin layer close to the growing top of the cloud. Also artificial mechanical impulses of technically reasonable size hardly can induce a downdraft within even a weakly active part of the cloud.

B. Large masses of environmental air (diameter ca 1 km or more) can at certain circumstances penetrate few hundreds meters downwards and/or nearly hover for several minutes at very low speeds (order of dm/s) before returnin£ definitely up or falling downwards (Figs 1b,2b) Their quasi-equilibrium is not a static equilibrium with environment - as postulated by Telford (Ref.4) - but essentially depends upon nfnamical interaction with the updraft and when the latter starts to weaken, they may turn to rapid downdrafts leading to total dissipation of the cloud. In such hovering state these masses may form a relative:y persistent cloudy environment for deveJ.opment of smaller scale spontanous Lowndrafts, such as discussed in Refs 3,4 or 8. In nature, such masses may evolve e.g. from large volumes of environmental air entrapped between rapidly growing Cu cong towers.

This suggests, that vertical mixing may be in fact a two-scale phenomenon consisting of a slow motion of large masses of environmental air dynamically interacting with the updraft, and faster, smaller scale spontanous downdrafts, which have no direct contact with it.

C. Nonbuoyant pressure field created by a developing updraft may essentially alter the conditions for downdraft development. Quasi equilibrium of the large scale motion mentioned in the point B may serve as an example of such an alteration. This problem calls for deeper investigation with use of multidimensional models.

5. REFERENCES

1. Byers, H.R. and Braham, R.R. 1949. The thunderstorm. Report of the Thunderstorm Project, u. Weathe Bureau, Washington, D.C., 31-38.

2. Squires, P., 1958a. The spatial variation of liquid water and droplet concentration in cumuli. Tellus, 10, 371-380.

3. Squires, P., 1958b. Penetrative downdraughts in cumuli., Tellus, 10, 381-385.

4. Telford, J.W., 1?75. Turbulence, entrainment and mi/4ing in cloud dynamics. Pure **Appl**. Geophys., 113, 1067-1084.

5. Paluch, I.R., 1979. The entrainment mechanism in Colorado cumuli. J. Atmos. -. 36, 2467-2478.

6. Boatman J.F. and Auer, A.H., Jr., 1983. The role of cloud :op entrainment in Cumulus clouds. J. Atmos. Sci., 40, 1517-1534.

7. Vulfson N.I., and Levin I.M., 1972. Razruzhenije razvivajushchsia kuchevych oblakov c pomoshchiju vzryvov, Izv. AN SSSR, se r. FAiO, VIII, 156-166.

8. Clark R.S., and al, 1972. Modification of Vlarm Convective Clouds by Hygroscopie and Hydrophylic Materials. Third Conference on Weather Modificat American Meteorological Society, Boston, 1979-1981.

9. Emanuel, K.A., 1981. A similarity theory for unsaturated downdrafts within clouds. J; Atm s. Sci., 38, 1541-1557.

10. Haman, K. 1973. On the Jpdraft-downdraft interaction in convective clouds, Acta Geophye. Pol. XXI, 215-253.

11. Haman K.E. and Niewiadomski M., 1980. Colw downdrafts in cumulonimbus clouds. Tellus, 32, 525 536.

THREE-DIMENSIONAL CONVECTIVE CLOUD DYNAMICS

- A NEW INTEGRATION SCHEME

Thomas H uf, Hartl!lut F311er, Ulrich Schumann

Deutsche Forschungs- und Versuchsanstalt fur Luft- und Raumfahrt
Oberpfaffenhofen
Institut flir Physik der Atmosphare
D-8031 WeJ3ling FRG

1.INTRODUCTION

The numerical simulation of convective cloud dynamic l and microphysical processes is one of the most challenging problems in present mesoscale meteorol**ogy**. Four basic problems can be identi;ied:

1. the formulation of the basic model equations
2. the application of eff·icient numerical algorithms and data processing techniques
3. the treatment of microphysical processes
4. the treatment of turbulent and other· subgrid scale processes.

The objective of this paper is to derive a new set of model equations suitable for 3-D numerical simulation of convective clouds, to discuss the advantages and implications of these equations and to develop an in:tegration scheme. The derivation of.the equations is mainly based on the postulate to u:se budget equations .. As a consequence the entropy **is** chosen as a prognostic variable and a new type of sound filtedng is necessary, which is different from the widely used Boussinesq apP.roximation.
These equations and the resulting·algorithm form **the** theoretical framework of the MESOSCOP model **(Mesoscale** Convection model Oberp£affenhofen), which is presently under development at our institute.

2. BASIC MODEL FEATURES

2. 1 The Use of Budget Equations

In numerical grid point models variables are calculated at fixed locations. Therefore, the Eulerian point of view is more appropriate than the Lagrangian. This means that the budget operator

D(pt/>)/Dt = a(p,j,)/at + **V•(pt/>V)**

should be used for all mass-specific quantities♦ instead of the total time derivative

pd$_{t/>}$/dt = p(a,p/at + **v•V,p)**

(with p density, V velocity).
It is easy to see, that V• (pV,j,) integrated over a gr'id-cell volume gives the net flux out of the cell, whereas an equivalent meaning of pv•Vtj, does not **exist**.
It should be· noted that both operators D(p$_{t/>}$)/Dt and pd,P/dt have identical values if the full continuity equation

$$Dp/Dt = ap/at + \mathbf{V \cdot pv} = o \qquad \mathbf{(1)}$$

is used in the m del. ln a sound filtered model, however, this is no longer the case a.:d both operators· can be used independently.
Consequently, the momentum equation has the foim

$$Dpv/Dt = apv/at + V\cdot(pvv) =$$
$$-Vp - pg - V\cdot J - 2pQxv \qquad (2)$$

(including pressure gradient, gravity, stress and Coriol;i.s force).
For each scalar mass-specific variable ti>of the model a budget equation **is used**

$$\mathbf{D\rho\psi/Dt + \nabla\cdot\rho\psi J_{\psi} = Q_{\psi}} \qquad (3)$$

(with $J_{t/>}$ diffusive flux and so·irces of ,j,).
Eq.(3) is used for entropy ,j,= s, and for the **mass** concentrations ,i,= m^{i} (dry air (i=0), water vapor (i=1), liquid water (i=2), ice (i=3)).
The asic system of equations is completed with equations of state

$$\psi = z_{\psi}(p,T,m^{k}) \qquad (4)$$

for entropy and density.

2.2 The Entropy as a Prognostic Variable

Commonly temperature is used as a prognostic variable and the heat equation is integrated. This, however, leads to several problems. First of all the heat equation is not of budget type. There is also an additional time derivative dp/dt which is nUl11erically difficult to handle. Furthermore the temperature field is not smooth across cloud boundaries and numerical noise is generated there.
Thus a new variable is looked for, which **satisfies a** budget equation, is smoother than **temperature at** cloud boundaries, but nevertheless allows the **calcu**lat ion of temperature.
The ice"liquid water potential temperature **(Ref. 1)** is an attempt to overcome these problems, but **this** quantity suffers from being not determined by a budget equation. In dry air the potential **temper**ature 0 is very often used and the problem with the second time derivative is solved. The variable 8, however, is not defined for cloudy air. Remembering that for dry air 0 is a measure for entropy s, with 5s = cpoln0, it is a straightforward concl si011 to use generally the entropy as a prognostic variable.
Entropy is governed by a budget equation (Ref.2):

$$D(\rho s)/Dt + \nabla\bullet(J^q/T - \mu_n J^n/T) =$$

$$= -J^n\mu_n/T - J^n\bullet\nabla\mu_n/T - 1/T^2 J^q\bullet\nabla T + 1/T\ J\bullet\bullet\nabla v \quad (5)$$

(with s mass-specific entropy, J^q heat flux, J^i diffusion flux of the i.th partial mass m^i, μ_i specific Gibbs potential, J^i phase flux, J momentum flux).

The r.n.s. of Eq.5 represents the nonnegative entropy source. Each term is the product of an irreversible flux c::ld the corresponding driving force. For reversible cases all irreversible fluxes vanish and therefore the total entropy source vanishes (Eq. 6). The entropy sources also equal zero if the driving forces vanish. This does not necessarily mean vanishing irreversible fluxes. If equilibrium is assumed between water vapor and liquid water, for instance, the driving force $\mu^2 - \mu^1$ vanishes but not the ,;:,ase flux J^1.

$$D\rho t/1/Dt = 0 \quad (6)$$

VB.Jlishing entropy sourc·. means that in this case entropy is smoother than Lemperature at cloud boundaries, as the ·,eat equation in all cases has a source term due to exchange of latent heat in contrast to entropy.

In cloudy air the state function for entropy is

$$s = z_s(p,T,m^k) =$$

$$= c_p \ln T/T^* - R_0 m^0 \ln p^0/p^* - R_1 m^1 \ln p^1/p^* \quad (7)$$

(with $c_p = c_{pn} m^n$ specific heat, R_i specific gas constant ($i=0,1$), p^i partial r-ressure ($i=0,1$), p^*, 'T"' reference value$).

Eq.7 can be so_lve'l. for the temperature, and 12 get

$$T = T^*\exp\{1/c_{v^*}[\sigma + R_0\rho^0\ln(\rho^0 R_0 T^*/p^*) +$$

$$+ R_1\rho^1\ln(\rho^1 R_1 T^*/p^*)]\} \quad (8)$$

(with $\sigma=\rho s$. $\rho^i = \rho m^i$ partial densities and $c_{v^*} = c_{v0}\rho^0 + c_{v1}\rho^1 + c_2\rho^2 + c_3\rho^3$, c_{vi} specific heat).

Thus the temperature can be calculated, if the entropy $\sigma=\rho s$ and the partial densities ρ^i are known.

Of all possible quantities, which may be used as prognostic variables, entropy seems to be most appropriate, as it incorporate,s the effects of the first as well as of the second law of thermodynamics.

2.3 The Filtering of Sound

The basic equations (1-4) describe not only processes of meteorological interest but also sound waves. Explicit numerical intcgration schemes are restricted to time steps 6.t<6.x/c, where !Ix is the grid spacing and c the speed of sound (CFL-criterion). Thus snund waves lead to uneconomically small time steps. Three solutions of this old problem exist:

1. explicit integration of the hyperbolic part of the equations with small time steps, while other terms may be recomputed at larger time steps for economical reasons (Ref. 3).

2. implicit, sound-damping integration of the hyperbolic part, which allows for larger time steps (Ref. 4),

3. filtering of sound by means of a diagnostic relationship between pressure, velocity and density (Ref.5).

If budget equations are used for all prognostic variables and if sound filtering is attempted, a suitable filtering equation is

$$\nabla\bullet\rho v = 0 \quad (9)$$

The often used filtering equation for shallow convection $\nabla\bullet v = 0$ cannot be used in this case as it yields an unphysical mode of sound waves and does not filter them (Ref.5).

It should be noted that the density p is a three-dimensional time-dependent variable and that the Boussinesq approximation is not applied in any form.

Filtering as well ap implicit integracion leads to a t'oisson or Helmholtz equation for the pressure p. These equations can be found by time derivation of the continuity equation (1), replacing the term V• pv/at with the momentum equation (2) and replacing the density derivative by means of an equation of state (4), or setting the density derivative to zero in the filtered case, respectively (cf.Eq.12 and 14). In both cases the resulting equation can be economically integrated with fast solution procedures (Ref. 6).

2.4 Cloud Microphysics

Because of the large computer storage and speed requirements of any three-dimensional cloud model microphysics can only be treated in parameterized form. The partial densities or water contents of the different kinds of particles are chosen as parameters beside pressure p and temperature T.

The liquid phase is represented by cloud droplets and raindrops, which may be produced or destroyed by water vapor diffusion, coalescence, freezing or riming. The solid cloud particles taken into accou...,t are frozen drops, plate-like ice crystals, graupels (rimed frozen drops, rimed ice crystals), ,snowflakes, dry hail and wet hail. Deposition nucleation, snowflake aggregation and melting have to be described in addition to the processes mentioned above.

Because the cloud model is intended to be u· ,d for a variety of applications, ph8:.e fluxes are treated in the general form as non-equilibrium proc sses.It has been pointed out for instance by Clark and Hall (Ref.7) that broadening of the droplet distribution occurs due to fluctuating supersaturation associated with fil.ite phase relaxation time scales of condensation.

To allow for the investigation o' such effects with the MESOSCOP r:idel no a prioi_ assumption a':out equilibrium conditions is made. Thus condensation is not restricted to saturation requirements, although for some applications this 'bulk-physical' assumption is more convenient as it reduces the numerical efforts.
The p ase fluxes being irreversible processes produce entropy.
Phase transformations as caused by water vapor diffusion depend on super- or subsaturation with respect to the phase considered, on environmental (p,T) properties but also on particle and spectral properties. Assuming certain spectral regularities (e.g. log-normal distributions, Marshall-Palmer spectra) it is possible to write them as functions of the model parameters or the water contents (Ref.7) respectively.
Coagulation of liquid drops is separ ted into autoconversion and accretion: Different formulations of the transfer rates will be compared, e.g. Kessler (Ref. 8), Wisner et al. (R.f. 9), or a one-parameter version of the scheme proposed by Holler (Ref.10), which also describes riming of ice crystals and droplet freezing. Accretional growth of hail is treated as in Ref.9, wet growth as ir, Ref.11, aggregation of snowflakes as in Ref.12.

3. DISCRETIZATION AND INTEGRATION SCHEME

The discretization of the model equations and the integration scheme are based on the following principles and arguments.

3. 1 Time Integration

One of the objectives of the MESOSCOP cloud physics program is the simulation of non-equilibrium processes. Therefore o diagnostic relationship exists between the partial densities. and which therefore are all forecasted by prognostic budget equations. The essential assumption for this method is that the time integration scheme' guarantees the positive definiteness of the partial densities. Thus an Euler-scheme is used with a correct d upwind scheme (Ref.13) for che partiai densities. Oxherwise, and in particular for momentum, the second-order accurate Adams-Bashforth scheme is.used.
A basic feature of the scheme is its implicit character. The divergence of momentum V•pv in the continuity equation (1) and the pressure gradient Vp in the momentum equation (2), as essential hyperbolic terms. responsible for sound waves, are, treated .implicitly (cf.Eq.13 and Eq.10).
The degree of impli itness can be controlled by parameters and il'(OS , il'Sl).
It should be noted that the discrete form of the Helmholtz or Poisson equation has to be defined such that it is consistent with the discretized continuity and momentum equation, especially in the implicit terms.

3. 2 Control of Filtering

In the unfiltered as well as in the filtered case a second order par ial differential equation of Helmholtz or Poisson type, has to be integrated. Only one term a;at(ap/at), which defines the difference between the Helmholtz and Poisson type of equation has to be changed in the integration scheme. So by setting a control parameter f to 0 or 1, two totally different fluid dynamical modes can be solved with the same model and the same integration technique. This technique is illustrated.in 3.3.

3.3 Integration Scheme

The integration procedure from times t_n to t_{n+1} ($n>1$) consists of two parts.
In th" first part all budget equations are solved beginning with the momentum equation:

$$(\rho v)^{n+1} = (\rho v)^n - \gamma\Delta t\ \mathrm{grad}\Delta p - \Delta t(\rho^{*n} - \rho^n)g -$$

$$\text{At } E\ [\mathrm{grad}\ p + \mathrm{div}(pVV) + pg + \mathrm{div}J + 2pQ\ v] \quad (10)$$

and followed by the budget equation (11) for entropy ($\mathcal{J} = s$, cf.Eq.5):

$$(p,P)^{n+1} = (p,P)^n -$$
$$- \text{At } E:(\mathrm{div}(p,PV) + \mathrm{div}J_{\mathcal{J}} - Q,p) \qquad (11)$$

and the continuity equations for the partial densities p^k resp. $P = m^k$.
It is·

$E:(f) = f^n$ in the Euler scheme

and

$E(f) = 3/2\ f^n - 1/2\ f^{n-1}$ for Adams-Bashforth.

The effects of microphysical processes (e.g. condensation) on concentrations and entropy are temporarily ignored and corrected afterwards in a special cloud physics procedure (2.4). For this reason temperature is determined with Eq.8.
In the second part pressure is calculated ••ith the Helmholtz equation:

$$f[ap/apJ^n Ap - At^2\ \text{il'}\mathrm{div}\ \mathrm{grad}(Ap) = q$$
$$p^{n+1} = p^n + Ap \qquad (12)$$

where f is the control parameter.for filtering.
Pressure equation and momentum equation are **solved** very closely within the integration sequence using identical values of the density.
Eq. 12 is derived, as previou ly stated, by combi - in.g the continuity equation:

$$\Delta\rho/\Delta t + \beta\mathrm{div}(\rho v)^{n+1} + (1-\beta)\mathrm{div}(\rho v)^n = 0 \qquad (13)$$

with the momentum equation (10) and using Eq. 14.
Den ity integration is treated differently. After a and p^k are known, the new d nsity p* is estimated at constant pressure (Ap=O) with a differential equation of stat-:,.:

$$\rho^{n+1} = [\partial\rho/\partial p]^n\Delta p + \Sigma[\partial\rho/\partial\psi^n]^n\Delta\psi^n + \rho^n \qquad (14)$$

$$= [\partial\rho/\partial p]^n\Delta p + \rho^{*n+1}$$

This estimate ρ^* is updated after the simulation of cloud microphysical processes.
For stability reasons the buoyancy term in Eq. 10 and in Eq.11 has to be computed with an estimate of the new density and thus ρ^* is used there. After pressure is known (Eq.12) the correct new value of the density can be calculated explicitly with Eq.14.
This scheme guarantees that buoyancy changes, caused by cloud microphysical processes, influence pressure and momentum immediately, using identical values.

3.4 Stability Analysis

Linear stability analysis shows that this scheme is stable if $\alpha \geq 0.5$ and $\beta \geq 0.5$ and Δt is less than the critical time step due to advection, diffusion and buoyancy.
For $\alpha = 0.5$, $\beta = 0.5$ the scheme is free of numerical damping; for $\beta = 1$, $\alpha = 1$ sound waves are damped; for $\alpha = 0$, $\beta = 1$ sound waves are totally suppressed.
If the fields of the previous time step or the initial fields deviate from the condition $\nabla \cdot \rho v = 0$, then they are corrected at the next time step so that the resulting fields of the new solution are again soundfree.

3.5 Spatial Discretization

We use the staggered grid as introduced by Harlow & Welch (Ref.14).

With index notation $[v = (u1,u2,u3)]$ and the standard finite difference and averaging operators $\delta_i, \overline{f}^i$ respectively, the differential operators are, approximated as follows:

$$\mathrm{grad}\, p \simeq \delta_i p, \quad \mathrm{div}(\rho V) \simeq \delta_i(\overline{\rho}^i u_i)$$

$$\mathrm{div}(\rho V\psi) = \mathrm{div}[(\rho V)\psi] \simeq \delta_i(\overline{\rho}^i u_i \overline{\psi}^i)$$

$$\mathrm{div}(\rho VV)_i = \mathrm{div}[V(\rho V)]_i \simeq \delta_j(\overline{\rho}^j \overline{u}_j^i \overline{u}_i^j)$$

The alternatives

$$\mathrm{div}(\rho V\psi) = \mathrm{div}[(\rho\psi)V] \simeq \delta_i(u_i \overline{\rho\psi}^i) \text{ and}$$

$$\mathrm{div}(\rho VV)_i = \mathrm{div}[(\rho V)V]_i \simeq \delta_j(\overline{\overline{\rho}^i u_i^j}\, \overline{u}_j^i)$$

cannot be recommended, because they do not cunserve quadratic quantities like the variance $1/2\rho\psi^2$ or kinetic energy $1/2\rho V^2$. This removes the ambiguity in the divergence term of the budget operator which is one implication of the use of budget equations.

4. RESULT

A set of basic equations and an integration scheme has been developed. It has been shown that the consequent use of budget equations has strong implications on the basic model variables, the type of sound filtering, the time integration scheme and the numerical algorithms employed. No use was made of the Boussinesq approximation. With the same integration scheme a sound filtered as well as a fully compressible fluid mode can be simulated. Entropy is used as a prognostic variable and an irreversibel treatment of cloud microphysical processes is attempted.

5. REFERENCES

1. Tripoli J J & Cotton W R 1981, The use of ice-liquid water potential temperature as a thermodynamic variable in deep atmospheric models, *Mon Wea Rev* 109, 1094 - 1102.

2. DeGroot S R & Mazur P 1969, *Grundlagen der Thermodynamik irreversibler Prozesse,* Mannheim, BI-Hochschultaschenbücher.

3. Klemp J B & Wilhelmsen R B 1978, The simulation of three-dimensional convective storm dynamics, *J Atmos Sci* 35, 1070 -1096.

4. Harlow F H & Amsden A A 1971, A numerical fluid. dynamics calculation method for all flow speeds, *J Computational Phys* 8, 197 - 213.

5. Hauf T 1980, Schallfilterung im konvektiven Scale, *Dissertation*, Johannes Gutenberg-Universitat Mainz.

6. Schumann U & Sweet R A 1976, A direct method for the solution of Poisson's equation with Neumann boundary conditions on a staggered grid of arbitrary size, *J Computational Phys* 20, 171-182.

7. Clark T L & Hall W D 1979, A numerical experiment on stochastic condensation theory, *J Atmos Sci* 36, 470 - 483.

8. Kessler E 1969, On the distribution and continuity of water substance in atmospheric circulations, *Meteor Monographs* 10, No. 32, 1 - 84.

9. Wisner C, Orville H D, Myers C 1972, A numerical model of a hail-bearing cloud, *J Atmos Sci* 29, 1160 -1181.

10. Holler H 1984, A paramerization-scheme of cloud microphysical processes, Proc *9th Int Cloud Physics Conf* Tallin.

11. Musil D J 1970, Computer modeling of hailstone growth in feeder clouds, *J Atmos Sci* 27, 474 482.

12. Chang C H 1977, Ice generation in clouds, *Master thesis,* Dept Meteor South Dakota School of Mines and Technology, Rapid City, 129 pp.

13. Smolarkiewicz P K 1983, A simple positive definite advection scheme with small implicit diffusion, *Mon Wea Rev* 1M, 479 - 486.

14. Harlow H H & Welch J b 1965, Numerical Calculation of time-dependent viscous incompressible flow with free surface, *The Physics of Fluids* 8, 2182 - 2189.

ON THE CONTIITIONS OF WARM RAIN FORMATION IN CUMULUS CLOUDS

Hu Zhijin
(Academy of Meteorological Sc·ienc·e,
State Meteorological Administration)
Beijing, People's, Republic· of China

1'. Introduction

In three sUllll!lers of 1963-65 in Jiujiang, Jiangxi Province 679 cumulus clouds were observed, using dual-theodolite, time lapse camera and radiosonds. The height, temperature and growth rate of cloud tops, cloud form, bass height, life time, initiation times of precipitation and graciation were recorded•. The observation shows that the probability of precipitation increases with the cloud top height (see fig.1). Comparison the cloud depthes with 50% probability of precipitation (l*) in various regions of the world shows apprecia e difference·. (see tab.1). For example H* was 5.71an in Jiujiang and 2.51an in Purto-R!ico. Data in tab. 11 11,re adapted from references(1'-12)and with different reliabilities. Battan (1) and Squires (12) showed the importance of the cloud base height (climate continentality) and cloud droplets spectrum (microphysical continentality). But these two.factors can hardly explain all -observed characters in tab.1. In this paper a simple mode is used to examine the relationship among H*, cloud base temperature, grow.th rate and microphysical continentality.

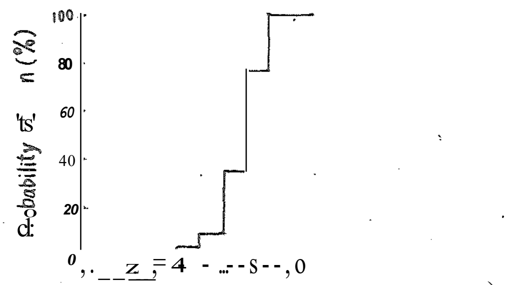

Cloud top height (km)

Fig.1. Precipitatiqn probability of clouds with various top heights

2. Model

The development of rain drops in a cloud parcel has 2 stag_es: 1• the cloud droplets spectrum (CDS) broadens, but there are no rain drops till a critical time T1; 2. after then raindrops are produced by autoconv:rsion and collection. After Berry (13) T1=(2+0.0266N/D/m)/m, where N, D are parameters of initial CDS, m--LWC. The production rate of rain water according to (14) is

$$\frac{d}{dt} = m((6+\frac{0.0200}{m}!)\frac{.}{D}\frac{.}{m}1ff,$$

the relaxation time of autoconversion has the same form as T1. So the full time of rain development will be T=k·T1, where k--coefficient (k>1).

The LWC increases with the rising of the cloud parcel, so height (H1), at which the first stage is accomplished, can be calculated from $\int^{H1}\frac{dH}{W}=1$, and the rain formation height Hp= k H1 •. After Warner (15), XprMAH (16) and based on airborne observations in Hunan Province LWC is ussumea to be one half of the adiabatic value, which is a function of clo d base temperature and height. The value of N/D is assumed to be 400 for marine clouds and 1200 for continental. H1 are calculated for all sites in tab.1, using observed data.

3. Results

1. The relationship between calculated H1 and observed cloud depth with 50% precipitation probability(H*) for 8 sites is shown in tab.1 and fig.2. The good correlation exceeds our expectations. The coefficient k=1.71 • Thie result shows the importance of wl1.rm rain process in the initiation of precipitation in cumulus with relatively warm base temperature.· It agrees with the observations of the first radar echo by Battan (17) and KoT06 (7).

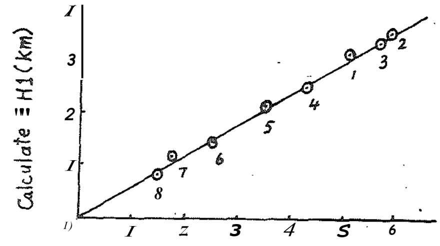

Observed H* (km)

Fig.2. Relationship between calculated H1 and observed cloud depth with 50% precipitation probability, H*.

?.. 'rhe relative importance of various factors in determing rainformation height (RFH) are analysed by this model. Results showed that the difference of RFH js due mainly to the cloud growth rate as .ell a, the continentality. (see tab.2). It agree with theoretical studies of Ludlb (1u) anc' ,'1&c-cready (11).

•P:,b.2. H* in various regions and its analyses

Regions for comparison	observed	due to W	To	N/D
Jiu,jiang Pur-Reco	2.3	1.65	1	1.4
Jiu,jiang Leningrad	1.6	1.9	0.B	1
Central USA Purto-Reco	2.4	1.55	1.1	1.4

3. The relationship between RFH and growth rates calculated by this model (cur e in fig.3) agrees with the observations of 64 cumulus clouds in Jiujiang. (see fig,3).

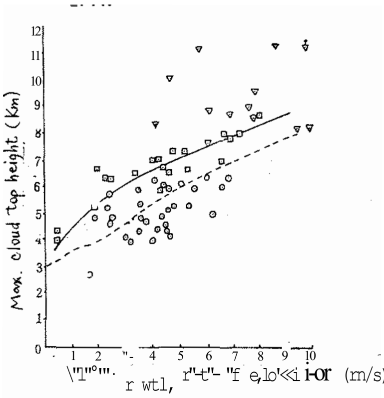

F,3. 3, Rel"Tionship b.:twee RFH - growth ""'- 0 (.).,\l'\11,(MASoui... rec... "ltet.! il, 0 with ra:;11, q ('.,I,.- Curve. lint..-- c. lood"iio"by ihis nlv:le/_

4. References

(1) Battan, **L.J.**, Braham, R.R., 1956, A st dy of convective precipitation based on cloud and rada= observations. J. Met., 13, 587.

(2) E.L.Harriagton, 1958, Observations on the **appearance** and growth of tropical cumuli, J.Met., 15, 127.

(3) S.A.Changnon, S.G.Bi,ler, 1957, On the observation of convective clouds mid the radar precipitation echoes within them, Bul. AMER. Meteo. Sc Soc., 38, 5, 279.

(4) BouT, Kop11vleH1<0, H.el<orqbic: aco'iieHHCC.Tvf rpou,ec..c.C1 cS"Q306"HtR oca,D,KcB 8 Kf'"leBb/X o8"MKOK , Tpy ,_Фl Yt<p-H1-1rMM, B n. /lg, up.61.

(5) Bou,;, KorHu HKo, Hel<o'Tpble. pe3,YllbTaT1,f CCAe,Llo6AH£-'.'l ,l\ H4"lH'--lec.,Ko e-rpyK,..Yfbl KyYeBb/X o'bl\o.KoB, il,id , Bbln. 82, e,11'·'72.

(6) k'opHweHtO' Ou,e.Htl,\ [303MO)!IHOC,T1,1 yGeA;J'{eH[,f;1 ocap,ICoB 113 Ky'ie8!,/)(Ob/\QKOB /303/Jiet, TBMeM C T8"€j'F'IM r/\€.,,IJ1C,\OTOM, i!,;cl, SIAn. 'J2, c;rr."/'2.

(7) Ko,a5, 1960, Pct;n,t>10MKau, oHHb/e xapanepwc.rnK'vf f\li!,HVl 1-l rro,, Tf)'A•I rro, bin.102, <.:.:rpb3.

(B) CeAe.mi Q, ,q,,l , 0 rp H1.11.1,c,x. u BepHIK11/\bHoi:i MOUjHOCT1.1 KO1-<6e.KTv!BHHX 00/\aKO13 , Tt)',O,bl ri- 0, sl-ln. p, "l'-i

(9) W,1LJ.1K11H, 1'j',0, He:J<6n>pble. pny/\0To,b1 vlcc.M.)J,061lHv!!I r•030Sbl/(" /\l-1BHe.6blX: (\01\ 0B' TP)",V,bl rro' ФhY_63 (/25)_

(10) **Byers**, H.R., Hall, **R.K.**, 1955, **A** census of cumulus-cloud height versus precipitation in the vicinity of Purto Rico during the winter ...nd spring of 1953-54, J. Meteo., 12, 176.

(11) Mac-cready et al., 1957, Nuclei, c mulus and seedability studies, Final Report of the Advisory Committee on Weather control, V. , part ,Ctimulu studies, 146.

(12) Squires P, 1958, The microstructure and colloidal stability of warm clouds, Tellus, 10, 2 256.

(13) Berry, E.X., 1968, Modification of the warm rain process, Proc. First Nat. Conf. on Wea, Mod.. Amer. Meteo. Soc.·, Albany, New York, 1968, 81.

(14) Hu Zhijin, 1980, A parameterized equation of warm rain formation in cumulus clouds, Proc. 8th International Confernce on cloud Physics, Clermont Ferrand 15-19 July 1980.

(15) Warner J., 1970, On steady-state one-dim nsional models of cumuius convection, J. Atmos. Sci., 27, 1035.

(16) Xpr G\H, oJ>,13uKO o/\C!KOB.

(17) Battan L.J., Observation on the formation and spread of precipitation in convective clouds, J.Meteo., 70,311.

(18) ason, B.J., 1971, The pr.ysics of clouds.

Tab.1. Characteristics of rainformation c·louds in various regions

	Region No.	1	2	3	4	5	6	7	8
	Latitude	35	40	30	50	60	20	20	20
	Microstructure	eont.	cont.	c·ont.	cont.	cont.	mar.	mar.	mar.
	Base height	3.6	1.6	1.3	1.7	0.9	0.5	o.6	0.6
	Base temper.ature	7	14	21	8.5	9	21	20	20
	Top growth rate	2.2	3.8	4.5	(1.5)	1.1	1.4	1.0	(0.25)
£_ -	Top height	8.7	7.5	7.0	6.0	4.5	3.0	2.4	2.1
..; Ll	Top tempel!'.	-24	-18	-8	-17	-10	8	7	9
3i; 1	Depth (H*)	5.1	5.9	5.7	4.3	(3.5)	2.5	1.8	15
alculated I	H1	3.1	3.5	3.3	2.5	2.2	1.5	1.2	00
	k H1	5.3	6.0	5.6	4.}	3.6	2.5	2.0	1.4

Region 1--New- Mexico. (1)(2); 2--Central U.S.A. (1)(3); 3--Jiujiang, China; 4--Ukraine (4--6); 5--Leningrad (7-9); 6--Purto-Reco (1)(2)(10); 7,8--marine cumulus and orographic c clouds in Hawaii (11-12).

538

NUMERICAL SIMULATION AND OBSERVATIONAL ANALYSIS OF CONVECTIVE CLOUDS IN THE .LOWER ALPINE REGION

Anne M. Jochum

Institut fur Physik der Atmosphare
Deutsche Forschungs- und Versuchsanstalt fur Luft- und Raumfahrt
Oberpfaffenhofen, D 8031 We6ling, FRG

1. INTRODUCTION

A time-dependent one-dimensional model with detailed microphysics including the ice-phase is used for case studies of convective clouds in the lower Alpine region.

It **is** the purpose of this paper to, discuss two selected case studies, one of shallow cumulus, and one of a deep. shower cloud which had been seeded with silver iodide.

"The model is based on Nelson's (Ref. 2) cloud model, with identical model physics and numerical methods. The initialization procedure as well as the code structure were modified in order to facilitate data handling and increase computational efficienc;y.

A short model description is given below.

Subsequently, two case studies are. presented to illustrate the broad range of possible applicatioqs. Case 1 of small cumulus compares model results to aircraft observations. Case 2 of an almost stationary cumulonimbus gives an analysis of radar data and compares them· with model results. The observed cloud had been seeded with silver iodide, and numerical seeding tests suggest that haii may indeed have been suppressed in this particular case.

2. THE MODEL

The cloud .model is time-dependent and one-dimensional. The simulated cloud is considered as a cylinder of fixed radius with its axis vertical in an environment otherwise at rest. Dependent variables are specified as functions of height along the cylinder and are assumed to represent -horizontal means taken over the updraft core. Turbulent diffusion and entrainment re parameterized using constant diffusion coefficients. The microphysical processes are incorporated in considerable detail. The space-time evolution of ·liquid- and solid-phase particle distribution functions is explicitly calculated. Each spectrum is resolved into 44 mass ranges (covering droplets from 2 µm to 4 mm, ic particles from 13.7 µm to 2.81 cm radius). Processes considered are nucleation, condensation, evaporation, sublimation, coalescence, break-up, riming, freezing and melting.

To initialize the model, the following input data are required: a temperature and humidity profile of the environment, an estimate of the conve tion initiating pulse of excess temperature and/or moisture and/or vertical momentum, the cloud base radius, the IN' (ice forming nuclei) spectrum, and the CCN (cloud condensation nuclei) spectrum or. an initial droplet spectrum.

3. CASE **1**

On 15. July 1982, several shallow cumuli were observed by aircraft in the northern foot-hills of the Alps. A detailed analysis of the data obtained from successive aircraft , penetrations and a description of the instrumentation .is given elsewhere in these proceedings (Ref. 1). Here, only the main features are reported.

Under generally anticyclonic conditions, with light winds from S-SE, there were forming small cumulus clouds around noon. The bases were observed around 1700 m agl, with tops rising to about 3200 m agl and average horizontai diameters of 2500 m. Maxlll!UIII updraft speed was ***3*** m/s at cloud base, 7 m/s .at 700 m above base.A maximum liquid water conteJlt of .2 g/m^3 was found at 700 m above base (. 1 g/m^1 at base).

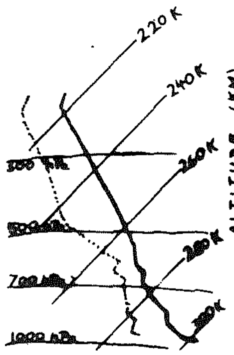

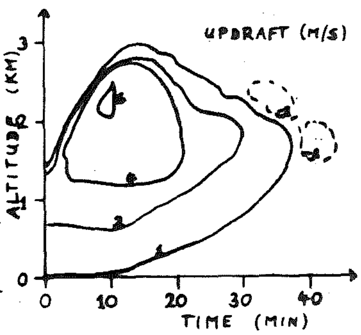

Figure 1. 15.7.82 Munich radiosonde.

Figure 2. Tillle-hejgbt profiles of model predicted updraft.

The radiosonde of Munich (100 km NE) at 12 GMT as depict-ad in Fig. 1 was used to initialize the model. A cloud base radius of 2000 m was derived from the observations. An initial pulse of .7 K excess temperature and light (1 **m/s)** vertical momentum was applied for 10 minute& at the lowest 600 m. The initial spectrum **was chosen** from droplet spectrometer measurements at cloud base.

The model generated a cloud with base at 1500 m agl rising to a top height of 3000 m after 10 minutes. A maximum updraft speed of 6 m/s was reached after 8 minutes at a height of 2400 m. The model cloud decayed after 35 minutes. The predicted evolution of droplet spectra shows little change, reaching maximum· radii of 16 µm (8 µm initially). Fig. 2 shows time-height profiles of computed updraft velocity. Cloud temperature and the overall features of cloud generation and decay are reproduced equally well.

4. CASE 2 - A SEEDING CASE?

On July 20, 1981, an isolated almost stationary cumulonicbus, 50 km SE of Munich, was observed by means of a conventional ***3*** cm weather radar. The cloud was almost 10 km deep and had a maxi.mum horizontal extension of 6 km. At ground there were 110 mm rain reported.

The radar is located at Oberpfaffenhofen, i.e. 45 km from the nearest edge of the cloud. A volume scan mode was employed with five elevation planes giving

a vertical resolution of 3 degrees. Horizontal radial and angular resolution are 150 m and 1 degree, respectively. Volume scans were performed every 7 minutes .
The data are interpolated on a three-dimensional cartesian grid of user selected resolution. In order to facilitate comparison with one-dimensional model results, horizontal mean values over the updraft core are computed at 100 m height intervals, and time-height profiles of radar reflectivity and liquid water content are drawn as shown in Figure 3.

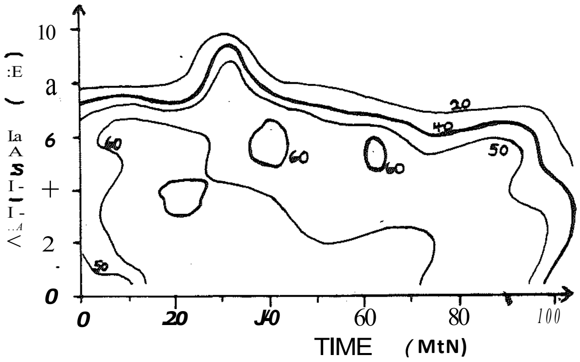

Figure 3. Time-height profiles of reflectivity (dBz) as computed from radar data.

The radiosonde of Munich at 12 GMT (Fig.4) is used to initialize the model. A cloud base radius of 4000 m is taken from observations, an average continental droplet spectrum is used as the initial spectrum. An excess temperature of 1.2 K and a vertical velocity disturbance of 2.5 m/s are applied at the lowest 600 m for 15 minutes.

POTENTIAL TE"PERRTURE INK

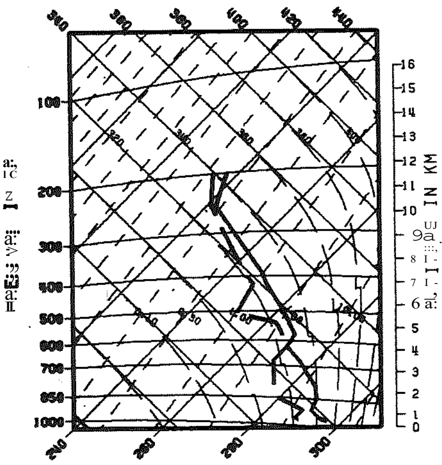

TEMPERATURE INK

Figure 4. /'lunich radiosonde 20.7.82 12 GNT.

The cloud had been seeded with silver iodide. Eventhough cloud seeding keeps being a highly speculative field we attempted numerical seeding tests for this particular case.
The model implementation of Agl seeding by supplying additional ice forming nuclei and decreasing the freezing temperature is described in Ref. 2. Beside this, model parameters for seeded and unseeded test cases were identical. A concentration of 100/1 AgI changes the computed precipitation rates at ground quite substantially as illustrated in Figure 5. Hail is redliced to a very high degree, whereas rain is slightly augmented.

A more detailed analysis of model computed hydrometeor spectra reveals a substantially. smaller _n ber of large liquid drops aloft than without seeding, and consequently practically no large frozen drops.

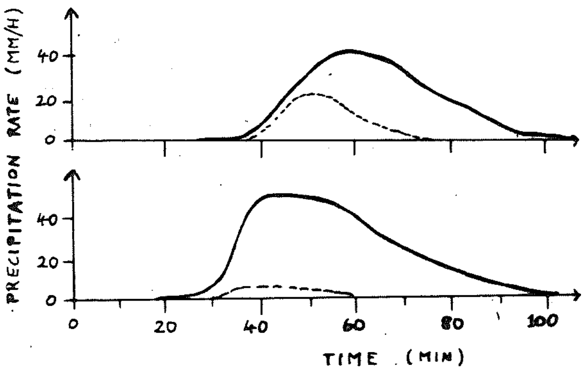

Figure 5. PrtJdicted precipitation ***rates at ground*** *for seeded (below) and unseeded (above) test case. Solid: rain, dot: hail.* For other numerical seeding tests performed with the model.Nelson (Ref. 2) concludes that for clouds having warm bases (with.base temperatures generally above 14[1]Celsius) the coalescence process forming large drops is dominant and leads preferentially to the formation of frozen-drop hail-embryo types. Under these conditions Agl seeding may result in hail suppression and is usually accompanied by rain decrease. Only for a small range of base temperatures rain augmentation may occur. In our case we apparently deal with an example of a warm-based (cloud base temperature was around 15°Celsius) cloud, where AgI seeding may have lead to significant hail suppression so that only light hail would have reached the ground. This agrees.with the observations.

5. CONCLUSIONS

Some results of numerical simulation of convective clouds using a time-dependent one-dimensional **model** with detailed microphysics were presented.
Case 1 is certainly close to the lower limit of the model's range of applicability but still compares well with aircraft observations. Case 2 gives rise to some speculations as does any kind of seeding experiment: Acc.epting the validity of the m.odel results for both unseeded and seeded conditions the model computations suggest that seeding was successful in. this particular case. According to the highly speculative nature of the matter great emphasis **was** laid on a most careful choice of initialization and other model parameters, taking into account the conclusions drawn from detailed parameter studies. All tests, however; confirm the fact that the model predicts hail suppression and slight rain augmentation. These results are in line with previous numerical seeding experiments performed with the same model (R f. 4), and they are consistent with obse:rvatio s.

6. REFERENCES

1. Meischner P, Bogel W, Horst H and Roth R 1984, Observational case study of microphysics in growing convective clouds near the Alps (see paper in these proceedings).

2. Nelson L D 1979, *Observations and Numerical* ***Sim****ulations of Precipitation Mechanisms in Natural and Seeded Convective Clouds.* University of Chicago, Technical Note 54.

Jun-ichi Shiino

Meteorological Research Institute, Tsukuba, Japan

1. INTRODUCTION

There has been a noticeable advance in this decade in our understanding on the evolution of droplets in cumulus clouds. Fruitful results on the physical mechanism of warm rain are obtained by Nelson(Ref.1), Ogura and Takahashi(Ref.2), Takahashi (Ref.3), Takeda(Ref.4), etc. They used one-dimensional time-dependent models of a warm cumulus in which cloud dynamical and microphysical interaction is to some extent taken into consideration and succeeded in a simulation of certain aspect of warm rain such as sudden outbreak, heavy and short-lived. Further improved studies by two- and three-dimensional models, in which more sophisticated and highly non-linear interaction is included, have been performed by Takahashi(Refs.5, 6, 7) and Soong(Ref.8). All of these researches clarified a role with great importance of the coalescence process of droplets as well as the existence of updraft for the development of warm rain.

One of the notable features in the evolutional process of droplets most of their results showed is the formation of a typical "bimodal" drop size-distribution composed of cloud droplets and drizzle sized drops, through which cloud droplets explosively grow into raindrops, being dominated by coalescence and almost always leading to an outbreak of rainfall. The existence of this "bimodal" distribution or the secondary peak in raindrop sizes is also supported by observations (Takahashi, Ref. 9). Therefore, the microphysical condition for the formation of the "bimodal" distribution would be recognized as the most essential problem in warm rain processes. The condition would be appropriate to be called as a "critical condition".

Scarcely any effort, however, has been devoted to the discussion of this kind of the critical condition. The main purpose of this paper is to investigate the "critical cundition" of vqrious microphysical parameters by an axisymnetric model of a maritime warm cunulus which includes highly non-linear interaction between cloud dynamics and microphysics. Another purpose is to investigate the feasibility of warm cloud modification (enhancement of precipitation) by a numerical experiment, in which the effectiveness of seeding small cunuli with water drops is examined.

2. GOVERNING EQUATIONS OF THE MODEL

The detail of the cloud model is presented in Shiino (Ref.10). The dynamical framework of the model is an anelastic system for deep moist convection. The basic equations consist of continuity equation of the air, horizontal and vertical equations of motion, thermodynamic equation and water vapour equation. Microphysical processes taken into account in the model are the formation of cloud droplets around cloud condensation nuclei, droplet growth by water vapour diffusion, coalescence, evaporation, sedimentation of droplets relative to the air, and drop breakup. Under consideration of these microphysical processes together with horizontal and vertical advection, and turbulent diffusion, the droplet size-distribution can be predicted every time step.

3. NUMERICAL PROCEDURES

The computational domain is 6.4 km in the vertical and 8 km in the horizontal with a grid interval of 400 m for both directions. Physical variables are arranged in a staggered system. The boundary conditions are rigid with free slip at all boundaries. The computational schemes are the forward difference in time, the modified upstream presented by Soong and Ogura(Ref.11) for advective terms except for vorticity, for which an ordinary upstream, and the centered difference for other space derivatives. The time increment is taken to be 20 sec. The scheme of numerical integration of the coalescence equation is due to Beny's(Ref.12) and breakup process of a large droplet follows Srivastava(Ref.13). As for collision efficiencies, the theoretical results obtained by Hocking(Ref.14) and Shafrir and Neiburger(Ref.15) are used in combination with an assumption. Terminal velocities of droplets are basically due to Gunn and Kinzer(Ref.16). In the present model, the evolutional process of droplets in both small-scale clouds, hereafter called as S-clouds, and well developed ones with higher cloud tops, which are dynamically more active in general than S-clouds and hereafter called as D-clouds, and its difference between the two are discussed for the present purpose. The vertical profiles of air temperature and moisture in the base state for S- and D-clouds are differentiated between the two with more intense conditional instability in the latter compared to the former. As an initial disturbance, a small and weak circulation accompanied by saturated water vapour is put into a lower portion of the atmosphere. The radius range of droplets considered is 4 to 4096 μ with 61 size-groups of water drops, which sufficiently eliminates numerical spreading of the size-distribution of droplets as examined by Shiino(Ref.10). The initial droplet spectrum formed by condensation is assumed to take a prescribed form in the present study. The normalized form is presented in Fig.1. Four kinds, being composed of two types, of spectrum are considered. The detail is to be refered to Shiino(Ref. 17). Among the four, type A with a dispersion of 0.364 and with a mean radius of 10 μ is used as a standard.

4. GENERAL DESCRIPTION OF THE MODEL CLOUDS

As soon as the initial disturbance is put into a region, the vertical velocity increases with time and reaches a maximum of 6.5 m sec⁻¹ in the D-cloud and 3.5 m sec⁻¹ in the S-cloud. Meanwhile, the maximum value of downdraft is 9.0 m sec⁻¹ in the D- and 2.9 m sec⁻¹ in the S-clouds. During the course of its development, the region with intense updraft is occupied by positive excess potential temperature, whose maximum is 3.2 °C in the D- and 0.8 °C in the S-clouds. The maximum height of the D-cloud through the life time is 5.8 km while it is 3.0 km in the S-cloud. One of the notable features which are contrast between the two clouds is that the maximum values of rain water and liquid water are realized at a mid-level (3.8 km) in the D-cloud, while they are observed near the cloud top in the S-cloud.

Vertical crosssections showing the features of the D-cloud in the developing, mature and decaying stages are illustrated in Shiino(Ref.10).

5. CONSIDERATION ON THE GROWTH OF DROPLETS

Figs.2a and 2b show the time-height variation of liquid water Q(upper) and the time variation of the droplet size-distribution in terms of water mass density g(lnR), where R is radius of a droplet, along the levels (A,B,C, ..) where liquid water takes a maximum at the central region of the D-(DA10) and the S-clouds(SA10). Meanwhile, Fig.3 represents the result of a budget analysis of water mass density of droplets, whose number density f(lnR) is governed by the following equation, at several points in D-cloud(Figs. 2a). ,...e. .I'

if__ 1L l..r.... j ;J f -,Lf)
at¯¯- -u. :Jr -w n + f- rf f VR)

+ (-%tl P + (fficia + (ft)co!I + (f k +Df,

where the thid term in the right hand side is the relative sedimentation, the fourth the formation of droplets by cloud condensation nuclei, the fifth the variation due to condensation growth or evaporation, the sixth the coalescence, the seventh the breakup and the last term the turbulent diffusion. The dynamical effect, (<19/;-;t)$_{y}$n , is defined as the sun of horizontal and vertical advection, relative sedimentation and the turbulent diffusion. In the early growing stage of the D-cloud, the droplet growth is gradual(A,B,C) since its dominant physical process is condensation of water vapour(Fig.3 , upper). However, as soon as small am:mnt of large droplets with. radius greater than 50 µ or so is produced(D) , these droplets being primarily produced by coalescence of droplets with udius 20 p. to 30 f (Fig.3, middle), the size-distribution shows remarkable change(E,F,G) and droplets grow rapidly to larger sizes by coalescence(Fig.3, lower).These large raindrops begin to fall against upward air lllJtion exe:c:..ing drag force to the current and then induce downdraft, which in turn accelerates downward lllJtion of the droplets, which is a highly nonlinear process between cloud dynamics and microphysics. On the other hand,in the S--cloud the droplet growth is as a whole fairly-gradual compared with the D-cloud. During the growing stage of the cloud, the growth of droplets is allllJst completely dominated by condensation and a typical bil!IJdal size-distribution which means the ascendancy of coalescence against condensation growth barely appears near the cloud top during the mature stage.

This diffe,ence in the evolutional process of droplets exerts significant influence on the behavior of droplets in the decaying stage of the clouds, which is discussed in Shiino(Ref.17).

6. HYPOTHESES ON THE FORMATION OF THE "BIM:JDAL" DROP SIZE-DISTRIBurION

As soon as the coalescence process comes into dominant, droplets grow explosively to larger sizes through a typical bim:Jdal size-distribution, allllJst always leading to an outbreak of r;::infalL However, the precipitation efficiency, maximum rainfall rate, etc. are significantly different between S- and D-clouds with c1:Lfferent dynamical properties . This is substantially due c:o the difference of the formative process of a typical bil!IJdal size-distribut".on between the clouds. Now, the essential problem which. should be solved is the critical condition, with which droplets favorably as well as promptly grow into a typical bil!IJdal size-distribution, of various cloud physical parameters.

First, the size-distributions at point D in the .D-cloud(DA10,Fig.2a) and point E in the S-cloud(SA10 , Fig.2b) are examined in detail. The selection of these points is exceedingly favorable for the present purpose since both of the simple distribution markedly change into a typical bim:Jdal size--"istribution within a few minutes. The analyzed result is given in Shiino(Ref.17) in terms of number density of droplets every 10 f- from 10 f- to 90 f . The lllJSt . striking feature is that droplets at these points exhibit. highly similar distributions in spite of their different growing histories._ This strongly suggests the existence of a general critical condition for the formation of the "bimodal" droplet size-distribution or the onset of a dominant coalescence process.

Then, the analysis is extended to all points of the clouds of SA10 and DA10 tmtil a typical bimodal size-distribution is fonned at the cloud center. The results are sumnarized in Fig.4, which represents a scatter diagram of the drop size-distribution in terms of mean radius(R inf) and dispersion(Ds). The data are selected every .three minutes up to 18 min. In the figure the number density of droplets with radius 60 /A (60 :!5 f), that with radius 80 f- (80 :!5 f) and liquid water are also superimposed..Based on a careful consideration of the drop size-distribution at the individual point, the diagram is divided into three regions, Simple Distribution{SD), Typical Bimodal Distribution(TBD) and Transitional Zone(TZ). According to the trajectories(black and white arrows),dispersion of droplets first decreases in contrast to the increase of mean radius and liquid water. Then, they change the tendency toward increasing ar0tmd the t:im: with liquid water exceeding 1 g kg-1 or so. The first decrease of dispersion is due to the cause that the growth of droplets is dominated by water vapour diffusion.

The beginning of a transitional distribution in TZ is different among the distributions depending upon the dispersion and mean radius. Droplets with relatively large mean radius easily enter into TZ even though the dispersion is relatively small,whi.le ·the distribution with smaller mean radius requires relatively large dispersion just before entering into TZ. However, the lllJSt significant feature, which is CO!lIDJil to all distributions at the instant of the onset of TZ, is that there already exists droplets whose radius is 60 f,Awith the concentration of 50 1:' or so, or those with radius 80 f', with the concentration of 1 .t-•. This is one of the hypotheses on the critical condition for the onset of the dominant coalescence process. The formation of droplets with radius of 40 f'- or so, which has been -taken as a kind of the criterion for the efficient evolution of droplets by incipient researchers, is not sufficient for the explosive growth of droplets. Restricting the present discussion to the distributions with liquid water exceeding 1.2 g kg^{1} or so, the onset of the· transitional distribut:lons in TZ is represented by a thick line, which is very closely related to the isopleth of 50 [$^{/}$ of 60 p. droplets or that of 1 [^{1} of 80 f droplets. The line is represented by the following eqll§:tion in terms of dispersion(Ds) and mean radius(R):

$$D_s = -0.018\,(R - 20) + 0.29\,,$$

for f'T< R < 513 f' • **(2)**

This is the second hypothesis on the critical condition for the -<='Jrmation of the typical "bimodal" drop size-distribution, with which droplets promptly grow to larger sizes by the dominant coalescence process, allllJst always leading to an outbreak of rainfall. Eq(2) means that droplets with mean radius of 20 f and dispersion of 0.29 can explosively grow to larger sizes by coalescence but droplets whose mean radius is smaller than this value require larger dispersion than 0.29 and vice versa:

7. A FEASIBILTIY STUDY OF WARM CLOUD MJDIFICATION

In principle it is supposed to be possible to enhance precipitation from warm clouds by seeding them with water drops by enhancing the efficiency of the collision-coalescence process. The possibility, however, is not substantiated at this t:im: of day. Here, a numerical experiment is presented to test the feasibility and the effectiveness of warm cloud lllJdification by seeding them with small water drops.

A cloud used for the seeding experiment is the S-cloud presented in the previous sections.The state of the cloud just before seeding is shown in Fig.5 in tenns of vertical velocity(W) , liquid water(Q) , mean radius(R) and dispersion(Ds); when the cloud is in the early period of the mature stage. Water drops whose normalized size-distribution is represented by the A type shown in Fig.1 and a mean radius Rti are seeded in a region where droplets are in a state just before changing into a bim:Jdal size-distribu- tion. The results of the seeding experiment are § umnarized in Fig. 6, which shows the dependency on Rī; of various physical quantities . Modification efficiency(Emo) is defined by the ratio of the total arrount of rainfall to that in the base state, seeding efficiency(Eseo\ ) by the ratio of the enhanced arrount of rainfall to the seeded am::iunt of water mass and precipitation efficiency(E p e) by the ratio of total am::iunt of rainfall to the total am::iunt of condensed together with seeded water. Rmox is the max:im.nn ramfall intensity through the life time. The results are enc0urag:fug of the.feasibility of warm cloud modification (enhancement of precipi- tation) by s·eeding them with water drops with radii around 100 I'· or so:

REFERENCES

1) Nelson,L.D. ,1971: A numerical study on the ini- tiation of warm rain. J.Atmos.Sci.; 28, 752- 762.
2) Ogura,Y., and T.1'akahashi,1973: The development of warm rain in a cumulus model. J.Atmos.Sci., 30, 262-277.
3) Takahashi, T. , 1973: Nt.nnerical sim.tlation of maritime warm cumulus. J.Geeiphys.Res., 78,. 6233-6247.
4) Takeda,T. ,1975: Evolution of a precipitating cloud and cloud droplets. Pageoph, 113, 891- 891-907.
5) Takahashi, T., 1974: Nt.nnerical sim.tlation of tropical showers. J.Atmos.Sci., 31, 219-232.
6) Takahashi,T. ,1975: Tropical showers in an axi- synmetric cloud model. J.Atmos.Sci., 32,.1318- 1330.
7) Takahashi,T. ,198lb: Warm rain study in a three- dimensional cloud model. J.Atmos.Sci., 38, 1991-2013.
8) Soong,S.T. ,1974: Nt.nnerical s:imJ.lation of warm rain development in an axisynmetric cloud model. J.Atmos.Sci., 31, 1261-1285.
9) Takahashi,T. ,198la: Warm rain study in Hawaii- rain initiaJ:ion. J.Atmos.Sci., 38, 347-369.
10) Shiino,J. ,1983: Coaparison of the parameterized •with non-parameterized microphysics. J.Met.Soc.Japan, 61, 629-655.
11) Soong,S.T., and Y.Ogura,1973: A ca:nparison bet- ween axisynmetric and slab-synmetric cun:ulus cloud model. J.Atmos.Sci., 30, 879-893.
12) Berry, E. X., 1967: Cloud droplet growth by collection. J.Atmos.Sci., 24, 688-701.
13) Srivastava, R. C., 1971: Size-distribution of raindrops generated by their breakup and coa- lescence. J.At:nos:Sci., 28, 410-415.
14) Hocking,L.M.,1959: The collision efficiency of small drops. Q.J.R.Met.Soc., 85, 44-50.
15) Shafrir,O., and M.Neiburger, 1963: Collision effici-encies of two spheres falling in 'a viscous medium.].Geophys.Res., 68, 4141-4148.
16) (}m,R., and G. D. Kinzer, 1949: The terminal velocity of fall for water droplPts in stagnant air. J.Meteor., 6, 243-248.
17) Shiino,J. ,1984: Evolution of raindrops in an axisynmetric cumulus model-Part II. The form- ation of a ''bim:Jdal" drop size-distribution. J.Met.Soc.Japan.(subrnitted).

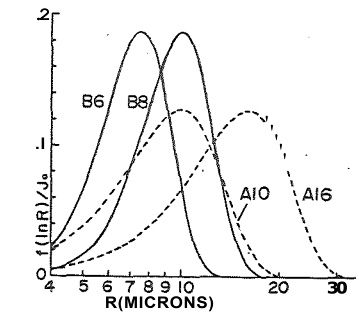

Fig. Normalized initial droplet size distribu- tions formed by condensation on •cloud conden- sation nuclei. A10 is used as a standard.

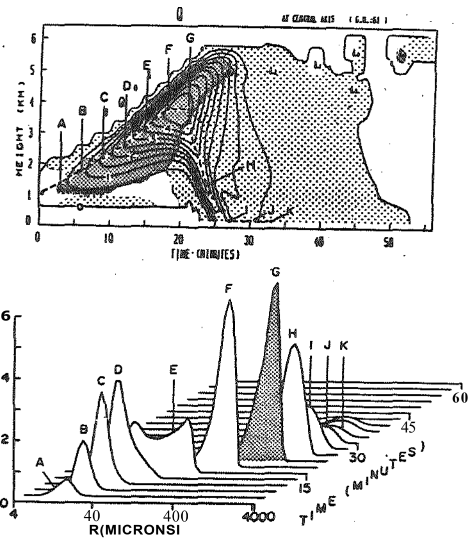

Fig.2a Time variation of the droplet size-distri- bution(lower) along the levels(A,B,C, ...) where liquid water (Q in g kg ,upper) takes a max:im.nn every three minutes at the ·central region of the D-cloud(DA10). In the darkly shaded area all of the condensation nuclei are activated. Thinly shaded area is the region where evaporation is taking place.

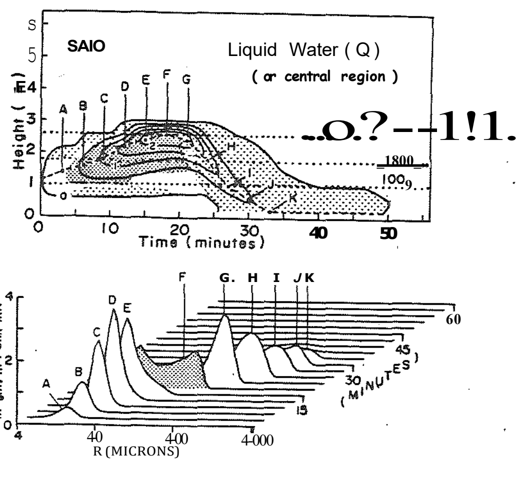

Fig.2b As in Fig.2a except for the S-cloud(SA10).

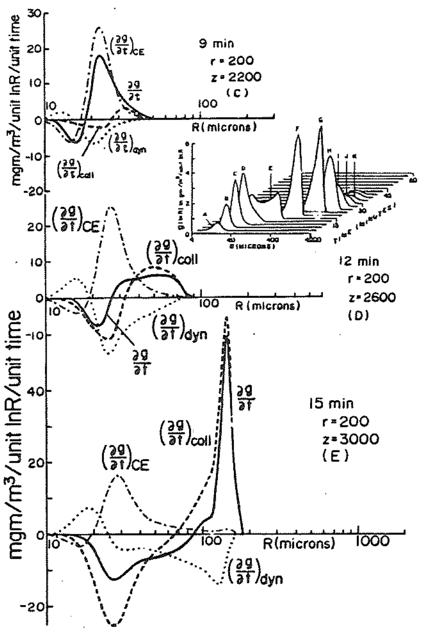

Fig.3 Balance of water mass density $g(\ln R)$ of droplets with radius greater than 10 μ in the unit of mg m^{-3} (unit lnR)$^{-1}$ sec^{-1} along the points with maximum liquid water (C,D,E in Fig.3a) in the D-cloud. Solid line is the net rate of change of water mass, dotted line is due to dynamical effect, broken line coalescence, and chain line condensation or evaporation.

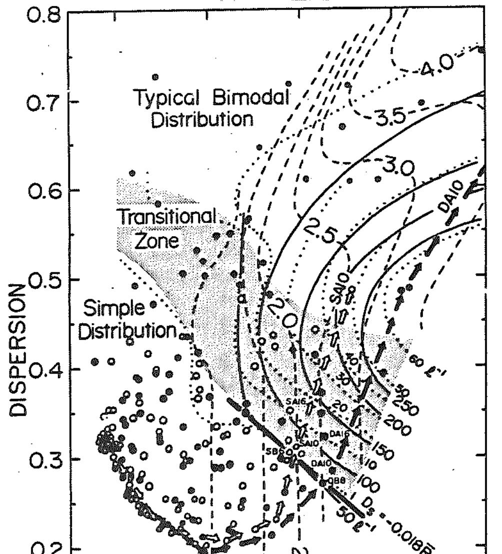

Fig.4 Scatter diagram of the droplet size-distributions for DA10(dots) and for SA10(circles) clouds in terms of mean radius($\bar{R}$) and dispersion (D_s). Solid lines are the concentration(in ℓ^{-1}) of droplets with radius 60 ± 5 μ, dotted lines those with radius 80 ± 5 μ and broken lines liquid water (in g kg^{-1}). Black arrows indicate the trajectory along the points with maximum liquid water at the central region of the D-cloud(DA10) up to 15 min and the white ones that for the S-cloud(SA10) up to 18 min. The shaded area is the Transitional Zone from the region of the Simple Distribution to the Typical Bimodal Distribution. See further detail in the text.

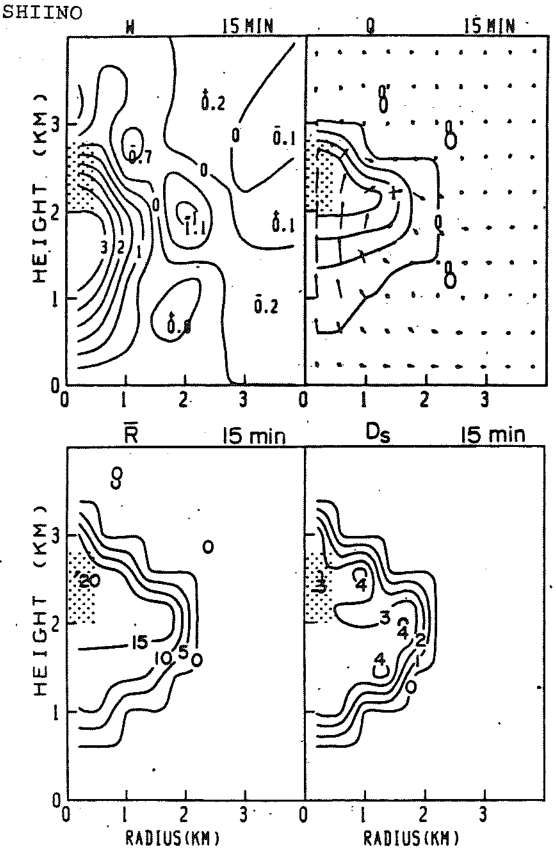

Fig.5 The state of the cloud just before seeding in terms of vertical velocity(W in m sec^{-1}), liquid water(Q in g kg^{-1}), mean radius(in μ) and dispersion(D_s, x0.1), when the cloud is in the early period of the mature stage. 0.1 g m^{-3} of small droplets is seeded in the shaded region.

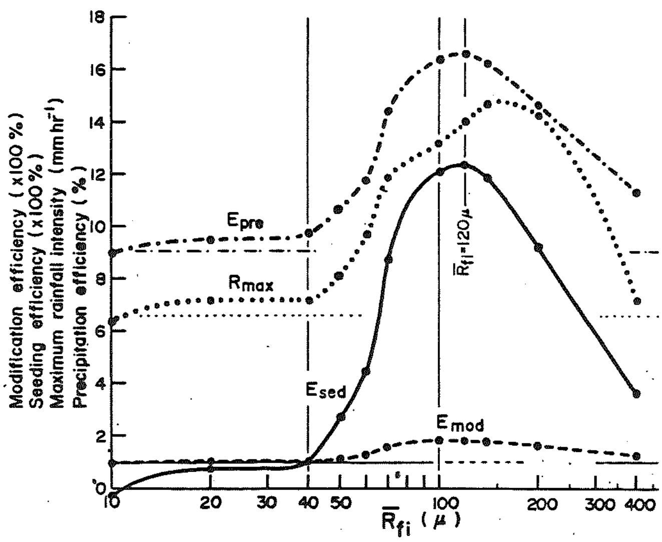

Fig.6 Dependency on $\bar{R}_{fi}$ of modification efficiency (E_{mod}), seeding efficiency(E_{sed}), precipitation efficiency(E_{pre}) and the maximum rainfall rate.

A NUMERICAL MODEL FOR A HAILSTORM

L.G. Kachurin, V.I. Bekrayev, M.V. Gurovitch
Leningrad Hydrometeorological Institute

A.I. Kartsivadze
Geophysical Institute of the Academy of Science
of the GSSR, Tbilisi

It has been previously reported about results of a numerical simulation of a hail process within a convection jet model (Refs.1-4). The model is based on the assumption of a convective storm, its active part to be exact, being a nonisothermal turbulent jet. The model has then undergone the development from a two- to three-dimensional distribution of parameters, from a stationary to quasi-stationary thermodynamics, from a simplified microphysical task to a direct solution of the kinetic equation for a three-phase storm.

The numerical model here discussed is designed to analyze heavy supercellstorms, in reference to which the assumptions about the existence of astationary phase are fairly justified. This phase is characterized by a practically stable radio echo form, preserved for several hours, an extended, almost unbroken hail path, distinct space distribution of upstream current areas (in a front region of a cloud) and intensive precipitation (in a rear part). The region of intensive precipitation is usually identified with a zone of an increased radar reflectivity. The above features of supercell prosses are successfully described by introducing a regeneration velocity of a moving hail centre, determined by its permanent renewal in a front part and dissipation in a rear one. The regeneration velocity is found as a vector difference of actual wind velocities at a condensation level and a hailstorm movement relative to the earth.

Summarizing observational results one more feature of heavy convective clouds can be rather distinguished as a rule than an exception - that is a Y-rotation of an upstream. The appearing eddy causes a differential pressure between the upstream and ambient air. To consider rotation effects in the model the main equation system is complemented by a third movement equation due to which parameter calculations of the storm jet are performed taking into account an outer wind change with height. The averaged parameters of the storm jet are transferred to their cross-section distribution, as was done before, using half-empirical relations satisfying balance requirements.

Thus, in the model there calculated three-dimensional fields of the main thermodynamical parameters and geometrical contours of the storm jet. Then, based on the quasi-stationary thermodynamics, precipitation particle trajectories as well as the size and concentration distribution in time and space are found. The model output characteristics used for a comparison with observation results, are based on calculations of radar reflectivity fields and the kinetic energy of rain and hail falling on the ground surface. Calculations are fulfilled within the model for a natural development of a hail formation process as well as for its transformation as a result of crystallized reagents being introduced.

Surely, having a number of simplified admissions and a conditional choice of empirical parameters used in the model its calculations cannot claim the immediate quantative comparison with experimental data. However, the comparative analysis of different parameters of a hailstorm, their dynamics and space distribution seem to allow the evaluation of the model fitness to physical phenomena.

For the last years complex investigations have been made experimentally on a number of heavy hail processes. The hail process (Ref.5) referred to as the "Fleming storm"in literature, seems to be one of the most studied. The storm was chosen for comparative evaluations and demonstrations of the numerical model possibilities.

Calculation results, obtained for characteristic parameters and conditions of the Fleming storm development are shown in Fig. 1,2. Horizontal planewise projection of the storm jet centre at a condensation level (Z = 2.8 km) is superposed with the origin of coordinates (X and Y cross point). This plane - the "ring platform" is situated at the sea level. The Earth surface is at the Z = 1.4km. In Fig.1 this height is marked with horizontal lines at the lateral sides of the ring and the axis positive direction is similar to the generally accepted one. The direction of the moving storm coincides with the X direction. Therefore the storm is depicted as it is seen by the observer who is in front of it or on its right. In Fig.2 the same storm is shown from behind and on the left (the positive XY direction, if compared to Fig.1, is turned to 180°).

In the left-hand part of Fig.1 and at the ring platform there depicted the hodograph curve of a wind motion constructed relative to the moving storm direction. The $\mathcal{U}_m$ vector reflects the actual velocity of the moving storm, and $\mathcal{U}_R$ is the regeneration speed vector. Axial jet section paral lel to X and Y give the idea about the geometry of the storm jet. In both Figures the storm contours in these sections are shown with dotted curves.

At the front side of the ring one can see the distribution of the water content S'_w(the O curve) with height and vertical velocity $\overline{W}$, averaged over the jet cross-section. The work (Ref.5) does not contain any solid data about the vertical distribution of these parameters. However, if one is oriented to the given in (Ref.6) field of velocities it would be possible to adopt $W(Z)_{max} \simeq 40$m/s as an evaluation of the vertical component maximum in the storm. The maximum average velocity $\overline{W}_{max}$ = 28m/s, calculated from the model when proceeding to the velocity distribution over the jet section, will give an agreable value of about 40m/s. The view of the given vertical velocity distribution over the cross section is shown for Z = 8km. Here one can see the distribution of the tangential component of the rotation velocity. The vertical profile of the $V_{t\,max}$ is shown using the coordinate system similar to $\overline{W}$. The triangles in this Figure indicate velocities of moving local reflectivity maxima determined as "hot points" by the authors in (Ref.5). They believe hot points to be tracers of the velocity field in the storm, at least its horizontal component. Only vertical and horizontal planewise projections of moving hot point trajectories are given in (Ref.5). The graph illustrates maximal velocities of hot points evaluated from comparison of the initial data (Ref.5).

Two other vertical walls of the ring in Fig.1 show the distribution of the radar reflectivity for cross sections parallel to X and Y, with X = -1km, and Y = -5km, respectively. Reflectivity calculations are made in the knots of a 2-km grid. Comparing these and other sections with observational results in (Ref.5), one may conclude that the reflectivity field structure is in a fair agreement with observations. The radioecho shed and overhang are remarkably noticeable, typical for heavy hail storms in the direction of their movement. The zone of the weak echo is clearly revealed in the central part of the upstream. The above features of the radioecho are typical of supercell hail storms. All these give way to a hope that the model is a good reflection of the distribution of main thermodynamical parameters, mechanisms for the development of storm and precipitation particles, and the character of the airmass circulation.

The movement of hailstones within the storm can be described by summarizing different factors, such as the distribution of the upstreams holding the hailstones, total horizontal air transfer in the storm jet, rotation and transfer velocity components, regeneration transfer of the storm as a whole. Fig.2 shows tragectories for three hailstones from the place where the appropriate hailstone was born (from freezing of a supercooled drop) to the falldown. Figures at the curves where the trajectories terminate indicate the size (diameter) of hailstones in centimeter. The Figure presents trajectories in a three-dimensional space and horizontal planewise projections of trajectories. The largest of the presented hailstones was born in the rear part of the storm. The hailstone is carried away by a horizontal flow to the centre of the upstream with a speed similar to that with which the upstream "leaves" the hailstone due to the regeneration mechanisms. The hailstone practically hangs in the storm under conditions of a great water content. It grows rapidly, then surpassing the upstream and falling down it appears outside the storm jet. A certain inconsistence between the model and nature lies in that the model does not reflect the region of downstream currents. It can be partly justified by the circumstance that the velocity of downstream currents in the precipitation region is usually substantially lower than that in the upstream flow. The hailstone formed on the right side of the storm jet is insolved in the area of great vertical velocities before it manages to reach a considerable size. Strong upstream currents throw it into the upper part of the storm, where the water content is small and the hailstone does not grow. Its growth is renewed only on the left side when going down the outlying area of the storm it repasses the supercooled part of the storm.

The examples presented in the Figure do not embrace all the variety of hail formation cases taking part in different regions of the storm. The summarizing feature of the hail concentration and sizes is seen in the field of a second kinetic energy of hail falling down on a unit surface square. This field is shown on the ring platform. It's easy to see that the precipitation field agrees with that of the radar reflectivity. As a typical feature of the Fleming storm, which was not noticeable during the similar calculations for other hail situations, the existence of two maxima for a hail intensity can be pointed out.

On the back side of the ring the total kinetic energy of hail falling on a unit square throughout the whole period of a hailstorm, is presented against the distance along the Y. This distribution for the Fleming storm proves to be bimodal. The obtained K maxima correspond to a very strong hailstorm.

It was slown earlier (Refs.1,2) that the effectiveness of influence on hail processes by crystallizing reagents considerably depended upon a powerful process and concentration of the introduced reagent. Below in the left-hand part of the Figure the dependence is shown of the maximal K(Y) on the concentration of artificial ice crystals n^* introduced in the storm. The calculations assume that the reagent would be introduced continuously and uniformly along the whole storm cross-section and it be activized at -7°C. The graph presents two curves for different initial drop spectra. The curve 1 is calculated similarly to all the rest parameters in Fig.1,2 for a comparatively wide drop spectrum in the lower part of the storm, with the power index in a two-parametrical Γ-distribution ν=0.6. The curve R is for ν=1.2. Thus the graph simultaneously characterizes the model sensitivity to the choice of the initial

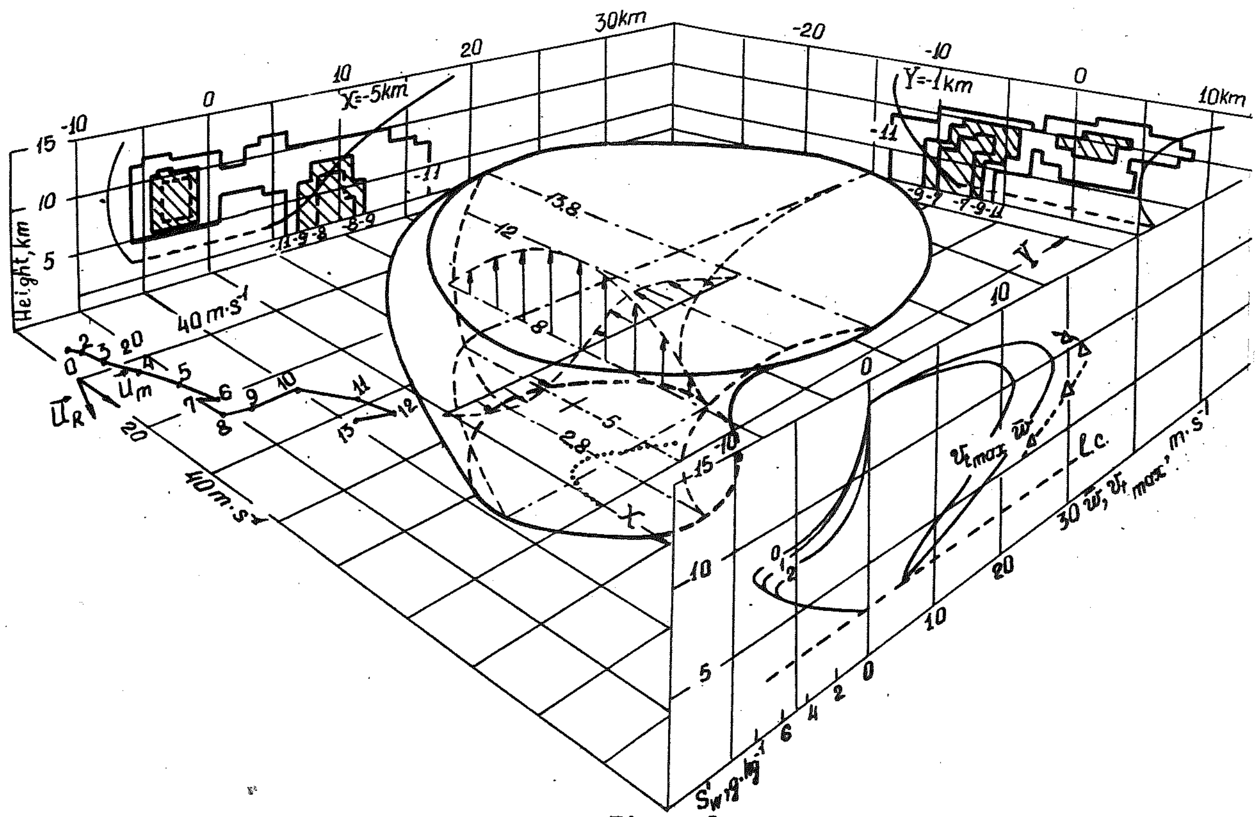

Figure 1

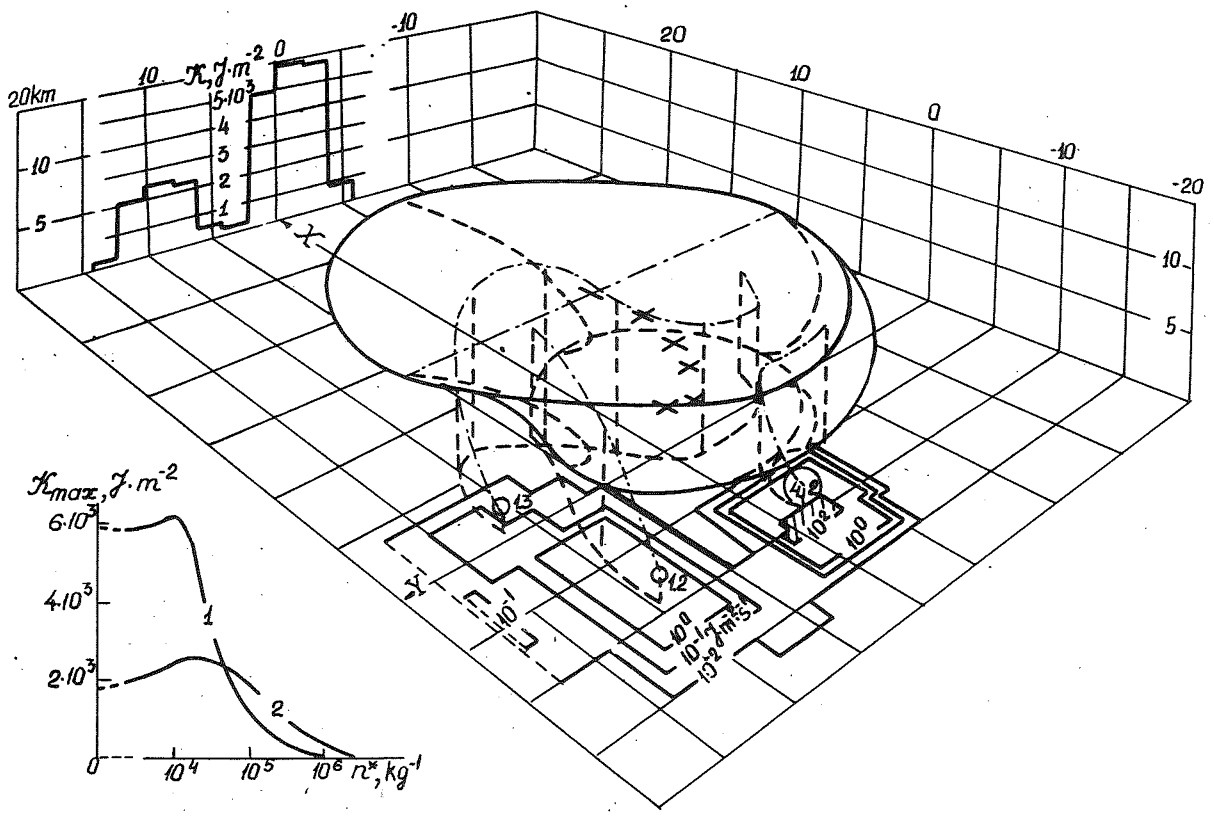

Figure 2

drop spectrum or the conditions for the hail process development which include continental or oversea air masses).

Despite some differences in the absolute K values curvature characteristics 1.2 imply a complex dependence of the hail danger upon the reagent concentration. With small concentrations of ice particles the intensity of the hailstorm increases then with the increasing n^* it reduces to 0. Similar dependences are also obtained for other hail processes. Speaking about a considerable or complete suppression of hail, calculations show that supercell storms of the Fleming type require a fairly great expence of the reagent. The absolute values obtained in the model being rather conventional, we may state, however, that powerful modern technical means of impact are not intended for the seeding of such intensity.

REFERENCE

1. Kachurin, L.G., Kartsivadze, A.I., Artemyeva N.D., Stojanov S.G. and Tekle M. 1974, Simulation of the natural process of hail formation and it's transformation under the influence of artificial crystallization, Proc. WMO/IAMAP Sci.Conf. on Weather Modific., Geneva.

2. Kachurin, L.G., Kartsivadze, A.I. 1976, On hail suppression possibility at the modern stage of the atmospheric processes modification means and techniques development, Proc. Second WMO Sci.Conf. on Weather Modific., Geneva.

3. Kachurin, L.G., Bekrayev, V.I. and Gurovich, M.V. 1980, Numerical simulation by means of crystallizing reagents, Paper presented at the Third WMO Sci.Conf. on Weather Modific, Geneva, 11, 695-699.

4. Kachurin, L.G., Bekrayev, V.I., 1982, Numerical simulation of supercell hailstorm. Int. Sci. Conf. on hail defeance., Sophia.

5. Browning, K.A. and Foote, G.B., 1976, Airflow and hail growth in supercellstorms and some implications for hail suppression, Quart J. Royal Met. Soc., 102, 435, 499-533.

6. Farley, R.D., Musil, D.I, Kopp, F.J., Orville, N.D. and Dennis, A.S., 1976, Final Report on the numerical simulation of hailstorm modification by competing embryos, Report 76-5 Inst. Atmosph. Sci, S. Dakota School of Mines and Technology, 56.

Figure 1. Results of Parameter Calculations for the Fleming storm (Ref.4).

In the centre of the ring there is a space disposition of the storm jet front and right-hand view. Arrows at 8km show the distribution over the radius of the storm jet of vertical and tangential velocity components. On the left side of the ring there is a hodograph curve for the wind velocity. Figures at break points indicate heights above the sea level in km. The front side show the distribution with height of the vertical velocity $\overline{W}$ and water content S_W. On the graph for the water content the 0 curve reflects a natural course of the process, and 1 and 2 curves the introduction of crystallizing reagents with $n^* = 10^4$ and $10^6 kg^{-1}$, respectively. The curve $V_{t,m}$ is for the distribution with height of tangential velocity maxima. Back sides show vertical sections of the radar reflectivity. Figures at the isolines are for reflectivity logarithms (sm^{-1}).

Figure 2. Calculation Results for the Trajectories and Kinetic Energy of Hail.

In the middle there is the space disposition of the storm jet, the view from the left and from behind. Pot-and-dash fat curves are hail trajectories, the dashed line is the projection of trajectories to the ring platform. On the ring there is the distribution of the second kinetic hail energy. On the back side there is the distribution over the Y of the total kinetic energy of hail falling down to a unit square throughout the hail period.

In the right-hand part below a change is shown of the maximal kinetic hail energy resulting from impact with different concentrations of artificial ice crystalls.

NUMERICAL SIMULATION OF TROPICAL SQUALL LINE

J.P. LAFORE and J.L. REDELSPERGER *

Etablissement d'Etudes et de Recherches Météorologiques
CNRM/Toulouse - FRANCE

1. INTRODUCTION

Convection is often organized in line like, for example, cloud streets, sea breeze clouds, frontal rainbands, tropical or mid-latitudes squall lines. During the french tropical deep convection experiment COPT 81 (Copt Organizing Committee, 1984) several squall lines were observed. The observational network was based principally on two Doppler radars, an acoustic sounder, a central meteorological station including satellite reception, rawindsounding and a network of ground meteorological stations. As part of this french tropical convection programme, a modeling effort was pursued. Lafore and Pircher (1983) proposed the use of mixed lateral boundary conditions (L.B.C.) to simulate, with a three dimensional cloud model (call after EERM'S model), such convection organized in line. This new type of L.B.C. uses cyclic L.B.C. in the line direction and open L.B.C. of Orlanski's type (976) in the other direction. At present time, we carry on these simulations with an other cloud model (Redelsperger and Sommeria 1984, see section 4) with important improvements, and some results will be presented during the oral presentation. Here we are going to present only some results of a squall line simulation accomplished with the EERM'S cloud model on a small domain.

2. THE SIMULATION IMPLEMENTATION

Owing to the use of fast Fourier transforms, the mixed L.B.C. has been easily introduced in the EERM'S model. It is a non hydrostatic compressible model with a classical parameterization of warm rain. A prognostic equation for the subgrid kinetic energy and a subgrid condensation scheme are used. The domain of integration has an extension of 30 km in both horizontal directions and 20 km in the vertical with a rather large grid of (1.5,1.5,0.8) km^3. Because the present upper boundary condition (null vertical velocity at the top) is reflective, we had to use horizontal damping above the tropopause (AT 16 km) to run the model during long integration time.

Among the different cases of squall lines observed during the COPT 81 experiment we chose to simulate the one observed the 23-24 June 1981, because it looks like a rather straight line of convective cells for its convective head part, propagating at about 50 km/h Southwest ward. The integration domain is orientated parallel to the observed squall line (at 40° from the North) and is translated at the mean propagation velocity, in order to keep the simulated squall line in the model boundaries. The stable environment in front of the squall line is illustrated by the sounding of 20 h 32 GMT (Fig. 1 and 2) taken 3 hours before the line passage (about 150 km before).

It is not possible, at present time, to initiate the simulation directly from the observed data, so special initialization has been used. The horizontally homogeneous profiles observed at 20 h 32 has been prescribed in the model and then a bidimensional bubble shaped temperature perturbation is introduced. During 45 mn (Phase I Fig.3) the model stays bidimensional and we obtain several cells which develop in front of the line. At 45 mn we introduce several random precipitation zones to destroy the bidimensional flow structure. After 95 mn the flow structure is fully three dimensional and in a first approximation the system seems to be in a permanent state (Fig. 3a). Analysis of this study phase is the object of the next section.

* On leave from Laboratoire de Météorologie Dynamique, Paris, FRANCE

3. RESULTS

From a morphological point of view, the simulated head part of the squall line appears as the superposition of several convective cells at different phases of their life cycle (Fig. 4). New elements (C_4) appear ahead the system. C_2 and C_3 are mature elements dissipating at the rear. In middle and high levels the convection appears tridimensional with several specified cells. On the contrary in the lowest levels up to 3 km after 2 h 45 of simulation, we have a typed structure (Fig. 5). The rain forms a continue band of precipitation associated with downward motion and cooling. This area is bounded ahead by a line of sharp temperature gradient. In front and along this frontal line we find a narrow band of strong convergence which feeds the mature convective elements (C_2, C_3). This structure appears after 2 h 45 and stays up to the simulation end. During this period we observe also a temperature gradient intensification and a widening of the precipitation band which reachs the domain back boundary after 3 h 20 of simulation.

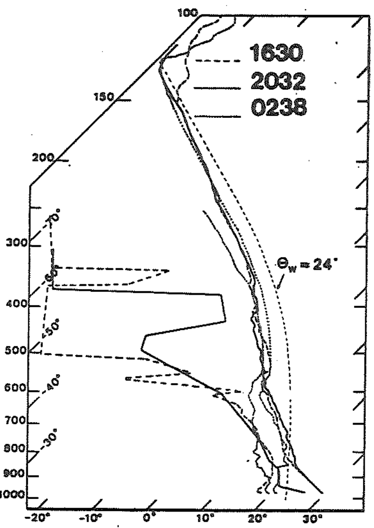

Figure 1. Thermodynamic soundings taken at COPT Central Site 1630 and 2032 UT on 23 June 1981 and 0238 on 24 June 1981 plotted on a skew-T log-P diagram. The dashed line represents the 24°C moist adiabat. The gust front passage of the squall line occured at 2340 UT on 23 June 81

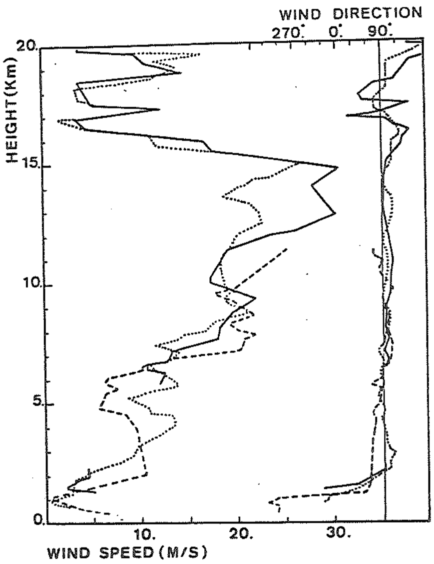

Figure 2. Vertical wind profiles (speed and direction) obtained by three soundings on 23 June 1981 at Korhogo before the squall line passage at 1630 (dotted lines) 2032 (solid lines) and 2333 UT (dashed lines)

The basic features of the simulation may be more clearly represented in term of bidimensional analysis. For that we computed the mean field for the different variables in a vertical cross section perpendicular to the line. So t'e stream function has been drawn for the mean flow (Fig. 6). We can distinguish several distinct parts :

- First an overturning updraft which depends on the propagation velocity and which reduced the stability ahead the system.
- Secondly a main jump updraft which contributes to change the thermodynamic and dynamic caracteristics of middle levels behind the squall line.
- Thirdly a part of the updraft which returns towards the ground in the rear part of the system to form a cold downdraft associated with the precipitations. The downdraft's origin cannot be explained only with the mean flow structure. The study of lateral fluctuations shows that local downdrafts issued from the cold and dry middle level in front of the system contribute to form this mean downdraft. - At last this later cold air spreading at ground flows out at the rear for one part, whereas the other one contributes to form a rotor helping to trigger the upward motion.

This general circulation is similar to those described previously by Zipser (1977) or Houze (1977) and partly to those simulated with a two dimensional model by Thorpe and al (1982). The sudden modification of the boundary layer corresponding to the passage of the gust front, observed by the ground stations is illustrated by Fig.7. The corresponding simulated results (Fig. 5 and 6) are very similar. We find also the temperature drop, the pressure jump and the wind gust, followed by the precipitations. Nevertheless the simulated windgust is twice larger that observed, because the first level of the model is higher above the ground (400 m). We notes also that in mean the rain is located just behind the gust front whereas the observed rain was rather about 20 km behind the gust.

The results show also that the simulated squall line does not reach really a permanent state. First the total precipitation rate is always growing, that corresponds to the widening of the precipitation band. Before 2 h 30 the system looks like a simple narrow line of convection with a low propagation speed of 11 m/s. Between 2 h 30 and 3 h the line structure changes quickly with the formation of the rotor and a simultaneous increasing of the temperature drop and the propagation velocity. After 3 h, the structure stays quite similar with only a broadening of the rotor. The propagation velocity (V_T) is around 14.5 m/s (V_T = 16 $\pm$ 2 m/s observed).

After four hours it was difficult to continue the simulation because boundary effects, the line width beeing too large in respect to the domain size.

4. CONCLUSION AND OUTLOOK

These later results show that using mixed L.B.C., a cloud model can simulate, at cloud scale, the convective part of a squall line. Although the simulation domain is too small to include the whole system, this simulation allowed to obtain a general circulation which is similar to those observed during the experiment (Chalon and al 84, Roux and al 84) and to those described by Zipser (77) or Houze (77).

However, its seems important to do some improvements in order to avoid the principal limitations of simulation results outlined above. Currents efforts consist to use a more elaborated model (Redelsperger and Sommeria 1984) with a larger domain (about 100 km in the horizontal direction). Two important shortcomings, noted in the previous section, will be so avoided. First, the model will have a top boundary

Figure 3. Extreme values of the vertical velocities W and temperature (ΔT) from the initial temperature profil, versus time.

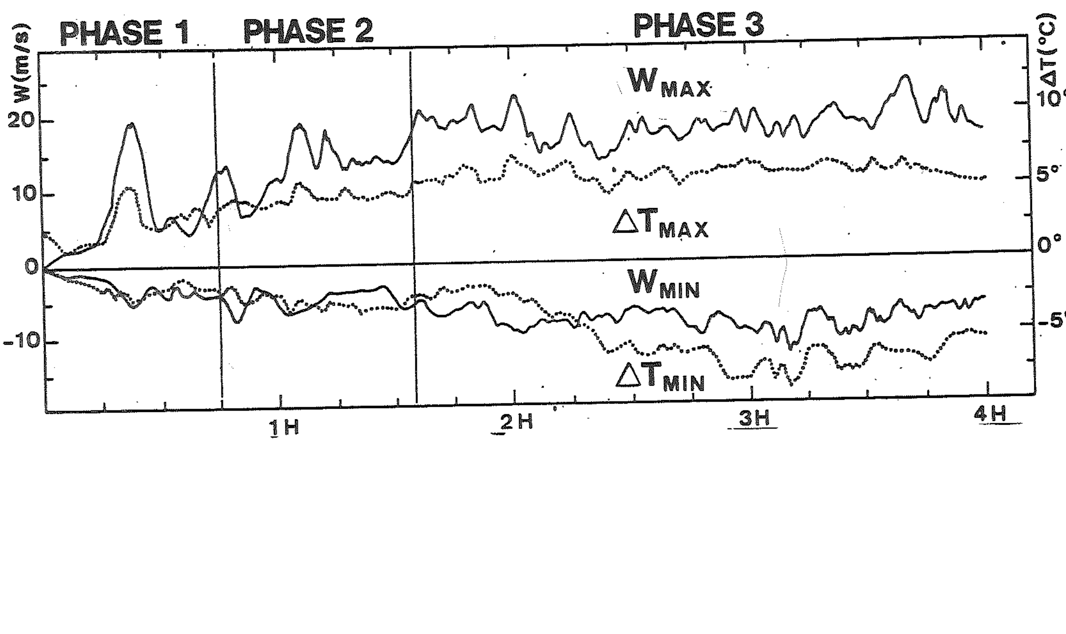

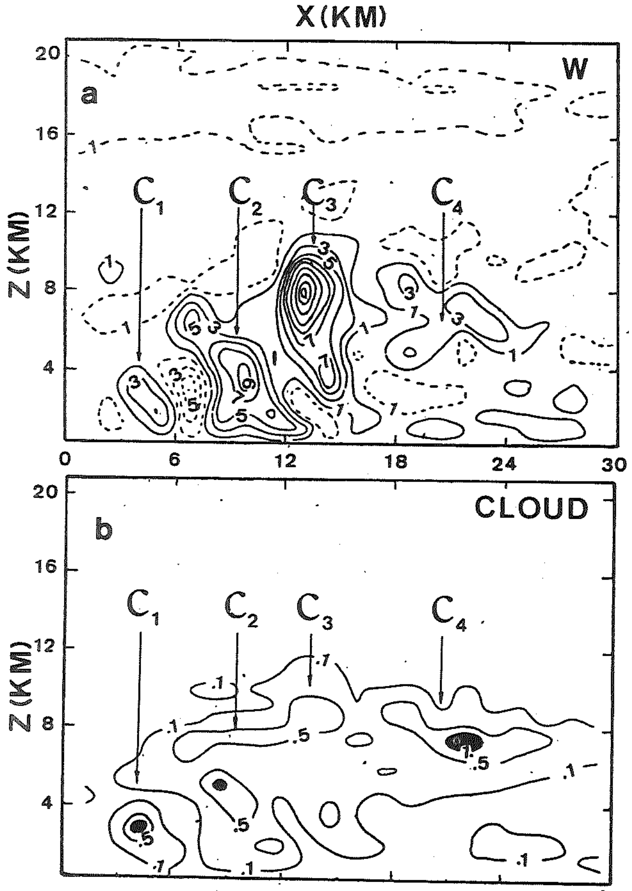

Figure 4. Vertical cross-section parallel to the propagation direction at 2h50 (simulation time)
a) For the vertical velocity W (m/s)
b) And for the cloud mixing ratio q_c (g/kg) at x = 7.5 km.

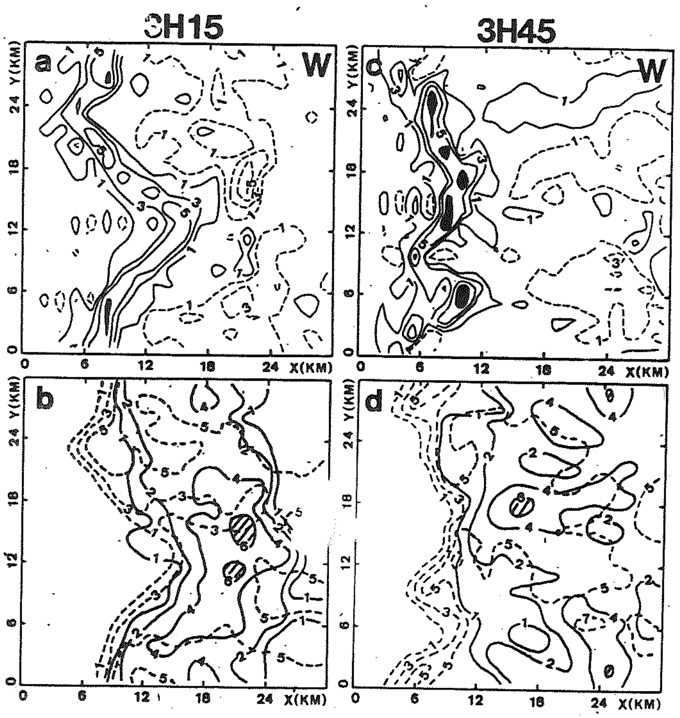

Figure 5. Horizontal cross sections at the lowest level of the model.
a) Vertical velocity W(m/s) at the altitude 0.8 km and at time 3 h 15
b) Temperature deviations T(°C) (dashed lines) and the precipitation mixing ratio q_c(q/kg) (solid lines) at level 0.4 km and at time 3 h 15
c) As figure a at time 3 h 45
d) As figure b at time 3 h 45

condition which will be non reflective ; secondly the boundary layer will be better represented in using a vertical mesh dimension varying with the altitude (increasing from 0,2 km at the lowest level to about 1 km at the top of the domain), conjointly with a sophisticated turbulence scheme and a realistic surface layer.

This current work will be presented at time of the conference in complement of the results presented in section 3.

5. REFERENCES

1. C.O.P.T. Organizing Committee (1982). "COPT 81 experiment designed for the study of dynamics and electrical activity of deep convection in continental Tropical regions". Conference on Cloud Physics. A.M.S Chicago p. 580.

2. Chalon J.P., Jaubert G. and Rossiaud D. (1984) Thermodynamic structure of an African Squall-line and its influence on the environment. Preprints Volume. IX International Conf. on Clouds Physics Tallinn : URSS

3. Houze R.A., (1977) : Structure and dynamics of a tropical squall line system. Mon. Wea. Rev. 105, 1540-1567.

4. Lafore J.P. and Pircher V. 1983 : Modélisation numérique tridimensionnelle à échelle fine d'une ligne de grains (submitted to Journal de Recherches Atmosphériques).

5. Lafore J.P. and Pircher V. 1984 : Three-dimensional simulation of the convective part of a tropical squall-line (to submit to J. Atmos. Sci).

6. Redelsperger J.L. and G. Sommeria, 1984 : Three-dimensional model of convective storm : sensitivity studies on subgrid parameterization and spatial resolution (to submit to J. Atmos Sci.).

7. Roux F. 1984 : Three-dimensional structure of a West African continental squall line observed during the experiment COPT 81. Preprints Volume. IX International Conf. on Clouds Physics, Tallinn URSS.

8. Thorpe A.J., Miller M.J., Moncrieff M.W., 1982 : Two-dimensional convection in non constant shear: a model of midlatitude squall-line. Quart. J.R. Soc. 108 p. 739.

9. Zipser E.I., 1977 : Mesoscale and Convective scale downdrafts as distinct components of squall-line structure. Monthly W.R, Vol. 105, pp 1568.

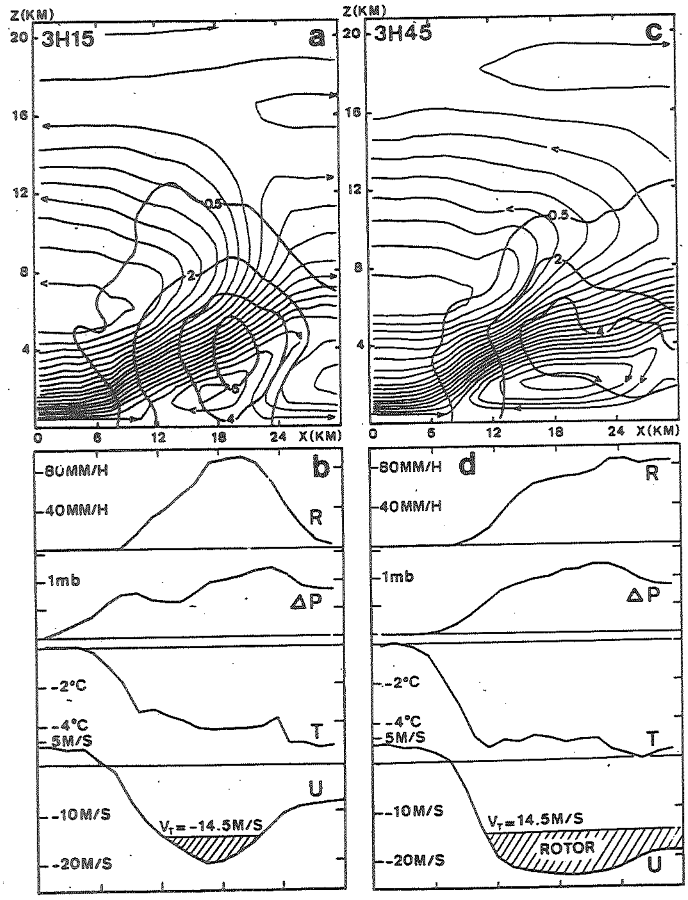

Figure 6. a) Stream function plotting (solid lines with arrows) mean circulation in the vertical plan parallel to the propagation direction, and the mean precipitation mixing ratio field q_r (g/kg) (heavy lines), at time 3 h 15. The system moves towards left of the figure at the propagation velocity of about 14.5 m/s (U_T).
b) The typical signature of the simulated squall line passage for four mean parameters at level 400 m : rain intensity (R), pressure (ΔP) temperature (T) and the wind gust (U) perpendicular to the line.
c) As figure a at time 3 h 45.
d) As figure b at time 3 h 45.

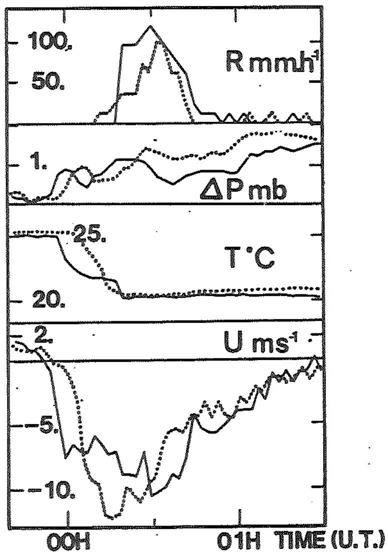

Figure 7. The typical signature of the squall line passage for four parameters (R, ΔP, T and U) as observed by two ground stations the 23-24 June 1981. To compare with simulation results (Figure 6), the system propagation velocity was around 50 km per hour.

NUMERICAL ONE-DIMENSIONAL MODEL OF A CONVECTIVE CLOUD AND PRECIPITATION FORECASTING

N.E. Lomidze, G.A. Nadibaidze
V.K. Seraphimov, $\boxed{\text{G.K. Sulakvelidze}}$

Transcaucasian Scientific Research Institute,
Hydrometeorological Centre of Georgian SSR,
Tbilisi State University, Tbilisi, USSR.

Works on hail prevention and precipitation increase are of great practical interest (Ref. 1). There are several methods of hail prevention and different approaches to the solution of the problems of artificial stimulation of precipitations, though experiments being carried out are not always equivalent. In this connection there appears the necessity for correct theoretical elaborations of modelling the processes of cloud and precipitation formation applied to vital practical problems.

The most successful models may more or less adequately describe some specific cases, but there are no comprehensive models, as even the increase of the space-dimensionality does not mean the necessary approach to more proper description of a cloud.

Numerical theory of convective precipitations and weather modifications with the aim of their prevention or stimulation requires the joint solving of equations describing the kinetics and thermohydrodynamics of cloud processes. However, in some cases even simpler models give the possibility to obtain results close to the real ones.

One-dimensional numerical operational model of a convective cloud describing the process of solid and liquid precipitation formation is suggested.

In mathematical aspect the process of precipitation formation in such a model is initiated by giving the source of drop water at the level of condensation. According to the data (Ref. 2, 3), drop water source intensity values at the level of powerful convective cloud base make on the average about some $g.m^{-2}s.^{-1}$. Profiles of temperature, updraught velocity and the value of source intensity are selected according to tropospheric radiosonde data.

Similarly to the estimation of rain development process described in (Ref. 4) out of drop distribution taken according to (Ref. 5) in unit volume at the base, a large drop of unit concentration is singled out growing subsequently at the expense of coagulation with small droplets. More water condensed during temperature decrease will be added to drop water, originated in the given volume at the condensation level as soon as the temperature rises. It is suggested that air masses follow continuously one after another forming updraughts. As soon as large drops are formed and moist air masses reach high levels in a cloud, where the velocity of updraughts and the velocity of drop sedimentation are equalled, the latters are precipitated out of the given volume, forming certain levels of accumulation of particles of proper sizes (initial step over the radius at the moment of level formation Δr = 1 mkm).

Distribution of large drops (and solid particles, arising in freezing large drops) according to their sizes at different heights subsequently will be determined by convective transfer and processes of their coagulation with small droplet fraction and fragments of breaking at lower levels by breaking and freezing large drops, melting solid particles below the level of zero isotherm.

Once the distribution of hydrometeors over heights has been determined (i.e. we may speak about these particles at the level of distribution function), further evolution of their spectra may be described by means of the following system of kinetic equations:

$$\frac{\partial f_1(v)}{\partial t} + \frac{\partial}{\partial z}\omega(v,z)f_1(v) = -f_1(v)\int_0^\infty \sigma(v,u)f'(u)\,du - f_1(v)\int_0^\infty \sigma(v,u)f_1(u)\,du - f_1(v)\int_0^\infty \sigma(v,u)f_2(u)\,du - f_1(v)P(v,T) + \int_0^v \sigma(v-u,u)f_1(v-u)f_1(u)\,du + \int_0^v \sigma(v-u,u)f_1(v-u)f'(u)\,du + F(v), \quad (1)$$

$$\frac{\partial f_2(v)}{\partial t} + \frac{\partial}{\partial z}\omega(v,z)f_2(v) = -f_2(v)\int_0^\infty \sigma(v,u)f_1(u)\,du - f_2(v)\int_0^\infty \sigma(v,u)f'(u)\,du + \int_0^v \sigma(v-u,u)f_2(v-u)f'(u)\,du + \int_0^v \sigma(v-u,u)f_2(v-u)f_1(u)\,du + f_1(v)P(v,T). \quad (2)$$

Here $f_1(v)=f_1(v,z,t)$, $f'(u)=f'(u,z,t)$, $f_2(v)=f_2(v,z,t)$ respectively, function of large and small droplet distribution according to their sizes (volumes); $\omega(v,z)$ -velocity of large drop movement; $\sigma(v,u)$ -function of particle collision probability with v and u volume (collection kernel); $F(v)$ characterizes number of particles with v volumes, arising and disappearing while breaking up (Ref. 6) in unit volume per unit time length; $P(v,T)$-probability of volume drop freezing at temperature T (considered according to (Ref. 7) and (Ref. 8).

The equation, describing the evolution of small droplets originated at the condensation level has the form of:

$$\frac{\partial f'(v)}{\partial t} + \frac{\partial}{\partial z} W(z) f'(v) = I(v, z_0) - f'(v)\int_0^\infty \sigma(v,u) f_1(u)\,du - f'(v)\int_0^\infty \sigma(v,u) f_2(u)\,du, \qquad (3)$$

where $W(z)$-vertical profile of updraught velocity, determined according to troposphere radiozonding data; I -intensity of the source (number of drops, originated in unit volume per unit time length at z_0 condensation level).

It should be noted that large drops which do not coagulate with each other and fragments of their break-up (which they may collide with) are described by the same function $f_1(v)$, as the sizes of fragments fall within the limits of acceptable sizes of large drops. Fragments of break-up grow at the expense of ascending small droplets.

Numerical solution of equations 1-3 is carried out by modelling the collision of large drops (solid particles) with a fragment under assumption of stochastic coagulation mechanism (it is suggested that large drops are broken up into 2-3 drops, as well) and with small droplets (continuous pattern of growth is used (Ref. 10).

Divergence of air flow above the level of maximum velocity is considered as well according to (Ref. 9).

To illustrate this, let us consider two clouds, characterized by the following parameters of updraught velocity:

$W_m = 16$ m.s.$^{-1}$, $H_K = 8.8$ km, $H_{W_m} = 4.0$ km,
$W_m = 26$ m.s.$^{-1}$, $H_K = 10.5$ km, $H_{W_m} = 5.5$ km,
$W_0 = 2$ m.s.$^{-1}$, $W_0 = 2$ m.s.$^{-1}$;

Here H_K, H_{W_m} heights of convection and maximum velocity levels, W_0 -value of velocity at the condensation level.

Under the first profile, the zone of large droplet fraction is originated (with a modal radius of drops $\simeq 0.14$ cm) with maximum water content value $q_m = 16$ g.m^{-3} by the 25 th min. above W_m level. Hereafter, the zone starts to collapse (this process lasts for 15 min), and falling precipitations make 5 mm.

In the second case, the zone of large droplet fraction accumulation was originated by the 50-th min. (modal radius of drops $\simeq 0.18$ cm). Maximum $q_m = 26$ g.m^{-3}. Collapsing of the zone lasts for 15 min. Altogether, falling precipitations make 20 mm.

The results of this relatively simple model are well consistent with the data of natural observations and basic results of numerical modelling of a nonstationary convective cloud, applying the same data of atmospheric thermodynamics as well (Ref. 11). Actually, in the first case, precipitations fallen out make 3.0 mm and $q_m = 10$ g.m^{-3}. In the second case, $q_m = 26$ g.m^{-3} while the total amount of precipitations $\simeq$ 20 mm.

In considering a heterogeneous freezing mechanism (Ref. 8) process of crystallization starts in a cloud by 7-10 min earlier than in the case of a homogeneous mechanism (Ref. 7). Duration of precipitation fall-out is decreased by 5-10 min, while the amount of solid precipitations is increased respectively.

The elaborated model had been tested in estimating the probability of hailstorm evolution during the period of May-June, 1983.

General expectations of the forecast equal to $\simeq$ 85 % within the radius of 100 km from the point of radiozonding. Application of a large amount of statistic data (for several years) with allowance for synoptic situations, will permit to specify the pattern of forecast and use it in practice.

REFERENCES

1. Sedunov, Yu.S. Effect of hydrometeorological processes. Problemy sovremennoi gidrometeorologii. L., Gidrometeoizdat, 1977, 314-343.
2. Auer, A.H., Marwitz, J.D. Estimates of air and moisture flux into hailstorms on the high plains. J.Appl. Meteorol. 1968, v.7, No. 2, 196-198.
3. Fankhauser, J.S. Subcloud air mass flux and moisture flux attending a northeast Colorado thunderstrom complex. Prepr. Conf. on cloud Physics, Tucson, Ariz., Am. Meteorol. Soc., Boston, Mass., 1974, 271-275.
4. Fletcher, N.H. The Physics of Rainclouds. Cambridge Univ. Press., 1962, 386 pp.
5. Borovikov, A.M., Mazin, I.P. Microstructure of drop clouds. Transactions of the 8-th All-Union Conference on Cloud Physics and Weather Modifications. L., Gidrometeoizdat, 1970, 13-21.
6. Srivastava, R.C. Size distribution of raindrops generated by their break-up and coalescence. J.Atm. Sci., 1971, 28, No. 3, 410-415.
7. Vorobiov, B.M. On the estimation of drop freezing in cumulus clouds. Trudy LGMI, 1972, 45, 93-107.
8. Vali, G. Quantitative evaluation of experimental results of the heterogeneous nucleation of supercooled liquids. J. Atm. Sci., 1967, v. 24, No. 4, 487-496.
9. Asai, T., Kasahara, A. A theoretical study compensating downward motions associated with cumulus clouds. J. Atm. Sci., 1967, v. 24, No. 4, 487-496.
10. Sulakvelidze, G.K. Shower-type precipitations and hail. L., Gidrometeoizdat, 1967, 412 pp.
11. Nadibaidze, G.A., Sulakvelidze, G.K. Some aspects of artificial modification of convective hailstorms. International Conference on Hail Prevention. Sofia, PRB, 1982, Theses, 113-114.

A COMPARISON BETWEEN OBSERVED AND COMPUTED PRECIPITATION OVER COMPLEX TERRAIN WITH A THREE DIMENSIONAL MESOSCALE MODEL INCLUDING PARAMETERIZED MICROPHYSICS

by

D. Médal*, E. Richard*, R. Rosset*, C. Obled**, E.C. Nickerson***

* (Laboratoire Associé de Météorologie Physique, Université de Clermont II, B.P. 45 63170 Aubière, France)

** (I.M.G., Université de Grenoble, B.P. 53 X, 38041 Grenoble, France)

*** (N.O.A.A.,E.R.L.,G.M.C.C., 325 Broadway, Boulder, Co 80303, U.S.A.

1. INTRODUCTION

A three dimensional mesoscale numerical model with parameterized microphysics (Refs 1, 2) has been used to investigate the role of complex orography in the distribution and evolution of the heavy rainfalls observed over the south eastern edge of the Central Massif in France (Cevennes ridge).

This area is subject to heavy precipitation : 2175 mm averaged yearly precipitation over Mount Aigoual located in the Cevennes ridge against 520 mm at Aigues Mortes located only 80 km away in the plain. These heavy rainfalls, driven mainly by surges of warm noist Mediterranean air interacting with the topography regularly occur during fall, giving rise to short episodes which sometimes lead to severe flash floods.

To simulate such an event, the model was run over a 250 km x 250 km area centered over the Cevennes ridge, thus allowing a quantitative comparison between observed and computed rainfall.

2. METEOROLOGICAL SITUATION

The meteorological situations inducing heavy rainfall episodes over the Cevennes ridge pertain to only a limited number of typical synoptic weather patterns (Ref. 3). The most frequent pattern (64 % of the cases) is characterized by a strong south-west to south south-west upper level flow of tropical air in association with an Atlantic trough located between Ireland and Portugal. At the surface a deep trough is found over the bay of Biscay while over Central Europe, a persistent continental high is protruding in the Po valley and in south-east France. Between these two surface centers, the flow is from the south-east. The meteorological situation of August 29th, 1976, selected for this study, fits into this description as can be seen in Fig. 1 (500 mb upper level chart) and in Fig. 2 (surface analysis).

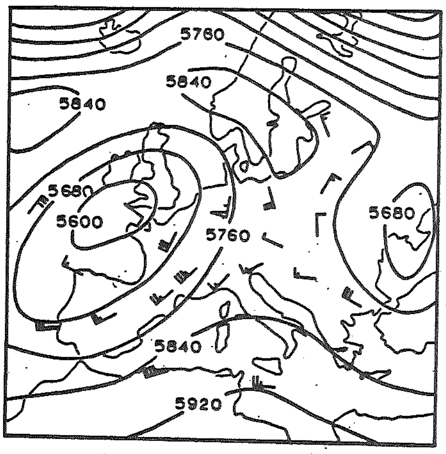

Fig. 1. 29-08-76, 0 h, 500 mb upper level chart.

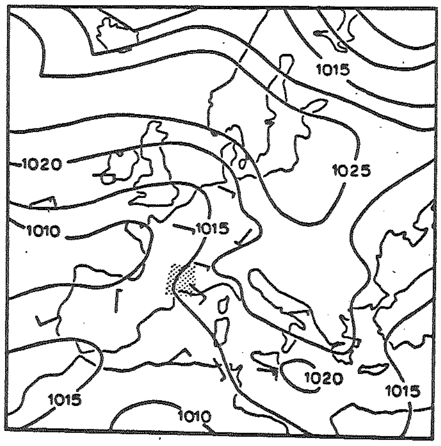

Fig. 2. 29-08-76, 0 h, surface analysis. The shaded area identifies the location of the model domain.

The shaded area in Fig. 2 is the 250 km x 250 km modelled area. A perspective view of the terrain is shown in Fig. 3. The Cevennes ridge on the west extends from sea level to 1600 m. On the eastern boundary, the western edge of the Alps is separated from the Central Massif by the Rhône valley. Fig. 4 depicts the height contours in the area. The dotted line rectangle in this figure corresponds to a dense rain-gauge network. For the case studied, Fig. 5 displays the evolution of hourly precipitation rates selected between 00 GMT and 07 GMT. Precipitation cores are distributed all along the ridge. The observed maximum intensities (1.8, 2.5, 2.1, 2.3 cm/hour) are not as variable as are the spatial localizations which display a great variability from one hour to the next.

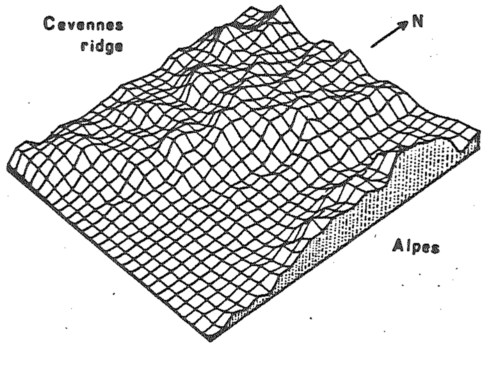

Fig. 3. A perspective view of the Cevennes terrain looking from south-east.

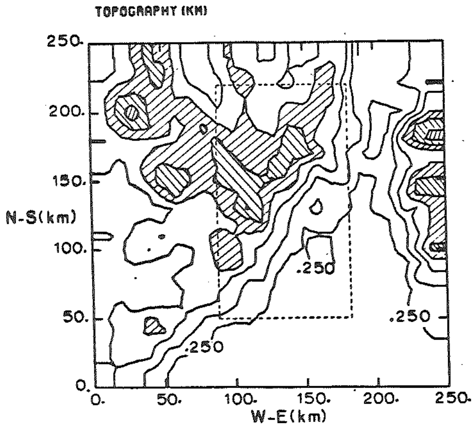

Fig. 4. Height contours in the model domain. The dashed areas indicate values in excess of 1 km. The dotted line identifies the limits of a zone (named P-zone) instrumented with a dense raingauge network.

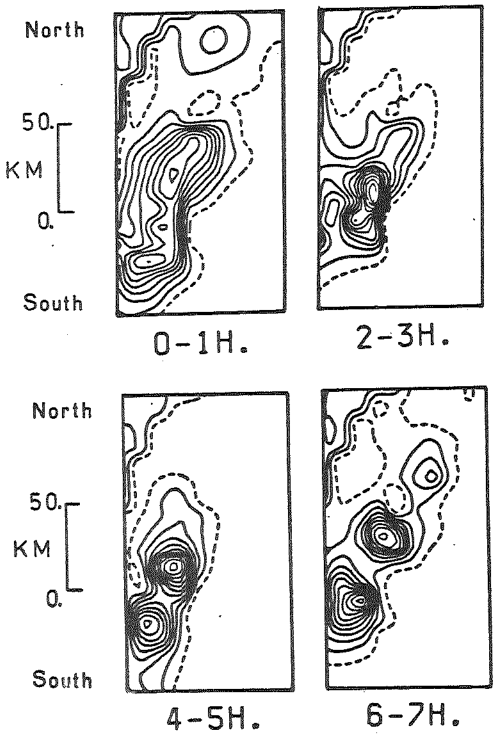

Fig. 5. Time sequence of the hourly observed precipitation rates in the P-zone defined in Fig. 4. The outer contour has a value of 0.2 cm/hour. The maximum values are 1.8, 2.5, 2.1, 2.3 cm/hour between 0.1 h, 2.3 h, 4.5 h, 6.7 h GMT respectively.

3. MODEL DESCRIPTION

The three dimensional hydrostatic mesoscale model is based upon primitive equations resolution. The 15 computational levels in a modified sigma coordinate system extend through the entire depth of the atmosphere. The horizontal grid length is 10 km and the time step is 15 seconds.

Explicit parameterizations of the following warm rain microphysical processes have been incorporated into the model : evaporation, condensation, autoconversion, self-collection and sedimentation.

Cloud water mixing ratio, q_{cw} is diagnosed from the predicted value of $q = q_v + q_{cw}$ (q_v : vapor mixing ratio) according to :

$$\begin{cases} q_v = q_{vs} \\ q_{cw} = q - q_{vs} \end{cases} \text{if } q > q_{vs} \quad \text{or} \begin{cases} q_v = q \\ q_{cw} = 0 \end{cases} \text{if } q \leqslant q_{vs}$$

where q_{vs} is the saturation mixing ratio.

Predictions are made of both rain water mixing ratio q_r and total number concentration N_r assuming a log-normal droplet distribution : the droplet concentration in the size range D to D + dD is given by :

$$dN_r = \frac{N_r}{\sqrt{2\pi}\,\sigma\, D} \exp\left(-\frac{1}{2\sigma^2} \mathrm{Ln}^2 \frac{D}{D_0}\right) dD \qquad (1)$$

where σ and D_0 are distribution parameters.

If the median droplet diameter D_0 is larger enough so that cloud size droplets contribute very little to the total number concentration, then integration of (1) over the entire spectrum of droplets of mass $\rho_w\ \pi D^3/6$ yields the following expression for the rain water mixing ratio :

$$q_r = \frac{N_r}{\rho} \left(\frac{\pi}{6} D_0^3\ \rho_w\right) \exp\left(\frac{9}{2} \sigma^2\right) \qquad (2)$$

where ρ and ρ_w represent the density of air and liquid water respectively. From (2) we see that there are two independant distribution parameters only one of which can be diagnosed from (2) given q_r and N_r. To close the system of equations, we assume σ is constant and compute D_0. For the model run reported on here $\sigma = 0.5$.

We have made extensive use of the work of Berry and Reinhardt (Ref. 4) in developping parameterizations for autoconversion, accretion and self-collection processes appropriate to the log-normal rain drop distribution. The prediction equations for q, q_r and N_r include the rates of conversion of cloud water to rain water by stochastic coalescence as well as the rate of accretion of cloud water by rain water. The self collection rate affects only the N_r equation.

Because cloud water formulation does not allow supersaturation with respect to liquid water, we assume that diffusional growth of raindrops can be neglected. In the case of evaporation, the necessary amount of rain water to maintain water saturation is evaporated after prediction, and the raindrop concentration reduced accordingly.

4. INITIAL CONDITIONS

The model wind fields were initialized with a single sounding from Nîmes at 00 GMT on the 29th of August, 1976. The predominant wind direction was from the south south-east in the low levels and from south south-west above 800 mb.

To initialize the temperature and moisture fields, an objective analysis made with three soundings within and around the studied area was used, so as to account for the observed north-south large scale gradient in moisture and temperature : i.e. the southern part of the domain is warmer and moister than its northern part.

Futhermore, the sea level pressure field was initialized with an analysis of all the available ground pressure data reduced to sea level.

5. MODEL RESULTS

The wind fields adjust to the underlying terrain in approximatively one hour after which the winds remain steady. Fig. 6 shows the difference between the wind field computed after 6 hours of simulation and the initial wind field at 18 m above the ground. Within the Rhône valley, the flow initially from south south-east has been accelerated while turning to a more southerly direction. A strong slow down can be observed over the Cevennes ridge.

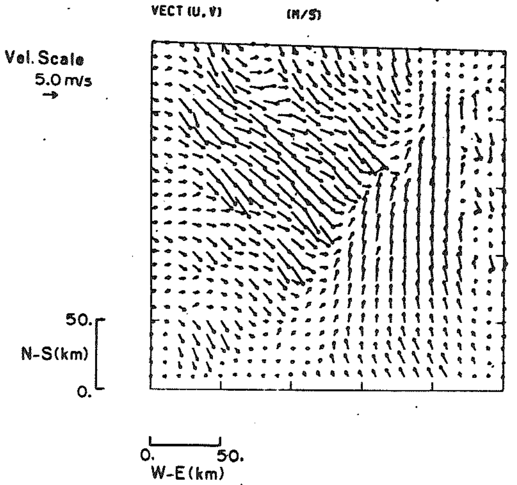

Fig. 6. Difference between the wind field predicted after 6 hours and the initial wind field at 18 m above the ground.

Clouds formed very rapidly in response to the orographic forcing at first over the highest mountains. Fig. 7 shows the vertically integrated cloud water defined by :

$$\overline{q_{cw}} = \int_0^\infty \rho \, q_{cw} \, dz$$

after 6 hours of model time. At this time, the clouds spnead out, even covering the northern part of the valley.

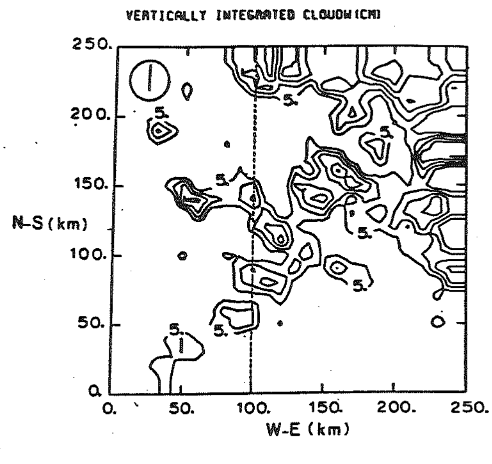

Fig. 7. Vertically integrated cloud water after 6 hours of model time. The dotted line identifies the location of the vertical cross section shown in Figs. 8, 9 and 10.

Fig. 8 is a north-south vertical cross section of the cloud water mixing ratio q_{cw} after 6 hours of model run along the dotted line in Fig. 7. Above the peaks, the model predicted the formation of a cloud layer extending from the ground to 4 km. The maximum value for this cross section is 0.43 g kg^{-1}. The corresponding values of rain water mixing ratio and total number concentration have been plotted in Fig. 9 and 10. The highest values, 1.35 g kg^{-1} and 480 rain drops/liter respectively, are found above the southern peak.

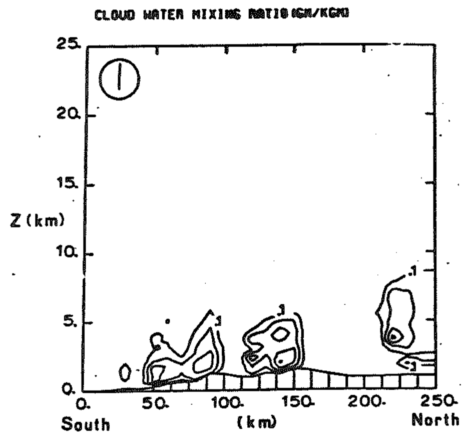

Fig. 8. Vertical cross section of cloud water mixing ratio along the dotted line in Fig. 7 after 6 hours of model time. The inner contour has a value of 0.4 g kg^{-1} while the outer contour has a value of 0.1 g kg^{-1}.

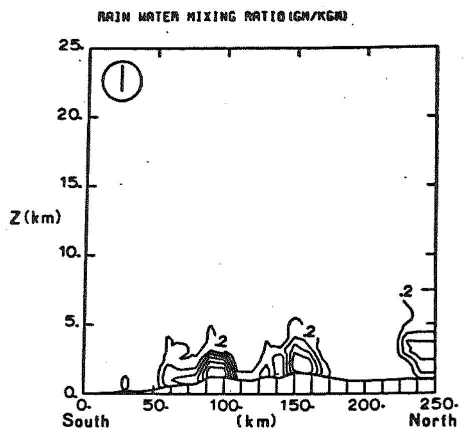

Fig. 9. Vertical cross section of rain water mixing ratio corresponding to Fig. 8. The inner contour has a value of 1.2 g kg^{-1} while the outer contour has a value of 0.2 g kg^{-1}.

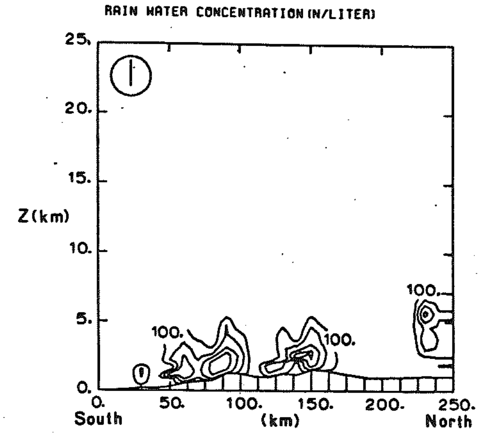

Fig. 10. Vertical cross section of rain water concentration corresponding to Fig. 8. The inner contour has a value of 400/liter while the outer contour has a value of 100/liter.

Fig. 11 shows the spatial distribution of the 6 hour cumulated precipitation over the whole area. The heaviest rainfall (7.9 cm) occurred over the Alps on the east of the domain. Heavy rainfalls were computed too, all along the Cevennes ridge. The maximum value (over 7 cm) is found in the northern part of the ridge, over Coiron peak.

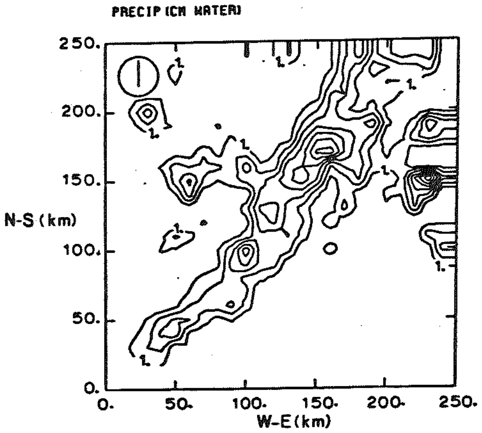

Fig. 11. Model predicted rainfall after 6 hour. The maximum value is 7.9 cm. The outer contour has a value of 1 cm.

6. DISCUSSION

In Fig. 5, we have previously noted the large variability in the position of the highest precipitation cores along the Cevennes ridge on a hourly basis from 00 GMT to 07 GMT. In Fig. 11, have been displayed the isohyets computed in the whole domain for cumulated rainfalls over a 6 hour period. A more consistent comparison between the observed and the computed results is made in Fig. 12. In this figure, the "observed" results refer to the hourly averaged rainfall rates computed over a period of 6 hours between 03 GMT and 09 GMT. As for the "computed" results, they are obtained at each grid point by dividing a factor of 6, the rainfall amounts calculated after the 6 hour run.

The main conclusion to be drawn from the two maps in Fig. 12 is their general good agreement. This agreement is better in the south of the domain where the rain cores are correctly localized together with equal rain amounts in the two maps.

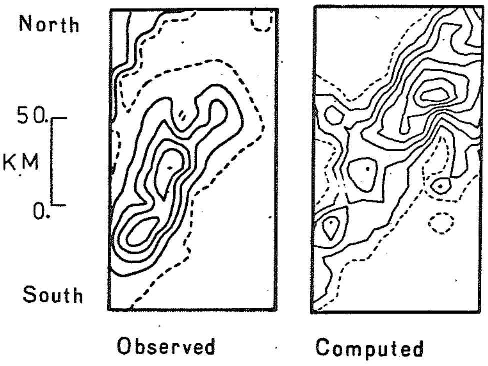

Fig. 12. Comparison between observed and computed hourly precipitation rates over the P-zone. The contours have been drawn every 0.2 cm/hour starting at 0.2 cm/hour (dashed line).

This agreement degrades somewhat in the north, particularly over the Coiron region where the calculated results are in excess over the observed ones. In fact, referring back to Fig. 5, one can see that rain appears in this region only after 06 GMT and later on.

The causes of discrepancies between the observed and computed results are at least twofold. First a large variability is always observed in the hourly sequences of severe rainfalls over the Cevennes and this cannot be accounted for by the single sounding used for initializing the model winds. Secondly, in the initialization procedure itself, two points need further improvement : a better initial humidity field using surface moisture data and non-zero initial vertical velocities (Ref. 5). New initialization techniques are presently being developped.

Nevertheless, our fine grid simulation largely improves present sub-synoptic rain forecasts in the region over such limited periods.

7. ACKNOWLEDGMENTS

We are indebted to P. Mascart, J. Duron, R. Pejoux and Y. Pointin for their help in programing graphic routines. We gratefully aknowledge C. Baraduc who did the typing.

8. REFERENCES

1. Nickerson E C 1979, On the numerical simulation of airflow and clouds over mountainous terrain, *Betr. zur Phys. der Atmos.* 54, 161-177.

2. Nickerson E C & Richard E 1981, On distribution and evolution of clouds and rain over the Vosges and Black Forest mountains : a three dimensional mesoscale simulation with parameterized microphysics, *Fifth Conf. Numerical Weather Predictions*, Monterey, Calif., November 2-6, 1981.

3. Rebotier R 1957, Le climat pluviométrique des basses Cevennes, *Monog. Météor. Nat.*, n°7, Paris.

4. Berry E X & Reinhardt R L 1973, Modeling of condensation and collection within clouds, *Desert Res. Inst.*, Phys. Sci. Pub. n° 16, University of Nevada.

5. Tarbell T C et al 1981, An example of the initialization of the divergent wind component in a mesoscale numerical weather prediction model, *Mon. Wea. Rev.* 109, 77-95.

ON THE ENTRAINMENT IN NONPRECIPITATING CUMULUS CLOUDS

Ivana Nemešová

Institute of the Physics of the Atmosphere
Czechosl. Acad. Sci., 14131 Prague, Czechoslovakia

1. INTRODUCTION

The paper presented here deals with a further test of the cloud top entrainment hypothesis of Squires and Telford (Refs. 1,2) on the basis of the works by Warner (Refs.3-5) and Paluch (Ref.6) for nonprecipitating cumulus clouds. For our purpose, the most interesting findings are the following :

The LWC/LWCA profile (LWC and LWCA denote the liquid water content and the adiabatic value of the LWC) seems to be indicative of the extent by which cloud entrainment and mixing have modified the cloud from an unmixed saturated parcel of air. The mean LWC/LWCA profiles exhibit a sharp drop in the magnitude as a function of height in the first kilometre above cloud bases, followed by a nearly constant magnitude of approximately 0.2 at higher levels. On the contrary, the value of the LWC for a given altitude is remarkably constant across a cloud.

The Telford's equilibrium approach appears to be a possible explanation of the observed LWC. We may consider the state in which the density at every level equals the density in the surroundings to be an approximation of a certain period in the life-time of a cumulus, excluding both the first growth and the decay stages.

In most case studies of nonprecipitating cumuli (Refs.6,7) the mixing involving two discrete levels only was found. The entrained air frequently originates from above the levels of observations.

The results of the present cloud models seem to depend on the way in which the mixing between clouds and their environments is described. It was found (Refs. 8,9) that all cloud simulations in a stagnant environment, one-, two-, even three-dimensional models, predicted LWC/LWCA profiles which exhibited very high magnitudes mainly in the upper third of the clouds, while simultaneously computed top levels agreed quite well with the observations. We may conclude that unless cloud models include a parametrization of the cloud interaction with the environment in a realistic manner, they are not likely to predict successfully liquid water contents in general.

In this paper we attempt to make an estimation of height levels in which the entrained air may originate throughout the vertical extents of model clouds on the basis of a thermodynamic treatment of Paluch and the equilibrium assumption.

2. PROCEDURES

The first step to have been carried out, was the choice of suitable convective days during past summer seasons. The term "suitable convective day" denotes the day on which nonprecipitating cumuli were observed at the Milešovka observatory and no frontal system passed Central Europe. We found over 50 days in summer seasons of 1980, 1981, 1982, a few of them were ruled out due to the fact that convective temperature exceeded the temperature maximum for the day, so that a convective condensation level (CCL) could not be found. We identified the CCL with the cloud base. For the remaining 50 days the cloud top levels were computed by the one-dimensional model with lateral entrainment, which predicts cloud tops quite satisfactorily (Refs.10,11); as input data served the 00 GMT soundings from the Prague-Libuš observatory. The computed LWC/LWCA ratios reach the magnitude of 0.8 at the upper parts of the clouds, which exceed the observed magnitudes by as much as a factor of 4. From the model results we used at first the determined vertical extents of the clouds; none exceeds the limit of 4 km. We suppose that the cloud of the known base and the top level contains the observed value of the LWC according to Warner's mean profile of the LWC/LWCA. The cloud is assumed to be in equilibrium relative to its surroundings, i.e. the cloud density at every height level above the cloud base equals the density in the environment. Under these assumptions we are able to determine the equilibrium temperature and the total water mixing ratio for each level inside the cloud.

Now we make use of the adiabatically invariant scalar quantities (Ref.6) which mix in a linear or nearly linear fashion. These two quantities are the total water content Q, when both precipitation-size and ice particles are absent, and the modified equivalent potential temperature Θ_q. Paluch measured these values within the clouds and plotted them together with an environmental sounding of the same quantities in $Q - \Theta_q$ coordinate system. The measurements frequently fall along a straight line connecting the points that represent the sub-cloud base air and an air parcel from above the observation level on the environmental curve. We can systematically use this finding in the following way. For all the clouds chosen, we compute the temperature Θ_q and total water contents Q from the equilibrium temperatures and the liquid water contents, supposing the air inside the cloud to be saturated. The cloud base air is assumed to be saturated with the zero value of the LWC and of the same temperature as the environmental clear air. Then, in the $Q - \Theta_q$ system, we numerically construct the straight lines that connect the points representing the cloud base air and the air inside the computed clouds for layers of an optional thickness up to the tops of the model clouds. The intersection points of those lines and the sounding curve may envisage the thermodynamic characteristics of the air which enters the mixture represented by the cloud mixed air. The described procedure is applied to all the 50 model clouds, giving for a succession of discrete points within vertical extent of each cloud the succession of vertical levels from which the entrained air is likely to originate.

As the vertical extent of the clouds ranges from 500 m up to 4 km, the height levels should be normalized to make comparison among the data feasible. We normalize any height level in the following manner. The height of the cloud base level is subtracted from the actual level and this difference is divided by the vertical extent of the cloud. This simple treatment now yields the non-dimensional parameter hn in the interval of $\langle 0,1 \rangle$ for all levels within the height interval of the cloud, while negative values of hn represent the levels below the cloud base and hn larger than 1 are ascribed to height levels above the cloud top. As regards the coordinate system $hn - hn_c$, where hn_c are the height levels within the cloud vertical extent ⟨0,1⟩, our procedure provides the successions of hn for the successions of hn_c which are chosen 0.1, 0.2 etc. up to 1.0. In this system the lateral entrainment is represented by the straight line hn = hn_c.

3. RESULTS

Our input data set contains 50 soundings and the same number of model clouds. The mean value of the cloud base heights, the cloud base temperature, the top height levels and the top temperatures are 1782 m (d=338), 8.6°C (d=4), 3382 m (d=1075), -1.6°C (d=7.7) respectively, d being the standard deviation. So the mean of the vertical extents amounts to 1600 m.

As expected, the computed series of hn depend on the vertical extents of the clouds. In the following we use the abbreviation VE for the vertical extent. Since our set of 50 cases is too small to be divided into subsets, only tentative conclusions can be drawn from the results. At first we divided the model clouds into 3 groups according to the magnitude of the VE : 0-1 km, 1-2 km, 2-4 km. The number of cases in these groups is in turn : 17, 20, 13. If we plot the mean values of hn as functions of hn_c, we can see that in the lower actually the upper parts of the cloud the entrained air originates from below in fact from above the actual level. If we examine the united group (1-4 km) of 33 cases, we can trace two types of relationship hn = f(hn_c) according to the levels of provenance of the entrained air. Type I contains only 6 cases in which the function hn = f(hn_c) intersects the lateral entrainment line in the lower half of a cloud; the entrained air seems to originate from above within the large part of the VE of the model clouds. We tried to determine conditions under which this situation occurs but we failed. The various combinations of characteristics including the wind shear were examined to determine those conditions; the findings appear to be inconclusive, possibly also due to the paucity of cases. We called the other cases in the group (1-4 km) type II (27 cases) and referred to the remaining clouds of the VE smaller than 1 km as type III (17 cases). Figure 1. shows curves for all the three types. The mean VE for types I, II, III is in turn 1780, 2200 and 645 m, so that the mean thickness of the layer Δ hn = 0.1 corresponds to : 178, 220, 64 m, respectively. The straight line represents the lateral entrainment. By the introduction of the parameter for mixing $\psi = mc/(mc + m)$, where mc and m denote the cloud and clear air masses, our procedure yields the dependance of ψ on hn_c for all the types. In Fig.2 we can see that the dilution of cloud air is smaller

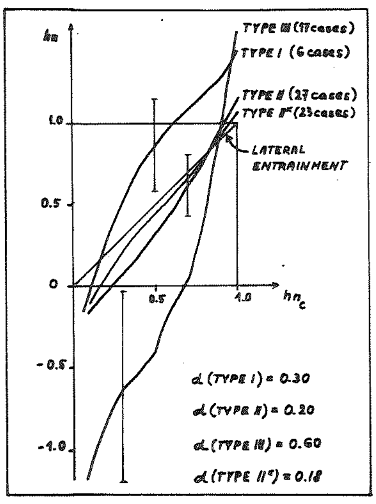

Fig. 1. The normalized height level hn = f(hn_c)

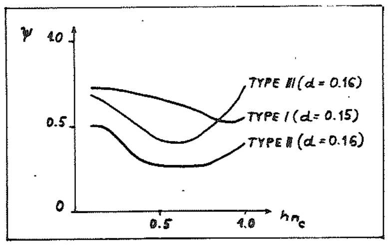

Fig. 2. The rate of dilution ψ = f(hn_c)

for type I as compared with type II and the maximum dilutions for types II and III occur in the middle parts of the model clouds.

If we divide our set into two groups only, one containing clouds of the VE smaller than 1.5 km and the other (II^x) with the cloud VE larger, the dispersion of hn values of group II^x is relatively small. The mean thickness of Δ hn = 0.1 corresponds to 250 m. Type II^x curve in Fig. 1 seems to be the nearest to the curve representing the lateral entrainment expecially in the middle parts of the model clouds.

As an accuracy in the determination of the cloud base level seemed to be important for all the computations, we tried to examine the effect of the height level of the cloud base on the magnitude of hn for type II^x. We found that for those 23 cases the (CCL-200 m) and (CCL+200 m) gave the mean hn differences of about +0.02 and -0.05 , i.e. comparatively small values.

4. CONCLUDING COMMENTS

The work has been undertaken to test the cloud top entrainment hypothesis by the indirect method using a set of soundings and model clouds. Since the number of cases is not representative from a statistical point of view all the conclusions should be regarded as tentative. Nevertheless, the limited results seem to point out the importance of the air entrainment from above the level of "observation" mainly in the upper third of model clouds. A dynamical model has been created to predict the subsidence time and the vertical velocity attained by a parcel under the effect of an evaporative cooling.

5. REFERENCES

1. Squires P.1958, Penetrative downdrafts in cumuli, Tellus 10, 381-389.
2. Telford J.W. 1975, Turbulence, entrainment and mixing in cloud dynamics,Pure Appl.Geophys.113, 1067-1084.
3. Warner J. 1955, The water content of cumuliform cloud, Tellus 7, 449-457.
4. Warner J. 1970, On steady-state one-dimensional models of cumulus convection,J.Atm.Sci. 27, 1035-1040.
5. Warner J. 1977, Time variation of updraft and water content in small cumulus clouds. J. Atm. Sci. 34, 1306-1312.
6. Paluch I. 1979, The entrainment mechanism in Colorado cumuli, J. Atm. Sci. 36, 2467-2478.
7. Boatman J.F., A.H.Auer 1983, The role of cloud top entrainment in cumulus clouds,J.Atm.Sci.40,1517.
8. Cotton W.R. 1975, On parametrization of turbulent transport in cumulus clouds,J.Atm.Sci.32,548-564.
9. Cotton W.R.,G.J.Tripoli 1978, Cumulus convection in shear flow-three-dimensional numerical experiments, J. Atm. Sci. 35, 1503-1521.
10. Nemešová I, E. Smítková 1982, A simple model of a builing cumulus cloud,Studia Geoph.et Geod.26,176.
11. Nemešová I. 1979, A steady-state model of a cumulus cloud, Studia Geoph. et Geod. 23, 368-379.

A COMPARISON OF CLOUD MODEL RESULTS AND AIRCRAFT OBSERVATIONS SOME FURTHER CONSIDERATIONS

H. D. Orville and L-M. Wu

Institute of Atmospheric Sciences
South Dakota School of Mines and Technology
Rapid City, South Dakota 57701

ABSTRACT (Revised)

A numerical cloud model is used to test the correspondence between the type of data produced by aircraft sampling of clouds and instantaneous plots of cloud variables available from cloud model integrations. Preliminary results are given for liquid water contents only and for a simulated aircraft flying at 100 m s^{-1}. The tentative conclusion is that the aircraft simulation data set and the cloud model instantaneous data sets will be in good agreement (correlation coefficients of about 0.90) if the time of penetration is within a minute of the instantaneous data set and the clouds are not changing "too rapidly."

Keywords: Cloud Model, Numerical Simulations, Aircraft/Cloud Model Comparisons

1. INTRODUCTION

As cloud models develop, the pressure to compare model results and observations increases. Commonly used comparisons have been radar echo patterns, accumulated rain and hail contents at the ground, and cloud top and base heights, among other things.

Aircraft observations of cloud variables are also prime candidates for comparison with cloud model characteristics. However, it should be noted that there is a basic difference between samples from an aircraft and the cross sectional printouts from a cloud model. An aircraft flying through a cloud makes observations that are functions of both space and time. The model results are printed out at one time and are essentially depictions of variations in space only. Printouts at several time steps are needed to show the time dependence of the various fields. Figures 1 and 2 illustrate the types of data plotted from aircraft passes and corresponding model results.

Figure 1 gives instantaneous cross sections of snow, graupel, and cloud water through the central cloudy region at various model times, 42 min-54 min, and at heights corresponding to the level at which a Queen Air aircraft flew. Comparison of this figure with Fig. 2 taken from the real data (illustrated as a time cross section, but with 1 min $\sim$4 km) shows the model disturbances to be of the same scale as those in nature, but to have too large cloud liquid water contents (even after allowance is made for the model values in g kg^{-1} to be converted to g m^{-3}). Also, the change of cloud water with flight direction and the associated change in ice particle concentration is clearly evident in Fig. 2, but not well represented in Fig. 1. In several locations in the model results, low liquid water contents correlate with high snow and graupel contents, as is also evident in the observations.

It was while working with results such as these that questions arose as to the differences between aircraft samples and cloud model cross sections.

The purpose of this study is to simulate the measurements of an aircraft (a/c) flying through clouds with speeds of 50, 70, and 100 m s^{-1} and to compare the results, which represent space and time changes, with model produced instantaneous "cross sections." The results of the study will indicate whether it is appropriate to compare the instantaneous model plots with time and space varying a/c observations.

For this preliminary study, the a/c is assumed to fly at constant altitude and to be affected to a negligible extent by the cloud motions. Consequently, model cross sections at constant altitude are used for the simulation study. In addition, our preliminary study uses model data at every 1-min interval. (Later studies, available at the conference, will report on simulated a/c plots prepared from data produced every time step; i.e., every few seconds.) Using the 1-min data requires that time and space interpolations be done to reproduce the simulated a/c traverses of the clouds.

2. BRIEF MODEL DESCRIPTION

The cloud model is two-dimensional, time-dependent (2DTD) with bulk water microphysics. The domain of the model is 19.2 km in both the X and Z dimensions with a 200 m grid interval. Atmospheric wind, potential temperature, water vapor, cloud liquid, cloud ice, rain, snow, and precipitating ice (in the form of ice pellets, frozen rain, and small hail) are the main dependent variables. The model has been developed from the works of Orville (Ref. 1), Liu and Orville (Ref. 2), Wisner et al. (Ref. 3), Orville and Kopp (Ref. 4), and Lin et al. (Ref. 5). Extension of the model to simulate deep convection has been made using a density weighted stream function (Ref. 6). The nonlinear partial differential equations constituting the model include the first and third equations of motion, a thermodynamic equation, and water conservation equations (for its three phases).

The production of cloud water, cloud ice, rain, snow, and precipitating ice is simulated using bulk water techniques. The production of rain from cloud water is simulated using equations based on the work of Kessler (Ref. 7) and Berry (Ref. 8). Precipitating ice may be formed by freezing rain to ice by means of an equation due to Bigg (Ref. 9) or by aggregation of snow or capture of snow or cloud ice by raindrops. An approximation to the Bergeron-Findeisen process is used to transform some of the cloud water into snow. Growth of

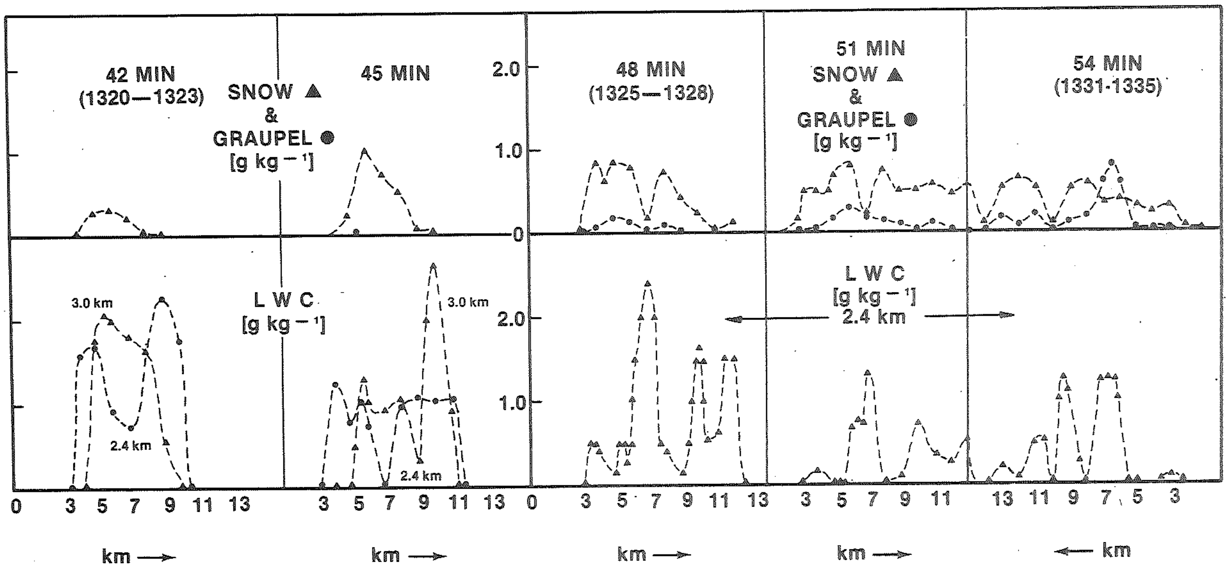

Figure 1. Model output of snow, graupel/hail, and cloud liquid water contents along a constant height corresponding to the aircraft sampling level. Model times are noted in each block with the corresponding aircraft penetration times in parentheses (as given in Fig. 2 and arbitrarily matched here). Abscissa gives values in km from the left border of the domain, except for the last block.

precipitating ice is governed by equations for wet and dry growth (Ref. 10). Cloud water may be transformed to cloud ice in the region between 0°C and -40°C using an equation developed by Saunders (Ref. 11). Homogeneous freezing takes place at the -40°C level. Rain, snow, and precipitating ice possess appreciable terminal fall velocities. Cloud water and cloud ice travel with the air parcels. Evaporation of all forms of hydrometeors and melting of snow and precipitating ice are also simulated.

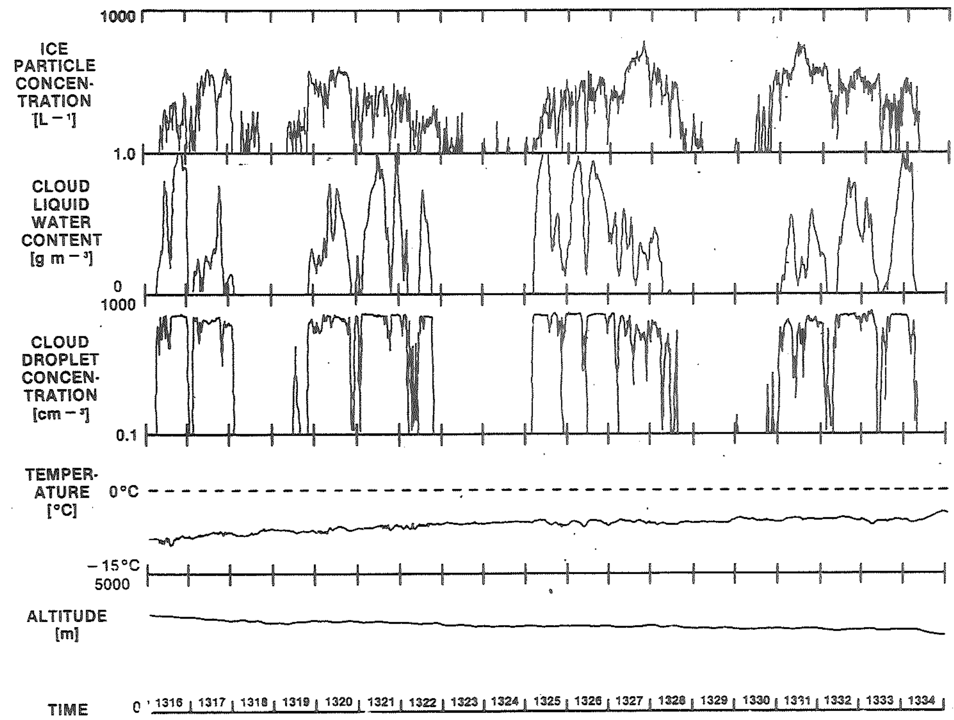

Figure 2. Sample of Wyoming Queen Air aircraft data for 14 May 1981 in the vicinity of Valladolid, Spain. The bottom two plots plus the LWC plot are linear; the other two are logarithmic along the ordinate. The aircraft penetrates in alternating directions from one segment to the next, starting with a south to north penetration. Times are in minutes and the tick marks about 4 km apart, corresponding to an aircraft speed of 70 m s^{-1}.

3. RESULTS

An atmospheric sounding from a cloud seeding experiment in the U.S. High Plains was used to initialize the cloud model. The 2000Z sounding for 24 July 1979 from Miles City, Montana, produced moderate size cumulus clouds limited in growth to the 5 to 6 km level.

Preliminary results regarding liquid water contents only are given here. Figures 3(a-d) illustrate the main points. Figure 3(a) shows a trace of LWC that would be obtained by an aircraft flying at a speed of 100 m s^{-1} at an elevation of 4.8 km above ground level. The a/c begins its traverse from the left border of the model domain at 47.0 min of simulated real time and finishes at a little past 50.0 min.

Figures 3(b), 3(c), and 3(d) show the instantaneous plots of LWC at 48.0, 49.0, and 50.0 min. Obviously, the simulated a/c pass gives a better representation of the cloud LWC field the closer in time the model output is to the a/c position. For example, the first cloud sampled (centered at about 8 km in from the left border) compares most favorably with that cloud on the 48.0 min cross section. That is the time at which the a/c begins its sampling of the cloud. The 49.0 and 50.0 min cross sections compare more favorably with the cloud elements on the right of the grid, the a/c position being at 12 km and 18 km at those times.

As a measure of the goodness of fit of the data, a linear correlation coefficient, r, was computed using a limited set of the data (taken primarily from the integer km points). Further, more complete correlations will be presented at the conference. The data confirm the obvious. The first cloud yields r-values of 0.89, 0.87, and 0.75 for the 48, 49, and 50 min data set correlated with the simulated aircraft pass. The second cloud mass yields r-values of 0.48, 0.61, and 0.87 for the same times, indicating better agreement as the "aircraft" approaches the cloud.

4. CONCLUSION AND DISCUSSIONS

Our general, tentative conclusion is that the aircraft simulation data set and the cloud model instantaneous data sets will be in good agreement ($r \approx 0.90$) if the time of penetration is within a minute of the instantaneous data set and the clouds are not changing rapidly.

This conclusion assumes little disturbance of the aircraft by the updrafts and downdrafts and an aircraft speed of 100 m s^{-1}. More vigorous clouds and slower speed aircraft would result in poorer correlations between aircraft and cloud model instantaneous data plots. We are in the process of programming an aircraft-type sampling process in our cloud model to provide comparisons with actual observational data, which could involve the rise and fall of the aircraft. However, we do not consider it possible to predict the actual details of any particular cloud. We do expect that general characteristics may be predicted.

Acknowledgments. We thank Mrs. Joie Robinson for her efforts in typing the manuscript and arranging the figures in the text. The aircraft data were provided by Gabor Vali of the University of Wyoming, whose help we appreciate.

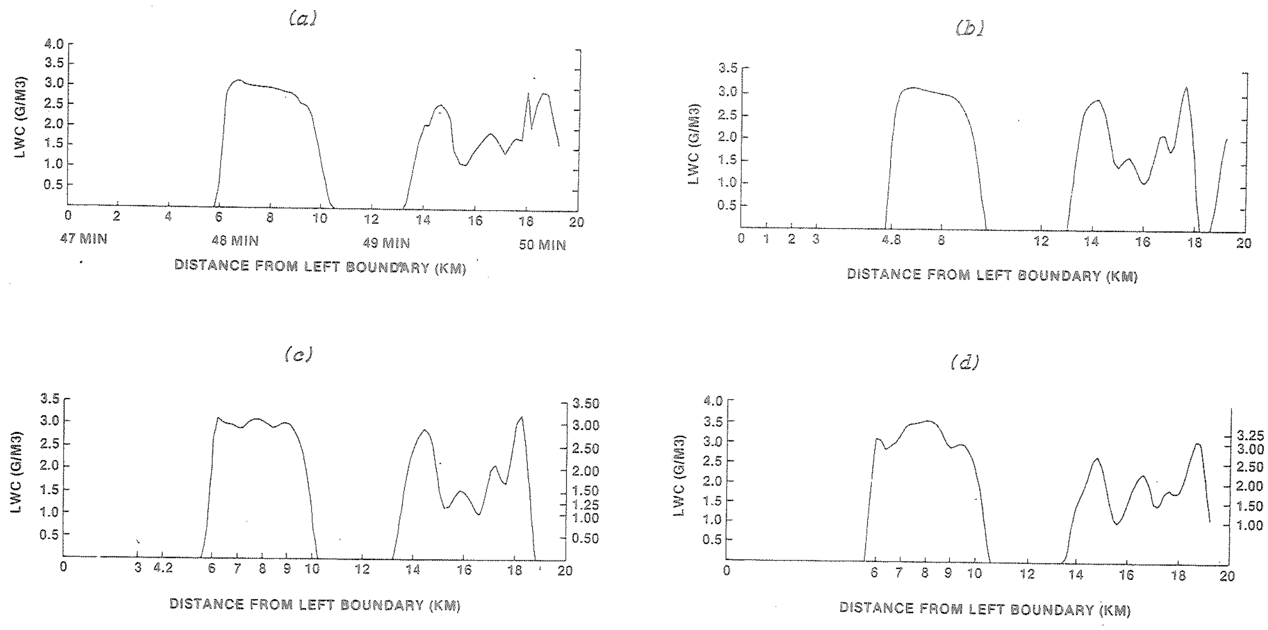

Figure 3(a-d). These graphs show the variation of liquid water content (LWC) across the model domain. The ordinate is in units of g m^{-3} and the abscissa is the distance in km from the left border of the domain. Figure 3(a) gives the plot of LWC as would be measured by an aircraft flying at 100 m s^{-1} at 4.8 km height and starting at 47 min of simulated real time at the left boundary. The time in minutes (48, 49, 50) above the km values in Fig. 3(a) indicates the position of the simulated aircraft. Figures 3(b-d) give the LWC graph from the cloud model data at 48.0, 49.0, and 50.0 min.

This work was supported by NSF Grant No. ATM-8311711. Data from the Precipitation Enhancement Project (PEP), sponsored by the World Meteorological Organization, initiated the study.

5. REFERENCES

1. Orville H D 1965, A numerical study of the initiation of cumulus clouds over mountainous terrain, *J Atmos Sci* 22, 684-699.

2. Liu J Y and Orville H D 1969, Numerical modeling of precipitation and cloud shadow effects on mountain-induced cumuli, *J Atmos Sci* 26, 1283-1298.

3. Wisner C, Orville H D and Myers C 1972, A numerical model of a hail-bearing cloud, *J Atmos Sci* 29, 1160-1181.

4. Orville H D and Kopp F J 1977, Numerical simulation of the history of a hailstorm, *J Atmos Sci* 34, 1596-1618.

5. Lin Y-L, Farley R D and Orville H D 1983, Bulk parameterization of the snow field in a cloud model, *J Climate and Appl Meteor* 22, 1065-1092.

6. Chen C H and Orville H D 1980, Effects of mesoscale convergence on cloud convection, *J Appl Meteor* 19, 256-274.

7. Kessler E 1969, On the distribution and continuity of water substance in atmospheric circulations, *Meteor Monogr* 10, 84 pp.

8. Berry E X 1968, Modification of the warm rain process, *Preprint Volume 1st Natl Conf Wea Modif*, Albany, Amer Meteor Soc, 81-88.

9. Bigg E K 1953, The supercooling of water, *Proc Phys Soc London* B66, 688-694.

10. Musil D J 1970, Computer modeling of hailstone growth in feeder clouds, *J Atmos Sci* 27, 474-482.

11. Saunders P M 1957, The thermodynamics of saturated air: a contribution to the classical theory, *Quart J Roy Meteor Soc* 83, 342-350.

NUMERICAL SIMULATION OF AIR-MASS CONVECTIVE CLOUD FIELDS

R.S. Pastushkov

Central Aerological Observatory, USSR State Committee for Hydrometeorology and Control of Natural Environment, Moscow, 123376, USSR

1. INTRODUCTION

The first numerical simulations of airmass convective cloud fields have been carried out by Chang and Orvill (Ref. 1) and by Hill (Ref. 2).

The results of these models have supported the observational fact of convective cloud field developing in the manner essentially different from that in the case of an isolated convective cloud. More recent numerical experiments by Drake et al. (Ref. 3), Pastushkov (Refs. 4, 6, 7), Kononenko et al. (Refs. 5, 8) have permitted to evaluate space and time nonhomogeneities of modeling convective systems, mutual dynamical interaction of individual convective clouds and the dependence of their thermodynamical structure on this interaction.

But all previous mathematical cumulus field models have been two-dimensional and no serious attempts towards the construction of a full three-dimensional model have been made. So the main purpose of the present study was to treat the development of convective cloud fields with horizontal sizes of 50 - 100 km in rectangular Cartesian three-dimensional co-ordinate system.

2. GOVERNING EQUATIONS. BOUNDARY AND INITIAL CONDITIONS

The model includes:
three equations of motion

$$\frac{\partial u_i}{\partial t} + u_j \frac{\partial u_i}{\partial x_j} = -\frac{1}{\rho_0}\frac{\partial \Pi}{\partial x_i} + \delta_{i3}\left(\lambda_1 \vartheta + \lambda_2 q + \lambda_3 q_{wr}\right) + \frac{\partial}{\partial x_j} K\left(\frac{\partial u_i}{\partial x_j} + \frac{\partial u_j}{\partial x_i}\right) \qquad (1)$$

the continuity equation

$$\frac{\partial(\rho_0 u_i)}{\partial x_i} = 0 \qquad (2)$$

the thermodynamic equation

$$\frac{\partial \vartheta}{\partial t} + u_j \frac{\partial \vartheta}{\partial x_j} = \alpha_1 u_3 + \frac{\partial}{\partial x_j} K\left(\frac{\partial \vartheta}{\partial x_j} - \delta_{j3}\alpha_1\right) \qquad (3)$$

the equation of conservation of all water substance

$$\frac{\partial q}{\partial t} + u_j \frac{\partial q}{\partial x_j} = \alpha_2 u_3 + \frac{\partial}{\partial x_3}(V_r q_{wr}) + \frac{\partial}{\partial x_j} K\left(\frac{\partial q}{\partial x_j} - \delta_{j3}\alpha_2\right) \qquad (4)$$

Eqs. 1-4 are completed by relations for:
the determination of saturation specific humidity

$$q_s = Q_{0s}(x_3)\exp\frac{L_c \vartheta}{R_v \Theta^2} - Q_0(x_3) \qquad (5)$$

the liquid water content

$$q_w = \begin{cases} 0 & \text{in the unsaturated region: } q<q_s \\ q - q_s & \text{in the saturated region: } q \geq q_s \end{cases} \qquad (6)$$

the separation of liquid water into cloud water droplets and rain drops

$$\begin{cases} q_{wc} = q_w \\ q_{wr} = 0 \end{cases} \quad \text{when } q_w < 10^{-3} \qquad (7)$$

$$\begin{cases} q_{wc} = 10^{-3} \\ q_{wr} = q_w - 10^{-3} \end{cases} \quad \text{when } q_w \geq 10^{-3} \qquad (8)$$

the determination of the terminal fall velocity of raindrops relative to the air (in m s^{-1})

$$V_r = \begin{cases} 4.5 \cdot 10^{3/2} q_{wr}^{1/2} & \text{when } q_{wr} < 4 \cdot 10^{-3} \\ 9 & \text{when } q_{wr} \geq 4 \cdot 10^{-3} \end{cases} \qquad (9)$$

and the calculation of eddy diffusion coefficients

$$K = K_0 + L_T^2 \sqrt{\left(\frac{\partial u_i}{\partial x_j} + \frac{\partial u_j}{\partial x_i}\right)^2} \qquad (10)$$

Here

$$\alpha_1 = \begin{cases} \gamma - \gamma_a = -\left(\frac{dT_0}{dx_3} + \gamma_a\right) & \text{when } q < q_s \\ \gamma - \gamma_{wa} = -\left(\frac{dT_0}{dx_3} + \gamma_{wa}\right) & \text{when } q \geq q_s \end{cases} \tag{11}$$

γ_a, γ_{wa} are the initial dry and wet adiabatic lapse rates:

$$\alpha_2 = -\frac{dQ_0}{dx_3} \tag{12}$$

u_i are components of air velocity; $\Pi = P + P_t$; ϑ, P, q, q_s are deviations of temperature, pressure and specific moisture content (specific humidity or saturation specific humidity plus specific liquid water content) and saturation specific humidity from initial reference values $T_0(x_3)$, $P_0(x_3)$, $Q_0(x_3)$; $\rho_0(x_3)$ is the initial value of air density; P_t is mean eddy pressure (Ref. 10); λ_1, λ_2, λ_3 are coefficients which equal g/θ, $0.61g$, $-1.61g$ (θ being initial vertical average of $T_0(x_3)$); $q_w = q_{wc} + q_{wr}$ is specific liquid water content, q_{wc}, q_{wr} being the water content in cloud droplets and raindrops; K_0 is constant initial value of K; L_T is average scale of turbulence; L_c is latent heat of condensation; R_v is gas constant of water vapour.

From Eqs. 1-2 may be derived the equation for pressure function Π:

$$\frac{\partial^2 \Pi}{\partial x_i^2} = \frac{\partial}{\partial x_i}\left(\rho_0 u_j \frac{\partial u_i}{\partial x_j}\right) + \frac{\partial}{\partial x_3}\rho_0\left(\lambda_1\vartheta + \lambda_2 q + \lambda_3 q_{wr}\right) + \frac{\partial^2}{\partial x_i \partial x_j}\rho_0 K\left(\frac{\partial u_i}{\partial x_j} + \frac{\partial u_j}{\partial x_i}\right) \tag{13}$$

The following boundary and initial conditions have been adopted:

at $x_3 = 0,\ L_z$:

$$\frac{\partial u_1}{\partial x_3},\ \frac{\partial u_2}{\partial x_3},\ u_3,\ q = 0 \tag{14}$$

$$\frac{\partial \Pi}{\partial x_3} = \rho_0\left(\lambda_1\vartheta + \lambda_2 q + \lambda_3 q_{wr} + 2\frac{\partial}{\partial x_i}K\frac{\partial u_3}{\partial x_3}\right)$$

at $x_3 = 0$: $\vartheta = \hat{\vartheta}(x_1, x_2, t)$ (15)

at $x_3 = L_z$: $\vartheta = 0$

at lateral boundaries:

$$\varphi(0, x_2, x_3) = \varphi(L_x, x_2, x_3)$$
$$\varphi(x_1, 0, x_3) = \varphi(x_1, L_y, x_3)$$
$$(\varphi \equiv u_i, \vartheta, q, \Pi)$$

at $t = 0$:

$$u_i, q = 0\ ;\ \vartheta = \hat{\vartheta}(x_1, x_2, 0) \tag{17}$$

Here $\hat{\vartheta}(x_1, x_2, 0)$ is the initial value of time dependent randomized function $\hat{\vartheta}(x_1, x_2, t)$. In Eqs. 1-17 the Einstein summation convention for indices was used.

3. COMPUTATIONAL SCHEME

The method for solution of governing equations consisted of centered time extrapolation of finite difference analogs of Eqs. 1, 3, 4 and exact (within round-off error) solution of the Poisson equation (Eq. 13) by splitting method (Ref. 11). The advective terms in Eq. 1 have been approximated by the Aralawa scheme and in Eqs. 3, 4 by the Lilly scheme (Ref. 12). The turbulence terms in all equations have been evaluated non-centrally with one time integration step lag.

The particular point of the model is the Poissen equation for pressure. Therefore the numerical solution method of this equation has been analysed both for precision and optimization.

Figs. 1, 2 show the rates of convergence of solution of Poisson equation for a different way of determination of the relaxation parameters. In this case the height of the base of the temperature disturbance was taken to be 3 km, its width and depth were 1 km. As it may be seen from these Figures, the most economical way of solving the Poisson equation for the mesoscale pressure fields is applying its discrete increasing spectrum of eigenvalues as relaxation parameters (curves 1 in Figs. 1, 2).

4. RESULTS OF NUMERICAL EXPERIMENTS

Several series of theoretical numerical experiments have been performed with different values of the basic parameters of the model.

The height of the domain under consideration was 4-12 km and its length was 50 km in both horizontal directions. Mesh sizes were 500-1000 m, the time interval was 20-30 s. Calculations were terminated 2-3 hours after the initialization of convection.

Fig. 3 shows the time variation of the relative error in the specific potential energy integral.

One case of the horizontal space distribution of modeling convective clouds is illustrated by Fig. 4. The initialization of this convective cloud field was performed by normally distributed space and time varied temperature pulsations at the ground.

The results of the performed numerical simulation show that the present model may be used for evaluation of airmass convective cloud field energy characteristics and their dependence on the parameters of atmosphere and earth surface, such as large-scale convergence-divergence, temperature-moisture lapse rates, space and time non-homogeneities of lowest atmospheric layer and the ground.

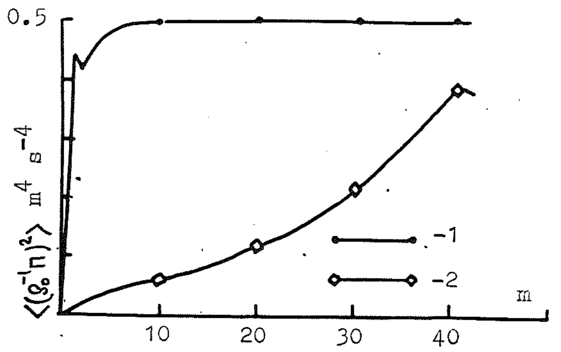

Figure 1. Speed of convergence of an iterative solution of three-dimensional Poisson equation by the splitting method. m -number of iterations, $\langle(\varrho_0^{-1}\Pi)^2\rangle$ - specific value of $(\varrho_0^{-1}\Pi)^2$. Relaxation parameters have been determined by a discrete spectrum of eigenvalues of finite difference analog of the Poisson equation. 1- increasing (2- decreasing) sequence of eigenvalues. The model covers a 52x52x52 km domain with a grid size of 1x1x1 km.

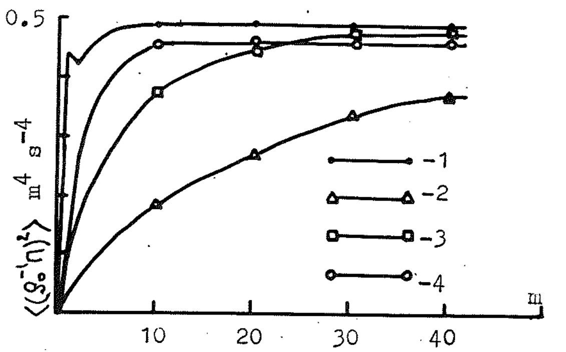

Figure 2. The same as in Fig. 1 but for various ways of determination of relaxation parameters. 1- relaxation parameters have been determined by discrete spectrum of eigenvalues, 2, 3, 4 - relaxation parameters are constant and equal $10\cdot10^{-7}$, $2.5\cdot10^{-7}$, $0.5\cdot10^{-7}$, respectively.

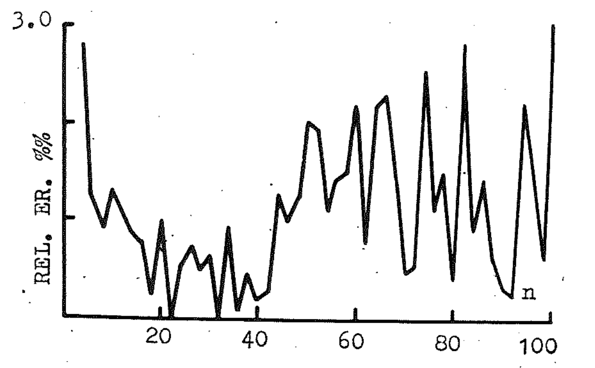

Figure 3. Time variation of the relative error in the specific potential energy integral. n -number of time step.

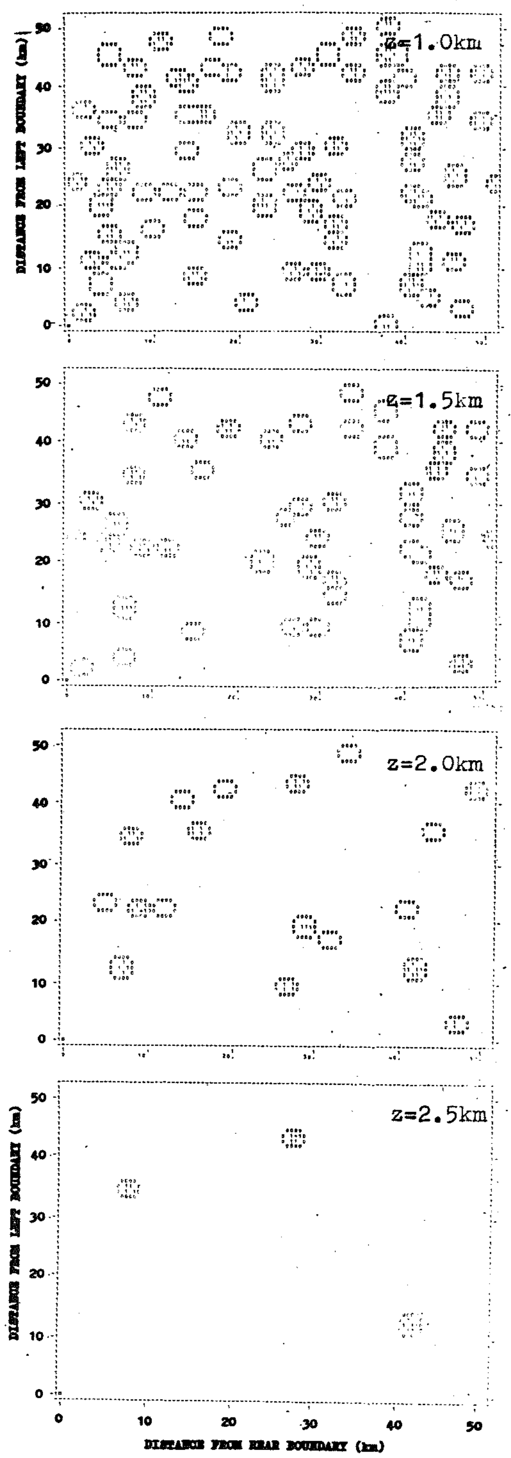

Figure 4. Horizontal cross-section of the domain under consideration at four subsequent heights. Zero-isolines are contours of modeling convective clouds and represent values of specific liquid water content 0.01 g kg^{-1}.

5. REFERENCES

1. Chang, S.W., Orville, H.D., 1973, Large-scale convergence in numerical cloud model. J. Atmos. Sci., 30, 947-950.
2. Hill, G.E., 1974, Factors controlling the size and spacing of cumulus clouds as revealed by numerical experiments. J. Atmos. Sci., 31, 646-673.
3. Drake, R.L., Coyle, P.D., Anderson, D.P., 1975, Interactive line thermals in convective layers: a numerical simulation. J. Atmos. Sci., 32, 302-319.
4. Pastushkov, R.S., 1976, Numerical simulation of convective cloud fields. Proceedings of All-union school "Mathematical modeling of atmosphere dynamics. Tashkent, Oct. 1976", USSR, 40-41.
5. Kononenko, S.M., Malbakhov, V.M., Pushistov, P.Y., 1978, Numerical model of irregular mesoscale convection in planetary Ekman layer. Trudy ZapSibNII, 41, 91-100.
6. Pastushkov, R.S., 1980, On the influence of space and time nonhomogeneities of the lowest atmospheric and oceanic surface layers on the development of convective clouds in ITCZ. Proc. int. conf. on scientific results of GATE. Kiev, Sep. 1980, USSR, 30-31.
7. Pastushkov, R.S., 1981, The evaluation of energy interaction of mesoscale fields of convective clouds with large-scale monsoonal processes. Int. conf. on early results of FGGE. Condensed papers and meeting reports. Tallahassee, Jan. 1981, USA, 1981, 7(41)-7(44).
8. Kononenko, S.M., Malbakhov, V.M., Pushistov, P.Y., Ginzburg, A.S., 1982, Numerical modeling of heat and moisture transfer by convection. Izv. Acad. Sci. USSR, Atmospheric and Oceanic Physics, 18, No. 7, 705-710.
9. Takeda, T., 1969, Numerical simulation of large convective clouds. McGill Univ., Stormy Weather Group Rep. NW-64, 100 pp.
10. Hinze, J.O., 1959, Turbulence. McGraw-Hill Book Co., 680 pp.
11. Marchuk, G.I., 1976, Numerical methods of weather prediction. Leningrad, Gidrometeoizdat, 356 pp.
12. Lilly, D.K., 1964, Numerical solutions for the shape-preserving two-dimensional thermal convective element. J. Atmos. Sci., 21, 83-98.

PRECIPITATION AND ELECTRIFICATION IN A COOL AXISYMMETRIC MODEL CLOUD

Tsutomu Takahashi

Cloud Physics Observatory
Department of Meteorology
University of Hawaii
Hilo, Hawaii, 96720 U.S.A.

ABSTRACT

Both precipitation and the accumulation of electrical charge are studied in a deep axisymmetric numerical cloud model which includes detailed microphysical and electrical processes. It was found that charge accumulation is strongly dependent on the graupel formation process. Most graupel form near the cloud top when snow crystals recirculate in the upper portion of the cloud.

Different charge accumulation processes appear to operate in three different cloud regions. Region 1 is near the cloud top (-30°C) where negative snow crystals, formed near the cloud top, re-enter the cloud along the upper boundary and add to the negative graupel, forming a strong negative space charge. Region 2 is near the -13°C level where negative snow crystals, form below the -10°C level, carried upward add to the falling negative graupel space charge. Region 3 involves charge separation between graupel and snow crystals newly created through ice multiplication at warmer temperatures (-6°C).

In continental clouds, a high concentration of graupel appears to form in a narrow region near the cloud top; the charge accumulation process of Region 1 therefore is predominant. In maritime clouds with a low ice nuclei concentration, strong charge accumulation is observed only at the -10°C level, probably due to the production of many snow crystals by ice multiplication. Numerical model results compare favorably with observations.

1. INTRODUCTION

It is a puzzling phenomenon that lightning, very common over continental land masses, is so infrequent in the region of Micronesia (Ref. 6). Geographical differences in electrical activity may be due to differences in the microphysical structure of various thunderclouds. A cloud model is used to study this problem. Since the electrical structure in winter thunderstorms is so similar to that in summer thunderstorms (Ref. 1), the charge separation processes which occur in winter thunderstorms probably represent the major charge separation processes. Under conditions thought to be similar to those found in winter thunderstorms, Takahashi's (Ref. 10) laboratory studies show that riming electrification is more effective in charge separation than either the Workman-Reynolds effect (Ref. 15) or the polarization charging mechanism. Thus, riming electrification is included in the numerical model as possibly the major charge separation mechanism.

2. MODEL CONSTRUCTION

Microphysical and charge separation processes in the model are similar to those used previously (Fig. 1, Refs. 9, 11). However, modifications were made to provide for point discharge from the ground (Ref. 3) and for the dependence of riming electrification on snow crystal size (Ref. 5).

The equations are deep-anelastic and the diffusion term is expressed in Reynolds' stresses, which are assumed to be proportional to the rate of strain of the large scale flow. The eddy diffusion coefficient is determined by a first-order closure system in which the coefficient in the equation was chosen as 0.4. The variables derived prognostically are vorticity, potential temperature, water vapor, Aitken nuclei, cloud condensation nuclei, ice nuclei, ice particles, number density function of water drops (30 classes), graupel (45 classes), snow crystals (21 classes of size, 5 classes of thickness), drop charge, graupel charge, snow crystal charge density functions, large ion and small ion concentrations. The calculation domain is 8 km in the vertical direction, 6.4 km in the radial direction. The domain is subdivided into 200 m intervals along both the z and r axes. The cloud nuclei concentration (CN) and ice nuclei concentration (CI) are varied to represent different geographical cloud systems.

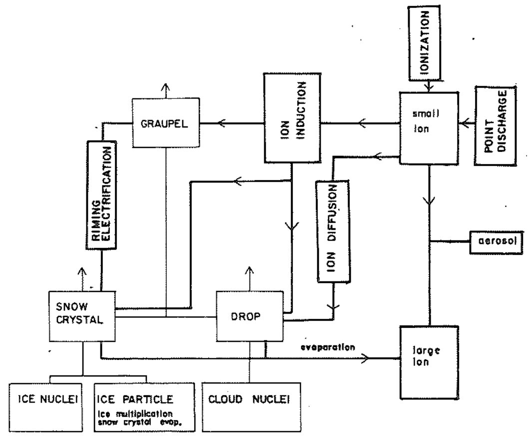

Figure 1. A schematic model of graupel formation and charge separation processes.

3. RESULTS

The updraft increased to 20 ms^{-1} during the 15 min after cloud development and then decreased gradually due to the increasing drag force of particles. A downdraft appeared initially at the cloud boundary, in the upper portions of the cloud

(15 min/18 min), and later moved down to the ground (31 m 40 s). This low-level downdraft appears to trigger new cloud development outside the original cloud cell. At 60 minutes, the downdraft covered a wide area.

During the developing stage, snow crystals grow within the updraft. They fall along the cloud boundary and are recirculated in the upper portion of the model cloud. The recirculated snow crystals are large enough to collect cloud droplets, thus forming graupel near the cloud top (15 min). Graupel first fall along the cloud boundary (18 min) and then at the cloud center as the updraft decreases (31 m 40 s). As graupel fall from the original cloud cell into the new cloud cell, ice particles are generated by the ice multiplication process (Hallett and Mossop, 1974) and snow crystals are nucleated. Relatively high snow crystal and graupel mixing ratios thus occur in the new cloud cell (60 min).

Graupel and snow crystals appear to be the major charge carriers except, perhaps, near the ground. Electricity in the cloud develops in parallel with the formation of graupel. In the developing stage, graupel are electrified negatively and snow crystals positively through riming electrification in the main cloud region. Negative graupel fall along the cloud boundary, while positive snow crystals are recirculated into the cloud. Thus the positive space charge increases in the upper portion of the cloud (15 min). As cloud top development ceases, the small cloud water content near the cloud top causes an increased area of positive graupel and negative snow crystals. The negative snow crystals are recirculated. The combined effect of the recirculated negative snow crystals and the negative graupel produce a strong negative space charge near the cloud top (18 min). As graupel fall, a relatively strong space charge separation occurs between the low-level negative graupel and the high-level positive snow crystals. As graupel fall beneath the -10^{o}C level, they are electrified positively (the snow crystals negatively) due to riming electrification. Negative snow crystals then are carried upward, increasing the negative space charge caused by graupel. Thus, a large negative space charge appears (31 m 40 s).

Near the ground, when the surface electric field is intense, both snow crystals and graupel change sign, due to ion induction. A strong charge separation process also occurs in the new cloud cell because of the large snow crystal concentration. Graupel are electrified positively and snow crystals negatively. A large space charge separation occurs due to gravitational separation (60 min).

Since positive charge accumulates in the developing stage, the electric potential gradient is positive within the cloud and negative near the cloud top (15 min). As the cloud reaches its maximum height, a very large positive potential gradient develops near the cloud top along the boundary of a 50 dBZ intensity radar echo (18 min, Fig. 2). As negative space charge accumulates in the cloud in later stages, a strong potential gradient is oriented outward along the boundary of 55 dBZ radar echo (31 m 40 s). In the new cloud cell, a slightly slanted negative potential gradient appears at lower levels (60 min), where the radar echo intensity is 35 dBZ. In the late stage of cloud life cycle, negative snow crystals evaporate as they fall, leaving negatively charged giant ions. Model results show a relatively large negative potential gradient near the ground, formed between the upper-level negative space charge and the lower-level positive ions supplied by point discharge.

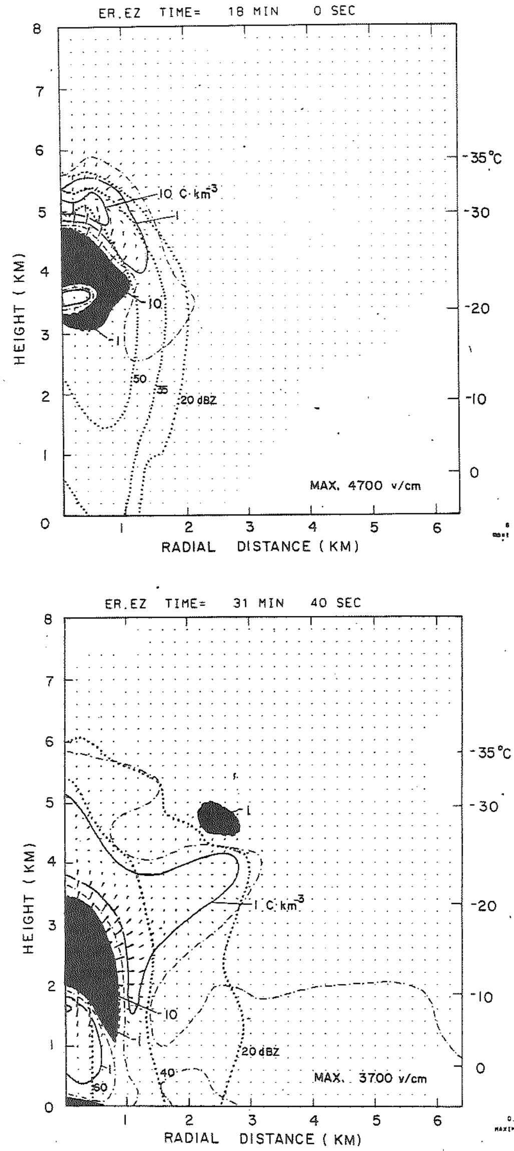

Figure 2. Model-derived magnitude and direction of the electrical potential gradient, and the radar echo intensity, as functions of the height and radial distance, at the various times shown. The net positive space charge is denoted by thin solid lines and the lightly shaded areas show regions within which the space charge is +1 $C\cdot km^{-3}$ or greater. The net negative space charge is denoted by thin dashed lines and the darkly shaded areas show regions within which the space charge is -1 $C\cdot km^{-3}$ or less. Radar echo intensities in units of dBZ are shown by dotted lines. The number in the lower right-hand corner of each diagram is the magnitude of longest arrow denoting the potential gradient.

4. SUMMARY

4.1. Graupel Formation and Charge Accumulation Zones

Graupel form near the cloud top through recirculation of snow crystals in the upper portion of the model cloud. The recirculated snow crystals are large enough to collect cloud droplets, thus forming graupel in the cloud. During this period, a strong electric charge accumulates near the cloud top. Through riming electrification in the main cloud region, graupel are electrified negatively while snow crystals acquire a positive charge. Near the cloud top, the low cloud water content tends to increase the positive graupel and negative snow crystals due to riming electrification. The negative snow crystals are recirculated. The combined effect of the recirculated negative snow crystals and the negative graupel produce a strong negative space charge near the cloud top (Region 1, Fig. 3). The first lightning discharge is observed near the $-30^{o}C$ level (Fig. 4).

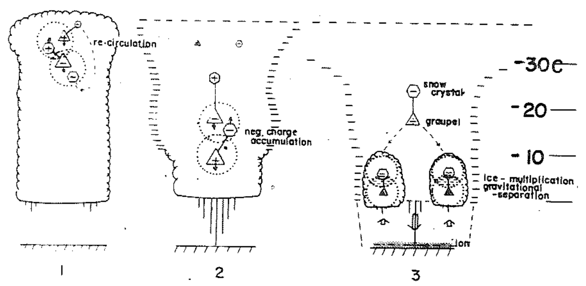

Figure 3. A schematic model showing the three major regions of charge accumulation in thunderstorms and related physical processes.

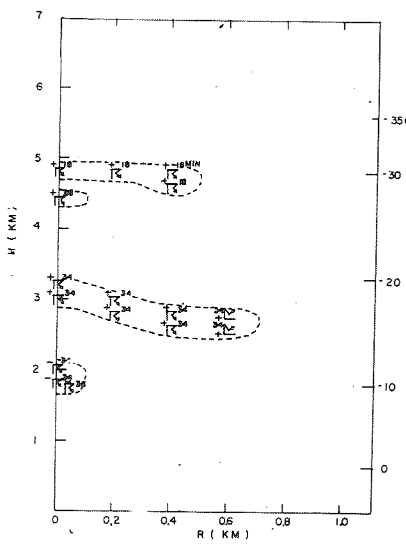

Figure 4. Model-derived lightning discharge sources ($CN=100\ cm^{-3}$, $CI=1\ cm^{-3}$). Conventional lightning symbols are used at each grid point where the calculated electric field is larger than the discharge field. Horizontal lightning sources are shown by 90^{o} rotation of the symbols. The left upper corner shows the sign of electric potential gradient and the right upper corner shows the time.

As graupel fall beneath the $-10^{o}C$ level, they are electrified positively (the snow crystals negatively) due to riming electrification. Negative snow crystals then are carried upward, increasing the negative space charge caused by graupel. Thus, a large negative space charge appears (Region 2, Fig. 3). Lightning develops near the $-18^{o}C$ level. Near the cloud boundary, horizontal lightning occurs (Fig. 4).

Strong charge separation also occurs in new cloud cells between positive graupel and negative snow crystals which are newly created through ice multiplication (Region 3, Fig. 3). Lightning occurs near the $-6^{o}C$ level.

4.2. Comparison with Observations

Observations show that the first lightning occurs near the cloud top, just after the radar echo starts to descend (Ref. 13). Lightning sources appear to occur in two separate regions ($-30^{o}C$ level and $-18^{o}C$ level) along a strong radar echo boundary (Ref. 4). The space charge distribution in the cloud is positive at upper levels and negative below (Ref. 7). The lowest-level positive space charge is due to positively charged graupel. Major charge carriers in the main space charge region are graupel (-50 pC) and snow crystals (+1 pC), both 3 mm in diameter. Near the ground, a strong ion space charge develops by point discharge (Ref. 8).

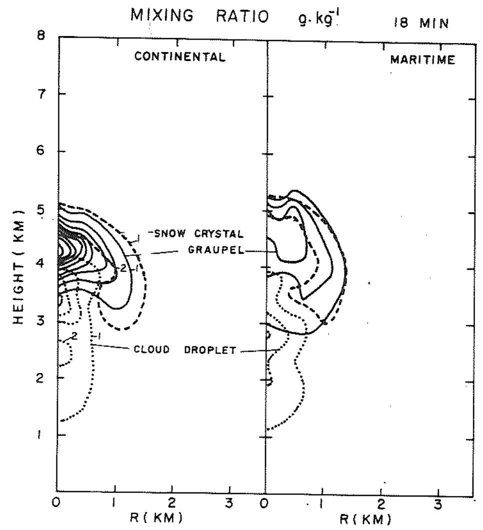

Figure 5. Model-derived mixing ratios of cloud droplets (dotted lines), snow crystals (dashed lines), and graupel (solid lines) at 18 min. Left: continental case, Right: maritime case.

4.3. Graupel Formation and Electric Charge Accumulation Processes in Other Cloud Systems

When the cloud nuclei concentration is increased to $1000\ cm^{-3}$, to represent continental clouds, while the ice nuclei concentration is held at $1\ cm^{-3}$, the drop growth rate is so slow that snow crystals can collect drops only near the cloud top. A large number of graupel form near the cloud top in a narrow region in comparison with the wider distribution of graupel in maritime clouds (Fig. 5). Thus, a very strong electric charge is calculated near the cloud top (Fig. 6). However, when an ice nuclei concentration of $0.01\ cm^{-3}$ is combined with a low cloud nuclei concentration (100 cm^{-3}), the accumulation of electrical charge is slow. An electric field stronger than the critical discharge field appears only near the $-10^{o}C$ level in late stages, due to snow crystal production through ice multiplication (Ref. 2). When the ice nuclei concentration is low (0.01 cm^{-3}) while the cloud nuclei concentration is high (1000 cm^{-3}), the slowest rate of electric charge accumulation occurs.

	CASES			
TIME (MIN)	A	B	C	D
5	+1(0)*	+1(0)	+1(0)	+1(0)
10	+1(0)	+1(0)	+1(0)	+1(0)
15	+147(3.2) (2, 10)**	+106(3.4) (3, 106)	+2(2.8) (0, 6)	+2(3.2) (0, 0)
16	+579(3.6) (31, 1400)	+675(3.6) (15, 8452)	+7(3.8) (0.4, 752)	+4(4.0) (0, 561)
18	+4187(4.8) (540, 2500)	+4908(4.4) (754, 8701)	+30(4.8) (0.2, 2300)	+26(4.6) (2, 303)
20	+2633(4.8) (640, 1600)	+27689(4.8) (745, 4262)	+44(5.0) (0.5, 1939)	+99(5.4) (2, 1003)
22	+1495(5.2) (634, 1100)	+23464(5.0) (653, 1793)	-52(5.4) (3, 625)	+157(5.0) (2, 1181)
24	+2112(4.2) (512, 744)	+14271(4.8) (642, 849)	-63(1.8) (3, 57)	+209(4.4) (5, 272)
26	+3962(4.4) (636, 837)	+11726(4.8) (640, 505)	-357(1.8) (15, 146)	+178(4.6) (6, 223)
28	+1457(3.8) (182, 721)	+10382(4.8) (641, 480)	-1097(1.8) (29, 211)	+207(3.8) (2, 145)
30	+2982(3.4) (117, 630)	+9154(4.6) (659, 399)	-2746(2.0) (41, 328)	+302(4.0) (5, 243)
32	+3791(3.0) (85, 547)	+9000(4.2) (350, 491)	-4577(1.8) (57, 427)	+415(3.8) (6, 240)
34	-3354(1.8) (45, 514)	+9800(3.4) (148, 321)	-4723(1.8) (66, 535)	+647(3.4) (7, 248)
36	-2933(1.8) (57, 603)	+9800(3.2) (87, 313)		+910(3.4) (11, 302)
38	-2744(1.6) (64, 610)	+8800(3.2) (96, 310)		+1259(3.2) (12, 339)
40	-2442(1.6) (55, 646)	+7500(3.2) (100, 285)		+1278(2.8) (12, 349)

A(CI=1 cm^{-3}, CN=100 cm^{-3}); B(CI=1, CN=1000);
C(CI=0.01, CN=100); D(CI=0.01, N=1000)
*: MAXIMUM ELECTRIC POTENTIAL GRADIENT (v cm^{-1}) AT CLOUD CENTER AND HEIGHT
**: (NUMBER CONCENTRATIONS OF SNOW CRYSTALS PER LITER AND GRAUPEL PER CUBIC METER)

Figure 5. Model-derived variables in the different cloud systems.

Specific concentrations of graupel and snow crystals seem to be critical in the formation of a strong electric field. A discharge field can develop only with 0.5(0.05) per cc and 2.5(0.6) per liter of snow crystals and graupel in the principal upper (lower) space charge regions (Fig. 5). In a new cloud cell, however, a lesser concentration (0.05 per cc and 0.05 per liter) will suffice, due to the narrower space charge distribution. The stronger electrical activity in the continental thunderstorm may depend upon higher graupel production than that which occurs in the maritime thunderstorms.

5. REFERENCES

1. Brook M and Krehbiel P 1982, The electrical structure of the Hokuriku winter thunderstorms, *J Geophys Res* 87, 1207-1215.

2. Hallett J and Mossop S C 1974: Production of secondary ice particles during the riming process, *Nature* 249, 26-28.

3. Jhawar D S and Chalmers J A 1965, Point discharge from multiple points, *J Atmosph Terr Phys* 27, 367-371.

4. Krehbiel P R, Brook M and McCrory R A 1979, An analysis of the charge structure of lightning discharges to ground, *J Geophys Res* 84, 2432-2456.

5. Marshall B J P, Latham J and Saunders C P R 1978, A laboratory study of charge transfer accompanying collision of ice crystals with a simulated hailstone, *Quart J Roy Met Soc* 104, 163-178.

6. Orville R E 1981, Global distribution of midnight lightning - September to November 1977, *Mon Wea Rev* 109, 391-395.

7. Simpson G C and Scrase F J 1937, The distribution of electricity in thunderclouds, *Proc Roy Soc London Ser A* 161, 309-352.

8. Standler R B and Winn W P 1979, Effects of coronae on electric fields beneath thunderstorms, *Quart J R Met Soc* 105, 285-302.

9. Takahashi T 1976, Hail in an axisymmetric cloud model, *J Atmos Sci* 33, 1579-1601.

10. Takahashi T 1978, Riming electrification as a charge generation mechanism in thunderstorms, *J Atmos Sci* 35, 1536-1548.

11. Takahashi T 1983a, A numerical simulation of winter cumulus electrification. Part 1: Shallow cloud, *J Atmos Sci* 40, 1257-1280.

12. Takahashi T 1983b, Electric structure of oceanic tropical clouds and charge separation processes, *J Meteor Soc Japan* 61, 656-669.

13. Workman E J and Reynolds S E 1949, Electrical activity as related to thunderstorm cell growth, *Bull Amer Met Soc* 30, 142-144.

14. Workman E J and Reynolds S E 1950, Electrical phenomena occuring during the freezing of dilute aqueous solutions and their possible relationship to thunderstorm electricity, *Phys Rev* 78, 254-259.

NUMERICAL SIMULATION OF THE EFFECTS OF STABLE LAYERS ALOFT ON THE DEVELOPMENT OF THERMAL CONVECTION

Sh. Tzivion(Tzitzvashvili)*, Z. Levin,** A. Manes*

*Israel Meteorological Service,Research and Development Division
**Tel Aviv University, Dept. of Geophysics and Planetary Sciences

1. INTRODUCTION

Conditions may often develop under which the atmosphere is potentially unstable, however, cloud development may be restricted due to the presence of one, or more, relatively shallow stable layers at the top of the atmospheric boundary layer.

The purpose of this study is to investigate the effects of such stable layers on the development of convection by means of numerical simulation. The effect of stable layers on the suppression of convection depends strongly on the extent of the potential instability of the atmosphere, on the height and depth of the suppressing stable layer and on the temperature gradient within the layer.

We would expect that the suppressing effect of stable layers is most strongly pronounced at the initial stages of convective development. To investigate this process it is,therefore, necessary to apply a model describing in detail and most accurately the initial stages of convective development. It is important to note that for the problem to be treated there is no need in detailed information regarding the microphysical cloud processes, which can thus be considered by relatively simple parameterization scheme.

2. MODEL DESCRIPTION

The inital system of equations describing the formation and evolution of an axisymetric convective cloud above a homogeneous boundary surface may be written in the following form:

$$\partial u/\partial t=F_d(u)-D(u)-\partial\pi/\partial r-\nu u/r^2 \quad (1)$$

$$\partial w/\partial t=F_d(w)-D(w)-\partial\pi/\partial r + g(\theta/\Theta_0- M) \quad (2)$$

$$\partial/\partial r(r\rho_0 u)+\partial/\partial z(r\rho_0 w)=0 \quad (3)$$

$$\partial\xi/\partial t=F_q(\xi)-D(\xi)-(\Theta_0/T_0\rho_0)\partial/\partial z((L/c_p)\rho_0 M_r\bar{\omega})+\Gamma_\theta w \quad (4)$$

$$\partial q/\partial t=F_q(q)-D(q)+(1/\rho_0)\partial/\partial z(\rho_0 M_r\bar{\omega})+\Gamma_q w \quad (5)$$

$$(1/r)\partial/\partial r(r\partial\pi/\partial r)+\partial^2\pi/\partial z^2=(1/r)\partial/\partial r(r(F_d(u)-D(u)))+\partial/\partial z(F(w)-D(w))-(1/r)\partial/\partial r(\nu u/r)+g\partial/\partial z(\theta/\Theta_0-M)-\partial/\partial t(\partial/\partial r(r\rho_0 u)+\partial/\partial z(r\rho_0 w)) \quad (6)$$

$$\xi=\theta-(L/c_p)(\Theta_0/T_0)M \quad (7)$$

$$q=q_v+M_{cl}+M_r \quad (8)$$

$$\nu_d=\nu_0+(C_t\Delta)^2|\mathrm{grad}(u^2+w^2)^{0.5}| \quad (9)$$

$$F_{d,q}(\phi)=(1/r)\partial/\partial r(\nu_{d,q}r\partial\phi/\partial r)+(1/\rho_0)*\partial/\partial z(\rho_0\nu_{d,q}\partial\phi/\partial z) \quad (10)$$

$$D(\phi)=(1/r)\partial/\partial r(ru\phi)+(1/\rho_0)\partial/\partial z(\rho_0 w\phi) \quad (11)$$

$$|\mathrm{grad}\phi|=((\partial\phi/\partial r)^2+(\partial\phi/\partial z)^2)^{0.5} \quad (12)$$

where:
ϕ-either function
F-turbulence operator
D-advection operator
|grad |-absolute value of the gradient operator
u and w - the radial and vertical velocity components, respectively
$\pi=p/\rho_0$
ξ - the perturbation of the virtual potential temperature which the cloudy air assumes if all droplets evaporate completely
q - perturbation of specific humidity
$M=(M_c+M_r)$ - specific water content
M_c - specific cloud water content
M_r - specific rain water content
Note: ξ and q are conservative functions with respect to phase transformations. The introduction of these parameters enables to write the energy and moisture transfer equations without explicit terms describing phase transformations
θ - perturbation of the virtual-potemtial temperature
T_0 and Θ_0 - the virtual temperature and virtual potential temperature of the non-perturbed atmosphere, respectively
Γ_θ - vertical gradient of the virtual potential temperature in the non-perturbed atmosphere
Γ_q - vertical gradient of the specific humidity in the non-perturbed atmosphere
$\bar{\omega}$ - weighted mean speed of a sinking rain droplet system
L - latent heat of condensation
Cp - specific heat at constant pressure
ν_d - turbulence coefficient for u and w
ν_q - turbulence coefficient for ξ and q
ν_0 - turbulence coefficient in the non-perturbed medium
$\nabla=(\nabla r\nabla z)^{0.5}$ - analog of mixing length, where ∇r and ∇z are grid lengths in radial and vertical directions, respectively
C_t - constant
r and z - radial and vertical coordinates, respectively and t - time.

Equation (6) with respect to the pressure perturbation is derived from the equations of motion (1) and (2), with the use of the continuity equation (3) The last term in equation (6) represents the local time derivative from the continuity equation, and,in general, should therefore be regarded as equal zero. It is not neglected, however, since in the finite-difference approximation of the continuity equation, the above term may be different from zero.

In equation (9) the turbulence coefficient in the form proposed by Monin (Ref. 6) is used.

The initial perturbation in temperature is given as an instantaneous point source:
with t=0 $\theta(r=150m,z=600m)=2.0^0c$ (13)
The initial perturbation is usually given in the form of a function decreasing with radius and height

(e.g. Ref. 8). However, in such cases the solution depends to some extent on the magnitude of the initial perturbation. If this perturbation is given in the form of a weak instantaneous point source,its magnitude does not affect the result, although the duration of cloud formation is somewhat increased.

Moveable side and upper boundaries are chosen as follows:

$$R(t)=L_R(t/t_{ch})^{\alpha} \text{ and } H(t)=H_z(t/t_{ch})^{\alpha} \qquad (14)$$

Where: $R(t)$ - side boundary, and L_R - the maximum value of the side boundary. $H(t)$ - the upper boundary, and H_z - the maximum value of the upper boundary. t_{ch} - characteristic time, about one hour, α - constant parameter, the value of which depends on the rate of convection development. In the numerical experiments carried out below it was assumed the value of 1/3 or 0.2.

The following boundary conditions were assumed:

$$\begin{aligned}
&w=\partial u/\partial z=\partial\xi/\partial z=\partial q/\partial z=0 \quad \text{for } z=0\\
&\partial u/\partial z=\partial w/\partial z=\partial\xi/\partial z=\partial q/\partial z=0 \quad \text{for } z=H(t)\\
&u=\partial w/\partial r=\partial\xi/\partial r=\partial q/\partial r=0 \quad \text{for } r=0\\
&\partial u/\partial r=\partial w/\partial r=\partial\xi/\partial r=\partial q/\partial r=0 \quad \text{for } r=R(t)
\end{aligned} \qquad (15)$$

The boundary conditions with respect to the gradients of the pressure perturbation can be derived directly from equations (1) and (2).

To solve equations (1), (2), (4) and (5) an explisit, straight-forward numerical computation scheme is applied. To avoid non-linear instability the approximation of the non-linear terms in the above equations is carried out according to the scheme suggested by Bryan (Ref. 1). The computation stability is achieved also by the proper choise of the turbulence coefficient.

Knowing the values of ξ and q, the values of θ and M can be determined from algebraic considerations. After determination of θ and M, the values of M_{CI}, M_T and $\bar{\omega}$ are derived in accordance with the parameterization scheme of Kessler (Ref. 3). No ice-phase is included in the model.To solve equation (6) with respeqt to the pressure perturbation the method of iterations based on Libman's eccelerated relaxation is applied (Ref. 5).

A horizontal grid is employed having a 150 meter step, whereas the vertical grid has a 300 meters step. The time steps are of 10 seconds. The total computational volume comprises of a cylinder with a radius of 5100 meters and 9000 meters height.

Numerical experiments were carrid out for an initial distribution of temperature-$T_0(^0K)$, and relative humidity $F_0(\%)$ given as follows:

$$\begin{aligned}
&-\partial T_0/\partial z=a-bz \ ; \ a=1.2*10^{-2} \ ; \ b=1.6*10^{-6} \ ;\\
&-\partial F_0/\partial z=cz \ ; \ c=4/3*10^{-6} \ ; \\
&\text{for } z=0 : T_o=295.6^0K,\ F_o=85\% \text{ and } P_o=1000\text{mb}.
\end{aligned} \qquad (16)$$

The results of numerical experiments, with the initial conditions (16), show that the computational stability is achieved for values of C_t within 0.95-1.15. Computational instability increases rapidly as more as the value of C_t deviates from the above limits. In these cases it was assumed that $\nu_q=\nu_d$.

3. EXPERIMENTS WITH STEDY-STATE SOLUTIONS

Assuming in equations (4)-(5) that $\bar{\omega}=0$, i.e., by neglecting the terms accounting for sedimentation of cloud droplets, the solution of the system of equations (1)-(9), with initial and boundary conditions given by (13)-(16), leads to a steady-state solution after a certain period of time. Numerical experiments under the assumption of $\bar{\omega}=0$ were carred out. The coefficient C_t was varied within the limits 0.2-1.2, and the the ratio ν_q/ν_d - within the limits of 1-3. For some specific values of these coefficients steady-state solutions were reached after about 35 minutes, however this regime remains only about 3-5 minutes. After about 40 minutes from initiation of conveqtion the solution fluctuates around the steady-state regime, with an amplitude increasing with time.In most cases computational stability is preserved within 55-60 minutes. However fluctuations can not be removed in any case.

Numerical experiments were carried out also by disregarding in equations (1)-(2) the pressure perturbation terms. In these cases as a rule steady-state solutions are reached. A persistant steady-state solution was obtained in two experiments, which is preserved for one hour or more. In one numerical experiment it was assumed that $\nu_q=\nu_d$, and $C_t=1.06$, and in the second experiment: $\nu_q=2.0\nu_d$ and $C_t=0.8$.

The results of these experiments are summarized in table 1.As can be seen from table 1, along the cloud axis the height distributions of vertical velocities and liquid water content remain almost constant during 40-80 minutes.

Steady-state solutions were also tested in case where the turbulence coefficient given as in Smagorinsky (Ref. 7):

$$\nu_d=(C_t\Delta)^2((\partial u/\partial z+\partial w/\partial r)^2+2((\partial u/\partial r)^2+(\partial w/\partial z)^2+(u/r)^2))^{0.5} \qquad (17)$$

In this case the dependence of the solution on the value of C_t was investigated by Hill (Ref.2) and Lipps (Ref.4). It was shown that varying this value within 0.22-0.63 strongly affected the solution.

Numerical experiments were carried out by using expression (17) and varying C_t within the values 0.1-1.0, and the ratio ν_q/ν_d within the values 1-3. In no case a satisfactory persistent steady-state regime, without fluctuations, was reached.

It seems that the demand for a persistent steady-state solution, in case the processes of cloud-droplet sedimentation and pressure perturbation are disregarded, may serve as an additional precondition for the choise of the value of C_t, corresponding to the given initial conditions, as well as for the testing of the stability of the computational scheme. Presumably, the system considered in case the pressure perturbations are accounted for, also should lead to a stedy-state regime. It seems, however, that the computational procedure applied for the solution of the pressure perturbation equation, does not provide the required accuracy. This may lead to the violation of the steady-state regime.

4. EXPERIMENTS IN THE PRESENCE OF STABLE LAYERS

The effect of elevated stable layers on the development of conveqtion is investigated by comparing the steady-state solutions with the inclusion of isothermal layers of 300 meters and 600 meters in depth, located at various heights, in the initial conditions (16).

Results of numerical experiments, with an isothermal layer of 300 meters depth, show that when the layer is located at the height ranges between 300-600 meters, 600-900 meters and 900-1200 meters, respeqtively, conveqtion as a rule develops up to the base of the isothermal layer. Within the isothermal layer conveqtion is weakened, while above this layer downdraft motion is observed. Relatively shallow clouds which occur during 20-25 minutes, are rapidly dissipated and the process is strongly nonstationary.

If the isothermal layer resides above the height of 1200 meters, convection penetrates it and proceeds further up. In all cases mentioned above persistent steady-state solutions are achieved. With the isothermal layer at higher altitudes its influence on the suppression of convection gradually diminishes and when it reaches height of 5100 meters, its presence hardlly afects the convection process at all. In the specific case when the isothermal layer occurs between the surface and the height of 300 meters, convection may develop above this layer, and the process reaches steady-state solution 40 minutes after initiation. However, the convection in this case is considerably less intense as compared with the case when a stable layer is absent. The height distributions of vertical velocities along the cloud axis, under steady-state regime, without the presence of stable layers aloft, and with stable layers at levels 0-300 meters, 1200-1500 meters and 3300-3600 meters, respectively, are presented in figure 1.

A similar qualitative pattern is observed when the depth of the isothermal layer is 600 meters. It was found that if the 600 meter isothermal layer occurs below the 1800 meter level, convection may reach a height of up 3000 meters, and above this level downdraft motion is observed, suppressing the convection. If the isothermal layer is within the altitude range of 1500- 2100 meters the updraft motion may reach a velocity as high as 11 m/sec. The cloud develops within 30 minutes up to an altitude of 3000 meters, and then dissipates within 20 minutes, with downdraft motion occuring in the whole layer.

With an isothermal layer occuring in the altitude range of 1800-2400 meters, or higher, the convection penetrates the isothermal layer and proceeds further. In all these cases the persistent steady-state solutions are reached. All numerical experiments indicate, as can be seen clearly in figure 2, that up to the lower boundary of the stable layer the haight distributions of vertical velocities and liquid water content are almost identical with the case when stable layer is absent. However, above the stable layer the convection is considerably suppressed. It seems that the stable layer affects only the dynamics of the layers above.

In those cases when the isothermical layer occurs in the altitude ranges of 600-900 meters, or 600-1200 meters, convection does not develop at all. For these specific cases numerical experiments were carried out with the aim to test the possible effect of a local and constant surface heat sourse on the enhancement of convection. The surfase heat source is assumed in the form:

$$\theta(r,z=o)= \delta[1-r/R(t)]^3 \qquad (18)$$

Where δ is a coefficient varying within 1.0-10.0. From the numerical experiments caried out it was possible to select the optimum values of δ for which convection may penetrate the isothermal suppressing layers and steady-state regime can be achieved. For an isothermal layer of 300 meters deep the optimal value of δ was founded δ=1.0, whereas for a 600 meter layer the value is δ=5.0. For values of δ below their optimal magnitudes, only relatively weak convection is developing, and after about 30-40 minutes an intensive fluctuation regime prevails, although computation stability is preserved within one howr. If the values of δ exceeds its optimum magnitude, the maximum vertical velocities, similar to those occuring with the optimum δ - value, are reached after 25-30 minutes. The vertical velocities continue to grow steadily until computational instability appears after about 50-60 minutes.

With the optimum value of the δ - coefficient the computation procedure is smooth, intense convection is developing, penetrating the stable layer, and a steady-state regime is reached within 35-40 minutes. It should be mentioned that in this case the steady-state regime is less persistent as compared to the case when a heat source is not present.

The height distribution of vertical velocities along the cloud axis, occuring under steady-state regime, under the influence of a surface heat source, and in the presence of isothermal layers at the heights between 600-900 meters, and 600-1200 meters, are shown in figures 1(e) and 2(d), respectively. As can be seen in these figures, in the presence of a stable layer aloft, but with addition of a surface heat source, convection develops as in the case when no stable layers and heat sources are available. However, in case of a heat source the convection process is slightly more intense.

5. SUMMARY AND CONCLUSIONS

Numerical simulations of thermal convection processes carried out in the present study have shown that if the sedimentation of cloud droplets, as well as pressure perturbations are disregarded, a persistent steady-state solution may be reached after about 35-45 minutes.

The numerical experiments show that in the presence of stable layer aloft, their effect on the process of convection development depends considerablly on the height of the base of the stable layer and its depth.

It is shown that in either case, an isothermal layer with a 300 meters deep and based at 900 meters or below, or with a 600 meters deep and based at 1800 meters or below, convection is completely suppressed above these layers. If an isothermal layer of 300 meters depth occurs above the 900 meter level, or an isothermal layer of 600 meters depth occurs above 1800 meters, then convection may penetrate these layers, and after some time the solution reaches a persistent steady-state regime. In this case the height distribution of the vertical velocities until the base of the stable layer is almost identical with the case when a stable layer is absent. Convection is weakened considerably above the stable layer. The extent of this weakening depends on the height and depth of the stable layer.

Numerical experimevts carried out with a permanently acting local surface heat source and in the presence of a low-based stable layer, 300 meters deep, the convection may penetrate this layer, provided that the surface at the center of the model domain is heated at least by 1^0c. An intense convective cloud develops in this case, the parameters of which appear to be almost identical with the case when no heat source, and suppressing stable layers occur aloft. Similar results are obtained also in the case the stable layer is 600 meters deep, however the surface heat source must give in this case a rise of about 5^0c in its center.

Acknowledgements. This study was supported in part by the Israeli Science Foundation, which is heartily appreciaited. The authors are grateful to Mr. Y.L. Tokatly, Director of the Israel Meteorological Service, for his attention and encouragement

TABLE 1 : Height distribution of vertical velocities - w and liquid water content - M along the cloud axis, 20, 40, and 80 minutes after convection has started for the folowing cases: (a) $C_t=1.06$, $\nu_q/\nu_d=1.0$ and (b) $C_t=0.8$, $\nu_q/\nu_d=2.0$

	(a) $C_t=1.06$ and $\nu_q=\nu_d$						(b) $C_t=0.8$ and $\nu_q=2.0\nu_d$					
Z(m)	w(m/sec)			M(gr/kg)			w(m/sec)			M(gr/kg)		
	20min	40min	80min	20min	40min	80min	20min	40min	80min	20min	40min	80min
300	2.4	2.5	2.5	0.2	0.2	0.2	2.5	2.8	2.8	0.2	0.2	0.2
1800	11.2	11.9	11.8	1.8	1.9	1.9	12.0	12.7	12.5	1.7	1.8	1.8
3300	16.5	18.5	18.4	3.3	3.5	3.5	16.8	19.6	19.4	2.8	3.2	3.2
4800	3.5	17.0	17.0	1.3	4.7	4.7	0.0	18.2	18.1	0.1	4.4	4.4
6300	0.0	-0.1	-0.1	0.0	0.0	0.0	0.0	-0.1	-0.2	0.0	0.0	0.0

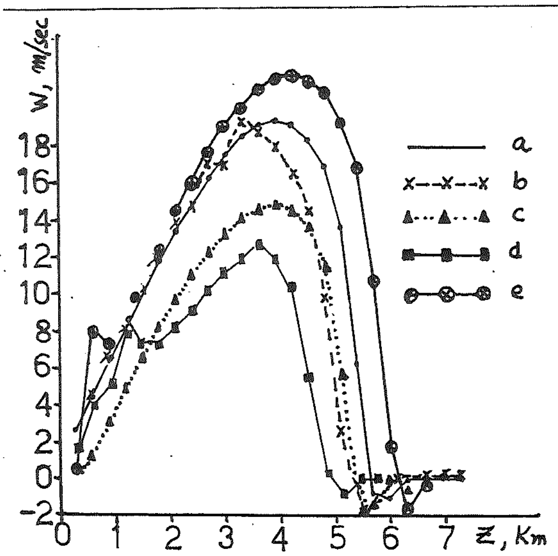

Figure 1. Height distribution of vertical velocities along the cloud axis under steady-state regime for: (a)-In the absence of stable layers aloft, (b)-Isothermal layer within height range of 3300-3600 meters, (c)-Isothermal layer within the 0-300 meters, (d)- Isothermal layer within 1200-1500 meters (E)- With a surface heat source, δ=1.0, and isothermal layer within the level 600-900 meters.

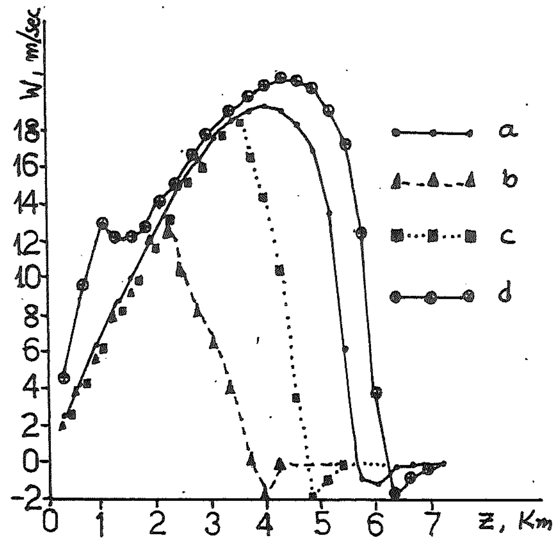

Figure 2. Height distribution of vertical velocities along the cloud axis under steady-state regime for: (a)- In the absence of stable layer aloft, (b)- Isothermal layer within height range of 1800-2400 meters, (c)- Isothermal layer within the 3000-3600 meters, (d)- With a surface heat source, δ=5.0, and an isothermal layer within the level 600-1200 meters.

6. REFERENCES

1. Bryan K 1966 , A scheme for numerical integration of the equations of motion on an irregular grid free of nonlinear instability, Month Weath Rev Vol 94, No1.
2. Hill G E 1974 , Factors controling the size and spacing of cumulus clouds as revaled by numerical experiments, J Atmos Sci 31, 646-673.
3. Kessler E 1969 , On the distribution and continuity of water substance in atmospheric circulations, Meteor Monogr No 32, Amer Meteor Soc.
4. Lipps F B 1977 , A study of turbulence parameterization in a cloud model, J Atmos Sci 34, 1751-1772.
5. Miyakoda K 1962 , Contribution to the numerical weather prediction-computation with finite difference, Japan J of Geophysics Vol 3, No 1.
6. Monin A C and Iaglom A M 1968, Statistical hidromechanics, Izdatelstvo " Nauka " M Vol 2.
7. Smagorinsky J 1983, General circulation experiments with the primitive equations, THe basic experiment, Month Weath Rev Vol 91, 99-164.
8. Soong S T and Ogura Y 1973 , A comparison between axisymmetric and slab-symmetric cumulus cloud models, J Atmos Sci 30, 879-893.

A STUDY OF HEAVY RAIN FORMATION BY USING NUMERICAL SIMULATION OF CLOUDPHYSICAL PROCESSES

Xu Huanbin Wang Siwei
(Academy of Meteorological Science, State Meteorological Administration of China)

1.Introduction

During 4-8th of August 1975 in Henan Province, China,extra-heavy rain occurred. The intensity of rainfall reached 189.5mm/hour;the rainfall during the whole process was 1631.3mm/five days. The question arises as,where did such a large amount of water come from? Of course the water is the product of vapour condensation, but the questions are what are the conditions that lead to the sufficient condensation and the rapid conversion from cloud water to rain, and how the rain passes through the updrafts to fall on the ground with strong intensity.

In study of heavy rain people have already noticed the interaction between the synoptical background and convective activity but we do not think the similar convective systems can give almost the same weather phenomena. Why? Because the factors and the processes which control what weather phenomena have to appear to be are not only the interaction between the background and cloudbody but also the cloudphysical processes in cloud. So that we should research more complex interactions among three aspects——synoptical background,cloudbody or convective system and its interior cloudphysical processes.

In order to study the formation of heavy rain from the point of view of physics of precipitation the following conditions are needed.

1.1 A structure of airflow in cloud that is represented by a framework of airflow or a profile of updraft distribution with height under circumstances of one dimension is not only able to condense a large amount of water but are also able to provide a favourite condition to stimulate the water drops growth through coalescence and multiplication through breakup mechanism. However, the updraft is not able to prevent raindrops from falling down through them. It seems that a"rectangle"profile is appropriate. Besides, we have another requirement, i.e. the height of 0°c level has to be on the upper position to keep the most part of cloudbody standing below it.

1.2 What we need to take into account are the processes of autoconversion of cloud droplets to raindrops,coalescence of raindrops among themselves, collection of cloud water by rain drops and freezing of raindrops. Particularly we should consider the multiplication of raindrops, that is the breakup of raindrops by impaction and natural breakup of raindrops. Moreover, each process operates so thoroughly and cooperates with the other so well, that the cloudbody will have continuous strong rainfall for a long time.

1.3 Solid precipitation particles may play an important role but there are some restraints. For example, when groups of ice particles are melted under 0°c level,the effects of cooling will not destroy the airflow framework of clouds or there is an addition of dynamic convergence. Otherwise the cloudbody will be dispersed.

Of course, a favourable synoptic situation is necessary, for instance, enough moisture, construction and reconstruction of instability, triggering mechanism and appropriate wind field etc.

In fact, the three requirements are of a detailed cloudphysics image of "sustained mechanism", "seeder" and"feeder"as indicated by T.Bergeron(1) in a case of convective rainfall. According to these requirements we have designed a heavy rain model which is described as following.

2.The description of the model

The model is one dimensional and time dependent and it employs parameterization for microphysical processes.The size distributions of liquid raindrops and total drops (which include frozen raindrops and liquid raindrops)are assumed to be exponential as given by

$$NrdD=NroE^{-\Lambda_L D}dD \qquad (1)$$

and

$$NadD=NroE^{-\Lambda D}dD \quad ; \qquad (2)$$

while frozen raindrop size distribution is assumed as

$$NidD=Nro(E^{-\Lambda D}-E^{-\Lambda_L D})dD \qquad (3)$$

and it is shown in figure 1. All the symbols are defined in the table 1. Here Nro, Λ_L and Λ are drop-size distribution parameters.They vary with time and height.Mr.Jiang Zhou-fan proved that the third type of distribution is reasonable in his measurements made in Lushan in 1981. Here we have

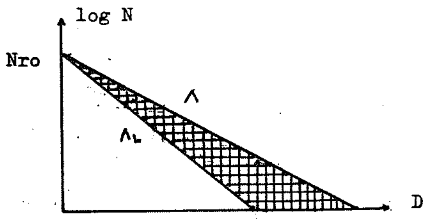

Figure 1.Schematic representation of size distribution of raindrops, frozen raindrops (shaded area) and total precipitation particles

removed the restriction of Nro which is assumed to be a constant at all the time in general parameterization models, therefore it could describe the change of rain drop-size distribution better. The model deals with the following microphysical processes: condensation of water vapour, autoconversion of cloud to rain in terms of specific content, coalescence of cloudwater by rainwater,accretion of cloudwater by frozen rain, accretion of rain by frozen rain, freezing of cloudwater and rain,evaporation of cloudwater and rain. The processes relating to the change of the density of raindrop number are:the autoconversion of cloud droplets to raindrops, coalescence of rain among themselves,accretion of rain by frozen rain, disappearence of raindrops by evaporation, natural raindrops breakup and breakup by impaction.On the basis of assumptions (1)-(3) we have developed all the formulae or equations for every process,which were parameterized.

The model's governing equations are the equations of motion and thermodynamics and equations of continuity for air, water vapour, cloudwater, rain water, frozen rainwater and density of raindrop number.

In this model the dynamic processes and microphysical processes are interacted,therefore under given conditions, the computed profiles of updrafts in cloud are possibly entirely different from the requirements as indicated in the introduction. Thus in order to satisfy these requirements we must adjust the environmental status. For convenience the temperature of environment is adjusted.

It means that the environmental temperature between cloudbody and synoptic background has to change in line with the example computed by the model.

From the statement mentioned above, we can comput the evolution of cloudbody and the change of environment around it. Therefore we may probably research the interaction between the cloudbody and background and seek a cloudphysical approach rather than the methods of statistics and model output statistics to understand the interior relationship between the synoptic situation and phenomena of heavy rain.

All the equations, and the program of adjustment, and the initial and boundary conditions of the model are given in refference(2).

The model run requires approximately 130 minutes CPU time in M-170 (HITAC) and the simulated real time is 88 minutes.

3.Results and discussions

3.1 We have calculated several cases.One of them is with heavy rain. Figure 2-4 displays the results of this case. The total precipitation given by model reaches 120mm within 56 minutes and the average intensity of rainfall is 24mm/10 minutes. The cloudbody remains stable for a long time while the rainfall intensity is approximately 23.4mm/10 minutes or 140mm/hour.

It is heavy rain case indeed,but it is difficult to get. If the parameters controlling the model are not appropriate, the cloudbodys would become either severe thunderstorms or weak cumulus. They would not be stable or would be stable but they would not produce heavy precipitation. It means that in study of heavy rain formation we should not only consider what situations may be reached in the interactions among the three aspects mentioned above but also find in which of these situations the heavy rain can be formed.

3.2 The profiles of updraft in cloud are computed at different times and indicated in figure 3 and so is the position of 0^oc level. It is found that these profiles are similar to a thin "rectangle". The values of updraft speed are less than the terminal velocity of raining and it is much less than in thunderstorm or hailstorm. The requirements as explained in the introduction are satisfied well.

3.3 Although the rainfall intensity is so strong the raindrop in cloudbody still keeps the concentration higher than 1/liter with average diameter of 1-2mm. It means that the mechanism of raindrop generation or multiplication and growth are very efficient and that the cloudbody is in very favourite status to supply enough condensation of vapour and to promote the formation of heavy rain. According to these results we are sure that these requirements are necessary for the formation of heavy rain.

3.4 The evolution of environmental temperature is given in figure 4. When condensation of water vapour occurs the environmental temperature has to increase, thus the buoyancy force decreases and further rise of cloudbody is damped. In other words, in order to satisfy the requirements of a heavy rain the development of cloudbody must be controlled by its own processes. For example, the development of cloudbody may lead to the increase of condensation, then the surplus heat of condensation may be used to heat up, the upper atmosphere while the cold rain and cooling effect caused by evaporation of rain may cool down the air temperature at lower part of atmosphere, and then instability decreases and development damps. It seems that this inhomogeneous heating controls the fashion of the transformation of instability energy into movement which leads to a stable and gentle cloudbody. Only in this case the surplus heat will be able to heat up the environment otherwise the heat will only heat up cloudbody itself; and only when heavy rainfall exists, can the surplus heat be obtained. Therefore we can say the heavy rain cloudbody must be a controlled convective system.

It appears that these ideas are quite similar to those obtained from the simulation of tropical cyclones. But this idea comes from the requirements of heavy rain physics and it has obvious physical significance.

Those results are also rather similar to that illustrated in a case analysis of heavy rain process over western Japan on June 27th, 1972.[3]

3.5 There are many restrictions since the model is one dimension, for example the airflow is illustrated by profile of updraft distribution instead of wind field. Thus the "seeder" and "feeder" have to remain in the same column of cloudbody. We have developed a two dimensional cloud model but we have not used it to investigate this subject. It will be done in the future.

Table 1, List of symbols

Symbol	Description	Units
D	Diameter of hydrometeor	cm
dD	Increment of Diameter	cm
Nr	Number density of raindrop in unit of Diameter and volume	cm^{-3}
Na	Number density of the precipitation particles (included raindrop and frozen raindrop) in unit of diameter and volume	cm^{-3}
Ni	Number density of frozen raindrop in unit of diameter and volume	cm^{-3}
Nro	Constant in parameterization of raindrop size distribution	cm^{-4}
Λ	Parameter in the parameterization of all the precipitation particle size distribution	cm^{-1}
Λ_L	Parameter in the parameterization of raindrop size distribution	cm^{-1}

References

1)Bergeron T., Problems and methods of rainfall investigation, Geoph. Monograph No.5,1960

2)Xu Huanbin and Wang Siwei, Some questions about the formation of heavy rain from the point of view of precipitation microphysics by the method of numerical simulation, Proceedings of Severe Convective Weather Conference, Meteo. Society of China, 1981, Hefai, Meteo. Press, 1983

3)Ninomiys K. and Yamazaki K., Heavy rainfalls associated with frontal depression in Asian subtropical Humid region (2) mesoscale features of precipitation, radar echoes and stratification, J.Meteo.S., Japan, Vol 57 No. 5 1979

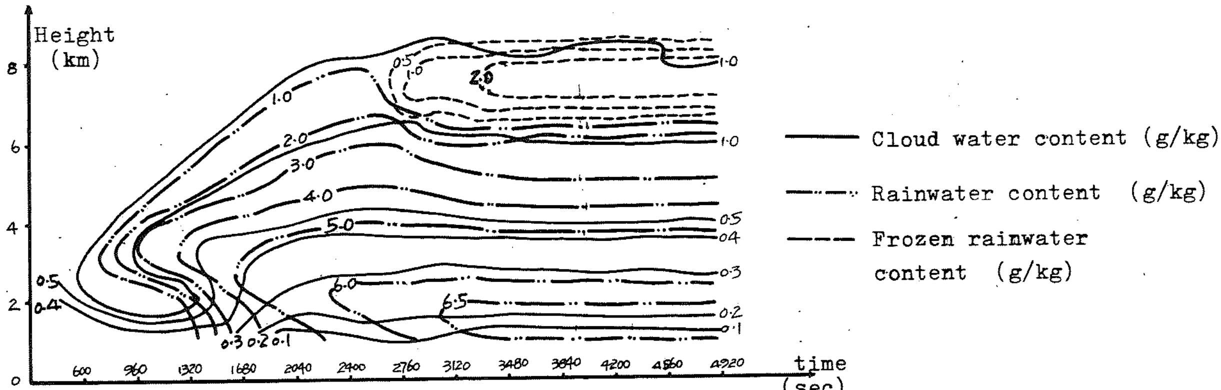

Figure 2. Height-time section of variables in cloudbody

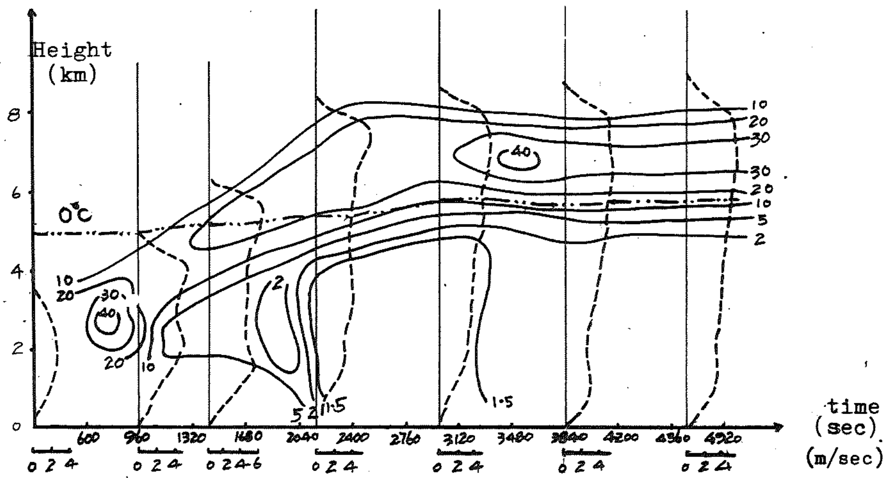

Figure 3. Height—time section of number density of raindrop (1/Litre, solid lines) and profiles of updraft distribution with height at different times (dashed)

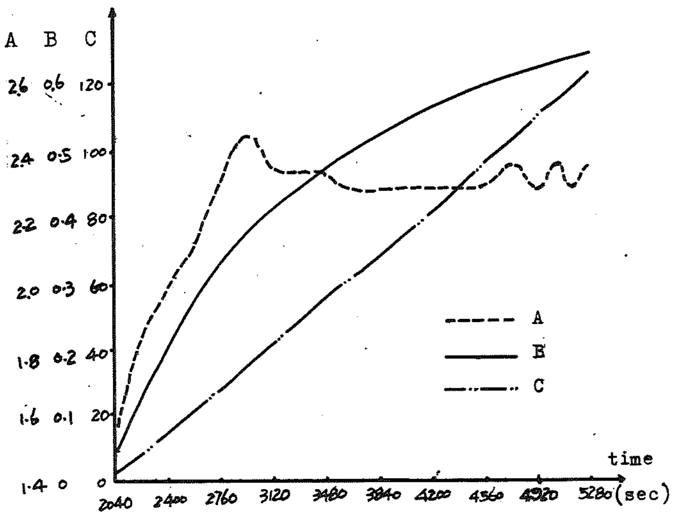

Figure 4 Intensity of rainfall (A, mm/10min.), Efficiency of precipitation(B) and Cumulative precipitation(C) versus time

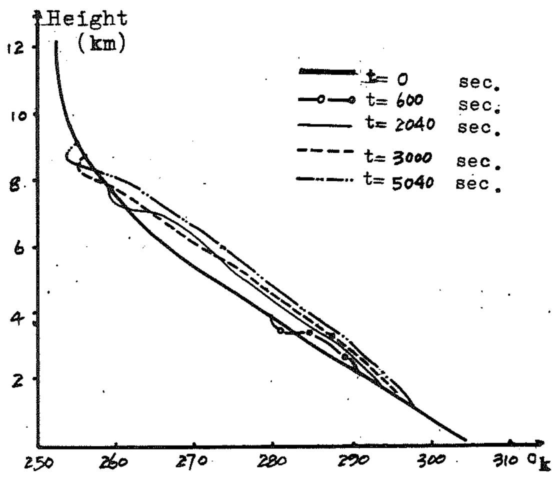

Figure 5 Changs of enviromental temperature at different times and heights

A STUDY ON THE GROWTH OF A POPULATION OF CLOUD DROPLETS BY CONDENSATION IN CUMULUS CLOUDS

Xu Huaying Huang Peiqiang
Huang Meiyuan and Hao Jingfu

Institute of Atmospheric Physics, Academia Sinica
Beijing, China

1. INTRODUCTION

The growth of cloud droplets by condensation is a fundamental process in the physics of cloud. It has been studied by many authors (Refs. 1, 2). In the early studies the parcel model was used. At first they supposed the parcel did not exchange with the circumstance. Since 1960 the rising parcel confused with circumstance has been considered (Refs. 3, 4, 5) and the rate of entrainment is given. In these models the Langrange method is used, so it can only discuss the change of meteorologcal elements and the distribution of cloud droplets spectrum with the rising parcel.

We use the Eular method to establish an one-dimensional time-dependent cylindrical model for the dynamics and thermodynamics of cumulus clouds, the salt particle and droplet range are divided into several classes. Therefore the growth of cloud droplets by condensation in cumulus clouds can be discussed and the evolution of concentrations and spectra of droplet as well as the salt content of particle in each level can be obtained.

2. FUNDAMENTAL EQUATION

An one-dimensional time dependent cylindrical model of cumulus clouds (Ref. 6) is used for studying the growth of cloud droplets by condensation.

The equation of vertical velocity

$$\frac{\partial w}{\partial t} = -w\frac{\partial w}{\partial z} - \frac{2\alpha^2 w}{a}|w| + \frac{2}{a}u_a(w - w_a) + \left(\frac{T_v - T_{ve}}{T_{ve}} - Q_w\right)g \quad (1)$$

The radial velocity can be obtained from the equation of mass continuity

$$\frac{2}{a}u_a + \frac{1}{\rho}\frac{\partial}{\partial z}(\rho w) = 0 \quad (2)$$

The thermal current equation

$$\frac{\partial T}{\partial t} = -w\frac{\partial T}{\partial z} - \Gamma_d w + \frac{2\alpha^2}{a}|w|(T_e - T) + \frac{2}{a}u_a(T - T_a) + \frac{L_v}{C_p}\frac{\delta Q_w}{\delta t} \quad (3)$$

The conservation equation of water vapor

$$\frac{\partial Q_v}{\partial t} = -w\frac{\partial Q_v}{\partial z} + \frac{2\alpha^2}{a}|w|(Q_{ve} - Q_v) + \frac{2}{a}u_a(Q_v - Q_{va}) - \frac{\delta Q_w}{\delta t} \quad (4)$$

The condensation spectra of cloud droplets are formed under a given spectra of salt particles in each levels. The salt particles and droplets range are divided into 102 classes using the exponential form for mass

$$X_I = X_0 \exp[3(I-1)/8.658] \quad (5)$$

where $X_0 = 2.76 \times 10^{-6}$ g is the mass of the smallest particle, I is the number of classes and X_I is the mass of the particle in class I.

The condensation growth equation of the particles with mass X_I is

$$\frac{dx_I}{dt} = \frac{4\pi r_I(S + 1 - A)G_I}{\frac{AL_e^2 M_w}{KRT^2 f_{3\alpha}} + \frac{1}{D\rho_{sw} f_{3\beta}}} \quad (6)$$

$$A = \exp\left(\frac{2\sigma' M_w}{\rho_L' R T r_I}\right)\left(1 + \frac{i m_I M_w}{W\left(\frac{4}{3}\pi r_I^3 \rho_L' - m_I\right)}\right)^{-\rho_L/\rho_L'}$$

The distribution of the number concentration of particles and droplets as well as the salt content of particles change under effected the current of air and can be expressed as

$$\frac{\partial F_I}{\partial t} = -(w - V_L)\frac{\partial F_L}{\partial z} + \frac{2\alpha^2}{a}|w|(-F_L) + \frac{2}{a}u_a(F_L - F_{La}) + \frac{F_L}{\rho}w\frac{\partial \rho}{\partial z} + \left(\frac{\delta F_L}{\delta t}\right)_c \quad (7)$$

$$\frac{\partial M_I}{\partial t} = -(w - V_L)\frac{\partial M_I}{\partial z} + \frac{2\alpha^2}{a}|w|(-M_I) + \frac{2}{a}u_a(M_L - M_{Ia}) + \frac{wM_I}{\rho}\frac{\partial \rho}{\partial z} + \left(\frac{\delta M_I}{\delta t}\right)_c \quad (8)$$

After condensation growth, the number concentration of cloud droplets in each class could be classified into new classes by Kovelz-Olund's (Ref. 7) method.

The water content can be obtained from suming up the particles in all of the classes.

$$Q_w = \frac{1}{\rho} \sum_I f_I x_I$$

Temperature and relative humidity at circumstance as the boundary conditions are given. The initial distribution of salt nuclei used in this model are the spectra of salt nuclei observed by woodcock (Ref. 8) and by us (Ref. 9) over the basin of Xin An River (Fig. 1).

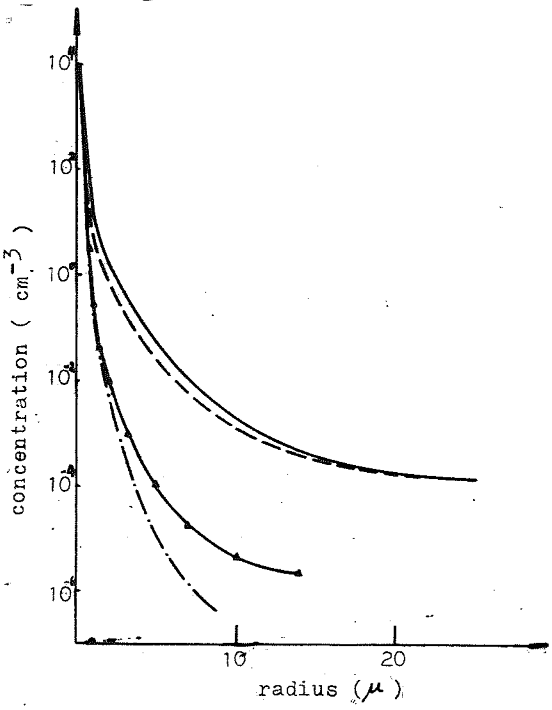

Fig. 1. The initial spectra of salt nuclei I and II are the spectra of salt nuclei observed by woodcock. I at the height of 200-1600m, II at 0-200m, III and IV are observed by us over the basin of Xin An River. III at 200-1600m, IV at 0-200m.

The initial disturbance of updraft and humidity is taken below 2 km. The model domain is 4 km. in the vertical direction with 200m grid interval. The model predicts the evolution of the vertical airflow, the temperature, the water vapor, the cloud liquid, the spectra of cloud droplets and the salt content of particles.

3. THE RESULTS OF CALCULATION

(1) The basic characteristics of the cloud droplets spectrum.

The spectrum of salt nuclei observed by woodcock is used as the fundamental initial condition. The evolution of the concentration of cloud droplets for four kinds of different size at 800m from cloud base is shown in Fig. 2. The concentration of each kind of cloud droplets changes quickly at the first five minutes. But only the concentration of larger droplets ($r > 20\mu$) increases continuously after the fifth minute, at that time the concentration of

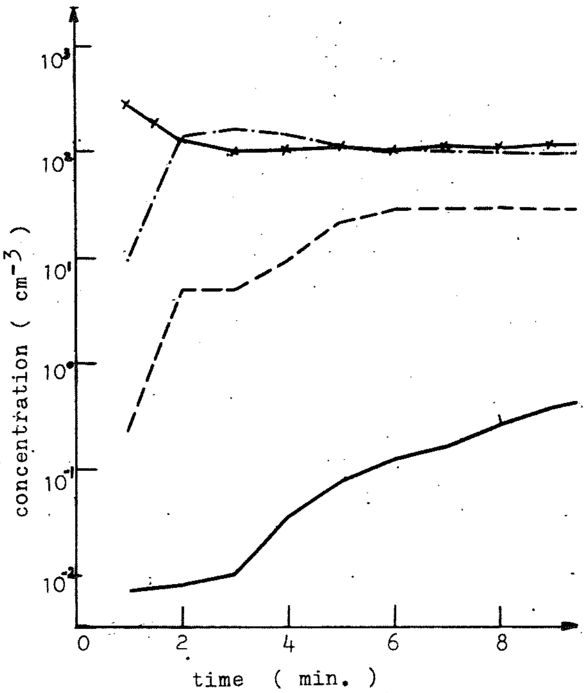

Fig. 2. The evolution of the concentration of cloud droplets for four kinds of different size at 800m from cloud base. $20\mu \le r < 40\mu$(solid line), $10\mu \le r < 20\mu$ (dashed line), $5\mu \le r < 10\mu$(point and dashed line), $1\mu \le r < 5\mu$(fork and dashed line).

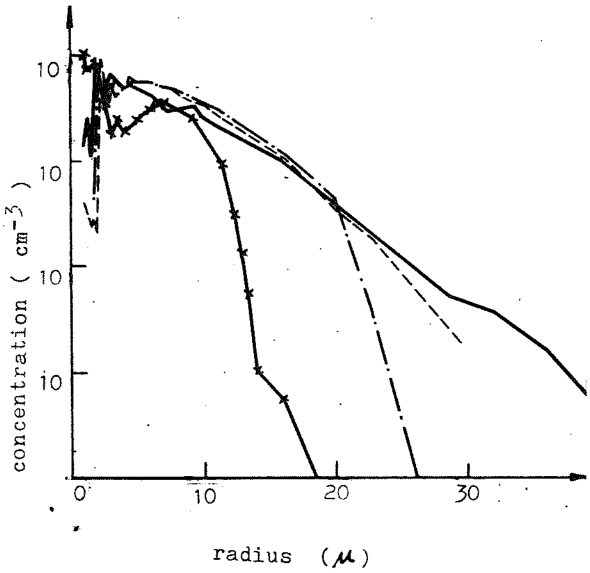

Fig. 3. The spectra of cloud droplets at four heights at the tenth minute. at the height of 400m (solid line), at the height of 800m (dashed line), at the height of 1200m (point and dashed line), at the height of 1600m (fork and dashed line).

small droplets vary constantly. An equable spectrum of cloud droplets is reached after five minutes. The spectra of cloud droplets at the tenth minute are taken to discuss as the equable spectrum.

Fig. 3. is the spectra of cloud droplets at 400m, 800m, 1200m and 1600m at the tenth minute. It can be seen that the concentration of droplets with $r > 1\mu$ at 800m is 249 cm^{-3} . 0.39 cm^{-3} is reached for $r > 20\mu$. The spectra below 1200m are wide, the concentration of cloud droplets larger than 16μ are more than 1 cm^{-3}. It is shown that the larger droplets can be grown in ten minutes by condensation.

(2) The effect of the concentration of salt particle on the formation of large cloud droplets

Three cases with different concentration of salt particle as initial condition are calculated. In first case we use the spectrum of salt particle observed by woodcock as the fundament spectrum, in second case the concentration of salt particle is a half of the fundamental spectrum, the concentration of salt particle in third case is 1/5 of the fundamental spectrum. The result of calculation shows that the concentration of cloud droplets with $r < 20\mu$ grown at the tenth minute by condensation are similar with the initial concentration of salt particles. That is, the largest is the 1 st case, smallest is in 3rd case. But for large droplets ($r > 20\mu$) it is different, in the third case its concentration is the largest (3cm^{-3}), in the second case is 1.4 m^{-3} , and in the first case only 0.5 cm^{-3} . Therefore the smaller concentration of salt particles is more favorable for the formation of large droplets by condensation.

(3) The effect of giant salt nuclei on the formation of large cloud droplets

To discuss the role of giant salt nuclei, we cut off the particle larger than 2.5μ in initial spectrum of salt particles. Calculations show that the spectrum of cloud droplets at 800m after ten minutes is the same as that growth from the fundamental spectrum. From this point out that the salt particle larger than 2.5μ only slightly influences the equable spectrum of condensation. In the case of initial nuclei spectrum without particles of $r > 2.5\mu$, the large cloud droplets of $r > 20\mu$ never appear until at the fourth minute, but in the case of spectrum with particles of $r > 2.5\mu$, the large droplets occur at the 1st min. of condensation. So the giant salt nuclei can promote to produce large droplets ahead of time.

If we cut off the nuclei larger than 1.5μ in the fundamental spectrum, it can be seen from table 1 that the droplets larger than 10μ do not appear by condensation even at the tenth minute. This is saying that the salt nuclei with radii of 1.5μ -2.5μ (their mass is about 10^{-11} gm) play an impartant role in the formation of large cloud droplets.

The salt nuclei observed over the basin of Xin An river(Ref. 9) is also used to calculate the growth of cloud droplets by condensation. In which the concentration of giant salt nuclei is two orders of magnitude smaller than that observed by woodcock. Calculation shows that the large cloud droplets do not appear in first five minutes, but the spectrum of cloud droplets at the 7th minute is wider than the spectrum calculated in the case of initial nuclei spectrum observed by woodcock.

Table 1
The concentration of cloud droplets and water content at 800m at the tenth minute

radii of cloud droplets (μ) / spectra of salt nuclei	concentration of cloud droplets (cm^{-3}) 1 - 5	5 - 10	10 - 20	20 - 40	water content Q_w (g/kg)
fundamental spectrum (fs)	109	108	32	0.39	0.51
same as fs but without nuclei of $r > 2.5\mu$	106	104	30	0.59	0.50
same as fs but without nuclei of $r > 1.5\mu$	56	0.1	0	0	0.09
concentration only 1/2 of fs	41	62	33	0.1	0.50
concentration only 1/5 of fs	9	20	24	2.3	0.45
$\alpha=1$ without leteral entrainment	0	2.16	0.69	2.50	0.24
$\alpha=0.7$ with lateral e ntrainment	87	121	47	2.38	0.77

Therefore less concentration of giant salt nuclei is more favorable to produce large droplets with $r > 20\mu$. Maybe the concentration of 10^{-3} cm^{-3} observed over the basin of Xin An River is suitable.

(4) The effect of turbulent exchange and entrainment on the equable spectrum of condensation

In Fig. 4. there are three spectra of cloud droplets grown after ten minutes at 800m. The point line shows the spectrum of droplets in the case of nuclei comming from cloud base and without entrainment around the cloud. In this case a bimodal spectrum is formed, the concentration of large droplets reaches 4 cm^{-3} which is larger than that in the case of with entrainment.

The dashed line shows the condition of the weak turbulent exchange (α =0.7). It can be seen that the droplets spectrum in case of α =0.7 is markedly wider than that in case of α =1.0 (solid line). so turbulent exchange can effect significantly the equable spectrum of condensation.

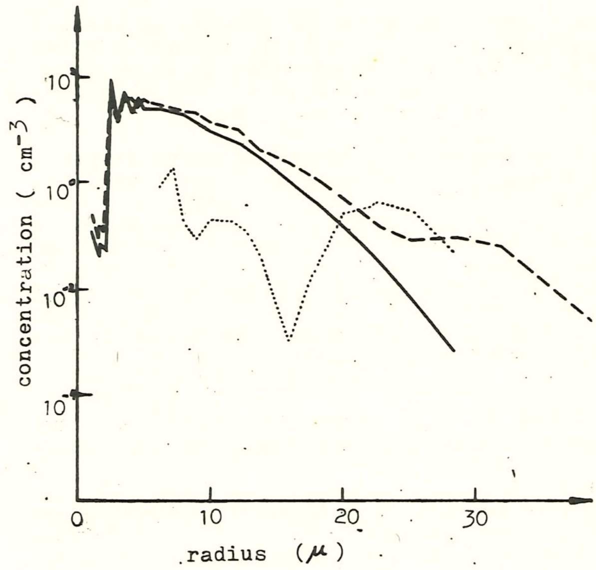

Fig. 4. The spectra of cloud droplets with different turbulent exchange and entrainment (at 800m at the tenth minute using fundamantal nuclei spectrum), the fundamental case (solid line), without entrainment (point line), weak turbulence (dashed line).

4. SUMMARY OF CONCLUSIONS

An one-dimensional time-dependent cloud model has been used to investigate the problems concerning condensation growth of a population of cloud droplets. The results from this study are summarized as following.

1. The giant salt nuclei with radii 1.5-2.5μ play an important role in the formation of large droplets by condensation. The existence of nuclei larger than 2.5μ only slightly influences the equable spectrum of condensation, but it can promote to produce large droplets ahead of time.

2. The extra large concentration of condensation nuclei is not favorable to produce large cloud droplets. And the concentration of 10^{-3} cm^{-3} for giant salt nuclei with radii 1.5 - 2.5μ is suitable.

3. The equable spectra of condensation may be wide, they are significantly influenced by entrainment and turbulent exchange between in cloud and out of cloud. The bimodal spectrum of droplets can appear in some conditions.

4. The effect of different spectra of salt nuclei on dynamics and themodynamics is very slight.

5. REFERENCES

1. Mordy, W., Tellus, 11, 16 - 44, 1959.
2. Fitzgerald, J. Atmos. Sci., 31, 1358 — 1367, 1974.
3. Mason, B. J. and Chien, C. W., Q. J. R. met. soc., 88, 136 —142, 1962.
4. Warner, J., J. Atmos. Sci., 30, 256 -261, 1973.
5. Lee In-young and Pruppacher, H. R., Pure Appl. Geophys., 115, 523-545, 1977.
6. Takahashi, T., J. Atmos. Sci., 30, 262-277, 1973.
7. Takahashi, T., J. Atmos. Sci., 33, 269-286, 1976.
8. Woodcock. A. H., J. Geophys. Res., 77, 5316-5321, 1972.
9. Huang Meiyuan, He Zhenzhen and Shen Zhilai, Scientia Atmospherica Sinica, 6, 301-307, 1982.

M.K. Yau and S. MacPherson

Department of Meteorology, McGill University, Montreal, Canada

1. INTRODUCTION

Radar analysis and hailstone trajectory calculation of hailstorms in Alberta have been reported by a number of authors (e.g., Chisolm and English, 1973; Marwitz, 1972a, b, c). These studies have yielded a wealth of information on the morphology, air flow patterns, and hailstone growth mechanism in these storms. With the advent of powerful computers, it is now possible to model explicitly the storm dynamical and microphysical processes (Orville and Kopp, 1977). It would be of interest to compare the results of the numerical simulations to those from data analysis. A more complete picture of the underlying mechanism of this violent phenomenon is expected to emerge from such an approach.

The purpose of this paper is to present some results of our first effort in the numerical modeling of an Alberta hailstorm. A simple ice phase microphysical parameterization scheme will be briefly described. The scheme has been incorporated into a convective cloud-scale model to simulate a hailstorm cell occurring on June 26, 1967. Results of comparison between observation and simulation will be highlighted.

2. DESCRIPTION OF THE MODEL

2.1. General

The three-dimensional cloud model is an outgrowth of the one developed by Steiner (1973). Warm rain processes have since been added and the model has been applied to different convective situations in the tropics (Turpeinen and Yau, 1981; Turpeinen, 1982) and the mid-latitudes (Yau and Michaud, 1982). Since the details and governing equations are described in the above references, only a brief summary of the major features is attempted here.

The model is based on the deep anelastic system of equations. A first order turbulence closure scheme which includes both the effects of deformation and buoyancy is included. For the present simulation, convection is initiated by a humidity impulse and the storm develops in a domain with periodic lateral boundary conditions but rigid and free-slip top and bottom surfaces.

2.2. The microphysical processes

A "bulk water" technique is used to treat the microphysics. Water substances are divided into five categories: vapor, cloud water, rain water, ice crystals/snow, and graupel/hail. The major processes are summarized in Fig. 1 and the abbreviation are defined as:

AC - Autoconversion of cloud to rain

CC - Collection of cloud by rain

CONTH - Initiation of graupel through raindrop freezing by contact with ice crystals

CONV - Conversion of ice particles to graupel

DEP(H) - Growth by vapor deposition for ice particles (graupel)

EVPC, EVPR - Evaporation of cloud water and evaporation of rain water,

GLAC - Glaciation of cloud water at temperature ≤ -35°C

HCOL - Rain accretion by graupel

MELT(H) - Melting of ice particles into cloud or rain water (melting of graupel into rain water)

NUCLEA - Nucleation of individual ice crystals from the vapor

PIFR - Initiation of graupel through Bigg's heterogeneous freezing of raindrops

RIM(H) - Riming of ice particles (graupel)

SUB(H) - Sublimation of ice particles (graupel)

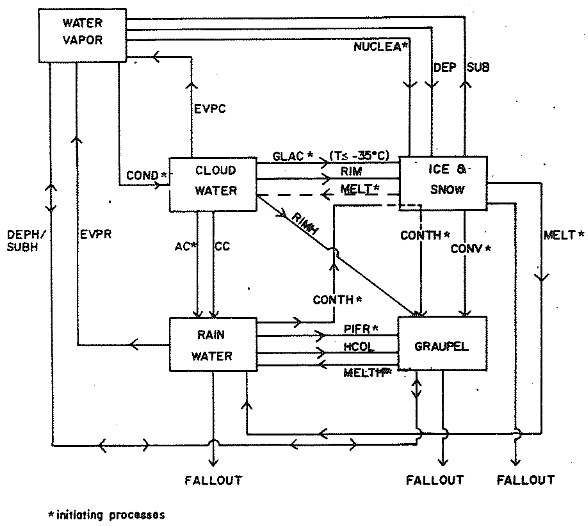

Fig. 1 The microphysical processes

The warm rain processes are modeled after the well-known scheme of Kessler (1969). For the ice processes, it is assumed that single ice crystals are initiated by nucleation from the vapor in the manner after Koenig and Murray (1976). Nucleation occurs when the air is saturated with respect to water and the temperature is below 0°C or when the air is saturated with respect to ice and the temperature below -12°C. Fletcher's curve is used to yield N_n, the maximum number of ice nuclei per gram of air activated as a function of supercooling. If there are already N_i ice crystals per gram of air present at a point, only the excess of N_n over N_i will be nucleated. The nucleated crystals are assumed to be monodisperse particles with a mass of 10^{-11} g (equivalent to an ice sphere of 3 μm radius).

Since the present method employs only one equation to treat single ice crystals and snowflakes a criteria must be chosen to distinguish between these two entities. Given an ice content q_i at a point, the scheme first assumed that it is composed of monodisperse crystals, whose mass m_i is calculated from the ratio of the ice content to the maximum number of ice crystals per gram of air (N_n) with a lower limit of 10^{-11} g, i.e.

$$m_i = \begin{cases} q_i/N_n & \text{for } q_i/N_n > 10^{-11} \text{ g} \\ 10^{-11} \text{ g}, & \text{otherwise} \end{cases}$$

If m_i turns out to be larger than a specified threshold value of 1.4×10^{-5} g (equivalent to an ice sphere of about 200 μm in size), then aggregation is assumed to have occurred and the ice content is now composed of snowflakes whose size is distributed exponentially.

For single crystals, the total deposition and sublimation rate are given by

$$DEP = [a_1 m_i^{a_2} (\frac{q_v - q_{si}}{q_{vs} - q_{si}})] N_i, \text{ if } q_v > q_{si}$$

$$SUB = -[a_1 m_i^{a_2} (\frac{q_v - q_{si}}{q_{vs} - q_{si}})] N_i, \text{ if } q_v < q_{si}$$

The term enclosed by the square brackets represents the deposition/sublimation rate of a single crystal taken from Koenig (1971). Here a_1 and a_2 are functions of temperature, q_{vs} and q_{si} are the saturation mixing ratio over water and ice respectively.

The total riming rate for single crystals is

$$RIM = \frac{\Pi D_m^2}{4} V_i (D_m) N_i E_i \rho_a q_i$$

where D_m is the melted diameter calculated from the mass of the ice crystal by assuming a bulk density of 0.5 g cm^{-3}, V_i is the crystal terminal fall speed from Langleben (1954), and E_i the collection efficiency is assumed a value of unity.

In the case of snowflakes with a size distributed as

$$N_i (D_m) = N_{oi} e^{-\lambda_i D_m}$$

The intercept N_{oi} and slope λ_i can be related to the snow content by using a relation between snowfall rate R_i and snow content given by Sehon and Srivastava (1970). Using

$$\rho_a q_i = 2.07 \times 10^{-3} R_i^{0.86} [R_i \text{ in mm hr}^{-1}]$$

it turns out that

$$N_{oi} = 2.45 \times 10^{-9} (\rho_a q_i)^{-1.09}$$

$$\lambda_i = 9.4 \times 10^{-3} (\rho_a q_i)^{-0.522}$$

The deposition/sublimation and riming rates for the exponential spectrum in terms of N_{oi} and λ_i are

$$DEP = a_1 (\frac{\Pi}{6} \rho w)^{a_2} \frac{N_{oi} \Gamma(3a_2 + 1)}{\rho a \lambda_i^{(3a_2 + 1)}} (\frac{q_v - q_{si}}{q_{vs} - q_{si}})$$

$$RIM = (\frac{\Pi}{4} a) (\frac{\rho w}{\rho_i})^{2/3} \frac{N_{oi} \Gamma(3 + b)}{\lambda i^{(3 + b)}} q_c$$

Where ρw is the density of water, a and b are constants in the expression for the terminal fallspeed of ice particles, and ρ_i is the density of ice.

When the temperature is warmer than 0°C, the entire ice crystal/snow content is melted instantaneously into either cloud droplets or raindrops, depending on the melted median volume diameter D_{oi}. If $D_{oi} < 200$ μm, then the ice is melted into cloud water. Otherwise, the rain category receives the melted ice.

If the temperature is below -35°C at a certain point, then all the cloud water at this point is isobarically frozen and the ice/snow content, water vapor mixing ratio, and temperature are isobarically adjusted to ice saturation using a process similar to that given in Stephens (1979) with minor modifications. Graupel particles are assumed to be distributed exponentially in size and the total number of particles in the spectrum is given by a constant value of 10^{-4}cm^{-3}. The graupel content at a point can be initiated by raindrop freezing (both contact and Bigg's freezing) and conversion from the ice/snow category. The expression for Bigg's freezing is taken from Orville and Kopp (1977). The entire ice/snow content at a point is transferred to graupel when the ice/snow median volume diameter exceeds a specified conversion threshold of 800 μm in diameter.

Once graupel is initiated at a point, the mean mass ($\bar{m}$) of the distribution is computed. This information is used to determine the type of graupel present. For $\bar{m} < 10^{-3}$g, the distribution is assumed to make up of small, light graupel particles of low density (0.1 g cm^{-3}). For $10^{-3} < \bar{m} < 2 \times 10^{-2}$, "heavy graupel" is assumed with a density of 0.6 g cm^{-3}. For $\bar{m} > 2 \times 10^{-2}$ g, the particle density is increased to 0.9 g cm^{-3} to model hailstones. After the type of graupel has been determined, the slope parameters are then calculated using the appropriate particle density along with the graupel content. The various rates and parameters used to determine the development of the graupel distribution are then computed after the expressions given in Stephens.

3. RESULTS

A 32 x 32 x 24 grid mesh was used. The grid lengths in the horizontal and vertical directions were 1 km and 0.5 km respectively. The model was initiated with a sounding from Penhold (Fig. 2), which lies approximately 70 km from the storm. Due to uncertainties in upper air data above 350 mb, information from a sounding at Edmonton, 206 km away, was used to obtain the temperature profile above this level. The environmental wind relative to the storm was rather weak. A mid-level "jet" in the u component occurred between 2 and 5 km.

Fig. 3 depicts the radar structure and air flow patterns of the simulated storm at 21, 31, and 46 minutes after initialization. The vertical sections represent the plane of maximum updraft velocity and the different times correspond roughly to the growing, maturing, and decaying stages of the hailstorm cell.

During the growing stage two major currents fed into the storm: an inflow of warm surface air from

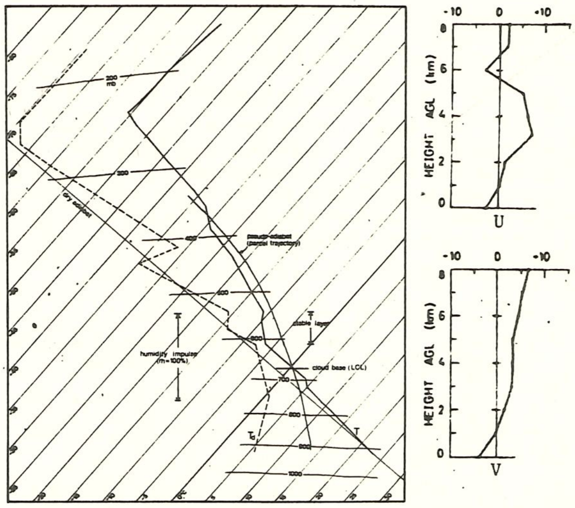

Fig. 2 Sounding from Penhold on June 27, 1967 (1617 M.S.T.) and wind relative to storm in m s^{-1}.

the southeast and a mid-level current from west-northwest. A slightly tilted updraft developed and a precipitation overhand emerged on the east side as a result of advection of condensate by the westerly flow over the region of surface inflow.

The top of the storm was just below the tropopause at the mature stage. Fallout of rain and graupel extended the reflectivity to the surface.

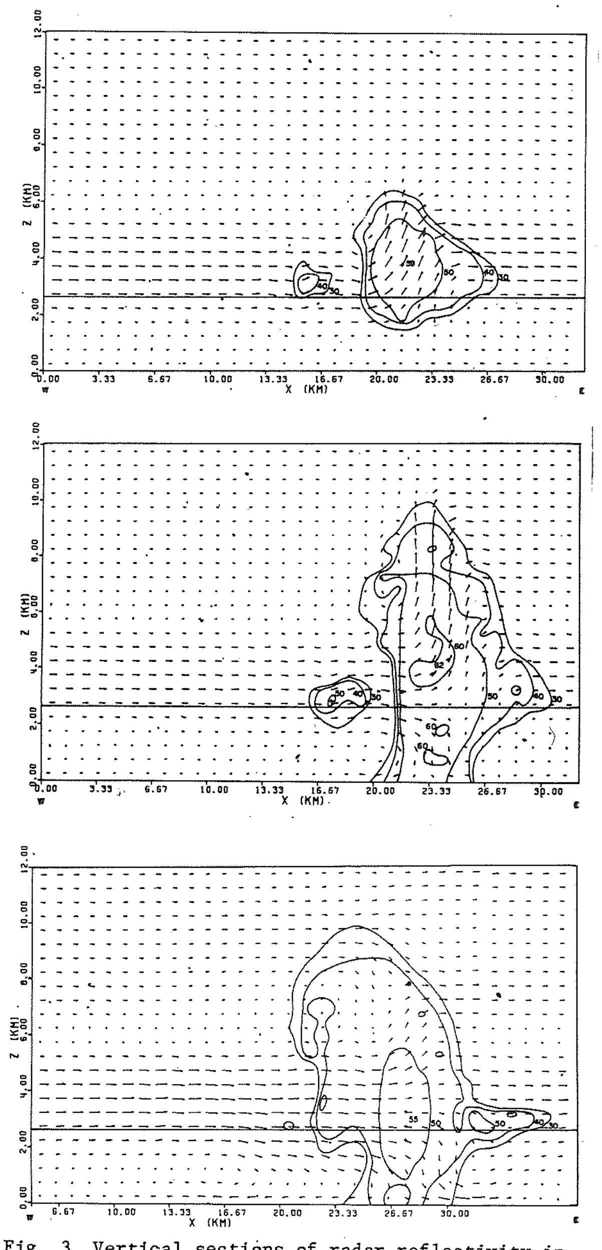

Fig. 3. Vertical sections of radar reflectivity in dBz and vector velocity at 21 min (top), 31 min (center), and 46 min (bottom). The magnitude of the longest arrow in the three panels are 7.7,13.0, and 7.9 ms^{-1} respectively.

The radar overhang became more evident and the gradient of reflectivity was steep on the west flank. The region of maximum updraft was located near the upper portion of the storm where a weak divergent flow also occurred. Below the 0°C isotherm, a downdraft developed and began to cut off the inflow near the surface. The storm was sustained mainly by the mid-level flow.

During the dissipating stage, the outflow near the ground spreaded out from all sides of the storm. Sinking motion occurred also in the upper portion. Although the reflectivity pattern remained erect, the storm continued its decline.

To gain insight into the microphysical processes in operation, the budgets for water substances are plotted in Fig. 4. Most of the ice processes were inactive before 10 min. Condensation (SCOND) and evaporation (SEVPC) regulated the production of cloud water (SCLD*). The storm broke through the relatively stable layer around 10 min and nucleation (SNUCLEA) increased substantially at altitudes between 3 to 4 km. The ice/snow content (SSNOW*) grew mainly by deposition (SDEP) and riming (SRIM) with some removal by melting (SMELT) and sublimation (SSUB). The continual growth of ice/snow led to their conversion (SCONV) to graupel particles (SHAIL*) around 13 min in the region of maximum cloud water.content near the center of the storm. Rain (SRAIN*) was initiated through autoconversion, but depleted by contact freezing (SCONTH) and collection by graupel (SHCOL) above the 0°C isotherm and by evaporation (SEVPR) below the cloud base.

By 25 min the storm has penetrated the -35°C level. Glaciation of the upper part of the storm occurred resulting in an increase in ice/snow content and a corresponding decrease in cloud water. Near the surface, rain (RCUM) and graupel (RCUMH) have arrived. The surface rainfall originated mainly from the melting of graupel (SMELTH).

The intensity of the storm started to diminish after 31 min. By 40 min, all forms of condensate were being depleted at a rate faster than the production. Evaporation, riming, glaciation and the ceasing of condensation continued to decrease the total cloud water. Melting of graupel still provided a source for rain but its removal was fast by evaporation and fallout. Nucleation has terminated, depositional growth of ice/snow is outweighed by conversion, sublimation and melting. Depletion of graupel through melting and fallout continued.

Chisholm (1970) analysed in detail one of the cells of this multicell hailstorm. Comparison of the results of the simulation and analysis indicated a fair amount of similarity in terms of the dimension and storm characteristics, the radar reflectivity structures, as well as the mode of development and motion of the storm. The model simulated well the radar overhang. The computed maximum updraft speed of 14.4 m s^{-1} agrees with the value of 16.4 ms^{-1} calculated from a loaded moist adiabatic model. However, the calculation indicates the absence of a weak echo region which might be present in the observation. Furthermore, the maximum median volume diameter of the hailstone calculated from the hail content (0.2 cm) is smaller than the reported maximum hailstone size of about 2 cm.

REFERENCES

Chisholm, A.J., and M. English, 1973: Meteor.Monogr.No. 14,Am. Meteor. Soc., 98 pp; Chisholm, A.J. 1970: Ph.D. thesis, Dept. of Meteor., McGill Univ., 237 pp; Kessler, E., 1969: Meteor. Monogr. No. 32, Am. Meteor.Soc., 84pp; Koenig, L.R., 1971: J. Atmos. Sci., 28, 226-237; Koenig, L.R., and F.W. Murray, 1976: J. Appl. Meteor., 15, 747-762; Langleben, M.P., 1954: Q.J.R.M.S., 80, 174-181; Marwitz, J.D., 1972 a,b,c: J. Appl. Meteor., 1,166-179, 180-188, 189-201; Orville, H.D., and F.J. Kopp, 1977: J. Atmos. Sci., 34, 1596-1618; Sekhon, R.S., and R.C. Srivastava, 1970: J. Atmos. Sci., 27, 299-307; Steiner, J.T., 1973: J. Atmos. Sci., 30, 414-435; Stephens, M.A., 1979: Atmos. Sci. Paper No. 319, Dept. of Atmos. Sci., Colorado State Univ., 122 pp; Turpeinen, O., and M.K. Yau 1981: Mon. Wea. Rev.,109,1495-1511; Turpeinen, O., 1982: Mon. Wea. Rev., 110, 1238-1254;Yau, M.K., and R.Michaud, 1982: J. Atmos. Sci., 39, 1062-1079.

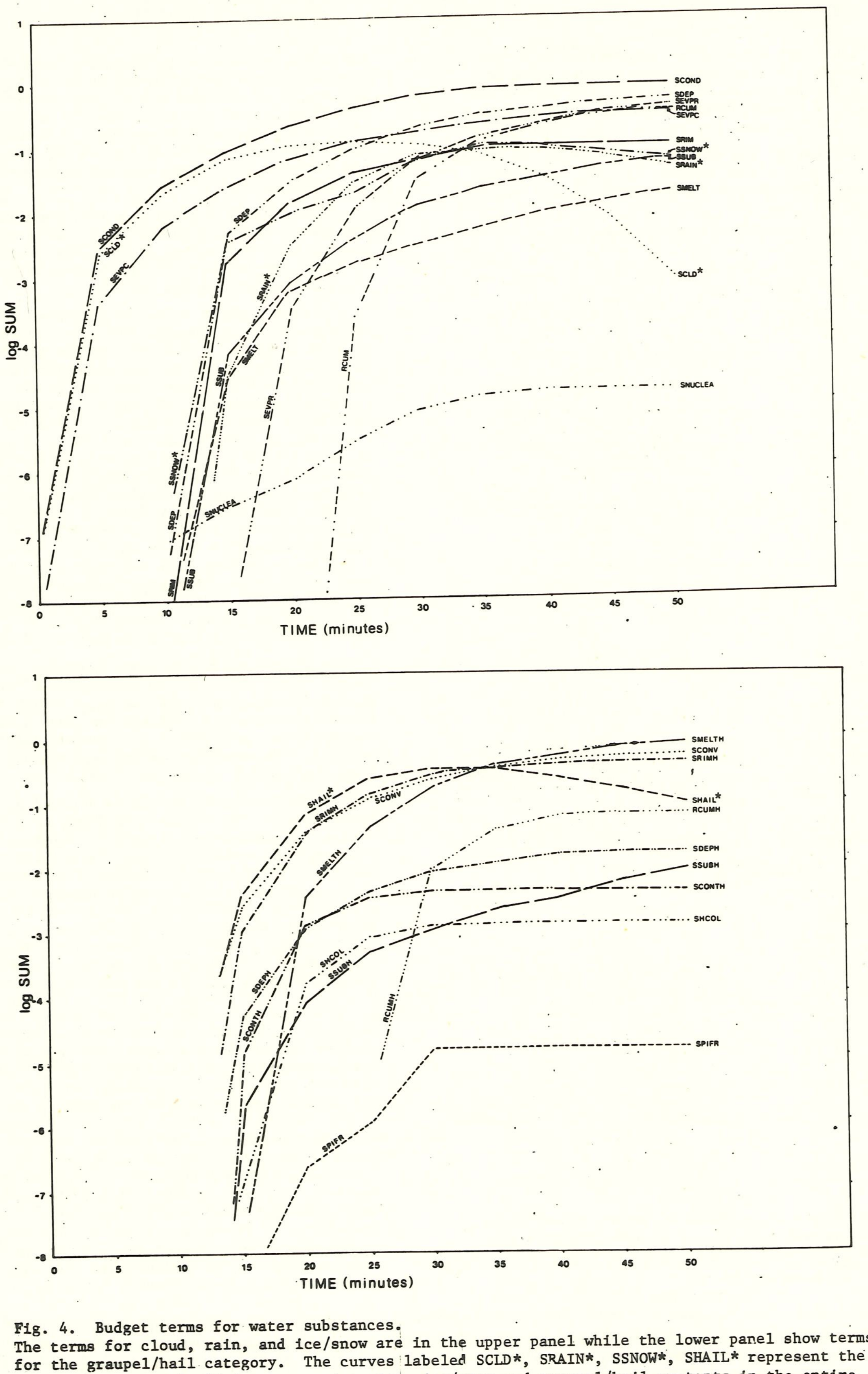

Fig. 4. Budget terms for water substances.
The terms for cloud, rain, and ice/snow are in the upper panel while the lower panel show terms for the graupel/hail category. The curves labeled SCLD*, SRAIN*, SSNOW*, SHAIL* represent the instantaneous total cloud water, rain water, ice/snow and graupel/hail contents in the entire domain. RCUM and RCUMH are the cumulative fallout of rain and graupel/hail. The remaining curves preceded by a letter S represent the cumulative sums of the various source/sink processes depicted in Fig. 1.

SESSION V

NUMERICAL SIMULATION OF CLOUD FORMATION PROCESSES

Subsession V-3

Orographic, stratiform and frontal clouds

NUMERICAL SIMULATION OF NATURAL EVOLUTION AND SEEDED PRECIPITATION FORMATION IN STRATIFORM CLOUDS

V.P. Bakhanov and A.A. Manjara

Ukrainian Scientific Research Institute, Kiev, USSR

1. MODEL DESCRIPTION

The purpose of the present investigation is a simulation of the seeded precipitation formation in supercooled stratiform clouds (SC). A time-dependent, two-dimensional microphysical model has been developed to calculate the fields of thermodynamical and microphysical characteristics of SC (Refs. 1, 2). Here this model is briefly described. The basis of a model is a system of equations for water vapor content (q) and temperature (T) transfer, cloud drop size and crystal size distributions (f_1 and f_2). The advection, updraft, horizontal and vertical turbulent diffusion, particle sedimentation, growth (evaporation) by deposition, coalescence of crystals with drops were taken into consideration. The motion field and turbulent characteristics are known in this model. The parametrization of droplet nucleation is used. The model is one-dimensional, if we consider the formation and natural evolution of supercooled SC (CNE-model). Under further consideration of an artificial crystallization spreading and seeded precipitation formation a model is two-dimensional (ACS-model). The dry ice seeding is simulated by introducing one or two instantaneous plane sources of ice nuclei.

In the model many cloud characteristics are calculated besides T, q, f_1, f_2. They are: supersaturation in respect of water (Δ_1) and ice (Δ_2), concentration of droplets (n_1) and ice crystals (n_2), liquid water and ice content (q_{L1} and q_{L2}), visibility (L), solid precipitation rate on the ground (j), precipitation amount (q_j) etc. An analysis was carried out in the coordinate system which moved with an average (for a cloud layer) wind velocity. The region of integration is a horizontal band with boundaries at heights z = 0 and z = 6 km (the grid spacing is Δz = 0.2 km). The variable spacing Δx (x is parallel to wind) and variable lateral boundary conditions have been used. The initial spacing Δx = 0.1-0.4 km and the initial width of the integration region equals 1.3 - 7.6 km. Subsequently Δx increases and a final integration region width sometimes equals 20 km. Variable values of the investigated functions on lateral boundaries were calculated with the aid of CNE-model. A more detailed model description was given in Refs. 1, 2.

2. NATURAL EVOLUTION OF SUPERCOOLED STRATIFORM CLOUDS

In this section we shall consider some numerical experiments with the next fixed parameters: CCN concentration $N_m = 0.5 \cdot 10^6$ g^{-1}, temperature on the ground T_o = +1 °C, initial humidity and humidity on the ground, q_{ro} = 80 %, initial temperature stratification gradient $\gamma_o = 0.6 \cdot 10^{-4}$ grad.cm^{-1}, vertical coefficient of eddy diffusion k_z = 5 m^2 s^{-1}. The updraft region has boundaries at z_1 = 975 m, z_2 = = 1425 m, the vertical velocity profile has a maximum value w_m.

As calculations show the time to initial condensation t_c is a very strong function of parameter w_m (for w_m = 5 cm s^{-1} t_c = = 9 h after model initiation, for w_m = = 2 cm s^{-1} - t_c = 26.9 h, for w_m = 1 cm s^{-1} - t_c = 65.5 h). Thus there is a minimum updraft velocity for supercooled SC forming. The calculated cloud thickness for some w_m values is depicted in Fig. 1. The criterion q_{l1} = 0.01 gm^{-3} is our definition of a cloud boundary. This definition explains a long time between t_c and timing to the first water content for small w_m. The dashed curves were obtained in that way. The maximum vertical velocity w_{m1} = 5 cm s^{-1} was fixed from t = 0 to t_{01} = 14 h. At t_{01} = 14 h w_{m1} was changed to w_{m2} and then CNE-calculations were continued for some time.

Characteristics of the calculated cloud for t_{01} = 14 h are: thickness $\Delta H \approx 700$ m, average liquid water content q_{l1} = 0.11 g m^{-3}, total mass of liquid water in the cloud layer Q_w = 75 g m^{-2}, cloud base temperature T_1 = -5.4 °C, cloud top temperature T_2 = = -9.3 °C. There is undersaturation ($\Delta_1 < 0$) in the lower third of this cloud. Fig. 1 shows that the subsequent evolution of this cloud is determined by value w_{m2}. The cloud

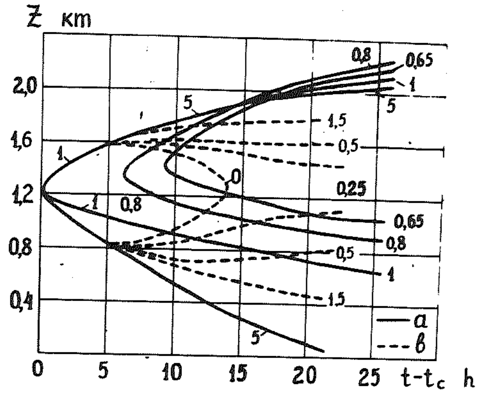

Figure 1. Cloud thickness as a function of time for different values of w_m. For a - w_m = Const (indicated near curves (in cm s^{-1})). For b - w_{m1} = 5 cm s^{-1} till t_{01} = = 14 h. At the time t_{01} = 14 h ($t_{01} - t_c$ = = 5 h) w_{m1} was changed to w_{m2} (indicated near curves).

continues to grow, if $w_{m2} >$ 0.5 - 0.6 cm s^{-1}. The cloud thickness is changed very little, if $w_{m2} \approx$ 0.5 - 0.6 cm s^{-1} (a steady-state cloud) and the cloud dissipates, if $w_{m2} <$ 0.5 cm s^{-1}. The considered cloud dissipates in 9 h for w_{m2} = 0, in 1-2 h for $w_{m2} < -2$ cm s^{-1} (Fig. 2). From Fig. 2 it is seen that a cloud stratification arises for $w_{m2} < -2$ cm s^{-1}. This stratification is explained by the inhomogeneous undersaturation profile.

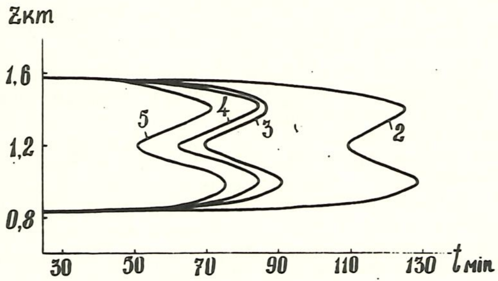

Fig. 2. The cloud evolution after the down-current starting. The absolute values of w_{m2} (cm s^{-1}) are near curves.

3. SIMULATION OF CRYSTALLIZATION KINETICS AND SEEDED PRECIPITATION FORMATION IN SUPERCOOLED STRATIFORM CLOUDS

3.1. Crystallization kinetics after single line seeding

The model described in the first section was used to carry out a great number of ACS calculations in supercooled clouds after the dry ice seeding (Refs. 1, 2, 3). We shall consider now an example of crystallization kinetics in a thick growing SC with the following characteristics: ΔH = 1.3 km, $\bar{q}_{L1}$ = 0.24 g m^{-3}, maximum liquid water content equals 0.44 g m^{-3}, Q_w = 300 g m^{-2}. This cloud has been calculated by NCE model with fixed parameter values, which were listed in the previous section. The updraft region has now the boundaries at z_1 = 975 m and z_2 = 1825 m, w_m = 5 cm s^{-1} (for z = 1.4 km). Fig. 3 illustrates the crystallization zone (CZ) evolution in this cloud layer after the single line seeding. The vertical wind shear equals 0.003 s^{-1}, the dry ice seeding rate M_s equals 5 kg km^{-1} (the correspondent linear concentration of ice nuclei N_s = 5.10^{14} km^{-1}). It has been suggested that the specific activity of the seeding agent is about 10^{11} g^{-1} (Refs. 4, 6). The criterion q_{L1} = 0.01 g m^{-3} is used for the definition of CZ boundaries. It has been suggested that the width of the two-dimensional CZ near cloud top (50-75 m lower) is adequate the effective CZ width Δx_{cr} which is observed in the aircraft sounding on the cloud top (Ref. 6).

Calculations show that $\Delta x_{cr} \approx$ 8 km at t = 30 min after seeding, $\Delta x_{cr} \approx$ 9.5 km at t = 50 min, $\Delta x_{cr} \approx$ 9 km at 70 min. It is seen from Fig. 3 that the continuous CZ arises at 30 min. Nevertheless the visibility of the ground from cloud top (H_2 = 2.1 km) is absent because the existence of dense ice haze. The improved visibility zone (with width 1.2 km) arised later at 50 min, when the haze disappeared. The continuous CZ disappeared at t = 70 min, because the liquid water wedges (z = 1.6 km) overlapped. The great inclination of CZ is the feature of the crystallization kinetics for $\Gamma \neq 0$. It has been shown that Δx_{cr} is approximately equal to the width of $q_{L2} >$ 0.05 g m^{-3} or $n_2 >$ 50 - 60 l^{-1} regions for early stages of ACS. It is better to estimate Δx_{cr} with the aid of $n_2 >$ 10 - 20 l^{-1} regions, when Δx_{cr} reaches the maximum. The seeded precipitation zone width Δx_q (the criterion $q_j >$ 0.1 mm) in the considered cloud was equal 2.7 km for Γ = 0 and 6 km for Γ = 0.003 - 0.004 s^{-1} (N_s = 5.10^{14} km^{-1}). Thus the precipitation zone width is by ~ 30 % less than the maximum CZ width $\Delta x_{cr,m}$.

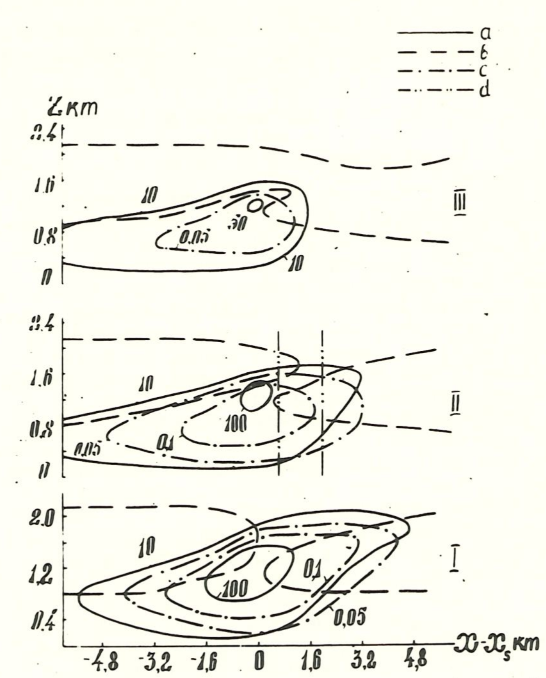

Figure 3. The crystallization zone evolution in the thick cloud layer (ΔH = 1.3 km, Q_w = 300 g m^{-2}, Γ = 0.003 s^{-1}, M_s = 5 kg km^{-1}) I - t = 30 min, II - t = 50 min, III - t = 70 min; a - ice crystals concentration n_2 = Const (10; 50; 100 l^{-1}); b - liquid water content q_{L1} = 0.1 g m^{-3}; c - ice content q_{L2} = Const (0.05 and 0.1 g m^{-3}); d - indicates boundaries of the improved visibility zone. x_s - the seeding line coordinate.

The calculations carried out in (Refs. 1, 2, 3) have proved that ACS velocity and $\Delta x_{cr,m}$ are strong by dependences on such parameters as M_s and Γ. The CZ characteristic dependence on k_x is important only in the case Γ = 0. In the case $\Gamma \neq 0$ the existence of the strong k_z - Γ interaction accelerates the horizontal crystal spreading (Ref. 5). The apparent horizontal diffusivity $\tilde{k}_x$ for instantaneous plane sources is equal to:

$$\tilde{k}_x = \Gamma^2 k_z t^2. \qquad (1)$$

It will be seen that for $\Gamma = 10^{-2}$ s^{-1}, k_z = 5 m^2 s^{-1}, t = 10 min coefficient $\tilde{k}_x$ equals 400 m^2 s^{-1} and k_x = 5 - 50 m^2 s^{-1} does not effect horizontal spreading of ice crystals for great values of Γ.

It has been shown that $\Delta x_{cr,m}$ reaches

4 - 5 km in the layers with parameters $\Delta H = 0.7$ km, $Q_w = 70 - 90$ m^{-2}, $M_s = 3 - 5$ kg km^{-1} and reaches 8 - 10 km in thick cloud layers ($\Delta H = 1.3$ km, $Q_w = 300$ gm^{-2}, $M_s = 5 - 10$ kg km^{-1}), if vertical shear equals 0.003 - 0.005 s^{-1}. Optimal for dispersal seeding rates obtained in (Refs. 1, 2, 3) are equal $3.10^{13} - 1.10^{15}$ km^{-1} (M = = 0.3 - 10 kg km^{-1}) and depend on microphysical and dynamical characteristics of clouds (especially on Γ and Q_w). Calculated crystallization zone characteristics are in agreement with the results of a recent experiment Refs. 7, 8). It is interesting to note that large dimensions of CZ ($\sim$ 9 km) were discovered in the aircraft crystal concentration measurements in seeded clouds (Ref. 8).

3.2. Precipitation field structure after mass seeding

In this section we shall consider the results of the precipitation formation modeling after the mass seeding of the thick SC ($\Delta H = 1.3$ km, $Q_w = 300$ g m^{-2}) considered in the foregoing section. Two lines were seeded with the seeding rate $M_s = 5$ kg km^{-1} ($N_s = 5.10^{14}$ km^{-1}). The vertical wind shear Γ and the distance between seeding lines l are varied. Fig. 4 illustrates the results of total precipitation calculations (the precipitation duration is equal to 1.5 - 2 hours). Distributions of $q_j(x)$ have two maxima for long distances l. For the case, if q_j - distribution has a bimodal structure, let ξ_q be the ratio of the minimum precipitation amount between two seeding lines to the maximum total precipitation. In the case $\Gamma = 0$ $\xi_q = 0.13$ for l = 3.2 km, $\xi_q = 0.45$ for l = 2.4 km, $\xi_q = 0.94$ for l = 1.6 km. If we accept the suggestion that ξ_q should be 0.6, the

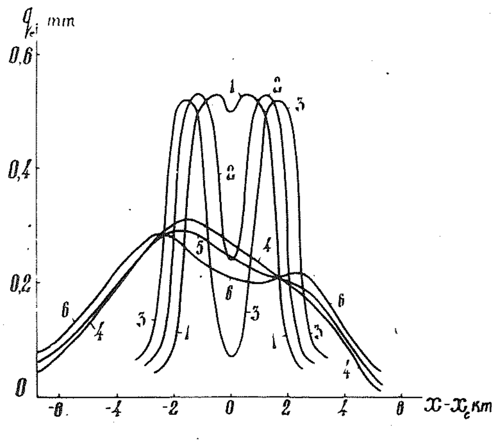

Fig. 4. The precipitation amount distribution after mass seeding ($\Delta H = 1.3$ km, $Q_w = 300$ g m^{-2}, $M_s = 5$ kg km^{-1}). $\Gamma = 0$ for 1; 2; 3; $\Gamma = 0.002$ s^{-1} for 4; 5; 6. For 1 - l = 1.6 km, 2 - l = 2.4 km, 3 - l = = 3.2 km, 4 - l = 3.2 km, 5 - l = 4 km, 6 - l = 4.8 km.

recommended distance between seeding lines l in the case $\Gamma = 0$ should be 2.2 km. In the case $\Gamma \neq 0$ the j(x, t) and $q_j(x)$ distributions are asymmetrical, the overlap of precipitation bands increases. For example, for $\Gamma = 0.002$ s^{-1} a bimodal structure appears only for l = 4.8 km (for this case $\xi_q = 0.69$).

3.3. Optimal mass seeding parameters

Many calculations were carried out to determine the optimal values of mass seeding parameters for different SC. The value $\xi_q = 0.6$ served as the criterion to optimal horizontal plane seeding rate $m_s^* = M_s/l^*$ in a precipitation enhancement modeling. Our calculations show that $\xi_q = 0.5 - 0.6$ correspond to a maximum of $\nu = m_s/q_j$ - a reagent utilization efficiency. The overlap of separate dispersal zones was the criterion in the SC dispersal simulation. The dimensionless recommended ratio m_s^*/Q_w is shown to be a universal dependence on Γ:

$$m_s^*/Q = (\alpha + \beta\Gamma)^{-1} + m_{s\infty} \quad (2)$$

where $\alpha = 1.5 \cdot 10^5$, $\beta = 2.5 \cdot 10^8$ s, $m_{s\infty} = 10^{-6}$ for seeded precipitation ($\tilde{\alpha} = 3.10^5$, $\tilde{\beta} = 5.10^8$ s, $\tilde{m}_{s\infty} = 3.3.10^{-6}$ for cloud dispersal). Optimal seeding parameters for precipitation are depicted in Table 1 for two SC ($\Delta H = 0.7$ km, $Q_w = 95$ g m^{-2}, $M_s = 1.5$ kg km^{-1} and $\Delta H = 1.3$ km, $Q_w = 300$ g m^{-2}, $M_s = 5$ kg km^{-1}; NS - numerical simulation, F - Eq. (2)).

It is demonstrated that the results obtained with different methods are in close agreement. It will be seen that optimal values m_s^* for precipitation formation must be 0.7 - 0.8 kg km^{-2} ($0.7 \cdot 10^{14} - 0.8 \cdot 10^{14}$ km^{-2}) per $Q_w = 100$ g m^{-2} for $\Gamma = 0$ and 0.2 - 0.3 kg km^{-2} ($2.10^{13} - 3.10^{13}$ km^{-2}) per $Q_w = 100$ g m^{-2} for $\Gamma \approx 0.005$ s^{-1}. Recommendations for n_s (in km^{-2}) corresponding to m_s do not depend on agent activity or on the kind of an agent. The simulations show that optimal distance l^* (for precipitation enhancement (for fixed M_s) is close to the maximum width $\Delta x_{cr,m}$ (for one seeding line).

4. CONCLUSIONS

1. In the case the updrafts are the main factors of a cloud formation there is the minimum value of a vertical velocity below which a cloud does not formate and an existing cloud is dissipating.
2. The stratification of cloud layers under a natural dissipation was found to depend on a great value of downcurrent velocity and inhomogeneous undersaturation profile.
3. The vertical wind shear is shown to have a strong effect on the acceleration of the horizontal crystal spreading and the formation of artificial precipitation.
4. Universal dependence of an optimal mass seeding rate on some stratiform cloud parameters for seeded precipitation enhancement has been obtained.

Table 1

Optimal mass seeding parameters (for precipitation)

ΔH km	Γ 10^{-3} s^{-1}	l^* km		m_p^* $\frac{g}{km^2}$		$\frac{m_p^*}{\Omega_w}$ $10^{-4} \frac{kg\ m^2}{km^2\ g}$	
		NS	F	NS	F	NS	F
1.3	0	2.2	2.2	2.27	2.31	76	77
	1	4.4	4.7	1.14	1.05	38	35
	2	6.2	6.6	0.81	0.76	27	25
	3	8.0	7.8	0.63	0.63	21	21
	4	10.0	9.7	0.57	0.56	17	19
0.7	0	2.0	2.1	0.75	0.73	79	77
	1	4.3	4.5	0.35	0.33	36	35
	3	8.0	7.5	0.19	0.20	19	21
	5	10.0	9.2	0.15	0.16	15	17

5. REFERENCES

1. Bakhanov, V.P., Buikov, M.V., Manjara, A.A. and Pirnach, A.M., 1981. A numerical model of supercooled stratiform cloud dispersal after the dry ice seeding. Trudy of Ukrainian Region. Inst. No. 185, 25-44.
2. Bakhanov, V.P., Manjara, A.A. and Kolezhuk, V.T., 1981. A simulation of an improved visibility zone formation in a supercooled stratiform cloud (the airborn dry ice seeding of one line). Trudy of Ukrainian Region. Inst. No. 185, 45-47.
3. Bakhanov, V.P. and Manjara, A.A., 1983. A numerical simulation of an artificial crystallization process in thick stratiform clouds after a mass seeding. Trudy of Ukrainian Region. Inst., No 203 (in press).
4. Jiusto, J.E. and Weickman, H.K., 1980. Cloud seeding agents and dispersal rates. Some viewpoints. Papers present at WMO Scient. Conf. on weath. mod., WMO-Geneva, 417-424.
5. Monin, A.S. and Yaglom, A.M., 1965. Statistical hydromechanics. Part 1. Moscow, Nauka, 639 pp.
6. Polovina, I.P., 1971. An artificial modification of air-mass stratiform clouds. Leningrad, Gidrometeoizdat, 215 pp.
7. Stewart, R.E. and Marwitz, J.D., 1982. Microphysical effects of seeding wintertime stratiform clouds near the Sierra Nevada mountains. Journ. Appl. Meteor., 21, No. 6, 874-880.
8. Sutherland, J.L., Thompson, J.R., Griffith, D.A. and Kunkel, B., 1982. Seeding tests on supercooled stratus using vertical fall pyrotechnics. Journ. Appl. Meteor., 21, No. 2, 248-251.

NUMERICAL MODEL OF MESOSCALE CIRRUS DYNAMICS

E.P.Borisenkov, T.A.Bazlova

A.I.Voeikov Main Geophysical Observatory
Leningrad, USSR

1. INTRODUCTION

Cloud formation and evolution involves micro-, meso- and macroscale processes the quantitative description of which is only possible based on numerical simulation. The present authors task was to develop a numerical model for describing the mesoscale cirrus cloud dynamics and to carry out a number of numerical experiments.

The cirrus clouds are mainly formed at 7-11 km heights at temperatures lower than -30°C and consist of ice crystals having predominant complex forms such as columns, bullets and bullet rosettes (Ref.1). As it is shown in a number of papers (Refs. 2-5), they influence greatly the radiative regime and dynamics of the atmosphere causing the tropospheric warming and changing the character of vertical motions. The microphysical and radiative properties of cirrus clouds being responsible for the above processes are highly changeable (Refs.6,7). Cirrus clouds transmit a considerable part of solar radiation, the global mean value is 88%, and have the global mean emissivity 0.475 (Ref.5). Unlike the cooling effect caused by low clouds, cirrus clouds increase atmospheric temperature as compared to a cloudless case due to greenhouse effect and a considerable part of transmitted solar radiation.

2. DESCRIPTION OF THE MODEL

The specific character of the numerical mesoscale cirrus dynamics model developed by the authors is that it is supposed to be included into some macroscale model using grid telescoping method (Ref.8) with one-sided interaction. The main idea of the method is to integrate a part of the model separately at the small-grid points and to take necessary nonstationary boundary conditions from the big-grid solution. When realizing the method, the problem of boundary conditions arises. The present paper presets boundary conditions at the inflow points calculates them at the outflow points according to advection from the region. The wind velocity components can be taken from the macroscale model or preset.

The model includes water vapor and ice phase transfer equations and the equation resulting from the first law of thermodynamics. Vertical motions, advection, turbulent diffusion, turbulent and phase flux divergencies are taken into account. The corresponding three-dimensional equations in isobaric coordinate system have the following form:

$$\frac{\partial q}{\partial t} + (u_i \nabla^i) q = K_H \nabla^2 q + g^2 \frac{\partial}{\partial p} K_v \rho^2 \frac{\partial q}{\partial p} - \frac{M}{\rho} \quad (1)$$

$$\frac{\partial \delta}{\partial t} + (u_i \nabla^i) \delta = K_H \nabla^2 \delta + g^2 \frac{\partial}{\partial p} K_v \rho^2 \frac{\partial \delta}{\partial p} + \frac{M}{\rho} \quad (2)$$

$$\frac{\partial \theta}{\partial t} + (u_i \nabla^i) \theta = K_H \nabla^2 \theta + g^2 \frac{\partial}{\partial p} K_v \rho^2 \frac{\partial \theta}{\partial p} + \frac{L M}{c_p \rho} \quad (3)$$

where u_i is wind velocity components, q is specific humidity, δ is specific ice content, θ is potential temperature, p is pressure, ρ is air density, K_H, K_v are horizontal and vertical turbulent diffusion coefficients, g is acceleration due to gravity, L is latent heat released on sublimation, c_p is heat capacity of dry air at constant p, M is sublimation rate, i.e. the mass if ice phase forming per unit time and per unit air volume.

The ice crystal growth equation with ventilation taken into account (Ref.9) is used for describing microphysical processes:

$$\frac{dm}{dt} = 4\pi C \mathcal{F} S \left(\frac{L^2}{K R_v T^2} + \frac{R_v T}{E_i(T) D} \right)^{-1} \quad (4)$$

where m is ice crystal mass, C is ice crystal capacity, $\mathcal{F}$ is ventilation coefficient, S is supersaturation with respect to ice, K is air thermal conductivity, R_v is the ideal gas content of water vapor, D is diffusivity of water vapor in the air, $E_i(T)$ is saturation vapor pressure over ice at temperature T.

Cirrus clouds are formed by freezing of supercooled droplets or by sublimation. With ice supersaturation, ice crystals grow by sublimation according to Eq.4. The sublimation rate is calculated then by the following formula:

$$M = \frac{dm}{dt} \cdot N \quad (5)$$

where N is concentration of ice crystals. The system of Eqs.1-5 is solved in the region: D= { x,y,p: 0≤x≤120km, 0≤y≤120km, 200mb≤p≤400mb } .

The q, δ, T- fields are preset at the initial time moment t=0 as original conditions. The initial values of concentration and ice particle dimensions are taken from experimental data. Some disturbance in the q-field is an impulse for cloud evolution.

The split integration scheme is used to solve the system. The numerical solution of equations obtained by splitting is made using the finite difference method.

3. RESULTS OF NUMERICAL EXPERIMENTS

The solution is determined at the points of the space grid with steps $\Delta x = \Delta y = 10$km, $\Delta p = 25$km and time step $\Delta t = 3$min. The horizontal turbulent coefficient is taken to be equal to $5 \cdot 10^4 \frac{m^2}{s}$. According to experimental data available on turbulent diffusion in Ci (Ref.1), K_V equals $16 \frac{m^2}{s}$.

Fig.1 presents the specific ice content of cirrus clouds developing in the atmosphere with wind shear depending on time.

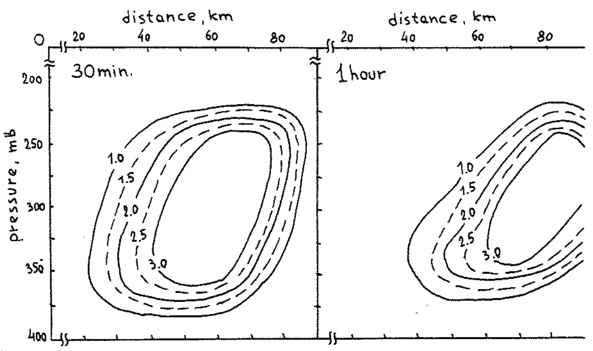

Figure 1. The vertical section of the specific ice content ($x10^{-4} \frac{g}{g}$) of cirrus cloud developing in the atmosphere with wind shear 0.1 m/s mb and at t=30min. and t=1hr. The section is made through the centre of a cloud in wind plane.

Numerical simulations have been carried out which show the effect of various meteorological factors (humidity, temperature, wind, turbulent diffusion heat advection) on cirrus cloud evolution. The humidity effect is illustrated in Fig.2.

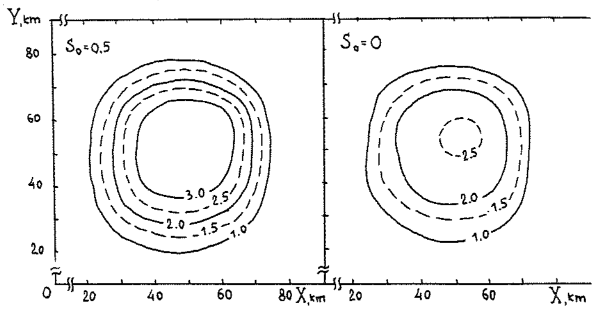

Figure 2. The horizontal section of the specific ice content ($x10^{-4} \frac{g}{g}$) of cirrus cloud at t=15min depending on the initial ice supersaturation S_0.

Numerical experiments enable one to observe cloud displacement caused by wind, cloud extention caused by turbulent diffusion, ice content increase and decrease depending on temperature and humidity as well as the corresponding temperature field distortions.

4. REFERENCES

1. Mazin I P Shmeter S M 1983. Clouds, their structure and physics of formation. Leningrad, Gidrometeoizdat, 307.

2. Borisenkov E P Efimova L K 1978. Theoretical evaluation of the effects of cirrus clouds and surface albedo on anti-cyclone dynamics. Trudy Glav Geofis Obs, 407, 101-111.

3. Borisenkov E P Meleshko V P Sokolov A P 1981. The effect of high clouds on the thermal regime and the circulation of the atmosphere. Meteorology and Hydrology, 11, 5-17.

4. Lion K N Gebhart K L 1982. Numerical experiments on the thermal equilibrium temperature in cirrus cloudy atmospheres J Meteor Soc Japan, 60, 570-582.

5. Lion K N Ou S C 1983. Theory of equilibrium temperatures in radiative--turbulent atmospheres. J Atmos Sci 40, 214-229.

6. Paltridge G W Platt C M R 1981. Aircraft measurements of solar and infrared radiation and the microphysics of cirrus cloud. Quart J Roy Meteor Soc 107, 367-380.

7. Platt C M R Dilley A C 1981. Remote sounding of high clouds. IV: Observed temperature variations in cirrus optical properties. J Atmos Sci 38, 1069--1082.

8. Hill G E 1968. Grid telescoping in numerical weather prediction. J Appl Meteor 7, 29-38.

9. Jayaweera K O L F 1971. Calculation of ice crystal growth. J Atmos Sci 28, 728-736.

A MODEL OF A MOUNTAIN CAP CLOUD

D J CARRUTHERS and T W CHOULARTON
Physics Department, UMIST,
Manchester M60 1QD, England

1. INTRODUCTION

We describe a 2-dimensional dynamic and microphysical model of a cap cloud forming over hills of moderate size and slope. The effects of 1) droplet loss to ground, 2) inhomogeneities in the condensation process near cloud base, 3) radiative cooling from cloud top, 4) dry air entrainment, are considered.

2. MODELLING OF CAP CLOUDS

2.1 The Model Formulation

2.1.1 Adiabatic model of cloud droplet evolution. This model calculates the cloud droplet size distribution of an air parcel subjected to adiabatic ascent. The dynamic model described below is used to calculate the altitude at which the air parcel has a relative humidity of 99%. At this level, a size distribution of droplets in vapour equilibrium calculated from the CCN activity spectrum is specified. The equations for this adiabatic model are based on those presented in Ref.1, the only difference being that the droplet growth equation has been modified so that only the CCN activity spectrum needs to be known, no explicit knowledge of the composition of the aerosols being required. These equations are presented in detail in Ref.2 so will not be repeated here. In this work, however, the equations have been modified to include the effects of radiative cooling and various mixing processes as required. As in (2), the equations were integrated using a simple forward difference technique.

2.1.2 Calculation of the Cloud Dynamics
In order to run the model, values of temperature and pressure at and below cloud base are required together with an updraught profile. The effect of condensation on the near surface flow is very small; thus, as long as the atmospheric boundary layer is near neutral in stability, which is often the case in the strong wind situations of interest, the three-layer model described in Ref.3 can be used to solve the airflow over the hill and so provide the required updraught profiles.

In this model, the atmosphere is idealised into three-layers: a boundary layer capped by an inversion at height I (-∞) upstream with less stable air above starting at J (-∞). The Helmholtz equation (Long's equation) for laminar flow is solved using non-linear boundary conditions. The near surface pressure field developed by the laminar flow model is used to calculate the mean velocities in the inner turbulent region using the theory of Ref.4. The cloud is assumed to form only in the lowest of the 3 layers in contact with the ground.

For the calculation of the updraughts, the hill profile used was $f(x) = h/(1 + (x/L)^2)$, where h is the hill height, x horizontal displacement from the summit and L the half-length. Since the vertical velocity varies rapidly with distance above ground, it was calculated using an averaging procedure. Following the analysis of Ref.4 where it was shown that, in the inner region, it is a reasonable approximation to assume that the turbulence is in local equilibrium, it was assumed that the rate of turbulent mixing was proportional to a local velocity scale $u_*(1 + \Delta S)$; where u_* is the friction velocity (taking its upstream value) and S the speed-up as defined in II. Air contained in a wedge with the following boundaries was considered to have an equal chance of passing close to the summit: the lower boundary was the hill surface, the upper boundary a plane such that, at a distance x from the summit, the time constant $\tau_M \approx \Delta z/[(1 + \Delta S)\sigma_w]$ for vertical turbulent mixing between the plane and the ground is approximately equal to the time for air to reach the summit $\tau_T \approx x/[(1 + \Delta S(x))u(\Delta \bar{z})]$. σ_w is the standard deviation of the vertical velocity, Δz the local height of the upper plane of the wedge above ground, x the distance from the summit and $\Delta \bar{z}$ a length scale used to calculate an average horizontal velocity through the width of the wedge. Since $\sigma_w \approx 1.2u_*$ (e.g Ref.5) and $u(\Delta \bar{z}) = (u_*/x)(1 + \Delta S)\ln(\Delta z/z_o)$ then

$$\Delta z \approx \frac{1.2kx}{\ln(\Delta \bar{z}/z_o)} \qquad (1)$$

where k is von-Karman's constant and z_o the roughness length.
Taking $\Delta \bar{z}$ = 60m for all x gives the thickness of the wedge

$$\Delta z = 0.06x \qquad (2)$$

The expression is insensitive to the value of x employed since the horizontal windspeed near the ground is approximately logarithmic and, with z_o = 0.02m (a typical value for hills such as GDF), varies only slowly for $\Delta \bar{z}$ > 10m. Updraughts at particular heights above cloud base were calculated using the three-layer model by averaging over horizontal bands contained in the wedge.

When $\Delta \bar{z}$ > p, where p is the thickness of the inner region, (= 80m for GDF), which occurs when x ≥ 1330m, the updraughts were calculated using a modified JH outer region solution.

2.2 Results

We now present some representative results which illustrate how the cloud droplet spectrum varies for the adiabatic model. We use hill parameters appropriate to GDF (h = 665m, L = 2km) throughout, making predictions appropriate to our measuring site about 4m above ground at the mountain top and comparing the results with observations made at this site. We also discuss the applicability of the results to other sites.

To illustrate the results from the model, we present the results obtained by applying the model with the following upstream parameters: height of inversion $I(-\infty) = 400m$, starting point of the less stable layer aloft $J(-\infty) = 800m$, stability of the inversion layer $\mu_2 = 1.2 \times 10^{-3} m^{-1}$ and stability aloft $\mu_3 = 0.7 \times 10^{-3} m^{-1}$ and the geostropic wind $U_G = 13m\ s^{-1}$. During the course of this case study, the cloud base lifted from 600m below the summit, early in the day, to near the mountain top. To illustrate the changing features of the adiabatic spectrum, the model was run for three cloud bases (a) 600m summit, (b) 420m, (c) 150m below the summit. Figures 1a,b,c show the calculated spectra for these cloud bases compared with the observed mountain top spectrum. The CCN activity spectrum used was very maritime, the spectrum measured on the day being approximated by the expression:

$$N = (400 \pm 130)S^{(0.46 \pm 0.15)} \qquad (3)$$

for the supersaturation $S \geq 0.1\%$ a maritime tail was fitted for $S \leq 0.1\%$ as described in Ref.2.

For the low cloud base case (Figure 1a), the updraught is initially low, so that the supersaturation peak is relatively small and only a few drops are activated. As the cloud flows up the hill, the updraught increases and the small number of drops are unable to prevent a rise in supersaturtion and consequently further activation of drops. This process continues until the updraught peak is reached just below the summit. The result is a fairly smooth broad peak in the summit spectrum in close agreement with observation. For higher cloud bases, Figures 1b and c, the cloud base updraught was much higher resulting in a larger sharp supersaturation peak at cloud base, with all the activation being concentrated in this region. A much narrower spectrum resulted at the mountain top with a substantially higher total number concentration in agreement with observations.

In each case, the calculated number concentration tends to exceed the observed number. This may be attributable to droplet loss to ground and an attempt to model this effect has been made.

2.3 Droplet Loss to Ground

The effect of loss of drops to ground by eddy diffusion and gravitational sedimentation was investigated by calculating the droplet flux F given by

$$F = k(z)\frac{\partial C(z)}{\partial z} + V_T C(z) = V_d(z)C(z) \qquad (4)$$

The droplet number concentration at our observation site (~4m above ground) is predicted to be about 2/3 of the value in the absence of loss to ground.

2.4 The Effect of Patchiness in the Vicinity of Cloud Base

Observations on GDF have shown that, close to cloud base, the liquid water content often varies by up to $0.2g\ m^{-3}$ on scales of several tens of metres. This variability decreases up the hill in the absence of mixing in of dry air from above the cloud. The patchiness is a consequence of humidity fluctuations (of order 1%) in the air approaching the hill and will have the effect of broadening the time-averaged drop size spectrum obtained within approximately 100m of cloud base, since parcels of air will contain droplet spectra in all stages of adiabatic growth. In the driest parcels these will be unactivated nuclei only whilst in the wettest there will be droplet distributions corresponding to the maximumn liquid water content observed of about $0.2g\ m^{-3}$.

As ascent continues, however, the effect will rapidly become less significant as the smaller drops catch up with the larger and the blobs lose their identity by turbulent mixing.

The mixing time constant T between neighbouring parcels may be estimated using the dimensional relation $T=(\lambda^2/\mathcal{E})^{\frac{1}{3}}$. Taking $\lambda \approx 20m$, $\mathcal{E} \approx 10^{-2}m^2sec^{-3}$ gives T 30 sec. Assuming an updraught of about $1m\ s^{-1}$ and the variation in the cloud bases of the different parcels of about 100m, it is likely that a significant number of drops will be mixed from the high liquid water content parcels into the drier parcels whilst they are close to 100% humidity, so that the evaporation from these drops will be insignificant. If they are few in number, however, they will be able to absorb water quickly as the supersaturation in the drier parcel develops. Thus,they will grow faster than their former neighbours in the high liquid water content parcel until the activated drops in the drier parcel reach a sufficient size to compete effectively for the available water and reduce the supersaturation. The presence of the larger drops in the drier parcel will somewhat reduce the peak supersaturation and hence the num-ber of drops activated there.

Figure 2 shows the calculated adiabatic spectrum 170m above cloud base. Curve B includes the effect of 1% humidity fluctuations on a scale of 20m spread over a vertical distance of 100m (5 different blobs were involved). A slight broadening of the peak of the spectrum and a reduction in the number of drops activated. A slight (for practical purposes insignificant) increase in the concentration of largest drops has occurred. The computations showed that further above ~~cloud base~~ the difference in spectral shapes decreased. This result was typical of a number of trials over 100m above cloud base. The effect on the spectral shape was always small although the concentration of drops activated was reduced by approximately 10%. The reason for the small size of the effect is that the activation of nuclei in the drier parcels when a large supersaturation begins to develop rapidly reduces it to small values again, hence any enhanced growth is small.

The broad spectrum in the cloud base region is illustrated by Figure 3. Hence this process is able to generate a drop size spectrum with a broader smoother peak than would occur in simple adiabatic growth when cloud base is only a few hundred metres below the mountain top.

2.5 The Effect of Dry Air Entrainment

2.5.1 The Effect of Displacing the Inversion on the Entrainment Rate

Assuming there is no initial shear in the stable layer capping the boundary layer before it is displaced, it can be shown from Long's equation that during a displacement of the layer over the hill the Richardson number will decrease and is given by

$$R_i = 1/\mu_2{}^2\xi^2 \qquad (5)$$

where ξ is the streamline displacement. Thus airflow over hills of the size of GDF may result in a reduction in Richardson number to values close to the critical value for turbulent breakdown ($Ri \simeq 0.2$). When a shallow very stable layer exists at the top of the cloud typically, a change of 4°C in 4m can occur.

In a shallow layer just above the cloud top with a windspeed of typically 10m s^{-1} in the layer, we have $\mu^2 = 5 \times 10^{-4}$ m^{-2} which implies a displacement of the interface of under 100m for $R_i < 0.2$.

2.5.2 Effect of Dry Air Entrainment of the Cloud Microphysics

Field data reported suggests that when large scale engulfing of dry air through a weak interface occurs, the entrainment tends to produce large reductions in both the water content and number concentration, with little change in spectral shape. These effects are especially important close to an entraining interface. In highly turbulent clouds, and when smaller scale entrainment occurs across a strong inversion, the evaporation effects tend to correspond to an intermediate description, in which liquid water fluctuation are a consequence of both fluctuations in droplet number concentration and droplet mean radius. These effects tend to be smaller in magnitude and to be more important at greater distances from the interface.

2.6 Radiative Cooling at Cloud Top

Close to the cloud top there is a large negative radiative flux divergence when the sky above the cap cloud is clear: in this region, drops grow by radiative cooling as well as by cooling due to ascent. The time T_R for which individual drops remain in the radiative cooling region is controlled by the depth of large radiative flux divergence (p_R) and the turbulence levels within it. An approximate expression for this time is

$$T_R \sim p_R/\sigma_w \qquad (6)$$

Ref.7 gives the equation for droplet growth due to radiative cooling for r > 5μm as

$$dr/dt = -RX \qquad (7)$$

where R is the nett radiation gain per unit surface area of drop and X is a temperature dependent coefficient.

At the top of the cap cloud with a typical liquid water content q_L of 0.5g m^{-3} R = −50W m^{-2} decreasing to −5W m^{-2} within 50m of cloud top (Ref.6) Thus, taking p_R = 50m and R = −25W m^{-2} then, in time T_R, the growth by radiative cooling will be

$$dr = 0.15/\sigma_w(\text{m s}^{-1})\ \mu\text{m} \qquad (8)$$

An approximate range of σ_w estimated from likely values of the scale of turbulent velocity near cloud top is σ_w = 0.1 to 0.4m s^{-1}. Therefore drops in the favoured region near cloud top may grow by amounts ranging from about 0.4μm ($T_R \approx$ 125sec) up to 1.5μm ($T_R \approx$ 500 sec). When the excess growth is significant ($T_R \sim$ 500 sec), the percentage of all cloud droplets involved is small since, over GDF, the transit time for the cloud to travel even from a low cloud base to the summit T_s is less than about 400 sec for $U_* \geq$ 0.1m s^{-1}. When the excess growth is small (σ_w = 0.4m s^{-1}) a large number of drops in the cloud, especially if it is shallow, experience this growth. Hence, this effect is likely to be detectable when the overlying sky is clear and the winds are light.

3. CONCLUSIONS

When an isolated cap cloud forms over hills of the size and scale of the Pennines, the dominant effect in determining the mean drop size distribution is the cloud condensation nucleus spectrum on which the drops form.

Near to cloud base, small scale fluctuations in the humidity of the airstream flowing up the hill will result in substantial structure in the liquid water content and a broad drop size distribution. These effects rapidly disappear more than 100m above cloud base. Turbulence near cloud base has no significant effect on the microphysical structure well above cloud base.

Radiative cooling from cloud top can cause a small but significant increase in the sizes of the larger drops; it is suggested that this could be of much greater significance in clouds with a longer life.

REFERENCES

1. Pruppacher H R & Lee I Y 1977 A comparative study of the growth of clouds by condensation using an air parcel model with and without entrainment. Pageoph, 115,523-545
2. Baker M B et al 1982 Field studies of the effect of entrainment on the structure of clouds at Great Dun Fell. Quart J Roy Met Soc, 108,899-916
3. Carruthers D J & Choularton T W 1982 Airflow over hills of moderate slope. Quart J Roy Met Soc, 108, 603-624
4. Jackson P S & Hunt J C R 1975 Turbulent windflow over a low hill. ibid, 101, 929-955
5. Bradley E F 1980 An experimental study of the profiles of wind speed, shearing stress and turbulence at the crest of a large hill. ibid, 106, 101-123
6. Caughey S J & Kitchen M 1983 Simultaneous measurements of the turbulent and microphysical structure of nocturnal stratocumulus cloud. Quart J Roy Met Soc (in press)
7. Roach W T 1976 On the effect of radiative exchange on the growth by condensation of a cloud or fog droplet. ibid, 102, 361-72

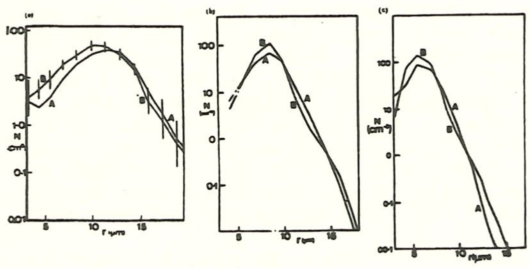

Figure 1. Comparisons of observed and calculated adiabatic spectra.
(a) A, observed high count spectrum for the period 0830-0845. $N=132cm^{-3}$, $q_L=1.08g\ m^{-3}$.
B, calculated spectrum for the same time. $N=196\pm50cm^{-3}$, $q_L=1.17g\ m^{-3}$.
The error bars result from the approximate uncertainty in the CCN distribution.
(b) A, observed high count spectrum for the period 1313-1330. $N=200cm^{-3}$, $q_L=0.55g\ m^{-3}$
B, calculated spectrum, $N=270\pm70cm^{-3}$, $q_L = 0.75g\ m^{-3}$
(c) A, observed high count spectrum for 1515-1528. $N=251cm^{-3}$, $q_L=0.29g\ m^{-3}$.

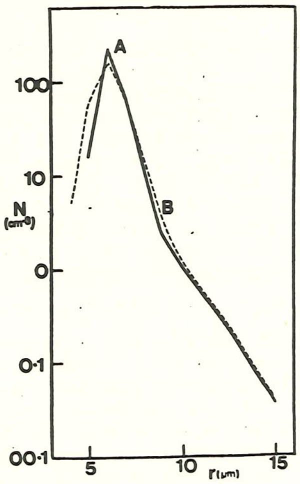

Figure 2. Calculated adiabatic spectra 170m above cloud base. The CCN distribution used is $N=400S^{0.46}$. The updraughts are calculated using the airflow model: $I(-\ )$ = 440m; $J(-\ )$ = 1900m; $u_2 = 1.2 \times 10^{-3}m^{-1}$; $u_3 = 0.7 \times 10^{-3}m^{-1}$; $u_0 = 13.0m\ s^{-1}$.
A Uniform cloud base; B Humidity fluctuations of 1% on scales of 20m at cloud base.

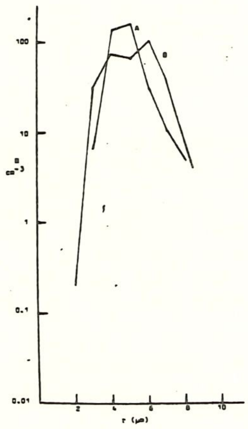

Figure 3 Calculated Silverband site spectra for a cloud base at 370m. Curve A simple adiabatic growth, curve B includes the effect of cloud base patches.

OROGRAPHIC ENHANCEMENT OF RAINFALL BY THE SEEDER-FEEDER MECHANISM

D J CARRUTHERS and T W CHOULARTON

Dept, of Applied Maths & Theoretical Physics
Univ. of Cambridge, England

Dept. of Physics, UMIST,
Manchester M60 1QD, England

1. INTRODUCTION

In warm sectors of depressions and close to surface fronts rainfall is frequently observed to be much greater over hills than over surrounding low ground. A mechanism for this effect was first put forward by Bergeron (Ref.1): he proposed that raindrops from pre-existing (seeder) clouds aloft wash out small droplets within low-level (feeder) clouds formed by ascent over the hills. This mechanism suggests that the amount of orographic enhancement is determined by the rate at which pre-existing precipitation washes out the feeder cloud and by the rate at which the feeder cloud is replenished by condensation. The largest enhancements would be expected to occur when the pre-existing precipitation rate is high and/or when pre-existing rain areas are accompanied by strong, near-saturated low-level flows. Support for this feeder-seeder mechanism has been provided by the recent theoretical studies (Ref.2,3,4). The model of Ref.3 incorporates simplifying assumptions, discussed later in this section, but it provides the most reasonable basis for further calculations.

Recently Ref.5 presented eight detailed case studies of orographic rain over the hills of S. Wales. The observations broadly supported the mechanism of Ref.1: more than 80% of the overall orographic enhancement was concentrated in the lowest 1500m. Agreement with the predictions of the model of Re.3 was reasonable: however, the observed rainfall rate was found to be more dependent on windspeed and less dependent on the pre-existing rainfall rate than the model predicted. Ref.3,5 suggest a number of possible explanations for these discrepancies. These included: (i) the modelling of the airflow structure over the hills; (ii) the effects of potential instability over the hills; (iii) wind drift of precipitation; (iv) the specified rainfall rate and distribution; (v) the specified cloud thickness and humidity. In sections 2 and 3 we illustrate with the use of a numerical model (Ref.6) the extent to which points (i), (iii) and (v) lead to inaccuracies Points (ii) and (iv) are discussed in detailed in Ref.6.

2. MODEL FORMULATION

2.1 Treatment of washout

Our description of the washout process is similar to that employed by Ref.3. However, we include the drift of precipitation as it falls through the feeder cloud and we have used a Marshall-Palmer raindrop size distribution (Ref.8). This results in an enhancement about 10% smaller than given by the Best distribution used by Ref.3 due to the lower concentration of small drops. The feeder cloud's drops are assumed to be monodispersed with radii r=10μm.

2.2 Treatment of airflow

For a representation of the airflow, and hence for the calculation of updraughts required for the washout model, we use dynamic models similar to those of Ref.8 (two) and Ref.9 (three) dimensions in which the atmosphere is divided into three layers of different but uniform stability. The effect of condensation in a layer can be considered following Ref.10.

A problem in modelling the airflow adequately is to include the effect of condensation without making the calculations inordinately complicated. The interfaces between cloudy and cloud-free regions are difficult to observe and probably would not coincide with the interfaces between the layers of different stabilities. Accordingly two extreme situations have been modelled: one in which the motion behaved as though the atmosphere was completely dry and the other in which the motion behaved as though the atmosphere was completely cloudy. The 'real' situation on any day must lie between these extremes and therefore model results should yield approximate upper and lower bounds for the enhancement. For further clarification we show results which include the effects of stratification for one atmospheric profile only, one which is broadly typical of cases in which heavy orographic rain has been observed. Details are given in Table 1, with, in the notation of Ref.7, $I(-\infty)$=800m and $J(-\infty)$=1500m. This is an approximate average of the eight profiles presented in Ref.5 which are characterized by a near-neutral boundary layer capped by a more stable mid-layer with less stable air above.

TABLE 1
Values of the moist and dry static stabilities used in the three-layer model

Layer	$N_d \times 10^2 (s^{-1})$	$N_e \times 10^2 (s^{-1})$
1	0.97	0
2	1.6	0.3
3	1.3	0.41

3. RESULTS

3.1 Choice of numerical models

Results are presented for several models:

Model	Dimensions	Wind drift
a. Bader-Roach	2-dimensional	wind drift included
b. Stratified model with moist stability (N_e^2)	2-dimensional	wind drift included
c. Stratified model with dry stability (N_d^2)	2-dimensional	wind drift included
d. Potential flow	2-dimensional	wind drift included
e. Potential flow	3-dimensional	wind drift included
f. Bader-Roach	2-dimensional;	no wind drift
g. Potential flow	2-dimensional;	no wind drift

The letters correspond to those on the figures where appropriate. The effects of stratification in three-dimensional flow were found to be small (smaller than in two dimensional flow) and are therefore not presented.

3.2 Choice of hill length and shape

The range of hill half-length (L) was 2 to 20km. This is the range for which the

Bergeron seeder-feeder mechanism (Ref.1) is most likely to be important. For hills exceeding 20km in length the coalescence processes within the orographic cloud may become important in producing rain. The heights chosen were up to 1000m; over higher hills, larger vertical displacements of air may change the structure of any existing mid-level precipitation.

For two-dimensional models, a bell-shaped hill was chosen with profile $f(x)= h[1+(x/L)^2]^{-1}$. For the three-dimensional model the hill profiles was $f(x,y)= h \exp[-(x/L)^2-(y/L)^2]$. The change of shape was necessary in order that the function had a simple Fourier transform; it is generally less representative of hills than the bell-shaped profile, but this does not change our conclusions.

3.3 Orographic enhancement over 'short' hills of a given height

Figure 1 shows the maximum calculated orographic enhancement over a short hill for two pre-existing precipitation rates. Collectively comparing curves a-e (wind drift included) with curves f,g (no wind drift) it is seen that the inclusion of wind drift greatly reduces the maximum enhancement. Again comparing curves a-d with f.g in Figure 2, which shows the enhancement as a function of distance over the hill, wind drift is seen to move the position of maximum enhancement from near the summit to 400m downwind (Ref.11,12).

The effect of wind drift is explicable in terms of two length scales:
(i) the horizontal drift of a raindrop radius r falling at speed V_r through a cloud of depth Z_c

$$L_d \approx Z_c u_o / V_r \qquad (1)$$

(ii) the scale length of horizontal variation in liquid water content (q)

$$L_q \approx q(\partial q/\partial x)^{-1} \approx L \qquad (2)$$

where L is the half-length of the hill. If $L_q \leq L_d$ (as over a short hill) the predominant effect of wind drift is to decrease the maximum value of the enhancement since no drops would fall exclusively in the region of highest liquid water content near the hill summit. The maximum value is also translated downwind a distance $x < L_d$. (The inquality applies since drops entering the cloud above the summit will on average pass through a much lower liquid water content than drops entering the cloud a distance $L_d/2$ upwind.) Finally the region of enhancement is extended downwind since drops entering the feeder cloud near the summit reach the ground downwind of the topography where the feeder cloud has evaporated.

Over the short hill when wind drift is included the efficiency of washout E_w, as defined in Ref.3 is very small: $E_w \approx 5\%$ for P_o=0.5mm h^{-1} rising to $\approx$12% for P_o =25.mm hr^{-1}. These values are approximately two thirds of the values obtained when wind drift is not included and so the total enhancement is also decreased.

Finally we refer only to the curves which include the effect of wind drift (a-e). The small differences in the enhancements are explicable entirely in terms of the vertical depth of the feeder cloud (Ref.6), e.g the Ref.3 model leads to the greatest cloud thickness and gives the greatest enhancement, which appears to be a small overestimate since when $u_o \gtrsim 15$m s^{-1} the differences beween the predictions of the two-dimensional dynamic models (b,c,d) are small and their average is smaller than the predictions of Ref.3. In particular the inclusion/exclusion of condensation effects in the airflow model has only a small effect on the enhancement and indeed the stratified models predict enhancements similar to the two-dimensional potential flow model. The three-dimensional model results in somewhat smaller enhancements due to some flow round rather than over the hill; this small decrease is, however, hardly observable.

3.4 Orographic enhancement over 'long' hills of a given height

Figures 3 and 4 present a similar set of graphs for a much longer less steep hill (L=20km, h=600m). In this case $L_q >> L_d$ (Eq. 1,2) and wind drift does not change the rainfall distribution, but it is translated downwind a distance L_d. The model of ref.3 (a) is seen to agree very well with the potential flow models (d and e) and three-dimensional effects are negligible. Models b and c, which include the effects of stratification with and without cloud, give smaller enhancements; however, assuming that the 'true' enhancement is aproximately the average of the two extremes, the difference is less than 0.5mm hr^{-1}. In all cases there is a slow approximately linear dependence of enhancement with windspeed but over this long hill the initial precipitation rate is relatively unimporant (Ref.5). The liquid water content of the feeder cloud was found to be extremely subadiabatic, corresponding to a high washout efficiency $E_w \approx 70\%$. Figure 4 shows that in all cases the maximum enhancement was upwind of the summit, at $x_\sim -L/5$ in the bases of Ref.3 and the potential flow models (d,e) and at $x_\sim -2L/5$ in cases b,c; the asymmetry of the flow caused by stratification has the effect of moving the maximum enhancement upwind. Over the long hill the airflow formulation of Ref.3 gives a good estimate of cloud depth. The effect of the longer hill is to increase the displacement of the streamlines. It is interesting that this would not have become apparent without the use of a non-hydrostatic airflow model.

3.5 <u>The influence of hill height and cloud depth</u>

Having established that potential flow solutions provide a sufficiently accurate description of the airflow for the modelling of orographic rain we performed further calculations to illustrate the sensitivity of the enhancement to hill height and feeder cloud depth. Comparisons of the potential flow models in two and three dimensions are presented (Figure 5) for the enhancement over short hills. The two- and three-dimensional solutions diverge for large h, as there is increased flow round rather than over the three-dimensional hill. This effect is not apparent over long hills.

On the short hill when Z_c > 1500m calculations showed that increasing the thickness of the feeder cloud does not alter the maximum precipitation since drops scavenging the top of the cloud reach the ground far downwind of the summit and so of the region of high liquid water content of the orographic cloud. Over a long hill there is a slow increase of precipitation maximum with increasing cloud depth.

4. CONCLUSIONS

(i) Wind drift moves the position of maximum enhancement downwind over long and short hills. It also reduces the total and maximum enhancement over short hills (L<10km); the magnitude of this effect suggests the need to carry out an observational experiment of the enhancement over short hills in warm sectors.

(ii) The model (Ref.3) slightly overestimates the enhancement over short hills; but is adequate for long hills. Thus, as supported by the calculations of Ref.5 we would expect the Ref.3 model to be sufficient for the hills of South Wales (L~10km).

(iii) The effects of stratification are small irrespective of hill length and of whether the effects of condensation on the airflow are or are not included. A potential flow model is sufficiently accurate to be used for hills of all lengths; neglect of stratification would lead only to a slight overestimate in the enhancement over long hills.

(iv) Three-dimensional effects are important over short steep hills (h/L≥0.3), but negligible over long hills.

(v) Both peak and total enhancements increase slowly with windspeed over long hills, but decrease over short hills.

(vi) The enhancement increases slowly with the pre-existing precipitation rate over both long and short hills.

(vii) The seeder-feeder process is a very efficient mechanism for washing out aerosol (in the feeder cloud). This can result in rainfall of very low pH in hilly regions.

REFERENCES

1. Bergeron T 1965 Suppl. Proc Int Conf Cloud Phys, Tokyo May 1965, 96-100
2. Storebø P B 1976 Tellus, <u>28</u> 45-59
3. Bader M J and Roach W T 1977 Quart J Roy Met Soc, <u>103</u>, 269-280
4. Gocho Y 1978 J Met Soc Japan, <u>56</u>, 405-423
5. Hill F F, Browning K A and Bader M J 1981 Quart J Roy Met Soc, <u>107</u>, 643-670
6. Carruthers D J and Choularton T W 1983 ibid <u>109</u>, 575-588
7. Carruthers D J and Choularton T W 1982 ibid <u>108</u>, 603-624
8. Pruppacher H R and Klett J D 1978 <u>Microphysics of clouds and precipitation</u> Reidel
9. Carruthers D J 1982 PhD dissertation, University of Manchester
10. Fraser A B, Easter R C and Hobbs P V 1973 J Atmos Sci, <u>30</u>, 801-812
11. Anderson P 1972 Yearbook for Bergen, Nat Naturv Series No 1
12 Utaaker K 1963 Univ Bergen Skrister <u>28</u>

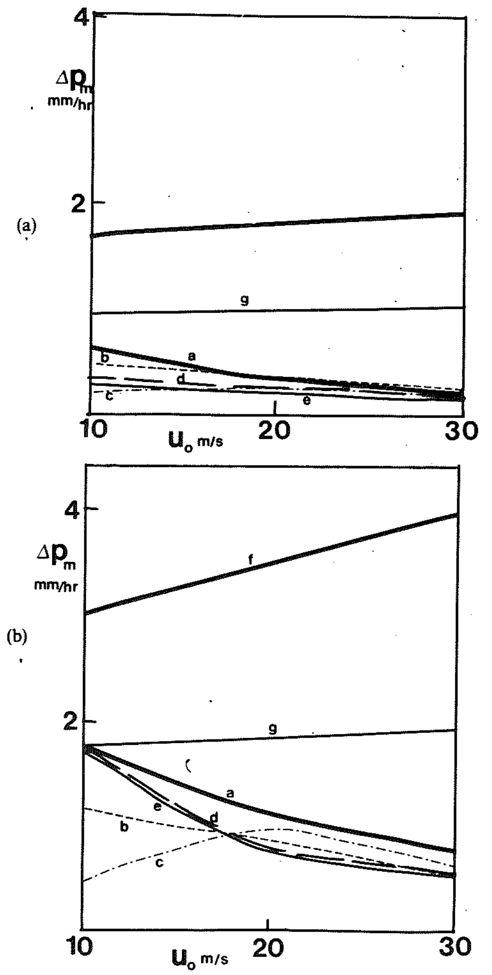

Figure 1. Maximum precipitation enhancement ΔP_m(mm hr^{-1}) as a function of windspeed and airflow model formulation for a short hill L=2000m, h=600m, Z_c=1500m.
(a) P_o = 0.5mm h^{-1}
(b) P_o = 2.5mm h^{-1}

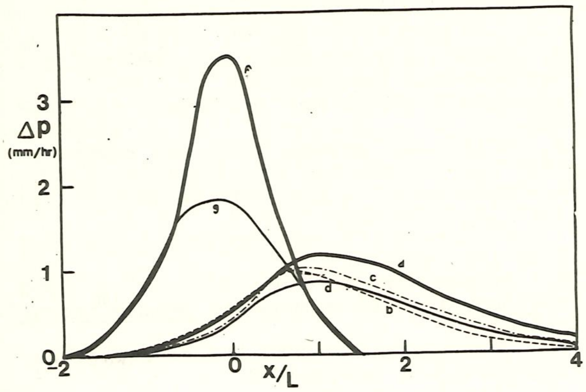

Figure 2. Precipitation enhancement as a function of distance over the short hill. P_o = 1.5mm h^{-1}

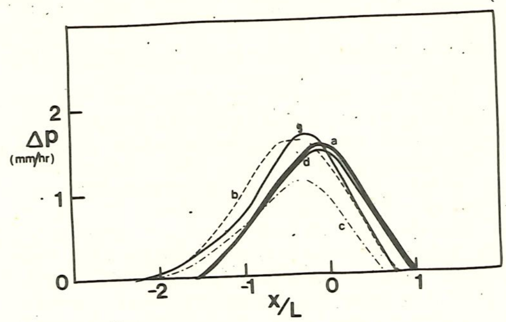

Figure 4. Precipitation enhancement as a function of distance over the long hill. P_o = 1.5mm h^{-1}

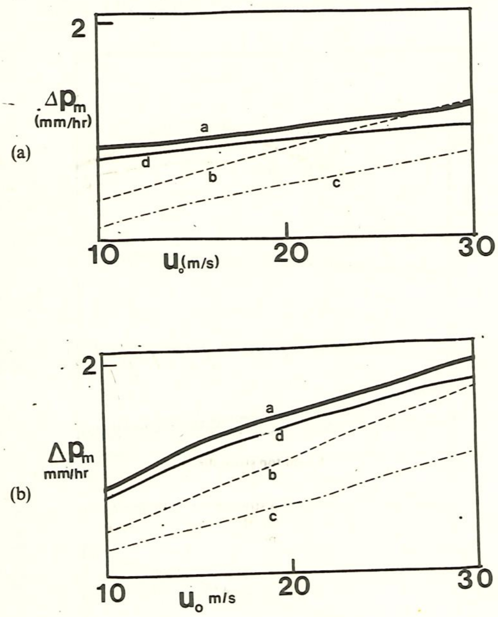

Figure 3. The variation of the maximum precipitation enhancement ΔP_m(mm h^{-1}) as a function of windspeed and airflow model for formulation for a long hill. L=20km, h=600m, Z_c =1500m. The 2D and 3D models give identical results.

(a) P_o = 0.5mm h^{-1}

(b) P_o = 2.5mm h^{-1}

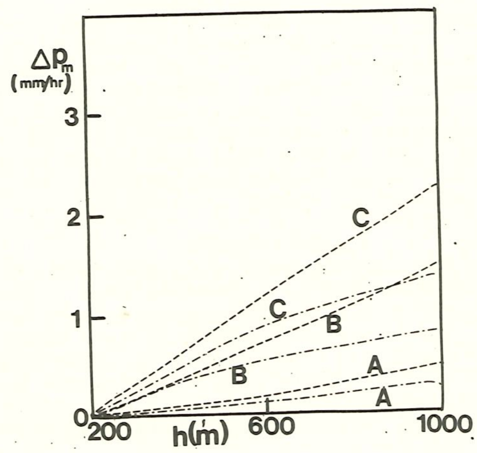

Figure 5. Maximum enhancement ΔP_m as a function of hill height. L=2000m, Z_c =1500m. Dashed line: 2D potential flow; dash-dot line: 3D potential flow.

CHARACTERISTICS AND EVOLUTION OF THE BOUNDARY LAYER CAPPED CLOUDS AS DETERMINED FROM 1D NUMERICAL SIMULATION

Chaing Chen and William R. Cotton
Dept. of Atmospheric Science
Colorado State University
Fort Collins, Colorado 80523
U.S.A.

1. INTRODUCTION

In order to simulate the stratocumulus-capped mixed layer, a one-dimensional stratocumulus model is developed. This model consists of five major p rts: (1) a one-dimensional (1D) option of the CSU Cloud/Mesoscale Model, (2) a partially-diagnostic higher-order turbulence model, (3) an atmospheric radiation model, (4) a partial condensation parameterization and (5) the drizzle precipitation.

This model is tested against the observed structure of the marine stratocumulus layer reported by Brost et al. (Refs. 1 and 2). The purpose of this paper is to investigate the interactions among the following physical processes: turbulence mixing, vertical wind shear, atmospheric radiation, drizzle precipitation, and large scale divergence.

2. MODEL DESCRIPTION

The current version of the CSU cloud/mesoscale model is a nonhydrostatic, multi-dimensional model which is evolved from a pure cloud model (Ref. 3). The stratocumulus model is just a special one-dimensional version of the "core" cloud/mesoscale model.

The second-order moment equations were derived by from Ref. 4. Ref. 5 is followed for the third-order moments and is also generalized to include the total water (r) and cloud water (r_c).

The radiation model consists of two parts: short-wave and long-wave radiation. The parameterization of long-wave radiation flux through a clear atmosphere follows Ref. 6. Refs. 7 and 8 introduced 'effective' emissivity of the cloud, where the cloud-layer emissivity is parameterized from observations. For the emissivity of an air column containing a clear and cloudy atmosphere (or a partially cloudy atmosphere), the 'mixed-emissivity' assumption (Ref. 9) is adopted.

The short-wave radiation model includes atmospheric molecular scattering and the parameterization of reflectance, transmittance and absorptance of a cloud layer (Ref. 8). The structure of the short-wave radiation model follows that of Ref. 10, which is a two-stream model (upward and downward flux). The 'equivalent transmittance' (Ref. 11) is employed to derived the reflectance, transmittance and absorptance of a 'clear-cloud mixed' atmosphere.

The 'all or nothing' condensation scheme is replaced by a 'partial condensation' parameterization. Two types of probability density function are tested in Ref. 12: (1) uniform distribution function Ref. 13 and (2) skewed distribution function (Ref. 14). In this paper, the gamma function is used as the probability density function.

In order to test the model against the observed structure of the marine stratocumulus layer (Refs. 1 and 2), the parameterization of rain and its fluxes are introduced and incorporated into the one-dimensional cloud/turbulence/radiation model. The governing equations for the warm rain parameterization is derived from Refs. 4 and 15 to deal with small mean radius of raindrops. The turbulence fluxes of rain are parameterized according to the scheme described by Ref. 4.

3. DESIGN OF THE NUMERICAL EXPERIMENTS

As we have mentioned before, the purpose of this paper is to test the CSU marine stratocumulus model against the observed structure of the marine stratocumulus layer (Refs. 1 and 2).

The initial and boundary conditions to start up the model are based on the field experiment off the California coast near San Francisco in June 1976. The details and the analysis of this experiment are described by Refs. 1 and 2.

Table 1 shows the sensitivity experiments for physical processes which include: 1) vertical wind shear; 2) long wave (L.W.) radiative cooling/warming; 3) large scale subsidence; and 4) drizzle precipitation. The experiments listed in Table 1 have one hour simulations.

TABLE 1

Design of the Sensitivity Experiments - Physical Processes

Exp	With Shear	L.W. Radiation Activated[1]	With Subsidence	With Drizzle	With Warmer Sea Surface Temp
STRS1	X	X		X	θ_s=285.16°K
SHEAR		X		X	"
RAD[2]	X	Not activated after 1800 sec		X	"
DRIZ[3]	X	X		X	"
DIV1[4]	X	X	Div=$5.0\times10^{-6}s^{-1}$	X	"
DIV2	X	X	Div=$1.0\times10^{-5}s^{-1}$	X	"

1. L.W. radiative model is activated every 60 sec
2. Experiment radiation
3. Experiment drizzle
4. Experiment divergence

4. SENSITIVITY EXPERIMENTS

4.1 Experiment STRS1

In Fig. 1, the maximum cloud water content occurs at 38 min with the magnitude around 0.357 g/kg. The cloud top starts to rise one grid after 45 min. From 45 min to 60 min the averaged cloud water content is around 0.2 g/kg. Although the fluctuation of cloud water content is incorporated in the parameterization of autoconversion the Exp. STRS1 still shows the overprediction of the cloud water content when it is compared with the observation.

In Fig. 2, a trace of pollutant is released below the top of the mixed layer. The pollutant does not have any terminal velocity or buoyancy and does not have any chemical reaction with the

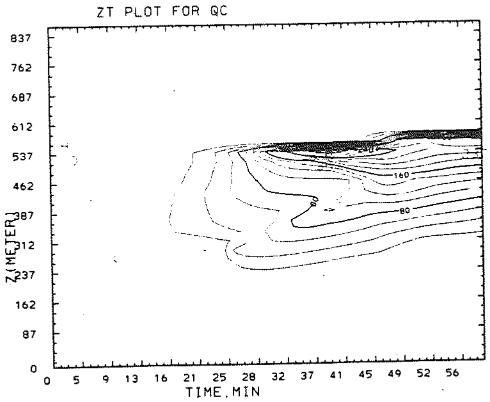

Fig. 1. The time-height contour for cloud water mixing ratio. The manitude of the maximum cloud water content is 0.357 g kg^{-1}. The interval of the contour is 0.02 g kg^{-1}.

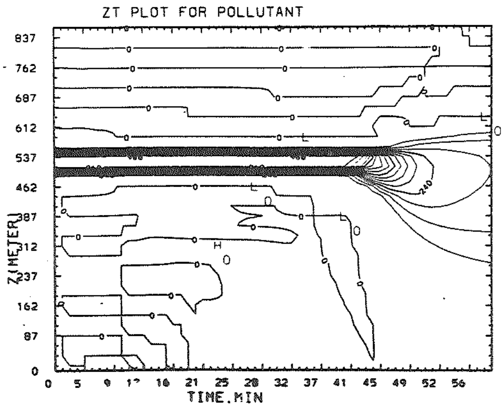

Fig. 2. The time-height contour for pollutant. The initial vaue for the pollutant is 1.0 g kg^{-1}. The interval of the contour is 0.06 g kg^{-1}.

radiation or the cloud liquid water. The total mass of the pollutant is found to be conserved all the time. From Figure 2 the pollutant abruptly commences to diffuse both upward and downward after 40 min. It is very interesting to investigate the reason why the pollutant diffuses after 40 min.

Figures 3, 4, 5 and 6 show the contour of four different kinds of Richardson number (R_{iv}, R_{ie}, R_{if}, R_{it}). R_{iv} and R_{ie} are the so-called gradient Richardson number. The flux Richardson number is defined by $R_{if} = -B/S$, Where the terms B and S represent the buoyancy production and shear production of the turbulence kinetic energy (TKE). In order to investigate a "transport instability", the transport Richardson number is proposed which can be defined by $R_{it} = -(B+D)/S$. Where the term D represents the vertical transport of TKE by eddies.

The cloud top entrainment processes are characterized by the indirect circulation. Energy is required to drive the indirect circulation. The energy comes from either the local shear or is vertically transported from the underlying mixed layer. The transport Richardson number is an index of the onset of the instability caused by vertical transport of turbulence kinetic energy and shear.

From Figures 3 and 4, the layer near the cloud top begins to develop thermal instability (negative

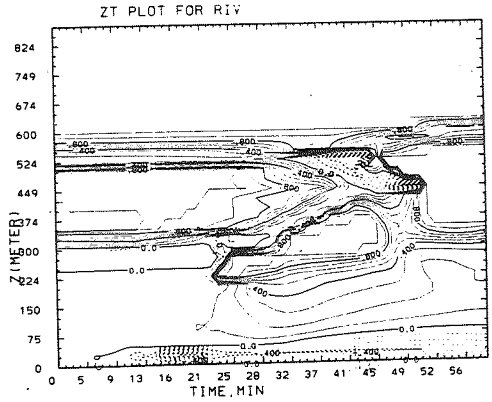

Fig. 3. The time-height contour for $\overline{\theta_v}$ Richardson number. The computation of R_{iv} is limited by $-1 \le R_{iv} \le 1$.

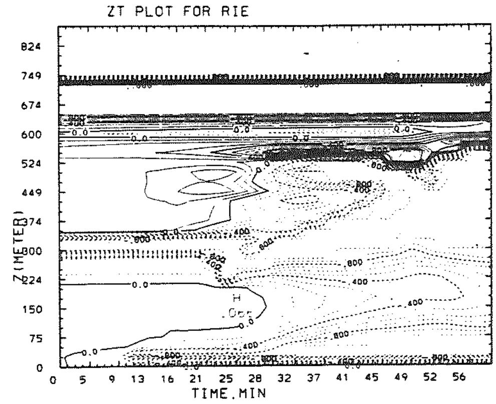

Fig. 4. As in Fig. 3, except for $\overline{\theta_e}$ Richardson number.

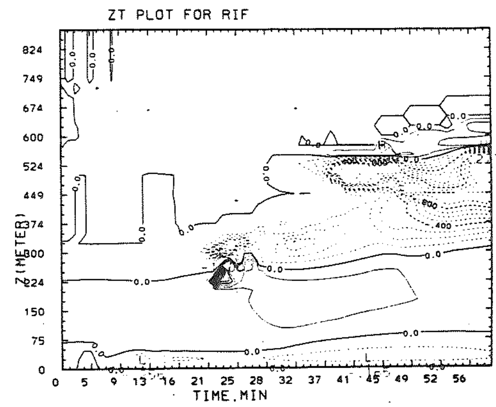

Fig. 5. As in Fig. 3, except for flux Richardson number. R_{if} is defined by $R_{if} = - B/S$, where B and S represent the buoyancy production and shear production of the turbulence kinetic energy.

R_{iv} and R_{ie}) after 30 min. This thermal instability is caused by the long wave (L.W.) radiative cooling. According to Figures 3 and 4, the layer above the cloud top is stable all the time. Both figures also show the intrusion of the warm air into the cloud layer at 45 min. It is obvious that the onset of the instability at 40 min. can not be explained by R_{iv} or R_{ie}. The contour of the flux Richardson as shown in Figure 5 also shows the similar behavior that has been found in Figures 3 and 4. However, the contour of the

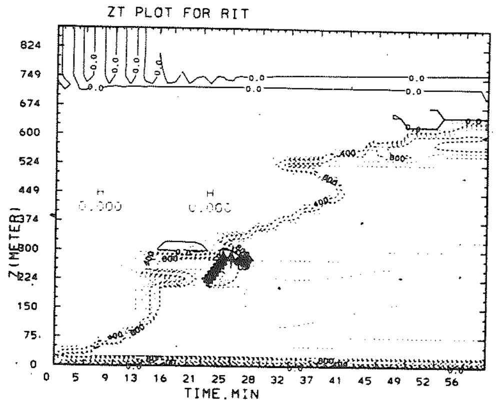

Fig. 6. As in Fig. 5, except for transport Richardson number, T_{it} is defined by R_{it} = -(B+D)/S. Where D represents the vertical transport of turbulence kinetic energy.

transport Richardson number (Figure 6) shows that the layer above the cloud top begins to show the development of the instability at 40 min.

The profiles of vertical heat flux ($\overline{w'\theta''_{il}}$, $\overline{w'\theta''_{v}}$) are shown in Figure 7. During the mature stage of cloud top thermal instability (45 min), the profile of $\overline{w'\theta''_{il}}$ is characterized by the large positive heat flux in the upper part of the cloud. At the mature stage of cloud top transport instability (60 min), a significant large negative heat flux can be found near the cloud top.

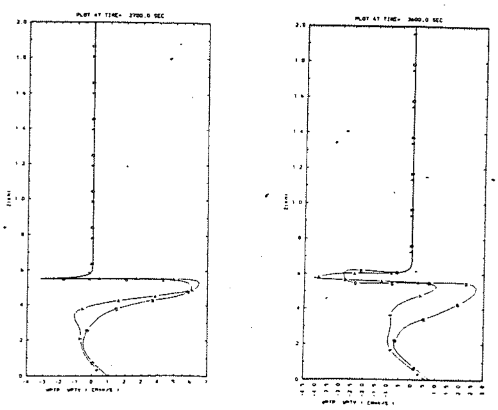

Fig. 7. The vertical profile of $\overline{w'\theta''_{il}}$ and $\overline{w'\theta''_{v}}$, at t = 2700 and 3600 seconds.

4.2 Experiment SHEAR

As shown in Table 1, the Exp. SHEAR is actually a sensitivity experiment without vertical wind shear. The maximum of the cloud water is 0.431 g/kg, which is 0.074 g/kg higher than that of the Exp. STRS1.

The onset of the transport instability can be identified after 45 min. The cloud top thermal instability is also believed to trigger the diffusion instability. Unlike the Exp. STRS1, the magnitude of the maximum negative heat flux during the entrainment instability is about -3.52 cm °K s^{-1} which is 2.85 cm °K s^{-1} smaller than that of the Exp. STRS1. The vertical thickness of the negative heat flux is also shallower than that of the Exp. STRS1. Therefore, the vertical wind shear across the cloud top not only promotes entrainment, but also increases the thickness of the entrainment interface layer.

4.3 Experiment RAD

According to Table 1, the L.W. radiation model is deactivated in Exp. RAD after 30 min. The purpose of applying the radiation model from 0 min to 30 min is to accelerate the formation of the cloud. After 30 min, the maximum of the cloud water is around 0.15 g/kg which is 0.207 g/kg lower than that of Exp. STRS1. Therefore, the cloud top radiative divergence is considered to be a controlling factor in the evolution of the stratocumulus mixed layer. From the results of Exp. STRS1, the stratocumulus mixed layer is found to be driven by buoyancy. Cloud top radiative cooling, however, is responsible for the production of buoyancy.

Figure 8 represents the vertical profiles of $\overline{w'\theta''_{il}}$ and $\overline{w'\theta''_{v}}$) at 45 min and 60 min. As shown in Figure 8, wind shear is very effective in producing the negative heat flux through the entire cloud layer. When Figure 8 is compared with Figure 7, the significant difference between the two experiments is that a positive heat flux exists below cloud top for the Exp. STRS1. The above mentioned positive heat flux is due solely to the cloud top L.W. radiative cooling. Therefore, the stratocumulus shown by Exp. RAD can be classified as a shear-driven cloud layer.

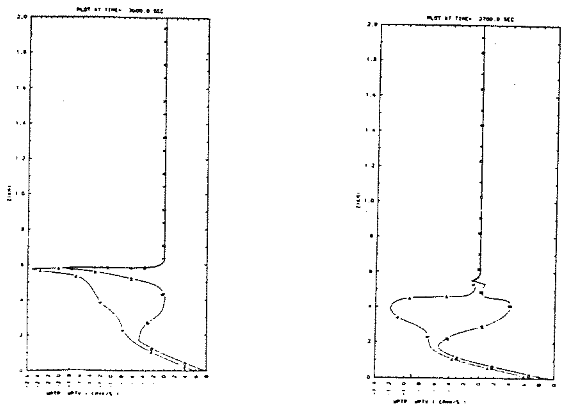

Fig. 8. As in Fig. 7, except for the Exp. RAD.

4.4 Experiment DRIZ

The drizzle process is deactivated for Exp. DRIZ. The deactivation of the drizzle precipitation produces more cloud water. The maximum cloud water content is 0.5 g/kg for Exp. DRIZ, while Exp. STRS1 has the maximum around 0.357 g/kg. Since the cloud top L.W. radiative cooling is determined by the cloud water path, the L.W. radiative cooling rate would be expected to be larger than that for the Exp. DRIZ. Exp. DRIZ exhibits 40°K/day larger cooling rate than the maximum L.W. cooling rate in Exp. STRS1 which contains drizzle.

In general, the Exp. DRIZ shows that the deactivation of the drizzle process enhances the buoyancy effect. The cloud layer simulated by the Exp. DRIZ can be considered as an extreme case of a "buoyancy-driven" stratocumulus capped mixed layer.

4.5 Experiment DIV1

The divergence Exp. DIV1 is 5.0 x 10^{-6} s^{-1} which can produce 0.25 cm s^{-1} subsidence at the height of 550 m. For a 10°K jump inversion, the layer with 25 m thickness can have 190°K/day entrainment warming due subsidence corresponding to $5.0 \times 10^{-6}\ s^{-1}$ divergence. Therefore, a significant part of the L.W. radiative cooling can be balanced partially by subsidence warming. The Exp. DIV1 produces less cloud water content (0.273 g kg^{-1}) than the Exp. STRS1 with the result of decreasing the buoyancy effect relative fo Exp. DIV1.

4.6 Experiment DIV2

In Exp. DIV2 a divergence of $1.0 \times 10^{-5}\ s^{-1}$ is imposed which is twice than that in Exp. DIV1. The maximum of the cloud water is around 0.162 g/kg. The height of the cloud top and cloud base is about 100 m ~ 150 m lower than that for the Exp. DIV1. Also the positive heat flux is insignificant for Exp. DIV2. Radiative cooling is obviously balanced by subsidence warming. The cloud layer simulated by Exp. DIV2 can be classified as a "shear driven" stratocumulus layer, which is similar to the cloud layer shown in the Exp. RAD.

5. CONCLUSIONS

In general, the Exp. STRS1 is quite successful in reproducing the profiles reported by Ref. 2. The thermal instability and the transport instability can be used to explain some of the characteristics shown in their paper.

The turbulence kinetic energy within the mixed layer is found to be produced by the destabilization of the layer at the cloud top. The L.W. radiative cooling is responsible for this destabilization. From the plot of the flux and transport Richardson, the thermal instability does exist at the cloud top. The onset of the thermal instability is also found prior to the onset of the transport instability. Therefore, the thermal instability can be considered as a trigger of the onset of transport instability.

The results from the sensitivity experiments for physical processes indicates:

1. The stratocumulus capped mixed layer is characterized by a "buoyancy-driven" cloud layer when vertical wind shear and drizzle precipitation are not present.
2. Without L.W. radiative warming/cooling, the stratocumulus cloud layer is totally controlled by wind shear. The character of the "shear-driven" cloud layer can also be found for the experiments with the activation of the large scale divergence and the existence of the upper level clouds.
3. Cloud top L.W. radiative cooling is the controlling factor to determine whether the cloud layer is "buoyancy-driven" or "shear-driven".

6. ACKNOWLEDGEMENTS

The authors wish to thank Dr. R.A. Brost for discussion. We also wish to thank Ms. Brenda Thompson for the word processing and typing. This work was supported under the Office of Naval Resarch (ONR) contract #N00014-83-K-0321 and the National Science Foundation grant #ATM-8312077. Computations were performed on the NCAR (National Center for Atmospheric Research) Cray-1 computer. NCAR is supported by the National Science Foundation.

7. REFERENCES

1. Brost, R.A., D.H. Lenschow and J.C. Wyngaard, 1982a: Marine stratocumulus layers. Part I: Mean conditions. J. Atmos. Sci., 39, 800-817.
2. Brost, R.A., J.C. Wyngaard, D.H. Lenschow, 1982b: Marine stratocumulus layers. Part II: Turbulence budgets. J. Atmos. Sci., 39, 818-836.
3. Cotton, W.R., and G.J. Tripoli, 1978: Cumulus convection in shear flow-- Three dimensional numerical experiments. J. Atmos. Sci., 35, 1503-1521.
4. Manton, M.J. and W.R. Cotton, 1977: Formulation of approximate equations for modeling moist deep convection on the mesoscale. Atmos. Sci. Paper No. 266, Dept. of Atmos. Sci., Colorado State University.
5. Zeman, O. and J.L. Lumley, 1976: Modeling buoyancy driven mixed layers. J. Atmos. Sci., 33, 1974-1988.
6. Rodgers, C.D., 1967: The use of emissivity in atmospheric radiation calculations. Quart. J. Roy. Meteor. Soc., 93, 43-54.
7. Stephens, G.L., 1978a: Radiation profiles in extended water clouds. I: Theory. J. Atmos. Sci., 35, 2111-2122.
8. Stephens, G.L., 1978b: Radiation profiles in extended water clouds. II: Parameterization schemes. J. Atmos. Sci., 35, 2123-2132.
9. Herman, G. and R. Goody, 1976: Formation and persistence of summertime arctic stratus clouds. J. Atmos. Sci., 33, 1537-1553.
10. Stephens, G.L. and Webster, P.J., 1979: Sensitivity of radiative forcing to variable cloud and moisture. J. Atmos. Sci., 36, 1542-1556.
11. Stephens, G.L., 1977: The transfer or radiation in cloudy atmosphere. Ph.D. Thesis. Meteorology Department, University of Melbourne.
12. Chen, C., and W.R. Cotton, 1983: A one-dimensional simulation of the stratocumulus-capped mixed layer. Boundary-Layer Meteorol., 25, 289-321.
13. Banta, R. and W.R. Cotton, 1980: On computing average cloud-water quantities in a partially cloudy region. J. de Rech. Atmos., 14, 487-492.
14. Bougeault, Ph., 1981: Modeling the trade-wind cumulus boundary layer. Part I: Testing the ensemble cloud relations against numerical data. J. Atmos. Sci., 38, 2414-2428.
15. Tripoli, G.J., and W.R. Cotton, 1982: The Colorado State University three-dimensional cloud/mesoscale model - 1981. Part I: General theoretical framework and sensitivity experiments. J. de Rech. Atmos., 16, 185-220.

A MODEL OF THE OROGRAPHIC ENHANCEMENT OF SNOWFALL

T W CHOULARTON and S J PERRY
Physics Department, UMIST, PO BOX 88,
Manchester M60 1QD, England

1. INTRODUCTION

In the seeder-feeder mechanism of precipitation enhancement it is envisaged that steady, relatively light precipitation is produced by a high-level seeder cloud which is unaffected by the presence of a low hill. However, when the moist low-level air is forced to rise over the hill a cloud is produced approximately 1km in depth which has a high liquid water content. The droplets in this cloud are small and so it is unable to produce precipitation itself: however, the seeder precipitation is able to very effectively sweep out the feeder cloud droplets giving rise to a substantial enhancement in the precipitation rate at the ground.

In a recent study (Ref.1) it is reported that low-level enhancement of snowfall, by a mechanism analagous to that of the seeder-feeder mechanism of the orographic enhancement of rainfall, resulted in a doubling of the snowfall rate over the hills of South Wales with a low-level easterly wind. Similar observations have been obtained by comparisons of the depth of snow accumulated on the Yorkshire Plain and on the Pennines after East wind snowfalls over Northern England. The density of the accumulated snow on the hills was similar to that on the lowlands and the snow falling consisted predominantly of vapour grown crystals (rather than heavily rimed particles) in both areas.

Hence it was decided to study the orographic enhancement of snowfall via the seeder-feeder mechanism found to be applicable to orographic rainfall, and to investigate the relative roles of growth of the seeder snow crystals by riming and vapour diffusion in the feeder cloud and to examine a possible role for secondary ice particle generation in the feeder cloud. In addition, the effects of wind-drift of precipitation and the stratification of the atmosphere may play crucial roles.

2. THE MODEL

2.1 Dynamics

This is based on the semi-linear airflow model (Ref.2) and incorporated into a model of orographic rainfall (Ref.3), in which it was shown that the incorporation of stratification had very little effect on the distribution and magnitude of the enhancement of rainfall, provided the flow didn't block. Accordingly a potential flow airflow model is used with a non-linear lower boundary condition as described in (Refs.2,3)

2.2 Microphysics

The air in which the feeder cloud is to form starts off upwind of the hill with a relative humidity of 90%. As this air is forced to ascend over the hill, the air cools, ice saturation is reached and the snowflakes can begin to grow by vapour diffusion.

The continuity equation for the available water q (q includes any liquid water present and the excess of water vapour over ice saturation) is given by

$$\frac{Dq}{Dt} = C - A \qquad (1)$$

where C is the rate at which water vapour becomes available and A the rate of absorbtion by precipitation. Assuming that the whole system is in a steady state then

$$\frac{D}{Dt} = \frac{U\partial}{\partial S} \qquad (2)$$

where U is the upwind velocity along a streamline trajectory S.

The rate at which water vapour becomes available C is given by

$$C = \frac{-W\partial\rho_s}{\partial z} \qquad (3)$$

where $\partial\rho_s/\partial z$ is the variacion of the saturated vapour pressure over ice with height.

Since the rate of removal of water from the cloud leads to the increase in precipitation rate then

$$A = \frac{-\partial P}{\partial z} \qquad (4)$$

where P is the precipitation rate. A itself is determined from the rate of growth of the crystals by vapour diffusion and riming. The latter can only occur if water saturation is reached in the feeder zone.

The model has so far been run with seeder precipitation consisting of unrimed radiating assemblage of dendrites. The mass/size relation and terminal velocity were obtained from Ref.4. The vapour growth of the snowflakes was calculated using the standard equation as found in, e.g. Ref.5 with the ventilation effect included.

The growth by accretion for a snowflake was calculated using the expression

$$\frac{dm_i}{dz} = \pi r^2 LEV \qquad (5)$$

where m_i is the mass of the snowflake, r its radius, L the liquid water content of the cloud, E the collection efficiency and V the terminal velocity of the flake. E was taken as 0.8.

2.3 Solving the equations

The accumulation of water by the snow in the feeder cloud was calculated in a grid covering the cloud with neighbouring elements along the same streamline. Starting at the upstream edge of the feeder cloud (where ice saturation is reached), the crystals fall through the top row and grow by vapour diffusion. The rate of release of water vapour is then calculated from the updraught in the grid element and offset against the loss due to vapour growth of the crystals to calculate the supersaturation with respect to ice in the neighbouring grid element along the top streamline. The growth of snow crystals falling through this element is then calculated and the process repeated along the streamline to the downstream edge of the cloud. The products of this will then be allowed to sediment through the next lowest set of grid elements and grow accordingly, with wind-drift taken into account, as described in Ref.3. If a supersaturation with respect to water developed in any grid element, this was converted to liquid water and the crystals were allowed to grow by riming.

3. RESULTS

These apply to a hill of the form

$$G(x) = \frac{h}{1 + \left(\frac{x}{L}\right)^2} \qquad (6)$$

where h is the hill height 600m, for the results presented below and L the half-length. The studies performed to date are for an upwind surface temperature of -3°C. The environmental lapse rate is dry adiabatic up to 150m and moist adiabatic above this level and the seeder cloud precipitation rate 1.5mm hr^{-1}. (All precipitation rates are rain equivalent values.)

It is found in general that for long hills $L \gtrsim 20$km water saturation is not reached and the growth of the precipitation is by vapour diffusion alone. For smaller hills, represented by L = 2km, liquid water is present and for L = 2km growth by accretion dominates for windspeeds ≥ 10m s^{-1}.

Figures 1 and 2 show the distribution of snowfall over the long hill (L = 20km) with a 1500m deep feeder cloud for windspeeds of 10m/s and 20m/s respectively. The doubling in windspeed nearly doubles the enhancement of the snowfall rate. This is due mainly to a large increase in the rate of supply of water vapour. Due to an increased wind-drift effect the maximum precipitation rate is moved slightly downwind; however, on this long hill the effects of wind-drift are small.

Increasing further the depth of the feeder cloud only causes a small further increase in the maximum precipitation rate as the effect of wind-drift becomes more important. The major effect is to produce an increasing tail of enhanced snowfall on the lee-slope (Figure 3).

Figures 4 and 5 show sample results for a short hill (L = 2km) over which growth by accretion is dominant, again with a 1500m deep feeder cloud and with windspeeds of 10m s^{-1} and 20m s^{-1} respectively. A large enhancement in the precipitation rate occurs just downwind of the summit and is comparable in magnitude to the values obtained over the long hill, but the precipitation arriving at the ground is heavily rimed and so of greater density. The larger updraughts on the short hill result in large values of liquid water contents near the summit which are offset by a larger wind-drift effect producing substantial enhancements downwind of the summit. The effects of wind-drift are partially reduced by the greater terminal velocity of the rimed particles.

4. CONCLUSIONS

It has been shown that the seeder-feeder mechanism is to be expected to produce substantial enhancement of snowfall over low hills. Over long hills water saturation is not established over much of the depth of the feeder cloud and the enhancement is due almost entirely to vapour growth. This result would seem able to explain the examples of low-level enhancement of snowfall cited in the introduction.

Over a long hill, increasing the windspeed up to 20m s^{-1} causes an increase in the maximum and total enhancements of precipitation rate. Increasing the feeder cloud depth beyond 1500m has little effect on the maximum enhancement due to an increase in the importance of wind-drift.

Over short hills substantial liquid water develops in the feeder cloud and growth of the precipitation is predominantly by riming with substantial enhancements confined to the region near the hill summit and downwind as wind-drift is very important.

We are currently working on a more detailed study of the enhancement process as a function of the upstream conditions and the size and shape of the hill. We are also investigating the possible role of ice multiplication resulting in growth by aggregation in clouds where substantial liquid water is produced.

REFERENCES

1. Browning K A 1983 Air motion and precipitation growth in a major snowstorm. Quart J Roy Met Soc, 109, 225-243
2. Carruthers D J and Choularton T W 1982 Airflow over hills of moderate slope. ibid, 108, 603-624
3. Carruthers D J and Choularton T W 1983 A model of the feeder-seeder mechanism of orographic rain including stratification and wind-drift effects. ibid, 109, 575-88
4. Locatelli J D and Hobbs P V 1974 Fall speeds and masses of solid precipitation particles. J Geophys Res, 79, 2185-97
5. Pruppacher H R and Klett J D 1978 Microphysics of Clouds and Precipitation D Reidel (pub)

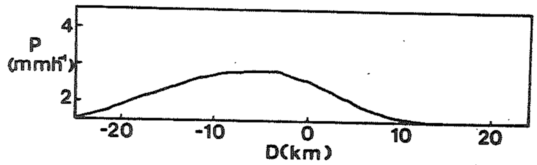

(1)

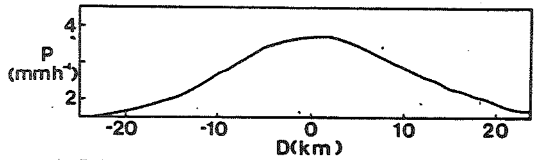

(2)

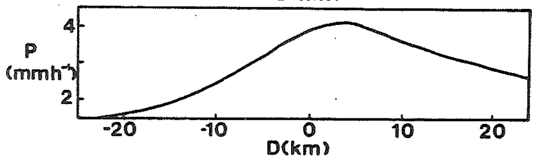

(3)

Figure 1. Precipitation rate (rain equivalent) in mm hr^{-1} against horizontal position over a hill with L = 20km. Feeder cloud depth = 1.5km, windspeed 10m s^{-1}.

Figure 2. As Fig.1 but with windspeed of 20m s^{-1}

Figure 3. As Fig.2 but with feeder cloud depth 2.5km.

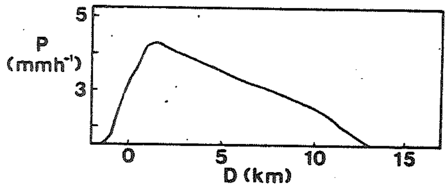

(4)

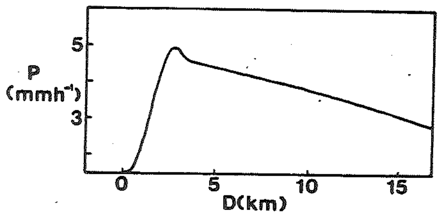

(5)

Figure 4. As Fig.1, but over a hill with L = 2km

Figure 5. As Fig.4, but with windspeed = 20m s^{-1}

A NUMERICAL SIMULATION OF THE EFFECTS OF SMALL SCALE TOPOGRAPHICAL VARIATIONS ON THE GENERATION OF AGGREGATE SNOWFLAKES

William R. Cotton, Gregory J. Tripoli and Robert M. Rauber
Dept. of Atmospheric Science
Colorado State University
Fort Collins, Colorado 80523
U.S.A.

1. INTRODUCTION

In an earlier study reported by Cotton et al. (Ref. 2), the CSU multidimensional cloud/mesoscale model was used to simulate the evolution of an observed orographic cloud. Intensive observations of this orographic precipitation event were made as part of the 1979 COSE (Colorado Orographic Seeding Experiment) field program and reported by Rauber (Ref. 1).

The results of that study suggested that the major deficiency of the model was its inability to predict adequate amounts of precipitation over the barrier crest. It was concluded that the deficiency could be largely attributed to the lack of a model of the ice crystal aggregation process. Rauber (Ref. 1) also speculated that local topographic features upstream of the main barrier crest creates "generating zones" which initiate aggregate embryos (small ice crystals) which can then aggregate and settle into the water rich regions along the upstream barrier crest.

Based on these results, it was decided to design a model experiment using actual topography. At the same time an ice crystal aggregation model was formulated along with a model for predicting ice crystal concentrations. In the following sections the formulation of the aggregation model is described, and the results of preliminary numerical experiments with this second-generation ice-phase model are presented.

2. SUMMARY OF THE MICROPHYSICAL MODEL

Water substance in the model is distributed among the variables total water mixing ratio r_T and the mixing ratios of water vapor r_v, cloud water r_c, raindrops r_r, ice crystals r_i, graupel particles r_g, and aggregates r_a. The mixing ratio of cloud droplets r_c, and water vapor are determined diagnostically. In addition, the concentration of ice crystals, N_i, is a prognostic variable. For the purposes of this paper, we shall concentrate on the prognostic equations for $\bar{r}_a$ and N_i, with the equations for the mixing ratios of other water quantities described in Ref. 2.

The conservation equation for the mean aggregate mixing ratio is:

$$\frac{\partial \bar{r}_a}{\partial t} = -\frac{\partial}{\partial x_j}\bar{u}_j\bar{r}_a - \frac{\partial}{\partial x_j}\overline{u_j''r_a''} - \frac{1}{\rho_o}\frac{\partial}{\partial z}\rho_o\bar{v}_a\bar{r}_a + \overline{VD}_{va} + \overline{CL}_{ca} + \overline{CL}_{ra} - \overline{ML}_{ar} - \overline{SH}_{ar} + \overline{CL}_{ia} + \overline{CN}_{ia} - \overline{CL}_{ag} - \overline{CN}_{ag} \tag{1}$$

Similarly, the conservation equation for ice crystal concentration is given by

$$\frac{\partial}{\partial t}\left[\frac{\bar{N}_i}{\rho_o}\right] = -\frac{\partial}{\partial x_j}\bar{u}_j\left[\frac{\bar{N}_i}{\rho_o}\right] - \frac{\partial}{\partial x_j}\left[\frac{\overline{u_j''N_i''}}{\rho_o}\right] - \frac{\bar{N}_i}{\rho_o^2}\frac{1}{\bar{r}_i}\frac{\partial}{\partial z}(\rho_o\bar{V}_i\bar{r}_i) + NNUA_{vi} + NNUB_{vi} + NNUC_{vi} + NNUD_{vi} + NSP_{vi} + NML_{iv} + NCN_{ig} + NCL_{ig} + NCN_{ia} + NCL_{ia} \tag{2}$$

The following notation is used to describe the various processes: VD_{ab} = vapor diffusion, CL_{ab} = collection, CN_{ab} = conversion, ML_{ab} = melting, NUA_{ab} = nucleation by deposition, NUB_{ab} = nucleation by Brownian collection, NUC_{ab} = nucleation by thermophoresis, NUD_{ab} = nucleation by diffusiophoresis, SP_{ab} = splintering formation of ice crystals and SH_{ab} = shedding

Subscripts of the above terms define the source (second subscript) and sink (first subscript) water categories between which the transfer is made, where v = vapor, c = cloud water, r = rain, i = ice crystals, g = graupel and a = aggregates.

In this paper we shall concentrate on the conversion and collection terms for aggregates, and the nucleation terms for pristine ice crystals.

The conversion rate of r_i to aggregates is given by

$$CN_{ia} = -\frac{\bar{m}_i}{\rho_o}\left.\frac{dN_i}{dt}\right]_{CN} \tag{3}$$

where the average crystal mass $\bar{m}_i$ is given by

$$\bar{m}_i = \frac{\bar{r}_i\rho_o}{N_i}.$$

The change in ice crystal concentration due to aggregation among a population of "pristine" ice crystals is given by

$$\left.\frac{dN_I}{dt}\right]_{CN} = -K_iN_i^2. \tag{4}$$

The collection kernel K_i is estimated from Passarelli and Srivastava's (Ref. 5) stochastic kernel for a distribution of particle densities of equal-sized crystals. This model reduces to

$$K_i = \frac{\pi D_i^2}{6}V_i\bar{E}_iX \tag{5}$$

where X is a measure of the variance of particle fall speed taken to be 0.25, D_i and V_i are the average crystal diameter and fall speed, respectively and E_i is the average collection efficiency among ice crystals.

Assuming that the aggregates once formed by conversion are distributed in the form

$$N(D) = \frac{N_T}{D_m} e^{-D/D_m} \tag{6}$$

where D_m is a "characteristic" diameter of the population estimated to be $D_m = 0.33$ cm, the rate of collection of ice crystals by mature aggregates is given by

$$CL_{ia} = 0.503\ \beta_1\ \rho_o\ E(a/i)\ |\overline{V_a} - \overline{V_i}|\ D_m^{-2.4} \times (2\ D_m^2 + 2\ D_i\ D_m + D_i^2)\ r_a\ r_i \tag{7}$$

where $\beta_1 = 0.015\ g\ m^{-2.4}$.

Both the rate of conversion (Eq. 3) and collection (Eq. 7) critically depend upon the collection efficiency E_i among ice particles.

In the following sections, the results of sensitivity experiments varying E_i is estimated from the temperature-dependent data reported by Hallgren and Hosler (Ref. 3) and Hosler and Hallgren (Ref. 4) [hereafter referred to as H-H]. In a second experiment, we assume a constant value of 1.4 over the temperature range -15°C and warmer based on Passarelli and Srivastava's (Ref. 5) aircraft estimate [hereafter referred to as PC]. A third experiment is performed in which we employ PC's estimate only in the temperature range -12 to -15°C and use HH's at warmer temperatures.

Since the initial rate of production of aggregates depends quadratically upon the concentration of ice crystals (Eq. 4), it is necessary to formulate more realistic models of ice crystal production. Use of the Fletcher (Ref. 6) deposition nucleation equation results in too few crystals at warm cloud temperatures for aggregation to occur. Thus, the Fletcher formula is combined with Young's (Ref. 7) models for contact nucleation by Brownian diffusion (NUB_{vi}), thermophoresis (NUC_{vi}) and diffusiophoresis (NUD_{vi}) to provide estimates for primary nucleation. We also estimate secondary production of ice crystals (NSF_{vi}) based on Gordon and Marwitz's (Ref. 8) parameterization of the Hallett-Mossop theory.

3. THE CASE STUDY

For this phase of the study we have selected a case from the 1982 COSE which occurred on 5 January 1982. The case was selected because it had cloud physics aircraft observations along with rawinsonde, Ku-Band radar, dual-channel microwave radiometer, surface mesonet and surface precipitation intensity and crystal observations during a quasi-steady period of a storm. A particularly outstanding feature of the sounding was the strong winds aloft. Westerly wind speeds ranged from 34 m s^{-1} to over 43 m s^{-1} from 500 mb to 200 mb. Winds weakened to 18 m s^{-1} from the southwest at 700 mb, however.

Based on the observations, four zones of particle growth were identified:

1) Colder than -15°C crystal growth was principally by diffusion. Crystal concentrations varied between 20 to 40 l^{-1} between -29 to -15°C;

2) Between -15°C and -12°C aggregate embryos were identified (i.e. double crystal aggregates) and ice crystal concentrations were as high as 100 l^{-1};

3) Between -10.5 to -9°C significant scavenging of the single crystal population by mature aggregates was prevalent.

4) From ridgetop level to the valley floor (-5°C) aggregate-aggregate collection/breakup processes prevailed though single crystal collection by aggregates continued.

4. EXPERIMENTAL DESIGN

The model was initialized with 30 minute topography along an east-west cross section of the Rocky Mountains at 40°N latitude. The domain generally ran from near the Colorado/Utah border to the High Plains to the east. The 30 min grid spacing corresponds to 718 m in the horizontal and a 500 m mesh was used in the vertical. The domain, illustrated in Fig. 1 is 367 km in the horizontal and 15.5 km high.

Lateral boundary conditions were the Klemp-Wilhelmson radiation condition with a mesoscale compensation region (see Ref. 9). The vertical boundary condition is the Klemp-Durran (Ref. 10) radiative boundary condition.

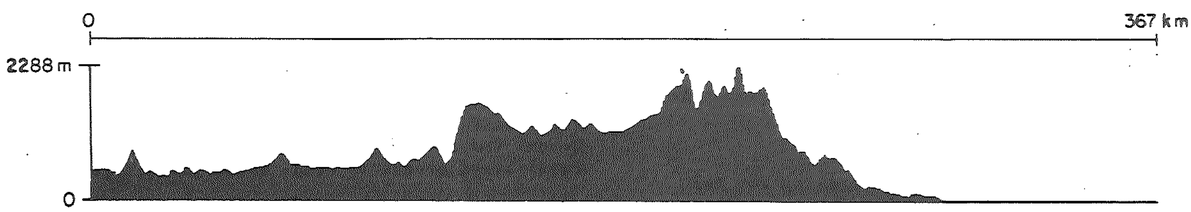

Fig. 1. Actual 30 minute topography used in the model. It represents west-east cross section extending from near the Colorado/Utah border (left side) to the Colorado High Plains. The first major ridge is the Park Range near Steamboat Springs, Colorado while the ridge further to the east is the Front Range just west of Fort Collins.

The model was initialized by adding the observed wind in increments for 30 min and then run for 2.5 hours to establish a quasi-steady mountain wave pattern. During this initialization phase, all microphysical tendencies were turned off. Each simulation was started from the same spin up result (at the end of the 3 hr. adjustment time) and run for an additional 2 hours.

The control experiment included all nucleation terms activated, and aggregation efficiencies based on HH and PC's estimate over the temperature range of -12 to -15°C.

5. SUMMARY OF RESULTS

For the control experiment, the largest supercooled liquid water contents were just over the upwind side of the Park Range (< 0.04 g kg^{-1}) and the Front Range (< 0.03 g kg^{-1}) with the highest liquid water contents (< 0.08 g kg^{-1}) being in the warmer lenticular cloud over the eastern plains.

Aggregates were initiated near the -15°C level but did not reach their highest mixing ratio (0.22 g kg^{-1}) until very near the ground over the Park Range. A similar profile was predicted over the Front range with the highest mixing ratio of aggregates being 0.16 g kg^{-1} (see Fig. 2). Near the surface, the principle process contributing to aggregate growth was CL_{ia}, aggregates collecting ice crystals while, CN_{ia} conversion was more than an order of magnitude smaller.

Near the ground over Steamboat Springs, the predicted ice crystal concentrations were approximately 10 l^{-1}. However, observed single crystal concentrations were typically less than one per liter. At the -14°C level the predicted single crystal concentrations were 1 to 10 l^{-1} which is about an order of magnitude less than observed values. At higher levels, the Fletcher deposition nucleation model resulted in consistently higher concentrations of ice crystals than observed. Model comparison with observed ice crystal concentrations is quite difficult however. Especially at warmer temperatures, there exists considerable variability in predicted crystal concentrations. This variability is also evident in the mixing ratio of pristine crystals as can be seen in Fig. 3. Thus, by moving an observer position left or right a few kilomters one could find predicted concentrations that are in better (or worse) agreement with observations. As a result of turning off deposition nucleation, the predicted concentration of ice crystals lowered to 0.3 l^{-1} at -14°C and the order of 1 l^{-1} at colder temperatures. This suggests that deposition nucleation is an important nucleation process, but its behavior is not well predicted by simple models such as the Fletcher formula.

As a consequence of defining aggregation efficiencies using H-H data, aggregation was reduced to only trace amounts (r_a < 0.02 g kg^{-1}) and that being only very close to the surface. This also resulted in higher concentrations of single crystals at the warmer temperatures.

Assuming $\overline{E_i}$ = 1.4 at all temperatures warmer than -15°C resulted in greatly enhanced aggregation in the stratified cloud upwind of the barrier crest. The resultant upstream precipitation led to progressive drying out of the atmosphere such that little supercooled water formed over the barrier crest. In addition, as time proceeded surface

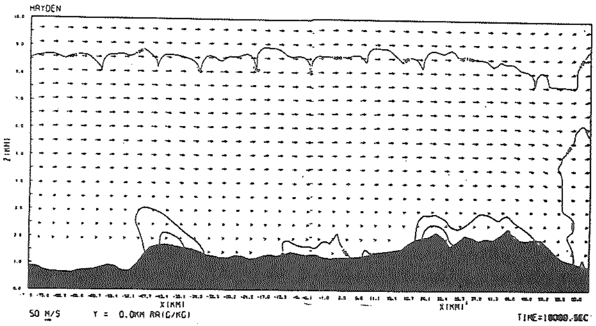

Fig. 2. Predicted wind vectors and contours of the mixing ratio of aggregates (r_a) after 1800 s of integration. Contour intervals are 0.1 g kg^{-1}. The dark contour line with the 100 label represents the zero threshold for aggregates.

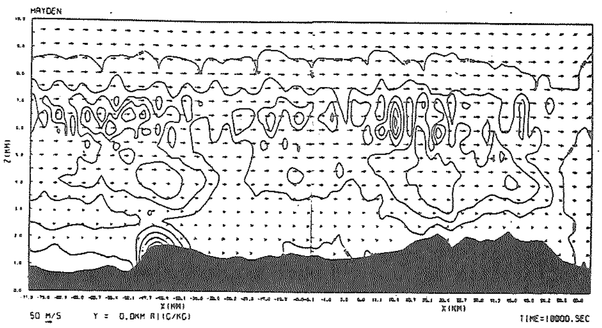

Fig. 3. As in Fig. 2 except contours are of the mixing ratio of pristine ice crystals (r_i). Contour intervals is 0.1 g kg^{-1}.

precipitation amounts diminished over the Park Range as well. Thus a combination of the H-H efficiencies and a constant $\overline{E_i}$ = 1.4 over the temperature range -12 to -15°C resulted in a predicted cloud structure most consistent with observation. Clearly, more observations and diagnostic studies are needed to further evaluate and refine the aggregation model.

6. CONCLUSIONS

The results of this study clearly illustrate the value of detailed observations in an orographic cloud environment to aid in the development and verification of models of precipitation processes. The temporal and spatial variability associated with turbulent cumulus clouds greatly reduces the likelihood of making definitive tests of a model.

The initial objective of this study was to examine the role of upstream hills in the initiation of precipitation processes affecting precipitation over the major orographic barriers. The upstream hills in the simulation are clearly triggering gravity waves aloft which initiate precipitation in the nearly saturated mid-tropospheric air mass. However, the two-dimensional model treats localized hills as ridges which can be expected to be a greater perturber of gravity waves than localized hills. Thus, a realistic appraisal of their importance requires three-dimensional simulations.

This study has strengthened the case for aggregation being a major contributor to surface precipitation and the water budget of orographic clouds. The aggregation model is very dependent upon the details of the model for aggregation collection efficiencies. The dendritic zone is viewed as the principle genesis region for aggregation. Mature aggregation evolves at warmer temperatures, however.

The predicted crystal concentrations also strongly modulate the rate of production aggregates. Our predictive ability for ice crystal concentration, unfortunately, is "at best" to within an order of magnitude and generally much poorer. The system, however is to some extent a self-regulating system. If primary nucleation is low, liquid water builds up allowing riming. The large rimed crystals can readily precipitate from the cloud system. If conditions are right (i.e., proper temperatures, etc.) the rimed crystals can also initiate secondary crystal production which can promote the formation of aggregates and contribute to precipitation. On the other hand, if initial crystal concentrations are high at warmer temperatures the resultant low-terminal velocity crystals might be expected to remain in the cloud for some time. However, as the concentration gets higher, the rate of production of embryos of aggregates get larger resulting in the tendency for the cloud to unload itself by precipitating aggregates. Thus, once a cloud is embedded within the aggregation zone (warmer than -15^{o}) precipitation can result over a broad range of ice crystal concentrations.

7. ACKNOWLEDGEMENTS

We thank Brenda Thompson for graciously typing the manuscript under the pressure of the deadline for submission of this paper. This research was supported by NSF Grants ATM8312077 and ATM8109590 and Air Force Contract #F19628-84-C-0005. The modelling was done on the NCAR CRAY-1 computer. NCAR is supported by the National Science Foundation.

7. REFERENCES

1. Rauber, Robert M., 1981: Microphysical processes in two stably stratified orograhic cloud systems. Atmos. Sci. Paper No. 337 (M.S. Thesis), Department of Atmospheric Science, Colorado State University, Fort Collins, CO 80523, 151 pp.

2. Cotton, W.R., M.A. Stephens, T. Nehrkorn, and G.J. Tripoli, 1982: The Colorado State University three-dimensional cloud/mesoscale model - 1982. Part II: An ice phase parameterization. J. de Rech. Atmos., 16, 295-320.

3. Hallgren, R.E. and C.L. Hosler, 1960: Preliminary results on the aggregation of ice crystals. Geo. Monogr., 5, 257-263.

4. Hosler, C.L. and R.E. Hallgren, 1960: The aggregation of small ice crystals. Disc. Farad. Soc., 30, 200-208.

5. Passarelli, R.E. and R.C. Srivastava, 1978: A new aspect of snowflake aggregation theory. J. Atmos. Sci., 36, 484-493.

6. Fletcher, N. H., 1962: Physics of Rain Clouds. Cambridge Univ. Press, London, Eng.

7. Young, K.C., 1974: A numerical simulation of wintertime, orographic precipitation: Part I. Description of model microphysics and numerical techniques. J. Atmos. Sci., 31, 1735-1748.

8. Gordon, G. and J. D. Marwitz, 1981: Secondary ice crystal production in stable orographic clouds over the Sierra Nevada. 8th Conf. on Inad. and Planned Wea. Mod., Reno, Nevada, Oct. 5-7, '81, pp. 62-63.

9. Tripoli, G.J., and W.R. Cotton, 1982: The Colorado State University three-dimensional cloud/mesoscale model - 1981. Part I: General theoretical framework and sensitivity experiments. J. de Rech. Atmos., 16, 185-220.

10. Klemp, J.B. and D.R. Durran, 1983: An upper boundary condition permitting internal gravity wave radiation in numerical mesoscale models. Mon. Wea. Rev., 111, 430-444.

A NUMERICAL MODEL OF STRATIFORM CLOUD

Hu Zhijin   Yan Caifan

(Academy of Meteorological Science, State Meteorological Administration of China, Beijing, People's Republic of China)

1. Model

A one-demensional time dependent model of precipitation development in stratiform clouds is developed. Water content of vapor and cloud droplets (Qv, Qc), water content and number concentration of ice crystals, snow flakes, graupels and raindrops (Qi, Ni, Qs, Ns, Qg, Ng, Qr, Nr) are calculated by equations in following form:

$$\frac{\partial M}{\partial t} = -(W-Vm)\frac{\partial M}{\partial Z} + K\frac{\partial^2 M}{\partial Z^2} - \frac{M}{\rho}\frac{\partial \rho Vm}{\partial Z} + \frac{\delta M}{\delta t}$$

where W--vertical air speed, Vm--average fall speed of M particles, K--turburent coefficient $\frac{\delta M}{\delta t}$ --transformation due to microphysical processes, M--any variable:

18 microphysical processes are considered: condensation of cloud droplets and raindrops (Svc, Svr), deposition of ice, snow and graupels (Svi, Svs, Svg), collection of cloud droplets by precipitation particles (Ccr, Cci, Ccs, Ccg), aggregation of ice particles (Cii, Cis, Css), collision and breakup of rain drops (Crr), conversions of cloud-rain, ice-graupel, snow-graupel (Acr, Aig, Asg), nucliation and multiplication of ice crystals (Pri, Pci).

$$\frac{\delta Qv}{\delta t} = -Svc - Svi - Svs - Svg - Svr - Pvi$$

$$\frac{\delta Qc}{\delta t} = Svc - Cci - Ccs - Ccr - Ccg - Pci - Acr$$

$$\frac{\delta Qi}{\delta t} = Svi + Cci - Cis - Cii - Aig + Pvi + Pci$$

$$\frac{\delta Ni}{\delta t} = NSvi - NCis - 2NCii - NAig + NPvi + NPci$$

$$\frac{\delta Qs}{\delta t} = Svs + Ccs + Cii + Cis - Asg$$

$$\frac{\delta Ns}{\delta t} = NSvs + NCii - NAsg - NCss$$

$$\frac{\delta Qg}{\delta t} = Svg + Ccg + Aig + Asg$$

$$\frac{\delta Ng}{\delta t} = NSvg + NAig + NAsg$$

$$\frac{\delta Qr}{\delta t} = Svr + Ccr + Acr$$

$$\frac{\delta Nr}{\delta t} = NSvr + NAcr + NCrr$$

Besides the index of cloud droplet spectrum width (Fc) and the riming index of ice and snow (Fi, Fs) are calculated. (Ref. 4).

$$\frac{\delta Fc}{\delta t} = \rho^2 Qc^2 \left(120\rho Qc + 1.6\frac{Nc}{Dc}\right)^{-1}$$

$$\frac{\delta Fi}{\delta t} = \left(\frac{Fi\cdot Qi + Cci\cdot\delta t}{Qi+(Cci+Svi)\delta t} - Fi\right)/\delta t$$

$$\frac{\delta Fs}{\delta t} = \left(\frac{Fs\cdot Qs + (Ccs + Fi\,(Cci + Cis))\delta t}{Qs + (Ccs + Cii + Cis + Svs)\,\delta t} - Fs\right)/\delta t$$

Equation for each microphysical process is deduced based on experimental and theoretical studies (1-5), assuming that the distribution of particles is in form of $dN = N_0 D^{\alpha} e^{-\lambda D} dD$, mass and fall speed of single particle is $m = Am\cdot D^{bm}$, $V = Av\cdot D^{bv}$, where D is diameter of particle, α, Am, bm, Av, bv are constants (see tab.1). N0 and λ are parameters. They are functions of N and Q, for example,

$\lambda_r = (6\cdot Amr\cdot Nr/Qr)^{\frac{1}{3}}$, $Nor = Nr\cdot\lambda r$.

Tab.1. Constants for various particles

	α	Am	bm	Av	bv
cloud droplets	2				
ice crystals	1	0.001	2	0.7	0.33
snow flakes	1	0.008	2	1.0	0.33
graupels	0	0.065	3	4.5	0.8
raindrops	0	0.524	3	21	0.8

$Svc = (Qv - Qsw)/Dt$ if $Qv > Qsw$, else

$$2\cdot\pi\cdot K_d\cdot\rho\,(Q_v - Q_{sw})\cdot\left(1+\frac{Lv\cdot K_d\cdot\rho\cdot Q_{sw}}{Kt\cdot T}\left(\frac{Lv}{RT}-1\right)\right)^{-1}\cdot 3\,N_c^{\frac{2}{3}}\left(\frac{Q_c}{10\pi}\right)^{\frac{1}{3}};$$

$$Svr = 2\pi K_d\,\rho\,(Q_v - Q_{sw})\cdot\left(1+\frac{Lv\cdot K_d\cdot\rho\cdot Q_{sw}}{K_t\cdot T}\left(\frac{Lv}{R\cdot T}-1\right)\right)^{-1}\cdot(6\cdot Amr)^{-\frac{1}{3}}\cdot Nr^{\frac{2}{3}}\cdot Qr^{\frac{1}{3}}\left(1+0.23\cdot\left(\frac{\rho\cdot Avr}{\mu}\right)^{\frac{1}{2}}\cdot(6\cdot Amr)^{-0.3}\cdot Nr^{-0.3}\,Q_r^{0.3}\cdot\Gamma(2.9)\right);$$

$$Svg = 2\pi K_d\cdot\rho\cdot(Q_v - Q_{si})\cdot\left(1+\frac{Lv\,K_d\cdot\rho\cdot Q_{sw}}{Kt\cdot T}\left(\frac{Lv}{RT}-1\right)\right)^{-1}\left(\frac{Q_g}{6\cdot Amg}\right)^{\frac{1}{3}}\cdot Ng^{\frac{2}{3}}\cdot\left(1+0.23\left(\frac{\rho\cdot Avg}{\mu}\right)^{\frac{1}{2}}\cdot\Gamma(2.9)\cdot(6\cdot Amg\cdot Ng)^{-0.3}\cdot Q_g^{0.3}\right);$$

$$Svi = 2\cdot A_1\frac{(Q_v - Q_{si})}{(Q_{sw} - Q_{si})}N_i^{(1-A_2)}\cdot Q_i^{A_2}\cdot 6^{-A_2};$$

$$Svs = 1.6\cdot A_1\frac{(Q_v - Q_{si})}{(Q_{sw} - Q_{si})}N_s^{(1-A_2)}\cdot Q_s^{A_2}\,6^{-A_2};$$

$$Ccr(Ccg) = \frac{\pi}{4}\Gamma(3.8)\cdot Av\cdot(6\cdot Am)^{-0.93}\cdot Q^{0.93}\cdot N^{0.07}\cdot\rho\cdot Qc\cdot E;$$

$$Cci(Ccs) = \frac{\pi}{4}\Gamma(4.33)\cdot Av\cdot(6\cdot Am)^{-\frac{7}{6}}\cdot Q^{\frac{7}{6}}\cdot N^{-\frac{1}{6}}\cdot\rho\cdot Qc\cdot Eci\cdot e^{-\alpha_1}\left(1+\alpha_1+\frac{\alpha_1^2}{2!}+\frac{\alpha_1^3}{3!}+\frac{\alpha_1^4}{4!}+\frac{\alpha_1^5}{5!}\right),$$

where $\alpha_1 = (10\pi Nc)^{\frac{1}{3}}\cdot Qc^{-\frac{1}{3}}\cdot D1$, ($D1 = 15\mu m$);

$$Pci = \frac{Nc}{250}e^{-\alpha_2}\cdot\left(1+\alpha_2+\frac{\alpha_2^2}{2}\right)\frac{Ccg}{Q_c}\cdot Qco;$$

if $265 \le T \le 270$; where $\alpha_2 = (10\pi Nc)^{\frac{1}{3}}Qc^{-\frac{1}{3}}D2$, ($D2 = 24\mu m$)

$$Pvi = -Bn\cdot Nn\cdot EXP(Bn\cdot(T_0 - T))\cdot W\cdot\frac{\partial T}{\partial Z}\cdot Qvo,\ \text{if } W>0,\ T<T_0;$$

$$Pvi' = Pvi\left(\frac{Qv - Qsi}{Qsw - Qsi}\right)^5,\ \text{if } Qv<Qsw;$$

$$Cii = \frac{\pi}{48}Avi\cdot(6\cdot Ami)^{-\frac{7}{6}}\cdot Q_i^{\frac{13}{6}}\cdot N_i^{-\frac{1}{6}}\cdot Kmii\cdot Eii\cdot\rho;$$

where $Kmii = \int_0^\infty\int_0^\infty e^{-(D_1+D_2)}D_1 D_2\,(D_1^2+D_2^2)(D_1+D_2)^2\,|D_1^{\frac{1}{3}} - D_2^{\frac{1}{3}}|\cdot dD_1\cdot dD_2$;

$$Cis = \frac{\pi}{24}Avs\,(6\,Ams)^{-\frac{7}{6}}Q_i\,N_s^{-\frac{1}{6}}\cdot Q_s^{\frac{7}{6}}\cdot Eii\cdot Kmis(\beta)\cdot\rho;$$

where $Kmis(\beta) = \int_0^\infty\int_0^\infty D_1\cdot D_2^3\,e^{-(D_1+D_2)}(D_1+\beta D_2)^2\,|D_1^{\frac{1}{3}} - \frac{Avi}{Avs}(\beta\cdot D_2)^{\frac{1}{3}}|\,dD_1\,dD_2$;

$$\beta = \left(\frac{Ams\cdot Ns\cdot Q_i}{Ami\cdot Ni\cdot Q_s}\right)^{\frac{1}{2}};$$

$Acr=$ if $Fc>1$ then $0.25\cdot\rho^2\cdot Q_c^3\cdot(360\cdot\rho Q_c+0.12\cdot\frac{Nc}{Dc})^{-1}$ else 0

$Aig=\frac{Q_i}{3}\cdot EXP(18\cdot(F_i-1))$;

$Asg=\frac{Qs}{3}\cdot EXP(18\cdot(Fs-1))$;

The changes in number concentration due to micro-processes are:

$NSvr=$ if Svr 0 then $Svr\frac{Nr}{Qr}$, else 0;

(NSvi, NSvs, NSvg are similar);

$NPvi=Pvi/Qvo$; $NPci=Pci/Qco$; $NAcr=Acr/Qro$;

$NCii=\frac{\pi}{4}KNii\cdot Avi\cdot Eii\cdot(6\cdot Ami)^{-\frac{7}{6}}\cdot\rho Ni^{\frac{5}{6}}\cdot Q_i^{\frac{7}{6}}$;

$$KNii=\int_0^\infty\int_0^\infty D_1\cdot D_2\cdot e^{-(D_1+D_2)}(D_1+D_2)^2|D_1^{\frac{1}{3}}-D_2^{\frac{1}{3}}|\cdot dD_1\cdot dD_2;$$

$NCis=\frac{\pi}{4}KNis(\beta)\cdot Avs\cdot Eii\,(6\cdot Ams)^{-\frac{7}{6}}\cdot\rho Ni\cdot Ns^{-\frac{1}{6}}\cdot Q_s^{\frac{7}{6}}$;

$$KNis=\int_0^\infty\int_0^\infty D_1\cdot D_2\cdot e^{-(D_1+D_2)}\cdot(D_1+\beta D_2)^2|D_1^{\frac{1}{3}}-\frac{Avi}{Avs}(\beta\cdot D_2)^{\frac{1}{3}}|\cdot dD_1\cdot dD_2;$$

$NCss=\frac{\pi}{8}KNii\cdot Avs\cdot Eii\cdot(6\cdot Ams)^{-\frac{7}{6}}\cdot Ns^{\frac{5}{6}}\cdot Q_s^{\frac{7}{6}}\rho$;

$NCrr=4\cdot10^{-8}\cdot\rho\cdot Nr^2\cdot\lambda_r^3(-EXP(-0.152\cdot\lambda_r)+Sr\cdot EXP(-0.23\cdot\lambda_r))$;

$$\lambda_r=(\frac{6\cdot Amr\cdot Nr}{Qr})^{\frac{1}{3}},\quad Sr=3;$$

$NAig=Aig\cdot\frac{Ng}{Qg}$, $NAsg=Asg\cdot\frac{Ns}{Qs}$.

Where Nc is the number concentration of cloud droplets, it is taken to be 200/g. Dc is the dispersion of initial cloud droplet spectrum, it is taken to be 0.167. Qvo, Qco, Qro are the mass of initial ice crystal and raindrop, produced by nucleation, multiplication and autoconversion. They are taken to be 10^{-10} g , 10^{-9}g and $5\cdot10^{-7}$g respectively. K_d, K_t, μ are the coefficients of water vapor diffusion, thermoconductivity and viscosity. A1, A2 are coefficients after Koenig(3). Sr is the average number of secondary drops produced by raindrop breakup. After Srivastava (5) Sr=3. E, Eci, Eii is the collection coefficient between drop-drop, drop-ice, ice-ice respectively. E=0.8 . Eci is the average value for droplets greater than D=15μm and taken to be a function of mean diameter of ice particles. It is assumed that only clouddroplets with D>15μm can be collected by ice or snow. Aggregation between ice particles was less studied, we took

$$Eii'=0.09\cdot EXP(0.2\cdot(T-T_0))+0.015\cdot EXP(0.085\cdot(T-T_0))/EXP(0.144\cdot(T-260)^2).$$

But calculations showed aggregation with this value was too fast, so $Eii=0.33\cdot Eii'$ is taken.

The main diameter of ice or snow $Dm=2.45\cdot\lambda^{-1}$, average fall speed

$$Vm=\frac{\Gamma(2+bm+bv)}{\Gamma(2+bm)}\cdot Av\cdot\lambda^{-bv}.$$

For graupels and raindrops $Dm=1.8\cdot\lambda^{-1}$,

$$Vm=\frac{\Gamma(1+bm+bv)}{\Gamma(1+bm)}\cdot Av\cdot\lambda^{-bv}$$

All ice particles are assumed to melt at temperature above 0°c; at the grid just below the 0°c level, Qi=Qs=Qg=0 ;

$$\frac{\delta Qr^*}{\delta t}=\frac{\delta Qr}{\delta t}+\frac{1}{\rho}\frac{\partial\rho QiVi}{\partial Z}+\frac{1}{\rho}\frac{\partial\rho QsVs}{\partial Z}+\frac{1}{\rho}\frac{\partial\rho QgVg}{\partial Z};$$

$$\frac{\delta Nr^*}{\delta t}=\frac{\delta Nr}{\delta t}+\frac{1}{\rho}\frac{\partial\rho NiVi}{\partial Z}+\frac{1}{\rho}\frac{\partial\rho NsVs}{\partial Z}+\frac{1}{\rho}\frac{\partial\rho NgVg}{\partial Z}.$$

Initial conditions: Qv=Qsi, Qc=Qi=Qs=Qg=Qr=0.

Upper boundary: Qv=Qsi, Qc=Qi=Qs=Qg=Qr=0, W=0 .

Bottom boundary: Qv=Qsi, W=Qc=0,

$$(\frac{\partial Qi}{\partial Z})_-=(\frac{\partial Qs}{\partial Z})_-=(\frac{\partial Qg}{\partial Z})_-=(\frac{\partial Qr}{\partial Z})_-=0\ .$$

Calculations run on DJS-6 computer of A.M.S. with DZ = 100---300m and Dt = 10s . The results of calculation with Dt = 10, 5, 2 s showed no significat difference.

2. Results

Model is varified in 6 cases observed by P.V. Hobbs (6)(7). The observed temperature and vertical profile of updraft are used as input to calculate the cloud microstructure and its development. For warm sector rain band (C1), cold front rain band 1 and 2 (c2, C3) the updraft profiles observed by Doppler radar are revised according to the airplane observations. Their max. updraft is taken to be 0.63, 0.6, 0.3 m/s respectively. For shallow warm cloud and warm front rainband 13 and 14 jan. 1975, (C4, C5, C6) observed updraft profiles are used. Comparison of calculated microstructure at 480 min., when the cloud reaches a stationary stage, with observations shows correspondence in many aspects. (see fig.).

1. LWC in cold region (0.1 g/m or less) is smaller than in warm region (less than 0.4 g/m). The largest cloud water content occures in warm cloud (0.8 g/m in C4). There is a max. LWC near the cloud top in some cases, which corresponds with observations (8).

2. Number concentration of ice particles (Ni+Ns +Ng) depends mainly on the vertical transport and the nucleation rate, which is a function of temperature and updraft in the upper part of the cloud and reaches a value of 10/kg S. Aggregation reduces the ice concentration significantly. (NCii+NCis+NCss=-1/kg S). The 'Hallett-Mossop' multiplication process operates only in warm sector cloud (C1) with a max. rate of 8/kg S near -5°c. Calculated profiles correspond with observations in C1,C2,C3,but disagree in C5, C6.

3. The riming is heavier, LWC is larger, more

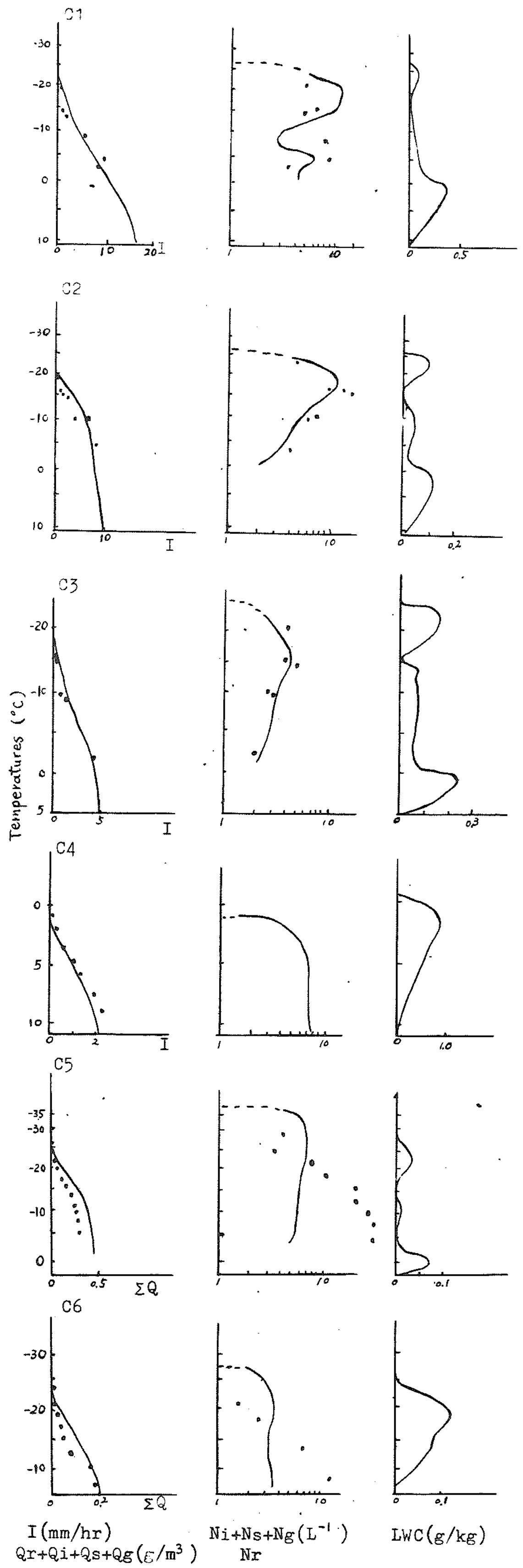

graupels (Ng = 4000/kg) occur and H-M multiplication is strong in C1, where the updraft speed is bigger and the cloud base is warmer.

4. The profiles of precipitation rate ($\Sigma\rho\cdot Q\cdot V$) or precipitation water content (Qi+Qs+Qg+Qr) agree with observations. It shows a "seeder-feeder" mechanism: In the upper part of the cloud high concentration of precipitation particles is produced, but their water content is only 20% of precipitation at cloud base. Deposition is the most important in precipitation growth in cold cloud (Svi+Svc+Svg=$8\cdot10^{-4}$g/kg S), and riming is important as well (Cci+Ccs+Ccg=5--$7\cdot10^{-4}$g/kg S).

5. Calculaed water content of snow flakes is very small in T<-20°c and become larger than ice in T>-15°c region. It agrees with observations except C5.

6. In shallow warm clouds (C4) precipitation was produced by warm rain process efficiently. The autoconversion runs mainly in the upper part of the cloud and produce sufficient number of raindrops, which grow up by collection($2\cdot10^{-4}$g/kg s) in the lower part. It seems to be another "seeder-feeder" mechanism.

7. Calculated precipitation rates correspond with observations.

3. References

1) B.J.Mason, 1971, The physics of clouds.

2) H.R.Pruppacher, J.D.Klett, 1978, Microphysics of clouds and precipitation.

3) Koenig L.R., 1972, Parameterization of ice growth for numerical calculations of cloud dynamics, Mon. Wea. Rev., 100, 417.

4) Hu Zhijin et al.1983, Numerical simulation of rain and seeding processes in warm layer clouds, Acta Meteorologica sinica (in Chinese), 41, 79.

5) R.C.Srivastava, 1978, Parameterization of rain drop size distributions, J. Atmos. Sci., 35, 108.

6) P.V.Hobbs et al., 1980, The mesoscale and microscale structure and organization of clouds and precipitation in midlatitude cyclones, 1: A case study of a cold front, J. Atmos. Sci. 37, 568.

7) P.H.Herzegh, P.V.Hobbs, 1980, 2: Warm-frontal clouds, J.Atmos. Sci., 37, 597.

8) Heymsfield A. J. 1977, Precipitation development in stratiform ice clouds, A microphysical and dynamical study, J. Atmos. Sci., 34, 367.

A NUMERICAL MODEL OF INTERACTION OF THE CELLULAR CUMULUS CONVECTION WITH THE LARGE-SCALE FLOW IN THE ATMOSPHERIC BOUNDARY LAYER

A.P. Khain, M.G. Yarmolinskaya

Hydrometeorological Center, 9-13 Bolshevistskaya Street, 123376 Moscow, USSR

L.H. Ingel

Institute of Experimental Meteorology, 82 Lenin Prospect, 249020, Obninsk, USSR

ABSTRACT

The interaction of the cellular convection with a large-scale accelerated flow is considered. The large-scale flow influences the convection by the mean subsidence and advection of heat and moisture. The convection has an effect on the large-scale flow by the latent heat release and vertical transport of heat and moisture. The terms in large-scale flow equations similar to the Reynold's stress are calculated directly by averaging the convection patterns.

Keywords: Mesoscale Meteorology, Cellular convection, Cloud bands, Large-scale flow, Boundary layer

1. INTRODUCTION

It is well known that parallel cloud bands are widespread in the unstably stratified boundary layer of the earth's atmosphere. The cloud bands were found to originate in convective layers with rather strong winds and a curved vertical velocity profile of rather uniform direction. A great majority of cumulus bands especially in trade wind layer is oriented parallel to the surface winds. The depth of convection layer is 1-2 km. It is topped with temperature inversion. This structure is shown in Fig. 1.

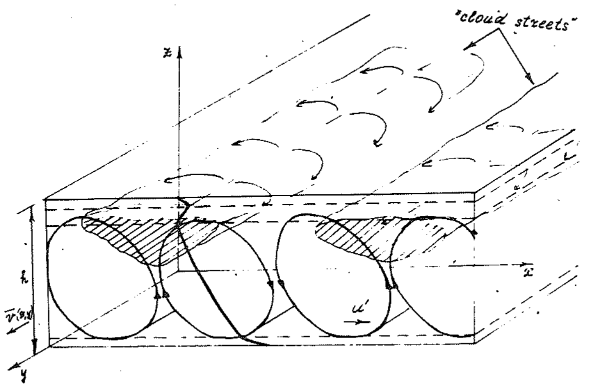

Figure 1. The schematic structure of convective layer with cloud bands (streets)

There are many two- or three-dimensional numerical models of dry and moist cellular convection. The boundary conditions in these models are similar to those of the classical Rayleigh convection problem. In such models the termperatures of upper and lower boundaries were fixed. It was assumed that the upper boundary coincided with the bottom of the inversion. The height and intensity of inversion were not calculated. Due to these considerations the results obtained were to some extent nonrealistic. It is desirable to set up this problem in such a way as to fit the structure in Fig. 1.

2. DESCRIPTION OF THE MODEL

2.1. Basic equations

We consider the lower layer of the atmosphere with the depth (h) of 2 km. Let y be the coordinate along the accelerated basic flow, x the coordinate perpendicular and to the left of the flow, z the vertical coordinate (Fig. 1). We must consider the interaction of the large-scale boundary layer flow with mesoscale cellular convection. These two processes have the same vertical extent but sufficiently different horizontal scales. These differences permit to separate the total set of equations into two simpler subsets. The idea of such separation for the case of horizontal uniform boundary layer was proposed by Pushistov (Ref. 1).

To achieve this separation we average the total three-dimensional equations in the x-direction. The averaging operator is defined by:

$$\overline{(\ )} = L^{-1}\int_0^L (\ )\,dx, \tag{1}$$

where L is the width of one or several convective cells.

Any arbitrary variable may be represented by the sum of the averaged value and the departure:

$$(\ ) = \overline{(\ )} + (\ )' \tag{2}$$

The value $(\ )'$ satisfies the following condition

$$\overline{(\ )'} = 0 \tag{3}$$

Normally condition (3) is not valid in convection models including cellular convection models where the deviations are calculated from the fixed basic state but not from the averaged value.

Let us begin our consideration with the continuity equation, which in our case can be written divV = 0, where V = (u,v,w) - velocity vector. By averaging this equation according to Eq. (1) and taking into account cyclic lateral boundary conditions in the x-direction, we get

$$\frac{\partial \bar{v}}{\partial y} + \frac{\partial \bar{w}}{\partial z} = 0 \tag{4}$$

and

$$\frac{\partial u'}{\partial x} + \frac{\partial w'}{\partial z} = 0 \tag{5}$$

In Eq. (5) we made use of $\frac{\partial v'}{\partial y} \ll \frac{\partial u'}{\partial x}$ on account of the scale difference in x and y-directions. Eq. (5) is the same as that usually used in two-dimensional shallow convection models.

In the same manner we can obtain the following set of basic flow equations:

$$\frac{\partial \bar{v}}{\partial t} + v\frac{\partial \bar{v}}{\partial y} + w\frac{\partial \bar{v}}{\partial z} = -\overline{\frac{1}{\rho}\frac{\partial p}{\partial y}} - \frac{\partial \overline{w'v'}}{\partial z} + \nu\frac{\partial^2 \bar{v}}{\partial z^2} \qquad (6)$$

$$\frac{\partial \bar{\theta}}{\partial t} + v\frac{\partial \bar{\theta}}{\partial y} + w\frac{\partial \bar{\theta}}{\partial z} = \frac{L}{c_p}\bar{\Phi} - \frac{\partial \overline{w'\theta'}}{\partial z} + \nu\frac{\partial^2 \bar{\theta}}{\partial z^2} \qquad (7)$$

$$\frac{\partial \bar{q}}{\partial t} + v\frac{\partial \bar{q}}{\partial y} + w\frac{\partial \bar{q}}{\partial z} = -\bar{\Phi} - \frac{\partial \overline{w'q'}}{\partial z} + \nu\frac{\partial^2 \bar{q}}{\partial z^2} \qquad (8)$$

$$\frac{\partial \bar{l}}{\partial t} + v\frac{\partial \bar{l}}{\partial y} + w\frac{\partial \bar{l}}{\partial z} = \bar{\Phi} - \frac{\partial \overline{w'l'}}{\partial z} + \nu\frac{\partial^2 \bar{l}}{\partial z^2} \qquad (9)$$

where θ, q, l - potential temperature, water vapor mixing ratio and liquid water content, correspondingly; ρ - density, p - pressure, Φ - rate of condensation, ν - eddy diffusion coefficient, L - specific heat of condensation, c_p - specific heat of dry air at constant pressure.

The effect of convective motions is described by the terms

$$-\frac{\partial \overline{w'v'}}{\partial z}, \quad -\frac{\partial \overline{w'\theta'}}{\partial z}, \text{ etc.}$$

In our case we cannot calculate v' and consequently $\frac{\partial \overline{w'v'}}{\partial z}$. This term was eliminated.

It is necessary to add the hydrostatic equation to the set of basic flow equations.

Let us consider the convective equations. The equations of motion may be written as following:

$$\frac{\partial u'}{\partial t} + u'\frac{\partial u'}{\partial x} + w'\frac{\partial u'}{\partial x} = -\frac{1}{\rho}\frac{\partial p'}{\partial x} - \frac{\partial u'}{\partial z} + \nu\nabla^2 u' \qquad (10)$$

$$\frac{\partial w'}{\partial t} + u'\frac{\partial w'}{\partial x} + w'\frac{\partial u'}{\partial z} = -\frac{1}{\rho}\frac{\partial p'}{\partial z} + g\frac{\theta'}{\bar{\theta}} + 0.61q'g - gl' + \nu\nabla^2 w' + G(w) \qquad (11)$$

where $G(w) = -\left(w'\frac{\partial \bar{w}}{\partial z} + \bar{w}\frac{\partial w'}{\partial z}\right) + \frac{\partial \overline{w'^2}}{\partial z}$

While deducing the Eq. (10-11) we used that

$$\bar{u}=0,\ u'\frac{\partial u'}{\partial x} \gg \bar{v}\frac{\partial u'}{\partial y};\ u'\frac{\partial w'}{\partial x} \gg \bar{v}\frac{\partial w'}{\partial y},$$

$$w' \gg \bar{w}$$

One can rewrite Eqs. (10-11) in terms of new variables

$$\eta\left(=\frac{\partial w'}{\partial x} - \frac{\partial u}{\partial z}\right) \text{ and } \quad \psi\left(u = -\frac{\partial \psi}{\partial z};\ w = \frac{\partial \psi}{\partial x}\right)$$

$$\frac{\partial \eta}{\partial t} + u'\frac{\partial \eta}{\partial x} + w\frac{\partial \eta}{\partial z} = \frac{g}{\bar{\theta}}\frac{\partial \theta'}{\partial x} + g\left(0.61\frac{\partial q'}{\partial x} - \frac{\partial l'}{\partial x}\right) - \frac{\partial \bar{w}\eta}{\partial z} + \nabla^2\eta \qquad (12)$$

$$\eta = \nabla^2\psi \qquad (13)$$

The Eq. (12) is similar to that used in Ref. 2, 3, except the term $-\frac{\partial \bar{w}\eta}{\partial z}$. It covers the effect of the basic flow. The equations of θ', q' and l' can be written:

$$\frac{\partial \theta'}{\partial t} + u'\frac{\partial \theta'}{\partial x} + w\frac{\partial \theta'}{\partial z} = \frac{L}{c_p}\Phi' + \nabla^2\theta' + \left(\frac{\partial \overline{w\theta'}}{\partial z} - \bar{w}\frac{\partial \theta'}{\partial z} - w'\frac{\partial \bar{\theta}}{\partial z}\right) \qquad (14)$$

$$\frac{\partial q'}{\partial t} + u'\frac{\partial q'}{\partial x} + w'\frac{\partial q'}{\partial z} = -\Phi' + \nabla^2 q' + \left(\frac{\partial \overline{w'q'}}{\partial z} - \bar{w}\frac{\partial q'}{\partial z} - w'\frac{\partial \bar{q}}{\partial z}\right) \qquad (15)$$

$$\frac{\partial l}{\partial t} + u\frac{\partial l}{\partial x} + w'\frac{\partial l}{\partial z} = \Phi' + \nabla^2 l' + \left(\frac{\partial \overline{w'l'}}{\partial z} - \bar{w}\frac{\partial l'}{\partial z} - w'\frac{\partial \bar{l}}{\partial z}\right) \qquad (16)$$

In accordance with Ref. 2-4 the terms $\bar{\Phi}$ and Φ' were eliminated from Eqs. (7-9) and (14-16) through introducing new variables A and B:

$$A = \begin{cases} \theta - \frac{L}{c_p}l & \text{if} \quad q > q_s\ (l > 0) \\ \theta & \quad\quad q \le q_s\ (l = 0) \end{cases}$$

$$B = \begin{cases} q + l & \text{if} \quad q > q_s\ (l > 0) \\ q & \quad\quad q \le q_s\ (l = 0) \end{cases} \qquad (17)$$

where q_s is saturated water vapor mixed ratio. The method of calculating θ, q and l from Eq. (17) has been described in detail in Ref. 4.

Thus the initial three-dimensional problem is reduced to some two-dimensional problems.

2.2. Boundary conditions

2.2.1. Basic flow

At the upper boundary (z = h): $\bar{p}$(y, h), $\bar{\theta}$(y, h) $\bar{q}$ (y, h) are given, $\bar{l}$ (y, h) = 0. The value $\bar{v}$ (y, h) is obtained from Eq. (6) by neglecting the nonstationary, eddy and convective terms. The boundary conditions at y = 0 consist of steady - state $\bar{v}$ (z), $\bar{\theta}$ (z), $\bar{q}$ (z); $\bar{l}$ (z) = 0. At the lower boundary (z = 0): $\bar{w}$ = 0. The fluxes of sensible and latent heat and surface stress are obtained by making use of the Monin-Obukhov similarity theory. The surface temperature is given as well.

2.2.2. Convective processes

Lateral boundary conditions are assumed to be cyclic in all variables. At the upper boundary (z = h) w' = 0, $\partial u'/\partial z$ = 0 or that appears to be the same η = 0, ψ = = 0. Furthermore, θ' = q' = l' = 0. At the lower boundary (z = 0), w' = 0 (ψ = 0). The convective fluxes must be obtained along with basic flow fluxes.

2.3. Computational scheme and initial conditions

Grid system is shown in Fig. 2.

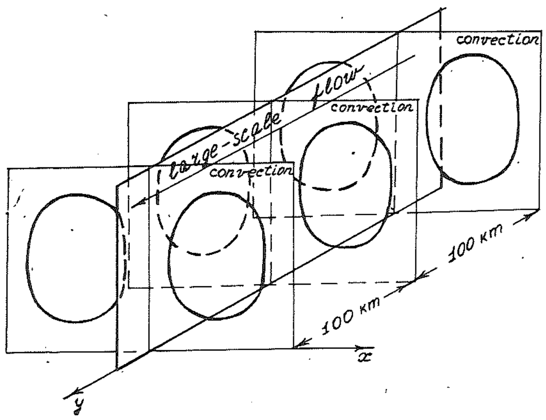

Figure 2. The structure of the grids of the model.

There is one basic flow grid (11x31 grid points, Δy = 50 km, Δz = 66.7 m) and three convective grids (33 x 31 grid points, Δx = 93 , 4 m, Δz = 66,7 m). A set of differential convective equations is transformed into the finite difference equations in the same way as in Ref. 2. Arakawa's method is used for space differentiation. Numerical time integration is carried out by Matsuno's method. The time increment is 30 s. The upstream finite-difference method is used for the basic flow. Time integration is also carried out by the Matsuno's method, however time increment is 60 s.

From the very beginning only the basic flow was calculated without including convection. The calculation of convective motions was included upon obtaining the stationary state of the basic flow. Later the integration of both the basic flow and convective sets of equations were carried out simultaneously.

3. RESULTS

To test the proposed model we solved the two-dimensional dry and moist cellular convection problem. This problem was treated by means of the method described in Ref. 2, 3. The results obtained by both methods coincided.

Here, however, the values $\frac{\partial \overline{w'\theta'}}{\partial z}$, $\frac{\partial \overline{w'q'}}{\partial z}$ and $\frac{\partial \overline{w'\ell'}}{\partial z}$ were calculated (Fig. 3).

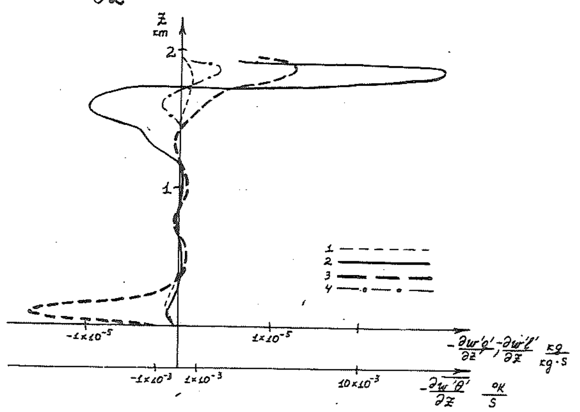

Figure 3. The profiles of $-\frac{\partial \overline{w'\theta'}}{\partial z}$, $-\frac{\partial \overline{w'q'}}{\partial z}$ and $-\frac{\partial \overline{w'\ell'}}{\partial z}$. 1. $-\frac{\partial \overline{w'\theta'}}{\partial z}$ - the case of the dry convection for Rayleigh number R = 3300 (free boundary conditions); 2. $-\frac{\partial \overline{w'\theta'}}{\partial z}$ - the case of moist convection with the same temperature gradient and initial relative moisture 60 %; 3,4 - $\frac{\partial \overline{w'q'}}{\partial z}$ and $-\frac{\partial \overline{w'\ell'}}{\partial z}$ correspondingly for the case of moist convection.

It can be seen that convective motions transfer heat and moisture from the surface layer to the upper part of convective layer. This transfer is very significant. Since the transfer of potential temperature is upgradient in significant part of the convective layer the convective effect on basic flow cannot be calculated in terms of the k-theory. We hope that the proposed method may be used in the weather prediction and convective parameterization problems.

4. REFERENCES

1. Pushistov, P.J., 1980. Application of splitting method and energy balance principle when setting up hydrodynamical local prediction problems (in Russian). Mathematical modelling of atmosphere and ocean dynamics. Pt. 2. Novosibirsk, 126-136.
2. Ivanov, V.N. and Khain, A.P., 1975. On dry and moist cellular convection in the atmosphere. Izv. Acad. Sci. USSR. Atmospheric and Oceanic Physics, 11, No. 12, 1211-1219.
3. Khain, A.P., 1976. On latent heat release effect on circulation structure of convective cell. Izv. Acad. Sci. USSR. Atmospheric and Oceanic Physics, 12, No. 2, 213-217.
4. Amirov, A.D., 1971. The methods for calculation temperature and moisture in the cumulus cloud model. Izv. Acad. Sci. USSR. Atmospheric and Oceanic Physics. 7, No. 7, 723-730.

A TWO-DIMENSIONAL TIME-DEPENDENT MODEL OF LOW CLOUDS AND FOGS WITH ACCOUNT FOR DYNAMICS, MICROPHYSICS, RADIATION AND ICE PHASE

V.I. Khvorostyanov, V.G. Bondarenko and O.P. Kotova
Central Aerological Observatory, Moscow, USSR

1. INTRODUCTION

Formation, evolution and dissipation of low clouds and fogs are governed by joint action of advective, radiative, turbulent and microphysical processes in the planetary boundary layer (PBL). These processes are interdependent and adequate description of the evolution of PBL with clouds and fogs demands their simultaneous consideration. It is a difficult task and different authors, while developing numerical models, either approximately accounted for some factors (e.g., time-dependence, advection, microstructure) or entirely disregarded them. The models are reviewed, for example, in Refs.1-4. This report, which is an expansion of the previous papers (Refs.5-7), describes a model which accounts for the processes mentioned above, on the basis of a closed system of equations.

2. MODEL DESCRIPTION

The structure of the model gives an opportunity to simulate low clouds and advection-radiation fogs, steam fogs, etc. The type of a simulated cloud or fog is determined by the physics of the process and is described in the model by variations in the initial and boundary conditions without changing of the basic equations.

2.1. The microstructure of fogs and clouds is numerically simulated through solving the kinetic equations for the droplet and crystal size distribution functions f_1, f_2, along with equations for the potential temperature θ and specific humidity q :

$$\frac{\partial f^{(i)}}{\partial t}+(u_j-v_s\delta_{j3})\frac{\partial f^{(i)}}{\partial x_j}+\frac{\partial}{\partial r_j}(\dot{r}_i f^{(i)})=\frac{\partial}{\partial x_j}K_j\frac{\partial f^{(i)}}{\partial x_j}+J^{(i)} \tag{1}$$

$$\dot{r}_i=\frac{D\Delta_i\rho_a K_{fi}}{\rho_i Q_i r_i \xi_i^2},\quad \varepsilon_{ci}=4\pi\rho_i\int_0^\infty r_i^2\dot{r}_i f_i\,dr_i \tag{2}$$

$$\frac{\partial\theta}{\partial t}+u_j\frac{\partial\theta}{\partial x_j}=\frac{\partial}{\partial x_j}K_j\frac{\partial\theta}{\partial x_j}+\sum_{i=1}^{2}\frac{L_i}{c_p}\varepsilon_{ci}+R_z \tag{3}$$

$$\frac{\partial q}{\partial t}+u_j\frac{\partial q}{\partial x_j}=\frac{\partial}{\partial x_j}K_j\frac{\partial q}{\partial x_j}-\sum_{i=1}^{2}\varepsilon_{ci} \tag{4}$$

where i=1(2) denotes droplets (crystals), r_i and $\dot{r}_i$ are the equivalent radius and the growth rate of the particle; Δ_1 the supersaturation; ε_{ci} the condensation or sublimation rate; R_z the radiative temperature change; K_{fi} accounts for the form of a crystal; v_{3i} is the sedimentation velocity; describes the activation of condensation and ice nuclei, and freezing of drops, according to Refs.3,4. The rest of the notations are the generally accepted ones. The repeated subscript j denotes summation over X, Z directions.

2.2. The dynamics of the PBL is described on the basis of second-order closure method. The equations of motion and continuity, turbulent energy b balance together with similarity and dimension relations, are used to determine wind speed components u, v, w and the turbulent diffusion coefficient K_z.

$$\frac{\partial u}{\partial t}+V_j\frac{\partial u}{\partial x_j}=\frac{\partial}{\partial x_j}K_j\frac{\partial u}{\partial x_j}+f_c v \tag{5}$$

$$\frac{\partial v}{\partial t}+V_j\frac{\partial v}{\partial x_j}=\frac{\partial}{\partial x_j}K_j\frac{\partial v}{\partial x_j}-f_c(u-G) \tag{6}$$

$$\frac{\partial b}{\partial t}+V_j\frac{\partial b}{\partial x_j}=K_z\left[\left(\frac{\partial V_j}{\partial x_j}\right)^2-\frac{g}{\theta}\frac{\partial\theta}{\partial z}\right]-\varepsilon+\frac{\partial}{\partial x_j}K_j\frac{\partial b}{\partial x_j} \tag{7}$$

$$\frac{\partial u}{\partial x}+\frac{\partial w}{\partial z}=0 \tag{8}$$

$$K_z=C_0 l b^{1/2},\ \varepsilon=cb^{3/2}/l,\ l=-\varkappa c^{1/4}\frac{b^{1/2}}{l}\Big/\frac{d}{dz}\frac{b^{1/2}}{l}$$

where G is the geostrophic wind speed, f_c the Coriolis parameter, l the mixing length, ε the dissipation rate of b.

2.3. To compute long-wave radiation (LWR), the variant of two-stream approximation is used, developed in Ref.8, where the window region of 8-13 μm has been shown to make a contribution of 90-95% to the radiative cooling of low clouds and fogs. Thus, the long-wave spectrum can be schematized by dividing it into two parts: 1) "effective window" region, which includes p_w=0.27 of the black-body radiation flux B, and where upward and downward fluxes $F_w^\uparrow$, $F_w^\downarrow$ can be computed using a two-stream approximation; 2) region beyond "effective window", where fluxes are equal to those of black-body radiation:

$$\frac{dF_w}{dz}=\pm\beta_l\rho_a\left(\alpha_v q+\sum_{i=1,2}\alpha_{Li}q_{Li}\right)\left(p_w B-F_w^{\uparrow,\downarrow}\right) \tag{9}$$

$$F_l^{\uparrow,\downarrow}=F_w^{\uparrow,\downarrow}+(1-p_w)B,\quad c_p\rho_a R_l=(F_l^\uparrow+F_l^\downarrow-2B) \tag{10}$$

$$\alpha_{Li}=\alpha_0\left[1-\frac{p_i+4}{p_i+1}\bar{r}_i C_{1i}+\frac{(p_i+4)(p_i+5)}{(p_i+1)^2}\bar{r}_i^2 C_{2i}\right] \tag{11}$$

where β_l=1.66; α_v=0.1 cm^2/g is the vapour mass absorption coefficient and α_{Li} are mass absorption coefficients of drops and crystals. The dependence of α_{Li} on cloud microstructure is described by (11), where $\bar{r}_i$, p_i are respectively the mean radii and parameters of gamma-distributions, by which the computed spectra are approximated at each time step; α_0=550 cm^2/g. This method is founded in Ref.8 on the basis of spectral calculations of LWR, an error being less than ≃10%. In fact, this is a further development of the famous Kondratyev's schematization of LWR spectrum for a cloudy atmosphere.

2.4. In order to calculate shortwave (solar) radiation (SWR), the method described in Ref.5 is used. Equations of SWR are solved using a two-stream approximation for 31 spectral intervals in order to resolve 8 main bands of water vapour in the region of λ = 0.4-4 μm.

$$\frac{1}{\sqrt{3}}\frac{dF^{\uparrow}_{s\lambda}}{d\tau_\lambda}=F^{\uparrow}_{s\lambda}-\frac{\omega_\lambda}{2}\left(F^{\uparrow}_{s\lambda}+F^{\downarrow}_{s\lambda}\right)-\frac{\Omega_\lambda}{2}\left(F^{\uparrow}_{s\lambda}-F^{\downarrow}_{s\lambda}\right) \quad (12)$$

$$-\frac{1}{\sqrt{3}}\frac{dF^{\downarrow}_{s\lambda}}{d\tau_\lambda}=F^{\downarrow}_{s\lambda}-\frac{\omega_\lambda}{2}\left(F^{\uparrow}_{s\lambda}+F^{\downarrow}_{s\lambda}\right)+\frac{\Omega_\lambda}{2}\left(F^{\uparrow}_{s\lambda}-F^{\downarrow}_{s\lambda}\right) \quad (13)$$

$$\omega_\lambda=\frac{\sum\sigma^{s}_{\lambda i}}{\sum(\sigma^{s}_{\lambda i}+\alpha_{\lambda i})+\alpha_{\lambda v}},\ \Omega_\lambda=\frac{\sum\sigma^{s}_{\lambda i}\langle\cos\theta\rangle_i}{\sum(\sigma^{s}_{\lambda i}+\alpha_{\lambda i})+\alpha_{\lambda v}} \quad (14)$$

$$\sigma^{at}_{\lambda i}=\sigma_{\lambda 0}\left[2+\frac{p_i+1}{p_i+2}\cdot\frac{1}{X^2_{\lambda i}}\cdot\frac{(m_{\lambda i}-1)^2-\varkappa^2_\lambda}{[(m_{\lambda i}+1)^2+\varkappa^2_\lambda]^2}\right] \quad (15)$$

$$\alpha_{\lambda i}=\sigma_{\lambda 0}\left[1-\left(1-\frac{2X_{\lambda i}\varkappa_{\lambda i}}{(p_i+1)}\right)^{-(p_i+3)}\right] \quad (16)$$

$$\sigma^{s}_{\lambda i}=\sigma^{at}_{\lambda i}-\alpha_{\lambda i},\ X_{\lambda i}=\frac{2\pi\bar{r}_i}{\lambda},\ \sigma_{\lambda 0}=\frac{3}{4\rho_w\bar{r}_i}\cdot\frac{p_i+1}{p_i+3} \quad (17)$$

where $F^{\uparrow\downarrow}_{s\lambda}$ are the upward and downward spectral fluxes of SWR; τ_λ the optical thickness; $\langle\cos\theta\rangle_i$ the asymmetry scattering factors. A single-scattering albedo ω_λ is expressed in terms of the scattering and absorption coefficients $\sigma^s_{\lambda i}$, $\alpha^s_{\lambda i}$ for droplets and crystals, respectively, which are described by using parameters of the gamma-distributions mentioned above; $m_{\lambda i}$, $\varkappa_{\lambda i}$ are real and imaginary parts of the refraction index.

2.5. Two situations are simulated: the formation of fogs and low clouds over land and the formation of steam fogs over sea. In the first case, surface boundary condition for temperature is found using the ground heat balance equation and the soil heat conductivity equation. The equality of turbulent and molecular fluxes of the water vapour serves as a lower boundary condition for humidity. In the second case, the prescribed values for the land and sea surface temperatures are used, and the humidity is supposed to be saturated at the sea surface. The wind speed is equal to zero at the roughness height and to geostrophic wind speed G at the top of the PBL. Methods of component-by-component splitting and splitting by physical processes are applied to solve this system of equations.

3. THE FORMATION OF CLOUDS AND FOGS OVER LAND

Consider an example of airmass transformation over a horizontally inhomogeneous underlying surface in wintertime. The initial surface temperature varies from T_{x1}= 265.15 K at the left boundary to T_{x2}= 260.15 K at the right one. The relative humidity varies from a saturated value at the snow surface to 80% on soil (see Fig.1), the geostrophic wind is G=12 m/s at the PBL top at z=1200 m. An advective or radiative cooling of airmass leads to formation of an inversion along the stream. Turbulence decreases along the x-axis, while two regions of ascending and descending currents appear (Fig.1). The turbulent cooling rate has a maximum at z=400-600 m, where the term $(\partial\theta/\partial z)\cdot(\partial K/\partial z)$ of the heat transport equation /4/ is negative and has a maximum of magnitude. The sum of turbulent and convective heat influxes is compensated by advective heating by one half its value. A moisture inversion is formed due to vapour sublimation at the surface. A moisture flux is directed downward, and the turbulent influx of q is negative up to 200-400 m. The advective influx of moisture and the heating rate are maximum at z = 300 - 500 m.

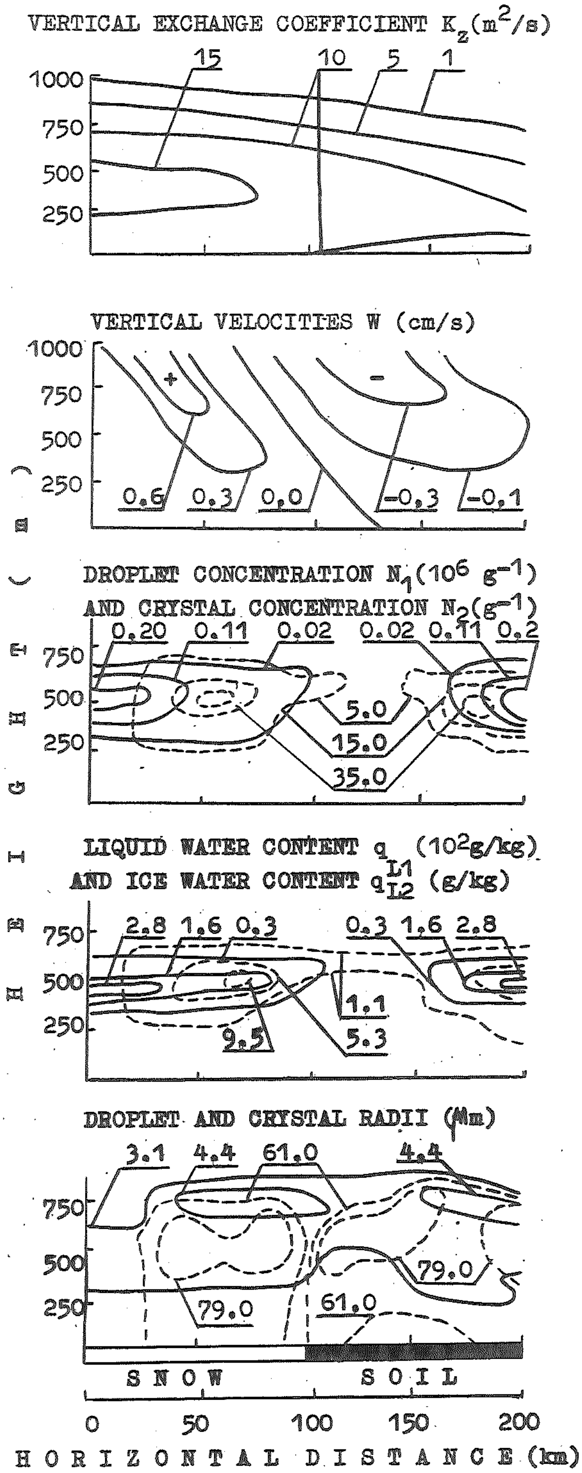

Figure 1. Fields of k , w , and the cloud microstructure characteristics of water (solid lines) and ice (dashed lines)

A simultaneous action of these processes results in a decrease of dew-point deficit over a large area. The cloud formation starts over snow after 7 hrs computation and 1 hour later over soil. Characteristics of the PBL and those of the cloud after 1 hr evolution are given in Fig.1. Two domains with a mixed microstructure exist (left and right). The generation rate of supersaturation Δ_1 as observed due to turbulent and radiative cooling and the rate of the subsequent transition of Δ_1 into the LWC are comparable with the rates of drop freezing and crystal growth. These domains are separeted by a zone with much lower LWC. This is caused by an increase in undersaturation at the snow-soil boundary and by downward motions near x=120 km. The rate of crystal generation through sublimation mode is much lower than that of crystal production by freezing. So, the microstructure of mixed St is sensitive to properties of the underlying surface and to the structure of vertical motions.

Figure 2 shows a typical cross-section of a cloud which is formed over dry soil in spring or autumn, after 6 hrs evolution. The cloud boundaries are at 300 and 700 m. Maxima of the LWC q_{L1} (0.3 g/kg), droplet concentration N_1 (160 g), longwave cooling R_L (-3.5 d/h), solar heating R_S(0.7d/h) are shifted towards the upper quarter of the cloud. Supersaturation Δ_1 is positive in the upper part of the cloud due to longwave cooling and it is negative in the lower part due to solar and turbulent heating. Thus, condensation takes place in the upper portion, while evaporation does in the lower portion, the droplet mean radius r_1 having two maxima. A further evolution of the cloud is determined by its interaction with the surface. Fig.3 illustrates the diurnal variations of heat balance components over a wet surface. The effective radiation R_0 is partly compensated by a turbulent flux H_T from the atmosphere and by a molecular flux H_S from the soil. The temperature T_0 decreases. After cloud formation, R_0 decreases by two orders of magnitude, fluxes H_T, H_S decrease or change of signs. After sunrise, the T_0 increases, R becomes positive, turbulent and latent heat fluxes into the atmosphere are comparable (sun's altitude $h_S(t)$ is calculated for the latitude of Moscow, September 21). The temperature T_0 increases until noon and remains constant. Solar heating and instability enhancement lead to turbulization of the PBL and to an increase of cloud top height up to 800-1000 m. A shift of the lower cloud boundary depends on surface properties, i.e., the lower boundary moves downward in daytime over a wet soil due to evaporation from the surface or due to a decrease in undersaturation over snow. The lower boundary moves up above a dry soil, thus a cloud can dissipate in several hours, when the sun is high enough.

Fog forms at lower values of the geostrophic wind G and at higher initial moisture. This fog can transform into cloud, become stable or dissipate, depending on G values, heat conductivity and soil moisture. Schemes of the cloud formation and of the mutual cloud and fog transformations are described in Refs.2-5.

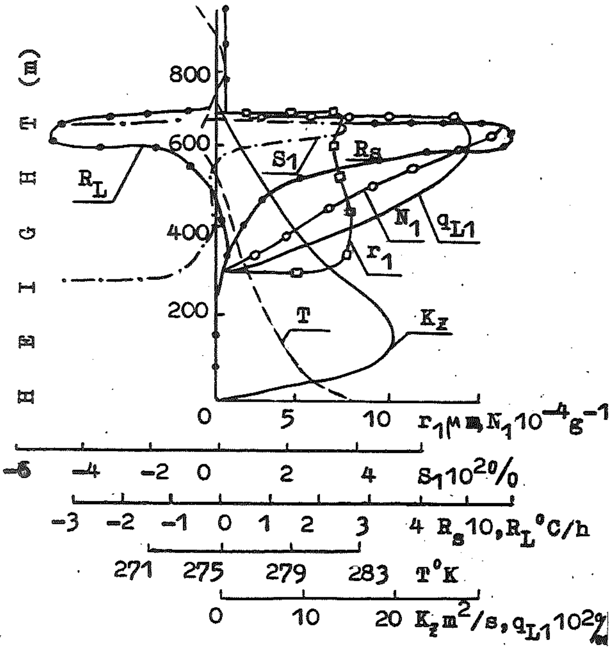

Figure 2. A vertical cross-section of the cloud over dry soil at 8 hr 30 min (2 hours after sunrise).
See notations in the text.

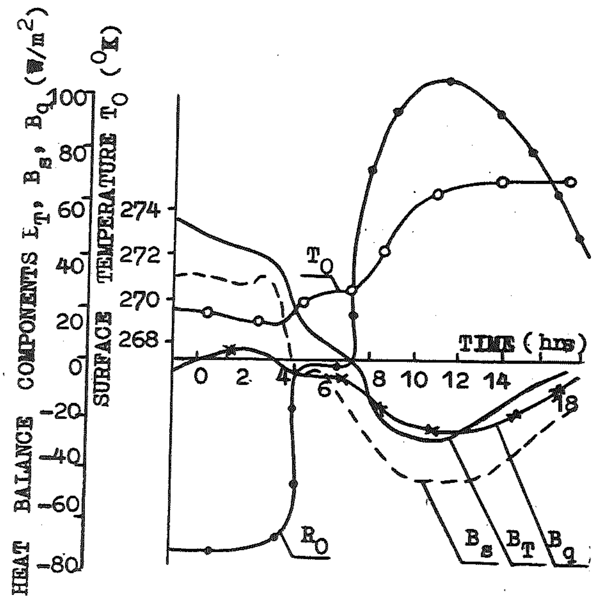

Figure 3. Diurnal variations of the surface temperature T and heat balance components during the cloud formation over a wet soil. H_T, H_q are the sensible and latent heat fluxes, H_S is the soil flux.

4. STEAM FOG FORMATION OVER SEA

The temperature of a coast surface(X=0) is equal, at the initial moment, to T_{X1} , decreasing with lapse rate γ = 6 /km, the relative humidity being $q_{r1}(z)$=const., T_{X2}= 0 C, q_{r2} =100% at the sea surface (X≠0).

We shall consider the difference $T=T \quad -T$ below. Calculations have been made for the case where $\Delta T=15C$, $G=3$ m/s, $q_{r1}=50\%$. The cold continental air gets warm due to motion above a warm sea surface, the inner boundary layer is seen to form, the turbulence coefficient increases by a factor of 3-5 (Fig.4). This increase causes the formation

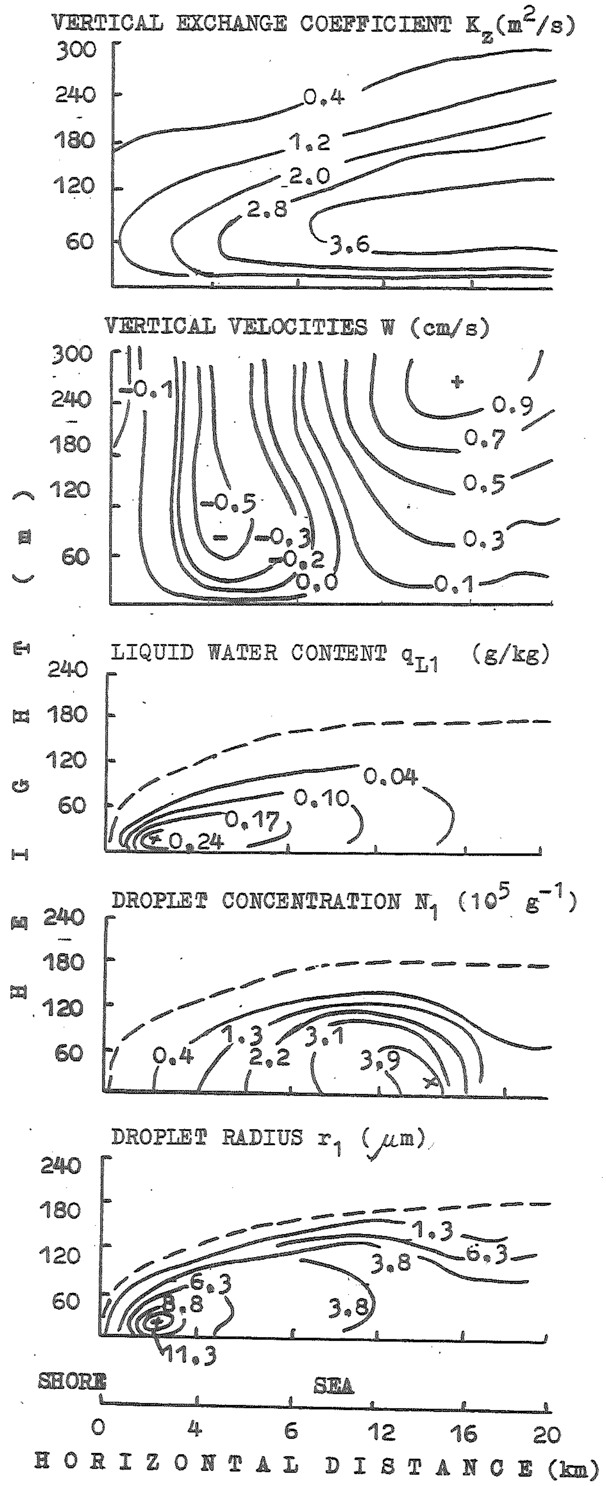

Figure 4. Fields of k_z, w, and the microstructure characteristics of maritime fog

of two regions of descending and ascending currents. This effect is opposite to that observed for the case with heat advection (see Fig.1). The values of W_{MIN}, W_{MAX}, K_{MAX} increase with increasing G, ΔT. Fog begins to form at the distance of 2 km off the shore. The upwind boundary of the fog approaches slowly to the coast, whereas the downwind boundary moves away from the coast much more rapidly. The characteristics of fog after 50 min evolution are shown in Fig.4. The LWC exhibits a maximum near the coast, the drop concentration being maximum at the distance of 16 km from the coast. These facts are related to a recent passage of condensation front. The mean droplet radius has two maxima: at x=2-4 km, z=0-60 m and at x=8-16 km, z=110 m, respectively. There are two maxima of supersaturation just in the same domains. The first maximum is caused by advective cooling, while the second one is accounted for radiative cooling which reaches its maximum value at 50-70 m below the fog top. So, when the thickness of a maritime steam fog exceeds 50-70 m, we can classify the fog as being of advection-radiation type. When q_{r1} decreases at ΔT=const. (or when ΔT decreases at q_{r1} = const), the time t_c and the horizontal coordinate X_c of fog formation increase. The thickness and LWC of fog increase with increasing q_{r1}, ΔT, G. A more detailed description of the effect of input parameters on the characteristics of fog is given in Refs.1-6.

REFERENCES

1. Matveev L.T.,1981, Cloud dynamics. Leningrad, Gidrometeoizdat, 311 pp.
2. Buikov M.V.,Khvorostyanov V.I.,1982, Modelling of clouds and fogs in atmospheric boundary layer(review). Obninsk, VNIIGMI-MCD Publ., issue 5, 67 pp.
3. Mazin I.P., and Shmeter S.M.,1983,Clouds, their structure and physics of formation. Leningrad, Gidrometeoizdat, 307 pp.
4. Kogan E.L.,Mazin I.P.,Sergeev B.N., Khvorostyanov V.I.,1984,Numerical simulation of clouds.Moscow,Gidrometeoizdat, 150 pp.
5. Khvorostyanov V.I.,1982,A two-dimensional non-stationary microphysical model of low level clouds and advection-radiation fogs. Meteorologia i gidrologia,No.7,p. 16-28.
6. Khvorostyanov V.I.,1983,Numerical simulation of maritime steam fogs and their modification. Meteorologia i gidrologia, No.12,p.44-52.
7. Khvorostyanov V.I.,1984,Numerical simulation of artificial crystallization and dispersal of supercooled fogs by the ground-based stationary source. Meteorologia i gidrologia,No.3,p.28-37.
8. Khvorostyanov V.I.,1981,Schematization of the atmospheric long-wave radiation spectrum for the models of clouds and fogs using data available from spectral calculations made with a high vertical resolution.Izv.Acad.Sci.USSR,Atmospheric and Oceanic Physics,17,No.10,p.1022-1030.

NUMERICAL SIMULATION OF THE FORMATION AND EVOLUTION OF FRONTAL STRATIFORM CLOUDINESS

B. Ya. Kutsenko

Central Aerological Observatory, Moscow, USSR

1. INTRODUCTION

With the introduction of more powerful computers it became possible to construct three-dimensional models of atmospheric fronts and their cloud systems. In spite of this two-dimensional models of atmospheric fronts and their cloud systems are still topical. They are continuously developed and used to investigate the structure of circulation in frontal zones and their influence on the formation, evolution and spatial characteristics of frontal stratiform cloudiness. They are also used to investigate and verify the new schemes of parametrization of microphysical, turbulent and radiation processes. Therefore this work treats two numerical models: a three-dimensional model of an atmospheric front and its cloud system evolution and a two-dimensional model of the formation and evolution of the frontal zone and its stratiform cloudiness.

The models are formed so as to ensure, along with dynamic, turbulent and radiation processes, direct modelling of cloud formation processes with their mutual influence.

2. A THREE-DIMENSIONAL MODEL OF THE FRONT AND CLOUD SYSTEM EVOLUTION

The governing equations of the model in a (x, y, σ, t) coordinate system may be written:

$$\frac{\partial(\pi u)}{\partial t} = -\frac{\partial(\pi uu)}{\partial x} - \frac{\partial(\pi vu)}{\partial y} - \pi\frac{\partial(u\dot\sigma)}{\partial\sigma} + fv\pi - \pi\frac{\partial\Phi}{\partial x} - \frac{\sigma\pi RT}{P_T+\sigma\pi}\frac{\partial\pi}{\partial x} + \pi_H F_u + \pi_V F_u \quad (1)$$

$$\frac{\partial(\pi v)}{\partial t} = -\frac{\partial(\pi uv)}{\partial x} - \frac{\partial(\pi vv)}{\partial y} - \pi\frac{\partial(v\dot\sigma)}{\partial\sigma} - fu\pi - \pi\frac{\partial\Phi}{\partial y} - \frac{\sigma\pi RT}{P_T+\sigma\pi}\frac{\partial\pi}{\partial y} + \pi_H F_v + \pi_V F_v \quad (2)$$

$$\frac{\partial(\pi T)}{\partial t} = -\frac{\partial(\pi Tu)}{\partial x} - \frac{\partial(\pi Tv)}{\partial y} - \frac{\partial(\pi T\dot\sigma)}{\partial\sigma} + \frac{RTw\pi}{c_p(P_T+\sigma\pi)} + \pi_H F_T + \pi_V F_T + \frac{\pi}{c_p}(LQ+R) \quad (3)$$

$$\frac{\partial(\pi q)}{\partial t} = -\frac{\partial(\pi uq)}{\partial x} - \frac{\partial(\pi vq)}{\partial y} - \pi\frac{\partial(\dot\sigma q)}{\partial\sigma} + \pi_H F_q + \pi_V F_q - \pi Q \quad (4)$$

$$\frac{\partial(\pi\delta)}{\partial t} = -\frac{\partial(\pi u\delta)}{\partial x} - \frac{\partial(\pi v\delta)}{\partial y} - \pi\frac{\partial(\dot\sigma\delta)}{\partial\sigma} + \pi_H F_\delta + \pi_V F_\delta + \pi Q \quad (5)$$

$$\frac{\partial\pi}{\partial t} = -\int_0^1\left(\frac{\partial(\pi u)}{\partial x} + \frac{\partial(\pi v)}{\partial y}\right)d\sigma \quad (6)$$

$$\frac{\partial\Phi}{\partial\sigma} = -\frac{\pi RT}{P_T+\sigma\pi} \quad (7)$$

$$\dot\sigma = \frac{\sigma}{\pi}\int_0^1\left(\frac{\partial(\pi u)}{\partial x} + \frac{\partial(\pi v)}{\partial y}\right)d\sigma - \frac{1}{\pi}\int_0^\sigma\left(\frac{\partial(\pi u)}{\partial x} + \frac{\partial(\pi v)}{\partial y}\right)d\sigma \quad (8)$$

$$w = \pi\dot\sigma + \sigma\left(\frac{\partial\pi}{\partial t} + u\frac{\partial\pi}{\partial x} + v\frac{\partial\pi}{\partial y}\right) \quad (9)$$

Here: $\sigma = (P-P_T)/\pi$ the vertical coordinate; $\pi = P_S - P_T$; P-pressure; P_T - pressure at the top of the model atmosphere; P_S - pressure at the bottom of the model atmosphere; Φ - geopotential; q, δ - specific humidity and cloud water, respectively; $\dot\sigma$, w - vertical σ and P velocities, respectively; ${}_HF$, ${}_VF$ - horizontal and vertical friction forces, respectively; Q - rate of condensation and evaporation per unit mass; R - rate of heating per unit mass due to net radiation. All other significations are generally accepted.

Water phase changes are calculated by the methods, developed in Ref. 1. Description of the surface boundary layer of the atmosphere is carried out on the basis of the similarity theory developed by Monin-Obukhov. The concrete methods of calculation of the fields of meteorological values in this layer are developed in Ref. 2. To calculate the profiles of vertical coefficients of turbulence in boundary layer the formulas, presented in Ref. 3 are made use of. The methods (Ref. 4) are used to account for the processes of radiation transfer at the formation and evolution of frontal stratiform cloudiness.

The system of equations is complemented by boundary and initial conditions. The conditions of wind velocity components equalling zero are given at a lower boundary. The temperature is determined through the heat balance at the surface. The upper boundary of the considered region is understood as a solid, smooth and thermoconductive surface.

To realize the model numerically a well-known at present "box-method" was used to approximate the non-lineal members. This representation of non-lineal members ensures preservation of energy and momentum.

3. A numerical two-dimensional model of formation and evolution of frontal zone and its stratiform cloudiness

The model, described in detail in Refs. 5, 6, is based on the solution of a system of primitive equations in the cartesian system of coordinates, composed of equations of motion, hydrostatics, continuity, thermodynamics, transfer of water vapour and cloud water. This model along with dynamic processes takes into account the processes of turbulence, water phase changes, radiation.

The fields of thermohydrodynamic parameters are represented in the form of the sum of two values: $f=\bar{f}+f'$. Here $\bar{f}$ is understood as undisturbed fields of meteorological elements, which is an approximate solution of original stationary lineal equations. The fields f' are a deviation from the large-scale distribution. It is assumed that the change of these fields does not depend on the direction along the frontal zone. Having introduced f into the original system of equations and subtracted from it respective equations of large-scale processes, we get a final system to calculate the formation and evolution of the frontal zone and its cloud system.

To calculate the rate of condensation of water vapour we use the method of invariants, described in Ref. 7. Vertical coefficients of turbulence for heat and momentum are understood as variable in space and time. Description of the surface boundary layer of atmosphere is made on the basis of the similarity theory by Monin-Obukhov. Concrete methods of calculating the fields of meteorological values are developed in Ref. 2.

The conditions of wind velocity components equalling zero were introduced on the lower boundary, while deviations of potential temperature and humidity were treated as the given functions of the coordinates. These conditions were used to determine the heat and momentum flux, which in fact were the actually used boundary conditions. The upper boundary of the area described was understood as a solid, smooth and thermoconductive surface. Since it is situated in the lower part of the stratosphere, specific humidity on it, according to experimental data, was assumed as equalling zero. Conditions of cross component of velocity disturbance obliteration were introduced on the side boundaries. Disturbance of fluxes of the longitudinal component of velocity, heat and specific moisture content were kept constant equalling their values at the initial point of time.

The field of potential temperature was introduced as initial data. It was separated by the sloping tropopause into two parts: the lower part (troposphere), where the temperature at fixed heights was growing from the north to the south, and the upper part (stratosphere), with the reverse trend of temperature. Fields of pressure, humidity, disturbances of the fields of velocities were other initial data of the model.

To approximate non-lineal members one of the variants of Arakawa-Lilly conservative scheme was used to realise the model numerically. This approximation ensured conservation of energy and momentum.

4. Results of calculation

The results of one of the numerical modellings of the front and its cloud system are given in Fig. 1. The figure shows that a sloping frontal zone (the region of potential temperature isoline thickening) was formed in the troposphere. The field of specific moisture content (dashed lines) also showed the formation of a sharp front, with the location of most sharp gradients in the field of specific moisture content coinciding with the maximum contrasts of other meteoelements in the frontal zone. The tongue of moist air was formed on the warm side of the frontal zone in the lower and middle troposphere, and the air on the cold side was growing drier due to descending motions of air.

The warm air mass over the frontal surface coinciding with the region of maximum vertical motions is the area of the formation and evolution of the frontal cloud sys-

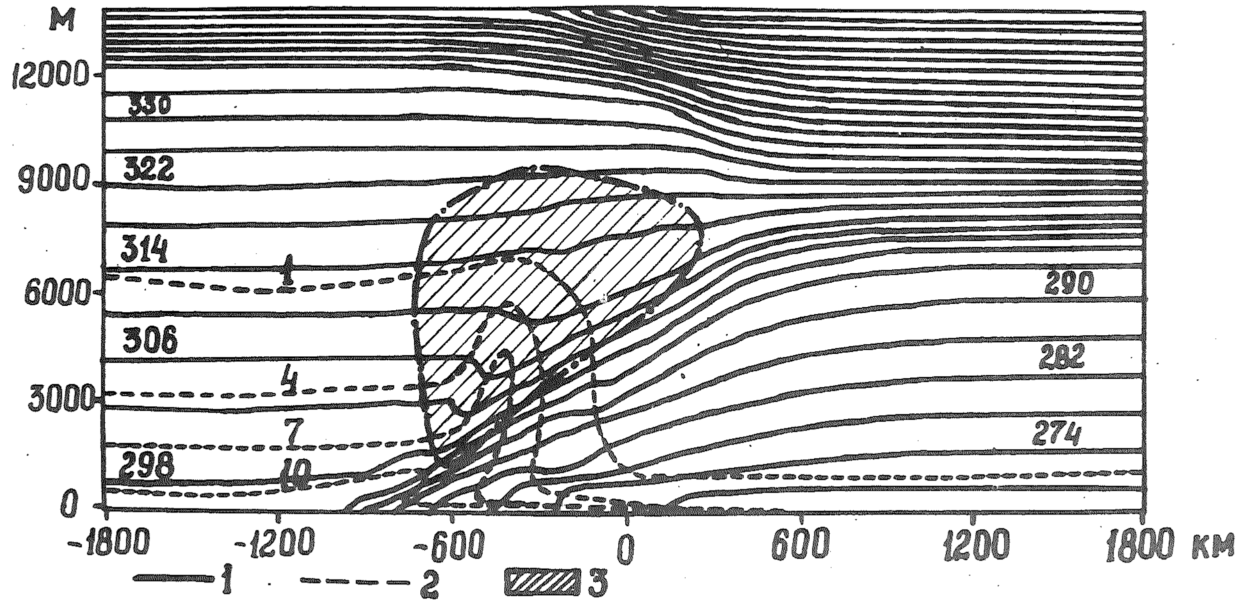

Figure 1. Vertical cross-section of tropospheric frontal zone and its cloud system. 1-isolines of potential temperature, 2-isolines of specific moisture content, 3-cloudiness.

tem. The cloudiness usually appears in two layers of the warm air mass (the appearance of specific liquid water content not equalling zero was taken for the start of cloudiness formation). The lower tier of cloudiness maximum liquid water content exceeds the analogous characteristic of the upper layer, but its vertical thickness is significantly less than in the upper layer. In the course of time the area of space taken by cloudiness is growing in both directions vertically and gradually expands horizontally. Cloudless layer gradually disappears and a system of frontal cloudiness with maximum liquid water content in the lower part is formed.

The characteristics of the frontal cloudiness being formed depend on many factors. Therefore, changing the initial data (the values of relative humidity and the temperature, their vertical and horizontal gradients), we obtain a possibility to model different conditions of the formation and structural peculiarities of frontal cloudiness. For example, growing contrast of temperatures between air masses, growing relative humidity in the boundary layer and reducing static stability of atmosphere are conductive to an early start of the frontal cloudiness formation. Increase in baroclinicity leads to the growing of both specific liquid water content maximum values and summary water content of the clouds, and is conductive to the formation of the upper layer of the clouds at a higher altitude.

4.1. The influence of radiation heat exchange on the formation and evolution of frontal stratiform cloudiness.

The results of the calculations (Ref. 4) showed a significant change in the cloud atmosphere temperature regime due to taking into account the radiation influx of heat, which may in some situations influence the development of dynamic processes. On the other hand, the contribution of radiation processes is diminishing with the growing intensity of vertical motions and the release of latent heat of condensation. It stands to reason that the final conclusion on the influence of radiation influx of heat on the hydrodynamics of fronts and their cloud systems may be drawn only after numerical experiments with the joint calculation of hydrodynamics considering the processes of cloud formation and radiation. Comparison of the results of these numerical experiments with the control ones (analogous parameters, but without taking into account radiation influxes of heat) makes it possible to appreciate the influence of radiation factors upon the structure of circulation in the frontal zone and its stratiform cloudiness.

Radiation losses of heat due to long-wave cooling-out in the upper boundary of stratiform cloudiness amount to several degrees per hour. They exceed to a large extent (except afternoon hours) the warming up due to the absorption of solar radiation. Therefore, it is considered correct to take into account first of all the heat influxes due to long-wave radiation transfer.

Fig. 2a shows isolines of vertical velocity field in the section perpendicular to the front line without account of radiation heat exchange. The initial data in this experiment are introduced in such a manner (Ref. 5) as to ensure front formation with the maximum rising motions not exceeding 1 cm/s. The figure shows that the warm side of the front is characterized by a rising motion, which cools the air and prevents sharp frontal zone formation in the middle troposphere, being at the same time one of the most potent factors regulating cloudiness formation and precipitation intensivity. The cold side of the front is characterized by descending motion warming up the air.

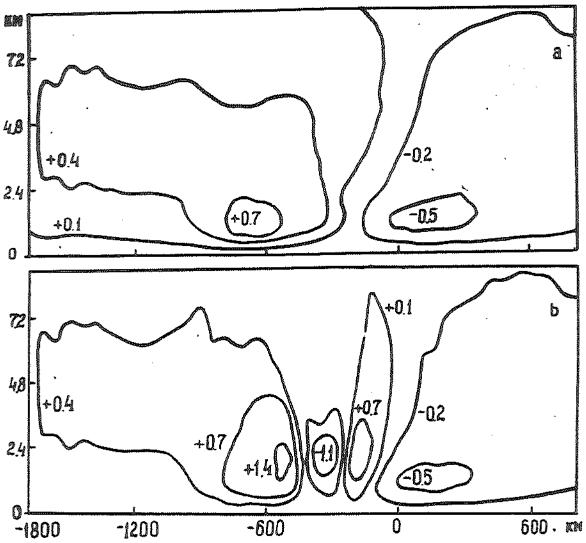

Figure 2. Vertical motions field (cm/s) in frontal zone.
a-without account of radiation heat exchange,
b-with account of radiation heat exchange.

Comparison of Fig. 3a and Fig. 3b clearly shows the changes, which have taken place in the spatial structure of circulation in the frontal zone. If long-wave radiation transfer processes are not taken into account, the frontal zone formation region has two cells of rising and descending motions of approximately equal width. With account of radiation factors the heat influxes, brought about by long-wave radiation generate heterogeneity of circulation on the warm side of the frontal zone (the region of formation and evolution of a cloud system). It is here, where the zones of alternating rising and descending motions are formed. Maximum descending and rising vertical velocities in comparison with the control variant have noticeably increased.

Fig. 3 showing isolines of the field of specific liquid water content in the section perpendicular to the front line illustrates the features of the spatial structure of frontal cloudiness system. If the radiation factors are not taken into account (Fig. 3a), it is homogeneous by its structure with the maximum of specific liquid water content located in the lower part of the cloud. The spatial size of cloudiness and the value quantities of specific liquid water content are in a qualitative agreement with those, obtained from the observations. Thus, for example, the quantity of maximum liquid water content equals 0.4 g/kg and is situated at the altitude of 1600 m.

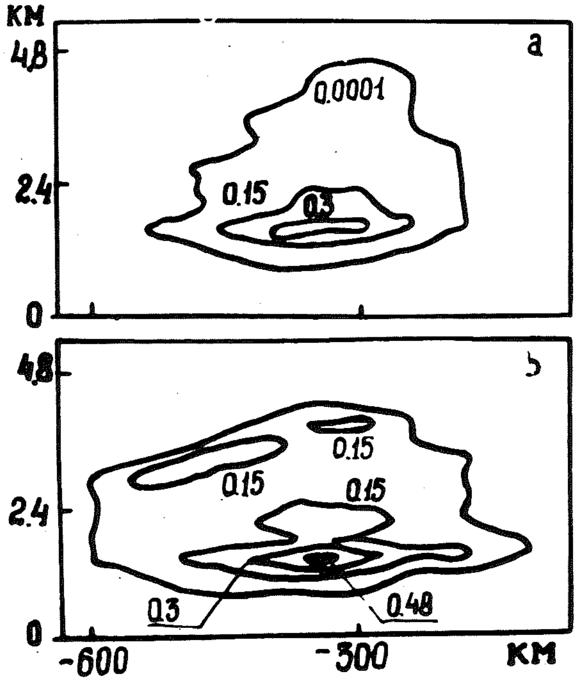

Figure 3. Isolines of specific liquid water content field (g/kg) in the frontal zone.
a-without account of radiation, b-with account of radiation.

Comparison of Fig. 3a and Fig. 3b shows that in case of a numerical experiment with radiation taken into account a more powerful stratiform cloudiness was formed. Its size expanded approximately by 150 km. Contrary to the variant without account of radiation factors, frontal cloudiness system here is heterogeneous by its structure. Local maximums of specific liquid water content equalling 0.15 g/kg are being formed in the upper part of the cloud. The liquid water content in the lower part of the cloudiness is also greater with its maximum by 0.1 g/kg exceeding that of the control variant.

Let us now consider the model of the formation and evolution of the frontal zone and its cloud system, where initial data are introduced in the way to ensure front formation with maximum rising motions, exceeding the quantity of the order of 1 cm/s. The analysis of the results obtained shows that the more intensive vertical motions are at the front, the less changeable are the characteristics of the vertical velocities field and frontal stratiform cloudiness with radiation factors taken into account. So, with the evolution of the front with maximum vertical velocities of the order of 5-10 cm/s, changes in the fields of thermohydrodynamic parameters, considering the radiation factors, in comparison with the control variant are practically not observed. The reason is that the radiation influx of heat in this case is a quantity, which is by far lower than the quantity of warming up due to the release of condensation heat.

Thus, results of numerical experiments show that the influence of long-wave radiation heat exchange on the characteristics of circulation in the frontal zone and its stratiform cloudiness is essential only in the cases with the evolution of the fronts, where the intensity of vertical motions brought about by dynamic factors, does not exceed the quantity of the order of 1 cm/s.

Recent years have seen many new experimental data obtained on the spatial structure of atmospheric fronts. Analysis of these data has made it possible to discover significant mesoscale heterogeneity of meteorological fields in the frontal zones, influencing greatly the fields of vertical motions and the intensity of precipitations. According to the results of numerical experiments described above, long-wave radiation influxes of heat are just one of the possible factors, determining the formation of heterogeneities in the fields of vertical motions and cloudiness.

5. REFERENCES

1. Lipps, F.B., 1977. A study of turbulence parameterization in a cloud model. J. Atmos. Sci., 34, 1751-1772.
2. Kazakov, A.L., and Lazriev, G.L., 1978. Parameterization of the atmospheric surface layer and the active soil layer. Izv. Acad. Sci., USSR, Atmospheric and Oceanic Physics., 14, No. 3, 257-265.
3. Delsol, F., Miyakoda, K., Clarke, R.H., 1971. Parameterized processes in the surface boundary layer of an atmospheric circulation model. Quart. J. Roy. Met. Soc., 97, No. 412, 181-209.
4. Feigelson, E.M., 1970. Long-wave radiation heat exchange and clouds. Leningrad, Gidrometeoizdat, 230 pp.
5. Kutsenko, B. Ya., 1981. Numerical studies of frontogenesis with account of phase transitions. Meteorology and Hydrology, No. 9, 23-34.
6. Kutsenko, B. Ya., 1982. Mathematical model of formation and evolution of a front and frontal stratus cloudiness. Trudy Tsentral. Aerolog. Obs., No. 148.
7. Matveev, L.T., 1959. Some aspects of the theory of formation and evolution of stratus clouds. Trudy Arctic and Antarctic Institute, 228, No. 1.

TWO-DIMENSIONAL NUMERICAL MODEL OF FRONTAL CLOUDS AND PRECIPITATION

G.V. Mironova, B.N. Sergeev

Central Aerological Observatory, Moscow, USSR

1. INTRODUCTION

Description of cloud and precipitation formation processes is an essential part of mathematical models intended for frontal system research and forecasting. These processes interact actively with flow field and may influence its structure owing to sources and sinks of phase change heat. For an adequate presentation of such interaction it is necessary to take correctly into account mass growth and evaporation rates of water and ice particles in clouds and precipitation and particle spatial transport rates. A parameterization method is developed for the description of these processes (Ref. 1). Concentrations and masses of the particles of the considered types are chosen as the main parameters. The method can be applied to numerical models of synoptic or mesoscale atmospheric processes and in forecasting schemes. The present paper deals with the description of the method and its application to numerical study of cloud and precipitation process interaction with flow field in a frontal region within the framework of a simple two-dimensional model.

2. GOVERNING EQUATIONS OF THE MODEL

Fields of meteorological variable are presented as a sum of large scale values and mesoscale perturbations. The large scale velocity field is the deformation field with the components $U_x=-Dx$, $U_y=Dy$, $U_z=0$, where D is constant. The x and y axes are directed across and along the front surface, respectively, the z axis is directed vertically upwards. The flow is homogeneous along the front line. The quasistatic approximation is assumed. The governing equations are written in terms of vorticity-streamfunction

$$\zeta = \frac{\partial u_x}{\partial z} - \frac{\partial u_z}{\partial x}, \tag{1}$$

$$\rho u_x = \frac{\partial \Psi}{\partial z}, \quad \rho u_z = -\frac{\partial \Psi}{\partial x} \tag{2}$$

$$\frac{\partial \zeta}{\partial t} = -\frac{\partial}{\partial x}(u_x\zeta) - \frac{\partial}{\partial z}(u_z\zeta) - \frac{\partial}{\partial x}(U_x\zeta) + \ell\frac{\partial u_y}{\partial z} - \frac{g}{\theta_0}\frac{\partial \theta}{\partial x} + A_x\frac{\partial^2\zeta}{\partial x^2} + \frac{\partial^2}{\partial z^2}A_z\zeta, \tag{3}$$

$$\frac{\partial}{\partial z}\frac{1}{\rho}\frac{\partial \Psi}{\partial z} = \zeta,$$

$$\frac{\partial u_y}{\partial t} = -u_x\frac{\partial u_y}{\partial x} - u_z\frac{\partial u_y}{\partial z} - U_x\frac{\partial u_y}{\partial x} - Du_y - \ell u_x + A_x\frac{\partial^2 u_y}{\partial x^2} + \frac{\partial}{\partial z}A_z\frac{\partial u_y}{\partial z}, \tag{4}$$

where ζ is vorticity, Ψ is streamfunction, u_x, u_y, u_z are components of velocity perturbation, ρ is the air density, ℓ is the Coriolis parameter, θ_0 is the mean potential temperature, θ is the potential temperature perturbation, A_z, A_x are coefficients of vertical and horizontal turbulent mixing.

The balance of heat is described by the equation

$$\frac{\partial \Pi}{\partial t} = -u_x\frac{\partial \Pi}{\partial x} - u_z\frac{\partial \Pi}{\partial z} - U_x\frac{\partial \Pi}{\partial x} - u_z\frac{\partial \Pi_f}{\partial z} + A_x\frac{\partial^2\Pi}{\partial x^2} + \frac{\partial}{\partial z}A_z\frac{\partial \Pi}{\partial z} + \frac{L_f}{C_p}J_{FT} \tag{5}$$

where $\Pi = T + \frac{L_c}{C_p}q$, T and q are the temperature and water vapor mixing ratio perturbations, L_c and L_f are latent heat of condensation and freezing, respectively, C_p is specific heat of air at constant pressure, $\Pi_f = T_f + \gamma_a z + \frac{L_c}{C_p}q_f$, T_f and q_f are background temperature and water vapor mixing ratio, J_{FT} is total rate of mass exchange by freezing, sublimation and melting.

The equation of the whole water content balance has the form

$$\frac{\partial S}{\partial t} = -u_x\frac{\partial S}{\partial x} - u_z\frac{\partial S}{\partial z} - U_x\frac{\partial S}{\partial x} - u_z\frac{\partial q_f}{\partial z} + \frac{\partial}{\partial z}V_wW + A_x + \frac{\partial}{\partial z}A_z\frac{\partial S}{\partial z} + J_{WE} \tag{6}$$

where $S = q + W$ is the perturbation of the whole water mixing ratio, W is liquid water mixing ratio, J_{WE} is the total rate of mass exchange by sublimation and accretion.

In the case of unsaturated air

$$q = S, \quad T = \Pi - (L_c/C_p)q \tag{7}$$

and in the opposite case

$$W = S + q_f - q_s, \quad T = \Pi - (L_c/C_p)(q_s - q_f) \tag{8}$$

where q_s is saturation mixing ratio.

3. PARAMETERIZATION OF CONVECTION

Convective clouds develop under conditions of potential instability release in the frontal region. Growing convective cells cause compensating descending motion and heating of environmental air. A dissipating cell mixes horizontally with the environment. The convection influence on the flow field caused by these processes is described by the one-dimensional time-dependent model of a convective cell.

The used parameterization scheme is analogous with the Kreitzberg and Perkey scheme (Ref. 2). The condition of potential instability existence is verified for the model levels corresponding to the low and middle troposphere. The convective cell parameters are calculated for the region of potential instability. The part of the area covered by convective cells is determined according to the condition of pressure change balance over the depth of the cell both within the cell and within the environment. The corrections to the temperature and vapor mixing ratio fields caused by convection are evaluated and the effects of subsidence, mixing and adjusting for hydrostatic balance and mass adjustment are taken into account.

4. THE PRESENTATION OF PRECIPITATION PROCESSES

The main processes of precipitation particle formation, growth and spatial transportation typical for frontal cloud of extratropical cyclones are taken into consideration. Ice crystals appear as a result of cloud drop freezing and deposition nuclei activation. Crystals have the form of plates or columns depending on the temperature of formation. In the frontal layer clouds precipitation forms under suitable conditions due to the Bergeron process. Ice crystals undergo the sublimation growth and fall relative to air. When the temperature is below 0 °C precipitation fall to the ground in the form of ice crystals. When the temperature near the ground is above 0 °C falling crystals melt and become raindrops, which continue their growth by accreting cloud water.

For convective cells formation and growth of graupel are taken into account but for processes mentioned above. Graupel growth is included in computation, if cloud water content is above 0,5 g/m^3 and crystal achieve the critical dimensions (plates of radius 150 μm and columns of length 100 μm). Large crystals accrete cloud water, which freezes on its surface. A crystal is takin_ spherical form and gradually becoming a graupel. The latter continues its growth by accretion. Graupels melt at the temperature above 0 °C and become raindrops.

If particles of any type get into unsaturated air, they evaporate.

The developed method of parameterization is based on the assumption that the particle size spectra have the form of the gamma-distribution. The mass spectra are given by

$$f(m) = \frac{N m^{\frac{\gamma-2}{3}}}{3\Gamma(\gamma+1)\beta^{\gamma+1}} \exp\left(-m^{1/3}\beta\right), \qquad (9)$$

where m is mass, N is particle concentration, β and γ are parameters, $\Gamma(x)$ is gamma function. Total particle concentration and mass for every considered particle type are chosen as the main parameters. The value of γ is proposed to be constant, where γ = 6 for cloud droplets, γ = 2 for raindrops and γ = 4 for ice crystals (Ref. 3).

Evolution of the concentration and mass fields by advection, gravitational settling, turbulent diffusion and by processes of particle production, growth and evaporation is described by the following equations:

$$\frac{\partial N^i}{\partial t} = -\vec{u}\nabla N^i + \frac{\partial}{\partial z}V_N^i N^i + A_x\frac{\partial^2 N^i}{\partial x^2} + \frac{\partial}{\partial z}A_z\frac{\partial N^i}{\partial z} - J_N^i + Q_N^i \qquad (10)$$

$$\frac{\partial M^i}{\partial t} = -\vec{u}\nabla M^i + \frac{\partial}{\partial z}V_M^i M^i + A_x\frac{\partial^2 M^i}{\partial x^2} + \frac{\partial}{\partial z}A_z\frac{\partial M^i}{\partial z} - J_M^i + Q_M^i \qquad (11)$$

where index i indicates the particle type (i = 1 corresponds to cloud droplets, i = 2 to plates, i = 3 to columns and i = 4 to graupels), $\vec{u}$ is wind vector, V_N^i and V_M^i are the weighted mean terminal velocities of particles, J_N^i and J_M^i are the growth or evaporation rates on N^i or M^i change, Q_N^i and Q_M^i are the production rates of N^i or M^i.

The weighted mean terminal velocity of particles is approximated as

$$V_N^i = \exp\left[\sum_{k=0}^{4} a_{Nk}^i(\ln\beta^i)^k\right](1000/P)^{0.5} \qquad (12)$$

where P is pressure, $\beta^i = [M^i/N^i(\gamma+3)(\gamma+2)(\gamma+1)]^{1/3}$. The same expression is used for V_M^i. The values of the coefficient a_{NK} and a_{MK} are presented by Sergeev (Ref. 1). The production rate Q_N for cloud droplets does not equal zero for the region of cloud boundary, where vertical velocity is $u_z \geq 0$. Q_N^1 is determined by formulas of initial condensation stage. The rate Q_{NF}^i of ice crystal formation by droplet freezing is expressed as (Ref. 4)

$$Q_{NF}^i = A\left(\frac{T}{T_0}\right)^{\delta}\frac{dT}{dt}, \qquad (13)$$

where T is temperature (°C), A, T_0, δ are parameters. The rate Q_{NS}^i of ice crystal formation on deposition nuclei equals (Ref. 4)

$$Q_{NS}^i = B\left(\frac{S_i}{S_0}\right)^{\varkappa}\frac{dS_i}{dt} \qquad (14)$$

where S_i is the vapor supersaturation over ice, B, S_0, $\varkappa$ are parameters.

It is assumed that plate type crystals form at T $\geq$ -3 °C or -20 $\leq$ T < 10 °C and column type crystals form at -10 $\leq$ T < -3 °C or T -20 °C.

The rate of concentration or mass change is approximated by the following formula

$$J_M^i = \pm\frac{N^i}{\Delta t}\exp\left(\sum_{j=0}^{4}\sum_{k=0}^{4} b_{Mjk}^i x^k y^j\right), \qquad (15)$$

where $x = \ln\beta^i + b_{Mx}^i$, $y = \ln(\Delta\tau) + b_{My}^i$, Δt is the time step of numerical model. The positive sign is attributed to particle growth, and the negative sign is attributed to particle evaporation. The table of coefficients b_{Mx}, b_{Mjk}, b_{My} is presented by Sergeev (Ref. 1). The parameter $\Delta\tau$ depends on the time step Δt, air pressure, temperature and humidity. It has different expressions for different microphysical processes. For example in the case of ice crystal growth or evaporation $\Delta\tau$ has the form

$$\Delta\tau = 4\pi A_i\int_0^{\Delta t} S_i\,dt \qquad (16)$$

where A_i is coefficient in the mass growth equation, S_i is supersaturation over ice.

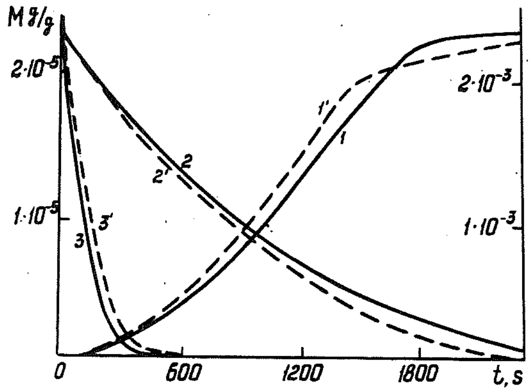

Figure 1. Comparison of the approximate (solid lines) and exact (dashed lines) mass dependences on time for the growth (1,1') and evaporation (2,2' and 3,3') of plate type crystals.

Checking of formula (15) is performed with the aid of the auxiliary microphysical model, which describes processes of particle growth or evaporator in a closed air parcel. The monodispersed particle spectrum is assumed in model computations. The variant of formula (15) attributed to $\gamma = 8$ is used for approximate computations. This case of the gamma-distribution (9) approaches to monodispersed spectrum. The comparison of some above-mentioned computation results is shown in Fig. 1. The growth (1,1) and evaporation (2,2'; 3,3') curves for plate type crystals are presented (T = -10 °C, p = 700 gPa, = 10^{-1} -10^{-2} m/s). It is assumed for the ice crystal evaporation that relative humidities are 90 % (curves 2,2') or 20 % (curves 3,3'). The left vertical scale describes the evaporation cases and the right scale describes the growth case. It may be seen that formula (15) gives physically correct and rather exact description of phase change dynamics in clouds.

A long time step up to 300 s may be used in formula (15). Because of that the developed parameterization scheme is more advantageous among others for using in models of a frontal cloud and precipitation evolution time of which is up to tens of hours.

5. BOUNDARY AND INITIAL CONDITIONS

Free slip and zero vertical velocity conditions are set at the lower and the upper boundary. Vertical turbulent flows of heat and moisture are proposed to be zero at that boundary. Open conditions (Ref. 5) are set at the lateral boundaries for ζ, u_y, Π, S.

Temperature and relative humidity vertical sections in the cross-front direction are set at the initial moment. The u_y component of velocity is initially in geostrophic balance with the temperature.

Initial fields of u_y und u_z components are computed by geostrophic momentum approximation.

6. NUMERICAL SCHEME

The equations (1)-(6) are solved over a 2560 km x 16 km domain with a 20 km grid interval in x direction and 250 m grid interval in z direction. The time step is 150 s. The leap-frog scheme combined with the Arakawa (Ref. 6) advection are used. Diffusion terms are shifted by one time step back. Central differences are used for other space derivatives. The Van Leer (Ref. 7) monotonic conservative scheme is used for solving equations (10)-(11). Vertical advection is calculated first and then horizontal advection.

7. SOME RESULTS OF MODELING

Computations are made for the initial temperature and humidity fields corresponding to some real cases of a warm front. Precipitation process influence on a flow field structure in the vicinity of a front is investigated. Some characteristics of the initial fields are varied keeping in view the aim of this investigation.

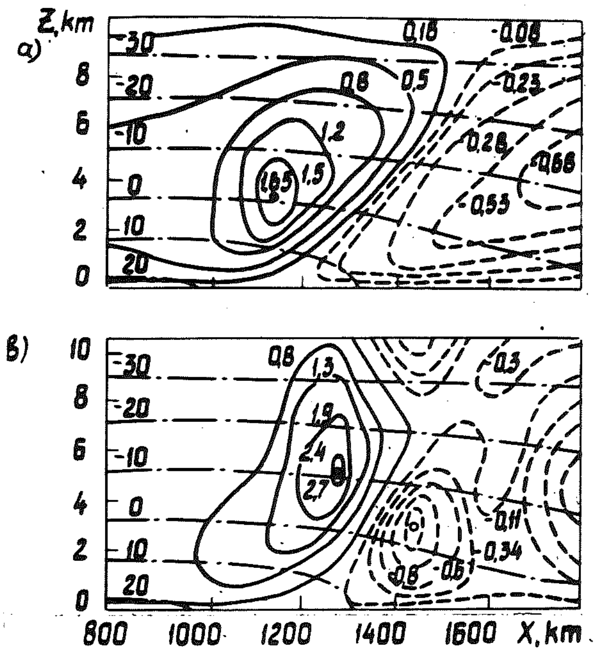

Figure 2. The vertical velocity field (cm/s) in frontal region. a. precipitation processes are omitted, b. precipitation processes are taken into account (t = 30 h).

According to the results process of cloud and precipitation formation essentially influences vertical frontal circulation. Vertical motions are intensified and its structure is changed. The examples of vertical velocity field in different cases for the time moment t = 30 h are shown in Fig. 2. As seen from Fig. 2a smooth circulation develops in the case of a moderate stratification stability ($\gamma = 5{,}5^{\circ}$ C/km), if processes of cloud, ice and precipitation formation are ignored. Heat sources and sinks connected with phase changes appear, if these processes are accounted. They give rise to inhomogeneous flow pattern, which manifests in cells of upward and downward motion in the regions, where ice grows and precipitation evaporates.

A time change of the cell parameter has a form of nonlinear oscillations provided cloud ice appears under the condition of saturation over water. Flow field fluctuations in our case are connected with the mass oscillations in the water vapor-liquid water-ice system existing in a cloud. These oscillations are revealed in the microphysical cloud models (Ref. 8). Oscillations of this type are essentially smoothed provided cloud ice appears at the humidities above ice saturation.

The liquid water and ice content fields of the frontal cloud system are presented in Fig. 3. The manifestations of the oscillations mentioned above are visible.

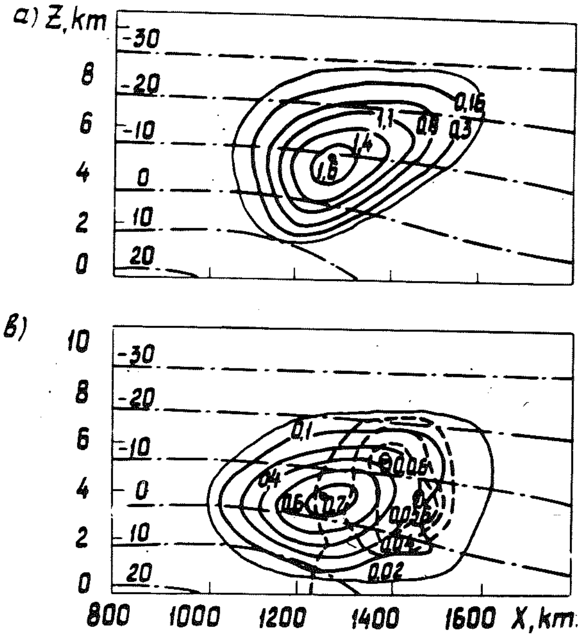

Figure 3. Parameters of the cloud and precipitation system. a. liquid water content in g/m^3 for the time t = 30 h, precipitation processes are omitted. b. liquid water content in g/m^3 (solid line), ice (T < 0 °C) and precipitating (T > 0 °C) water content in g/m^3 (dashed line) for the time t = 30 h, precipitation processes are taken into account.

Flow field and microphysical parameter inhomogeneities lead to precipitation field inhomogeneities. As an example the precipitation intensity time dependence is shown in Fig. 4 for the two discussed cases of the assumption about ice formation.

The presented results show the interaction of precipitation processes with flow field in the region of an atmospheric front may play significant role in the formation of flow and precipitation field structure. This structure is sensitive to the details of ice formation processes.

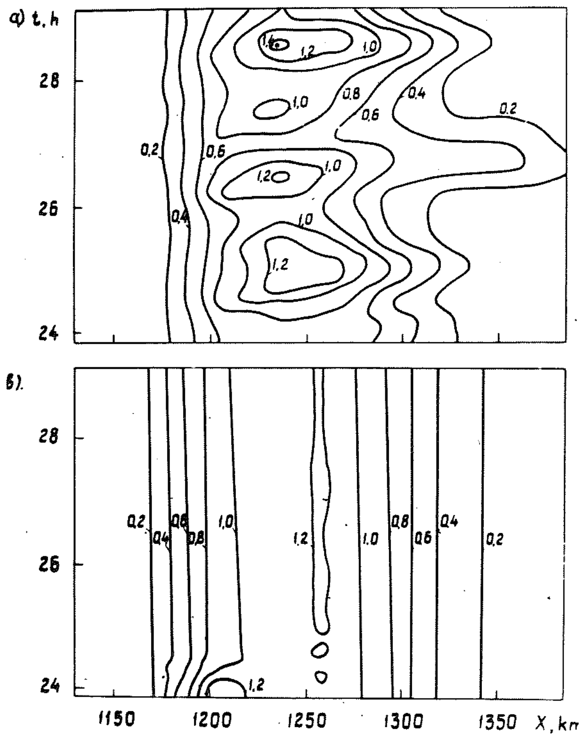

Figure 4. Time dependence of the precipitation intensity (in mm/h) spatial distribution. a. ice formation under the condition of saturation over water. b. ice formation at humidities above ice saturation.

8. REFERENCES

1. Sergeev, B.N., 1983. Numerical modeling of an atmospheric front with a cloud system and precipitation (in Russian). Meteorol. and Hydrolog., No. 4, 21-29.
2. Kreitzberg, C.W., Perkey, D.J., 1976. Release of potential instability: Part I. A sequential plume model within a hydrostatic primitive equation model. J. Atmos. Sci., 33, 456-475.
3. Litvinov, I.V., 1974. Structure of atmosperic precipitation (in Russian). Leningrad, Gidrometeoizdat, 180 pp.
4. Vali, G., 1975. Remarks on the mechanism of atmospheric ice nucleation. Proc. VIII Int. Conf. on Nucleation, Moscow, Gidrometeoizdat, 265-269.
5. Orlanski, J., 1976. A simple boundary condition for unbounded hyperbolic flows. J. Comp. Phys., 21, No. 3.
6. Arakawa, A., 1966. Computational design for long-term numerical integration of the equations of fluid motion: Two dimensional incompressible flow. Part I. J. Comput. Phys., 1, 119-143.
7. Van Leer, B., 1974. Towards the ultimate conservative difference scheme. II Monotonicity and conservation combined in a second order scheme. J. Comp. Phys., 14, 361-370.
8. Buykov, M.B., Pirnach, A.M., 1975. Numerical modeling of microphysical precipitation forming processes in mixed layered clouds (in Russian). Izv. Acad. Sci. USSR, Atmospheric and Oceanic Physics, 11, No. 5.

A NUMERICAL SIMULATION OF THE INTERACTION OF DYNAMICAL AND MICROPHYSICAL PROCESSES IN FRONTAL CLOUDS

A.M. Pirnach

Ukrainian Scientific Research Institute, Kiev, USSR

1. INTRODUCTION

A two-dimensional time-dependent model was used to study the interaction between dynamical and microphysical processes in winter frontal cloud systems. The above frontal systems were examined considering 1) the feature of the cloud formation process and evolution of cloudiness and precipitation in different regions of the frontal system, 2) sources and sinks of moisture in relation to a front, 3) the air motion associated with the frontal cloud system, 4) the effect of cloudiness on the development of atmospheric front in space and time.

2. DESCRIPTION OF THE MODEL

The formation and development in space and time of cloud systems in the frontal zones are simulated by integration of the following set of primitive equations:

$$\frac{\partial \rho u}{\partial x} + b_2 \frac{\partial \rho v}{\partial y} + \frac{\partial \rho w}{\partial z} = 0. \quad (1)$$

$$P = \rho R T. \quad (2)$$

$$\frac{\partial s_i}{\partial t} + u\frac{\partial s_i}{\partial x} + b_i v \frac{\partial s_i}{\partial y} + w_i \frac{\partial s_i}{\partial z} = F_i + k_x \frac{\partial^2 s_i}{\partial x^2} + k_z \frac{\partial^2 s_i}{\partial z^2},$$

$$i = 1,2,\ldots,7. \quad (3)$$

$$(s_1, s_2, \ldots, s_7) = (u, v, w, q, t, f_1, f_2) \quad (4)$$

$$(w_1, w_2, \ldots, w_7) = (w, w, w, w, w, w - v_1, w - v_2). \quad (5)$$

$$(b_1, b_2, \ldots, b_7) = (1, 1, 1, 0, 0, 0, 0). \quad (6)$$

$$F_1 = lv - \frac{1}{\rho}\frac{\partial P}{\partial x}. \quad (7)$$

$$F_2 = -c_1 lu - c_2\left(lu_f + \frac{1}{\rho}\frac{\partial P}{\partial y}\right). \quad (8)$$

$$F_3 = -\frac{\partial P}{\partial z} - g. \quad (9)$$

$$F_4 = -E_1 - E_2. \quad (10)$$

$$F_5 = \frac{L_1}{c_p}E_1 + \frac{L_2}{c_p}E_2 - \gamma_a w. \quad (11)$$

$$F_6 = -\frac{\partial f_1 r_{1k}}{\partial r} + I_a - I_f. \quad (12)$$

$$F_7 = -\frac{\partial f_2 r_{2k}}{\partial r} + I_s + I_f. \quad (13)$$

There is an assumption that a coordinate system itself is moving and its velocity is u_f at $t = 0$.

u_f is horizontal velocity of a front.

x, y, z, r, t are respectively horizontal coordinates perpendicular and parallel to a front, height above sea level, cloud particle size and time.

u, v, w are wind components in the x, y, z direction, respectively.

The other symbols defined as follows:

T	air temperature
P	air pressure
ρ	air density
q	specific humidity
f_i	size distribution function of drops (i=1) and ice particles (i=2)
v_i	terminal velocity of drops (i=1) and ice particles (i=2)
L_i	condensation (i=1) and crystallization heat (i=2)
c_p	specific heat at constant pressure of dry air
γ_a	dry-adiabatic gradient
l	Coriolis parameter
g	acceleration due to gravity
R	gas constant of dry air
k_x, k_z	turbulence eddy coefficients in x and z directions, respectively (Ref. 3)
E_i	rates of the change of q due to condensation or evaporation (Refs. 1, 3). i=1,2
r_{i_k}	rate of the change of r due to condensation or evaporation
I_a, I_s	sources of the origin of drops and ice particles, respectively (Refs. 1, 3)
I_f	freezing rate of drops (Refs. 1, 3)
u_1	$u_f + u$
c_1, c_2	parameters

Two methods were used to compute the initial data: 1) the time-independent two-dimensional theoretical models of the frontal systems (Refs.3), 2) the serial rawinsonde data were used to construct cross-sections through the frontal systems passing over the area (Ref. 5).

The boundary conditions may be obtained using Eq. 3, if one sets

$w = b_i = F_i = k_x = k_z = 0$ at $z = 0$;

$\frac{\partial s_i}{\partial z} = w = 0$ at $z = Z$; $i = 1,2,\ldots,7$;

$\frac{\partial s_i}{\partial x} = 0$ at $x = 0$ and $x = X$;

$\frac{\partial s_i}{\partial y} = 0$ at $y = 0$ and $y = Y$.

X, Y, Z are maxima of x, y, z respectively. The solution schemes of nonsteady differential Eqs. 1-13 were given in Ref. 3.

3. RESULTS OF NUMERICAL EXPERIMENTS

Numerical integration of the model equations has been carried out and analyzed for many frontal situations. In the interest of space, only one case will be discussed at length here, although some reference will be made to the results obtained in the other cases. More details can be obtained from Refs. 2-6. In this report, the analysis is based on the results obtained with numerical models described above in section 2. The initial data obtained with the models are described in Ref. 5.

The occluded frontal system which we observed was approaching the MPG (Meteorological Proving Ground of Ukrainian Scientific Research Institute, Jovtneve, USSR) on 11-12 January, 1976. This frontal system was embedded in a westerly upper-level flow. A broad zone of precipitation and cloudiness was encompassing it. The peak of precipitation rate was 1.5 mm/h.

A vertical cross-section through the occluded frontal system which passed over MPG rawin-sonde site at 0 h MST 12 January, 1976 is shown in Fig. 1. Location of the front was determined with the help of a vertical cross-section of temperature shown

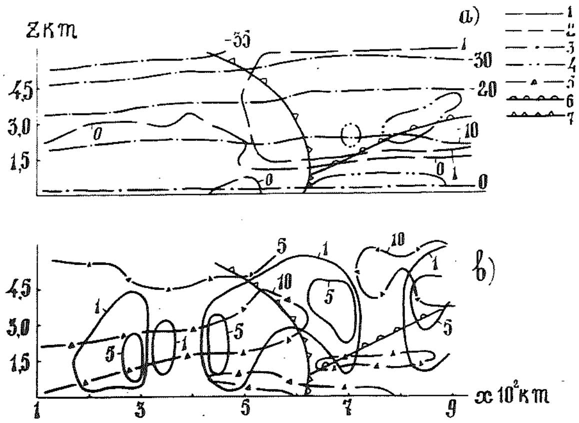

Figure 1. Vertical cross section through the occluded frontal system. 12 January, 1976 at 03 h MST. a) isotherms (T), water supersaturation (Δ_1), ice supersaturation (Δ_2); b) wind components u_1 and w. The numbers near isoline indicate the following 1) W cm/s, 2) Δ_2 g/kg, 3) T °C, 4) $\Delta_1 = 0$, 5) u_1 m/s, 6) warm front, 7) cold front.

in Fig. 1a. The occluded frontal system which moved over MPG on 12 January was first characterized by the passage of a warm front located between $1 \leqslant z \leqslant 3$ km $600 \leqslant x \leqslant 900$ km at 03 h. This warm front was followed by a well-defined cold front located between $0 \leqslant z \leqslant 5$ km and $450 \leqslant x \leqslant 600$ km. The frontal system is moving with the velocity $u_f = 10$ m/s. The values of horizontal wind component u were mainly less than zero and $u_1 < u_f$. The cold front was located in the 300 km section of upward motion including two peaks of 8 cm/s and over the warm front surface it was peak updrafts of 7 cm/s. From Fig. 1a, it is evident that the primary source of moisture for the frontal clouds was in the warm air mass, which contained the regions with $\Delta_1 > 0$ and $\Delta_2 > 0.1$ g/kg ($\Delta_i = q - q_{mi}$, $i = 1,2$; q_{mi} is saturation specific humidity in relation to water and ice respectively). The sinks of moisture with $\Delta_2 < 0$ occurred behind the cold frontal surface and below the warm frontal surface. The development in space and time of the dynamic and microstructure of frontal cloud systems in their interrelationship was calculated with the aid of Eqs. 1-13. In this case it is assumed that $B_i = 0$, $c_1 = 1$, $c_2 = 0$. The values of other parameters and constants are given in Ref. 3. The time change of the dynamic and cloud microphysics of the frontal system was shown in Figs. 1-3. The temperature field was gradually changing (Figs. 2a and c). In the warm front the intensity of the horizontal temperature gradients was decreasing. Computed air motion (Figs. 2a, c) showed that the field of vertical motions consisted all the time of a few cells. Three peak updrafts were in the frontal system, two peaks were found in the warm air mass and one peak was behind the cold frontal surface. A peak downdrafts was found near the cold frontal surface. Results of numerical experiments for warm fronts given in Refs. 2-6 showed that in these fronts both the cells of updraft and downdraft are present during existence of the front, but the warm front was keeping the only peak updrafts in the warm air mass. The occluded front was evidently keeping a peak updrafts due to the warm front and two peaks due to the cold front. The frontal cloudiness associated with the regions of the stable maximum upward motions.

The cloudiness existed for many hours. In our case at t = 1 h a mixing cloud was found in the warm air mass with two peaks of the cloud liquid water content up to 0.23 g/kg and 0.15 g/kg. We have also to mixing cloud behind the cold front with the maximum liquid water content $q_{l\ 1m} = 0.17$ g/kg.

At t = 12 h clouds and strong precipitation were located behind the cold front. The main sources of moisture with $0.1 \leqslant \Delta_2 \leqslant 0.25$ g/kg and $q_{l1m} = 0.5$ g/kg were accumulating at $300 \leqslant x \leqslant 550$ km. The mois-

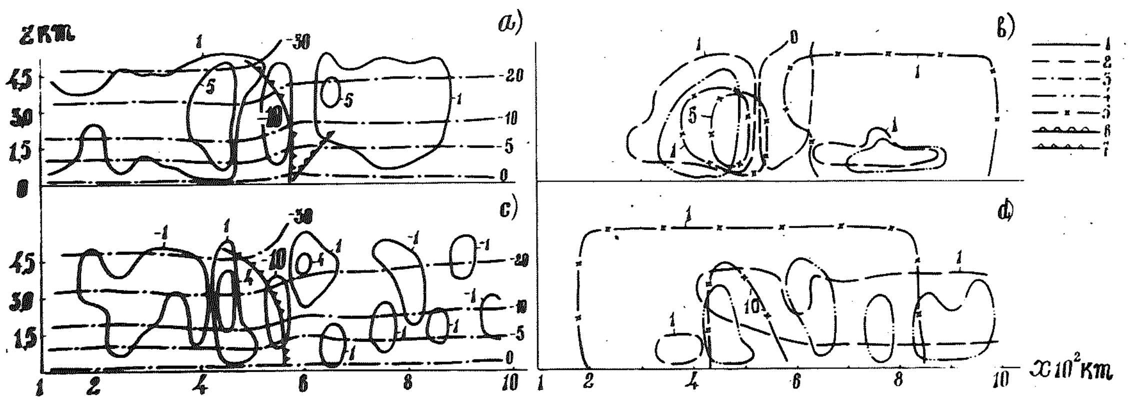

Figure 2. Vertical cross section of the frontal cloudiness (a,b) at t = 12 h, (c,d) at t = 24 h.
The numbers near isoline indicate the following: 1) W cm/s, 2) Δ_2 10^{-1} g/kg, 3) T °C, 4) $\Delta_1 = 0$, 5) q_{l2} 10^{-1} g/kg, 6) warm front, 7) cold front.

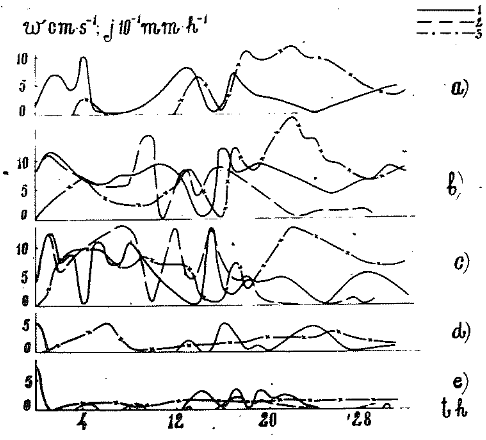

Figure 3. The time development of precipitation rate (3), maximum updrafts in both cases, with and without cloudiness (1 and 2), respectively, at x equates 400 (a), 450 (b), 500 (c), 600 (d), 700 (e) km.

ture accumulation has resulted in a precipitation rate of 0.6 mm/h at $400 \leqslant x \leqslant 500$ km (Figs. 2-3). In warm mass sources of moisture were located at $650 \leqslant x \leqslant 850$ km. In this case $j \leqslant 0.1$ mm/h.

At t = 24 h the cloud front was present, signs of the warm front were not observed. The field of the vertical motion of the warm front consisted of many cells. In the cold front the peak updraft of 5 cm/s occurred above the cold frontal surface at 4.5 km altitude. The widespread region of upward motions was located behind the cold front with peak updrafts of 5 cm/s. Downdrafts were found near the cold frontal surface, its peak of 14 cm/s occurred at 3 km altitude. The regions with $\Delta_2 > 0.1$ g/kg were found both in the warm and cold air masses. Behind the cold front $q_{l1m} = 0.44$ g/kg, in the warm air mass $q_{l1m} = 0.16$ g/kg. Both the peak ice water content q_{l2m} and peak precipitation rate j_m were found behind the cold front, $q_{l2m} = 0.14$ g/kg, $j_m = 1.5$ mm/h.

It can be seen from Table 1 that the stable mixing clouds with the maximum liquid and solid water content were located at $450 \geqslant x \geqslant 500$ km. In the warm mass the mixing clouds were less stable and their liquid water content was weaker than behind the cold front. The precipitation seemed to originate in a region about 150 km wide, which was located at $3 \geqslant z \geqslant 4$ km, near x = 450 km. In this region $j_m = 1.9$ mm/h.

Results for various cases of the warm frontal systems described in Refs. 2-5 showed that both the most stable updrafts and the main cloud region were located in the warm air mass above the frontal surface. They were unstable, when the warm front was decreasing. Evidently, in this case the front was decreasing also.

Table 1 and Fig. 3 show that the liquid water content, ice water content, ice concentration, precipitation updraft are oscillating in time and space. The amplitudes and the periods of such oscillations depend on the location of the clouds in relation to the front.

Table 1

Change in direction x and time of maximum liquid water content, maximum ice water content and ice particle concentrations

t, h	x km: 300	400	450	500	600	650	700	800
			q_{l1m}	10^{-3} g/kg				
4	68	277	400	484	2	0	0	67
8	0	128	502	501	0	92	14	29
12	0	215	486	356	2	89	23	51
16	238	144	187	234	0	0	0	16
20	57	197	423	380	0	150	98	20
24	0	20	362	436	95	134	135	154
28	0	20	258	338	17	110	110	78
32	87	318	600	522	0	46	5	2
			q_{l2m}	10^{-3} g/kg				
4	5	40	89	109	40	23	10	24
8	0	0	41	70	15	14	18	18
12	0	26	95	74	13	15	16	17
16	41	18	95	73	16	17	13	9
20	61	104	140	91	23	20	14	9
24	64	94	143	134	28	18	12	10
28	23	50	66	69	19	23	11	11
32	16	34	90	78	10	20	10	8
			N_{2m}	g^{-1}				
4	0	3	6	10	3	1	0	1
8	0	0	1	52	2	0	1	1
12	0	0	9	15	5	1	0	0
16	2	5	85	14	1	0	0	0
20	1	4	14	4	1	0	0	0
24	1	1	4	3	6	0	0	0
28	0	0	2	2	0	1	0	0
32	0	2	20	2	1	0	0	0

The stable updrafts were found at x = 450 km. Both the w_m and j oscillations were alike. The precipitation oscillations at $x \geqslant 600$ km were similar to those at x = 450 km, but their amplitude was smaller than at $400 \leqslant x \leqslant 500$ km, $j_m = 0.5$ mm/h. Evidently in the frontal system the main cloud region has determined the precipitation rate.

Table 2 and Fig. 3 illustrated the effect of the phase state of the cloudiness upon the air motion of the occluded front. In the case of the cloudless front the values f_1 and f_2 are assumed to be zero. It is evident from Fig. 3 that the period of oscillation w_m in both cases with and without cloudiness was different from each other.

It is noted that at x = 450 km in the region of the stable condensation the cloudiness was intensifying ascending motions. At x = 500 km where the condensation processes were often changing to the evaporation processes the ascending motions in the clouds were found to be weakening.

The space distribution of difference δw between w for the cases with and without cloudiness at t = 12 h is shown in Table 2.

Table 2

Change in space of vertical air motions at t = 12 h. 1) Calculations with clouds, 2) Calculations without clouds

z km	No.	x km 300	400	450	500	600	650	700	800
5	1	2	-3	1	7	-4	1	-1	0
	2	1	2	4	1	-2	3	1	1
4	1	5	-9	4	15	-7	1	-3	-0
	2	1	5	8	1	-4	5	2	2
3	1	6	-13	4	16	-7	1	-4	-1
	2	2	6	8	-1	-6	5	2	2
2	1	6	-13	5	14	-4	2	-5	-2
	2	1	6	8	-4	-5	1	1	2
1	1	3	-9	4	9	-2	1	-4	-0
	2	1	3	5	-3	-0	-3	0	1

Comparing Table 2 with Fig. 2 we see, as expected, that the upward motion was intensified in the region of intensive condensation at x = 450 km. The intensive evaporation of drops weakened the descending motion at x = 500 km. The greatest value of w may be explained by coincidence of the extreme values of w in time and space. A ratio of the maximum values of w_m in Fig. 3 was 60 - 70 %. The cloudiness effect on δ temperature T was $-3 < T < 3^{\circ}$. Mainly the $\delta T < 0$ relationship was found. The effect of evaporation was more intensive. The time and space oscillations of δw, δu, δT etc. were found.

4. CONCLUSIONS

Two-dimensional nonstationary numerical models of atmospheric fronts were constructed. Using the above models the evolution of the dynamics and microstructure of the front cloud systems were calculated, considering their interrelations.

Calculations of the horizontal structure and development of the frontal systems showed the following:

1) The dynamics, cloud microphysics and precipitations of the frontal systems may oscillate in time and space, the periods and amplitudes of these oscillations were found to depend on the values of model parameters and on the distance from frontal surface.

2) On atmospheric fronts of the winter season one or a few stable sources of moisture associated with the stable updraft regions are always existing.

3) The fields of vertical motion and frontal cloud system were shown to consist of many cells. The number of cells is increasing on the decreasing fronts.

4) The cloudiness may both intensify and weaken the ascending and descending motion in the cloud and in the nearcloud environment by 60 - 70 % in dependence on the phase of the cloud.

5. REFERENCES

1. Buikov, M.V., Pirnach, A.M., 1975. A numerical simulation of precipitation in mixed stratiform clouds taking into account its microstructure. Izv. AN USSR, FAO, v. 2. No. 5, 469-480.
2. Buikov, M.V., Pirnach, A.M., 1976. A numerical simulation of the frontal cloud systems. Trudy of Ukrainian Regional Res. Ins., No. 146, 3-23.
3. Pirnach, A.M., 1984. A numerical simulation of interaction of the dynamical and microphysical process in frontal clouds of the winter season. Trudy of Ukrainian Regional Res. Ins., No. 199 (in press).
4. Pirnach, A.M., 1983. A numerical model of cloudiness effect on atmospheric fronts. Meteorology and Hydrology, No. 9, 33-42.
5. Akimov, N.M., Palamarchuk, L.V., Pirnach, A.M., 1983. A study of precipitation associated with the winter frontal cloud system in the specified synoptical situations. Trudy of Ukrainian Regional Res. Ins., No. 203 (in press).
6. Pirnach, A.M., 1984. A study of dynamics and microphysics in the frontal cloud systems. A numerical experiments. Trudy Ukrainian Regional Res. Ins., No. 206, (in press).

OBSERVATIONAL AND NUMERICAL STUDIES OF CLOUD AND PRECIPITATION PROCESSES IN RAINBANDS IN EXTRATROPICAL CYCLONES

Steven A. Rutledge
Department of Atmospheric Sciences, Oregon State University
Corvallis, Oregon 97331 U.S.A.

and

Peter V. Hobbs
Department of Atmospheric Sciences, University of Washington
Seattle, Washington 98195 U.S.A.

1. INTRODUCTION

The regions of heaviest precipitation in extratropical cyclones usually occur in the form of mesoscale rainbands (Refs. 1-4). Several types of rainbands have been identified according to their location and orientation within extratropical cyclones (Refs. 2, 5). Since 1973 radars, aircraft, and other facilities have been used in the CYCLES (CYCLonic Extratropical Storms) Project to document rainbands in extratropical cyclones in the Pacific Northwest of the U.S.

From these field studies, conceptual models have been developed that show the relationship between the air motions, cloud structures and precipitation mechanisms in the various types of rainbands (Refs. 3, 5). Recently, we have conducted numerical modeling studies to test the validity of the conceptual models and to provide a better quantitative understanding of the precipitation processes operating within the rainbands. To date the modeling studies have focused on warm-frontal and narrow cold-frontal rainbands.

2. MODEL DESCRIPTION

The manner in which microphysical processes are handled in cloud models can be classified into two categories, parameterized or explicit. In this study we use a parameterized approach to inporate microphysical processes into our diagnostic model. Such a model requires the input of various initial fields and numerical values which are available directly from well-documented case studies.

The model is two dimensional with coordinates x-z where x is the horizontal distance perpendicular to the rainband and z is height. A complete description of the model is given in Refs. 9, 10. Model variables include temperature and the mixing ratios of water vapor, cloud water, cloud ice, rain, snow and graupel. The fields of rain, snow and graupel are precipitating fields since they are allowed to fall relative to the updraft. The size distributions of these fields are each assumed to follow an inverse exponential distribution (Refs. 6-8). The particles comprising the fields of cloud water and cloud ice are each assumed to be monodisperse in size. Continuity equations for all fields are written in Eulerian form where local changes with time of a particular quantity are computed for each time step due to advection as well as the production or destruction of the quantity due to microphysical processes.

Microphysical mechanisms in the model include processes such as condensation, deposition, collection, accretion and melting. Where required, the continuous collection equation is used to compute all collection or accretion processes. Small cloud ice crystals are initiated from the vapor phase as described in Ref. 11. Continued growth of these crystals by deposition can lead to snow initiation provided the average diameters of the cloud ice crystals exceeds 500 μm. Again we follow Ref. 11 for this formulation. The initiation of rain by the autoconversion of cloud water follows the parameterization given in Ref. 12. The threshold cloud water value is set at 0.7 g kg^{-1}.

Three graupel initiation mechanisms are included in the model. Graupel is initiated due to snow-cloud water collisions (riming) only when cloud water and snow exceed minimum threshold values (0.5 g kg^{-1} for cloud water and 0.1 g kg^{-1} for snow). If these thresholds are not met, the growth of snow by collecting cloud water is computed. The second graupel initiation mechanism occurs when collisions between snow and rain take place (for $T<0°C$) provided the mixing ratios of snow and rain both exceed 0.1 g kg^{-1}. If these conditions are not satisfied, snow increases in mass by accreting rain. The third graupel initiation mechanism results from collisions between rain and cloud ice. Graupel is initiated when rain collides with cloud ice provided the rain mixing ratio exceeds 0.1 g kg^{-1}. When these conditions are not satisfied the frozen drops are considered to be a source for snow.

The diagnostic model we use requires the input of several initial fields as well as knowledge of various numerical values in the parameterization. The initial thermodynamic fields that are specified in the x-z plane (horizontally uniform at the beginning of the model integration) include temperature, pressure and the water vapor mixing ratio. Furthermore, the air motion pattern in the x-z plane, derived from Doppler radar scans is input and held constant during the model integration. The model is run until steady-state conditions are achieved.

3. OBSERVATIONAL AND NUMERICAL STUDIES OF WARM-FRONTAL RAINBANDS

Warm-frontal rainbands are mesoscale features within which the widespread precipitation associated with the warm air advection in a cyclone is enhanced. Field studies of warm-frontal rainbands (Refs. 3,5 13-15) indicate that precipitation forms through a "seeder-feeder" process (Ref. 16). This mechanism involves ice crystals, produced aloft in "seeder" clouds (composed of small, convective cells), growing as they fall through lower-level "feeder" clouds (deep stratiform clouds).

Our modeling studies for warm-frontal rainbands are broken into two categories based on observed differences in the feeder cloud vertical motion pattern. This ascent may occur over horizontal distances of 100 km or more within and beneath the frontal zone aloft with magnitudes ~10 cm s^{-1} (Refs. 5, 14), or over shorter horizontal distances (30 km) with greater intensity (50-90 cm s^{-1}), as described in Ref. 15. The TYPE 1 category consists of a feeder cloud with weak vertical motions on the frontal scale while the TYPE 2 category models the case where the feeder cloud vertical motion is more intense and organized on the mesoscale. The model simulations consist of specifying this air motion pattern and thermodynamic fields throughout the x-z plane where the feeder zone is located. The seeder zone is parameterized by specifying a steady flux of snow into the top of the feeder zone. This flux is determined by applying a M-Z relationship (where M is the ice content and Z the radar reflectivity factor) to reflectivity data available from the particular case studies. For these warm-frontal simulations the microphysical model has been altered by eliminating the graupel category. This exclusion is based on airborne observations of particle types in warm-frontal rainbands (Refs. 5, 14-15).

3.1 Model results for the TYPE 1 case

As stated earlier this model relies heavily upon a well-documented case study to provide model input data (thermodynamic fields and air motion pattern). The case study we use for the TYPE 1 study is discussed in Ref. 14. The feeder cloud in this case extends from the 2 km level (0°C) upward to 5.5 km (-17°C). Here we assume the input of snow at this level due to the presence of the seeder clouds. The model domain is 100 km in the horizontal and 6 km in the vertical.

The simulation was begun by switching on the air motion pattern and the steady-state line source of snow at the 5.5 km level. Approximately 8000 s were required for the model to reach a steady-state. For this simulation we discuss the vertical profile of the precipitation rate in the seeder-feeder region. Precipitation rates range from 0.5 mm h^{-1} at the top of the feeder zone (the amount due to input from seeder clouds) to peak values of 1.8 mm h^{-1} just prior to melting (this level also corresponds to the base of the feeder zone). Surface rainfall rates were 1.2 mm h^{-1}. The lower surface rainfall rates are due to evaporation between cloud base and the surface. The model indicates that the increase in precipitation rates within the feeder zone was due to "seed" ice particles growing by vapor deposition.

The importance of the seeder clouds becomes clear when this simulation is compared with the case when seeder clouds are absent (the steady line source of snow at the top of the feeder zone is not permitted). In this case the precipitation rate is only 1.0 mm h^{-1} at the base of the feeder zone, compared to 1.8 mm h^{-1} at this level in the combined seeder-feeder case. Since the precipitation rate at the top of the feeder zone was 0.5 mm h^{-1} due to the presence of seed crystals, evidently less condensate is being converted to precipitation in the feeder zone in the absence of seed particles (hence the deficit of 0.3 mm h^{-1}). This condensate appears as cloud water in the upper regions of the feeder zone. Peak cloud water contents were nearly 0.1 g kg^{-1} located near the 4.5 km level. When seeder clouds were present, cloud water was suppressed since sufficient quantities of ice were available (namely the seed ice particles) to remove the available condensate.

The model results are in accord with the field measurements. For example, the model indicates that 70% of the precipitation present at the base of the feeder zone was due to the growth of seed ice particles by deposition within the feeder cloud (compared with 80% deduced from the field measurements). Also the model precipitation rates at the surface below the seeder-feeder region (1.2 mm h^{-1}) agree reasonably well with measured rates (1.2-2.0 mm h^{-1}).

3.2 Model results for the TYPE 2 case

In this TYPE 2 case we use the case study presented in Ref. 15 to provide required model input data. The feeder zone in this case extends from the 1 km level upward to 3.5 km (-4°C) where the horizontal line source of snow (seeder zone) is located.

Shown in Fig. 1 are the precipitation rates in the seeder-feeder region for this simulation. The width of the seeder zone extends from 30 to 70 km and the mesoscale zone of strong vertical motions (50-90 cm s^{-1}; see Ref. 15 for the distribution of w in the x-z plane) extends from 50-80 km. Outside this zone a uniform vertical motion of 5 cm s^{-1} is imposed.

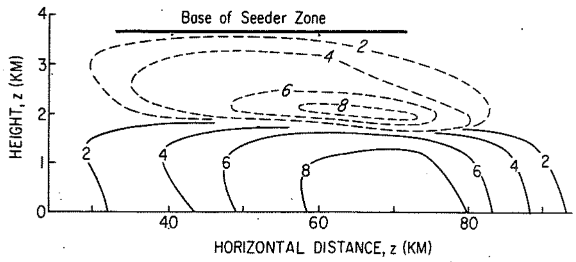

Figure 1. Precipitation rates for the TYPE 2 simulation. Dashed line is precipitation rate due to snow (mm h^{-1} of water) and solid line is precipitation rate due to rain (mm h^{-1}). Heavy line indicates base of the seeder zone.

The precipitation rate at the top of the feeder zone is 2 mm h^{-1} due to input from seeder clouds. Precipitation rates then increase rather rapidly to $\geq$ 8 mm h^{-1} just prior to melting. The maximum precipitation rate in the snow region immediately above the 0°C level is 8.5 mm h^{-1} (located near x=70 km). The peak precipitation rate at cloud base (1 km level) was 9.3 mm h^{-1}, so therefore the growth of precipitation between the 0°C level and cloud base was small. Hence the bulk of the precipitation growth in the feeder cloud took place in the layer between 3.5 and 2 km.

The model indicates that the rapid increase in precipitation rates within the feeder zone occurred due to snow collecting cloud water immediately above the 0°C level. Appreciable amounts of cloud water were present in the feeder zone with values between 0.1-0.3 g kg^{-1} located between the 1.5 and 3 km levels. The larger cloud water contents occurred near the 2 km level. Hence in this TYPE 2 case, a substantial amount of cloud water is present in the feeder zone, as a result of the strong, mesoscale updraft.

In this case the precipitation was a direct result of seed ice particles sweeping out the available cloud water. The average surface precipitation rate beneath the rainband was 7.4 mm h^{-1} compared to a measured average rate of 8.0 mm h^{-1}. The dominant precipitation growth mechanism is riming which is in agreement with the conclusions given in Ref. 15.

4. OBSERVATIONAL AND NUMERICAL STUDIES OF NARROW COLD-FRONTAL RAINBANDS

The narrow cold-frontal rainband often contains the most intense precipitation within a cyclonic storm. This rainband has been shown to consist of a series of small, ellipsoidally-shaped "cores" that straddle the surface cold front (Refs. 3, 17, 18). Precipitation rates are high in these core areas but markedly depressed in the "gap" regions between the cores (Ref. 19).

The air motion pattern within this rainband is dominated by a narrow, intense updraft located directly above the surface cold front. Updraft speeds of 10 m s^{-1} are common (Refs. 5, 19). These intense updrafts produce relatively high cloud water contents (1-2 g m^{-3}) and riming is considered to be the dominant precipitation growth mechanism.

The model studies for the narrow cold-frontal rainband are conducted in a similar manner to those discussed in Sec. 3 in that a well-documented case study provides required model inputs (Ref. 19). In the case studies described in Refs. 5, 19, the rainband was embedded either within light stratiform precipitation or within a wide cold-frontal rainband. Since the airflow ahead of the rainband is dominated by strong low level inflow, it appears likely that particles originating within these stratiform clouds could be swept up into the updraft region and perhaps affect the precipitation process. In-situ airborne sampling in these rainbands supported this "seeding" since particles at low levels in the updraft region consisted of large crystals and aggregates which are unlikely to have originated within the warm, shallow updrafts. Our model studies include this source of snow ahead of the rainband by assuming a steady vertical line source of snow to be present immediately ahead of the rainband. The magnitude of the snow content in this vertical profile is deduced from radar reflectivity measurements available in Ref. 19. Available from the observational study are the requisite thermodynamic and air motion fields required as model inputs. The peak updraft velocity in this case was 7 m s^{-1}. The cloud microphysical model in this case does not exclude graupel.

Shown in Fig. 2 are several model output quantities for this case. Cloud water is confined to a relatively narrow region above the surface cold front since it is within this region that the strongest vertical motions are found. The cloud water contour indicated roughly corresponds to the 1 m s^{-1} vertical velocity contour. The peak cloud water content is 0.9 g kg^{-1} compared to measured values ranging from 0.7 to 1.5 g kg^{-1} in this region.

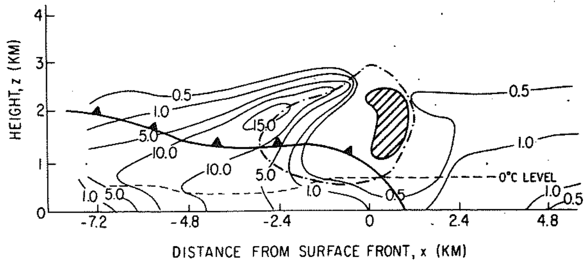

Figure 2. Precipitation rate (mm h^{-1}, solid line), cloud water contour (≥ 0.5 g kg^{-1}, dash-dot line), and graupel initiation zone (hatching). The cold front is indicated by the usual symbol.

The hatched region in Fig. 2 indicates the graupel initiation region. Here graupel is initiated by snow-cloud water collisions (riming). The snow that is converted to graupel in this region does not originate in the updraft region but rather is supplied by the stratiform clouds ahead of the rainband. The other possible graupel initiation mechanisms were not activated as both require a rain content exceeding 0.1 g kg^{-1}, peak values were only 0.03 g kg^{-1}. The rain content was kept small due to accretion by both graupel and snow. Furthermore, the relatively low amounts of rain in the updraft region prevented appreciable snow initiation which can occur when rain freezes upon colliding with cloud ice. This together with the general smallness of other snow initiation mechanisms in the updraft region results in graupel forming along the leading edge of the updraft region, upon ice particles that originate in the stratiform clouds ahead of the rainband. The continued growth of graupel is dominated by the collection of cloud water in the updraft region.

Next we turn to a brief discussion of the precipitation pattern produced by the model shown in Fig. 2. Ahead of the surface front the precipitation rate is fairly uniform, with surface rates ~1 mm h^{-1}. The precipitation in this region is due to the vertical source of snow (located at x=5 km). The second precipitation zone is located between x=1.2 and x=-1.2 km. The precipitation rate in this region is nearly zero everywhere. Because of the strong updrafts in this region, precipitation particles are moving upward instead of falling to the surface. The third precipitation zone is located where x ≤ -1.2 km and is characterized by rapidly increasing precipitation rates with a peak value of 12.3 mm h^{-1} located 5 km to the rear of the surface front. The precipitation above the 0°C level in this region consists mainly of graupel. Rapid melting of graupel occurs below the 0°C level, hence the surface precipitation is mostly rain. This variation in the surface precipitation rate predicted by the model agrees well with observations (Ref. 5). In addition the average surface precipitation rate from the rainband predicted by the model (9.0 mm h^{-1}) agrees well with field measurements (8.0 mm h^{-1}). The maximum surface precipitation rate was located 4 km to the rear of the surface front in the field measurements. This relatively good agreement between the model results and field measurements lends confidence to these results.

4. CONCLUSIONS

In the warm-frontal simulations precipitation growth occurred through vapor deposition in the feeder zone when the vertical motions were weak and organized on the frontal scale. When the vertical motions in the feeder zone were strong and organized on the mesoscale, precipitation growth occurred through riming. In both cases the role of the seeder clouds was to supply sufficient quantities of ice to efficiently remove condensate available in the feeder zone.

Model studies for the narrow cold-frontal rainband indicate that graupel forms in this rainband when ice particles, that originate in the stratiform clouds ahead of the rainband, grow rapidly by riming when they enter the strong updraft (and hence region of high liquid water content). When this source of input ice particles are absent, somewhat weaker graupel precipitation occurs. Graupel forms in this case when small frozen drops grow by riming. The drops form in the updraft region through autoconversion and subsequently freeze when collisions with cloud ice occur. The production of frozen drops is much smaller when ice particles enter the updraft region due to larger accretional growth rates. The snow particles from the surrounding stratiform clouds allow large quantities of cloud water to be removed from the updraft through riming. Hence the surrounding stratiform clouds act as a seeder zone in this case, supplying ice particles to the convective updraft region (a feeder zone). This is the inverse of the seeder-feeder process in warm-frontal rainbands where convective clouds act as the seeder zone and stratiform clouds serve as the feeder zone.

5. REFERENCES

1. Browning K A 1974, Mesoscale structure of rain systems in the British Isles, *J. Meteor. Soc. Japan* 50, 314-217.

2. Houze R A Jr et al 1976, Mesoscale rainbands in extratropical cyclones, *Mon. Wea. Rev.* 104, 868-878.

3. Hobbs P V 1978, Organization and structure of clouds and precipitation on the mesoscale and microscale in cyclonic storms, *Rev. Geophys. and Space Phys.* 16, 741-756.

4. Houze R A Jr & Hobbs P V 1982, Organization and structure of precipitating cloud systems, *Adv. in Geophysics* 24, 225-315.

5. Matejka T J et al 1980, Microphysics and dynamics of clouds associated with mesoscale rainbands in extratropical cyclones, *Quart. J. Roy. Meteor. Soc.* 106, 29-56.

6. Marshall J S & Palmer W McK 1948, The distribution of raindrops with size, *J. Meteor.* 5, 165-166.

7. Gunn K L S & Marshall J S 1958, The distrbution with size of aggregate snowflakes, *J. Meteor.* 15, 452-461.

8. Houze R A Jr et al 1979, Size distributions of precipitation particles in frontal clouds, *J. Atmos. Sci.* 36, 156-162.

9. Rutledge S A & Hobbs P V 1983, The mesoscale and microscale structure and organization of clouds and precipitation in midlatitude cyclones. VIII: A model for the "seeder-feeder" process in warm-frontal rainbands, *J. Atmos. Sci.* 40, 1185-1206.

10. Rutledge S A & Hobbs P V, 1983, The mesoscale and microscale structure and organization of clouds and precipitation in midlatitude cyclones. XII: A numerical study of precipitation development in narrow cold-frontal rainbands, *J. Atmos. Sci.* (submitted).

11. Stephen M A 1979, A simple ice phase parameterization, *Paper No. 319. Dept. of Atmos. Sci.* Colo. State Univ., Ft. Collins, CO, 122 pp.

12. Kessler E III 1969, On the distribution and continuity of water substance in atmospheric circulations, *Meteor. Monogr. 32*, 84 pp.

13. Hobbs P V & Locatelli J D 1978, Rainbands, precipitation cores and generating cells in a cyclonic storm, *J. Atmos. Sci.* 35, 230-241.

14. Herzegh P H & Hobbs P V 1980, The mesoscale and microscale structure and organization of clouds and precipitation in midlatitude cyclones. II: Warm-frontal clouds, *J. Atmos. Sci.* 37, 597-611.

15. Houze R A Jr et al 1981, The mesoscale and microscale structure and organization of clouds and precipitation in midlatitude cyclones. III: Air motions and precipitation growth in a warm-frontal rainband, *J. Atmos. Sci.* 38, 639-649.

16. Bergeron T 1950, Uber der mechanisum der ausgeibigen Niderschlage, *Ber. Dtsch. Netterdien Stes.* 12, 225-232.

17. Hobbs P V & Biswas K R 1979, The cellular structure of narrow cold-frontal rainbands, *Quart. J. Roy. Meteor. Soc.* 105, 723-727.

18. James P K & Browning K A 1979, Mesoscale structure of line convection at surface cold fronts, *Quart. J. Roy. Meteor. Soc.* 105, 371-382.

19. Hobbs P V & Persson P O G 1982, The mesoscale and microscale structure and organization of clouds and precipitation in midlatitude cyclones. V: The substructure of narrow cold-frontal rainbands, *J. Atmos. Sci.* 39, 280-295.

A THREE-DIMENSIONAL NUMERICAL SIMULATION OF THE BREAKUP OF A MARITIME STRATUS-CAPPED BOUNDARY LAYER

Paul M. Tag and Steven W. Payne

Naval Environmental Prediction Research Facility
Monterey, California 93943 U.S.A.

1. INTRODUCTION

The planetary boundary layer (PBL) bridges the gap between the solid boundary of the earth's surface and the free-flowing atmosphere above. As such, the PBL controls the evolution of the large scale weather features familiar to all weather forecasters. More important, the PBL is that area where we all live and are concerned with the sensible weather elements of temperature, precipitation, and wind.

In terms of predicting numerically the highly nonlinear interaction between the PBL and the free atmosphere, the handling of the PBL is the most difficult. Whereas the free atmosphere can reasonably be approximated by grid points separated by tens, or even hundreds, of kilometers, the use of such large horizontal spacing for the PBL is less justified. Terrain, land/water interfaces, and surface conditions can all change on very fine scales. One could argue that large oceanic expanses which are comparatively devoid of fine-scale surface variations would thus be ideal for large horizontal grid spacing in the PBL.

Although the preceding argument sounds plausible, the regional or global modeler will be quick to point out that the oceanic PBL is anything but uniform. He or she will point to a satellite photo speckled with oceanic cumulus clouds, with hundreds of clouds existing within the confines of one numerical grid. This same modeler will tell you that the correct parameterization of a nonuniform layer of clouds poses a large problem in large scale atmospheric modeling. Because the role of the stratocumulus or cumulus is to transport energy from the surface to higher levels, inaccuracies in the simulation of PBL cloud populations or their breakup will lead to inaccuracies in the firing of the atmospheric heat engine.

2. STATEMENT OF THE PROBLEM

For this presentation we will concentrate on the evolution of a homogeneous stratus layer into a broken field of stratocumulus, and further on to complete dissipation. This transition is important for two reasons, the first of which is obvious. Many a forecast user would like to know the timing of a stratus breakup. More important to our purpose here, an understanding with regard to regional or global modeling, the behavior and effect of a homogeneous deck of clouds is much different from a broken layer. As a result, the correct timing of a breakup is important.

Specifically, we will explore the breakup of a stratus layer through cloud top entrainment. Deardorff (Ref. 1) and Randall (Ref. 2) have both derived theoretically the criteria for onset of cloud top instability. Randall defines this instability as CIFKU (CIFK upside-down), as a variation of CIFK (conditional instability of the first kind). CIFKU is a downward-directed instability in which dry air from above cloud top is 1) mixed into the cloud top, 2) becomes heavier due to evaporation of cloud water into the parcel, and 3) continues to accelerate downward. Deardorff defines one criterion for CIFKU onset in terms of the equivalent potential temperature:

$$\Delta\theta_e < (\Delta\theta_e)_{crit.} \qquad (1)$$

where

$$(\Delta\theta_e)_{crit.} = \frac{\bar{\theta}\Delta q_w}{\alpha} .$$

In this expression, q_w is the total water specific humidity, α is a variable with a value typically near one-half, and Δ represents the above-cloud to the in-cloud difference. The equivalent potential temperature is defined as

$$\theta_e = \theta(1 + \frac{L}{C_p T} q),$$

where the symbols have their usual definitions. It is our purpose to determine whether the criterion of Eq. 1, or any criterion for stratus breakup, can be applied to the mean condition across an area which is much larger than individual cloud elements.

3. NUMERICAL MODEL

The NEPRF three-dimensional PBL model (DIMEN3) was chosen for this study. DIMEN3 was developed to explore BL development over the open ocean or near land and adjacent ocean. Although fully three-dimensional, our model can be run in one or two dimensions also.

DIMEN3 is a system of partial differential equations solved on a staggered (Arakawa Scheme C) grid (Ref. 3). We have differential equations for u, v, w, θ, r_v, and r_c (three wind components, potential temperature, and vapor and cloud mixing ratios). The potential temperature and mixing ratios are handled in normal eulerian fashion until condensation occurs, at which time the advection process is switched to a Lagrangian scheme. Such a scheme is conceptually more straightforward for phase changes, which occur in a highly implicit way (Ref. 4).

The important physical processes with respect to marine PBL simulations are turbulent mixing and radiation. The radiation package was adapted from the work of Ref. (5) and includes both short and long wave radiation. The vertical turbulent mixing is the most important component of a successful stratus simulation and is based on K-theory here. Above the surface boundary layer (as specified by Barker and Baxter's formulation (Ref. 6) of the Businger et al. data (Ref. 7)), values of the eddy mixing coefficient K_M are a function of local wind shear and buoyancy (Ref. 8). In a recent comparison of five numerical fog/stratus prediction models (ranging in sophistication from a higher order closure (HOC) model to a mixed layer "slab" model), DIMEN3 came in second, right behind the NEPRF HOC model (Ref. 9). As a result of this testing, we have some confidence in the use of this model for our study here.

4. NUMERICAL SIMULATIONS

Deardorff (Ref. 1) conducted a three-dimensional simulation of stratus breakup. Because of cloud interaction with the top of his domain, however, he stopped the computation before the stratus had broken into scattered cumuli. We intend to present a stratus breakup with both two and three-dimensional simulations. We will follow Deardorff's method of generating a stratus deck and then initiating cloud top instability by cooling the air above the cloud. In our simulations, however, we will include radiative flux divergence.

Variations in the homogeneous stratus layer will be generated through variations in the ocean surface temperature. One initial experiment with a one degree step function has been successful in stimulating variations in the stratus layer. In sensitivity experiments we intend to vary not only the amplitude but also the frequency of the variation. Our primary goal, however, is to determine if the conditions which define stratus breakup across a variable-temperature surface are equivalent to the breakup conditions for a corresponding constant mean surface temperature. The answer to this question is of particular interest to the large-scale modeler and will dominate the conference presentation.

5. REFERENCES

1. Deardorff J W 1980, Cloud top entrainment instability, *J Appl Meteor*, 37, 131-147.

2. Randall D A 1980, Conditional instability of the first kind upside-down, *J Atmos Sci*, 37, 125-130.

3. Tag P M & Rosmond T E 1980, Accuracy and energy conservation in a three-dimensional anelastic model, *J Atmos Sci*, 37 2150-2168.

4. Murray F W 1970, Numerical models of a tropical cumulus cloud with bilateral and axial symmetry, *Mon Wea Rev*, 98, 14-28.

5. Oliver D A & Lewellen W S 1979, The A.R.A.P. atmospheric radiation model. Appendix C of status report on low-level atmospheric turbulence model, final report, Aeronautical Research Associates of Princeton, Inc., Princeton, NJ, 116 pp.

6. Barker E H & Baxter T L 1975, A note on the computation of atmospheric surface layer fluxes for use in numerical modeling, *J Appl Meteor*, 14, 620-622.

7. Businger, J A et al 1971, Flux-profile relationships in the atmospheric surface layer *J Atmos Sci*, 28, 181-189.

8. Tag P M 1983, Marine fog/stratus forecasting with a 3-D boundary layer model. Preprints of papers presented at the Sixth Conference on Numerical Weather Prediction, American Meteorological Society, 45 Beacon St., Boston, MA, 74-76.

9. Mack E J et al 1983, An evaluation of marine fog forecast concepts and a preliminary design for a marine observation forecast system. Project SEA FOG IX Final Report, Naval Air Systems Command Contract No. N00019-81-C-0102, Room 472 Jefferson Plaza, No. 1, Washington, DC 20361, 73 pp. plus Appendices.

NUMERICAL MODEL OF COLD FRONT CONVECTIVE CLOUDS

S.A. Vladimirov, R.S. Pastushkov

Central Aerological Observatory, USSR State Committee for Hydrometeorology and Control of Natural Environment
Moscow, 123376, USSR

1. INTRODUCTION

Most numerical investigations which deal with frontal structures and their evolutions have concentrated on problems of frontogenesis (Refs.1-3). In these cases, initially smooth baroclinic zones are distorted to form a frontal zone through an imposed synoptic deformation field. However, although these studies provide a complete picture of the frontal formation, they are not so successful in describing a fully developed front after frontogenesis has occured.

Another approach to numerical investigations of fronts is to study the already formed mature frontal system (Refs.4-6). In such models, the initial conditions do not contain the synoptic deformation fields, but rather include the velocity components fields. So both the movement of front and the characteristic jet distribution of the velocity component parallel to front can be taken into consideration.

All the previous numerical models of fronts have included the hydrostatic assumption. Therefore, the convective processes associated with a cold front cannot be represented well enough in these models. However, convective processes are playing an essential role in the dynamics of fronts, especially in the case of the cold ones.

Therefore, we shall not use the hydrostatic assumption in the present model. Moreover, we shall use the second abovementioned approach in frontal modelling and shall not consider the initial phase of the front development.

2. GOVERNING EQUATIONS. BOUNDARY AND INITIAL CONDITIONS

The present two-dimensional numerical model employs the free convection assumption of the thermohydrodynamical equations of atmosphere, with a set of thermodynamical and parameterizational relations. The equations are written in the Cartesian coordinates with the y coordinate running parallel to the axis of the front. All the used variables are uniform in y, except for the quantity θ_g, where $\partial\theta_g/\partial y$ is only a function of z. To represent the velocity field in the x-z plane we use a streamfunction ψ, along with a vorticity ω.

The model includes the equation of vorticity

$$\frac{\partial \omega}{\partial t} + \frac{\partial (u\omega)}{\partial x} + \frac{\partial (w\omega)}{\partial z} = -f\frac{\partial V}{\partial z} + g\frac{\partial}{\partial x}\left(\frac{\vartheta}{\theta_0} + 0.61q - 1.61L\right) + \frac{\partial}{\partial x}K_x\frac{\partial \omega}{\partial x} + \frac{\partial}{\partial z}K_z\frac{\partial \omega}{\partial z}, \qquad (1)$$

the equation of velocity component parallel to the front

$$\frac{\partial V}{\partial t} + \frac{\partial (uV)}{\partial x} + \frac{\partial (wV)}{\partial z} = -f(u - v_0) + \frac{\partial}{\partial x}K_x\frac{\partial V}{\partial x} + \frac{\partial}{\partial z}K_z\frac{\partial V}{\partial z}, \qquad (2)$$

the thermodynamic equation

$$\frac{\partial \vartheta}{\partial t} + \frac{\partial (u\vartheta)}{\partial x} + \frac{\partial (w\vartheta)}{\partial z} = -V\frac{\partial \theta_g}{\partial y} + \alpha_1 W + \frac{\partial}{\partial x}K_x\frac{\partial \vartheta}{\partial x} + \frac{\partial}{\partial z}\left(\frac{\partial \vartheta}{\partial z} - \alpha_1\right), \qquad (3)$$

the equation of conservation of all water substance

$$\frac{\partial q}{\partial t} + \frac{\partial (uq)}{\partial x} + \frac{\partial (wq)}{\partial z} = \frac{\partial}{\partial z}(V_r L_r) + \alpha_2 W + \frac{\partial}{\partial x}K_x\frac{\partial q}{\partial x} + \frac{\partial}{\partial z}K_z\left(\frac{\partial q}{\partial z} - \alpha_2\right), \qquad (4)$$

the diagnostic relation between vorticity and streamfunction

$$\frac{1}{\rho_0}\frac{\partial^2 \psi}{\partial x^2} + \frac{\partial}{\partial z}\frac{1}{\rho_0}\frac{\partial \psi}{\partial z} = -\omega . \qquad (5)$$

A streamfunction is defined as

$$\rho_0 u = \frac{\partial \psi}{\partial z} \qquad \rho_0 W = -\frac{\partial \psi}{\partial x} \qquad (6)$$

The equations (1) to (5) are completed by the following parameterizational and physical relations:

$$\alpha_1 = \begin{cases} \gamma - \gamma_d \\ \gamma - \gamma_w \end{cases}, \quad L = \begin{cases} 0, & \text{when } q < q_s \\ q - q_s, & \text{when } q \geq q_s \end{cases} \qquad (7)$$

$$\alpha_2 = -\frac{dQ_0}{dz}, \qquad (8)$$

$$L_r = \begin{cases} 0, & \text{when } L \leq 10^{-3} \\ L - 10^{-3}, & \text{when } L > 10^{-3} \end{cases} \qquad (9)$$

$$V_r = \begin{cases} 4.5 \cdot 10^{3/2} L_r^{1/2}, & \text{when } L_r < 4 \cdot 10^{-3} \\ 9, & \text{when } L_r \geq 4 \cdot 10^{-3} \end{cases} \qquad (10)$$

$$q_s = Q_{0s} \exp\frac{L_c \vartheta}{R_v \theta_0^2} - Q_0(z), \qquad (11)$$

$$K_z = K_0 + L_T^2 \cdot Def \quad , \quad K_x = K_z \left(\frac{h_x}{h_z}\right)^{4/3} . \tag{12}$$

Here u, v, w are the x (across the front)-, y (along the front)-, and z (vertical)- components of the velocity; v_0 is the initial value of u; f is the Coriolis parameter; ϑ, q, q_s are the deviations of temperature, specific moisture content, saturation specific humidity from their initial reference values in the prefrontal region (at the right boundary) $T_0(z)$, $Q_0(z)$ (θ_0 being vertical average of $T_0(z)$); L, L_r are the specific all liquid water and water content in raindrops; V_r is the terminal rainfall velocity; γ, γ_d, γ_w are the initial (at the right boundary), the dry and wet adiabatic lapse rates; K_x, K_z are the x - and z - eddy diffusion coefficients (K_0 being constant initial value of K_z, L_T - average scale of turbulence, Def - velocity field deformation); $\rho_0(z)$ is the initial stratified air density; $Q_{os}(z)$ is the initial saturation specific humidity; L_c is the latent heat of condensation; R_v is the gas constant of water vapor.

In addition, in Eq. 2 the assumption

$$-\frac{1}{\rho_0}\frac{\partial P}{\partial y} = f v_0 \tag{13}$$

and geostrophic relation

$$\frac{\partial \theta_g}{\partial y} = -f\frac{\theta_0}{g}\frac{\partial v_0}{\partial z} \tag{14}$$

have been used. The total temperature field was assumed to be of the form

$$T(x,y,z,t) = T_0(z) + \vartheta(x,z,t) + \theta_g(y,z). \tag{15}$$

The initial field of the velocity component parallel to the front was defined according to (Ref. 4), the initial velocity across the front was only a function of z, and the initial vertical velocity was equal to zero.

To define the initial field of temperature the geostrophic relation has been used

$$\frac{\partial \vartheta^\circ}{\partial x} = \frac{f\theta}{g}\frac{\partial V^\circ}{\partial z} \tag{16}$$

To evaluate the influence of the heat and radiative properties of the surface on the frontal dynamics the bottom boundary conditions for the temperature in the form of the heat balance equation of the surface have been adopted

$$C\frac{\partial T_*}{\partial t} + R_* + H_* + LM_* = 0 \tag{17}$$

Here C is the heat capacity of the effective water layer, which parameterize the heat flux to the ground, T_* is the surface temperature, H_*, LM_* are the heat and the latent heat fluxes to the atmosphere, parameterized according to (Ref. 7), R_* is the total radiative flux from the surface determined according to (Ref. 8).

The other bottom and top boundary conditions were

at $z = 0$

$$\omega = a^\circ, \quad \psi, q = 0 \qquad V = V^\circ(x,0), \tag{18}$$

at $z = H$

$$\omega = a \qquad \psi = \frac{aH^2}{2} \qquad \vartheta, q, v = 0. \tag{19}$$

The formulation of the lateral boundary conditions is a more difficult problem. These conditions must be open-type and allow disturbances to "radiate" out of the domain under consideration without reflection. There are several versions of such conditions. In this paper the next ones have been used (Ref. 9):

at $x = 0$ ("inflow" boundary)

$$\frac{\partial \omega}{\partial t} = 0 \qquad \frac{\partial \varphi}{\partial x} = 0 \qquad (\varphi \equiv \psi, \vartheta, q, v), \tag{20}$$

at $x = L_x$ ("outflow" boundary)

$$\varphi_{I+1}^{n+1} = 2\varphi_I^n - \varphi_{I-1}^{n-1} . \tag{21}$$

3. COMPUTATIONAL SCHEME

To minimize computational instability and to keep the conservation properties of the governing set of equations the advective terms in the vorticity Eq. 1 were represented by the algorithms of Arakawa and the advective terms in Eqs. 3-4 were represented by algorithms of Lilly. Centered space and time difference approximations were used to represent the other space and time derivatives. The turbulent terms were approximated by the Duffort-Francel scheme.

The finite difference form of Eqs. 1-5 with the Richardson-Shuman notations may be written as follows

$$\delta_t \overline{\omega}^t + \delta_x \overline{(\overline{u}^z \omega)}^x + \delta_z \overline{(\overline{w}^x \omega)}^z = -f\delta_z V + \delta_x g\overline{\left(\frac{\vartheta}{\theta_0} + 0.61q - 1.61L\right)}^{xzz} + \left[\delta_x(K_x\delta_x\omega) + \delta_z(K_z\delta_z\omega)\right]_{DF} \tag{22}$$

$$\delta_t \overline{V}^t + \delta_x(\overline{u}^{xz}\overline{V}^x) + \delta_z(\overline{w}^{xz}\overline{V}^z) = f(u - v_0) + \left[\delta_x(K_x\delta_x V) + \delta_z(K_z\delta_z V)\right]_{DF} \tag{23}$$

$$\delta_t \overline{\vartheta}^t + \delta_x(\overline{u}^{xz}\overline{\vartheta}^x) + \delta_z(\overline{w}^{xz}\overline{\vartheta}^z) = -v\frac{f\theta_0 a}{g} + \alpha_1\overline{w}^z\left[\delta_x(K_x\delta_x\vartheta) + \delta_z(K_z(\delta_z\vartheta - \alpha_1))\right]_{DF} \tag{24}$$

$$\delta_t \overline{q}^t + \delta_x(\overline{u}^{xz}\overline{q}^x) + \delta_z(\overline{w}^{xz}\overline{q}^z) = \delta_z\overline{(V_r L_r)}^{xzz} + \alpha_2\overline{w}^z\left[\delta_x(K_x\delta_x q) + \delta_z(K_z(\delta_z q - \alpha_2))\right]_{DF} \tag{25}$$

$$\delta_{xx}\psi + \delta_z(\delta_z - \rho_0^{-1}\delta_z\rho_0) = -\rho_0\omega \tag{26}$$

The diagnostic Eq. 26 was solved by the Nemchinov method (Ref. 11). According to Ref. 12 the linear stability conditions for Eqs. 22-26 are

$$\Delta t < \min\left[\frac{\min(h_x, h_z)}{\max(|u| + |w|)}, \frac{\min(h_x^2, h_z^2)}{4K_{max}}\right] \tag{27}$$

4. RESULTS OF COMPUTATIONS

A series of the experiments with the present model were run to study the evolutions of the cold front and its convective cloud system. The results obtained show a sufficient accuracy of the computations. For instance, the errors of satisfaction of the energy equations are of the order 5-10 %.

The integration process consisted of two stages. Such procedure was used in Ref. 5, too. On the initial stage we have used the equations without moisture. The results of this "dry" integration are shown in Fig. 1. On the second stage we have integrated the total set of equations.

The "dry" integration was performed with the horizontal grid size of 4 km. In the "moist" case this size was 2 km. The vertical and the time increments were 0.5 km and 30 s in both cases. The domain under consideration was 600 km in horizontal and 8.5 km in vertical.

The results of the experiments presented here were obtained for the case of the specific profile of the relative humidity. There was a layer with a very high value (0.95). The purpose of using such profile of the relative humidity was to obtain the cloudiness just at the beginning of the "moist" integration.

Fig. 2 shows that the cloud appearence has occurred just on the initial time steps of the "moist" integration. The further evolution of the frontal cloudiness depends on the values of the parameters used in the model, in particular on the turbulent exchange. If the mean vertical turbulent coefficient is of the order 100 $m^2 \cdot s^{-1}$ (the mean horizontal coefficient is 5000 $m^2 \cdot s^{-1}$) the frontal cloud grows initially in the horizontal direction and then at some moment begins to break into smaller clouds in the region close to the frontal surface. (See Fig. 3). At the time 1.5 h these small clouds develop to the system of six convective clouds with the top height up to 3.5 km. In the case of larger turbulent intensity all these effects are smoothed. The cloudiness grows more slowly and does not transform into convective cells at least up to the time 2.5 h.

A comparison of the "moist" integration results with the "dry" ones shows the essential moisture effects on the dynamics of the frontal circulation.

In conclusion it is worth pointing out that some of our results correspond to the really observed phenomena. In particular the zero temperature departure contour stretched to the frontal movement direction (Fig. 2) corresponds to the well-known phenomenon of the midtropospheric temperature fall above a warm sector a few hundreds of kilometers in front of the cold front (Ref. 13). The radar data also show that frontal rain, as a rule, does not form a single area, but pass as two or three bands with 1-2 hour intervals (Ref. 14). This fact corresponds to transformation of our main frontal cloudiness to the system of the convective cells. (Fig. 3).

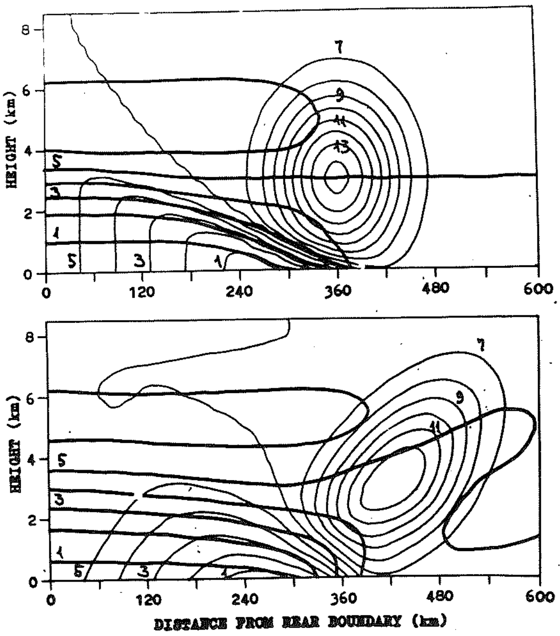

Figure 1. The evolution the "dry" frontal circulation. The upper frame shows the temperature deviation ϑ (thick solid lines) and the velocity component parallel to the front V (thin solid lines) at the initial moment. The lower frame shows the same variables at time 6 h. Contour intervals are $\Delta\vartheta$ = 1 °C, ΔV = 3 $m \cdot s^{-1}$. Initial contours are ϑ_1 = -4 °C, V_1 = = 15 $m \cdot s^{-1}$.

5. REFERENCES

1. Williams, R., 1967. Atmospheric frontogenesis: a numerical experiment. J. Atmos. Sci., 24, 627-641.
2. Hoskins, B., 1971. Atmospheric frontogenesis model; some solution. Quart. J. Roy. Met. Soc., 97, 412.
3. Kutsenko, B. Ya., 1981. Numerical studies of frontogenesis with account of phase transitions. Meteorology and Hydrology, No. 9, 23-34.
4. Orlanski, I., Ross, B., 1977. The circulation associated with a cold front. Part 1: dry case. J. Atmos. Sci., 34, 1691-1733.
5. Orlanski, I., Ross, B., 1978. The circulation associated with a cold front. Part 2: moist case. J. Atmos. Sci., 35, 445-465.
6. Orlanski, I., Ross, B., 1982. The evolution of an observed cold front. Part 1: numerical simulation. J. Atmos. Sci., 39, 296-327.
7. Corby, G., 1974. Global 5-level general circulation model. GARP Publ. Ser., No. 14, 113-126.
8. The report of the third international conference of experts on the radiation program of GATE, 1975, Leningrad, 186-188.
9. Elvius, T., Sundsröm, A., 1979. Numerical methods in atmospheric models, GARP Publ. Ser. No. 17, 379-416.

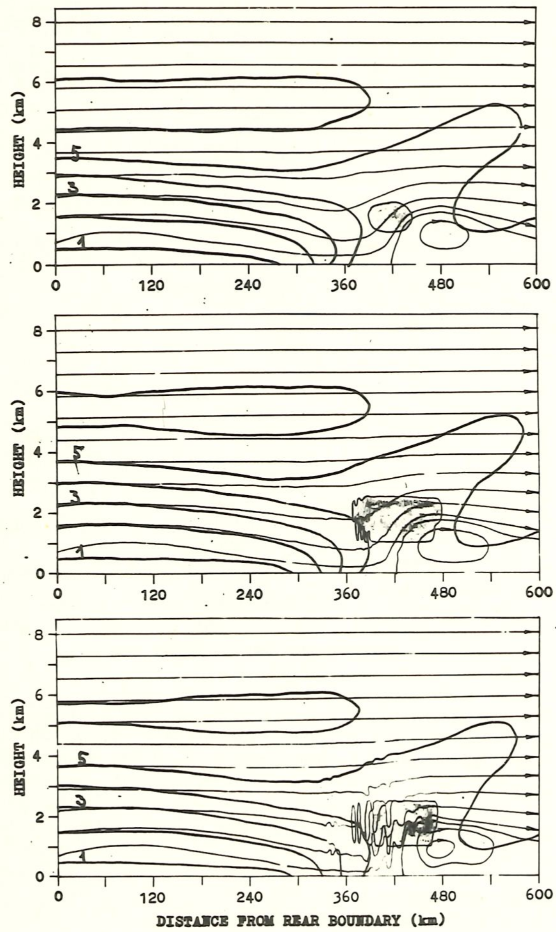

Figure 2. The evolution of the "moist" frontal circulation from the position given in the lower frame of Fig. 1. The upper frame shows the temperature deviation ϑ (thick solid lines), the streamfunction ψ (thin solid lines) and liquid water content L (shaded areas) at the time 2.5 min after the beginning of "moist" integration. The middle and the lower frames show the same variables at the times 32.5 and 55 min, respectively. Contour intervals are the same as in Fig. 1 for ϑ and variable for ψ

10. Lilly, D., 1964. Numerical solutions for shape-preserving two-dimensional convective element. J. Atmos. Sci., 21, 83-98.
11. Nemchinov, S.V., 1967. On the solution of boundary problems for elliptical second-order differential equations by grid method. J. Comp. Math. and Math. Phys., 2, No. 3, 418-436.
12. Fromm, J., 1967. Unstable flow of incompressible viscous liquid. The numerical methods in hydrodynamics. Moskwa, Mir.
13. Khromov, S.P., 1948. The Synoptical Meteorology, Leningrad, Gidrometeoizdat, 696 pp.
14. Borovikov, A.M. et al., 1961. The Cloud Physics, Leningrad, Gidrometeoizdat, 460 pp.

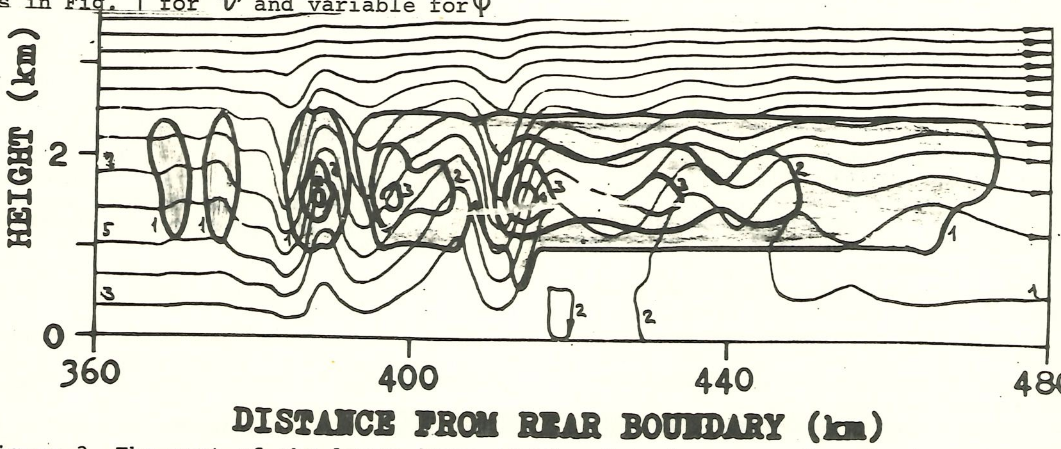

Figure 3. The part of the lower frame of Fig. 2 in larger scale. The liquid water content L and streamfunction ψ are shown by thick and thin solid lines, respectively. Contour intervals are ΔL = 0.1 $g \cdot kg^{-1}$, $\Delta\psi$ = 500 $m^2 \cdot s^{-1}$.

AUTHOR INDEX
of Volume II